GEOLOGIJA

2023 | št.: **66/1**

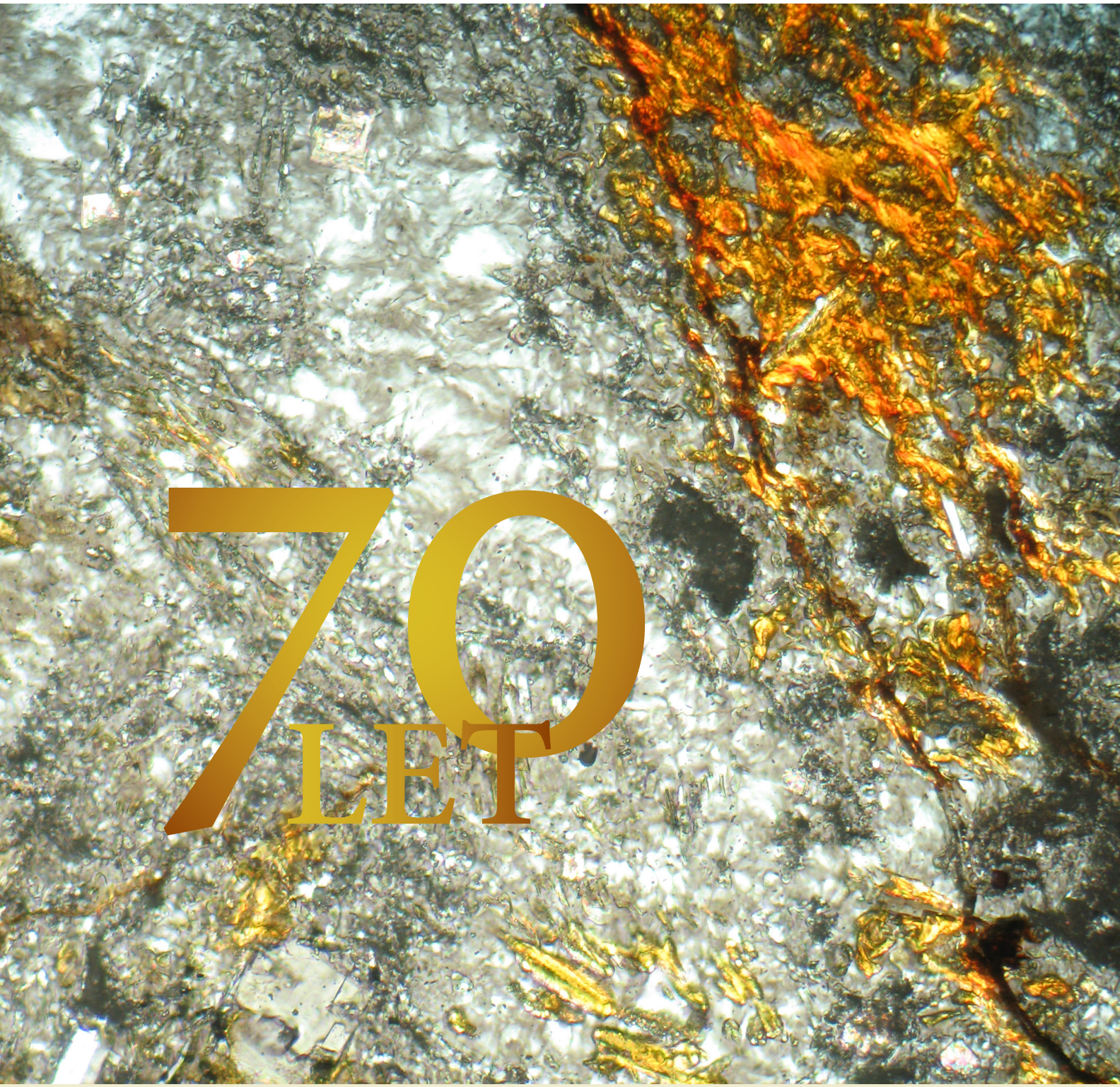

GeoZS
Geološki zavod
Slovenije

ISSN
Tiskana izdaja / Print edition: 0016-7789
Spletna izdaja / Online edition: 1854-620X

GEOLOGIJA

66/1 – 2023

GeoZS
Geološki zavod Slovenije

GEOLOGIJA	2023	66/1	1-198	Ljubljana

GEOLOGIJA
ISSN 0016-7789

Izdajatelj: Geološki zavod Slovenije, zanj direktor Miloš Bavec
Publisher: Geological Survey of Slovenia, represented by Director Miloš Bavec
Financirata Javna agencija za raziskovalno in inovacijsko dejavnost Republike Slovenije in Geološki zavod Slovenije
Financed by the Slovenian Research and Innovation Agency and the Geological Survey of Slovenia

Naslov uredništva / Editorial Office: GEOLOGIJA Geološki zavod Slovenije / Geological Survey of Slovenia
Dimičeva ulica 14, SI-1000 Ljubljana, Slovenija
Tel.: +386 (01) 2809-700, Fax: +386 (01) 2809-753, e-mail: urednik@geologija-revija.si
URL: https://www.geologija-revija.si/

GEOLOGIJA izhaja dvakrat letno. / GEOLOGIJA is published two times a year.
GEOLOGIJA je na voljo tudi preko medknjižnične izmenjave publikacij. /
GEOLOGIJA is available also on exchange basis.

Izjava o etičnosti
Izdajatelji revije Geologija se zavedamo dejstva, da so se z naglim naraščanjem števila objav v svetovni znanstveni literaturi razmahnili tudi poskusi plagiatorstva, zlorab in prevar. Menimo, da je naša naloga, da se po svojih močeh borimo proti tem pojavom, zato v celoti sledimo etičnim smernicam in standardom, ki jih je razvil odbor COPE (Committee for Publication Ethics).

Publication Ethics Statement
As the publisher of Geologija, we are aware of the fact that with growing number of published titles also the problem of plagiarism, fraud and misconduct is becoming more severe in scientific publishing. We have, therefore, committed to support ethical publication and have fully endorsed the guidelines and standards developed by COPE (Committee on Publication Ethics).

Baze, v katerih je Geologija indeksirana / Indexation bases of Geologija: Scopus, Directory of Open Access Journals, GeoRef, Zoological Record, Geoscience e- Journals, EBSCOhost

Cena / Price

Posamezni izvod / Single Issue	Letna naročnina / Annual Subscription
Posameznik / Individual: 15 €	Posameznik / Individual: 25 €
Institucija / Institutional: 25 €	Institucija / Institutional: 40 €

Tisk / Printed by: TISKARNA JANUŠ d.o.o.

Slika na naslovni strani: Na sliki je oligocenski tuf s Smrekovškega vulkanskega kompleksa, zbrusek v presevni polarizirani svetlobi, med navzkrižnimi nikoli. Beli in sivi minerali so heulandit, v njem so tudi drobni minerali z visokim reliefom, ki pripadajo analcimu. Oranžno-rumeni filosilikatni minerali so glineni minerali z zmesno strukturo vrste corrensit-klorit (foto: Polona Kralj).

Cover page: The image shows thin section of Oligocene tuff from the Smrekovec Volcanic Complex, north-eastern Slovenia, plain-polarised light, crossed nicols. White and light-grey minerals are heulandite, which includes tiny minerals of analcime characterised by very high relief. Orange-yellow phyllosilicate minerals belong to randomly mixed-layered corrensite-chlorite (photo: Polona Kralj).

GEOLOGIJA 66/1, 1-198, Ljubljana 2023

VSEBINA – CONTENTS

Gosar, M.
Uvodnik - 70 let revije Geologija 5

Placer, L., Rižnar, I. & Novak, A.
Transverse Dinaric zone of increased compression between the Kraški rob and Hrušica Regions, NE Microadria 9
Prečnodinarska cona povečane kompresije med Kraškim robom in Hrušico, NE Mikroadrija

Čadež, F.
Geološka spremljava poskusnega odkopa uranove rude na Žirovskem vrhu 73
Geological control of trial excavation of Uranium ore in Žirovski vrh

Spatzenegger, A. & Poltnig, W.
Taxonomic and stratigraphic remarks on *Placites urlichsi* Bizzarini, *Pompeckjites layeri* (Hauer), *Carnites floridus* (Wulfen) and *Sageceras haidingeri* (Hauer) 87
Taksonomija in stratigrafski razpon vrst *Placites urlichsi* Bizzarini, *Pompeckjites layeri* (Hauer), *Carnites floridus* (Wulfen) and *Sageceras haidingeri* (Hauer)

Oselj, K., Kolar-Jurkovšek, T., Jurkovšek, B. & Gale, L.
Microfossils from Middle Triassic beds near Mišji Dol, central Slovenia 107
Mikrofosili iz srednjetriasnih plasti pri Mišjem Dolu, osrednja Slovenija

Rajver, D. & Adrinek, S.
Overview of the thermal properties of rocks and sediments in Slovenia 125
Pregled toplotnih lastnosti kamnin in sedimentov v Sloveniji

Koren, K., Brajkovič, R., Bajuk, M., Vraničar, Š. & Fabjan, V.
Hydrogeological characterization of karst springs of the white (*Proteus anguinus anguinus*) and black olm (*Proteus anguinus parkelj*) habitat in Bela krajina (SE Slovenia) 151
Hidrogeološka karakterizacija kraških izvirov na območju habitata belega (*Proteus anguinus anguinus*) in črnega močerila (*Proteus anguinus parkelj*) v Beli krajini (JV Slovenija)

Zhyrnov, P. & Solomakha, I.
Geological-genetic structure of Irpin city, the role of lithological factors during engineering-geological zoning and construction assessmenta 167
Geološko-genetska zgradba mesta Irpin, vloga litoloških dejavnikov pri inženirsko-geološkem določanju con in oceni gradnje

Khalili, R., Satour, L. & Mennad, S.
Borers and epizoans on oyster shells from the upper Tortonian, Lower Chelif Basin, NW Algeria 185
Vrtalci in epizoji na zgornjetortonijskih ostreidnih lupinah iz Spodnjega Chelif bazena, SZ Alžirija

GEOLOGIJA 66/1, 5-7, Ljubljana 2023

https://doi.org/10.5474/geologija.2023.000

GEOLOGIJA 70 LET

70 let revije Geologija

Revija Geologija je bila ustanovljena leta 1953 kot slovenska znanstvena revija za področje geologije.

Po drugi svetovni vojni so bile potrebe po mineralnih surovinah precejšnje. Jugoslavija je ubrala samostojno pot kolikor se je le dalo neodvisno od Sovjetske zveze. Zato je jugoslovanska politika želela, da bi bili samozadostni. Takratna generacija geologov je imela veliko in pomembno nalogo: zagotoviti čim več mineralnih surovin. Za to je bilo potrebno dobro poznavanje geološke zgradbe. Prva povojna generacija geologov je imela tako polne roke dela. Naša najpomembnejša rudnika kovin, Idrija in Mežica, sta takrat proizvajala velike količine dragocenih kovin in tako izdatno polnila državno blagajno. Razcvet so doživljali tudi premogovniki. To je bil tudi čas, ko je bilo treba po razdejanju med vojno na novo zgraditi državo. Za gradnjo novih stanovanjskih objektov in ostale infrastrukture so potrebovali ogromne količine nekovinskih mineralnih surovin. Vse to je zahtevalo veliko geoloških raziskav in hkrati terjalo precejšnje napore takratne skromne generacije geologov. Geologov je v tistem času močno primanjkovalo. Veliko jih je delalo in študiralo obenem, poleg tega pa so delali tudi na pomembnih geoloških in rudarskih projektih po celi Jugoslaviji in tudi v tujini.

Da si bomo lažje predstavljali, kako dolgo že izhaja naša revija, osvežimo znanje zgodovine in poglejmo, kaj vse se je dogajalo leta 1953. James D. Watson in Francis Crick z Univerze v Cambridgeu sta razvozlala kemijsko zgradbo molekule DNK, britanski pisatelj Ian Fleming je izdal prvi roman o Jamesu Bondu, Edmund Hillary in šerpa Tenzing Norgay sta kot prva človeka osvojila vrh Mount Everesta. To je bil čas, ko geologi še niso vedeli za teorijo o tektoniki plošč, in moja starša se še nista poznala.

Kljub temu, da to obdobje ni bilo zelo naklonjeno poglobljenemu znanstvenemu delu in publiciranju, vsaj ne na področju geologije, se je vodstvo takratnega Geološkega zavoda Ljubljana, predhodnika današnjega Geološkega zavoda Slovenije, skupaj s stanovskimi kolegi, združenimi v Slovenskem geološkem društvu, odločilo, da je treba ustanoviti slovensko znanstveno revijo za področje geologije. Že takrat so se zavedali velikega pomena znanstvenega publiciranja in z ustanovitvijo Geologije omogočili objavljanje znanstvenih dognanj s področja geologije v domači reviji.

Znanost je ena izmed temeljnih človekovih dejavnosti. Od nje je odvisen razvoj družbe, saj ga poganjajo prav znanstvena dognanja. Rezultate znanstvenega dela pa je treba predstaviti znanstveni in širši javnosti. Zato je objavljanje v znanosti izjemno pomembno in pravzaprav predstavlja precejšen del našega dela. To je kratko in jedrnato v eno misel strnil ameriški založnik in znanstveni urednik več znanstvenih revij Gerard Piel, ki je leta 1986 v uvodniku revije Science zapisal: »Neobjavljena znanost je mrtva znanost.« Znanstveniki se zavedamo, da je vsakršno znanstveno dognanje – najsibo še tako izvirno – nepopolno in nedokončano, dokler rezultati niso objavljeni.

Človeštvo se med seboj sporazumeva od nekdaj, znanstveno komuniciranje pa je relativno mlado. Prve znanstvene revije so nastale konec 17. stoletja. Takrat je najverjetneje nastalo tudi prvo znanstveno delo s področja geologije. Nicolas Steno je spoznal, da je v zemeljski skorji zapisana zgodovina geoloških dogodkov, ki jo je mogoče razvozlati s skrbnim preučevanjem plasti in fosilov, in to leta 1669 zapisal v svojem doktorskem delu.

V 19. stoletju je pričelo število znanstvenih revij hitro naraščati. Načela znanstvenega publiciranja pa so se začela razvijati v začetku 20. stoletja. Filozofija znanosti temelji na dejstvu, da morajo biti izsledki znanstvenih raziskav objavljeni. To pomeni, da morajo biti primerno dokumentirani, interpretirani in predstavljeni ter dosegljivi mednarodni znanstveni javnosti. Samo tako jih je mogoče prepoznati, preveriti, jih vključiti v obstoječe znanstveno vedenje ter jih tudi uporabiti za nadaljnje raziskave. Ko znanstveniki objavijo rezultate svojih raziskav in njihovo interpretacijo, raziskovalnemu okolju omogočijo, da presodi, kakšno znanstveno vrednost imajo. Znanstveni članki so namenjeni deljenju rezultatov lastnega izvirnega raziskovalnega dela z drugimi znanstveniki ali pregledu raziskav določene teme. Zato so ključnega pomena za razvoj sodobne znanosti, v kateri delo enega znanstvenika oziroma ene skupine nadgrajuje delo drugih.

Pri znanstvenikih, zlasti naravoslovcih, je zanimivo, da večinoma ne pišejo zelo radi. Že Charles Darwin je zapisal: »Kako srečno bi bilo življenje naravoslovca, ko bi le opazoval in nikoli pisal.« Je pa res, da je pisanje člankov obrt, ki se je moramo naučiti.

Motivi za objavljanje člankov so se skozi zgodovino spreminjali. Poleg prej naštetih, ki so vsekakor trden temelj, so se pojavili še mnogi drugi, kot na primer: pridobiti izkušnje oz. usvojiti pisanje člankov, rešiti težavo, omogočiti spoznanje, interes za razvoj znanstvenega področja, pa tudi postati viden, (samo)promocija, izpolnitev pogojev za pridobitev naziva ali za habilitacijo ali za zagovor doktorskega dela, nabiranje 'točk' ... Žal je tako, da živimo v zelo tekmovalni dobi, kar je Saša Pavček v knjigi Živi ogenj gledališča komentirala z naslednjimi besedami: »Oh, tekme, primerjave, rezultati, prosim, ne!«. Pisala je o režiserjih in igralcih, a menim, da v znanosti ni prav nič drugače. Včasih pa brez tega ne gre, zato v nadaljevanju sledi nekaj statistike v zvezi z objavami v Geologiji. Naj nam popestrijo pogled v zgodovino izdajanja Geologije in naj ne služijo tekmovalnosti.

V vseh 70 letih (1953–2022) je Geologija objavila 1157 člankov in dve monografiji, pri tem je sodelovalo 1835 avtorjev. Poleg tega je bilo objavljeno še 63 nekrologov, 156 raznih poročil in 133 ocen novih publikacij. V tem času je največ člankov (52) napisal Anton Ramovš, sledi Vasja Mikuž s 50 članki in potem Bogdan Jurkovšek z 31 članki. Zanimivo je, da je deset najbolj dejavnih avtorjev sodelovalo pri kar 334 člankih.

V zadnjih desetih letih je bilo največ avtorjev zaposlenih na Univerzi v Ljubljani, teh je bilo kar 85. Večinoma delujejo na Oddelku za geologijo Naravoslovnotehniške fakultete. Iz Geološkega zavoda Slovenije je bilo 76 avtorjev, ostali so bili zaposleni na Agenciji republike Slovenije za okolje (18), Institutu »Jožef Stefan« (17), Znanstvenoraziskovalnem centru Slovenske akademije znanosti in umetnosti (13) ter v drugih organizacijah doma in v tujini.

V naši reviji so bile objavljene vsebine, ki so pomembne za razvoj geoloških znanosti. V prvih desetletjih so pisali o novih spoznanjih v zvezi z geološko zgradbo Slovenije in rudnih nahajališčih. Dognanja o nastanku, razvoju in geoloških razmerah v naših najpomembnejših rudiščih so bila objavljena v številnih člankih v Geologiji in so bila tudi temelj za ugotavljanje novih zalog rude in s tem za uspešno izkoriščanje rude v teh rudiščih. V monografiji »Nastanek rudišč v SR Sloveniji«, ki so jo 1980 napisali Matija Drovenik, Mario Pleničar in Franc Drovenik, so zbrani podatki o naših rudiščih, zato predstavlja temelj za vsa naslednja dela na tem področju. Drugo monografijo z naslovom »Mikrofacies mezozojskih karbonatnih kamnin Slovenije« je leta 2011 napisal Bojan Ogorelec. Ker karbonatne kamnine mezozojske starosti v Sloveniji zavzemajo okoli 40 % ozemlja in je njihova celotna skladovnica debela preko 5000 metrov, je natančen pregled njihovega razvoja in njihovih značilnosti zelo relevantna tema. Delo pa je pomembno tudi zato, ker v mikrofaciesu apnencev in dolomitov prepoznamo skoraj vse strukturne tipe, saj so nastajali v različnih sedimentacijskih okoljih, značilnih za karbonatne kamnine. Zato je ta monografija tudi odličen pripomoček pri študiju. Med najpogosteje navajanimi deli pa so članki o geotektonski zgradbi Slovenije avtorja Ladislava Placerja.

V Geologiji so bila objavljena pomembna dognanja, pridobljena v okviru diplomskih, magistrskih in tudi doktorskih raziskav. Verjetno je mnogo slovenskih geologov svoj prvi znanstveni članek objavilo prav v Geologiji. Zato ima naša revija pomembno vlogo pri vzgoji mladih geologov.

Geologijo so vodili štirje uredniki: Štefan Kolenko 1953–1982 (30 let), Stanko Buser 1983–1997 (15 let), Bojan Ogorelec 1998–2009 (12 let) in Mateja Gosar od 2010 dalje. Tehnično pomoč urednikom je do leta 1999 zagotavljala Metka Karer, ki je poskrbela tudi za tehnično brezhibnost večine slikovnega in tabelaričnega gradiva za objave. Edina uradna tehnična urednica je Bernarda Bole, ki to funkcijo zelo skrbno in z osupljivo natančnostjo opravlja od leta 1999. Torej že 24 let. Spomnim se besed, s katerimi me je bodril Bojan Ogorelec, ko je predajal uredništvo v moje roke: »Mateja, naj te ne bo strah, saj bo šlo, imela boš Bernardo, ona obvlada tekoče uredniško delo in ti bo pomagala. Ti pa veš kam moraš Geologijo peljati.« Bernardi sem iskreno hvaležna za odlično sodelovanje.

Članki so bili v vseh letih pisani v tujih jezikih, pretežno angleščini, in tudi v slovenščini. Zelo pomembno je, da imajo vsi članki povzetek v tujem in tudi v slovenskem jeziku. Tako skrbimo, da se razvija tudi slovenska geološka terminologija.

Znanstvene revije morajo sodelovati s strokovnjaki, ki opravijo recenzijo prejetih del. Recenzija je kritična in objektivna presoja prikazanih raziskav, predstavljenih rezultatov in zaključkov. Prav vsi, ki delujemo v znanosti, se zavedamo izjemnega pomena ocenjevalcev pri vseh fazah našega dela: od ocenjevanja projektnih prijav na razpisih doma in v svetu do ocenjevanja naših del. Vendar se vsi soočamo z

izjemnim pomanjkanjem strokovnjakov, ki bi to delo opravili. Zato smo zelo hvaležni kolegicam in kolegom, ki se odzovejo na našo prošnjo za recenzijo in potem to recenzijo tudi objektivno in vestno opravijo v predvidenem roku. V zadnjem desetletju so se pri recenzentskem delu še posebno izkazali (navajam v abecednem vrstnem redu): Mihael Brenčič, Luka Gale, Špela Goričan, Petra Jamšek Rupnik, Miloš Miler, Nina Rman, Boštjan Rožič, Timotej Verbovšek in Nina Zupančič.

Uredništvo sledi trendom v svetovni znanstveni publicistiki in potrebam slovenskih raziskovalcev. Naj omenim le najpomembnejše novosti, ki smo jih uvedli v zadnjih desetih letih. Geologija je revija z diamantnim odprtim dostopom. Člankom v Geologiji pripisujemo DOI (identifikator digitalnega objekta), s čimer je vsak članek enoznačno označen in omogoča trajno povezavo besedila do njegove lokacije na internetu ter enostavno spremljanje njegovega citiranja. Oblikovanje in postavitev vsebine Geologije je prevzelo uredništvo. To že vrsto let uspešno opravlja Vida Pavlica. Članki so objavljeni pod licenčnim pogojem CC BY. Ta priznava avtorstvo, podpira prosto izmenjavo, iskanje in ponovno uporabo. Najpomembnejši dosežek je bil vključitev revije Geologija v multidisciplinarno bibliografsko zbirko s citatnim indeksom Scopus, ki jo gradi založniški velikan Elsevier. V zvezi s tem se moram še posebno zahvaliti Ireni Trebušak, ki mi je z nasveti in širokim znanjem pomagala, da smo premagali neštete ovire in leta 2014 dosegli ta pomemben mejnik. Opravljena je bila digitalizacija in indeksacija vsebin, objavljenih v Geologiji v vseh 70 letih. Hvaležna sem, da je to obsežno delo prevzel naš Geološki informacijski center pod vodstvom Jasne Šinigoj. Za uspešno izpeljano digitalizacijo je zaslužen predvsem Maks Šinigoj, ki je skrbno pregledal vse digitalizirane letnike ter izjemno vestno in dosledno popravljal številne napake vseh vrst. Za to si zasluži posebno pohvalo. Naša stara internetna stran je bila prenesena na sistem OJS (Open Journal Systems), za kar gre zasluga Marku Zakrajšku. S tem je odprto dostopno vse, kar je bilo kadarkoli objavljeno v naši reviji, in omogočeno je iskanje po celotnem arhivu revije. Ker se zavedamo, kako pomembna je dostopnost podatkov in kakšno vlogo imajo pri tem znanstvene revije, letos uvajamo rubriko 'podatkovni članek'.

Zagotovo je še veliko novosti in ljudi, ki so prispevali k dobremu delovanju Geologije. Ne moremo omeniti vseh, smo pa vsem, ki sodelujejo z uredništvom, hvaležni.

Uredba o izvajanju znanstvenoraziskovalnega dela v skladu z načeli odprte znanosti, ki je bila sprejeta konec letošnjega maja, zahteva odprto dostopnost znanstvenih publikacij in zagotavlja, da se pri vrednotenju dosežkov vrednoti bistvene vsebinske dosežke dela, in ne mesta objave oziroma metrik revije ali založnika. To je vsekakor v prid objavljanju v reviji Geologija, ki izpolnjuje vse zahteve te uredbe.

Zavedamo se, da so pred nami novi izzivi. Danes, ko je umetna inteligenca v razvitejši fazi svojega razvoja (ChatGPT in drugi podobni tehnološki programi) in kot valjar melje in spreminja praktično vse, kar si predstavljamo pod družbeno realnostjo, so bojazni zaradi umetne inteligence povsem realne, tudi v znanosti in še posebno pri znanstvenem publiciranju.

Zahvala za finančno podporo gre Javni agenciji za znanstvenoraziskovalno in inovacijsko dejavnost Republike Slovenije (ARIS) in vsem njenim predhodnikom. Najpomembnejše finančno breme revije Geologija pa vsekakor nosi založnik Geološki zavod Slovenije. Hvaležni smo, da razumevajoče podpira delovanje uredništva, in finančno poskrbi, da revija preživi, in to ne glede na to, ali smo v letih suhih ali debelih krav.

Spoštovane raziskovalke in raziskovalci s področja znanosti o Zemlji, Geologija je naša revija, pravzaprav revija vseh generacij povojnih slovenskih geologov in seveda tudi širše. Vsak od nas je dodal kamenček ali dva v mozaik, ki predstavlja 70 let njenega delovanja. Hvaležno se spominjamo starejših kolegic in kolegov, ki jih danes ni med nami, so pa s svojim delom postavili trdne temelje na katerih smo lahko gradili. Zavedajmo se, da prav vsi lahko prispevamo, da bo naša Geologija še naprej dobro delovala, da nam bo vsem koristila pri znanstvenoraziskovalnem delu, da se bo razvijala v koraku s časom, ki prihaja, in da bo v ponos tudi bodočim generacijam.

Mateja Gosar, glavna in odgovorna urednica Geologije

GEOLOGIJA 66/1, 9-71, Ljubljana 2023

https://doi.org/10.5474/geologija.2023.001

Transverse Dinaric zone of increased compression between the Kraški rob and Hrušica Regions, NE Microadria

Prečnodinarska cona povečane kompresije med Kraškim robom in Hrušico, NE Mikroadrija

Ladislav PLACER[1], Igor RIŽNAR[2] & Ana NOVAK[1]

[1]Geološki zavod Slovenije, Dimičeva ul. 14, SI-1000 Ljubljana, Slovenija;
e-mails: ladislav.placer@telemach.net, ana.novak@geo-zs.si
[2]Geološke ekspertize Igor Rižnar s. p., SI-1000 Ljubljana, Slovenija; e-mail: igor.riznar@telemach.net

Prejeto / Received 21. 3. 2023; Sprejeto / Accepted 29. 6. 2023; Objavljeno na spletu / Published online 4. 8. 2023

Key words: NE Microadria (Adria Microplate), Istra peninsula, Istra Pushed Area, Črni Kal Anomaly, Kraški rob – Mt. Hrušica Traverse, stacked structure, envelope fault

Ključne besede: NE Mikroadrija (Jadranska mikroplošča), Istra, istrsko potisno območje, črnokalska anomalija, traverza Kraški rob – Hrušica, zložbena zgradba, ovojni (envelopni) prelom

Abstract

The Kvarner fault divides the Microadria (Adria microplate, the Adria stable core) into the Po and Adria segments. The Istra block, which is sandwiched between the right-lateral Kvarner Fault and the left-lateral Sistiana Fault lies at the extreme eastern edge of the Po segment. Both faults run transversely to the Dinarides and reach their thrust boundary in the east. The Microadria has been moving towards the Dinarides since the Middle Miocene. The movement of the Istra block is exposed in relation to the neighbouring blocks, so an extensive pushed area (the Istra Pushed Area) was formed in the External Dinarides, which is bent towards the northeast. It is defined by two flexural zones, one lying in the extension of the Sistiana Fault and the other in the extension of the Kvarner Fault. The structure of the Dinaric thrust border on the north-eastern side of the Istra block is complex. Its prominent structural element is the Črni Kal Anomaly, due to which a zone of increased compression developed within the Istra Pushed Area and transversely to the Dinarides (Kraški rob – Hrušica Traverse), which lies between the Sistiana and Kvarner Flexural Zones. In terms of kinematics, it differs greatly from these two, and various geomorphologically responsive deformations have occurred within it. Mt. Vremščica (1027 m), which represents a transpressive anticline within the wider zone of the Raša Fault is the most prominent. In order to understand the genesis of the Classical Karst relief, it is important to know that the Mt. Vremščica ridge rose from the levelled karst surface.

Izvleček

Kvarnerski prelom deli Mikroadrijo (Jadranska mikroplošča, stabilno jedro Adrije) na padski in jadranski segment. Na skrajnem vzhodnem robu padskega segmenta leži istrski blok, ki je umeščen med desnozmični Kvarnerski in levozmični Sesljanskim prelom. Oba preloma potekata prečno na Dinaride in segata do njihove narivne meje. Mikroadrija se že od srednjega miocena naprej pomika proti Dinaridom, premikanje istrskega bloka je nasproti sosednjim blokom eksponirano, zato se je v Zunanjih Dinaridih izoblikovalo obsežno potisno območje (istrsko potisno območje), ki je usločeno proti severovzhodu. Določata ga dve upogibni coni, ena leži v podaljšku Sesljanskega, druga v podaljšku Kvarnerskega preloma. Zgradba narivne meje Dinaridov na severovzhodni strani istrskega bloka je zapletena, njen izstopajoči strukturni element je črnokalska anomalija, zaradi katere se je v istrskem potisnem območju in prečno na Dinaride razvila cona povečane kompresije (traverza Kraški rob - Hrušica), ki leži med sesljansko in kvarnersko upogibno cono. V kinematskem smislu od obeh močno odstopa, v njej so nastale različne geomorfološko odzivne deformacije, najbolj vidna med njimi je Vremščica (1027 m), ki predstavlja transpresivno antiklinalo znotraj širše cone Raškega preloma. Za razumevanje geneze reliefa Klasičnega krasa je pomembno vedeti, da se je greben Vremščice dvignil iz uravnanega kraškega površja.

Introduction

Blašković & Aljinović (1981), and Blašković (1991; 1999) already showed that the Dinaric foothills in the Istra and Kvarner are moving towards the Dinarides, and a more specific structural justification for the movement of Istra was given in the discussion on the basics of understanding the tectonics of the north-western Dinarides and Peninsula Istra (Placer et al., 2010) and in discussion of the Sistiana Fault and Sistiana Bending Zone (Placer et al., 2021b). In these discussions, it was established that Istra, which is part of the Microadria (Adriatic microplate), lies in a block (the Istra block) between two strike-slip faults: the left-lateral Sistiana Fault in the northwest and the complex right strike-slip Kvarner Fault in the southeast (Fig. 1). Both faults lie transversely to the Dinarides and extend only as far as the Dinaric Thrust Belt boundary. In the Dinarides, their influence is reflected in the clockwise Sistiana and anticlockwise Kvarner Flexural Zones, which run in the direction of both faults. In this article, the term Sistiana Bending Zone is replaced by the term Sistiana Flexural Zone because it better corresponds to the tectonic terminology. The part of the Microadria northwest of the Sistiana Fault was designated as the Friuli block, which is less exposed to the Dinarides than the Istra block. The movement of the Istra block is compensated by the lateral bending of the External Dinarides towards the northeast and by underthrusting in the area of their thrust boundary. This is how the Istra-Friuli Thrust-Underthrust Zone and the Istra Pushed Area, defined by both flexural zones, were formed. The process of pushing is more important

Uvod

Da se Dinarsko predgorje na območju Istre in Kvarnerja premika proti Dinaridom sta opozorila že Blašković in Aljinović (1981) ter Blašković (1991; 1999), določnejša strukturna utemeljitev premikanja Istre pa je bila podana v razpravi o osnovah razumevanja tektonike severozahodnih Dinaridov in Istre (Placer et al., 2010) ter v razpravi o Sesljanskem prelomu in sesljanski upogibni coni (Placer et al., 2021b). V teh razpravah je bilo ugotovljeno, da leži Istra, ki je del Mikroadrije (Jadranske mikroplošče), v bloku (istrski blok) med dvema zmičnima prelomoma, levozmičnim Sesljanskim prelomom na severozahodu in desnozmičnim Kvarnerskim prelomom na jugovzhodu. Oba preloma ležita prečno na smer Dinaridov in segata le do njihove narivne meje. V Dinaridih se njun vpliv odraža v levosučni sesljanski in desnosučni kvarnerski upogibni coni, ki potekata v smeri obeh prelomov. Del Mikroadrije severozahodno od Sesljanskega preloma je bil označen kot furlanski blok, ki pa je proti Dinaridom manj izpostavljen od istrskega bloka. Premikanje istrskega bloka je kompenzirano z bočnim upogibom Zunanjih Dinaridov proti severovzhodu in s podrivanjem v območju njihove narivne meje. Tako sta nastala istrsko-furlanska podrivna cona in istrsko potisno območje, ki ga določata obe upogibni coni. Proces potiskanja je pomembnejši od podrivanja. V podrivni coni naj bi se paleogenski narivi, ki označujejo konec dinarske narivne faze, transformirali v neogenske do recentne podrive. Recentno dviganje krovnih grud v območju

Fig. 1. Tectonic subdivision of Istra penninsula and its Dinaric hinterland. Updated after Placer et al. (2010, Fig. 3; 2021b, Fig. 1).
Sl. 1. Tektonska rajonizacija polotoka Istre in dinarskega zaledja. Dopolnjeno po Placer et al. (2010, sl. 3; 2021b, sl. 1).

1 Dinarides. External Dinaric Thrust Belt: T – Trnovo Nappe, H – Hrušica Nappe, S – Snežnik Nappe / Dinaridi. Zunanjedinarski narivni pas: T – Trnovski pokrov, H – Hrušiški pokrov, S – Snežniški pokrov

2 Dinarides. External Dinaric Imbricated Belt / Dinaridi. Zunanjedinarski naluskani pas

3 Microadria: stable core, imbricated borderland (autochton *sensu lato*) / Mikroadrija: stabilno jedro, naluskano obrobje (avtohton *sensu lato*)

4 Microadria: stable core (autochton *sensu stricto*) / Mikroadrija: stabilno jedro (avtohton *sensu stricto*)

5 Southern Alps / Južne Alpe

6 Southern Alps thrust boundary / narivna meja Južnih Alp

7 External Dinaric Thrust Belt boundary, nappe bondary / meja Zunanjedinarskega narivnega pasu, meja pokrova

8 Thrust plane within Dinaric thrust boundary / nariv v coni narivne meje Dinaridov

9 Istra-Friuli Thrust-Underthrust Zone (Placer et al., 2010, Istra-Friuli Underthrust Zone) / istrsko-furlanska narivno-podrivna cona (Placer et al., 2010, istrsko-furlanska podrivna cona)

10 BuF – Buje reverse Fault / BuF – Bujski reverzni prelom

11 Anticlinoria: a – Čičarija Anticlinorium, b – Trieste-Komen Synclinorium, c – Ravnik Anticlinorium / antiklinoriji: a – Čičarijski antiklinorij, b – Tržaško-Komenski antiklinorij, c – Ravenski antiklinorij

12 Synclinoria: d – Brkini Synklinorium, e – Vipava Synclinorium / sinklinoriji: d – Brkinski sinklinorij, e – Vipavski sinklinorij

13 Important sub-vertical fault: SF – Sistiana Fault, KF – Kvarner Fault, RF – Raša fault, IF – Idrija Fault / pomembnejši subvertikalni prelom: SF – Sesljanski prelom, KF – Kvarnerski prelom, RF – Raški prelom, IF – Idrijski prelom

14 Microadria structural block: A – Istra block (A1 – South Istra Structural Wedge, A2 – North Istra Structural Wedge), B – Friuli block / strukturni blok Mikroadrije: A – istrski blok (A1 – južnoistrski strukturni klin, A2 – severnoistrski strukturni klin), B – furlanski blok

15 Relative movement direction of the fault block / relativna smer premika prelomnega krila

16 General direction of South Istra Structural Wedge movement / generalna smer premikanja južnoistrskega strukturnega klina

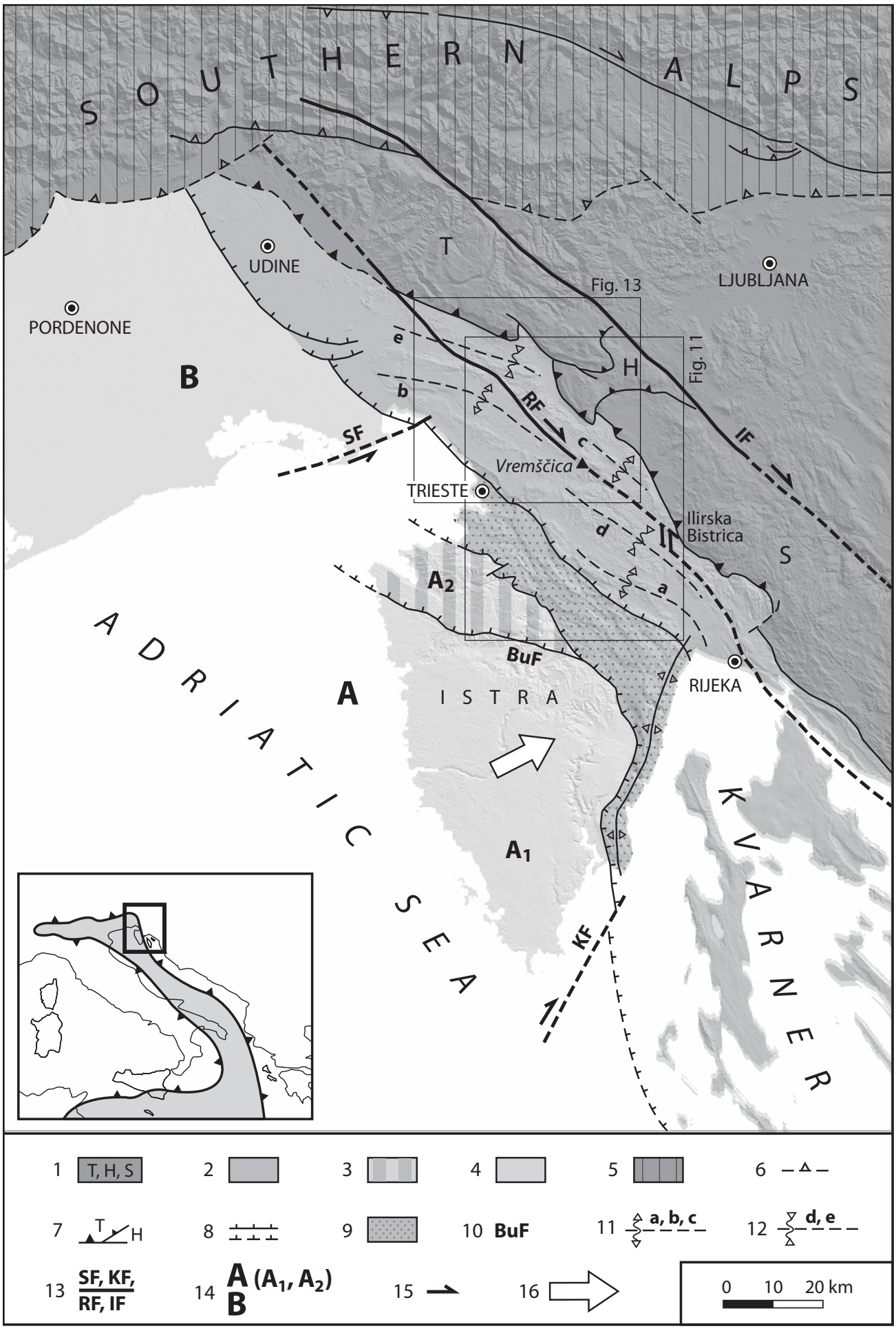
SOUTHERN ALPS
T
H
S
UDINE
LJUBLJANA
PORDENONE
Fig. 13
Fig. 11
B
e
b
RF
c
SF
IF
Vremščica
TRIESTE
Ilirska Bistrica
d
a
A2
BuF
A
ISTRA
RIJEKA
ADRIATIC SEA
A1
KVARNER
KF
1 T, H, S
2
3
4
5
6
7 T H
8
9
10 BuF
11 a, b, c
12 d, e
13 SF, KF, RF, IF
14 A (A1, A2) B
15
16
0 10 20 km

than underthrusting. In the underthrust zone, the Paleogene thrusts, which mark the end of the Dinaric thrust phase, are supposed to transform into Neogene to recent thrusts. The recent uplift of the Paleogene nappes in the Istra-Friuli Thrust-Underthrust Zone was determined in Istra by the reambulation of levelling lines (Rižnar et al., 2007).

Istra is a visible part of the Istra block, divided into the South Istra and North Istra Structural Wedges (Fig. 1). According to the established directions of movement and parallel deformations, the South Istra Structural Wedge should move towards the Dinarides faster than the northern one.

The above-mentioned fundamental findings stimulated a series of focused researches: the recent movement of Istra towards the Dinarides was proven by GPS measurements (Weber et al., 2010), the more intense movement of the tip of the South Istra Structural Wedge towards the Dinarides was confirmed by measurements of the local rotation of magnetic poles in cave sediments in the thrust units of the Dinarides (Vrabec et al., 2018); large sub-recent gravity phenomena in the area of the Istra Pushed Area were investigated (Placer et al., 2021a), and more precisely the Sistiana Flexural Zone was investigated (Placer et al., 2021b). Publications regarding the seismicity of the area in question are not covered here.

Geophysical surveys of the seabed of the Gulf of Trieste have shown that the mapped structures from Istra continue to the northwest. In this sense, the articles published after the discovery of the Buzet Thrust (Placer et al., 2004), which forms the south-western border of the Istra-Friuli Thrust-Underthrust Zone, are important. The subsea structure is shown in the articles by Carulli (2006; 2011), Busetti et al. (2010a; 2010b; 2012; 2013), Trobec et al. (2017), and Novak et al. (2020).

The findings of the aforementioned research are shown in Figure 1 within the structure of this part of the Dinarides.

When studying the geomorphology of the Istra Pushed Area, it was shown that the movement of the Istra block caused not only lateral faulting, but also contraction of the Dinarides. Thus, the folds folded more intensively, and the blocks adapted to the contraction by moving along the existing discontinuities. Therefore, it is necessary to solve the structure of geological objects within the Pushed Area in two stages: firstly, the structural geometry in the Paleogene at the end of thrusting must be determined, and then the successive deformations that occurred during the phase of Neogene-recent thrusting according to the Paleogene structural pre-set. Among the studied features, e.g. Kras (Trieste-Komen

istrsko-furlanske podrivne cone, je bilo v Istri ugotovljeno z reambulacijo nivelmanov (Rižnar et al., 2007).

Istra je vidni del istrskega bloka, razdeljena na južnoistrski in severnoistrski strukturni klin (sl. 1). Po ugotovljenih smereh gibanja in vzporednih deformacijah, naj bi se južnoistrski strukturni klin premikal proti Dinaridom hitreje od severnega.

Zgoraj omenjene temeljne ugotovitve so vzpodbudile vrsto usmerjenih raziskav: z meritvami GPS je bilo dokazano recentno premikanje Istre proti Dinaridom (Weber et al., 2010), intenzivnejše premikanje konice južnoistrskega strukturnega klina proti Dinaridom je bilo potrjeno z meritvami lokalne rotacije magnetnih polov v jamskih sedimentih, ki ležijo v narivnih enotah Dinaridov (Vrabec et al., 2018), raziskani so bili veliki subrecentni gravitacijski pojavi v območju istrskega potisnega območja (Placer et al., 2021a), natančneje je bila raziskana sesljanska upogibna cona (Placer et al., 2021b). Objave o seizmiki obravnavanega prostora tu niso zajete.

Geofizikalne raziskave podmorja Tržaškega zaliva so pokazale, da se kartirane strukture iz Istre nadaljujejo proti severozahodu. V tem smislu so pomembni članki, ki so bili objavljeni po odkritju Buzetskega nariva (Placer et al., 2004), ki tvori jugozahodno mejo istrsko-furlanske podrivne cone. Zgradbo podmorja prikazujejo članki Carulli-ja (2006; 2011), Busetti-jeve in sodelavcev (2010a; 2010b; 2012; 2013), Trobčeve in sodelavcev (2017) in Novakove in sodelavcev. (2020).

Ugotovitve omenjenih raziskav so v okviru zgradbe tega dela Dinaridov prikazane na sliki 1.

Pri proučevanju geomorfologije istrskega potisnega območja se je pokazalo, da premikanje istrskega bloka ni povzročilo le bočne usločitve, temveč tudi krčenje Dinaridov. Tako so se gube intenzivneje nagubale, bloki pa so se krčenju prilagodili s premiki po obstoječih diskontinuitetah. Zato je potrebno zgradbo geoloških objektov znotraj potisnega območja reševati dvostopenjsko, najprej je treba določiti strukturno geometrijo v paleogenu ob koncu narivanja, potem pa nasledstvene deformacije, ki so nastale v fazi neogensko-recentnega potiskanja po paleogenskem strukturnem predrisu. Izmed proučenih objektov, npr. Krasa (Tržaško-Komenskega antiklinorija), Škocjanskih jam, Brkinov (Brkinskega sinklinorija) ali Čičarije (Čičarijskega antiklinorija), po kompleksnosti dogajanja izstopa osameli hrbet Vremščice (1027 m). V tej razpravi je opisano zaporedje deformacij, ki je privedlo do nastanka omenjenega hrbta.

Anticlinorium), Škocjan caves, Brkini (Brkini Synclinorium) or Čičarija (Čičarija Anticlinorium), the isolated ridge of Mt. Vremščica (1027 m) stands out in terms of complexity. This discussion describes the sequence of deformations that led to the formation of the aforementioned ridge.

Instead of the term Istra-Friuli Underthrust Zone, the term Istra-Friuli Thrust-Underthrust Zone is used in this discussion, which better illustrates the role of this zone in the process of Paleogene thrusting and Neogene-recent underthrusting.

The structural geometry, kinematics, and geomorphology of Istra

The visible part of Istra consists of the South Istra (A_1) and North Istra Structural Wedges (A_2), which rest on the Istra-Friuli Thrust-Underthrust Zone (Fig. 1). Due to the movement of this part of Microadria, and thus also Istra, both units behave differently towards the Dinarides, so it makes more sense to name them according to their dynamic characteristics. Thus, we introduce the terms South Istra Pushed Wedge and North Istra Extrusion Wedge (Fig. 2): the first moves with its tip towards the Dinarides, while the other is being extruded to the northwest towards the Gulf of Trieste. Both of them created corresponding structural and resulting geomorphological forms. The boundaries of the two dynamic units are not entirely identical to their formal structural boundaries on the surface, so the designation Ad_1 is introduced for the South Istra Pushed Wedge, and Ad_2 for the North Istra Extrusion Wedge.

South Istra Pushed Wedge Ad_1

The South Istra Structural Wedge is bounded by the Buje reverse Fault in the north, and in the east by the Kvarner Fault and the segment of the outer boundary of the Istra-Furlania Thrust-Underthrust Zone between the Kvarner and Buje Faults. It is built of Jurassic, Cretaceous, Paleocene, and Eocene carbonate rocks and Eocene clastics. The bedding forms a gently buckled anticline, the axis of which plunges very gently to the east-northeast, but its direction is impossible to determine precisely because the dip of the bedding is so low. Given the location of the anticline between the Buje and Kvarner Faults, where the main geomorphological object is the Limska draga (Lim channel/dry valley), it is called the Lim Anticline. It should not be confused with the north–south trending West Istra Anticline, which lies offshore, west of Istra. The Lim Anticline is discussed in more detail later.

A closer examination of the structural wedge boundaries showed that the reverse Buje Fault

Namesto izraza istrsko-furlanska podrivna cona, je v tej razpravi uporabljen izraz istrsko-furlanska narivno-podrivna cona, ki bolje ponazarja vlogo te cone v procesu paleogenskega narivanja in neogensko-recentnega podrivanja.

Strukturna geometrija, kinematika in geomorfologija Istre

Vidni del Istre sestavljata južnoistrski (A_1) in severnoistrski strukturni klin (A_2), ki se naslanjata na istrsko-furlansko narivno-podrivno cono (sl. 1). Obe enoti se zaradi premikanja tega dela Mikroadrije, in s tem tudi Istre, proti Dinaridom, obnašata različno, zato ju je smiselneje imenovati tudi po njunih dinamskih značilnostih, tako uvajamo termina južnoistrski potisni klin in severnoistrski iztisni klin (sl. 2), prvi se s konico premika proti Dinaridom, drugi pa se iztiska (izriva) na severozahod proti Tržaškemu zalivu. Oba sta pri tem ustvarila ustrezne strukturne in iz njih izhajajoče geomorfološke oblike. Meje obeh dinamičnih enot niso povsem identične z njunimi formalnimi strukturnimi mejami na površini, zato je za južnoistrski potisni klin uvedena oznaka Ad_1 , za severnoistrski iztisni klina pa Ad_2.

Južnoistrski potisni klin Ad_1

Južnoistrski strukturni klin je na severu omejen z Bujskim reverznim prelomom, na vzhodu pa s Kvarnerskim prelomom in segmentom zunanje meje istrsko-furlanske narivno-podrivne cone med Kvarnerskim in Bujskim prelomom. Zgrajen je iz karbonatnih kamnin jurske, kredne, paleocenske in eocenske starosti ter iz eocenskih klastitov. Plasti tvorijo rahlo usločeno antiklinalo, katere os zelo blago tone proti vzhodu do severovzhodu, vendar je njeno smer natančneje nemogoče določiti, ker je vpad plasti majhen. Glede na lego antiklinale med Bujskim in Kvarnerskim prelomom, kjer je glavni geomorfološki objekt Limska draga, jo imenujemo Limska antiklinala. Menimo, da je ne smemo zamenjevati z Zahodnoistrsko antiklinalo, ki leži v podmorju zahodno od Istre v smeri sever-jug. Limska antiklinala bo natančneje obravnavana pozneje.

Natančnejši pregled mej strukturnega klina je pokazal, da Bujski reverzni prelom ne kaže znakov sekundarnega premikanja, vendar ga na zahodu seka Zambratijski prelom in več njemu vzporednih za katere domnevamo, da naprej proti vzhodu-jugovzhodu potekajo južno od Bujskega preloma. Zambratijski prelom ima vidne horizontalne drse (sl. 2, točka 1; sl. 5/1) iz

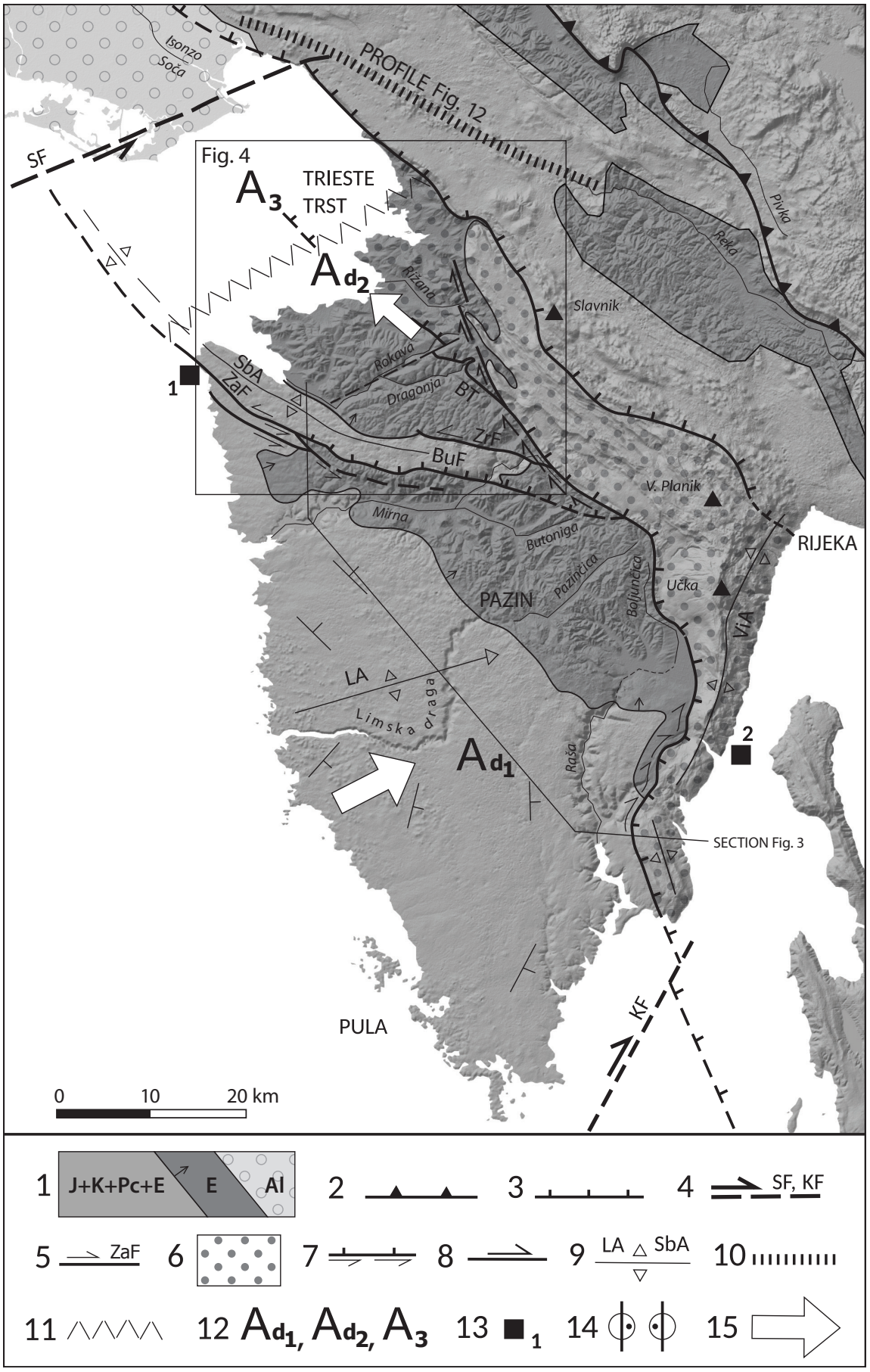

Fig. 2. Istra structural sketch and hydrographic network.
Sl. 2. Strukturna skica Istre in hidrografska mreža.

shows no signs of secondary movement, but it is cut in the west by the Zambratija Fault and several parallel ones, for which we assume continue south of the Buje Fault to the east-southeast. The Zambratija Fault has visible horizontal slickensides (Fig. 2, point 1; Fig. 5/1), from which it was not possible to determine the direction of the movement. It was determined on the basis of the rotation of the paleomagnetic poles in the vicinity of the fault, from which it indirectly follows that it is a left lateral strike-slip fault (Placer et al., 2010, fig. 4). The reverse Buje Fault did not become a left-lateral strike-slip, probably due to its uneven horizontal cross-section, which is manifested in a large bulge-like protrusion north of the lower Mirna River, which inhibited its movement. The Istra-Friuli Thrust-Underthrust Zone is morphologically strongly expressed in eastern Istra and runs almost parallel to the eastern Istrian coast, and thus also parallel to the Kvarner Fault. From the viewpoint above the Flanona Hotel in Plomin (Fig. 2, point 2), a south-easterly dipping fault plane (110/30) with prominent subhorizontal slickenides (Fig. 5/2), indicating dextral strike-slip (Placer et al., 2010, fig. 4) were found. It is obviously a Paleogene thrust plane rotated clockwise along the right strike-slip Kvarner Fault in the Neogene and then transformed into a strike slip fault plane. From these facts follows that the left-lateral strike-slip Zambratija Fault and several parallel ones formed next to the reverse Buje Fault, from which the left-lateral strike-slip Zambratija Zone was formed. Along the right-lateral strike-slip Kvarner Fault, the Istra-Friuli Thrust-Underthrust Zone bent to the south-southwest and became parallel to

katerih pa ni bilo mogoče ugotoviti smisla premika, ta je bil določen na podlagi rotacije paleomagnetnih polov v bližini preloma iz česar posredno izhaja, da gre za levo zmikanje (Placer et al., 2010, sl. 4). Bujski reverzni prelom ni postal levozmični verjetno zato, ker mu je to preprečeval njegov neravni horizontalni presek, ki se kaže v veliki trebušasti izboklini severno od spodnje Mirne. Istrsko-furlanska narivno-podrivna cona je v vzhodni Istri morfološko močno izražena in poteka skoraj vzporedno z vzhodno obalo Istre, s tem pa tudi s Kvarnerskim prelomom. Na razgledišču nad hotelom Flanona v Plominu (sl. 2, točka 2) je bila odkrita ploskev v smeri 110/30 z izrazitimi subhorizontalnimi drsami (sl. 5/2), ki kažejo na desno zmikanje (Placer et al., 2010, sl. 4). Očitno gre za paleogensko narivno ploskev, ki je bila v neogenu ob desnozmičnem Kvarnerskem prelomu zasukana v smeri urinega kazalca in nato transformirana v zmično ploskev. Iz dejstev torej izhaja, da je ob Bujskem reverznem prelomu nastal Zambratijski levozmični prelom in nekaj njemu vzporednih, iz katerih se je oblikovala zambratijska levozmična cona. Ob Kvarnerskem desnozmičnem prelomu se je istrsko-furlanska narivno-podrivna cona upognila proti jugo-jugozahodu in se postavila vzporedno s prelomom. Nastala je kombinirana kvarnerska desnozmična cona.

Da obstaja južnoistrski potisni klin potrjujejo tudi podatki paleomagnetnih raziskav jamskih sedimentov v Čičariji, ki kažejo na levo in desno krajevno omejeno rotacijo enot istrsko-furlanske narivno-podrivne cone. Konica klina je delovala

1 J + K + Pc + E – Jurassic, Cretaceous, Paleocene, and Eocene carbonates, E – Eocene flysch, Al – aluvium. Bedding strike and dip / J + K + Pc + E – jurski, kredni, paleocenski in eocenski karbonati, E – eocenski fliš, Al – aluvij. Vpad plasti

2 External Dinaric Thrust Belt boundary / meja Zunanjedinarskega narivnega pasu

3 Thrust plane within Dinaric thrust boundary: BuF – reverse Buje Fault, BT – Buzet Thrust / nariv v coni narivne mejne Dinaridov: BuF – Bujski reverzni prelom, BT – Buzetski narivni prelom

4 Strike-slip fault in the Microadria area: SF – Sistiana Fault, KF – Kvarner Fault / zmični prelom v območju Mikroadrije: SF – Sesljanski prelom, KF – Kvarnerski prelom

5 Lateral strike-slip faults: ZaF – Zambratija Fault, ZrF – Zrenj Fault / zmični prelomi: ZaF – Zambratijski prelom, ZrF – Zrenjski prelom

6 Istra-Friuli Thrust-Underthrust Zone / istrsko-furlanska narivno-podrivna cona

7 Neogene-recent right lateral strike-slip movements in the Paleogene thrust zone / desnozmični neogensko-recentni premiki v paleogenski narivni coni

8 Right lateral strike-slip fault in the Črni Kal Anomaly / desnozmični prelom v črnokalski anomaliji

9 Anticlines: LA – Lim Anticline, SbA – Savudrija-Buzet Anticline, ViA – East Istra Anticline / antiklinale: LA – Limska antiklinala, SbA – Savudrijsko-Buzetska antiklinala, ViA – Vzhodnoistrska antiklinala

10 Profile in Fig. 12 / Profil na sl. 12

11 North Istra Extrusion Wedge extrusion boundary / meja iztiskanja severnoistrskega iztisnega klina

12 Istra block: Ad1 – South Istra Pushed Wedge, Ad2 – North Istra Extrusion Wedge, A3 – Trieste parallelepiped / istrski blok: Ad1 – južnoistrski potisni klin, Ad2 – severnoistrski iztisni klin, A3 – tržaški paralelepiped

13 Observed evidence of strike-slip movement: 1 – Zambratija, 2 – Flanona / mesta vidnih dokazov zmikanja: 1 – Zambratija, 2 – Flanona

14 Strike–slip in the section in Fig. 3: left lateral strike-slip, right lateral strike-slip / zmični premik v profilu na sl. 3: levozmični prelom, desnozmični prelom

15 General direction of pushing, extrusion / generalna smer potiskanja, iztiskanja

the fault. Thus, a combined right-lateral strike-slip Kvarner Zone was formed.

The existence of the South Istra Pushed Wedge is also confirmed by the data from paleomagnetic research of the cave sediments in Čičarija, which indicate left and right locally limited rotation of the units of the Istra-Friuli Thrust-Underthrust Zone. The tip of the wedge worked so that the thrust units in front of it bent, with some rotating to the left and some to the right (Vrabec et al., 2018).

The structure of the South Istra Pushed Wedge is given in the sketch of the Lim Anticline cross-section in Figure 3, where the simplified structures of the Zambratija and Kvarner shear zones, and the Lim Anticline with the dry Limska draga are presented in dark hatch, and the surface flows of Mirna River with Butoniga and Raša River with Boljunčica are present in the anticline limbs. The reverse Buje Fault abuts on the Zambratija Fault at depth, with its left-lateral movement related to the Zambratija Fault or to its zone. The Kvarner Fault abuts on the outer border of the Istra-Friuli Thrust-Underthrust Zone, with dextral displacement along the Kvarner Fault and along the transformed segment of the Istra-Friuli Thrust-Undrethrust Zone.

We cannot yet speak more precisely about the age of the individual structural elements and geomorphology of the South Istra Pushed Wedge, but we can determine the sequence of their formation. There was no deposition in Istra in the Oligocene (Basic Geological Map - OGK sheets: Trieste, Ilirska Bistrica, Rovinj, Labin, Pula, Cres), so we assume that the area rose to the surface at the beginning of the Oligocene and a period of erosion

tako, da so se narivne enote pred njo upognile, del se je zasukal v levo, del pa v desno (Vrabec et al., 2018).

Zgradba južnoistrskega potisnega klina je podana v skici prečnega prereza Limske antiklinale na sliki 3, tu se vidi poenostavljeni strukturi zambratijske in kvarnerske zmične cone, Limsko antiklinalo s suho Limsko drago v temenu in površinska tokova Mirne z Butonigo in Raše z Boljunčico v krilih gube. Na Zambratijski prelom se v globini naslanja Bujski reverzni prelom, levozmični premik je vezan na prvega, oziroma na njegovo cono. Kvarnerski prelom se naslanja na zunanjo mejo istrsko-furlanske narivno-podrivne cone, desnozmični premik se dogaja ob Kvarnerskem prelomu in ob transformiranem segmentu istrsko-furlanske narivno-podrivne cone.

O starosti posameznih elementov strukture in geomorfologije južnoistrskega potisnega klina še ne moremo natančneje govoriti, lahko pa določimo zaporedje njihovega nastajanja. V Istri niso bile odložene oligocenske plasti (OGK, listi: Trst, Ilirska Bistrica, Rovinj, Labin, Pula, Cres), zato domnevamo, da se je v začetku oligocena območje dvignilo na površje in pričelo se je obdobje erozije v katerem se je izoblikovala primarna rečna mreža. Pričetek premikanja Mikroadrije proti Dinaridom še ni natančneje določen, domnevamo, da se je začelo v srednjem miocenu, kljub temu pa lahko razpravljamo o zaporedju dogodkov. Zaradi napredovanja klina med konvergentnima prelomoma (Kvarnerski prelom, Zambratijski prelom) proti severo severovzhodu je pričela rasti Limska

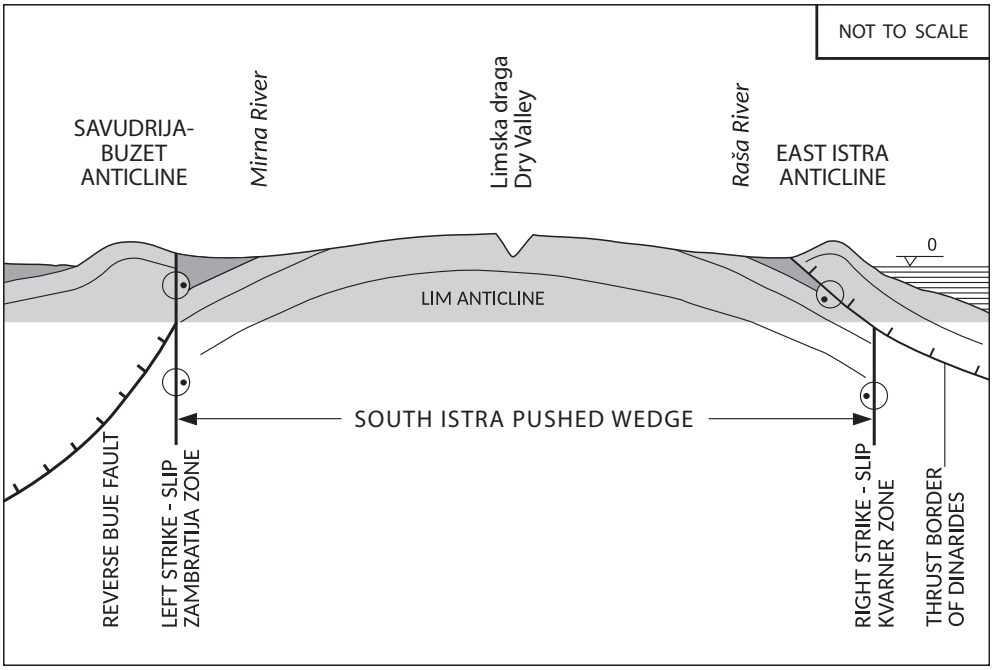

Fig. 3. Lim Anticline transversal cross section. Cross section trace in Figure 2. *Legend in Figure 2.*

Sl. 3. Skica prečnega profila Limske antiklinale. Potek profila na sl. 2. *Legenda na sliki 2.*

began, during which the primary river network (was) formed. The beginning of the Microadria movement towards the Dinarides is not yet precisely determined. It is assumed that it started in the middle Miocene; however, we can discuss the sequence of events. Due to the progress of the wedge between the convergent faults (Kvarner Fault, Zambratija Fault) towards the north-northeast, the Lim Anticline began to grow, and the Paleo-Mirna and Paleo-Raša flows, which were directed along the thrust wedge shear boundaries, submitted to its geometry. The Paleo-Pazinčica River flow, however, remained trapped in the crest of the anticline where it carved a deep valley. The karst surface peneplanation of southern Istra is today slightly buckled, as its uplift along the anticline axis was faster than the erosion of the Paleo-Pazinčica, which is why it retreated underground. The process of formation of the current geomorphological image of the South Istra Pushed Wedge was either continuous or multi-stage, but without detailed research it is impossible to determine this.

The South Istra Pushed Wedge geometry and dynamics are also strengthened by the springs of the most important rivers at its tip, Mirna and Butoniga rivers, Raša with its former tributary the Boljunčica river, and Pazinčica.

In the immediate hinterland of the pushed wedge tip is the highest peak of Čičarija, Mt. Veliki Planik (1272 m). Nearby is Mt. Vojak (1394 m), Mt. Učka's peak, which lies in the East Istra Anticline. It was formed from multiple structural units as a consequence of Paleogene thrusting and subsequent Neogene to recent movements along the Kvarner Fault.

North Istra Extrusion Wedge Ad_2

Formally, the North Istra Structural Wedge (Figs. 2 and 4A) is a unit between the reverse Buje Fault (BuF) and the Istra-Friuli Thrust-Underthrust Zone, more precisely the Buzet thrust Fault (BT), along its south-western border. The reverse Buje Fault lies under the Istra-Friuli Thrust-Underthrust Zone in the Buzet area. This point formally represents the tip of the wedge. The North Istra Structural Wedge is built of Cretaceous, Paleocene, and Eocene carbonates overlain by Eocene clastites; carbonates are exposed in the Savudrija-Buzet Anticline, which is an accompanying structure of the reverse Buje Fault, and in the tectonic window or half-window at Izola, which is an accompanying structure of the Križ Thrust (KT). The flysch beds plunge below the Istra-Friuli Thrust-Underthrust Zone.

antiklinala, njeni geometriji sta se podredila tokova paleo-Mirne in paleo-Raše, ki sta se usmerila vzdolž zmičnih meja potisnega klina, tok paleo-Pazinčice pa je ostal ujet v temenu antiklinale kjer je urezoval globoko dolino. Kraška uravnava južne Istre je danes rahlo usločena, njeno dviganje je bilo v osi antiklinale hitrejše od erozije paleo-Pazinčice, zato se je ta umaknila v podzemlje. Proces nastajanja sedanje geomorfološke podobe južnoistrskega potisnega klina je bil ali kontinuiran ali večstopenjski, brez detajlnih raziskav tega ni mogoče ugotoviti.

Geometrijo in dinamiko južnoistrskega potisnega klina utrjujejo tudi izviri pomembnejših rek v njegovi konici, Mirne in Butonige, Raše z nekdanjim pritokom Boljunčico in Pazinčice.

V neposrednem zaledju konice potisnega klina se nahaja najvišji vrh Čičarije, Veliki Planik (1272 m). V bližini je vrh Učke, Vojak (1394 m), ki pa leži v Vzhodnoistrski antiklinali. Ta je sestavljena iz več strukturnih enot in je nastala v prepletu učinkov paleogenskega narivanja in neogensko-recentnih premikov ob Kvarnerskem prelomu.

Severnoistrski iztisni klin Ad_2

Severnoistrski strukturni klin (sl. 2 in 4A) je v formalnem smislu enota med Bujskim reverznim prelomom (BuF) in istrsko-furlansko narivno-podrivno cono, natančneje Buzetskim narivnim prelomom (BT), ki leži na njeni jugozahodni meji. Na območju Buzeta leži Bujski reverzni prelom pod istrsko-furlansko narivno-podrivno cono. Ta točka formalno predstavlja konico klina. Severnoistrski strukturni klin je zgrajen iz krednih, paleocenskih in eocenskih karbonatov, ki jih prekrivajo eocenski klastiti; karbonati izdanjajo v Savudrijsko-Buzetski antiklinali, ki je spremljajoča struktura Bujskega reverznega preloma in v tektonskem oknu ali poloknu v Izoli, ki je spremljajoča struktura Križnega narivnega preloma (KT). Flišne plasti tonejo pod istrsko-furlansko narivno-podrivno cono.

V dinamičnem smislu je južna meja severnoistrskega iztisnega klina identična s severno mejo južnoistrskega potisnega klina, obstaja pa možnost, da je poleg zambratijske levozmične cone levozmično aktiven tudi Zrenjski prelom na severni strani Savudrijsko-Buzetske antiklinale. Severovzhodna meja severnoistrskega iztisnega klin pa ni identična z Buzetskim narivnim prelomom, temveč poteka poševno na do 12 km široko istrsko-furlanske narivno-podrivne cono,

In a dynamic sense, the southern border of the North Istra Extrusion Wedge is identical to the northern boundary of the South Istra Pushed Wedge, but there is a possibility that, in addition to the strike-slip Zambratija Zone, the Zrenj Fault on the north side of the Savudrija-Buzet Anticline is active as well. The north-eastern border of the North Istra Extrusion Wedge is not identical to the Buzet Thrust, but runs obliquely to the 8 to 12 km-wide Istra-Friuli Thrust-Underthrust Zone, approximately from the upper Mirna to the lower Glinščica/Rosandra rivers in a SSE-NNW direction. This boundary is not represented by only one structural element, but rather by a complex fault zone in which subvertical faults in the SSE-NNW direction are the most important (Figs. 2 and 4A).

Before describing the zone between the upper Mirna and lower Glinščica/Rosandra rivers, let's look at the most important signs of lateral thrusting within the North Istra Extrusion Wedge (Figs. 2 and 4A). The most important is the normal Rokava Fault, which runs transversely to the wedge and indicates the direction of extrusion towards the Gulf of Trieste. The middle Dragonja and Rokava valleys were formed along the Rokava Fault (Placer et al. 2004; Placer, 2005). A large part of the upper Dragonja valley also runs transversely to the extrusion približno od zgornje Mirne do spodnje Glinščice v smeri SSE-NNW. Te meje ne predstavlja le en element strukture, temveč kompleksna prelomna cona v kateri so najpomembnejši deznozmični subvertikalni prelomi v smeri SSE-NNW (sl. 2 in 4A).

Preden opišemo cono med zgornjo Mirno in spodnjo Glinščico, si oglejmo najpomembnejše znake bočnega izrivanja znotraj severnoistrskega iztisnega klina (sl. 2 in 4A); na prvem mestu je Rokavin normalni prelom, ki poteka prečno na klin in kaže na smer iztiskanja proti Tržaškemu zalivu. Po njem sta se izoblikovali dolini srednje Dragonje in Rokave (Placer et al., 2004; Placer, 2005). Prečno na iztisni klin poteka tudi večji del doline zgornje Dragonje in pa številne doline potokov, ki med srednjo Dragonjo in Bračano ponikajo v apnencu Savudrijsko-Buzetske antiklinale. Prečno na klin teče tudi srednja Mirna preko Savudrijsko-Buzetske antiklinale. Severozahodno od Rokavinega preloma ne prevladujejo več prečne doline, tu so spodnja Dragonja, Drnica, Badaševica, Rižana in Osapska reka poglobile svoje struge po drugih elementih strukture. Glede na to izgleda, da se je severozahodni del klina iztisnil kot sorazmerno homogen blok.

Fig. 4. North Istra Extrusion Wedge: A. North Istra structural sketch (updated and symplified after Placer, 2005, Fig. 1; 2007, Fig. 2; Placer et al., 2010, Fig. 5). B. Neogene to recent extrusion evidence in the northern Istra relief.

Sl. 4. Severnoistrski iztisni klin: A. Strukturna skica severne Istre (dopolnjeno in poenostavljeno po Placer, 2005, sl. 1; 2007, sl. 2; Placer et al., 2010, sl. 5). B. Znaki neogensko-recentnega iztiskanja v reliefu severne Istre.

1 K + Pc + E – Cretaceous, Paleogene and Eocene carbonates, E – Eocene flysch. Bedding strike and dip / 1 K + Pc + E – kredni, paleocenski in eocenski karbonati, E – eocenski fliš. Vpad plasti

2 Paleogene reverse and thrust faults: BuF – reverse Buje Fault, BT – Buzet Thrust KT – Križ Thrust IT – Izola Thrust / paleogenski reverzni in narivni prelomi: BuF – Bujski reverzni prelom, BT – Buzetski narivni prelom, KT – Križni narivni prelom, IT – Izolski narivni prelom

3 Paleogene backthrust fault (Strunjan structure) / paleogenski povratni reverzni prelom (Strunjanska struktura)

4 Neogene-recent reverse fault / neogensko-recentni podrivni reverzni prelom

5 Istra-Friuli Thrust-Underthrust Zone / istrsko-furlanska narivno-podrivna cona

6 Larger sub-vertical fault with prevailing strike-slip component, extrusion boundary: proved ZaF – Zambratija Fault, inferred ZrF – Zrenj Fault / večji subvertikalni prelom s prevladujočo zmično komponento, meja iztiskanja: dokazano ZaF – Zambratijski prelom, domnevno ZrF – Zrenjski prelom

7 Right lateral strike-slip faults in the Črni Kal Anomaly zone, extrusion boundary: 3 – Gračišče series, 4 – Kastelec series / desnozmični prelomi v območju črnokalske anomalije, extrusion boundary: 3 – gračiški niz, 4 – kastelski niz

8 Right lateral offset in the Neogene to recent underthrust reverse fault, extrusion boundary / desnozmični premik v ploskvi neogenskega do recentnega podrivnega reverznega preloma, meja iztiskanja

9 Normal fault. Proved, inferred: RoF – Rokava Fault / normalni prelom. Ugotovljen, domneven: RoF – Rokavin prelom

10 Extensional crack (Gračišče) / ekstenzijska razpoka (Gračišče)

11 Neogene antiformal deformation of the Paleogene thrust plane: a – Glinščica/Rosandra, b – Varda, c – Črni Kal, d – Movraž, e – Perci village near Buzet / v neogenu antiformno deformirane paleogenske narivne ploskve: a – Glinščica, b – Varda, c – Črni Kal, d – Movraž, e – Perci pri Buzetu

12 Spatialy restricted folds : Strunjan structure, Tinjan structure or Tinjan Extrusion Wedge / gube prostorsko omejenega obsega: strunjanska struktura, tinjanska struktura ali tinjanski iztisni klin

13 Larger folds: SbA – Savudrija-Buzet Anticline, BaA – Bazovica Anticline, LiS – Lipica Syncline / večje gube: SbA – Savudrijsko-Buzetska antiklinala, BaA – Bazovska antiklinala, LiS – Lipiška sinklinala

14 Extrusion direction / smer iztiskanja

15 Extrusion evidence locations: 1 – Zambratija, 3 – Gračišče, 4 – Kastelec / mesta z dokazi iztiskanja: 1 – Zambratija, 3 – Gračišče, 4 – Kastelec

16 A saddle above Trieste between Mt. Mai/Maj and Mt. Mote Calvo/Globojnar at elevation point 416 m / sedlo nad Trstom med Majem (Mai) in Globojnarjem (Monte Calvo) na koti 416 m

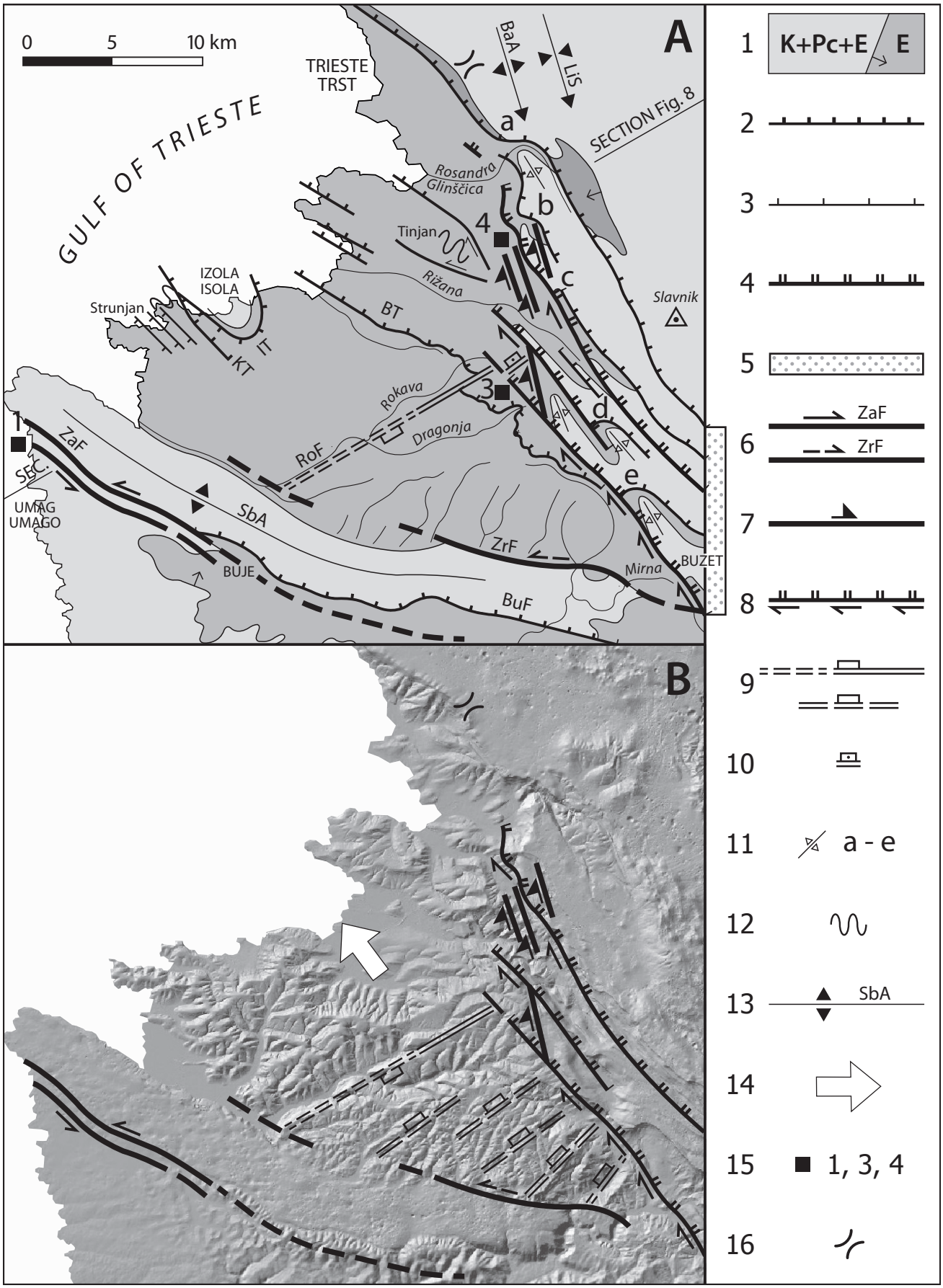
A
B
0 5 10 km
TRIESTE
TRST
GULF OF TRIESTE
BaA
LiS
SECTION Fig. 8
Rosandra
Glinščica
Tinjan
Rižana
IZOLA
ISOLA
Strunjan
BT
KT
Slavnik
Rokava
Dragonja
RoF
ZaF
SbA
ZrF
BuF
BUJE
UMAG
UMAGO
Mirna
BUZET
a
b
c
d
e
1
3
4
1 K+Pc+E E
2
3
4
5
6 ZaF
ZrF
7
8
9
10
11 a - e
12
13 SbA
14
15 1, 3, 4
16

wedge, as well as numerous valleys of streams that sink between the middle Dragonja and Bračana rivers in the limestone of the Savudrija-Buzet Anticline. The middle Mirna also flows transversely across the wedge and the Savudrija-Buzet Anticline. Northwest of the Rokava Fault, transverse valleys no longer dominate: here the lower Dragonja, Drnica, Badaševica, Rižana and Osapska reka rivers have deepened their beds along other structural elements. Based on this, it appears that the north-western part of the wedge was extruded as a relatively homogeneous block.

Now let's take a look at the north-eastern border of the North Istra Extrusion Wedge between the upper Mirna and lower Glinščica/Rosandra rivers. In order to understand the causes of the shear zone formation that runs obliquely in the direction of thrusting, or underthrusting, we need to take a closer look at the Istra-Friuli Thrust-Underthrust Zone structure. In the Čičarija, it consists of several similar structural duplexes. The anticlines in the fronts of duplexes are composed of Paleogene limestone followed by the transitional marl or by flysch in some places. Each duplex is covered by the Pg limestone core of the next duplex of the same structure. The axes of the frontal limestone anticlines regionally plunge towards the northwest, so that in the north-western part of the Istra-Friuli Thrust-Underthrust Zone, the Paleogene limestones are no longer at the surface, but the transitional marl or flysch of the upper duplexes is thrust on the transitional marl and flysch of the lower ones. The described conditions can be seen on the OGK (sheet Trieste), simplified on the tectonic sketch of northern

Oglejmo si zdaj severovzhodno mejo severnoistrskega iztisnega klina med zgornjo Mirno in spodnjo Glinščico. Da bi razumeli vzroke nastanka zmične cone, ki poteka poševno na smer narivanja, oziroma podrivanja, si moramo podrobneje ogledati zgradbo istrsko-furlanske narivno-podrivne cone. Ta je na območju Čičarije sestavljena iz več podobnih narivnih lusk. V njenem jugovzhodnem delu ležijo v čelih lusk čelne antiklinale iz paleogenskega apnenca na katerem ležijo prehodni laporji in ponekod tudi fliš, ki ga prekriva paleogenski apnenec, ki gradi čelo naslednje luske enake zgradbe. Osi čelnih antiklinal iz apnenca regionalno tonejo proti severozahodu, tako da v severozahodnem delu istrsko-furlanske narivno-podrivne cone paleogenski apnenci niso več na površju, temveč je prehodni lapor ali fliš zgornjih lusk narinjen na prehodni lapor in fliš spodnjih lusk. Opisane razmere so vidne na OGK (list Trst), poenostavljeno na tektonski skici severne Istre, kjer je fliš označen s sivim odtenkom (sl. 2 in 4A). Severozahodni boki karbonatnih antiklinal v čelih lusk se na površju izklinjajo v pasu med zgornjo Mirno in spodnjo Glinščico v smeri SSE-NNW, narivne ploskve pa potekajo naprej po flišu proti NW. Potek narivnic v flišu na sliki 4A ni izrisan, temveč le nakazan v bližini morske obale, kjer narivnice praviloma ležijo v dnu zalivov, kar pomeni, da so ti nastali po tektonsko prizadetih conah. Narivnice v flišu med obalo in zmično cono v smeri SSE-NNW niso izrisane zato, ker jih je potrebno detajlno geološko skartirati. Karbonatne antiklinale v čelih lusk med zgornjo Mirno in spodnjo Glinščico

Fig. 5. Structural peculiarities of Istra and Istra-Friuli Thrust-Underthrust Zone.

Sl. 5. Strukturne posebnosti Istre in istrsko-furlanske narivno-podrivne cone.

1 Left-lateral strike-slip Zambratija Fault: sub-horizontal slickensides on the plane 30/90 (Fig. 2, location 1; Fig. 4A, location 1) / Zambratijski levozmični prelom: subhorizontalne drse v ploskvi 30/90 (sl. 2, točka 1; sl. 4A, točka 1)

2 Right-lateral strike-slip Kvarner Zone: right-lateral strike-slip along the plane 110/30, which was primarily parallel to the Dinarides. Above Flanona Hotel near Plomin (town) (Fig. 2, location 2) / kvarnerska desnozmična cona: desno zmikanje v ploskvi 110/30, ki je imela prvotno smer Dinaridov. Nad hotelom Flanona pri Plominu (sl. 2, točka 2)

3 Extensional crack in direction 340/50 at Gračišče (Fig. 4A, location 3) / ekstenzijska razpoka v smeri 340/50 pri Gračišču (sl 4A, točka 3)

4 Fault zone in flysch in direction 50/50 zone of Neogene-recent underthrust reverse faults above Gabrovica village (Fig. 4A, location »c«; Fig. 8, Istra-Friuli Thrust-Underthrust Zone) / prelomna cona v flišu v smeri 50/50 cona neogensko-recentnih podrivnih reverznih prelomov nad Gabrovico (sl. 4A, točka »c«; sl. 8, istrsko-furlanska narivno-podrivna cona)

5 Antiformally bent paleogene thrust plane in the Varda road cut (Fig. 4A, location »b«) / antiformno usločena paleogenska narivna ploskev v cestnem useku Varda (sl. 4A, točk »b«

6 Antiformally bent paleogene thrust plane above Movraž village (Fig. 4A, location »d«) / antiformno usločena paleogenska narivna ploskev nad Movražem (sl. 4A, točka »d«)

7 Fault zone in flysch in direction 25/45 Paleogene thrust with stepped oblique cut, Valmarin (Škofije). Structural type of disordered jump (Fig. 7D) / prelomna cona v flišu v smeri 25/45 cona paleogenskega nariva, ki ima stopničasti poševni rez, Valmarin (Škofije). Strukturni tip neurejenega preskoka (sl. 7D)

8 Backthrust in the Strunjan structure in direction 230/60 (Figs. 4A and 8) / povratni reverzni prelom v strunjanski strukturi v smeri 230/60 (sl. 4A in 8)

9 Transverse folding in the Tinjan Extensional Wedge. Axial planes in direction 310/90 .Construction cave for the water reservoir at Slatine village (Fig. 4A, location 4) / prečno gubanje v tinjanskem iztisnem klinu. Osna ravnina gub v smeri 310/90 Izkop za vodohran v Slatinah (sl. 4A, točka 4)


1


2


3


4


5


Movraž
6


7


8


9

Istra, where the flysch is marked with a grey hatch (Figs. 2 and 4A). The north-western flanks (if a simple fold is determined e.g. by the northern and the southern limbs and an axial plane between them we are missing the term to describe the western and the eastern part of the fold. As there is no adequate term for these in the literature, a term flank is used here. Flank and limb should therefore not be interchangeable terms) of the carbonate anticlinesin the fronts of the duplexes pinch out on the surface in the SSE-NNW trending belt between the upper Mirna and the lower Glinščica/Rosandra, and the thrust planes continue in flysch towards the NW. The course of the thrusts in the flysch in Fig. 4A is not drawn, but only indicated near the sea coast, where thrust planes generally lie at the bottom of bays, which means that they were formed along tectonically affected zones. Thrusts in the flysch between the coast and the shear zone in the SSE-NNW direction are not fully drawn because they need to be geologically mapped in detail. The carbonate anticlines in the fronts of the duplexes between the upper Mirna and the lower Glinščica/Rosandra lie in an echelon series, which in reality represents a wider zone and not just a single set of duplexes.

The north-western edges of the echelon-arranged frontal carbonate anticlines are accompanied by the SSE-NNW trending subvertical right-lateral faults. These were mapped at the highway construction site in two areas (Placer, 2003; 2004): between the lower entrance to the Kastelec tunnel and the upper entrance to the Dekani tunnel (260/90, 250/90, 240/80) (Fig. 4A, point 4) and in the vicinity of Gračišče, where a fault (70/80) was measured, otherwise without visible slickensides, but in its western flank there are pronounced extensional fractures in the 350-0/70 direction, which indicate extrusion towards the north-northwest (Fig. 4A, point 3; Fig. 5/3). These two groups are referred to as the Kastelec and Gračišče sets of right-lateral strike-slip faults throughout the article. To understand their meaning, let's look at the structural analysis of the relationship between these faults and the thrust duplexes of the Istra-Friuli Thrust-Underthrust Zone, with frontal anticlines composed of Paleogene limestone and Eocene flysch in the Figure 6. In the analysis, we proceed from the idealized echelon arrangement of duplexes and frontal anticlines (Fig. 6A), where in the ground plane the edges of the Paleogene limestone anticlines are connected to form an envelope »e«, which runs in a 340° direction. This direction was chosen because it illustrates the location of the right-lateral strike-slip

ležijo torej v ešalonskem nizu, ki pa ni linearen, oziroma ne obsega le enega niza lusk, temveč zajema širšo cono.

Severozahodne robove ešalonsko razporejenih čelnih karbonatnih antiklinal spremljajo subvertikalni desnozmični prelomi v smeri SSE -NNW. Ti so bili na delovišču avtoceste kartirani na dveh območjih (Placer, 2003; 2004); med spodnjim vhodom v predor Kastelec in zgornjim vhodom v predor Dekani 260/90, 250/90, 240/80 (sl. 4A, točka 4) in v okolici Gračišča, kjer je bil izmerjen prelom 70/80, sicer brez vidnih drs, toda v njegovem zahodnem krilu nastopajo izrazite ekstenzijske razpoke v smeri 350-0/70, ki kažejo na iztiskanje proti severo-severozahodu (sl. 4A, točka 3; sl. 5/3). V nadaljevanju članka ti dve skupini imenujemo kastelski in gračiški niz desnozmičnih prelomov. Da bi razumeli njihov pomen, si na sliki 6 oglejmo strukturno analizo odnosa med temi prelomi in narivnimi luskami istrsko-furlanske narivno-podrivne cone v čelu katerih ležijo antiklinale iz paleogenskega apnenca in eocenskega fliša. V analizi izhajamo iz idealizirane ešalonske razporeditve lusk in čelnih antiklinal (sl. 6A), kjer so v tlorisni ravnini robovi antiklinal iz paleogenskega apnenca povezati z ovojnico ali envelopo »e«, ki poteka v smeri 340°. Ta smer je bila izbrana zato, ker ponazarja lego desnozmičnih prelomov kastelskega in gračiškega niza. Ovojnica ali envelopna »e« leži v ravnini, ki jo imenujemo ovojna ali envelopna ravnina »E«. Da bi ugotovili njen vpad je bila iz terenskih podatkov določena srednja lega paleogenskih narivnih ploskev »P«, ki znaša 50/30 in srednja lega plasti »D« v krilu čelne antiklinale, ki znaša 35/20. Konstruirana presečnica »s« na sliki 6B ima smer 341/11, zaokroženo 340/10, kar je enako smeri envelope »e« na sl. 6A. To pomeni, da ležita ovojnica »e« in presečnica »s« v ovojni ravnini »E«, ki ima smer 340 ° in vpad 90 °. V našem primeru je ovojna ravnina »E« konstruirana meja med območjem, kjer v luskah prevladuje paleogenski apnenc in območjem, ki je zgrajeno iz mehkejšega fliša, zato predstavlja labilno cono po kateri bi lahko nastal zmični prelom.

Konstrukcija na sliki 6 je idealizirana, vendar dobro ponazarja razmere v pasu med zgornjo Mirno in spodnjo Glinščico. Ovojna ravnina »E« ponazarja vzroke za nastanek kastelskega in gračiškega niza subvertikalnih desnozmičnih prelomov v smeri SSE-NNW, le da v naravi ne gre za eno ovojno ravnino ali zmični prelom, temveč za cono, ki je sestavljena iz več podobnih ešalonskih segmentov. Izločena sta kastelski

faults of the Kastelec and Gračišče series. The envelope »e« lies in a plane called the envelope plane »E«. In order to determine its elements (azimuth and dip), the middle position of Paleogene thrust surfaces »P« was determined from the field data, which is 50/30, and the middle position of layer »D« in the limb of the frontal anticline, which is 35/20. Constructed intersection »s« in Figure 6B has a bearing of 341/11 rounded to 340/10, which is parallel to the direction of envelope »e« in Figure 6A. This means that envelope »e« and the intersection »s« lie in the envelope plane »E«, which has a 340° bearing and vertical dip. In our case, the enveloping plane »E« is a constructed boundary between an area dominated by duplexes of Paleogene limestone and an area built of softer (less rigid) flysch, so it represents a labile zone along which a strike-slip fault could occur.

The construction in Figure 6 is idealized, but it well illustrates the conditions in the belt between the upper Mirna and lower Glinščica/Rosandra rivers. The enveloping plane »E« illustrates the causes of the formation of the SSE–NNW trending Kastelec and Gračišče series of subvertical right-lateral strike-slip faults, except that *in-si*tu it is not a single enveloping plane or strike-slip fault, but a zone consisting of several similar echelon segments. Kastelec and Gračišče series are obliterated here because they are emphasized in the Figure 4A due to their importance.

Echelon-arranged carbonate anticlines, as presented in Figue 6A, represent a stack of competent blocks in a less competent medium, therefore we propose introducing the name stacked structure, and envelope fault for the fault that occurred along the envelope plane of the stacked structure.

The complex dextral strike-slip zone between the upper Mirna and the lower Glinščica/Rosandra, which is characterized by a stacked structure and enveloping faults, is called the Črni Kal Anomaly. The regional cause of its formation is explained in the chapter on the formation of the North Istra Extrusion Wedge and the South Istra Pushed Wedge.

In addition to the Paleogene thrust faults, reverse faults (Figs. 4A and 5/4) also occur in the Istra-Friuli Thrust-Underthrust Zone, representing the leading structures of the Kraški rob (geographic region along the SW margin of the Čičarija plateau between the villages of Socerb and Mlini Fig. 11) recent uplift. Next to them, the Paleogene thrusts planes are anticlinally bent (Fig. 5/5). In Fig. 4A, some examples of such deformation are marked with the letters »a« (Glinščica/Rosandra), »b« (Varda, Fig. 5/5), »c« (Črni Kal), »d« (Movraž,

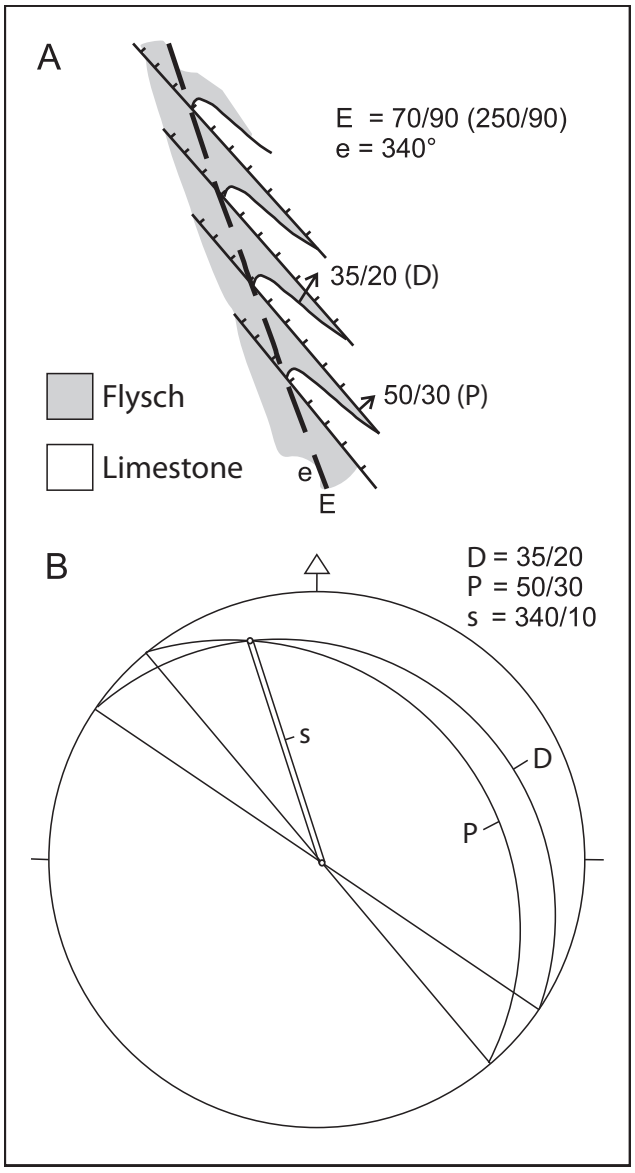

Fig. 6. Formation of Kastelec and Gračišče series of faults.
Sl. 6. Nastanek prelomov kastelskega in gračiškega niza.

A. Stacked structure: ideal echelon arrangement of Paleogene limestone and flysch duplexes.

The north-western edges of the thrusted frontal anticlines of Paleogene limestone form an echelon series whose »e« envelope is straight and runs due NNW (340°), which is oblique to the trust planes running NW (50°). / Zložbena zgradba: idealni ešalonski niz narivnih lusk iz paleogenskega apnenca in fliša. Severozahodni robovi čelnih antiklinal iz paleogenskega apnenca tvorijo ešalonski niz, katerega ovojnica »e« ali envelopa je ravna in poteka v smeri NNW (340°), kar je poševno na narivne ploskve lusk, ki potekajo v smeri NW (50°).

B. Construction of the intersection between the middle position of the thrust surfaces of the scales (»P« = 50/30) and the middle position of the bedding (»D« = 35/20). The intersection »s« lies in the direction 341/11, rounded 340/10, with its direction identical to the direction of the envelope »e«, which means that both lines lie in a single plane. It is vertical and called the enveloping plane »E«, which lies in the direction 70/90, (or 250/90). / Konstrukcija presečnice med srednjo lego narivnih ploskev lusk (»P« = 50/30) in srednjo lego plasti (»D« = 35/20). Presečnica »s« leži v smeri 341/11, zaokroženo 340/10, njena smer je identična s smerjo ovojnice ali envelope »e«, kar pomeni, da ležita obe premici v eni ravnini. Ta je vertikalna. Imenujemo jo ovojna ali envelopna ravnina »E«, ki leži v smeri 70/90, oziroma 250/90.

Fig. 5/6) and »e« (Perci near Buzet). Some of these Paleogene thrust surfaces show a certain degree of metamorphosis (verbally communicated by Dr. Bogomir Celarc, 2021), which, in addition to being folded, undoubtedly indicates their inactivity and that the reverse faults are younger, i.e. of Neogene-recent age. Unlike the others, they are called underthrust reverse faults. The antiformly bent thrust surface in Glinščica/Rosandra a, marked with »a«, is probably related to the Bazovica Anticline.

In the area of the Črni Kal Anomaly, there are SSE–NNW trending (Kastelec and Gračišče series) subvertical right-lateral strike-slip faults and SE-NW trending reverse underthrust faults. The relationship between them is multi-phased, in some places the first intersect the others, in others it is the other way around. In the zones characterised by reverse underthrust faults, signs of sub-horizontal extrusion towards the northwest to north-northwest are also found in the area of the Črni Kal Anomaly.

Based on the geometrical conditions on the tip of the North Istra Extrusion Wedge, we conclude that there exists an underthrusting reverse fault between Gračišče and Buzet, which is occasionally active also as a right-lateral strike-slip. The underthrusting kinematics next to it is indicated by the anticlinal folding »e«, while the extrusion is indicated by the transverse valleys parallel to the Rokava Fault (Fig. 4B). The Rokava Fault also terminates next to this underthrusting fault (Fig. 4A, point 3), due to which the Rokava valley suddenly turns to the southeast, and the Buzet Thrust also leans on it.

We assume that the oscillation between subhorizontal dextral strike-slip and underthrusting is a characteristic of the Istrian Pushed Area. With this mechanism and intermediate variants, we can explain large tectonic mirrors in the Raša fault zone mentioned in the chapter on the Raša fault in this article.

The discovery of the underthrust reverse faults requires a new geological mapping of the Istra-Friuli Thrust-Underthrust Zone, especially the part that takes place in flysch. The sketch of its already published (thrust) structure (Placer et al., 2004, Fig. 1; 2010, Fig. 5; Placer, 2005, Fig. 1; 2007, Fig. 2), is based on knowledge of the Buzet Thrust, examined from Buzet to the Gulf of Trieste coast and takes place exclusively in flysch layers (Placer et al., 2004). The Buzet Thrust Thrust plane on the surface obliquely intersects the strata everywhere at an angle of around 30°, and beds are folded into a flanking fold along the thrust plane, thus we

in gračiški niz, ki sta zaradi svojega pomena poudarjena na sliki 4A.

Ešalonsko razporejene karbonatne antiklinale, kot je to predstavljeno na sliki 6A, predstavljajo skladovnico ali zložbo kompetentnih blokov v manj kompetentnem mediju, zato predlagamo, da se uvede naziv zložbena zgradba ali zložbena struktura, za prelom ki je nastal po ovojni ravnini zložbene strukture pa ovojni ali envelopni prelom. Izraz zložbena zgradba izvajamo iz skladovnice drv, ki so zložena v zložbo, izraz skladovna zgradba bi bil neprimeren, ker se prekriva s skladi, oziroma plastmi.

Kompleksno desnozmično cono med zgornjo Mirno in spodnjo Glinščico, za katero je značilna zložbena zgradba in ovojni prelomi, imenujemo črnokalska anomalija. Regionalni vzrok za njen nastanek bo razložen v poglavju o nastanku severnoistrskega iztisnega in južnoistrskega potisnega klina. Poleg paleogenskih narivnih prelomov nastopajo v istrsko-furlanski narivno-podrivni coni tudi reverzni prelomi (sl. 4A in 5/4), ki predstavljajo vodilne strukture recentnega dviganja kraškega roba. Ob njih so ploskve paleogenskih narivov antiklinalno usločene (sl. 5/5). Na sliki 4A so nekateri primeri takih usločitev označeni z malimi črkami »a« (Glinščica), »b« (Varda, sl. 5/5), »c« (Črni Kal), »d« (Movraž, sl. 5/6) in »e« (Perci pri Buzetu). Nekatere paleogenske narivne ploskve od teh kažejo določeno stopnjo metamorfoze (ustno posredoval dr. Bogomir Celarc 2021), kar poleg tega, da so nagubane, nedvomno kaže na njihovo neaktivnost in da so reverzni prelomi mlajši, torej neogensko-recentne starosti. Za razliko od drugih jih imenujemo podrivni reverzni prelomi. Antiformna usločitev narivne ploskve v Glinščici, ki je označena z »a« je verjetno povezana z Bazovsko antiklinalo (Bazovica, bazovski: Merku, 2006, 42).

V območju črnokalske anomalije torej nastopajo subvertikalni desnozmični prelomi smeri SSE-NNW (kastelski in gračiški niz) in podrivni reverznimi prelomi smeri SE-NW. Odnos med njimi je večfazen, ponekod prvi sekajo druge, ponekod je obratno. V conah podrivnih reverznih prelomov najdemo v območju črnokalske anomalije tudi znake subhorizontalnega iztiskanja proti severozahodu do severo-severozahodu.

Po geometrijskih razmerah na območju konice severnoistrskega iztisnega klina sklepamo, da obstoja med Gračiščem in Buzetom podrivni reverzni prelom, ki je postal občasno tudi desnozmičen. Na podrivno kinematiko ob njem kaže antiklinalna usločitev »e«, na iztiskanje

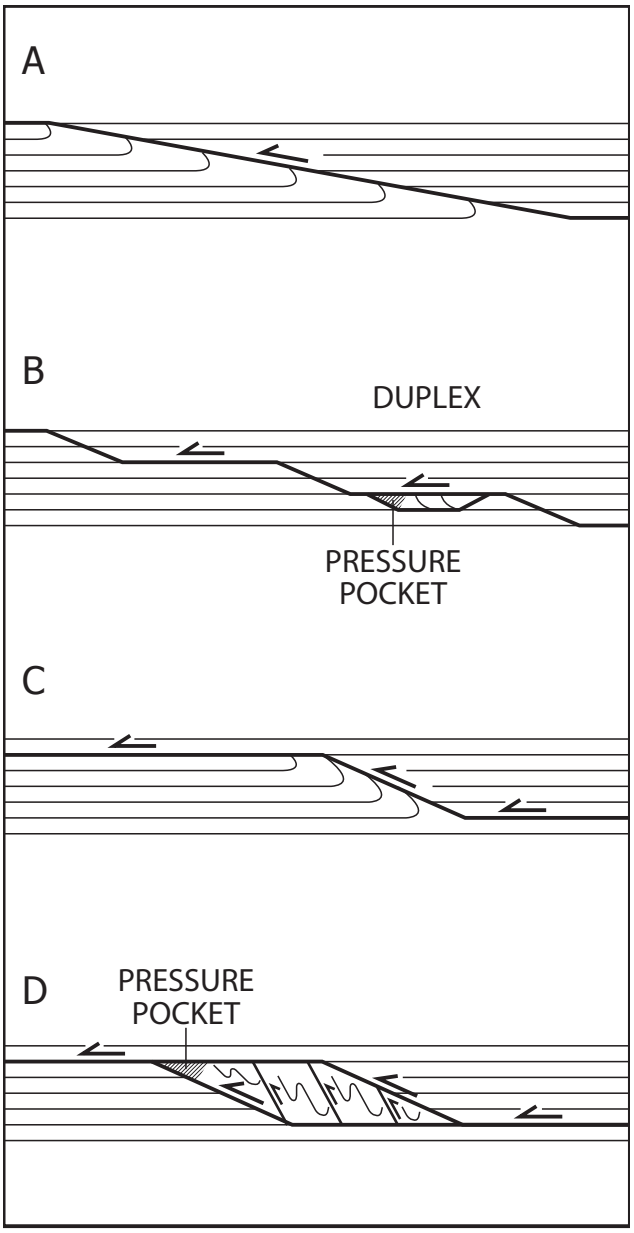

Fig. 7. The course of the thrust plane in flysch layers. Profile. A. Straight oblique cut. B. Stepped oblique cut. C. Jump with natural folds. D. Disordered jump (Fig. 5/7).

Sl. 7. Potek narivne ploskve v flišnih plasteh. Profil. A. Premi poševni rez. B. Stopničasti poševni rez. C. Preskok z obnarivnimi gubami. D. Neurejeni preskok (sl. 5/7).

conclude that it is the same in depth. An example of an oblique cut is presented in Figure 7A. Other thrust faults in the flysch within the Istra-Friuli Thrust-Underthrust Zone have so far been interpreted in accordance with the structure of the Buzet Thrust. During later detailed research of this area, it was shown that the oblique cut in the flysch is not always straight, but is often stepped (Fig. 7B), which means that the thrust plane sometimes runs between the layers, and sometimes obliquely to them. The thrust plane dip in such a case is somewhat steeper. When it passes between layers, identical parallel interlayer deformations appear next to it, and locally duplexes may evolve, and when they

kažejo prečne doline potokov, ki so vzporedne Rokavinemu prelomu (sl. 4B). Ob njem se izklinja tudi Rokavin prelom (sl. 4A, točka 3), zaradi česar dolina Rokave nenadoma zavije proti jugovzhodu. Nanj se naslanja tudi Buzetski narivni prelom. Domnevamo, da je nihanje med subhorizintalnim desnim zmikanjem in podrivanjem značilnost istrskega potisnega območja, s tem mehanizmom in vmesnimi variantami lahko razložimo velika tektonska zrcala v prelomni coni Raškega preloma, ki jih v tem članku omenjamo v poglavju o Raškem prelomu.

Odkritje podrivnih reverznih prelomov terja ponovno geološko kartiranje istrsko-furlanske narivno-podrivne cone. Zlasti tistega dela, ki poteka v flišu. Skica njene narivne zgradbe, ki je bila doslej večkrat objavljena (Placer et al., 2004, sl. 1; 2010, sl. 5; Placer, 2005, sl. 1; 2007, sl. 2) je izhajala iz poznavanja Buzetskega narivnega preloma, ki je bil pregledan od Buzeta do obale Tržaškega zaliva in poteka izključno v flišnih plasteh (Placer et al., 2004). Njegova narivna ploskev na površju povsod poševno seka plasti pod kotom okoli 30°, ob njej so plasti večinoma povite v obnarivno gubo, zato sklepamo, da je tako tudi v globini, na sliki 7 ga predstavljamo kot primer premega poševnega reza. Ostale narivne prelome v flišu znotraj istrsko-furlanske narivno-podrivne cone, smo doslej interpretirali v skladu z zgradbo Buzetskega narivnega preloma. Pri poznejših detajlnih raziskavah tega ozemlja pa se je pokazalo, da poševni rez v flišu ni vedno raven, zelo pogosto je stopničast (sl. 7B), kar pomeni, da poteka narivna ploskev nekaj časa med plastmi, nekaj časa poševno nanje. V takem primeru je vpad narivne ploskve nekoliko bolj strm. Ko poteka med plastmi, nastopajo ob njej identične vzporedne medplastne deformacije, ponekod pa se razvijejo dupleksi. Pri preskoku iz enega nivoja plasti v drugega se pojavljata dva tipa zgradbe prelomne cone. V prvem primeru so se plasti zasukale v obprelomno gubo (sl. 7C), v drugem se razvije neurejeno zaporedje skoraj izoklinalnih gub in reverznih prelomov (sl. 7D in 5/7). Struktura drugega ali neurejenega tipa preskoka je na moč podobna novonastalim conam podrivnih reverznih prelomov (sl. 5/4). Pomemben kriterij razlikovanja so strukturni žepi, ki se nahajajo v čelih narivnih struktur neurejenega tipa (sl. 7D) in dupleksov (sl. 7B). V njih običajno nastopajo močno stlačene pretrte kamnine ali zgoščine, ki imajo glede na okoliški pretrti medij povečano volumsko gostoto. Obravnavane žepe imenujemo tlačni strukturni žepi, skrajšano tlačni žepi, ki predstavljajo novost v

jump from one level to another, two types of fracture zone structure appear. In the first case, the layers are twisted into a fold along the fault (Fig. 7C), in the second a disordered sequence of almost isoclinal folds and reverse faults develops (Figs. 7D and 5/7). The structure of the second or disordered type of jump is very similar to newly formed zones of underthrust reverse faults (Fig. 5/4).

An important distinguishing criterion is the structural pockets located in the faces of thrust structures of disordered type (Fig. 7D) and duplexes (Fig. 7B). They usually contain highly compressed crushed rocks or clusters, which are denser compared to the surrounding crushed (but not compressed as in the pressure pocket) medium. Said pockets are structural pressure pockets, abbreviated as pressure pockets representing a novelty in the case of the thrust duplexes of the described type. Pressure pockets of this type were observed in thrust zones, while other zones of underthrust reverse faults have not been explored in this sense. However, they do not form in duplexes, which accompany the phenomena of underwater synsedimentary gravitational sliding. An exceptional example of the latter can be seen in the flysch cliff of Simonov zaliv (Simon bay) near Izola, which does not feature a pressure pocket at the head of the landslide, but a relaxed intertwining of layers that were only partially lithified at the time of sliding along the inclined seabed. Due to the importance of this phenomena, the structure is named the Kane landslide after the nearby hamlet and cape. In the Summaries and Excursions for the 4th Slovenian Geological Congress in Ankaran in 2014, the mentioned landslide was shown as an example of a thrust duplex structure (Vrabec & Rožič, 2014, 84-91).

The task of re-mapping is to take into account all these peculiarities; above all it is necessary to distinguish the zones of disordered jump of step thrust surfaces (Figs. 7B and 5/7) from the Neogene-recent zones of reverse thrust faults (Fig. 5/4).

The structural relationships in the North Istra Extrusion Wedge are sketched in profile in Figure 8. The Paleogene thrusts (Buzet Thrust, Izola Thrust, Križ Thrust, antiformally folded thrusts of the Kraški rob) and the reverse Buje Fault with its backthrusts. The left-lateral strike-slip Zambratija Fault, enveloping or envelope right-lateral strike-slip faults of the Črni Kal Anomaly, and underthrust reverse faults are also of Neogene-recent age.

Underthrusting occurs only in the north-eastern part of the profile along the underthrust reverse faults, where their hanging blocks are being uplifted. This is geomorphologically manifested

primeru narivnih dupleksov opisanega tipa. Tlačne žepe tega tipa smo opazovali v narivnih conah, medtem ko so ostale cone podrivnih reverznih prelomov v tem smislu neraziskane. Ne nastajajo pa v dupleksih, ki spremljajo pojave podvodnega singenega gravitacijskega drsenja, izjemen primer slednjega je viden v flišnem klifu Simonovega zaliva v Izoli, kjer se v čelu plazu ne nahaja tlačni žep temveč sproščeni preplet plasti, ki so bile v času polzenja po nagnjenem morskem dnu le delno strjene. Predlagamo, da ta primer poimenujemo po bližnjem zaselku in rtiču plaz Kane. V Povzetkih in ekskurzijah za 4. slovenski geološki kongres v Ankaranu leta 2014, je bil omenjeni plaz prikazan kot primer strukture narivnega dupleksa (Vrabec & Rožič, 2014, 84–91).

Naloga ponovnega kartiranja je upoštevati vse te posebnosti, predvsem je potrebno ločiti cone neurejenega preskoka stopničastih narivnih ploskev (sl. 7E in 5/7) od con neogensko-recentnih podrivnih reverznih prelomov (sl. 5/4).

Strukturni odnosi v severnoistrskem iztisnem klinu so skicirani v profilu na sliki 8. Paleogenske starosti so narivi (Buzetski, Izolski, Križni nariv, antiformno usločeni narivi Kraškega roba) in Bujski reverzni prelom s povratnimi narivi. Neogensko-recentne starosti so Zambratijski levozmični prelom, desnozmični ovojni ali envelopni prelomi črnokalske anomalije in podrivni reverzni prelomi.

Podrivanje se dogaja le v severovzhodnem delu profila ob podrivnih reverznih prelomih, ob katerih se dvigujejo njihove krovninske grude. To se geomorfološko kaže kot dviganje Kraškega roba, kar je povzročilo antiformni upogib paleogenskih narivnih ploskev. Aktualno dviganje kraškega roba dokazuje kontrolni izračun nivelmanskega vlaka preko Kraškega roba (Rižnar et al., 2007).

V profilu na sliki 8 je shematsko prikazana tudi lega desnozmičnih ovojnih prelomov. Njihov odnos do podrivnih reverznih prelomov je ambivalenten, prva opažanja so pokazala, da prevladujejo podrivne strukture z drsami po vpadu, vendar najdemo znake desnega zmikanja tudi v conah podrivnih reverznih prelomov. Domnevamo, da je v začetni fazi razvoja severnoistrskega iztisnega klina prevladovalo iztiskanje, pozneje podrivanje, verjetno pa se občasno še vedno pojavlja tudi iztiskanje.

V jugozahodnem delu profila pri kartiranju površja nismo našli neogensko-recentnih podrivnih struktur. V tem primeru je zanimiva primerjava seizmičnega profila morskega dna

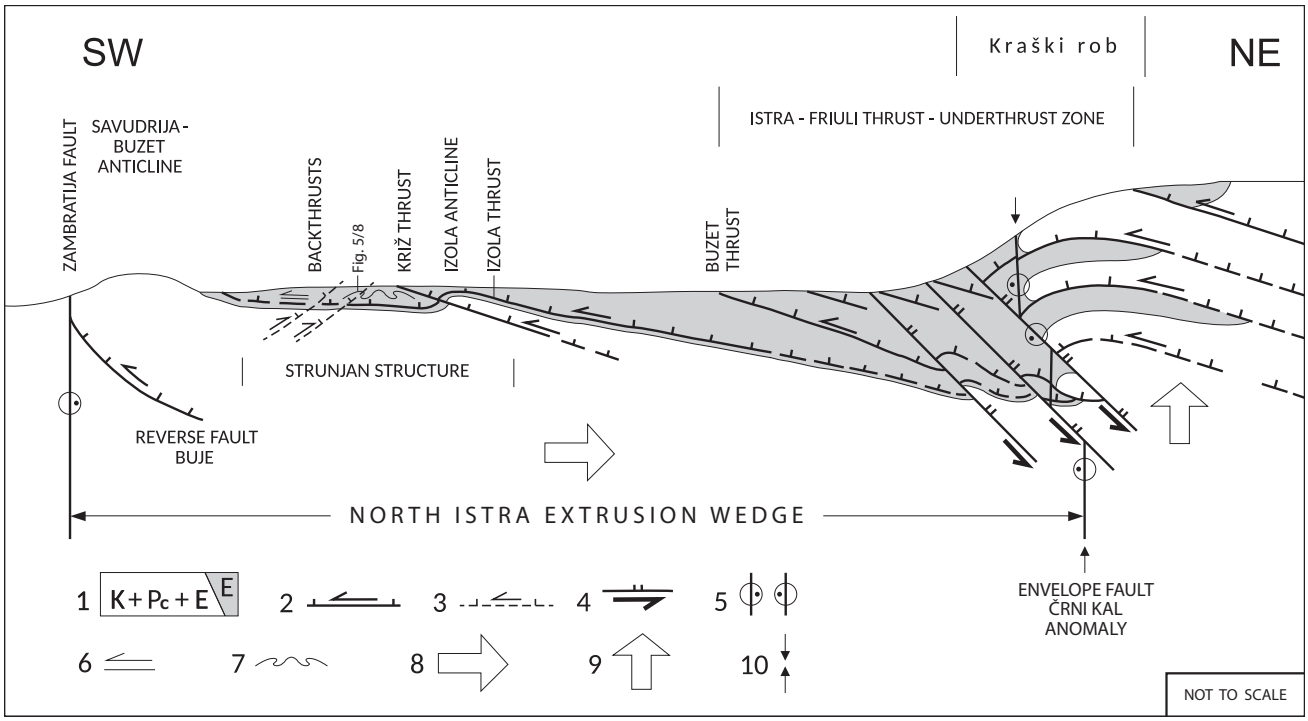

Fig. 8. Sketch of the cross-section of the North Istra Extrusion Wedge. The course of the profile in Fig. 4A. Adapted after Placer et al. (2010, Fig. 6).

Sl. 8. Skica prečnega profila severnoistrskega iztisnega klina. Potek profila na sl. 4A. Dopolnjeno po Placer et al. (2010, sl. 6).

1 K + Pc + E – Cretaceous, Paleocene and Eocene carbonates, E – Eocene flysch / K + Pc + E – kredni, paleocenski in eocenski karbonati, E – eocenski fliš

2 Paleogene reverse and thrust fault: reverse Buje Fault, Izola Thrust, Križ Thrust, Buzet Thrust / paleogenski reverzni in narivni prelom: Bujski reverzni prelom, Izolski narivni prelom, Križni narivni prelom, Buzetski narivni prelom

3 Paleogene backthrust fault / paleogenski povratni reverzni prelom

4 Neogene-recent underthrust reverse fault / neogensko-recentni podrivni reverzni prelom

5 Left strike-slip Zambratija Zone, a set of right strike-slip faults of the Črni Kal Anomaly (envelope faults) / zambratijska levozmična cona, niz desnozmičnih prelomov črnokalske anomalije (ovojni ali envelopni prelomi)

6 Area of interlayer movements in the Strunjan structure (Placer et al., 2010, Figs. 18 and 19) / območje medplastnih premikov v strunjanski strukturi (Placer et al., 2010, sl. 18 in 19)

7 Mirror folded area in the Strunjan structure / zrcalno nagubano območje v strunjanski strukturi

8 Direction of the Neogene-recent movement of the Istra block / smer neogensko-recentnega pomikanja istrskega bloka

9 Recent uplift of the Kraški rob / recentno dviganje kraškega roba

10 Sketch of the envelope faults position within the Črni Kal Anomaly / skica lege ovojnih (envelopnih) prelomov znotraj črnokalske anomalije

as the uplift of the Kraški rob, which caused the antiform bending of the Paleogene thrust surfaces. The current uplift of the Kraški rob is evidenced by the recalculation of the levelling lines across the Kraški rob (Rižnar et al., 2007).

The position of the right-lateral strike-slip envelope faults is schematically presented in profile in Figure 8. Their relationship to underthrust reverse faults is ambivalent: first observations showed that underthrust structures with slickensides along (parallel to) the bedding predominate, but evidence of dextral slip are also observed in underthrust reverse fault zones. It is assumed that extrusion was dominant in the initial phase of the North Istra Extrusion Wedge development, followed by underthrusting, but extrusion probably still occurs from time to time.

prečno na Izolsko antiklinalo (Busetti et al., 2013, sl. 3) z odsekom profila na sliki 8 med Savudrijsko-Buzetsko in Izolsko antiklinalo. Kartiranje je pokazalo, da sta poleg Izolske antiklinale vidna še medplastni nariv v prehodnem laporju antiklinale, ki smo ga poimenovali Izolski nariv in Križni nariv za katerega na kopnem ni bilo mogoče ugotoviti v kakšnem strukturnem odnosu je z Izolsko antiklinalo. Med Savudrijsko-Buzetsko antiklinalo in Križnim narivom ležijo povratni narivi, ki so spremljajoča struktura Bujskega reverznega preloma. V bloku med povratnimi narivi in Križnim narivom je fliš zrcalno simetrično naguban. V seizmičnem profilu se Izolska antiklinala nagiba proti jugozahodu, kar kaže na paleogensko čelno narivno gubo, ki je najbližja Križnemu narivu. Vendar ta

In the south-western part of the profile, no Neogene-recent underthrust structures were found during surface mapping. In this case a comparison of the seismic profile of the seabed transverse to the Izola Anticline (Busetti et al., 2013, Fig. 3) with the section of the profile in Figure 8 between the Savudrija-Buzet and Izola Anticlines is interesting. Geological mapping showed that there are also interlayer thrusts (the Izola, and the Cross Thrusts) visible in the transitional marl, in the Izola Anticline. It was not yet possible to determine their structural relationship with the Izola Anticline. Backthrusts and related structures between the Savudrija-Buzet Anticline and the Križ Thrust belong to the reverse Buje Fault. The flysch is mirror-symmetrically folded in the structural block between the backthrusts and the Križ Thrust. The Izola Anticline is tilted to the southwest in the seismic profile, indicating a Paleogene frontal thrust fold, which is closest to the Križ Thrust. The thrust fault is not visible in the seismic profile, so we assume that only a fold has developed there, which has not yet been broken by the thrust plane. Post-Paleogene reactivation is mentioned in the description of the seismic profile that only affected subvertical faults without significant impact on the structure. A fold in the flysch along the reverse underthrust indicates the symmetry of fold vergence in the Strunjan structure between the reverse thrusts and the Križ Thrust and is presented in Figure 5/8. This was formed successively: first, folds formed in the Križ Thrust footwall, then along backthrusts. Justification of the sequence of events is given in the chapter on the formation of the North Istra Extrusion Wedge and the South Istra Pushed Wedge. The Kane landslide in Simonov zaliv lies in the area of the Strunjan structure, but, as we have already mentioned, it is not a tectonic formation in origin, but rather a synsedimentary phenomenon in the flysch. The landslide slid in a direction of roughly 310°, while signs of Paleogene thrusting show a direction of some 220°.

The important question – the amount of displacement along the Paleogene thrusts, which represent the boundary of the Dinaric thrust structure – remains unanswered. While it could be relatively large, the debates regarding the structure of the Dinarides have failed to produce an acceptable solution.

Interpretation of the profile in Figure 8 represents some progress in understanding the mechanism of movement of the Microadria towards the External Dinarides, which includes thrusting and underthrusting. The progress is obvious after comparison with the Umag - Kozina profile (Placer et al., 2010, fig. 6), where the underthrusting was

v seizmičnem profilu ni viden, zato domnevamo, da se je na območju geofizikalnega profila razvila le guba, ki je narivna ploskev še ni pretrgala. V opisu seizmičnega profila je omenjena popaleogenska reaktivacija, ki pa je zajela le subvertikalne prelome brez pomembnega vpliva na zgradbo. Na sliki 5/8 je prikazana guba v flišu ob povratnem narivu, ki kaže na simetrijo vergence gub v strunjanski strukturi med povratnimi narivi in Križnim narivom. Ta je nastala zaporedoma, najprej so se razvile gube v talnini Križnega nariva, nato ob povratnih narivih. Utemeljitev zaporedja dogodkov je podana v poglavju o nastanku severnoistrskega iztisnega in južnoistrskega potisnega klina. Plaz Kane v Simonovem zalivu leži v območju strunjanske strukture, vendar, kot smo že omenili, po izvoru ni tektonska tvorba, temveč je sinsedimentarni pojav v flišu. Plaz je drsel v smeri okoli 310°, medtem ko kažejo znaki paleogenskega narivanja na smer okoli 220°.

Odprto ostaja vprašanje dolžine premika ob paleogenskih narivih, ki predstavljajo mejo dinarske narivne zgradbe. Ta bi bil lahko sorazmerno velik, vendar nam dosedanje razprave o zgradbi Dinaridov o tem še ne dajejo sprejemljivega odgovora.

Interpretacija profila na sliki 8 pomeni napredek pri razumevanju mehanizma premikanja Mikroadrije proti Zunanjim Dinaridom, ki zajema potiskanje in podrivanje. Napredek je viden po primerjavi s profilom Umag - Kozina iz leta 2010 (Placer et al., 2010, sl. 6), ko se je podrivanje obravnavalo kot reaktivacija paleogenskih narivnih ploskev v nasprotni smeri. Antiklinalno usločene paleogenske narivne ploskve ob podrivnih reverznih prelomih, ki so na sliki 4A označene z »a«, »b«, »c«, »d« in »e«, nastopajo tudi v jugovzhodnem delu istrsko-furlanske narivno-podrivne cone, npr. nad Brestom pod najvišjim vrhom Čičarije, Velikim Planikom (1272 m). V tem smislu predstavlja strukturni izziv tudi zgradba Učke, zato je potrebno ponovno strukturno obdelati celotno narivno-podrivno cono med Tržaškim in Reškim zalivom.

Narivi in prelomi znotraj severnoistrskega iztisnega klina se nadaljujejo proti severozahodu. Iz strukturne rekonstrukcije podmorja Tržaškega zaliva (Carulli, 2011, sl. 3) in geofizikalnega profila v smeri SW-NE (Busetti et al., 2012, sl. 2) je moč sklepati, da se zahodno od Savudrije os Savudrijsko-Buzetske antiklinale obrne proti severozahodu (sl. 2). O Zambratijskem prelomu ni podatkov, domnevamo pa, da spremlja Savudrijsko-Buzetsko antiklinalo v podmorju Bujski

considered as a reactivation of Paleogene thrust planes in the opposite direction. Anticlinally deformed Paleogene thrust planes next to underthrust reverse faults, shown in Figure 4A, marked with »a«, »b«, »c«, »d« and »e«, also occur in the south-eastern part of the Istra-Friuli Thrust-Underthrust Zone, e.g. above Brest under Mt. Veliki Planik (1272 m), the highest peak of Čičarija. In this sense, Mt. Učka also represents a structural challenge, so it is necessary to structurally remap the entire thrust-underthrust zone between the Gulf of Trieste and the Gulf of Rijeka.

Thrusts and faults within the North Istra Extrusion Wedge continue to the northwest. From the structural reconstruction of the Gulf of Trieste seabed (Carulli, 2011, fig. 3) and the geophysical profile in the SW-NE direction (Busetti et al., 2012, fig. 2), it can be concluded that the axis of the Savudrija-Buzet Anticline west of Savudrija turns to the northwest (Fig. 2). There is no information about the Zambratija Fault, but we assume that the reverse Buje Fault follows the Savudrija-Buzet Anticline, and Carulli (ib.) also assumed the same. The change of direction occurs also on the opposite side of the extrusion wedge. Here the SSE-NNW trending Črni Kal Anomaly (the complex shear zone between the upper Mirna and lower Glinščica/Rosandra rivers), turns due SE-NW. The Bazovica Anticline and the Lipica Syncline north-northwest of the lower Glinščica/Rosandra (Fig. 4A) have the same direction, so we believe that they probably represent the extreme structural limit of the Črni Kal Anomaly. This is also indicated by the change in the Kraški rob trend on the saddle between Mt. Mai /Maj (~ 443 m) and Mt. Monte Calvo/Globojnar (~ 442 m) above Trieste, where the Kraški rob turns from the SSE-NNW to the SE-NW direction (Fig. 4). Despite the apparently well-defined boundary on the mentioned saddle (elevation 416 m), it is quite clear that it is correct to speak only of the belt between the upper Mirna and the lower Glinščica/Rosandra, since the Črni Kal Anomaly cannot be strictly bounded.

The North-Istra Extrusion Wedge thus transits into a parallelepiped roughly between Savudrija and Trieste, which is called the Trieste parallelepiped block or the Trieste parallelepiped. It is clear that due to the parallelopiped shape, the effect of extrusion is completely absent, therefore the space between Savudrija and Trieste is also the north-western limit of the extrusion wedge (Fig. 2). The Trieste parallelepiped (A3) formally lies in the extension of the North Istra Extrusion Wedge (Ad2) and represents its south-eastern margin extrusion boundary, so it makes sense to use the term only in the discussion of block dynamics.

reverzni prelom. Podobno je domneval tudi Carulli (ib.). Sprememba smeri se dogodi tudi na nasprotni strani iztisnega klina, tu se črnolakska anomalija, oziroma kompleksna strižna cona med zgornjo Mirno in spodnjo Glinščico v smeri SSE-NNW, obrne v smer SE-NW. Severo-severozahodno od spodnje Glinščice se nahajata Bazovska antiklinala in Lipiška sinklinala (sl. 4A), ki imata enako smer, zato menimo, da verjetno predstavljata skrajno strukturno mejo črnokalske anomalije. Na to kaže tudi sprememba smeri Kraškega roba na sedlu med Majem (Mai, okoli 443 m) in Globojnarjem (Monte Calvo, okoli 442 m) nad Trstom, kjer se kraški rob iz smeri SSE-NNW obrne v smer SE-NW. Kljub na videz dokaj natančno določeni meji na omenjenem sedlu (kota 416 m), pa je povsem jasno, da je korektno govoriti le o pasu med zgornjo Mirno in spodnjo Glinščico, saj črnokalske anomalije ni mogoče ostro omejiti.

Severnoistrski iztisni klin preide torej približno med Savudrijo in Trstom v paralelepiped, ki ga imenujemo tržaški paralelepipedni blok ali tržaški paralelepiped. Jasno je, da je zaradi paralelepipedne oblike povsem izostal učinek iztiskanja, zato je prostor med Savudrijo in Trstom hkrati tudi severozahodna meja iztisnega klina (sl. 2). Tržaški paralelepiped (A_3) leži formalno v podaljšku severnoistrskega iztisnega klina (Ad_2), vendar predstavlja njegovo jugovzhodno stranico meja iztiskanja, zato je termin smiselno uporabljati le v diskusiji o dinamiki blokov.

Glede na dinamiko severnoistrskega iztisnega klina bi bilo povsem mogoče, da bi zaradi ekstenzije v jugovzhodni polovici klina in blokade nasproti tržaškemu paralelepipedu, prišlo v severozahodni polovici iztisnega klina do gubanja prečno na iztiskanje, podobno kot v tinjanskem iztisnem klinu (Placer, 2005, sl. 3), kjer so te gube lepo razvite (sl. 4A in 5/9). Tinjanski iztisni klin je miniaturni pendant severnoistrskega iztisnega klina, zato bi tudi pri slednjem pričakovali med Rokavinim prelomom in jugovzhodno mejo tržaškega paralelepipeda več gub, ali pa vsaj eno veliko. Pri kartiranju površja teh nismo odkrili.

Geofizikalne raziskave Tržaškega zaliva so pokazale, da je predplio-kvartarna (večinoma flišna) kamninska podlaga prekrita z nekaj deset do nekaj sto metri plio-kvartarnega sedimenta (Busetti et al., 2010a, 2010b; Morelli & Mosetti, 1968; Trobec et al., 2018) Relief flišne podlage v skrajnem vzhodnem delu zaliva je bil v večji meri izoblikovan med mesinijsko

Considering the dynamics of the North Istra Extrusion Wedge, it would be quite possible that due to the extension in the south-eastern half of the wedge and the blockage opposite the Trieste parallelepiped, folding transverse to the extrusion would occur in the north-western half of the extrusion wedge, much like the Tinjan Extrusion Wedge (Placer, 2005, Fig. 3), where these folds are well developed (Figs. 4A and Fig. 5/9). The Tinjan Extrusion Wedge is a miniature pendant of the North Istra Extrusion Wedge, so we would expect several folds, or at least one large one between the Rokava fault and the south-eastern Trieste parallelepiped boundary, but these were not detected at surface mapping.

Geophysical surveys of the Gulf of Trieste have shown that the Pre-Plio-Quaternary bedrock (mostly flysch) is covered by tens to several hundred meters of Plio-Quaternary sediment (Busetti et al., 2010a, 2010b; Morelli and Mosetti, 1968; Trobec et al., 2018). The relief of the flysch substrate in the easternmost part of the bay was formed to a great extent during the Messinian erosion phase and to a lesser extent during a shorter Pliocene erosion episode (Busetti et al., 2010a, 2010b). The complex formation of the relief indicates that the surface currents during periods of erosion generally flowed westward (Morelli and Mosetti, 1968), which is comparable to the direction of the present-day river network in the extreme north-western part of Istra (i.e. Dragonja, Rižana, Glinščica/Rosandra, etc.). The youngest Late Pleistocene sedimentary sequences, deposited just before the last transgression in the eastern and central part of the area of the present-day Gulf of Trieste, show the general direction of the water currents towards the south, with one channel even running roughly parallel to the present-day coastline of the eastern part of the Gulf of Trieste (Novak et al., 2020; Ronchi et al., 2023; Trobec et al., 2017). It is very difficult to compare Late Quaternary river networks with river networks on flysch due to the far younger geomorphology, where sedimentation plays a greater role in shaping the surface compared to erosion. The shape of the river network in the Late Pleistocene was largely influenced by the topography of the time (Ronchi et al., 2023), since in the area of the present-day Gulf of Trieste, the terrain rose to the northwest (Trobec et al., 2018) due to the Soča megafan from the last glacial maximum (Fontana et al., 2014, 2010, 2008), which also covers the south-eastern part of the Gulf of Trieste. Possible transverse folding in the south-eastern part of the Gulf of Trieste could therefore only be determined from the structural map of the contact between carbonates and flysch.

erozijsko fazo ter deloma med krajšo pliocensko erozijsko epizodo (Busetti et al., 2010a, 2010b) Kompleksna izoblikovanost reliefa nakazuje, da so površinski tokovi v obdobjih erozije v splošnem tekli proti zahodu (Morelli & Mosetti, 1968), kar je primerljivo s smerjo današnje rečne mreže v skrajnem severozahodnem delu Istre (i.e. Dragonja, Rižana, Glinščica, itd.). Najmlajša poznopleistocenska sedimentna zaporedja, ki so se odložila tik pred zadnjo transgresijo na vzhodnem in osrednjem delu današnjega območja Tržaškega zaliva, pa kažejo generalno smer vodotokov proti jugu, pri čemer je en kanal tekel celo približno vzporedno z današnjo obalno črto vzhodnega dela Tržaškega zaliva (Novak et al., 2020; Ronchi et al. 2023; Trobec et al., 2017). Poznokvartarne rečne mreže zelo težko primerjamo z rečno mrežo na flišu, saj gre za precej mlajšo geomorfologijo, kjer ima sedimentacija večjo vlogo pri izoblikovanju površja v primerjavi z erozijo. Na obliko rečne mreže v poznem pleistocenu je v večji meri vplivala takratna paleotopografija (Ronchi et al., 2023), saj se je na območju današnjega Tržaškega zaliva teren dvigal proti severozahodu (Trobec et al., 2018) zaradi Sočine megapahljače iz zadnjega glacialnega viška (Fontana et al., 2014, 2010, 2008), ki prekriva tudi jugovzhodni del Tržaškega zaliva. Morebitno prečno gubanje v jugovzhodnem delu Tržaškega zaliva, bi bilo torej mogoče ugotoviti le iz strukturne karte stika med karbonati in flišem. To je sicer objavil Carulli (2011, sl. 3), vendar je njegov izdelek pregleden, zato ga ni mogoče uporabiti v ta namen.

Prečnodinarska cona povečane kompresije v zaledju črnokalske anomalije

V tem poglavju so opisane deformacije, ki so v istrskem potisnem območju nastale zaradi dinamike severnoistrskega iztisnega klina. Tu je med črnokalsko anomalijo, ki je prostorsko blizu Kraškemu robu in Hrušico nastala cona povečane kompresije, ki v celoti prečka Zunanjedinarski naluskani pas in sega še v čelni del Zunanjedinarskega narivnega pasu. Zaradi njune specifične zgradbe in zaradi nasledstvenega značaja novih deformacij, so te v vsaki enoti opisane posebej. Samostojno poglavje je namenjeno Raškemu prelomu, ker je v njegovi prelomni coni povečana kompresija povzročila nastanek transpresivne antiklinale, ki se je iz kraške uravnave dvignila kot Vremščica (1027 m).

This was published by Carulli (2011, Fig. 3), but as his work represents a review article it cannot be used for this purpose.

Transverse Dinaric zone of increased compression in the hinterland of the Črni Kal Anomaly

This chapter describes the deformations that occurred in the Istra Pushed Area due to the North Istra Extrusion Wedge dynamics. Here, between the Črni Kal Anomaly, which is close to the Kraški rob, and Mt. Hrušica a zone of increased compression has formed, which crosses the entire External Dinaric Imbricated Belt and extends into the frontal part of the External Dinaric Thrust Belt. Due to their specific structure and due to the hereditary nature of the new deformations, they are described separately in each unit. A separate chapter is devoted to the Raša Fault, because the increased compression of its fault zone caused the formation of a transpressive anticline, which rose from the karstic levelled terrain as Mt. Vremščica (1027 m).

External Dinaric Imbricated Belt

The External Dinaric Imbricated Belt in the territory under consideration is bounded by the Istra-Friuli Thrust-Underthrust Zone and the External Dinaric Thrust Belt boundary. (Fig. 1). The term »imbricated belt« is inappropriate for this part of the Dinarides because it doesn't consist of imbricates (horses) but of folds. Nevertheless, the term is acceptable because horses characterize the rest of this belt in the External Dinarides. The Istra hinterland is made up of large, folded units, the Trieste-Komen and Čičarija Anticlinoria and the Vipava and Brkini Synclinorium. There is also slightly smaller Ravnik Anticlinorium.

All of the listed units represent an example of complete (ideal) folding and are spatially displaced across compartments (Placer, 2005, Fig. 2), which means that equivalent folded structures do not lie in consecutive compartments but skip across the width of the compartment. The Vipava Synclinorium continues in its direction into the Ravnik Anticlinorium, the Trieste-Komen Anticlinorium into the Brkini Synclinorium, and the Čičarija Anticlinorium is exposed and does not transit into the synclinorium. In theory, complete folding is expressed in sets of linear folds displaced for a compartment (a set width). It usually covers larger homogeneously constructed areas, but there are only two folded sets with a frontal anticlinorium and a rear synclinorium that are being displaced (offset). The term frontal refers to the thrust structure of the Dinarides: the Trieste-Komen frontal Anticlinorium

Zunanjedinarski naluskani pas

Zunanjedinarski naluskani pas je na obravnavanem ozemlju omejen z istrsko-furlansko narivno-podrivno cono in mejo Zunanjedinarskega narivnega pasu (sl. 1). Termin »naluskani pas« je za ta del Dinaridov neustrezen, ker ga ne sestavljajo luske temveč gube, vendar je kljub temu sprejemljiv, ker so luske značilne za preostali del tega pasu v Zunanjih Dinaridih. Zaledje Istre je zgrajeno iz velikih nagubanih enot, Tržaško-Komenskega in Čičarijskega antiklinorija ter Vipavskega in Brkinskega sinklinorija. Tu je še Ravniški antiklinorij, ki je nekoliko manjši.

Vse naštete enote predstavljajo primer popolnega gubanja in so prostorsko zamaknjene po predalih (Placer, 2005, sl. 2), kar pomeni, da ekvivalentne nagubane strukture ne ležijo v zaporednih predalih, temveč preskakujejo za širino predala. Vipavski sinklinorij se po smeri nadaljuje v Ravniški antiklinorij, Tržaško-Komenski antiklinorij v Brkinski sinklinorij, Čičarijski antiklinorij pa je izpostavljen in se ne izteka v sinklinorij. V teoriji se popolno gubanje izraža v linearnih in predalčno zamaknjenih gubah in običajno zajema obsežnejša homogeno zgrajena območja, tu pa gre za specifičen primer, kjer obstojata le dva nagubana niza s čelnim antiklinorijem in začelnim sinklinorijem, ki sta zamaknjena. Termin čelni se nanaša na narivno zgradbo Dinaridov, Tržaško-Komenski čelni antiklinorij se previje v začelni Vipavski sinklinorij, Čičarijski čelni antiklinorij se previje v začelni Brkinski sinklinorij, ta pa v Ravniški antiklinorij (sl. 9A).

Predalčna nagubana zgradba ima določene zakonitosti, ki so zastopane tudi v našem primeru, pomembne so tri: 1. prehod antiklinale (antiklinorija) v sinklinalo (sinklinorij) in obratno, po smeri, se dogodi s cepljenjem gub, 2. v pravilni predalčni nagubani zgradbi se gube cepijo v prečno ležeči coni, imenovani cona cepljenja gub (sl. 9A in 9B), 3. ekvivalentne strukture v predalčno nagubani zgradbi se povezujejo z navzkrižnimi povezovalnimi gubami (nov termin), ki imajo usločeno os (undacija). Predalčno zamaknjeni antiklinali povezuje prečna antiklinala s konkavno usločeno osjo, sinklinali povezuje sinklinala s konveksno usločeno osjo (sl. 9C). Cona cepljenja gub je nasproti predalčnim gubam manj deformabilna (sl. 9D).

Vzrok za nastanek predalčne nagubane zgradbe v Zunanjedinarskem naluskanem pasu tiči v zgradbi in dinamiki Zunanjedinarskega narivnega pasu. Prečnodinarska cona cepljenja gub se namreč nahaja v podaljšku stika Snežniškega in Hrušiškega pokrova proti

folds into the rear Vipava Synclinorium, and the Čičarija frontal Anticlinorium folds into the rear Brkini Synclinorium, which in turn folds into the Ravnik Anticlinorium (Fig. 9A).

The compartment-like folded structure has certain regularities (rules), which are also presented in our case, of which three are important: 1. the transition of an anticline (anticlinorium) to a syncline (synclinorium) and vice versa, according to direction, occurs by the splitting of folds. 2. in the correct crosswise-connecting folds, the folds are split in a transverse zone called the folds splitting zone (Figs. 9A and 9B). 3. equivalent structures in the crosswise-connecting folds are connected by crosswise-connecting folds (new term), which have a folded (buckled) axis (undation). The anticlines displaced by a compartment connect transverse anticlines with a concave folded axis, while synclines connect a syncline with a convex folded axis (Fig. 9C). The splitting folds zone is less deformable compared to the longitudinal folds (Fig. 9D).

The cause of the formation of the compartment-like folded structure in the External Dinaric Imbricated Belt lies in the structure and dynamics of the External Dinaric Thrust Belt. The Transverse Dinaric folds splitting zone is located in the extension of the contact between the Snežnik and Hrušica Nappes towards the southwest in the direction of thrusting. There is no similar phenomenon in the extension of the contact between the Hrušica and Trnovo Nappes, which could mean two things: that the position of the Transverse Dinaric folds splitting zone is accidental, or that the Hrušica Nappe extends far to the northwest under the Trnovo Nappe, and both nappes act together as a single unit. In contrast, the Snežnk Nappe under the Hrušica Nappe is expected to pinch out over a relatively short distance. That such an explanation is possible is shown by the hydrological connection between the Vipava River spring in the Hrušica Nappe and the sinks east of the Postojna basin in the Snežnik Nappe (Petrič et al., 2020). The Trnovo and Hrušica Nappes are older than the Snežnik

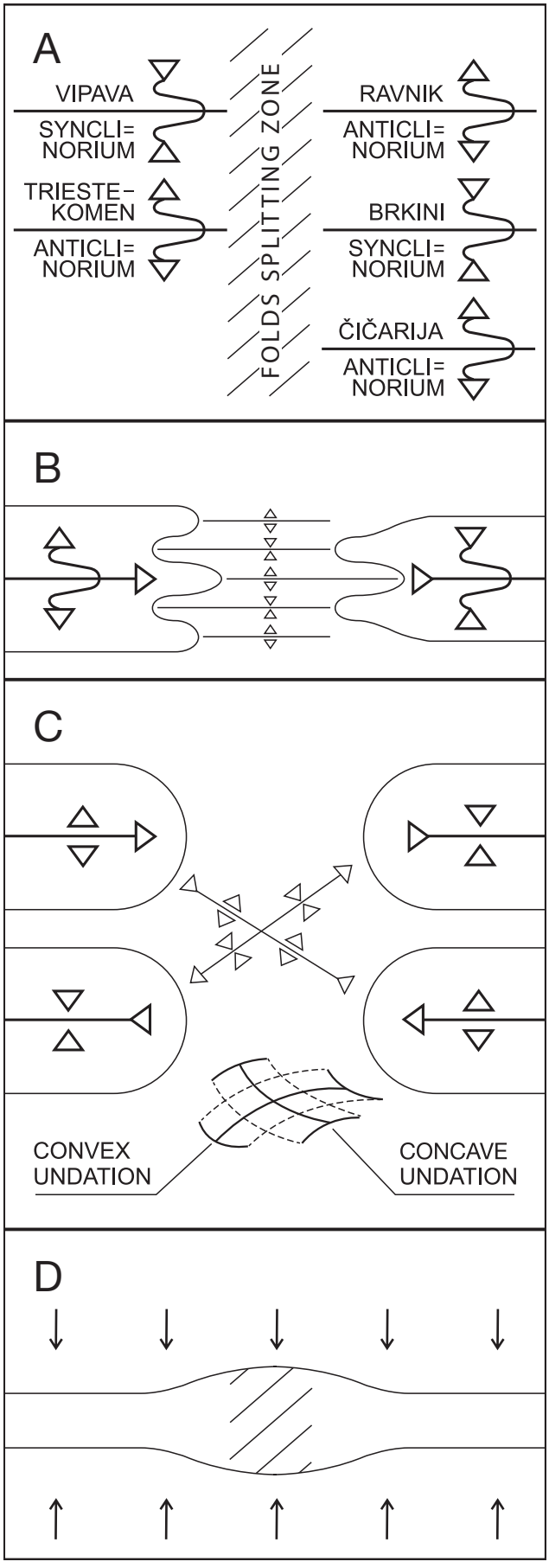

Fig. 9. Compartment-like folded structure, folds splitting and crosswise connecting folds: A. Structural sketch of the compartment-like folded territory of the External Dinaric Imbricated Belt. B. Folds splitting. C. Crosswise connecting folds: concavely bent anticline axis, convexly bent syncline axis; D. Reduced compressibility of the Senožeče Folds Splitting Zone.

Sl. 9. Predalčna nagubana zgradba, cepljenje gub in navzkrižno-povezovalne gube: A. Strukturna skica predalčno nagubanega ozemlja Zunanjedinarskega naluskanega pasu. B. Cepljenje gub. C. Navzkrižno-povezovalne gube: konkavno usločena os antiklinale, konveksno usločena os sinklinale; D. Zmanjšana stisljivost senožeške cone cepljenja gub.

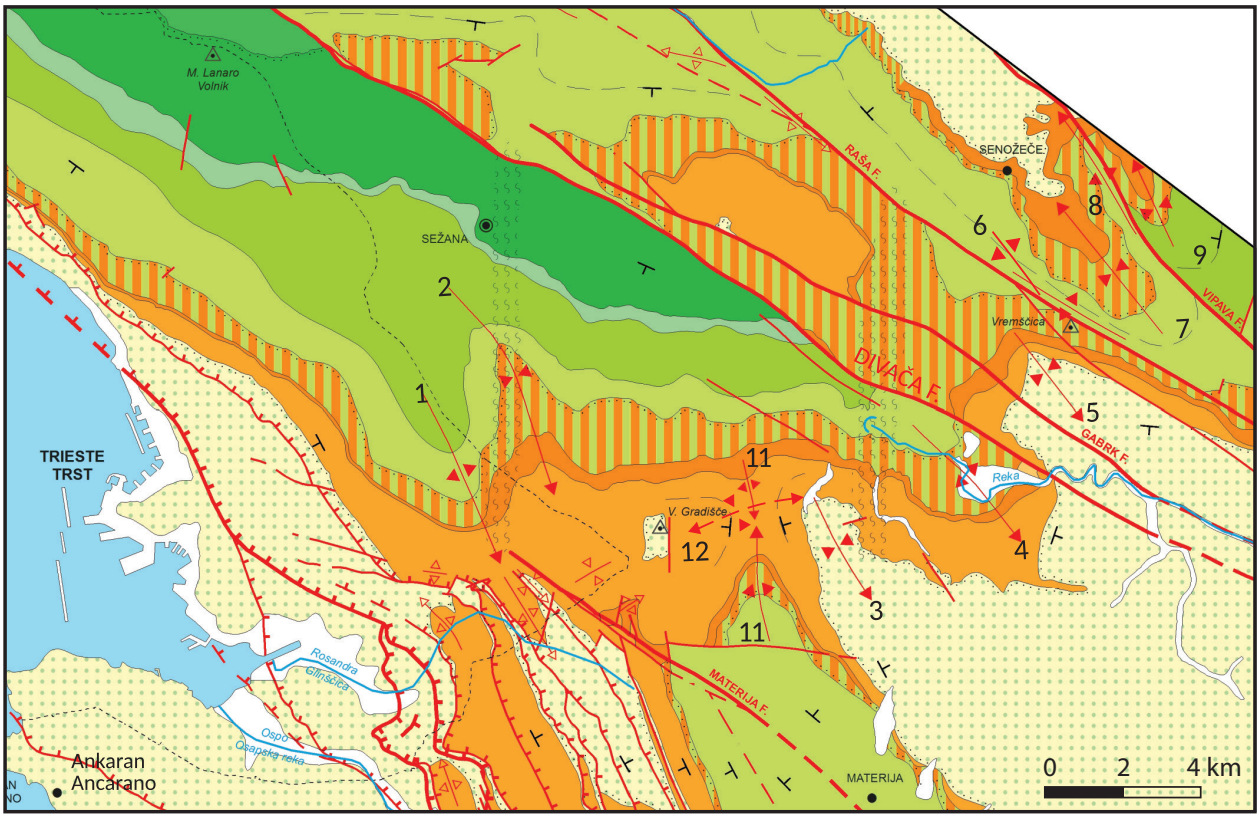

STRATIGRAPHIC CHART after / STRATIGRAFSKA TABELA po: Jurkovšek, B. et al. 2013

AGE STAROST			FORMATION FORMACIJA		MAP KARTA
QUATERNARY KVARTAR			KV		
TERTIARY - TERCIAR	PALEOGENE PALEOGEN	EOCENE EOCEN	F	PP	
			ANA		
		PALEOCENE PALEOCEN	TF	TF2	KRAS GROUP KRAŠKA GRUPA
				TF1	
			LIB		
CRETACEOUS - KREDA	UPPER CRETACEOUS ZGORNJA KREDA	MAASTRICHTIAN MAASTRICHTIJ			
		CAMPANIAN CAMPANIJ	LF		
		SANTONIAN SANTONIJ			
		CONIACIAN CONIACIJ	SF		
		TURONIAN TURONIJ	RF		
		CENOMANIAN CENOMANIJ	PF		
	LOWER CRETACEOUS SPODNJA KREDA	ALBIAN ALBIJ			
		APTIAN APTIJ	BF		
		VALANGINIAN VALANGINIJ			

DESCRIPTION OF FORMATIONS after / OPIS FORMACIJ po: Jurkovšek, B. 2008

KV: Quaternary deposit
Kvartarni nanos

F: FLYSCH. Alternation of marlstone, sandstone, breccia and conglomerate. Calcarenite intercalations and olistostromes. In the basis Transitional Beds (PP): breccia and basal marl
FLIŠ. Menjavanje laporovca, peščenjaka, breče in konglomerata. Vložki kalkarenita in olistostrome. V podlagi prehodne plasti (PP): breča in bazalni lapor

ANA: ALVEOLINID-NUMMULITID LIMESTONE. Bedded and massive limestone
ALVEOLINSKO-NUMULITNI APNENEC. Plastnati in masivni apnenec

TF: TRSTELJ FORMATION. Upper Trstelj Beds (TF2): Bedded calcarenite with foraminifers. Lower Trstelj Beds (TF1): Bedded, mainly miliolid limestone
TRSTELJSKA FORMACIJA. Zgornje trsteljske plasti (TF2): Plastnati kalkarenit s foraminiferami. Spodnje trsteljske plasti (TF1): Plastnati, pretežno miliolidni apnenec

LIB: LIBURNIA FORMATION. Bedded limestone, marly limestone and limestone breccia
LIBURNIJSKA FORMACIJA. Plastnati apnenec, laporasti apnenec in apnenčeva breča

LF: LIPICA FORMATION. Bedded and massive limestone with rudist biostromes and bioherms. Intercalations of platy and laminated Tomaj Limestone with chert
LIPIŠKA FORMACIJA. Plastnati in masivni apnenec z rudistnimi biostromami in biohermami. Vmes ploščasti in laminirani tomajski apnenec z rožencem

SF: SEŽANA FORMATION. Bedded limestone with rare rudist biostromes. Intercalations of bedded Pliskovica Limestone with chert and with pelagic microfossils and platy laminated Komen Limestone with chert. In the basis bedded limestone with oncoids and desiccation pores and thickly bedded to massive limestone with large amount of rudists
SEŽANSKA FORMACIJA. Plastnati apnenec z redkimi rudistnimi biostromami. Vmes plastnati pliskovški apnenec z rožencem in pelagičnimi mikrofosil ter ploščasti in laminirani komenski apnenec z rožencem. V podlagi plastnati apnenec z onkoidi in izsušitvenimi porami ter debeloplastnati do masivni apnenec z veliko količino rudistov

RF: REPEN FORMATION. Bedded limestone with chert and pelagic microfossils. Intercalations of platy and laminated Komen Limestone with chert and pelagic microfossils. In the basis massive, partly recrystallized Kopriva Limestone with displaced, locally broken and rounded rudist shells
REPENSKA FORMACIJA. Plastnati apnenec z rožencem in pelagičnimi mikrofosili. Vmes ploščasti in laminirani komenski apnenec z rožencem in pelagičnimi mikrofosili. V podlagi masivni in delno rekristalizirani koprivski apnenec s premeščenimi, mestoma zdrobljenimi in zaobljenimi lupinami rudistov

PF: POVIR FORMATION. Bedded, locally platy limestone with thicker dolomite intercalations and with rare intercalations of dolomitic breccia and limestone breccia. In upper part platy and laminated Komen Limestone with chert. In the basis emergence breccia
POVIRSKA FORMACIJA. Plastnati, lokalno ploščasti apnenec z debelejšimi vložki dolomita in redkimi vložki dolomitne breče ter apnenčeve breče. V zgornjem delu ploščasti in laminirani komenski apnenec z rožencem. V podlagi emerzijska breča

BF: BRJE FORMATION. Bedded limestone and dolomite with intercalations of dolomitic breccia and limestone breccia
BRSKA FORMACIJA. Plastnati apnenec in dolomit z vložki dolomitne in apnenčeve breče

Fig. 10. Structural-geological map of the Senožeče Folds Splitting Zone. Updated after Jurkovšek et al. (1996; 2008; 2013) and Placer (2015). The updates do not interfere with the thrust structure. *The key for the naming of the folds in Fig. 11.*

Sl. 10. Strukturno-geološka karta senožeške cone cepljenja gub. Dopolnjeno po Jurkovšek et al. (1996, 2008, 2013) in Placer (2015). Dopolnitve ne posegajo v narivno zgradbo. *Legenda poimenovanja gub na sl. 11.*

Nappe; this corresponds to the spatial lag between the Trieste-Komen and the Čičarija Anticlinoria, as well as a temporal lag, since in the nappe structure the younger units are formed below the older ones. In the Glinščica/Rosandra area, where the Trieste-Komen and Čičarija Anticlinoria meet, the thrust structures of the latter lie below the thrust structures of the former.

The area of the described splitting of folds is shown on a simplified structural map of the considered territory (Fig. 10), from where it is transferred to the digital model of the relief in Figure 11. Based on previous research, we conclude (OGK, sheets: Gorica, Postojna, Ilirska Bistrica; Jurkovšek et al., 1996; Placer, 2015) that there are three major folds on the south-eastern margin of the Trieste-Komen Anticlinorium, which are also part of the north-western margin of the Brkini Synclinorium. For the sake of easier discussion, we have now named them. In Figures 10 and 11 they are marked with numbers, the Artviže (3) and Gornje Ležeče Synclines (5), and the Famlje Anticline (4). Senožeče (7) and Laže Syncline (9), and Jelenje (8) and Razdrto Anticline (10) are clearly visible at the junction of the Vipava Synclinorium and the Ravnik Anticlinorium. The latter is presented only in Figure 11. Between the Gornje Ležeče and Senožeče Synclines, there is an anticline that also belonged to this group of split folds; however, it lies in the wider zone of the Raša Fault and is therefore strongly deformed. In Figures 10 and 11 it is only symbolically presented and named after the Vremščica Paleo-Vremščica Anticline (6).

jugozahodu v smeri narivanja. V podaljšku stika Hrušiškega in Trnovskega pokrova ni podobnega pojava, kar bi lahko pomenilo dvoje, da je lega prečnodinarske cone cepljenja gub slučajna, ali pa, da se Hrušiški pokrov razteza pod Trnovskim pokrovom še daleč proti severozahodu in delujeta obe krovni enoti skupaj kot enotna narivna gruda. V nasprotju s tem pa naj bi se Snežniški pokrov pod Hrušiškim kmalu izklinil. Da je taka razlaga mogoča, kaže hidrološka povezava med izvirom reke Vipave v Hrušiškem pokrovu in ponori vzhodno od Postojnske kotline v Snežniškem pokrovu (Petrič et al., 2020). Trnovski in Hrušiški pokrov sta starejša od Snežniškega; to ustreza prostorskemu zamiku med Tržaško-Komenskim in Čičarijskim antiklinorijem, pa tudi časovnemu zamiku, saj v krovni zgradbi mlajše enote nastajajo pod starejšimi. Na območju Glinščice, kjer se stikata Tržaško-Komenski in Čičarijski antiklinorij, narivne strukture slednjega ležijo pod narivnimi strukturami prvega.

Območje opisanega cepljenja gub je prikazano na poenostavljeni strukturni karti obravnavanega ozemlja (sl. 10), od koder je preneseno na digitalni model reliefa na sliki 11. Po dosedanjih raziskavah povzemamo (OGK, listi: Gorica, Postojna, Ilirska Bistrica; Jurkovšek et al., 1996; Placer, 2015), da nastopajo na jugovzhodnem obrobju Tržaško-Komenskega antiklinorija tri večje gube, ki so hkrati tudi del severozahodnega obrobja Brkinskega sinklinorija. Zaradi lažjega pogovora smo jih zdaj poimenovali, na

Fig. 11. Geomorphology of the Senožeče Folds Splitting Zone.

Sl. 11. Geomorfologija senožeške cone cepljenja gub.

1 External Dinaric Thrust Belt boundary, nappe boundary, nappe unit (T – Trnovo Nappe, H – Hrušica Nappe, S – Snežnik Nappe) / meja Zunanjedinarskega narivnega pasu, meja pokrova, pokrov (T – Trnovski pokrov, H – Hrušiški pokrov, S – Snežniški pokrov)

2 Istra-Friuli Thrust-Underthrust Zone / istrsko-furlanska narivno-podrivna cona

3 Črni Kal Anomaly / črnokalska anomalija

4 Two folds in the Črni Kal Anomaly influence zone: 1 – Bazovica Anticline, 2 – Lipica Syncline / gubi v vplivnem območju črnokalske anomalije: 1 – Bazovska antiklinala, 2 – Lipiška sinklinala

5 Subvertical NW striking faults (»Dinaric trend«) with a predominant shear offset component: IF – Idrija Fault, PF – Belsko Fault, RF – Raša Fault / subvertikalni prelomi dinarske smeri s pretežno zmično komponento premika: IF – Idrijski prelom, BF – Belski prelom, RF – Raški prelom

6 Compartment-like folded area: a – Čičarija Anticlinorium, b – Trieste-Komen Anticlinorium, c – Ravnik Anticlinorium, d – Brkini Synclinorium, e – Vipava Synclinorium / predalčno nagubano ozemlje: a – Čičarijski antiklinorij, b – Tržaško-Komenski antiklinorij, c – Ravniški antiklinorij, d – Brkinski sinklinorij, e – Vipavski sinklinorij

7 Splitting folds: 3 – Artviže Syncline, 4 – Famlje Anticline, 5 – Gornje Ležeče Syncline, 6 – Paleo-Vremščica Anticline, 7 – Senožeče Syncline, 8 – Jelenje Anticline, 9 – Laže Syncline, 10 – Razdrto Anticline / cepilne gube: 3 – Artviška sinklinala, 4 – Fameljska antiklinala, 5 – Gornjeležeška sinklinala, 6 – Paleovremška antiklinala, 7 – Senožeška sinklinala, 8 – Jelenja antiklinala, 9 – Laženska sinklinala, 10 – Razdrška antiklinala

8 Cross-connecting folds: 11 – Rodik-Preloka Anticline, 12 – Pared Syncline / navzkrižno-povezovalne gube: 11 – Rodiško-Preloška antiklinala, 12 – Paredska sinklinala

9 Undation of the nappe units: I – Nanos-Čaven antiform, II – Hrušica-Trnovo synform / undacija krovnih enot: I – nanoško-čavenska antiforma, II – hrušiško-trnovska sinforma

10 Sistiana Flexural Zone / sesljanska upogibna cona

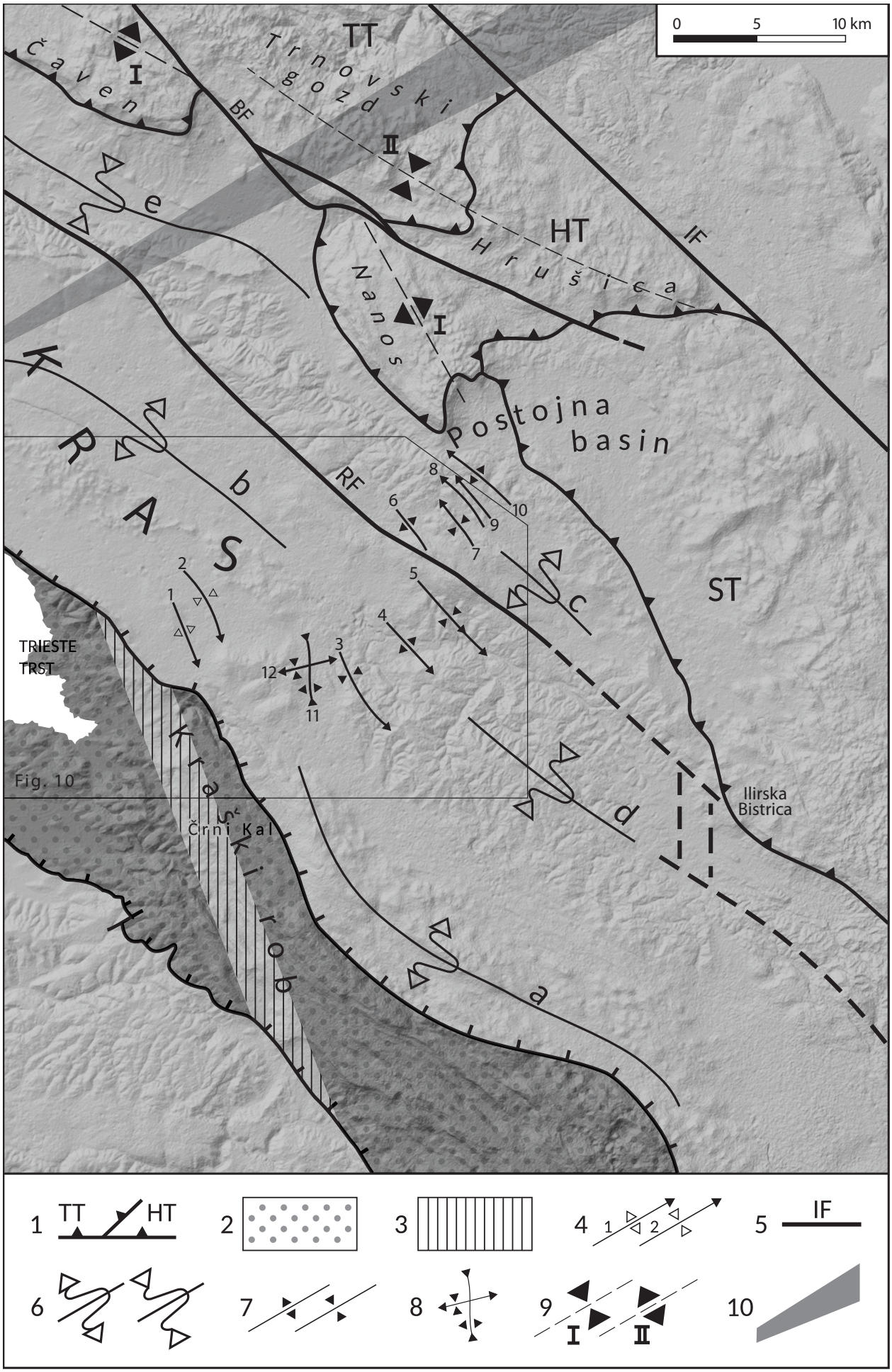
0 5 10 km
TT
Trnovski gozd
Čaven
I
II
BF
HT
Hrušica
IF
Nanos
I
Postojna basin
KRAS
RF
8
6
9
10
7
2
1
5
4
3
12
11
ST
TRIESTE
TRST
Fig. 10
Kraški rob
Črni Kal
Ilirska Bistrica
a
b
c
d
e
1 TT HT
2
3
4 1 2
5 IF
6
7
8
9 I II
10

The considered folds splitting zone is several kilometres wide and lies transversely in the direction of the Dinaric fold axes. It is named after the village of Senožeče – the Senožeče Folds Splitting Zone.

The cross-connecting folds are partially preserved between the Trieste-Komen and Čičarija Anticlinoria, and the Brkini Synclinorium and the flysch depression in front of the Trieste-Komen Anticlinorium. They can be seen in the junction between the Rodik and Preloka Anticlines, named the Rodik-Preloka Anticline (11), which has a concave folded axis, and a convexly folded syncline lying transversely to it, which runs between the Brkini Synclinorium and the depression in front of the Trieste-Komen Anticlinorium. We named it the Pared Syncline (12). The degree of curvature of the axes of cross-connecting folds is weak, so in some places they are not mapped at all. Between the Trieste-Komen and Ravnik Anticlinoria and the Vipava and Brkini Synclinoria the cross-connecting folds are deformed along the Raša Fault.

As was already noted, the Lipica Syncline (2) and the Bazovica Anticline (1) on the margin of the Trieste-Komen Anticlinorium do not belong to the theoretical model of the Senožeče Folds Splitting Zone. This assumption is also confirmed by the general structural setting, since there are no folds connecting the lagged Trieste-Komen and Čičarija Anticlinoria southwest of the cross-connecting Rodik-Preloka Anticline (11) and Pared Syncline (12). The formation of the two mentioned folds (1 and 2) is related to the Črni Kal Anomaly, presumably with the antiformly bent Paleogene thrust surface in Glinščica/Rosandra area (Fig. 4A, area »a«).

Deformations that cannot be related to folds splitting but rather to an increased compression northeast of the Črni Kal Anomaly occur in the Senožeče Folds Splitting Zone. The connection to the increased compression is obvious, as the general structures of the south-western part of the Senožeče Folds Splitting Zone run parallel to the Črni Kal Anomaly (Fig. 11), which applies to the extreme north-western part of the Čičarija Anticlinorium and the Artviže Syncline (3) in the Brkini Synclinorium and also for the Lipica Syncline (2) and Bazovica Anticline (1). The cross-connecting folds of the Rodik-Preloka Anticline (11) and the Pared Syncline (12) also have a modified position. We will not discuss the kinematic mechanism of the adjustment of the mentioned structures in the direction of the Črni Kal Anomaly herein, but it would certainly be necessary to conduct some

slikah 10 in 11 so označene s številkami, tu ležijo Artviška (3) in Gornjeležeška sinklinala (5) ter Fameljska antiklinala (4). Na stiku Vipavskega sinklinorija in Ravniškega antiklinorija so lepo vidne Senožeška (7) in Laženska sinklinala (9) ter Jelenja (8) in Razdrška antiklinala (10). Slednja je vidna le na sliki 11. Med Gornjeležeško in Senožeško sinklinalo je obstajala antiklinala, ki je tudi pripadala tej skupini cepilnih gub, vendar leži v širši coni Raškega preloma in je zaradi tega močno deformirana. Na sliki 11 je le simbolno zabeležena in poimenovana po Vremščici Paleovremška antiklinala (6) (Paleovremščica anticline). Izognili smo se izrazu Paleovremščiška, ker je neroden, izraz paleoantiklinala Vremščice pa bi odstopal od pridevniške rabe za ostale gube, ki je prijaznejša do slovenščine.

Obravnavana cona cepljenja gub je široka nekaj kilometrov in leži prečno na osi gubanja Dinaridov. Imenujemo jo senožeška cona cepljenja gub.

Navzkrižno-povezovalne gube so delno ohranjene med Tržaško-Komenskim in Čičarijskim antiklinorijem ter Brkinskim sinklinorijem in flišno udorino pred Tržaško-Komenskim antiklinorijem. Vidimo jih v povezavi med Rodiško in Preloško antiklinalo, poimenovano Rodiško-Preloška antiklinala (11), ki ima konkavno usločeno os in prečno nanjo ležečo konveksno usločeno sinklinalo, ki poteka med Brkinskim sinklinorijem in udorino pred Tržaško-Komenskim antiklinorijem. Poimenovali smo jo Paredska sinklinala (12). Stopnja ukrivljenosti osi navzkrižno-povezovalnih gub je šibka, zato ponekod sploh niso kartirane. Med Tržaško-Komenskim in Ravniškim antiklinorijem ter Vipavskim in Brkinskim sinklinorijem sta navzkrižno-povezovalni gubi deformirani ob Raškem prelomu.

Kot je bilo že rečeno, Lipiška sinklinala (2) in Bazovska antiklinala (1) na robu Tržaško-Komenskega antiklinorija, ne sodita v teoretski model senožeške cone cepljenja gub. To predpostavko potrjujejo tudi splošne razmere, saj jugozahodno od navzkrižno-povezovalnih Rodiško-Preloške antiklinale (11) in Paredske sinklinale (12) ni gub, ki bi povezovale zamaknjena Tržaško-Komenski in Čičarijski antiklinorij. Nastanek obeh omenjenih gub (1 in 2) je povezan s črnokalsko anomalijo, domnevno z antiformno usločitvijo paleogenske narivne ploskve v Glinščici (sl. 4A, območje »a«).

V senožeški coni cepljenja gub nastopajo deformacije, ki jih ne moremo povezovati s cepljenjem temveč s povečano kompresijo severovzhodno od

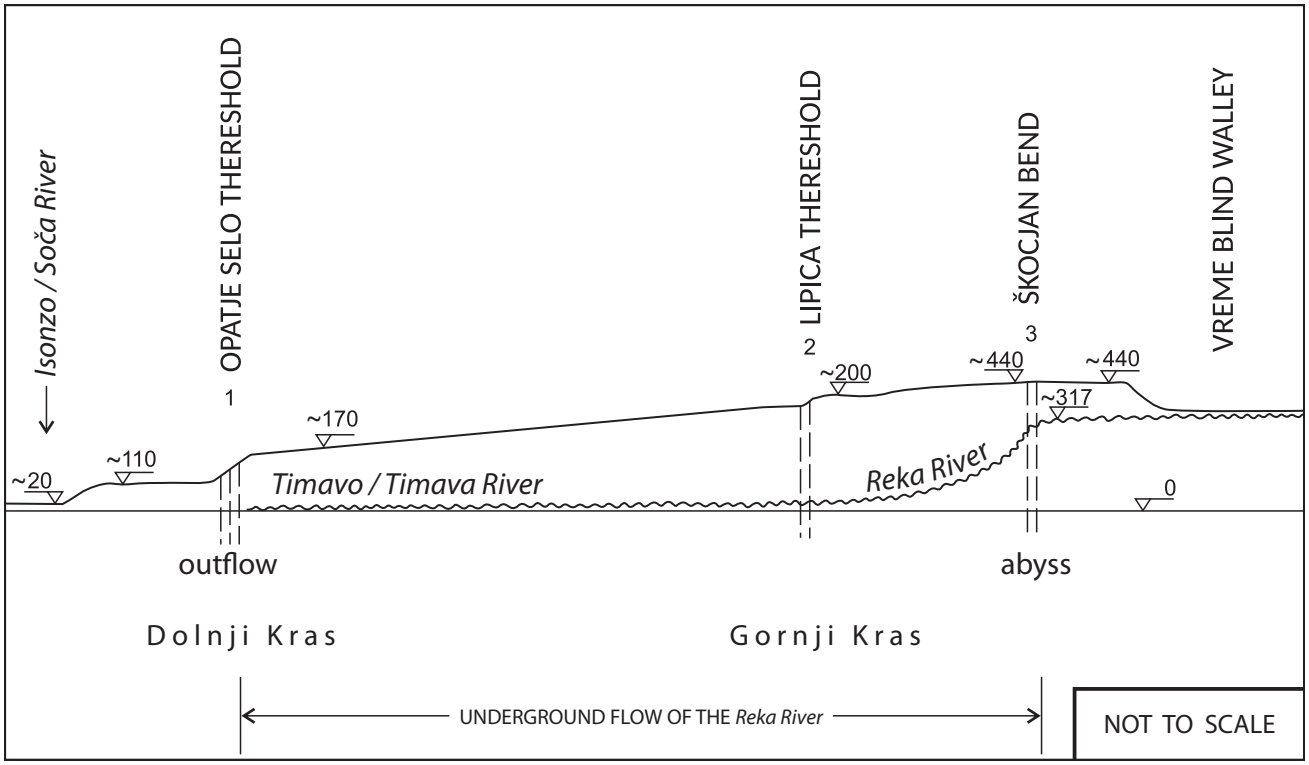

Fig. 12. Sketch of the longitudinal geomorphological cross section of Kras region. Position of the profile in Fig. 2.
Sl. 12. Skica vzdolžnega geomorfološkega profila Krasa. Lega profila na sl. 2.

detailed structural research before answering this question.

The effect of locally increased compression in the Dinaric hinterland of the Črni Kal Anomaly is also reflected in the longitudinal geomorphological profile of the Kras region (Fig. 12). Initially, the original peneplanation of the Trieste-Komen Plateau was sub-horizontal, whereas today it is inclined. From the Doberdob Plateau on the Spodnji Kras at an elevation of about 110 m, it gradually rises towards Gornji Kras to about 440 m on the Divača Kras, where the rise terminates at the Matavun Fault Zone, along which the Škocjan structural bend was formed (Placer, 2015). Behind the Škocjan structural bend lies the plateau of Goriče Kras (after the village of Goriče near Famlje), which is not inclined but remains horizontal at around 440 m. Somewhat below this settlement, at an elevation of about 400 m, lies the Naklo level, as a remnant of the blind Vreme valley highest terrace. The Škocjan structural bend played an active role in the formation of the present Notranjska Reka (river) sinking area and the longitudinal profile of the Škocjan Caves. In the simplified structural map of the Karst (Placer, 2015), the term Škocjanski prag (Škocjan treshold) was used for the structural bend, but it is not an elevation level, only an escarpment, which requires a new corresponding term.

črnokalske anomalije. Povezava je očitna zato, ker so generalne strukture jugozahodnega dela senožeške cone cepljenja gub vzporedne črnokalski anomaliji (sl. 11), to velja za skrajni severozahodni del Čičarijskega antiklinorija in za Artviško sinklinalo (3) v Brkinskem sinklinoriju in za Lipiško sinklinalo (2) in Bazovsko antiklinalo (1). Spremenjeno lego imata tudi navzkrižno-povezovalni gubi Rodiško-Preloška antiklinala (11) in Paredska sinklinala (12). Kakšen je bil kinematski mehanizem prilagoditve omenjenih struktur smeri črnokalske anomalije v tem članku ne bomo razpravljali, vsekakor pa bi bilo potrebno pred odgovorom na to vprašanje, izvesti detajlne usmerjene strukturne raziskave.

Učinek lokalno povečane kompresije v dinarskem zaledju črnokalske anomalije se odraža tudi v vzdolžnem zbirnem geomorfološkem profilu Krasa (sl. 12). Prvotna uravnava Tržaško-Komenske planote je bila ob svojem nastanku subhorizontalna, danes je nagnjena. Od Doberdobske planote na Spodnjem Krasu na višini okoli 110 m, se proti Gornjemu Krasu polagoma dviga do okoli 440 m na Divaškem Krasu, kjer se dviganje ustavi ob matavunski razpoklinsko-prelomni coni, po kateri je nastal škocjanski pregib (Placer, 2015). Za škocjanskim pregibom leži uravnava Goriškega Krasa (po vasi Goriče pri Famljah), ki ni nagnjena temveč ostaja na enaki višini okoli

External Dinaric Thrust Belt

Figure 11 also shows part of the External Dinaric Thrust Belt with the Snežnik, Hrušica and Trnovo Nappes. According to the regional research data (OGK, sheets: Tolmin, Videm, Kranj, Gorica, Postojna; Mlakar, 1969), we conclude that the overlying thrust plane of the Trnovo Nappe bends transversely to the Dinarides, so that from southwest to northeast the Trnovo synform, the Idrija antiform, Žiri synform and the Poljane-Vrhnika antiform (Placer et al., 2021a) stand out. In Figure 11, only a part of the Trnovo synform (II) is visible, the axis of which continues towards the southeast into the Hrušica Syncline. It is not possible from the data on the geologic map to determine whether the underlying Hrušica Nappe thrust plane is also synformly bent.

In the article on the relationship between tectonics and gravity phenomena at the boundary of the External Dinaric Thrust Belt (Placer et al., 2021a), it was established that the underlying thrust surfaces of the Hrušica Nappe below Nanos and the Trnovo Nappe below Mt. Čaven are convexly folded. The new terms Nanos and Čaven antiforms were introduced. Both therefore lie at the head of both thrust fronts, but they differ in amplitude – in the first it is around 250 m, in the second around 30 m.

The Nanos and Čaven antiforms at the head of the Hrušica and Trnovo Nappe belong to the same antiform unit (Placer et al., 2021a), so it makes sense to introduce the term Nanos-Čaven antiform (Fig. 11, I). The relationship between them is not clear because the intervening space is denuded, and the Sistiana Flexural Zone also passes through it (Placer et al., 2021b), due to which the axis of the antiform is bent laterally and its convex part rests on the Belsko Fault (formerly Predjama fault, Placer et al., 2021a). The lateral bending of the Nanos-Čaven antiform and the unusual change of the Belsko Fault trace are the result of the crossing of two Transverse Dinaric deformation zones in this area, the flexural zone of the Sistiana Fault and the now described zone of increased compression in the Dinaric hinterland of the Črni Kal Anomaly. A more detailed description of the effect of the aforementioned deformations in this area is beyond the scope of this article, and to prove the existence of a zone of increased compression it is important to note that the Nanos segment of the Nanos-Čaven antiform has a significantly larger amplitude than the Čaven segment.

440 m. Nekaj pod to uravnavo leži na koti okoli 400 m nakelski nivo, ki je ostanek najvišje terase Vremske slepe doline. Škocjanski pregib je imel dejavno vlogo pri nastajanju sedanjega ponornega območja notranjske Reke in vzdolžnega profila Škocjanskih jam. V poenostavljeni strukturni karti Krasa (Placer, 2015) je bil za škocjanski pregib uporabljen termin škocjanski prag, vendar ne gre za višinsko stopnjo temveč le za pregib, ki terja ustrezno spremembo naziva.

Zunanjedinarski narivni pas

Na sliki 11 je viden tudi del Zunanjedinarskega narivnega pasu s Snežniškim, Hrušiškim in Trnovskim pokrovom. Po podatkih dosedanjih regionalnih raziskav povzemamo (OGK, listi: Tolmin in Videm, Kranj, Gorica, Postojna; Mlakar, 1969), da krovna narivna ploskev Trnovskega pokrova undira prečno na Dinaride, tako da od jugozahoda proti severovzhodu izstopajo trnovska sinforma, idrijska antiforma, žirovska sinforma in poljansko-vrhniška antiforma, oziroma poljansko-vrhniški nizi (Placer et al., 2021a). Na sliki 11 je od naštetih viden le del trnovske sinforme (II), katere os se proti jugovzhodu nadaljuje v Hrušiško sinklinalo, medtem ko iz podatkov na karti ni mogoče ugotoviti ali je sinformno usločena tudi krovna narivna ploskev Hrušiškega pokrova.

V članku o odnosu med tektoniko in gravitacijskimi pojavi na meji Zunanjedinarskega narivnega pasu (Placer et al., 2021a) je bilo ugotovljeno, da sta krovni narivni ploskvi Hrušiškega pokrova pod Nanosom in Trnovskega pokrova pod Čavnom konveksno usločeni. Uvedena sta bila termina nanoška in čavenska antiforma. Obe torej ležita v čelu obeh pokrovov, vendar se razlikujeta po velikosti amplitude, pri prvi znaša okoli 250 m, pri drugi okoli 30 m.

Nanoška in čavenska antiforma v čelu Hrušiškega in Trnovskega pokrova pripadata isti antiformni enoti (Placer et al., 2021a), zato je smiselno uvesti termin nanoško-čavenska antiforma (sl. 11, I). Odnos med njima je nejasen zato, ker je vmesni prostor denudiran, preko njega pa poteka tudi sesljanska upogibna cona (Placer et al., 2021b), zaradi katere je os antiforme bočno upognjena, njen izbočeni del pa se naslanja na Belski prelom (prej Predjamski prelom, Placer et al., 2021a). Bočni upogib nanoško-čavenske antiforme in nenavadna sprememba smeri Belskega preloma sta posledica križanja dveh prečnodinarskih

Raša Fault

In order to understand the deformations along the Raša Fault in the area of the Transverse Dinaric zone of increased compression between the Kraški rob and Hrušica, it is necessary to look at its trace from a greater distance. The Raša Fault trace (Fig. 1) is drawn on the Italian side according to Carulli's (2006) data. On the Slovenian side, it is interpreted anew between Gorica and Dornberk, and from here to Vremščica by Poljak (2007), Jurkovšek et al. (1996), Jurkovšek (2010); Placer (2015), Placer et al. (2021b), and according to OGK data (sheets: Gorica, Trieste, Postojna and Ilirska Bistrica). Southeast of Vremščica, the Raša Fault trace is drawn on the basis of an exposed fault zone in the Stržen stream valley (Fig. 13) and on the basis of the interpretation of the formation of the pull-apart Ilirska Bistrica coal basin, which is said to have formed along the Raša Fault (Placer & Jamšek, 2011). In Figure 1, the visible part of the fault trace is marked with a solid line, and the invisible or presumed part with a dashed line.

For the purposes of this article, it is important to show in greater detail the conditions along the Raša Fault between Gorica and Vremščica (Fig. 13) and the Stržen valley. The damage zone is exposed in several places, in the village of Brdo near Dornberk (village) (Fig. 13, point 1), in the ravines and on the intermediate ridges between Tabor and Cvetrož village (Fig. 13, point 2), in the Zajčica road cut on the highway near Senožeče (Fig. 13, point 3), in three sand pits »V žlebu« (toponime) above Čepno beneath the Mt. Vremščica slope (Fig. 13, point 4) and along the Stržen (Fig. 13, point 5). There are also several small sand pits in the Raša valley next to the Raša Fault.

The structure of the Raša Fault is best visible in the Zajčica terraced road cut on the highway near Senožeče (Fig. 13, point 3; Fig. 14), and was also revealed in a large, abandoned sand pit near the road cut. The entire fault zone, about 80 m wide, is exposed in the east wall of the road cut (Fig. 14A). Its major part is enlarged in Figure 14B. Here, an anticlinal fold is still visible in the third terrace. The anticline can be detected upon closer inspection of the entire roadcut. The first terrace riser is already built up and covered with grass, which is why Figure 14C shows the mirror image of the western wall of the road cut at the height of the first terrace, which is no longer there today but the mentioned anticline was clearly visible here. In Figure 14D, the structure of the section is sketched with the stratigraphic data from Jurkovšek et al. (1996); on the left half, there is bedded Lipica Formation limestone ($LF/K_2^{4\text{-}5}$),

deformacijskih con na tem prostoru, upogibne cone Sesljanskega preloma in sedaj opisovane cone povečane kompresije v dinarskem zaledju črnokalske anomalije. Natančnejši opis učinka omenjenih deformacij na tem prostoru presega okvir tega članka, za dokazovanje obstoja cone povečane kompresije pa je pomembno, da ima nanoški segment nanoško-čavenske antiforme bistveno večjo amplitudo od čavenskega segmenta.

Raški prelom

Za razumevanje deformacij ob Raškem prelomu v območju prečnodinarske cone povečane kompresije med Kraškim robom in Hrušico, je potrebno pogledati na njegov potek z nekoliko večje razdalje. Trasa Raškega preloma (sl. 1) je na italijanski strani potegnjena po podatkih Carulli-ja (2006). Na slovenski strani je od Gorice do Dornberka interpretirana na novo, od tu do Vremščice pa po podatkih Poljaka (2007), Jurkovška et al. (1996), Jurkovška (2010), Placerja (2015) in Placerja et al. (2021b), ter po podatkih OGK (listi Gorica, Trst, Postojna, Ilirska Bistrica). Jugovzhodno od Vremščice je potegnjena na podlagi vidne prelomne cone v dolini potoka Stržena (sl. 13) in na podlagi interpretacije nastanka ilirskobistriškega premogovnega pull apart-skega ali razmičnega bazena, ki naj bi nastal ob Raškem prelomu (Placer & Jamšek, 2011). Na sliki 1 je vidni del trase označen s polno črto, nevidni ali domnevni del pa s prekinjeno črto.

Za ta članek je pomembno, da podrobneje prikažemo razmere ob Raškem prelomu med Gorico in Vremščico (sl. 13) ter dolino potoka Stržena. Zdrobljena cona je vidna na več mestih, v naselju Brdo pri Dornberku (sl. 13, točka 1), v grapah in na vmesnih grebenih med Taborom in Cvetrožem (sl. 13, točka 2), v useku Zajčica na avtocesti pri Senožečah (sl 13, točka 3), v treh peskokopih »V žlebu« nad Čepnim pod Vremščico (sl. 13, točka 4) in ob potoku Strženu (sl. 13, točka 5). Tudi v dolini Raše je ob Raškem prelomu več manjših peskokopov.

Najlepše je vidna zgradba Raškega preloma v terasastem useku avtoceste Zajčica pri Senožečah (sl. 13, točka 3; sl. 14), razkrita pa je bila tudi v veliki jami nekdanjega peskokopa blizu useka. Na sliki 14A je fotografija vzhodne stene useka, kjer je vidna celotna zdrobljena cona preloma, široka okoli 80 m. Njen večji del je povečan na sliki 14B, tu je v ježi tretje terase kljub porušenosti še opazna antiklinalna guba, ki jo je pri bolj natančnem pregledu mogoče zaznati na celotni višini useka. Ježa prve terase je že podzidana in zatravljena, zato je na sliki 14C prikazana

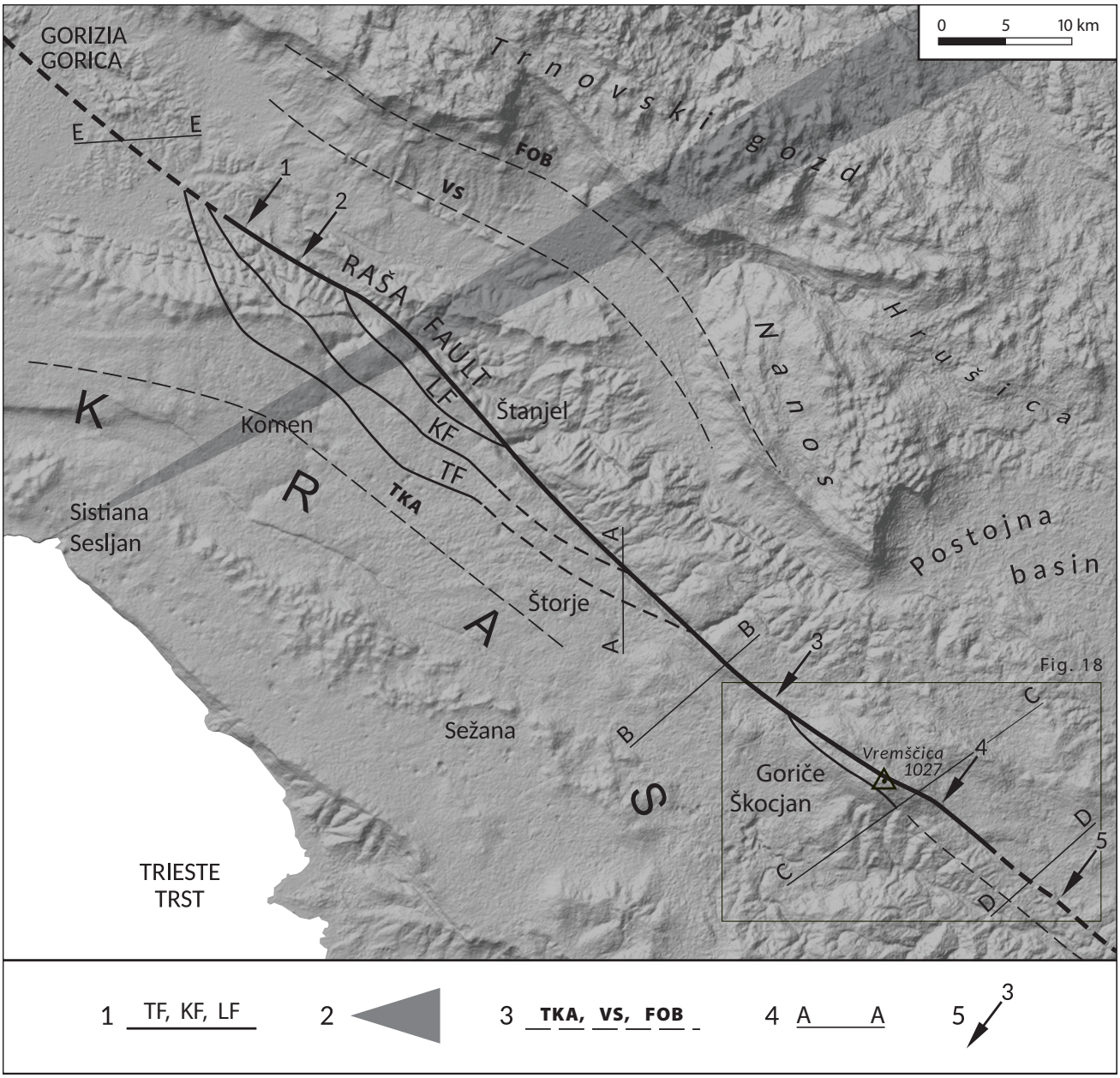

Fig. 13. Raša Fault between Gorica and the Stržen stream.

Sl. 13. Raški prelom od Gorice do potoka Stržen.

1 Adjusting faults: TF – Tomačevo Fault, KF – Kobjeglava Fault, LF – Lukovec Fault / izravnalni prelomi: TF – Tomačevski prelom, KF – Kobjeglavski prelom, LF – Lukovski prelom

2 Sistiana Flexural Zone / sesljanska upogibna cona

3 Bent structures in the Sisitiana Flexural Zone: TKA – Trieste-Komen Anticlinorium axis, VS –Vipava Synclinorium axis, FOB – External DinaricThrust Belt front / upognjene strukture v sesljanski upogibni coni: TKA – os Tržaško-Komenskega antiklinorija, VS – os Vipavskega sinklinorija, FOB – čelo Zunanjedinarskega narivnega pasu

4 Profiles across the Raša Fault: A – A Štorje - Stomaž, B – B Povir - Griško polje, C – C Vremska dolina - Mt. Vremščica - Ravnik, D – D Košanska dolina, E – E Brezavščak stream valley / profili preko Raškega preloma: A – A Štorje - Stomaž, B – B Povir - Griško polje, C – C Vremska dolina - Vremščica - Ravnik, D – D Košanska dolina, E – E Dolina potoka Brezavščka

5 Observation sites of the Raša Fault: 1 – Brdo near Dornberk, 2 – Saksidi, 3 – Zajčica, 4 – Čepno, 5 – Stržen / mesta opazovanja Raškega preloma: 1 – Brdo pri Dornberku, 2 – Saksidi, 3 – Zajčica, 4 – Čepno, 5 – Stržen

gently dipping to the northeast, followed by two stronger subvertical fault planes with an intermediate tectonized block, then the block folded into an asymmetric anticline slightly inclined to the southwest. Its wavelength is 20 m to 25 m with an amplitude of about 8 m. Towards the southwest, zrcalna podoba zahodne stene useka v višini ježe prve terase, ki je danes ni več. Tu je bila omenjena antiklinala lepo vidna. Na sliki 14D je zgradba useka skicirana, stratigrafski podatki so navedeni po Jurkovšku et al. (1996); na levi polovici so plasti Lipiške formacije (LF/K_2^{4-5}), ki

the anticline limb lies on a subvertical fault plane, behind which lies a block of tectonized beds of the Lipica Formation. It is completed by a set of several parallel fault surfaces, behind which lie Liburnia Formation beds (LIB/K-Pc), already a part of the south-western block of the Raša Fault. As the Liburnian Formation makes a part of the Karst Group of Formations, the KGF is used instead of the LIB/K-Pc designation in Figure 14D. In the sand pit, right-lateral strike slip fault surfaces with sub-horizontal slickensides and several completely flat subvertical tectonic mirrors, from a few metres to 25 m^2 in size, were observed in the Lipica Formation limestones. Tectonic mirrors were polished to a high gloss, and clearly indicate periodic polygonal movement of the fault blocks, confirmed also by barely visible striae in different directions. Signs of polygonal movement of the fault blocks were also observed in the fault zone of the Idrija Fault (Placer, 1980, fig. 12) and in the thrust plane of the Hrušica Nappe in the sand pit near Planina (Placer, 1994/95).

In the profile sketch (14D), it is necessary to draw attention to the compatibility of the geological structure and the surface: on the left, the gentle slope of the upland adapts to the gently inclined bedding; the top of the upland lies above the top of the extruded anticline; and the steep slope on the right lies in the inner fault zone. From the conditions in the profile, we conclude that the relief here is the result of tectonic formation.

Three successive sand pits opened in the limestones of the Lipica and Liburnia Formations (LF/K_2^{4-5}, LIB/K-Pc), separated by the main fault plane of the damage zone of the Raša Fault in the »V žlebu« valley above Čepno village (Fig. 13, point 4). The most telling are the fault surfaces in the middle sand pit, where horizontal tectonic slickensides occur, which indicate right-lateral strike slip motion and vertical slides with block movements in different directions. Other directions are also present.

Flysch rocks occur in outcrops of the Raša Fault damage zone at Brdo near Dornberk (Fig. 13, point 1), between Tabor and Cvetrož (Fig. 13, point 2) and near Stržen (Fig. 13, point 5). In all cases, the main fault plane dips steeply towards the northeast; next to it lies a cut reverse flexure, which at first glance would indicate a simple reverse movement, but conditions at Zajčica and Čepno show that other movements also exist, so conclusions based on a limited set of data can be deceptive. Without detailed research of different parts of the fault zone, it is not possible to discuss the kinematics of the blocks along the Raša Fault.

položno vpadajo proti severovzhodu, sledita dve močnejši subvertikalni prelomni ploskvi z vmesnim zdrobljenim blokom, zatem blok naguban v asimetrično antiklinalo, ki je rahlo nagnjena proti jugozahodu. Njena valovna dolžina znaša okoli 20 m do 25 m, amplituda okoli 8 m. Proti jugozahodu se krilo antiklinale naslanja na subvertikalno prelomno ploskev, za katero je blok iz zdrobljenih plasti Lipiške formacije. Zaključi ga snop več prelomnih ploskev za katerimi ležijo plasti Liburnijske formacije (LIB/K-Pc), ki že pripadajo jugozahodnemu bloku Raškega preloma. Na sliki 14D je namesto Liburnijske formacije oznaka KGF (Kraška grupa formacij), katere del je tudi Liburnijska formacija. V peskokopu so bile v apnencih Lipiške formacije zabeležene desnozmične prelomne ploskve s subhorizontalnimi tektonskimi drsami in več povsem ravnih, od nekaj do 25 m^2 velikih subvertikalnih tektonskih zrcal, ki so bila polirana do visokega sijaja, kar jasno kaže na občasno poligonalno premikanje prelomnih kril, ki so ga potrjevale tudi komaj vidne strije v različnih smereh. Znaki poligonalnega premikanja prelomnih kril so bili opazovani tudi v prelomni coni Idrijskega preloma (Placer, 1980, sl. 12) in v narivni ploskvi Hrušiškega pokrova v peskokopu pri Planini (Placer, 1994/95).

V skici profila (14D) je potrebno opozoriti na skladnost geološke zgradbe in površja; na levi se položno pobočje vzpetine prilagaja položnim plastem, vrh vzpetine leži nad vrhom izrinjene antiklinale, strmo pobočje na desni leži v coni glavne prelomne ploskve. Iz razmer v profilu povzemamo, da je relief na tem mestu posledica tektonskega oblikovanja.

»V žlebu« nad Čepnim (sl. 13, točka 4) so odprti trije zaporedni peskokopi v apnencih Lipiške in Liburnijske formacije (LF/K_2^{4-5}, LIB/K-Pc), ki ju razdvaja glavna prelomna ploskev Raškega preloma. Najbolj povedne so prelomne ploskve v srednjem peskokopu, kjer nastopajo tektonske drse horizontalne smeri, ki kažejo na desno zmikanje in vertikalne drse z različno usmerjenimi premiki blokov. Prisotne pa so tudi druge smeri.

Izdanki zdrobljene cone Raškega preloma v Brdu pri Dornberku (sl. 13, točka 1), med Taborom in Cvetrožem (sl. 13, točka 2) ter ob Strženu (sl. 13, točka 5), so v flišnih kamninah. V vseh primerih glavna prelomna ploskev strmo vpada proti severovzhodu, ob njej leži pretrgana reverzna fleksura, kar bi na prvi pogled kazalo na enostavni reverzni premik, vendar Zajčica in Čepno kažeta, da obstojajo tudi drugačni premiki, zato je sklepanje na podlagi omejenega

A

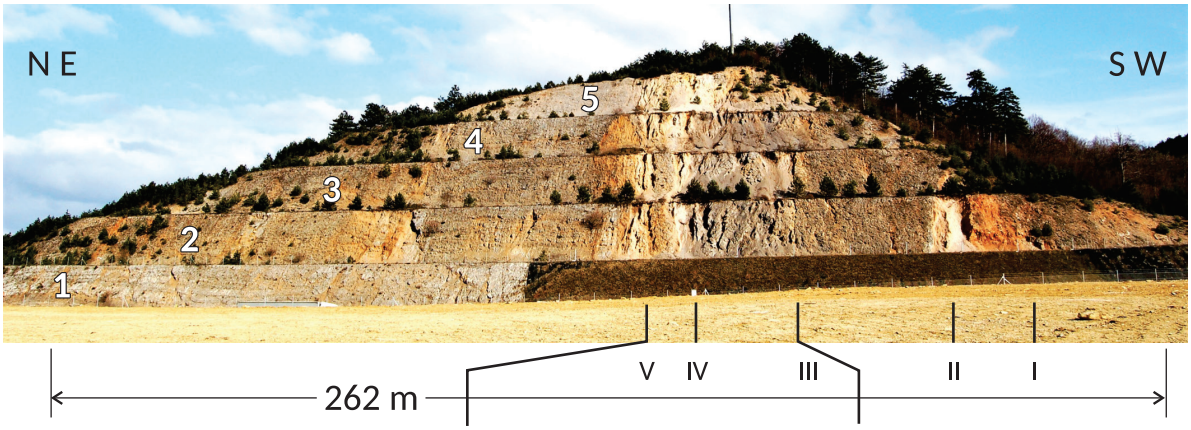
N E
S W
1
2
3
4
5
V
IV
III
II
I
262 m

B


5
4
3
2

C


1
V
IV
III
75 m

D

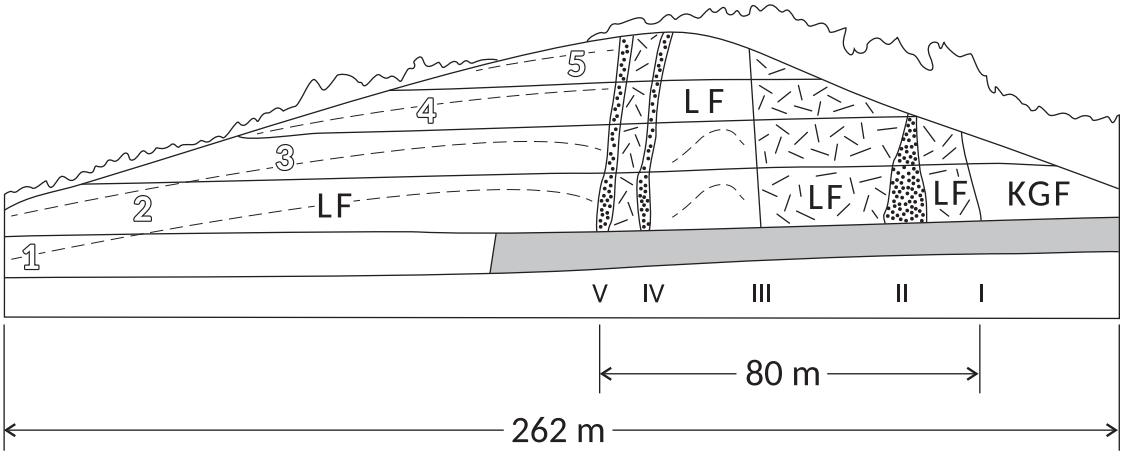
1
2
3
4
5
LF
LF
LF
LF
KGF
V
IV
III
II
I
80 m
262 m

Only faulted rocks were observed in the outcrop next to Stržen (Fig. 13, point 5), but not the structure of the fault zone or the kinematics.

Displacements along the Raša Fault have not yet been investigated more precisely, but Jurkovšek et al. (1996, profile A – B) provides relatively reliable information about the vertical displacement between the two fault blocks in the profile between the villages of Štorje and Stomaž, which amounts 150 to 200 m (measured from the cross-section on the map). The direction of the horizontal component of the displacement is right-lateral, but its magnitude has not yet been determined.

In this article we are interested in the section of the Raša Fault, where the vertical uplift of its north-eastern block was measured (Jurkovšek et al., 1996, profile A – B). This profile is shown again (Fig. 15, profile A – A) for the sake of understanding the topic under discussion. The mentioned offset of 150 m to 200 m is significant because it was determined on the basis of systematic mapping and a good knowledge of the thickness of the strata. However, since we are studying the relationship between tectonics and geomorphology, it was necessary to check whether a similar vertical movement also exists in the karst formations between the two blocks of the Raša Fault.

A single karst ridge extends from Štanjel to Goriče pri Famljah, and plunges gently to the northwest in the south-western block of the Raša Fault in Figure 13. In the north-eastern block, there are fewer peneplained areas, which are found only in the vicinity of Senožeče, Volče and in Košanska dolina valley (Fig. 18). For a comparison with profile A – A it was necessary to choose a control profile as close as possible to that of Štorje for the sake of credibility. As such, the B – B profile from Povir village through the Divača-Sežana lowland (about 390 m), the Mt. Sopada ridge, the Senadolski dol (a dol is usually an elongated shallow valley in Dinaric Karst), the Mt. Selivec ridge, and the flat Griško polje field (about 540 m) below Mt. Veliki Ognjivec (636 m) seemed suitable (Fig. 15, profile B - B). The difference in the peneplane elevations between the Divača - Sežana lowland and the Griško polje field is around 150 m. The bottom of Senadolski dol is not

števila podatkov lahko varljivo; brez detajlnih raziskav različnih predelov prelomne cone ni mogoče govoriti o kinematiki blokov ob Raškem prelomu. V golici ob potoku Strženu (sl. 13, točka 5) je bila zabeležena le prelomna porušitev, ne pa tudi zgradba prelomne cone ali kinematika.

Premiki ob Raškem prelomu še niso bili natančneje raziskani, vendar podajajo Jurkovšek et al. (1996, profil A – B) sorazmerno zanesljiv podatek o vertikalnem premiku med obema prelomnima kriloma v profilu med Štorjami in Stomažem, ki znaša okoli 150 m do 200 m (izmerjeno iz profila na karti). Smer horizontalne komponente premika je desna, vendar njena velikost še ni določena.

V tem članku nas zanima odsek Raškega preloma, kjer je bil izmerjen vertikalni dvig njegovega severovzhodnega krila (Jurkovšek et al., 1996, profil A – B). Zaradi razumevanja obravnavane teme, ta profil ponovno prikazujemo (sl. 15, profil A – A). Omenjeni skok 150 m do 200 m je pomemben zato, ker je bil določen na podlagi sistematičnega kartiranja in dobrega poznavanja debeline plasti. Ker pa proučujemo razmerje med tektoniko in geomorfologijo, je bilo potrebno preveriti ali obstoja podoben vertikalni premik tudi pri kraških uravnavah med obema kriloma Raškega preloma.

Na sliki 13 se v jugozahodnem krilu Raškega preloma razteza enotna kraška uravnava od Štanjela do Gorič pri Famljah, ki neznatno visi proti severozahodu. V severovzhodnem krilu je uravnanih površin manj, najdemo jih le v okolici Senožeč, v Volčah in v Košanski dolini (sl. 18). Za primerjavo s profilom A – A je bilo potrebno zaradi verodostojnosti izbrati kontrolni profil čim bliže Štorjam. Kot tak se je zdel primeren profil B – B od Povirja preko Divaško-Sežanskega podolja (okoli 390 m), grebena Sopade, Senadolskega dola, grebena Selivca in uravnanega Griškega polja (okoli 540 m) pod Velikim Ognjivcem (636 m). Razlika v koti uravnav med Divaško-Sežanskim podoljem in Griškim poljem znaša tu okoli 150 m. Dno Senadolskega dola ni primerno za primerjavo, ker je preoblikovano ob

Fig. 14. Raša fault in the Zajčica roadcut (highway) (Figs. 13 and 18): A. Photo of the section. B. Part of the damage zone. C. Oblique anticline within the damage zone indicating reverse movement of the northeast limb. D. Sketch of the section: about 80 m wide Raša Fault damage zone. I – Southwestern boundary fault plane, which is also the main one; II, III, IV – internal fault planes; V – northeastern boundary fault plane. *Key for the stratigraphic markers in Fig. 15.*

Sl. 14. Raški prelom v useku avtoceste Zajčica (sl. 13 in 18): A. Fotografija useka. B. Del zdrobljene cone. C. Poševna antiklinala znotraj zdrobljene cone, ki kaže na reverzni premik severovzhodnega krila. D. Skica useka: okoli 80 m široka zdrobljena cona Raškega preloma. I – jugozahodna mejna prelomna ploskev, ki je hkrati glavna; II, III, IV – notranje prelomne ploskve; V – severovzhodna mejna prelomna ploskev. *Legenda stratigrafskih oznak na sl. 15.*

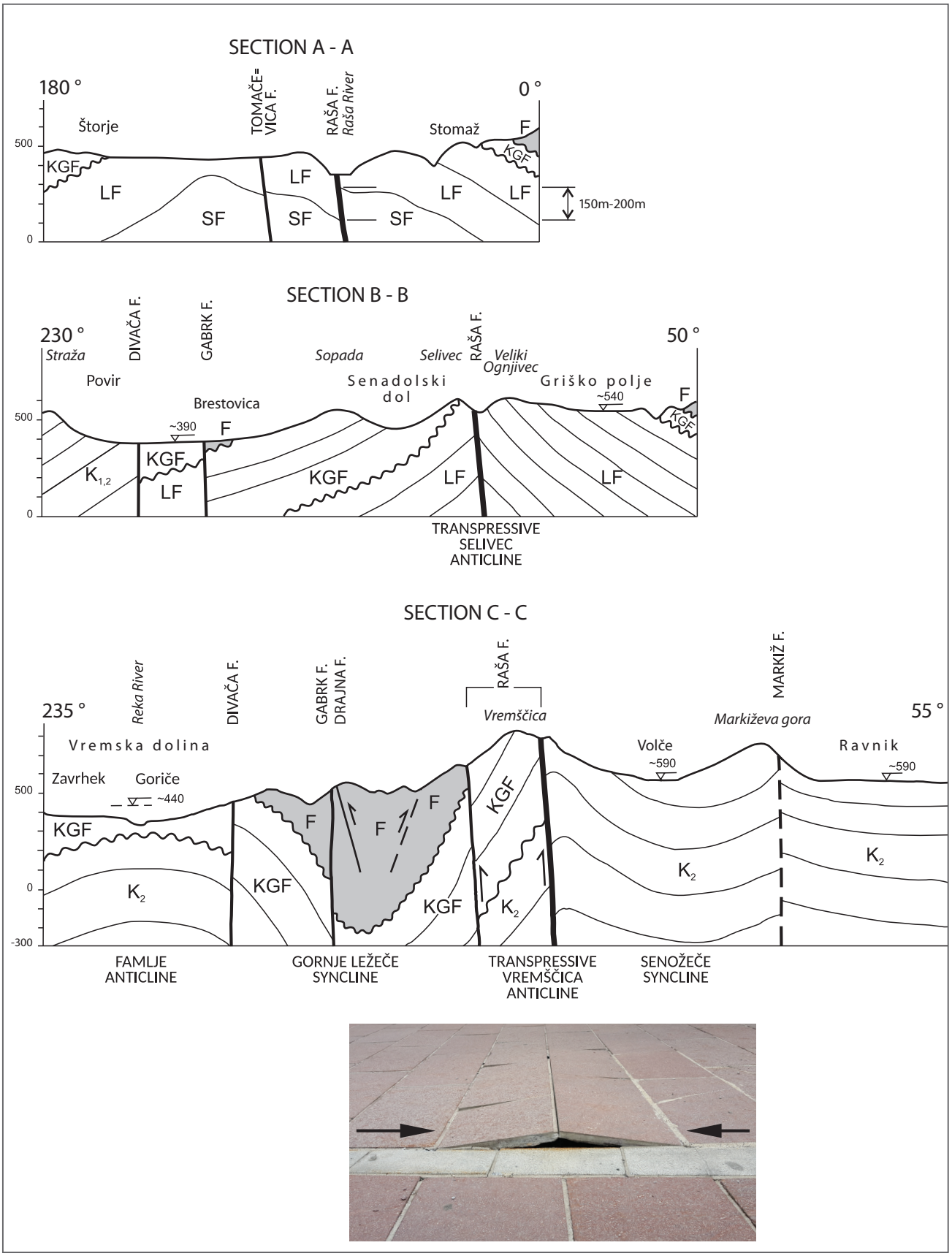

Fig. 15. Profiles across the Raša Fault: A – A Štorje - Stomaž (after Jurkovšek et al. 1996, profile A – B); B – B Povir - Griško polje; C – C Vremska dolina - Vremščica - Ravnik, in the photo a handy model of the transpressive Vremščica Anticline; D – D Košanska dolina; E – Brezavščck stream valley. 1 Approximate level of comparative peneplanation.

Sl. 15. Profili preko Raškega preloma: A – A Štorje - Stomaž (po Jurkovšek et al. 1996, profil A – B). B – B Povir - Griško polje; C – C Vremska dolina - Vremščica - Ravnik, na fotografiji priročni model Vremške transpresivne antiklinale; D – D Košanska dolina; E – E dolina potoka Brezavščka. 1 približni nivo primerjalne uravnave.

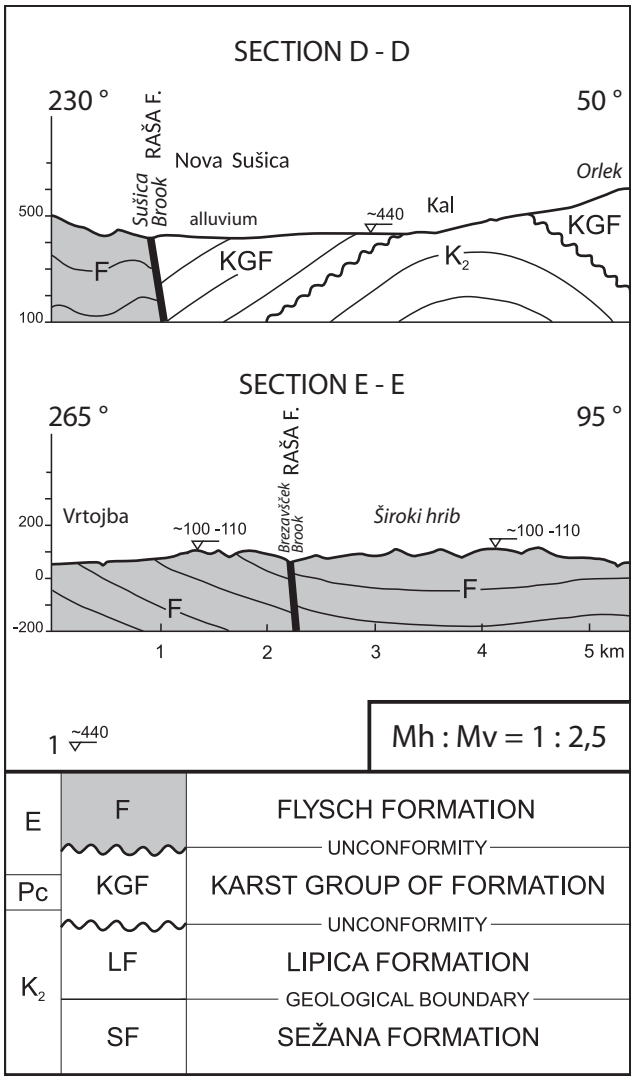

Fig. 15. continuation
Sl. 15. nadaljevanje

suitable for comparison, because it was transformed by the Raša Fault, nor is the flood plain near Dolenja vas village, which was transformed and deepened by the Senožeški potok stream. The second control profile C – C runs from Zavrhek village through the Vreme valley, across the Vremščica ridge to the part of the plateau at Volče (around 590 m) and over Mt. Markiževa gora to Ravnik peneplain (around 590 m) northeast of here (Fig. 15, profile C – C). The starting peneplanation level in the south-western block lies in the vicinity of Goriče pri Famljah village (around 440 m), but the profile does not cover it, so its projection on the profile plane is indicated. Also in this profile, the difference in the height of the settlements between Goriče, Volče, and Ravnik peneplain is about 150 m. Both control profiles therefore indicate that the difference in the height of the peneplained territory between the north-eastern and south-western blocks of the Raša Fault is comparable to the geological offset in the A – A profile between Štorje and Stomaž.

Raškem prelomu, primerna pa ni tudi naplavna ravnica pri Dolenji vasi, ki jo je preoblikoval in poglobil Senožeški potok. Drugi kontrolni profil C – C poteka od Zavrhka preko Vremske doline, čez greben Vremščice na del uravnave pri Volčah (okoli 590 m) in preko Markiževe gore na Ravnik (okoli 590 m) severovzhodno od tod. Izhodiščna uravnava v jugozahodnem krilu je v okolici Gorič pri Famljah (okoli 440 m), vendar je profil ne zajema, zato je nakazana njena projekcija na profilno ravnino. Tudi v tem profilu znaša razlika v višini uravnav med Goričami ter Volčami in Ravnikom okoli 150 m. Oba kontrolna profila torej kažeta na to, da je razlika v višini uravnanega ozemlja med severovzhodnim in jugozahodnim krilom Raškega preloma primerljiva z geološkim skokom v profilu A – A med Štorjami in Stomažem.

Profila D – D in E – E kažeta drugačno podobo. Profil D – D poteka prečno na Raški prelom jugovzhodno od Vremščice mimo Nove Sušice, ki leži na uravnavi Košanske doline. Ta je v celoti v severovzhodnem krilu Raškega preloma, trasa samega preloma pa poteka od Gornje Košane na golico št. 5 (sl. 13 in 18) ob strugi Strženа. Med Gornjo Košano in Strženom Raški prelom ni zaznan v geomorfologiji terena, preseneča pa kota uravnave Košanske doline, ki znaša pri Novi Sušici okoli 440 m, kar je toliko kot v okolici Gorič pri Famljah severozahodno od Vremščice, to pa praktično pomeni, da se severovzhodno krilo Raškega preloma med Gornjo Košano in Strženom ni dvignilo nad jugozahodnim krilom. Koti uravnav Košanske doline (okoli 440 m) in v okolici Gorič (okoli 440 m) sta približno enaki.

Podoben ali enak, je podatek v profilu E – E preko doline Brezavščka med Gorico in Volčjo Drago, v katerem so povezani najvišji uravnani grebeni flišnega gričevja v jugozahodnem krilu Raškega preloma (Martinjak okoli 100 m, Bukovnik okoli 100 m in 110 m), s tistimi v severovzhodnem krilu (Široki hrib okoli 100 m, Lamovo okoli 100 m). Uravnana slemena in vrhovi na približno enako nadmorsko višino kažejo na večje uravnano flišno ozemlje, ki ga seka Raški prelom, vendar brez vidnega vertikalnega premika. Flišna uravnava na tem območju ni povezana z uravnanim Krasom, vendar je odnos med obema kriloma Raškega preloma mogoče primerjati med seboj. Obravnavana flišna uravnava je omejenega obsega in se proti severu kmalu konča ob geomorfološki meji v smeri zahod-vzhod. Ni raziskano ali gre za tektonsko ali erozijsko mejo.

Profiles D – D and E – E provide a different picture. Profile D – D runs across the Raša Fault southeast of Mt. Vremščica past Nova Sušica village, which lies on the Košana valley plateau entirely on the north-eastern block of the Raša Fault (Fig. 15, profile D – D). The Raša Fault trace runs from Gornja Košana village to outcrop No. 5 (Figs. 13 and 18) along the Stržen. The Raša Fault is not detected in the geomorphology of the terrain between Gornja Košana and Stržen, but the elevation of the Košana valley is surprising, which is roughly 440 m near Nova Sušica village, as much as in the vicinity of Goriče pri Famljah northwest of Mt. Vremščica, which in practical terms means that the northeast block of the Raša Fault between Gornja Košana and Stržen did not rise above the south-western block. The peneplanation elevations of the Košana valley (around 440 m) and in the vicinity of Goriče (around 440 m) are approximately the same.

The information in the profile E – E across the Brezavščck valley between Gorica and Volčja Draga village is similar or identical (Fig. 15, profile E – E), where the highest levelled ridges of the flysch hills in the south-western block of the Raša Fault (Mt. Martinjak about 100 m, Mt. Bukovnik about 100 m and 110 m) are connected, with those in the north-eastern block (Mt. Široki hrib about 100 m, Mt. Lamovo about 100 m). Level ridges and peaks at approximately the same altitude indicate a larger peneplained flysch area cut by the Raša Fault, but without visible vertical displacement. The peneplained flysch in this area is not related to the peneplained Karst, but the relationship between the two blocks of the Raša Fault can be compared with each other. The discussed peneplanation of flysch formation is of limited extent and soon ends to the north at the geomorphological boundary in the E–W direction. The question whether it is a tectonic or erosional boundary has not been investigated.

Let's return again to profiles B – B and C – C in Fig. 15. In profile B – B, in addition to the already mentioned peneplanation in both blocks of the Raša Fault, there are four more hills, Mt. Straža (542 m) above Povir village, Mt. Sopada ridge, Mt. Selivec ridge, and Mt. Veliki Ognjivec ridge (636 m). Mt. Straža among the Tabor hills was formed due to selective corrosion and is built from less soluble rocks of the upper part of the Povir Formation (dolomite). As a result of selective corrosion, Mt. Sopada was also formed, as until recently it was covered by flysch, which is still visible along the Gabrk Fault (Jurkovšek et al., 1996). The formation of Mt. Selivec and Mt. Veliki Ognjivec,

Vrnimo se ponovno k profiloma B – B in C – C na sliki 15. V profilu B – B so poleg že omenjenih uravnav v obeh krilih Raškega preloma še štiri vzpetine, Straža (542 m) nad Povirjem, greben Sopade, greben Selivca in greben Velikega Ognjivca (636 m). Straža v Taborskih gričih je nastala zaradi selektivne korozije, zgrajena je iz manj topnih kamnin zgornjega dela Povirske formacije (dolomit). Zaradi selektivne korozije je nastala tudi Sopada, saj jo je še do nedavnega pokrival fliš, ki je še viden ob Gabrškem prelomu (Jurkovšek et al., 1996). Drugačen je nastanek Selivca in Velikega Ognjivca, med katerima leži Raški prelom. V prelomnih krilih vpadajo plasti v nasprotnih smereh in so ob Raškem prelomu najbolj strme, ko se pa od preloma oddaljujemo, je vpad vse manjši, pri tem pa je pomembno, da je hkrati z bolj strmo lego plasti dvignjen tudi relief. Pred seboj imamo transpresivno antiklinalo, ki se je dvignila iz uravnanega sveta zaradi predisponirane lege plasti v coni Raškega preloma, imenujemo jo Selivška transpresivna antiklinala. Po zdrobljeni coni preloma je erozija ustvarila grapo, ki se izteka v dolino Raše. Grebena Selivca in Velikega Ognjivca sta ostanek vrha transpresivne antiklinale, ki jo je erozija po grapi med dviganjem razdelila na dva dela.

Po taki analizi se Senadolski dol pokaže kot netipična asimetrična kraška depresija, njegovo jugozahodno pobočje je del Sopade in je nastalo zaradi selektivne korozije, severovzhodno pobočje pa predstavlja krilo Selivške transpresivne antiklinale, zaradi katere se je že uravnano površje izbočilo. Senadolski dol je torej kombinirana tvorba, ki v strukturnem smislu predstavlja korozijsko modificirano krilo tranapresivne antiklinale. Podobnih in drugačnih dolov je na Krasu kar nekaj, brez dvoma pa bi jih našli tudi drugod, zato je smiselno, da tak genetsko mešani ali kombinirani kraški dol poimenujemo nevtralno, predlagamo termin kombinirani dol, kombidol ali komdol. Genetskih kombinacij, ki so prispevale k nastanku dolov je več, zato je nemogoče najti za vsako specifično kombinacijo posebno ime. Pred kratkim imenovani genetski tip dola razdol (Placer et al., 2021a), je nastal po snopu razpok ali po razpoklinski coni in je genetsko vezan samo na en fenomen. Ker gre za kraške pojave, je korozija dejavnik, ki ga ni treba vključevati v termin. Termin pradol, ki so ga predlagali Diercks et al. (2021) je rečnoerozijska tvorba, tu imata struktura in korozija drugoten pomen.

between which lies the Raša Fault, is different. Layers in both fault blocks plunge in opposite directions and are steepest at the Raša Fault and become continuously less steep as we move away from the fault. It is important that with increased dip of the bedding, the relief is also raised. The described structure is a transpressive anticline, which rose from the peneplained relief due to the predisposed position of the strata in the Raša Fault zone, hence the transpressive Selivec Anticline. Along the damage zone erosion carved a canyon that runs into the Raša valley. The Mt. Selivec and Mt. Veliki Ognjivec ridges are the remains of the top of the transpressive anticline, divided into two parts by erosion along the fault during uplift.

According to such analysis, Senadolski dol appears as an atypical asymmetric karst depression, its south-western slope is part of Mt. Sopada and was formed by selective corrosion, while its north-eastern slope represents the limb of the transpressive Selivec Anticline, due to which the already levelled surface bulged. Senadolski dol is therefore a combined formation, which structurally represents a corrosion-modified limb of a transpressional anticline. There are a number of similar and different dols in the Kras, and can no doubt be found elsewhere as well, so it makes sense to name such a genetically combined karst dol neutrally, thus we suggest the term combined dol called komdol (new term). There are several genetic combinations that contributed to the formation of dols, so it is impossible to find a special name for each specific combination. Razdol, one recently-named genetic type of dol (Placer et al., 2021a) was formed in a fracture system or in a fault zone and is genetically related to only one phenomenon. Since these are karst phenomena, corrosion is a factor that does not need to be included in the term. The term pradol proposed by Diercks et al. (2021) is used for a dol formed by river erosion. Structure and corrosion are of secondary importance here.

On this occasion, it makes sense to point out that there are also dols that are entirely the result of folding: for example, »Vrhpoljski dol« between the Krvavi potok stream and the village of Vrhpolje near Kozina, which is not a name given by the locals but represents a valley along the syncline, which is a secondary formation of the Materija Fault. Here we have a nice example of a folded primary peneplanation, but since it is a karst relief, this type of valley or dol could be called a synclinal valley or sindol (new term).

From the interpretation of the relief in profile B – B, it therefore follows that before the formation

Ob tej priliki je smiselno poudariti, da obstojajo tudi doli, ki so v celoti posledica gubanja. Tak je npr. »Vrhpoljski dol« med Krvavim potokom in Vrhpoljem pri Kozini, ki ga domačini sicer tako ne imenujejo, predstavlja pa dolino po sinklinali, ki je sekundarna tvorba Matarskega preloma. Tu imamo lep primer nagubane primarne uravnave, ker pa gre za kraški relief, bi ta tip doline ali dola lahko imenovali sinklinalni dol ali sindol.

Iz razlage reliefa v profilu B – B torej izhaja, da je pred nastankom Raškega preloma, na nivoju profila, obstajala enotna kraška uravnava iz katere sta se dvigala samo grebena Taborskih gričev in Sopade. Po nastanku Raškega preloma in v fazi transpresije se je severovzhodno krilo preloma dvignilo, hkrati pa je nastala tudi transpresivna antiklinala, ki jo je omogočila ugodna lega plasti v krilih preloma, ki so že pred nastankom Raškega preloma tvorile antiklinalo v sestavi senožeškega pasu cepljenja gub (sl. 11). Grapa po grebenu transpresivne antiklinale je lahko nastala samo v primeru, da je bila erozijsko dejavna že pred transpresivnim dvigom, saj je ob dviganju izgubila hidrografsko zaledje.

V profilu C – C je prikazana zgradba Vremščice, ki je podobna Selivcu, le da je izhodna struktura izrazitejša, ker se Vremščica, oziroma območje, ki ga prikazuje profil C – C, nahaja bliže osrednjega dela senožeškega pasu cepljenja gub. V njem sta zajeti Gornjeležeška in Senožeška sinklinala, med katerima je pred nastankom Raškega preloma ležala Paleovremška antiklinala. Po nastanku cepilnih gub je bilo celotno ozemlje, skupaj s Fameljsko in Paleovremško antiklinalo, uravnano. Za tem je poševno na Paleovremško antiklinalo (okoli 20°) nastal zmični Raški prelom, ob katerem se je, tako kot v primeru Selivca, v fazi transpresije dvignila transpresivna guba ob hkratnem dvigu severovzhodnega krila preloma. Gubo imenujemo Vremška transpresivna antiklinala. V primeru Vremščice je zaradi obstoja vzporednega kraka ob Raškem prelomu, verjetno prišlo tudi do izrivanja vmesnega bloka. Tako pri Selivcu kot pri Vremščici, je bilo dviganje severovzhodnega krila Raškega preloma in transpresivne antiklinale, lahko enofazen ali večfazen proces, v vsakem primeru pa je Vremška transpresivna antiklinala nasledstvena struktura Paleovremške antiklinale. V profilu C – C je tik ob Raškem prelomu še vidno njeno sleme. Fotografija pod profilom poenostavljeno ponazarja mehanizem nastanka Vremške antiklinale; položene talne plošče na tleh predstavljajo uravnano ozemlje, dve sta se

of the Raša Fault, at the level of the profile, there was a single karstic peneplanation from which only the ridges of the Tabor hills and Mt. Sopada rose. After the formation of the Raša Fault and during the transpression phase, the north-eastern block of the fault rose, and at the same time a transpressive anticline was formed, which was made possible by the favourable position of the bedding in the fault blocks that already formed an anticline in the Senožeče Folds Splitting Zone before the formation of the Raša Fault (Fig. 11). The ravine along the crest of the transpressive anticline could only have formed if it was erosively active before the transpressive uplift, as it lost its hydrographic hinterland during the uplift.

Profile C – C shows the building of Mt. Vremščica, which is similar to Mt. Selivec, except that the outgoing structure is more pronounced because Mt. Vremščica, or the area shown by profile C – C, is located closer to the central part of the Senožeče Folds Splitting Zone. It includes the Gornje Ležeče and Senožeče Synclines, between which the Paleo-Vremščica Anticline took place before the formation of the Raša Fault. After the formation of split folds, the entire territory, together with the Famlje and Paleo-Vremščica Anticlines, was levelled (peneplained). Afterwards, the Raša Fault was formed obliquely (around 20°) to the Paleo-Vremščica Anticline, along which, as in the case of Mt. Selivec, a transpressive fold rose during the transpression phase at the same time as the north-eastern block of the Raša Fault rose. The fold is called the transpressive Vremščica Anticline. The intermediate block was probably pushed out in the case of Mt. Vremščica, due to the existence of a parallel fault branch along the Raša Fault. Both at Mt. Selivec and at Mt. Vremščica, the uplift of the north-eastern flank of the Raša Fault and the transpressive anticline may have been a single-phase or multiphase process, but in any case, the transpressive Vremščica Anticline is the successor structure of the Paleo-Vremščica Anticline. In profile C – C, its hinge is still visible right next to the Raša Fault. The photo below the profile illustrates the formation mechanism of the Mt. Vremščica Anticline; laid floor slabs on the ground represent a levelled area, with two of them later rising due to the shrinkage of that part of the bridge construction on which the slabs are laid. The contact between them illustrates the role of the Raša Fault.

The transpressive Vremščica Anticline is separated from the Selivec Anticline by a saddle, which is conditioned by a less pronounced anticlinal

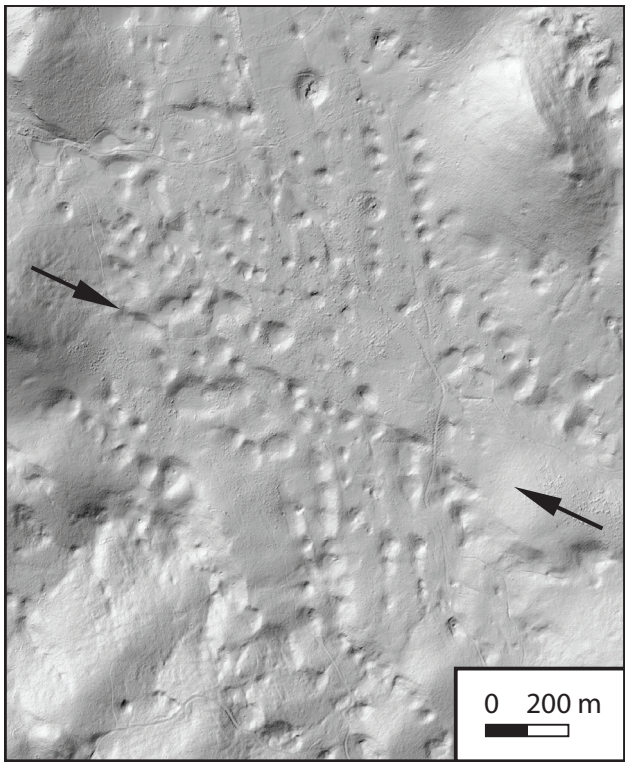

Fig. 16. Markiž Fault. Position in Fig. 18.
Sl. 16. Markižev prelom. Lega v prostoru na sl. 18.

pozneje dvignili zaradi krčenja dela konstrukcije mostu, na katerem so plošče položene. Stik med njima ponazarja vlogo Raškega preloma.

Vremška transpresivna antiklinala je od Selivške ločena s sedlom, ki je pogojeno z manj izrazito antiklinalno lego plasti. Sedlo leži v bližini useka Zajčica (sl. 14) in nima imena, vendar ga zaradi lažjega sporazumevanja imenujemo Senadolsko sedlo. Transpresivna guba tu ni odsotna temveč le manj izrazita, profil Zajčica lepo pojasnjuje njegovo zgradbo.

Domnevamo, da je zaradi transpresije dvignjena tudi Markiževa gora med uravnavama okoli Volč in na Ravniku (sl. 15, profil C – C) . Razteza se ob Markiževem prelomu vzporedno z Vremščico, le da je dvig tu skromnejši in asimetričen. Na obstoj Markiževega preloma posredno kažeta smer Markiževe gore in njeno dolgo, ravno, strmo severovzhodno pobočje, ki je verjetno zaradi hitrega dviga skoraj v celoti prekrito z deluvijem. Obstoj preloma podpira tudi izstopajoči linearni niz vrtač v smeri WNW -ESE, ki poteka preko manjše uravnave severozahodno od Markiževe gore proti Senožečam (sl. 16). Da gre za pomembnejšo mejo nakazujejo nizi vrtač v smeri NNW-SSE do N-S, ki se naslanjajo na omenjeni niz in so razviti v obeh krilih. Prostorska lega Markiževega preloma je vidna na sl. 18.

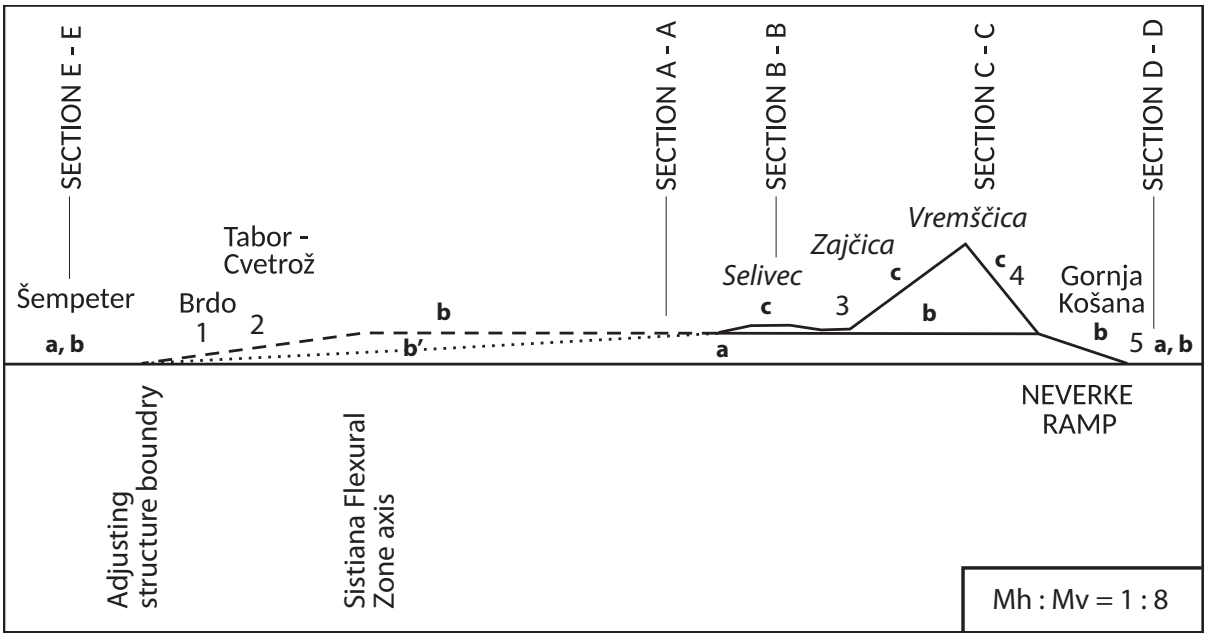

Fig. 17. Vertical displacement along the Raša Fault, based on the difference in elevation of the levelled areas: a – idealized starting level in the southwestern block of the Raša Fault; b – elevation level in the northeastern block of the Raša Fault (b´ – variant); c – Selivec and transpressive Vremščica Anticlines ridge level; 1 to 5 – observation sites along the Raša Fault.

Sl. 17. Vertikalni premik ob Raškem prelomu, ki temelji na razliki v višinskem nivoju uravnav: a – idealizirani izhodiščni uravnani nivo v jugozahodnem krilu Raškega preloma; b – nivo uravnav v severovzhodnem krilu Raškega preloma (b´ – varianta); c – nivo slemena Selivške in Vremške transpresivne antiklinale; 1 do 5 – opazovalna mesta ob Raškem prelomu.

position of the strata. The saddle is located near the Zajčica section (Fig. 14) and has no name, but for ease of communication we called it the Senadole saddle (after the village of Senadole). The transpressive fold is not absent here, but only less pronounced; the Zajčica profile nicely explains its structure.

We assume that Mt. Markiževa gora was also raised between the levelled relief around Volče and on Ravnik peneplain (Fig. 15, profile C – C) due to transpression. It stretches along the Markiž Fault parallel to Mt. Vremščica, except that the rise here is less pronounced and asymmetrical. The existence of the Markiž Fault is indirectly indicated by the direction of Mt. Markiževa gora and its long, flat, steep north-eastern slope, which is probably almost entirely covered by deluvium due to rapid uplift. The existence of the fault is also supported by a prominent linear series of dolines (usually round sinkholes) in the WNW-ESE direction, which runs over a small plane northwest of Mt. Markiževa gora towards Senožeče (Fig. 16). The importance of the boundary is indicated by the series of dolines in the NNW-SSE to N-S direction, which rest on the mentioned series and are developed in both fault blocks. The position of the Markiž Fault is presented in Figure 18.

Before the uplift of Mt. Vremščica, the area around Goriče, Volče and Ravnik was levelled, as in the case of Mt. Selivec. Since it is more or less obvious that Mt. Selivec, Mt. Vremščica, and Mt.

Tako kot pri Selivcu je tudi pri Vremščici prvotno uravnano površje pred nastankom Vremščice, združevalo območja Gorič, Volč in Ravnika. Ker je več ali manj očitno, da so Selivec, Vremščica in Markiževa gora nastali zaradi povečane transpresije, domnevamo, da so zaradi nasledstvenih deformacij ob povečani transpresiji nastale tudi nekatere druge pozitivne in negativne reliefne oblike okoli danes obstoječih uravnav. Kraški relief opisovanega ozemlja je torej seštevek primarno uravnanega ozemlja, selektivne korozije, erozije in nasledstvene tektonike, kar pomeni, da je treba h genezi reliefa posameznih območij pristopati kompleksno. V profilu C – C je zajeta tudi flišna Gornjeležeška sinklinala, ki pripada Brkinskemu sinklinoriju, zato jo je potrebno obravnavati drugače po litološki in strukturni plati. V sorazmerno stisnjeni sinklinali so bili ugotovljeni znaki vertikalnega izrivanja jedra, ki ga povezujemo z učinkom transpresije. Ob regionalni cesti Vremska dolina - Ribnica je nasproti vodarne Draga viden reverzni prelom 65/60, ki poteka v smeri osi Gornjeležeške sinklinale. Ob njem je videti tudi prevrnjene plasti. Območje ni detajlno kartirano, zato le sklepamo na obstoj konjugiranih dislokacij. Zaradi pomena omenjenega preloma za razumevanje zgradbe ozemlja, ga po bližnjem Drajnem potoku (sl. 18) imenujemo Drajni reverzni prelom.

Markiževa gora were formed due to increased transpression, we assume that some other positive and negative relief forms around the existing levelled areas were also formed due to successive deformations in the zone of increased transpression. The karst relief of the described area is therefore the sum of a primarily regulated territory, selective corrosion, erosion, and successive tectonics, which means that the genesis of the relief of individual areas must be approached with this complexity in mind. The Gornje Ležeče Syncline, covered in the C – C profile, belongs to the Brkini Synclinorium, so it needs to be treated differently in terms of lithology and structure. Signs of vertical core extrusion were found in the relatively tight syncline, associated with the transpression effect. A reverse fault 65/60 is exposed, running in the direction of the Gornje Ležeče Syncline axis along the Vremska dolina (Vreme valley) - Ribnica regional road, opposite the Draga water reservoir. Inverse bedding can also be seen next to it. The area is not mapped in detail, so we only infer the existence of conjugate dislocations. Due to the importance of the aforementioned fault for understanding the structure of the territory, it is called the reverse Drajna Fault after the nearby Drajna Stream (Fig. 18).

The Divača and Gabrk Faults, visible in profiles B – B and C – C, are older than the Raša Fault. No deformation was found in the area that could be definitively related to successional offsets.

The transverse profiles data is supplemented by a longitudinal schematically comparative geomorphological profile, which combines the two fault blocks of the Raša Fault (Fig. 17). Such comparison does not deal with real geomorphological data, but instead is meant to show the differences in the absolute elevation of the compared levelled areas between the two fault blocks: between those in the south-western block are shown with a horizontal line »a«, and with a dashed line »b« in the north-eastern block, which in the individual profiles is offset from the line »a« as much as the difference in the absolute elevation of the levelled areas. The two lines completely overlap in the area between Gorica and Volčja Draga, and there is no comparative data on the villages of Volčja Draga and Štorje, but in the vicinity of Štorje they are already well apart, at around 150 m to 200 m. From Štorje to Volče, the lines illustrating the elevations are separated, with the difference in elevation between them around 150 m everywhere. They are reunited in the Košana valley.

Line »a« is not only a construction aid but is very close its natural state, as the elevations of the

Divaški in Gabrški prelom, ki sta vidna v profilih B – B in C – C, sta starejša od Raškega preloma. Na obravnavanem prostoru ob njima nismo opazili deformacij, ki bi jih brez vsakega dvoma lahko pripisali nasledstvenim premikom.

Podatki prečnih profilov so dopolnjeni z vzdolžnim shematskim primerjalnim geomorfološkim profilom, ki združuje obe prelomni krili Raškega preloma (sl. 17). Tu ne gre za stvarne geomorfološke podatke temveč za prikaz razlik v absolutni višini primerjanih uravnav med obema prelomnima kriloma; tiste v jugozahodnem krilu so prikazane z vodoravno črto »a«, v severovzhodnem krilu s črto »b«, ki je v posameznih profilih toliko odmaknjena od črte »a«, kolikor znaša razlika v absolutni koti uravnav. Črti se povsem prekrivata na območju med Gorico in Volčjo Drago, od Volčje Drage do Štorij ni primerjalnih podatkov, vendar sta v bližini Štorij že krepko narazen, okoli 150 m do 200 m. Od Štorij do Volč sta črti, ki ponazarjata uravnave ločeni, višinska razlika med njima je povsod okoli 150 m. V Košanski dolini sta ponovno združeni.

Črta »a« ni le konstrukcijsko pomagalo, temveč je zelo blizu stanja v naravi, saj sta koti uravnav na območju Gorič in Košanske doline zelo blizu, okoli 440 m. Območje doline Brezavščka med Gorico in Volčjo Drago je izven take primerjave, vendar vseeno ustreza kriteriju vertikalnega premika.

Kakšen je potek črte »b« med Volčjo Drago in Štorjami ne vemo, lahko pa sklepamo, da se loči od črte »a« že daleč pred Štorjami, brez dvoma pa se ji ponovno priključi v Gornji Košani. Preden spregovorimo o tem si oglejmo strukturno skico Košanske doline na sliki 18. Raški prelom se od peskokopov »V žlebu« nad Čepnim (sl. 18, točka 4) spusti po geomorfološko močno odzivni grapi do Gornje Košane, od tu naprej proti strugi Sušice (sl. 18, točka 5) pa ga praktično na površju ni mogoče zaznati. Skrivnost nenadne spremembe v geomorfologiji tiči v reverznem prelomu, ki se v Gornji Košani odcepi od Raškega preloma in ga je potem mogoče slediti pod robom Košanskega hriba (589 m) najprej proti vzhodu in nato vzhodu-jugovzhodu do potokov Sušice in Stržena. Imenujemo ga Košanski reverzni prelom, v katerega čelu se je razvila Košanska antiklinala. Velikost premika ob Košanskem prelomu se od Raškega preloma proti vzhodu naglo zmanjšuje, kar pomeni, da gre za sekundarno tvorbo v širši coni Raškega preloma. Pomik ob Košanskem prelomu je pomemben zato, ker kaže, da se je prvotno enotno uravnano območje v severovzhodnem krilu preloma razdelilo na zgornji

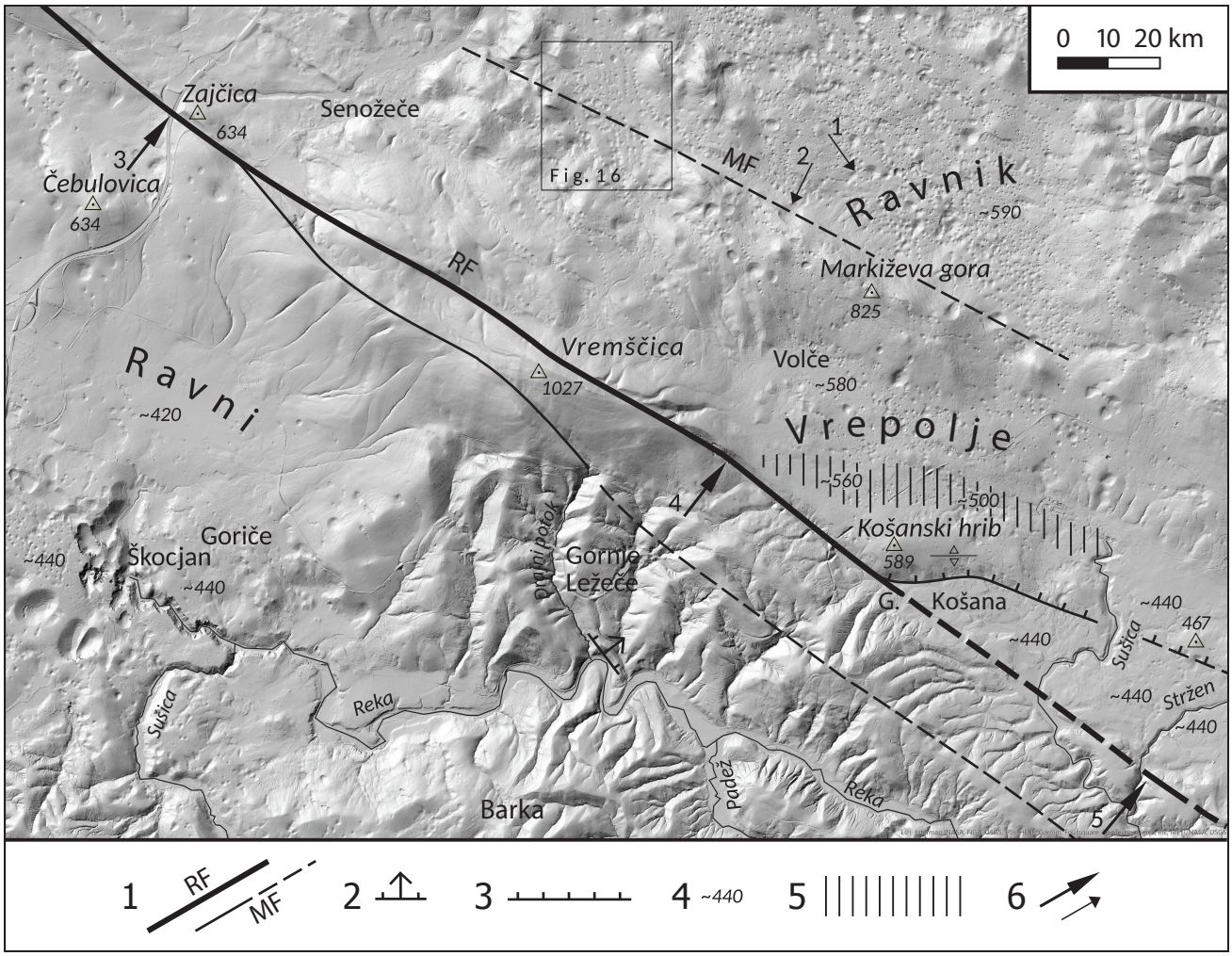

Fig. 18. Structural-geomorphological sketch of the Košana valley.

Sl. 18. Strukturno-geomorfološka skica Košanske doline.

1 Fault: RF – Raša Fault, MF – Markiž Fault / prelom: RF – Raški prelom, MF – Markižev prelom

2 Reverse Drajna Fault / Drajni reverzni prelom

3 Reverse Košana Fault / Košanski reverzni prelom

4 Approximate adjustment level (approx. 440 m) / približna kota uravnave (ok. 440)

5 Neverke ramp / neverška klančina (rampa)

6 Observation site: 3 – AC Zajčica section, 4 – sand pits »V žlebu« above Čepno, 5 – Stržen valley / opazovalno mesto: 3 – usek AC Zajčica, 4 – peskokopi »V žlebu« nad Čepnim, 5 – dolina Stržena

levelled areas of Goriče and the Košana valley are, at around 440 m, very close. The area of the Brezavšček valley between Gorica and the Volčja Draga valley is beyond such comparison, but still meets the criterion of vertical movement.

We do not know what the course of line »b« is between Volčja Draga and Štorje, but we can conclude that it separates from line »a« long before Štorje, and rejoins it at Gornja Košana village. Before we talk further about it, let's take a look at the structural sketch of the Košana valley in Figure 18. The Raša Fault descends from the »V žlebu« sand pits above Čepno village (Fig. 18, point 4) along a geomorphologically strongly responsive ravine to Gornja Košana; from here in the direction of the Sušica riverbed (Fig. 18, point 5) it is practically impossible to detect it on the surface. The secret

nivo okoli Volč (okoli 580 m) in spodnji nivo v Košanski dolini (okoli 440 m). Povezuje ju pas danes nagnjene uravnave severno od Košanskega hriba. Nagnjeni povezovalni pas nekdaj enotne uravnave imenujemo po bližnjem naselju Neverke neverška klančina ali neverška rampa. Vzhodno od stika neverške klančine z uravnavo Košanske doline se v krovni grudi Košanskega reverznega preloma dviga vzpetina, katere del je viden na sliki 18 (kota 467), ki ne potrjuje koncepta pojemanja reverznega premika ob tem prelomu proti vzhodu. Anomalija je slej ko prej povezana s prelomom v smeri SW-NE, ki poteka preko sedla med dolinama reke Pivke in notranjske Reke (OGK, list Ilirska Bistrica; Šebela, 2005, sl. 1). Nanj se naslanja Košanski reverzni prelom. Natančnejša razlaga presega okvir tega članka.

of the sudden change in geomorphology lies in the reverse fault, which splits off from the Raša Fault at Gornja Košana village and can then be followed under Mt. Košanski hrib (589 m) first to the east and then east-southeast to the Sušica and Stržen streams. We named it the reverse Košana Fault, at the head of which the Košana Anticline developed. The offset along the Košana Fault rapidly decreases from the Raša Fault to the east, which means that it is a secondary formation in the wider zone of the Raša Fault. The offset along the Košana Fault is important because it shows that the originally uniformly levelled area in the north-eastern block of the fault was divided into an upper level around Volče (around 580 m) and a lower level in the Košana valley (around 440 m). They are connected by a belt of what is today the inclined plane north of Mt. Košanski hrib. The inclined connecting belt is called Neverke ramp after the nearby village of Neverke. An elevation rises in the hanging wall of the reverse Košana Fault, part of which can be seen in Figure 18 (elevation point 467), to the east of the junction of the Neverke ramp with the levelled Košana valley, which does not confirm the concept of a decrease in the offset along this reverse fault to the east. The anomaly is in one way or another related to a fault in the SW-NE direction, which runs across the saddle between valleys of the Pivka and Reka rivers (OGK, sheet: Ilirska Bistrica; Šebela, 2005, fig. 1) and terminates at the reverse Košana Fault. A more detailed explanation is beyond the scope of this article.

Line »b« in the longitudinal profile in Figure 17 therefore joins line »a« along the Neverke ramp.

The discussion about where northwest of Štorje the effect of transpression along the Raša Fault should cease is theoretically interesting. A direct comparison with the Neverke ramp is not possible, but a hypothetical discussion is possible, for which we find a basis in the discussion of the Sistiana Flexural Zone (Placer et al., 2021b). The left-lateral strike-slip Sistiana Fault in the seabed of the Gulf of Trieste has a WSW-ENE trend in the area of Sistiana Bay. The fault is wedged out at the north-eastern boundary of the Istra-Friuli Thrust-Underthrust Zone. Further to the northeast, a flexural zone was formed in that direction, where the Trieste-Komen Anticlinorium, the Vipava Synclinorium, and the frontal part of the External Dinaric Thrust Belt are clearly bent (Fig. 13). The bending was the result of the movement of the Istran block towards the Dinarides, as its axis runs from Sistiana Bay towards the village of Spodnja Branica and Ajdovščina (Fig. 1). The Dinarides between the Sistiana and Kvarner Flexural Zones

Črta »b« v vzdolžnem profilu na sliki 17 se torej priključi črti »a« po neverški klančini.

Razprava o tem, kje severozahodno od Štorij naj bi izzvenel učinek transpresije ob Raškem prelomu, je teoretično zanimiva. Neposredna primerjava z neverško klančino ni mogoča, možna pa je hipotetična obravnava za katero najdemo osnovo v razpravi o sesljanski upogibni coni (Placer et al., 2021b). Sesljanski levozmični prelom v podmorju Tržaškega zaliva poteka v smeri WSW-ENE, na območju Sesljanskega zaliva se izklini ob severovzhodni meji istrsko-furlanske narivno-podrivne cone, naprej proti sevrovzhodu pa se je v njegovi smeri izoblikovala upogibna cona v kateri sta se lateralno vidno upognila Tržaško-Komenski antiklinorij, Vipavski sinklinorij in čelni del Zunanjedinarskega narivnega pasu (sl. 13). Os upogiba poteka od Sesljanskega zaliva proti Spodnji Branici in Ajdovščini, nastala pa je zaradi pomikanja istrskega bloka proti Dinaridom (sl. 1). Območje Dinaridov med sesljansko in kvarnersko upogibno cono je bilo torej izpostavljeno povečani transpresiji in učinku raznolike nasledstvene tektonike. Ker je v sesljanski upogibni coni bočno usločen tudi Raški prelom, bi se v apikalnem delu usločitve, torej na območju Spodnje Branice, vsaj teoretično črta »b« lahko odcepila od črte »a«. Vendar os upogibne cone ni ozka, niti natančno določena, v najširšem smislu bi njen vpliv proti severozahodu lahko segal do severovzhodne meje izravnalne zgradbe Raškega preloma, torej do stičišča Tomačevskega preloma z Raškim prelomom (sl. 13). V tem primeru bi se črta »b« lahko odcepila od črte »a« že na območju Volčje Drage. Za tako možnost govori deformacija flišnih plasti v Brdu pri Dornberku (sl. 13, točka 1). Za potrditev hipoteze bi bilo potrebno opraviti usmerjene terenske in modelne raziskave. Na sliki 17 sta za potek črte »b« od Selivca do meje izravnalne zgradbe Raškega preloma nakazani dve možnosti, »b« in »b´«.

Dvig Selivca in ekstremni dvig Vremščice je na sliki 17 prikazan s črto »c«, ki shematsko sledi njunemu slemenu in Senadolskemu sedlu med obema vzpetinama. Razmere na profilu na sliki 17 torej kažejo, da je transpresija dosegla največji učinak na območju Vremščice.

Poleg strukturnih kazalcev, da so Selivec, Vremščica in Markiževa gora antiklinalne, ali bolje antiformne deformacije prej uravnanega kraškega površja, obstajajo tudi krasoslovni pokazatelji, ki pa še niso dovolj raziskani, da bi bili zanesljivi. Najpomembnejše so vrtače, ki so na uravnanem ozemlju pogoste, na znatno nagnjenem

were therefore exposed to increased transpression and the effect of diverse successional tectonics. Since the Raša Fault trace is also laterally bent in the Sistiana Flexural Zone, in the apical part of the folding, i.e. in the area of Spodnja Branica, line »b« could, at least theoretically, split off from line »a« (Fig. 13). However, the Sistiana Flexural Zone axis is neither narrow nor precisely defined; in the broadest sense its influence towards the northwest could extend as far as the north-eastern border of the Raša Fault adjusting structure i.e. to the junction of the Tomačevo Fault with the Raša Fault (Fig. 13). In this case, line »b« could split off from line »a« already in the area of Volčja Draga village. The deformation of the flysch beds at the village of Brdo near Dornberk supports such a possibility (Fig. 13, point 1). To confirm the hypothesis, it would be necessary to carry out focused field and model research. In Figure 17, two options are indicated for the course of line »b« from Mt. Selivec to the boundary of the Raša Fault adjusting structure, »b« and »b'«.

The uplift of Mt. Selivec and the extreme uplift of Mt. Vremščica are represented by line »c« in Figure 17, which schematically follows their ridge and the Senadole saddle between the two elevations. The conditions on the profile in Figure 17 therefore show that the transpression reached its greatest effect in the Mt. Vremščica area.

In addition to the structural indicators that Mt. Selivec, Mt. Vremščica and Mt. Markiževa gora are anticlinal, or rather antiform deformations of the previously levelled karst surface, there are also karstological indicators that have not yet been sufficiently studied as to be considered reliable. The most important are dolines, which are common on flat land, yet absent or markedly rarer on a significantly tilted relief. Two tentative conclusions can be drawn from this: 1. dolines do not develop on slopes or only exceptionally under special conditions, and 2. dolines only develop on levelled relief and eventually disappear if the levelled relief tilts. The second assumption is more likely, because dolines are often found on antiform hinges, which is a kind of confirmation of what has been said, since the antiform hinge maintains a more or less horizontal (untilted) position, but there are no dolines or there are significantly fewer on the slopes. The rare dolines on the slopes could be the remnants of the larger ones from the previous peneplanation, while the smaller ones may have already disappeared. In this sense, we could interpret the situation on Mt. Markiževa gora above the village of Volče (Fig. 18): its north-eastern slope is conditioned by a fault, so it is steep and covered with

svetu jih ni ali pa so bistveno bolj redke. Iz tega je mogoče postaviti dva začasna sklepa: 1. vrtače se na pobočjih ne razvijejo ali le izjemoma kadar nastopijo posebni pogoji in 2. vrtače se razvijejo le na uravnanem svetu in sčasoma izginejo, če se uravnano ozemlje nagne. Verjetnejša je druga domneva, pogosto namreč najdemo vrtače na slemenih antiform, kar je svojevrstna potrditev povedanega, saj ohrani sleme antiforme več ali manj vodoravno lego, na pobočjih jih pa ni ali jih je bistveno manj. Redke vrtače na pobočjih bi lahko bile ostanki večjih vrtač prvotne uravnave, medtem ko so manjše morda že izginile. V tem smislu bi lahko interpretirali razmere na Markiževi gori nad Volčami (sl. 18), njeno severovzhodno pobočje je pogojeno s prelomom, zato je strmo in pokrito z deluvijem, jugozahodno pobočje pa položnejše, na njem je nekaj manjših vrtač, vendar bistveno manj kot spodaj na uravnanem Vrepolju pri Volčah, na slemenu pa sta dve večji vrtači. Lahko bi torej dejali, da so redke vrtače na jugozahodnem pobočju preostanek večjih vrtač, ki so obstajale pred dvigom. Pas ob Volčah in navzdol proti Košanskemu hribu je kultiviran in ni primeren za primerjavo. Preko Ravnika se na severovzhodni strani Markiževe gore vleče niz vrtač, ki kaže na brezstropo jamo (1), konča se ob severovzhodnem pobočju z veliko udorno tvorbo podobno zatrepu (2). Ta pokriva celotno severno pobočje in del grebena, kar pomeni, da je nastala po dvigu Markiževe gore in je verjetno posledica sekundarnih procesov, zato ne ruši predlagane interpretacije.

Vremščica in Selivec sta praktično brez večjih vrtač, obstajajo pa manjše, ki so na lidarju komaj zaznavne.

Razmeroma enostavna razlaga pa je manj prepričljiva za Sopado za katero smo ugotovili, da ni nastala zaradi tektonskega dviga temveč zaradi selektivne korozije, saj je Sopado dolgo časa prekrival pokrov flišnih kamnin, katerega ostanek je še viden ob Gabrškem prelomu v Brestovici pri Povirju (sl. 15, profil B – B). Če zanemarimo udornico Petnjak nad Brestovico, preseneča ena velika vrtača in nekaj manjših ter nizi vrtač v grapah. Vsi ti pojavi bi lahko nastali zaradi posebnih pogojev pri postopnem umikanju flišnega pokrova od slemena Sopade navzdol, vendar bi bilo treba to možnost še preučiti.

Korelacija

V coni povečane kompresije med črnokalsko anomalijo in Hrušico (sl. 11) so zaporedoma razvrščene naslednje strukturno-geomorfološke posebnosti: 1. deformirani severozahodni robovi

deluvium, while the south-western slope is flatter with a few small dolines, but significantly fewer than further below, on the levelled Vrepolje field near Volče, and there are two larger dolines on the ridge. It could therefore be said that the rare dolines on the south-western slope are the remnants of larger dolines that existed before the uplift. The zone along Volče and down towards Mt. Košanski hrib is cultivated and not suitable for comparison. A series of dolines stretches across the Ravnik plane north of Mt. Markiževa gora and indicate an unroofed cave (1), ending on the north-eastern slope with a large collapse form similar to a steephead (2). It covers the entire northern slope and part of the ridge, which means that it was formed after the uplift of Mt. Markiževa gora and is probably the result of secondary processes, so it does not affect the proposed interpretation.

Mt. Vremščica and Mt. Selivec are practically free of larger dolines, but there are smaller ones that are barely detectable on the lidar.

A relatively simple explanation, however, is less convincing for Mt. Sopada, which we found to have been formed not by tectonic uplift but by selective corrosion, as Mt. Sopada was covered by flysch rocks for a long time, so flysch remnants can still be seen next to the Gabrk Fault at the village of Brestovica pri Povirju (Fig. 15, profile B – B). Ignoring the collapse doline Petnjak above Brestovica pri Povirju, one large and several smaller dolines and series of dolines in the ravines are surprising. All these phenomena could have formed due to special conditions during the gradual retreat of the flysch cover from the Mt. Sopada ridge down, but such a possibility should still be studied.

Correlation

In the zone of increased compression between the Črni Kal Anomaly and Mt. Hrušica (Fig. 11), the following structural-geomorphological peculiarities are sequentially classified: 1. the deformed north-western edges of the Brkini Synclinorium and the Čičarija Anticlinorium, 2. the Škocjan structural bend, which represents the highest part of the NW-tilted levelled karst surface (Fig. 12), 3. transpressive Selivec and Vremščica Anticlines (Fig. 15, profile B – B, profile C – C; Fig. 17) and 4. the Nanos part of the Nanos-Čaven antiform, which has a larger amplitude than the Čaven part. The interdependence of the described structural-geomorphological peculiarities is shown on the correlation diagram (Fig. 19), where their position on the common imaginary axis in the direction of N25° is given schematically. It is roughly perpendicular to the local trend of the larger Dinaric

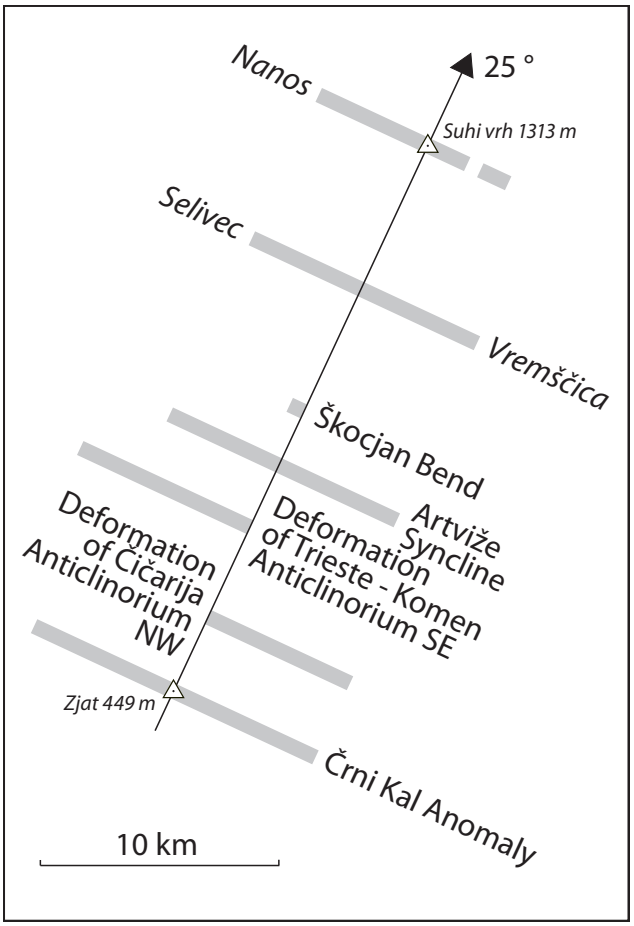

Fig. 19. Corelation diagram.
Sl. 19. Korelacijski diagram.

Brkinskega sinklinorija in Čičarijskega antiklinorija, 2. škocjanski pregib, ki predstavlja najvišji del proti NW nagnjene uravnave Krasa (sl. 12), 3. Selivška in Vremška transpresivna antiklinala (sl. 15, profil B – B, profil C – C; sl. 17) in 4. nanoški del nanoško-čavenske antiforme, ki ima večjo amplitudo od čavenskega dela. Soodvisnost opisanih strukturno-geomorfoloških posebnosti je prikazana na korelacijskem diagramu (sl. 19), kjer je shematsko podana njihova lega na skupni namišljeni osi v smeri 25°. Ta je približno pravokotna na tukajšnjo smer večjih dinarskih struktur in poteka med hribom Zjat (449 m) na Kraškem robu nad Podpečjo in najvišjim vrhom Nanosa, Suhim vrhom (1313 m). V spodnjem delu diagrama je prikazano vplivno območje črnokalske anomalije. Vse omenjene strukturno-geomorfološke posebnosti na korelacijskem diagramu ležijo v coni, ki je dolga okoli 40 km in široka okoli 10 km do 15 km. Zaradi prekrivanja strukturnih in geomorfoloških vrhuncev uvajamo namesto opisnega termina prečnodinarska cona povečane kompresije med črnokalsko anomalij in Hrušico, skrajšani termin traverza Kraški rob

structures and runs between Zjat hill (449 m) on the Kraški rob above the village of Podpeč and the highest peak of Mt. Nanos, Mt. Suhi vrh (1313 m). The influence area of the Črni Kal Anomaly is shown in the lower part of the diagram.

All of the mentioned structural-geomorphological features on the correlation diagram lie along a zone some 40 km long and 10 km to 15 km wide. Due to the overlap of structural and geomorphological peaks, instead of the descriptive term Transverse Dinaric zone of increased compression between the Črni Kal Anomaly and Mt. Hrušica«, we introduce the abbreviated term Kraški rob – Hrušica Traverse. For the sake of simplified use, we replaced the term Črni Kal Anomaly with the term Kraški rob (Žitko, 1990; Placer, 2007), with which it mainly overlaps (Fig. 11). The aforementioned zone of increased compression is not an exception within the Istra Pushed Area, as there is a disproportionately larger unit located in the hinterland of the South Istra Pushed Wedge. The Črni Kal Anomaly is a peculiarity, a special feature, which was the cause of the North Istra Extrusion Wedge formation. Without the discovery of the Črni Kal Anomaly and the zone of increased compression, we would not be able to explain the formation of Mt. Vremščica and other structural-geomorphological peculiarities in it, e.g. structural characteristics of the Škocjan Caves sinking area.

The Kraški rob - Hrušica Traverse spatially overlaps with the Senožče Folds Splitting Zone. The overlap is not accidental, as the Črni Kal Anomaly between the fronts of the Trieste - Komen and Čičarija Anticlinorium is an integral part of the Senožeče Folds Splitting Zone. If we look at the problem from the point of view of space shortening, the folds splitting zone is more (deformed) than the synclinorium and anticlinorium next to it (Fig. 9D), so the deformations are more pronounced in it.

In this article, we did not deal with the deformation kinematics of the north-western edges of the Brkini Synclinorium and the Čičarija Anticlinorium, which is related to the Črni Kal Anomaly. The exposed position of the Ravnik Anticlinorium could also be the result of increased compression, as it lies in the traverse zone. There are still some problems, but the tectonic geomorphology of the Istra Pushed Area is still in its infancy.

Formation of the North Istra Extrusion Wedge and South Istra Pushed Wedge

The main cause of the formation of the North Istra Extrusion Wedge and the South Istra Pushed Wedge is the structure of the border area between - Hrušica. Izraz črnokalska anomalija smo zaradi poenostavljene rabe zamenjali s pokrajino Kraški rob (Žitko, 1990; Placer, 2007) s katero se v glavnem prekriva (sl. 11). Omenjena cona povečane kompresije ni izjema znotraj istrskega potisnega območja, saj se neprimerno večja nahaja v zaledju konice južnoistrskega potisnega klina, posebnost je črnokalska anomalija, ki je bila vzrok za njen nastanek. Brez odkritja črnokalske anomalije in cone povečane kompresije ne bi mogli razložiti nastanka Vremščice in drugih strukturno-geomorfoloških posebnosti v njej, npr. strukturnih značilnosti ponornega območja Škocjanskih jam.

Traverza Kraški rob - Hrušica se prostorsko prekriva s senožeško cono cepljenja gub. Prekrivanje ni slučajno, saj je črnokalska anomalija med čeloma Tržaško-Komenskega in Čičarijskega antiklinorija sestavni del senožeške cone cepljenja gub. Če gledamo na problem s strani krčenja prostora, je cona cepljenja gub bolj toga od sinklinorijev in antiklinorijev ob njej (sl. 9D), zato so deformacije tu povečane.

V tem članku se nismo ukvarjali s kinematiko deformacije severozahodnih robov Brkinskega sinklinorija in Čičarijskega antiklinorija, ki je povezana s črnokalsko anomalijo. Tudi izpostavljena lega Ravniškega antiklinorija bi lahko kazala na posledico povečane kompresije, saj leži v območju traverze. Problemov je še nekaj, vendar je tektonska geomorfologija istrskega potisnega območja šele v povojih.

Nastanek severnoistrskega iztisnega in južnoistrskega potisnega klina

Glavni vzrok nastanka severnoistrskega iztisnega klina in južnoistrskega potisnega klina je zgradba mejnega območja med Mikroadrijo in Dinaridi v Istri v katerem ima posebno vlogo črnokalska anomalija. Uvodoma si najprej oglejmo standardni horizontalni presek ene izmed manjših narivnih lusk, ki so sestavni del istrsko-furlanske narivno-podrivne cone (sl. 20). Vzorčna narivna luska je omejenega obsega. Njeno čelo ima obliko loka, zato se bočno izklinja, premik ob narivni ploskvi je največji v njenem srednjem delu, kjer se razvije čelna antiklinala, ki tone proti obema bokoma (sl. 20A), lahko pa se plasti preprosto naslanjajo na narivno ploskev brez izrazite čelne antiklinale (sl. 20B). Med narivanjem so zgornje luske s svojo težo izzvale nastanek spodnjih lusk, tako da se je izoblikoval splet lusk, ki je prikazan na sl. 20C. Iz tega sledi, da ležijo mlajše luske pod starejšimi. Taka zgradba je značilna za čičarijski del istrsko-furlanske

Microadria and the Dinarides in Istra, in which the Črni Kal Anomaly plays a special role. As an introduction, let us first take a look at the standard horizontal section of one of the smaller duplexes that are an integral part of the Istra-Friuli Thrust-Underthrust Zone (Fig. 20). The sample thrust duplex is limited in scope. Its front has the shape of an arch, so it curves laterally, and the offset along the thrust plane is largest in its central part, where a frontal anticline develops and its axis (gently) plunges towards both flanks (Fig. 20A), but the layers can simply rest on the thrust plane without a distinct frontal anticline (Fig. 20B). During thrusting, the upper duplexes provoked the formation of the lower scales with their weight, so that the scales-like network of duplexes was formed, which is shown in Fig. 20C. It follows that the younger scales lie below the older ones. Such a structure is typical for the Čičarija part of the Istra-Friuli Thrust-Underthrust Zone. The frontal anticlines (the duplex cores) are from the oldest layers that come to the surface, in our case Paleogene limestone.

The formation of the North Istra and South Istra Structural Wedges and their dynamic versions is shown schematically in Figure 21 in four sketches A, B, C and D. The first three show what happened in the Paleogene, the last one in the Neogene, which extended into the recent period.

Figure 21A shows the Trieste-Komen and Čičarija frontal Anticlines in the initial stage of the formation of the Trieste-Komen and Čičarija Anticlines. The two frontal anticlines had already shifted in the beginning, which is described in the chapter on thestructure of the External Dinaric Imbricated Belt.

Figure 21B shows the beginning of the development of a single thrust zone, when two anticlinoria formed from the two anticlines. From the present-day structure it can be concluded that there was no direct connection between the frontal thrusts of the two offset folds, but that a series of thrust duplexes of monotonous structure was formed between them, in which the north-western edges of the frontal anticlines of the Paleogene limestone were arranged in an echelon series. In the figure, the situation is simplified, whereby a situation developed where the envelope of the north-western flanks of the Paleogene limestone frontal anticlines was linear in two-dimensional space, and the subvertical plane or enveloping plane »E« in three-dimensional space. The spatial arrangement of frontal anticlines from Paleogene limestone can be compared to a stack of firewood, where the sawn surfaces of individual logs create a constructed plane. That this is possible is shown

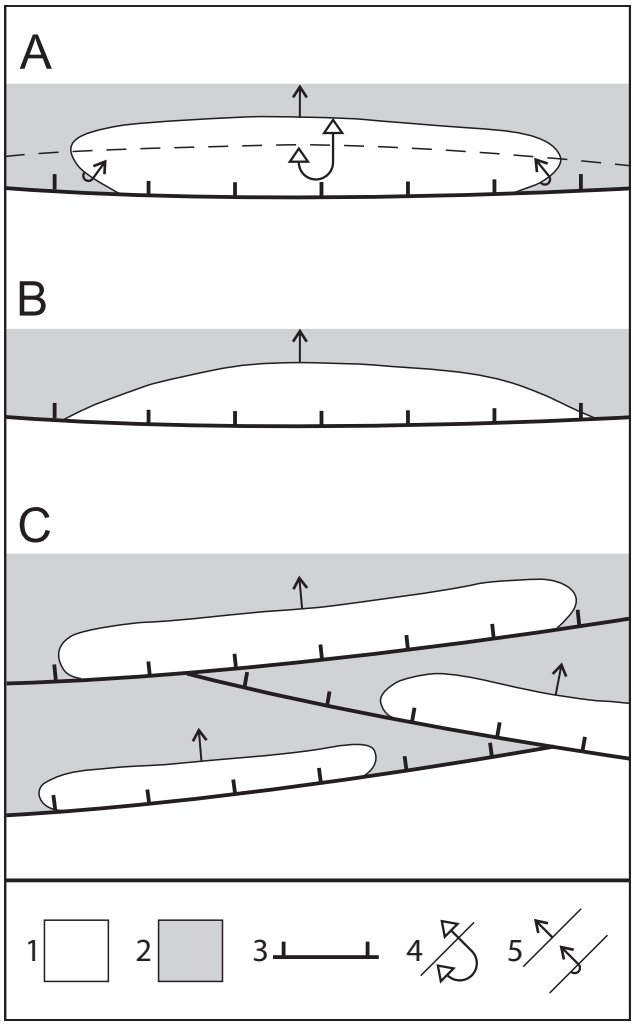

Fig. 20. Imbrication geometry: A. Ideal thrust sheet, variant with frontal anticline. B. Ideal thrust sheet, variant without frontal anticline. C. Imbricated zone (zone of multiple thrust sheets).

Sl. 20. Geometrija luskanja: A. Idealna narivna luska, varianta s čelno antiklinalo. B. Idealna narivna luska, varianta brez čelne antiklinale. C. Narivna cona iz narivnih lusk.

1 Carbonates / karbonati

2 Flysch / fliš

3 Thrust plane / narivna ploskev

4 Overturned Anticline / prevrnjena antiklinala

5 Bedding: normal, inverse / plasti: normalne, inverzne

narivno-podrivne cone. Čelne antiklinale so iz najstarejših plasti, ki izdanjajo na površje, v našem primeru je to paleogenski apnenec.

Nastanek severnoistrskega in južnoistrskega strukturnega klina ter njunih dinamskih izvedenk je shematsko prikazan na sliki 21 v skicah A, B, C in D, prve tri kažejo dogajanje v paleogenu, zadnja v neogenu, ki se je podaljšalo v recentno obdobje.

Na sliki 21A sta narisani Tržaško-Komenska in Čičarijska čelna antiklinala v začetni fazi nastajanja Tržaško-Komenskega in Čičarijskega antiklinorija. Čelni antiklinali sta bili zamaknjeni že v začetku, kar je opisano pri zgradbi Zunanjedinarskega naluskanega pasu.

in the structural diagram in Figure 6. Therefore, a special type of building was created, for which we proposed the term composite building.

Figure 21C shows the further development of the thrust structure. Erosion thrusts developed in front of the thrust zone front, such as the Isola Thrust, which initiated the formation of interlayer thrust surfaces in the flysch (Fig. 8). As the last thrust unit of the Dinarides in this area, the reverse Buje Fault, or the Buje Thrust Sheet, was formed, which has all the characteristics of the initial thrust unit, except that it is larger (Fig. 20). Five structural features indicate this:

1. The Savudrija-Buzet Anticline is the frontal anticline of the Buje Thrust Sheet, whose carbonate core is visible from the Savudrija peninsula to the Mirna valley before Buzet, where the limestone is covered by flysch layers in such a way that is typical for the carbonate cores of the initial thrust scales frontal folds in Figures 20A and 20C. The Savudrija-Buzet Anticline continues from Savudrija towards the northwest in the Gulf of Trieste seabed (Carulli, 2011, Fig. 3). The anticline is also indicated by the geophysical profile in the WSW-ENE direction (Busetti et al., 2012, Fig. 2). Figures 21C shows its presumed position at the time of its formation in the Paleogene.

2. The steep position of the reverse Buje Fault corresponds to the initial stage of thrust development.

3. Northeast verging reverse faults are visible in the cliff of the south-western coast of Strunjan Bay (Figs. 4A and 8). Judging by their position, they are related to the backthrusting in the hinterland of the Buje reverse Fault.

4. Thicker sub-horizontal layers of calcarenite are visible in the flysch cliff between Piran and Fiesa, i.e. in the uplifted block between the reverse Buje Fault and its backthrusts. Internal rotation is developed along the internal structures parallel to lamination in these layers via interlayer slips (Placer et al., 2010, fig. 19). The slips of the hanging wall beds are directed in a southwestern direction (Figs. 4A and 8). The data is not evidence of thrusting or underthrusting, but interlayer slipping could have been established only before the formation of the reverse Buje Fault and its backthrusts. The reverse Buje Fault is therefore related to the Paleogene thrusting. An interlayer thrust was discovered in the sub-horizontal bedding of the transitional marl between Paleogene limestone and flysch in Izola, which is the apparent equivalent of interlayer offsets in the cliff between Piran and Fiesa, which we named the Izola Thrust (Figs. 4A and 8).

Na sliki 21B je viden pričetek razvoja enotne narivne cone, ko sta iz antiklinal nastala antiklinorija. Iz današnje zgradbe je moč sklepati, da ni prišlo do neposredne povezave med čelnima narivoma obeh zamaknjenih gub, temveč, da je med njima nastal niz narivnih lusk monotone zgradbe, v katerih so se severozahodni robovi čelnih antiklinal iz paleogenskega apnenca razporedili v ešalonski niz. Na sliki so razmere poenostavljene, razvilo se je stanje, ko je ovojnica (envelopa) severozahodnih bokov čelnih antiklinal iz paleogenskega apnenca bila v dvodimenzionalnem prostoru lineara, v tridimenzionalnem prostoru pa subvertikalna planara ali ovojna ravnina (envelopna ravnina) »E«. Prostorsko razporeditev čelnih antiklinal iz paleogenskega apnenca lahko primerjamo s skladovnico drv, kjer žagane ploskve posameznih polen ustvarjajo konstruirano ravnino. Da je to mogoče je pokazano na strukturnem diagramu na sliki 6. Nastal je torej poseben tip zgradbe za katerega smo predlagali termin zložbena zgradba.

Na sliki 21C je prikazan nadaljnji razvoj narivne zgradbe. V predčelju narivne cone so se razvili erozijski narivi, kot npr. Izolski nariv, ki so injicirali nastanek medplastnih narivnih ploskev v flišu (sl. 8). Kot zadnja narivna enota Dinaridov na tem prostoru je nastal Bujski reverzni prelom, oziroma Bujska narivna luska, ki ima vse značilnosti inicialne narivne enote, le da je velikih dimenzij (sl. 20). Na to kaže pet strukturnih značilnosti:

1. Savudrijsko-Buzetska antiklinala je čelna antiklinala Bujske narivne luske, njeno karbonatno jedro je vidno od Savudrijskega polotoka do doline Mirne pred Buzetom, kjer karbonat prekrijejo flišne plasti na tak način, kot je značilno za karbonatna jedra čelnih gub inicialnih narivnih lusk na sliki 20A in 20C. Savudrijsko-Buzetska antiklinala se od Savudrije proti severozahodu nadaljuje v podmorju Tržaškega zaliva (Carulli, 2011, sl. 3). Na antiklinalo kaže tudi geofizikalni profil v smeri WSW – ENE (Busetti et al., 2012, sl. 2). Na sliki 21C je prikazana njena domnevna lega ob nastanku v paleogenu.

2. Strmi vpad Bujskega reverznega preloma ustreza inicialnemu stadiju razvoja nariva.

3. V klifu jugozahodne obale Strunjanskega zaliva so vidni reverzni prelomi, ki vergirajo proti severovzhodu (sl. 4A in sl. 8). Po prostorski legi sodeč, kažejo na povratno narivanje v zaledju Bujskega reverznega preloma.

4. V flišnem klifu med Piranom in Fieso, torej v dvignjeni grudi med Bujskim reverznim prelomom in njegovimi povratnimi narivi, so

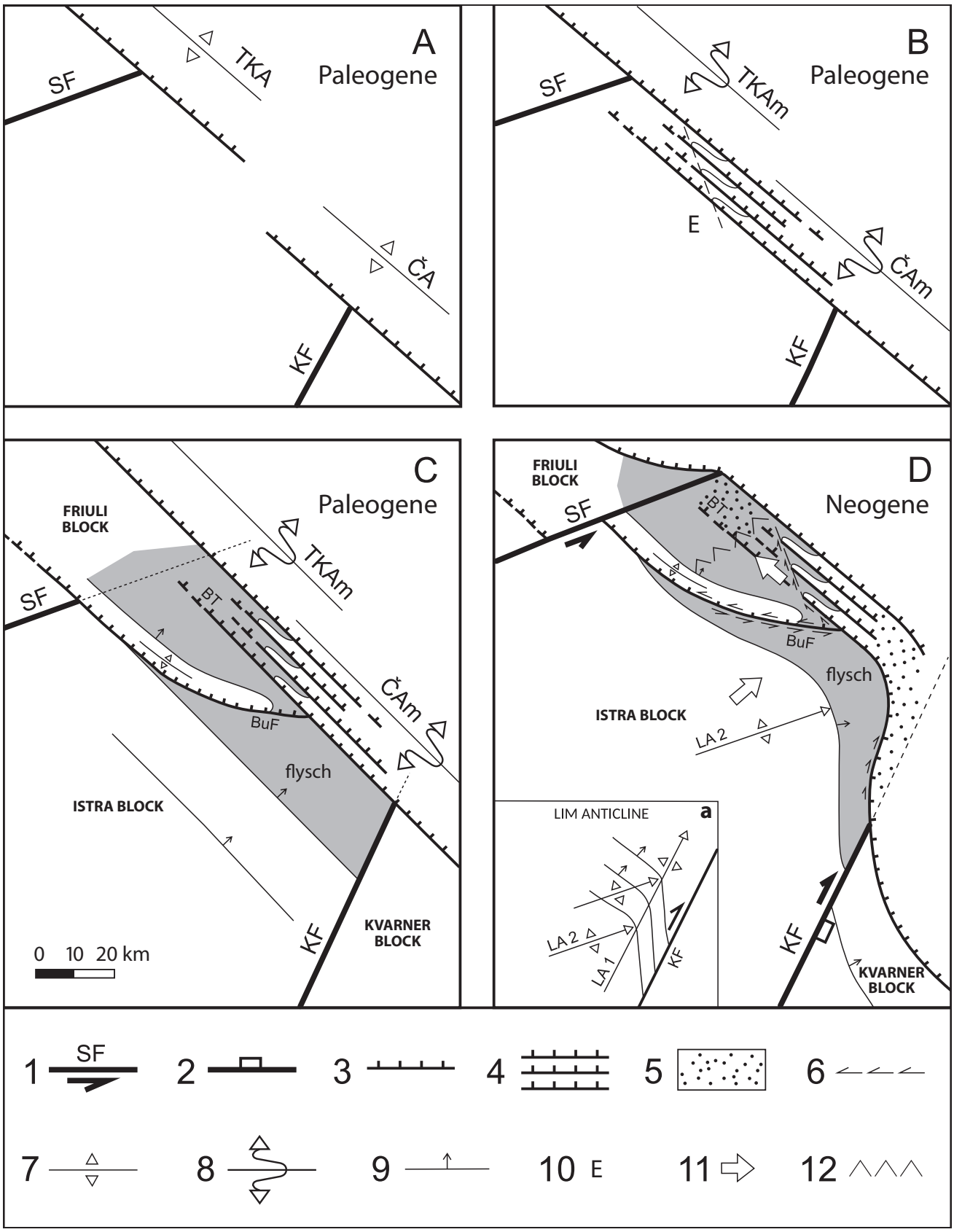

Fig. 21. Formation of the Črni Kal Anomaly, the North Istra Extrusion Wedge and the South Istra Pushed Wedge.
Sl. 21. Nastanek črnokalske anomalije, severnoistrskega iztisnega klina in južnoistrskega potisnega klina.

5. Folds are developed in the flysch between the reverse Buje Fault backthrusts and the Križ Thrust (Figs. 4A and 8). The Križ Thrust is a Paleogene structure associated with the interlayer Izola Thrust which represents an example of the interweaving of subhorizontal thrust planes in the flysch and interlayer thrust planes. The vergence of the folds in the intermediate space between the reverse Buje Fault backthrusts and the Križ Thrust is mirror-like. In this case, the symmetry is not evidence of simultaneous formation, but indicates that the older folds were formed together with the Križ Thrust. Later, when the reverse Buje Fault backthrusts were formed, the folds that create the impression of symmetry were also formed. A broader explanation is given in the description of Figure 8.

The Buje Thrust Sheet did not develop into a nappe thrust with a large offset along a subhorizontal or gently sloping thrust plane but remained as its aborted unit at the end of the Dinarides thrust. Its extreme south-eastern part is today the

vidne debelejše subhorizontalne plasti apnečevega peščenjaka. V njih je po internih strukturah vzporednih laminam, razvita interna rotacija, ki je nastala zaradi medplastnih zdrsov (Placer et al., 2010, sl. 19). Zdrsi krovninskih slojev so usmerjeni proti jugozahodu (sl. 4A in 8). Podatek ni dokaz za narivanje ali podrivanje, toda medplastno drsenje se je lahko uveljavilo samo pred nastankom Bujskega reverznega preloma in njegovih povratnih narivov. Povezujemo ga torej s paleogenskim narivanjem. V Izoli je bil v subhorizontalnih plasteh prehodnega laporja med paleogenskim apnencem in flišem odkrit medplastni nariv, ki je pojavni ekvivalent medplastnih premikov v klifu med Piranom in Fieso, imenovali smo ga Izolski nariv (sl. 4A in 8).

5. Med povratnimi narivi Bujskega reverznega preloma in Križnim narivnim prelomom so v flišu razvite gube (sl. 4A in 8). Križni narivni prelom je paleogenska struktura, povezujemo ga z Izolskim medplastnim narivnim prelomom, ki predstavlja

Paleogene thrusting:

A. Formation of shifted primal anticlines of the Trieste-Komen and Čičarija Anticlinoria and frontal reverse faults.

B. Anticlines develop into anticlinoria. A jump of movements from the frontal thrust of the Čičarija Anticlinorium to the frontal thrust of the Trieste-Komen Anticlinorium is formed via an echelon set of reverse faults. A stacked structure is formed (updated after Placer et al., 2010, Fig. 25 A). A composite building is created.

C. A segmented thrust zone is finally formed, the Buje Thrust Sheet is formed, which is the last (the most external) unit of the thrust structure of this part of the Dinarides with reverse Buje Fault in its front. The South Istra and North Istra Structural Wedges are formed (updated after Placer et al., 2010, Fig. 25 B).

Paleogensko narivanje:

A. Nastanek zamaknjenih izvornih antiklinal Tržaško-Komenskega in Čičarijskega antiklinorija ter čelnih reverznih prelomov.

B. Iz antiklinal se razvijeta antiklinorija. Oblikuje se preskok premikov s čelnega nariva Čičarijskega antiklinorija na čelni nariv Tržaško-Komenskega antiklinorija preko ešalonskega niza reverznih prelomov. Nastane zložbena zgradba (dopolnjeno po Placer et al., 2010, sl. 25 A).

C. Dokončno se oblikuje segmentirana narivna cona, nastane Bujska narivna luska, ki je zadnja enota narivne zgradbe tega dela Dinaridov. V njenem čelu Bujski reverzni prelom. Nastaneta južnoistrski in severniostrski strukturni klin (dopolnjeno po Placer et al., 2010, sl. 25 B).

Neogene underthrusting and pushing:

D. Formation of the South Istra Pushed and North Istra Extrusion Wedges.

Neogensko podrivanje in potiskanje:

D. Nastanek južnoistrskega potisnega in severnoistrskega iztisnega klina.

1 The segmented Microadria strike-slip faults: SF – Sisitiana Fault, KF - Kvarner Fault / zmični prelom segmentirane Mikroadrije: SF – Sesljanski prelom, KF – Kvarnerski prelom

2 Subsided fault block / ugreznjeno prelomno krilo

3 Paleogene thrust, reverse fault: BT – Buzet Thrust, BuF – reverse Buje Fault / paleogenski nariv, reverzni prelom: BT – Buzetski nariv, BuF – Bujski reverzni prelom

4 Paleogene thrust zone / paleogenska narivna cona

5 Neogene-recent Istra-Friuli Thrust-Underthrust Zone / neogensko-recentna istrsko-furlansla narivno-podrivna cona

6 Lateral slipping along primary thrust surfaces, along reverse faults and along envelope faults in the Črni Kal Anomaly / zmikanje po primarnih narivnih ploskvah, po reverznih prelomih in po ovojnih ali envelopnih prelomih v črnokalski anomaliji

7 Anticlines: TKA – Trieste-Komen Anticline, ČA – Čičarija Anticline, LA –Lim Anticline, a flanking asymetric fold along the Kvarner Fault (LA1 – axis in the axial plane, LA2 – axis in one of the bisector planes) / antiklinale: TKA – Tržaško-Komenska antiklinala, ČA – Čičarijska antiklinala, LA – Limska antiklinala, obprelomna asimetrična guba ob Kvarnerskem prelomu (LA1 – os v osni ravnini, LA2 – os v eni izmed simetralnih ravnin)

8 Anticlinoria: TKAm – Trieste-Komen Anticlinorium, ČAm – Čičarija Anticlinorium / antiklinoriji: TKAm – Tržaško-Komenski antiklinorij, ČAm – Čičarijski antiklinorij

9 Geological boundary, dip direction / geološka meja, smer vpada

10 Stacked structure / zložbena zgradba

11 Rellative offset direction / smer relativnega premikanja bloka

12 North Istra Extrusion Wedge extrusion boundary / meja izrivanja severnoistrskega iztisnega klina.

North Istra Structural Wedge. We assume that Microadria was already segmented in the Paleogene. This is indicated by the absence of the Oligocene in Istra, which is very likely related to the post-thrust uplift of Istra along the Kvarner Fault. From the above data, it follows that the South Istra Structural Wedge was also formed in the Paleogene.

In the Neogene, the movement of Istra, or rather this part of Microadria, towards the Dinarides began, which resulted in the development of pushing and underthrusting structures. The origin and direction of the deformations now change radically and run in the opposite direction of thrusting. In this process, the segmented Microadria faults also came to life, the most important of which are the Kvarner Fault and the Sistiana Fault in the territory under consideration, between which lies the Istra block. Structural mapping of the selected areas showed that the degree of thrusting and underthrusting of the Istra block increases from northwest to southeast, which is illustrated by the degree of tectonization of the Istra-Friuli Thrust-Underthrust Zone. This movement is smaller in the area of the Trieste parallelepiped, larger in the area of the North Istra Extrusion Wedge, and largest in the tip of the South Istra Pushed Wedge. Pushing and underthrusting is reflected in the formation of »pushed« reverse faults and in the folding of Paleogene thrust units. Both caused the uplift of the Kraški rob and the deformation of the Dinarides. The mechanism of folding and uplift of the Dinarides due to underthrusting and pushing of the Microadria has not yet been described in detail.

Sketch D (Fig. 21D) shows the hypothesis of the formation of the South Istra Pushed and North Istra Extrusion Wedges and envelope faults in the area of the Črni Kal Anomaly. The arcuate shape of the reverse Buje Fault trace and the resulting wedge-shaped south-eastern block should therefore have been designed already in the Paleogene (Fig. 21C). The Neogene movement of the Istra block towards the Dinarides provoked the development of the left-lateral strike-slip Sistiana and right-lateral strike-slip Kvarner Flexural Zones and the formation of pushed and underthrust zones. Within the Istra block itself, the wedge-shaped south-eastern part of the Buje Thrust Sheet provoked an extrusion process that did not follow the disjunctive boundaries of the wedge. Its south-western margin slipped along the newly formed strike-slip Zambratija Zone at the head of the Buje Thrust Sheet, while its north-eastern margin slipped along the newly formed dextral strike-slip zone in the enveloping plane of the Črni Kal Anomaly. The graphic in Figure 21D is a rough schematic of the reverse

primer prepletanja položnih narivnih ploskev v flišu in medplastnih narivnih ploskev. Vergenca gub v vmesnem prostoru med povratnimi narivi Bujskega reverznega preloma in Križnim narivnim prelomom, je zrcalna. Simetrija v tem primeru ni znak hkratnega nastanka, temveč kaže na to, da so starejše gube nastale skupaj s Križnim narivom, ob nastanku povratnih reverznih prelomov Bujskega reverznega preloma, pa so zatem nastale tudi gube, ki ustvarjajo podobo simetrije. Pri opisu sliki 8 je podana širša razlaga.

Bujska narivna luska se ni razvila v krovni nariv z daljšim premikom in položnejšim vpadom, temveč je ob zaključku narivanja Dinaridov ostala kot njihova abortirana enota. Njen skrajni jugovzhodni del predstavlja danes severnoistrski strukturni klin. Predpostavljamo, da je bila Mikroadrija v paleogenu že segmentirana, na to kaže odsotnost oligocena v Istri, kar je zelo verjetno povezano s postnarivnim dvigom Istre ob Kvarnerskem prelomu. Iz naštetih podatkov izhaja, da je bil v paleogenu zasnovan tudi južnoistrski strukturni klin.

V neogenu se je pričelo premikanje Istre, oziroma tega dela Mikroadrije, proti Dinaridom, v katerih so se zaradi tega razvile strukture potiskanja in podrivanja. Izvor in smer deformacij se sedaj radikalno spremenita in potekata v nasprotni smeri narivanja. V tem procesu oživijo tudi prelomi segmentirane Mikroadrije, pomembnejša med njimi sta na obravnavanem ozemlju Kvarnerski in Sesljanski prelom med katerima leži istrski blok. Strukturno kartiranje izbranih območij je pokazalo, da se stopnja potiskanja in podrivanja istrskega bloka povečuje od severozahoda proti jugovzhodu. To se najlepše vidi v stopnji porušenosti istrsko-furlanske narivno-podrivne cone. Na območju tržaškega paralelepipeda je manjša, na območju severnoistrskega iztisnega klina večja, največja na območju konice južnoistrskega potisnega klina. Potiskanje in podrivanje se odraža v nastajanju potisnih reverznih prelomov in v gubanju paleogenskih narivnih enot. Oboje je povzročilo dvig kraškega roba in deformacijo Dinaridov. Mehanizem gubanja in dviganja Dinaridov zaradi podrivanja in potiskanja Mikroadrije še ni bil podrobneje opisan.

Na skici D (sl. 21D) je podana hipoteza nastanka južnoistrskega potisnega in severnoistrskega iztisnega klina ter ovojnih ali envelopnih prelomov v območju črnokalske anomalije. Ločna oblika Bujskega reverznega preloma in iz tega izhajajoča klinasta oblika njegovega jugovzhodnega boka, naj bi bila torej zasnovana že v

Buje Fault area, so it also appears in Figure 22. The formation of the South Istra Pushed Wedge is therefore the result of the movement of the North Istra Extrusion Wedge. The amount of displacement along the edges of the North Istra Extrusion Wedge is the same, but it is asymmetric along the edges of the South Istra Pushed Wedge; along the strike-slip Zambratija Zone it is equal to the displacement of the North Istra Extrusion Wedge and is relatively small, while it is incomparably larger along the strike-slip Kvarner Fault. This is externally reflected in the formation of the extensive sigmoidal structure of the Kvarner Flexural Zone and the asymmetric Lim Anticline.

The dynamics of this process are also confirmed by recent GNSS (Global Navigation Satellite System) data, according to which the part representing the South Istra Pushed Wedge is moving north-northeast, i.e. parallel to the Kvarner Fault (Brancolini et al., 2019, fig. 1). A large asymmetrical anticlinal fold, called the Lim Anticline, developed along the Kvarner Fault. Its asymmetrical structure is presented in Fig. 21D, sketch a; the axis in the axial plane is marked as LA1; and the axis in one of the symmetry planes is marked as LA2, and there are as many of these as there are layers. Due to a gentle bedding dip it is easy to determine anticline axis on the geological map only in the symmetry plane of the unconformity between the Eocene carbonates and clastites (Fig. 21D, fold LA2; Fig. 2), while the axis of the LA1 axial plane can only be constructed. When interpreting the current shape of the Lim Anticline it is also necessary to take into account the deformation due to movement along the left-lateral strike-slip Zambratija Zone. The Lim Anticline shape (Figs. 2 and 3) is therefore a combination of a flanking fold along the right-lateral strike-slip Kvarner Zone and the left-lateral strike-slip Zambratija Zone.

By describing the role of the reverse Buje Fault, or the Buje Thrust Sheet it is, in the dynamic scheme of Istra, possible to answer the question of where the border of the Dinarides lies northwest of the Kvarner Fault. Formally, it would lie along the reverse Buje Fault, which is the most distal thrust of the Dinarides which, however, did not experience its full development. Which is why the Buje Thrust Sheet became a part of Microadria in the process of its underthrusting. Thus, the formal thrust boundary of the Dinarides in eastern Istra represents the south-western or external edge of the Istra-Friuli Thrust-Underthrust Zone, and in the area of the Gulf of Trieste its north-eastern or inner edge. The Kvarner Fault extends to the external edge, the Sistiana Fault to the internal edge, and with this the

paleogenu (sl. 21C). Neogensko premikanje istrskega bloka proti Dinaridom je izzvalo razvoj sesljanske levozmične in kvarnerske desnozmične upogibne cone ter nastajanje potisne in podrivne cone. Znotraj samega bloka je klinasta oblika jugovzhodnega dela Bujske narivne luske izzvala proces iztiskanja, ki pa ni sledil disjunktivnim mejam klina. Njegov jugozahodni rob je zdrsel po novonastali zambratijski levozmični coni ob čelu Bujske narivne luske, severovzhodni rob pa po novonastali desnožnični coni v envelopni ravnini črnokalske anomalije. Grafika na sl. 21D je v območju Bujskega reverznega preloma grobo shematska, tako je tudi na sl. 22. Nastanek južnoistrskega potisnega klina je torej posledica premika severnoistrskega iztisnega klina. Velikost premika ob robovih severnoistrskega iztisnega klina je enaka, ob robovih južnoistrskega potisnega klina pa je asimetrična; ob zambratijski levozmični coni je enaka premiku severnoistrskega iztisnega klina in sorazmerno majhna, ob Kvarnerskem desnozmičnem prelomu pa neprimerljivo večja. Ta se navzven odraža v nastanku obsežne sigmoidalne zgradbe kvarnerske upogibne cone in Limske asimetrične obprelomne antiklinale.

Dinamiko tega procesa potrjujejo tudi recentni podatki GNSS (Global Navigation Satellite System) po katerih se del, ki predstavlja južnoistrski potisni klin, premika proti severo-severovzhodu, torej vzporedno s Kvarnerskim prelomom (Brancolini et al., 2019, sl. 1). Razvila se je obsežna obprelomna guba, oziroma obprelomna antiklinala, ki smo jo poimenovali Limska. Njena zgradba je asimetrična (sl. 21D, skica a), os v osni ravnini je označena z LA1, os v eni izmed simetrijskih ravnin pa z LA2, teh je toliko kolikor je plasti. Na površinski karti Istre je zaradi blagega vpada plasti mogoče hitro in enostavno določiti le os v simetralni ravnini diskordančnega stika med eocenskimi karbonati in eocenskimi klastiti (sl. 21D, guba LA2; sl. 2), medtem ko je mogoče os osne ravnine LAl le konstruirati. Pri razlagi sedanje oblike gube pa je potrebno upoštevati tudi deformacijo zaradi premika ob zambratijski levozmični coni, Limska antiklinala na slikah 2 in 3 je torej kombinacija obprelomne gube ob kvarnerski desnozmični coni in zambratijski levozmični coni.

Z opisom vloge Bujskega reverznega preloma, oziroma Bujske narivne luske, v dinamični shemi Istre, je mogoče dati odgovor na vprašanje, kje poteka meja Dinaridov severozahodno od Kvarnerskega preloma. Formalno po Bujskem reverznem prelomu, ki je skrajni zunanji nariv

Črni Kal Anomaly acquires a meaning that must be investigated from other aspects as well, e.g. sedimentological. At the moment, we can only suggest that the informal and temporary boundary between the Dinarides and the Adriatic promontory runs along the Črni Kal Anomaly.

Considering the offset between the Trieste-Komen and the Čičarija Anticlinoria, which caused the Črni Kal Anomaly, we believe that the Istra-Friuli Thrust-Underthrust Zone is only so wide in the Istra block. The Zone should therefore be narrower northwest of the Sistiana Fault, but this aspect has not yet been investigated.

Dynamic model

A structural geometry of the Istra block and the south-western part of the Istra Pushed Area sketch is presented in Figure 22. At first glance, the relation between the autochthon (*sensu stricto* and *sensu lato*), that is, Microadria, and the Dinarides is noticeable. The only original deformations of the autochthon *sensu stricto* are the Sistiana and Kvarner Faults, both of which lie transversely to Dinaridov, vendar ta ni doživel popolnega razvoja. Zato je Bujska narivna luska v procesu podrivanja Mikroadrije postala njen aktivni del. Tako predstavlja formalno narivno mejo Dinaridov v vzhodni Istri jugozahodni ali zunanji rob istrsko-furlanske narivno podrivne cone, na območju Tržaškega zaliva pa njen severovzhodni ali notranji rob. Kvarnerski prelom sega do zunanjega roba, Sesljanski prelom do notranjega roba, s tem pa dobi črnokalska anomalija pomen, ki ga je treba raziskati tudi z drugih vidikov, npr. sedimentološkega. V tem trenutku lahko le predlagamo, da poteka neformalna in začasna meja med Dinaridi in jadranskim predgorjem po črnokalski anomaliji.

Glede na zamik med Tržaško-Komenskim in Čičarijskim antiklinorijem, zaradi katerega je nastala črnokalska anomalija, menimo, da je istrsko-furlanska narivno-podrivna cona tako široka le na območju istrskega bloka. Severozahodno od Sesljanskega preloma naj bi bila torej ožja, vendar je v tem smislu še neobdelana.

Fig. 22. Dynamic model of the Kraški rob - Hrušica Traverse formation.

Sl. 22. Dinamski model nastanka traverze Kraški rob - Hrušica.

1 Thrusting classification: autochthon *sensu stricto,* autochthon *sensu lato,* allochthon / narivna razčlenitev: avtohton *sensu stricto,* avtohton *sensu lato*, alohton

2 External Dinaric Thrust Belt boundary / meja Zunanjedinarskega narivnega pasu

3 A thrust (plane) in the External Dinaric thrust boundary zone: BuF – reverse Buje Fault, BT – Buzet Thrust / nariv v coni narivne meje Dinaridov: BuF – Bujski reverzni prelom, BT – Buzetski narivni prelom

4 Istra-Friuli Thrust-Underthrust Zone / istrsko-furlanska narivno-podrivna cona

5 Črni Kal Anomaly, the informal boundary between autochthon *sensu lato* and allochthon / črnokalska anomalija, neformalna meja avtohtona *sensu lato* in alohtona

6 The segmented Microadria strike-slip faults: SF – Sistiana Fault, KF – Kvarner Fault / zmični prelom segmentirane Mikroadrije: SF – Sesljanski prelom, KF – Kvarnerski prelom

7 Secondary subsided block of the Kvarner Fault / sekundarno ugreznjeno krilo Kvarnerskega preloma

8 Right lateral strike-slip longitudinal faults: RF – Raša Fault, IF – Idrija Fault / dinarski desnozmični longitudinalni prelom: RF – Raški prelom, IF – Idrijski prelom

9 Direction of secondary strike-slip movement / smer sekundarnega zmikanja

10 Axis of the flexural zone and the inferred position of the Sistiana and Kvarner Faults beneath nappe units of the External Dinarides: SFZ – Sistiana Flexural Zone, KFZ – Kvarner Flexural Zone / os upogibne cone in domnevna lega Sesljanskega in Kvarnerskega preloma pod narivnimi enotami Zunanjih Dinaridov: SFZ – sesljanska upogibna cona, KFZ – kvarnerska upogibna cona

11 Anticline: LA2 – Lim Anticline (axis in one of the bisector planes), SbA – Savudrija- Buzet Anticline, ViA – East Istra Anticline / 11 antiklinala: LA2 – Limska antiklinala (os po eni od simetralnih ravnin), SbA – Savudrijsko-Buzetska antiklinala, ViA – vzhodnoistrska antiklinala

12 Anticlinorium, synclinorium: a – Trieste-Komen Anticlinorium, b – Čičarija Anticlinorium, c – Ravnik Anticlinorium, d – Vipava Synclinorium, e – Brkini Synclinorium / 12 antiklinorij, sinklinorij: a – Tržaško-Komenski antiklinorij, b – Čičarijski antiklinorij, c – Ravniški antiklinorij, d – Vipavski sinklinorij, e – Brkinski sinklinorij

13 Area of the Kraški rob - Hrušica Traverse / območje traverze Kraški rob - Hrušica

14 Structural-geomorphological trajectory / strukturno-geomorfološka trajektorija

15 North Istra Extrusion Wedge limit of extrusion / meja izrivanja severnoistrskega iztisnega klina

16 External boundary of the Mesozoic carbonate platform / zunanja meja mezozojske karbonatne platforme

17 Relative direction of movement of the South Istra Pushed and North Istra Extrusion Wedges / relativna smer premikanja južnoistrskega potisnega in severnoistrskega iztisnega klina

18 Exposed peaks: SV– Mt. Suhi vrh (1313 m), V – Mt. Vremščica (1027 m), A – Mt. Ajdovščina (804 m) and Mt. Artviže (817 m), S – Mt. Slavnik (1028 m), U – Mt. Učka (1394 m), VP – Mt. Veliki Planik (1272 m), G – Mt. Gomila (1241 m), VS – Mt. Veliki Snežnik (1796 m) / izpostavljeni vrhovi: SV – Suhi vrh (1313 m), V – Vremščica (1027 m), A – Ajdovščina (804 m) in Artviže (817 m), S – Slavnik (1028 m), U – Učka (1394 m), VP – Veliki Planik (1272 m), G – Gomila (1241 m), VS – Veliki Snežnik (1796 m).

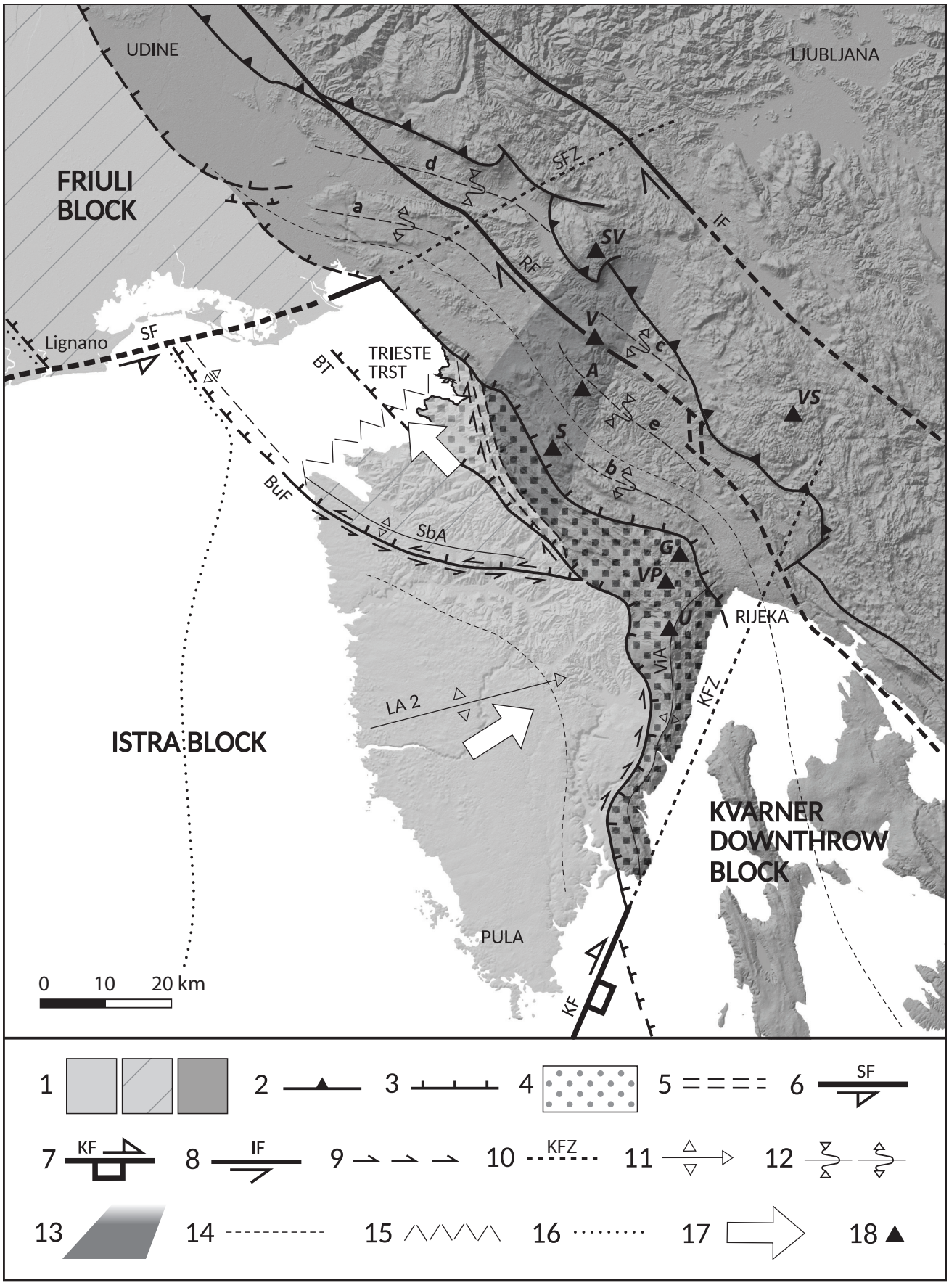
UDINE
LJUBLJANA
FRIULI BLOCK
Lignano
SF
TRIESTE
TRST
BT
BuF
SbA
SFZ
IF
RF
a
d
c
e
b
SV
V
A
S
VS
G
VP
U
RIJEKA
ViA
KFZ
LA 2
ISTRA BLOCK
KVARNER DOWNTHROW BLOCK
PULA
KF
0 10 20 km
1
2
3
4
5
6
SF
7
KF
8
IF
9
10
KFZ
11
12
13
14
15
16
17
18

the Dinarides, while the reverse Buje Fault, or rather the Buje Thrust Sheet, is part of the Dinaric thrust structure, which became part of the autochton (*sensu lato*) in the Neogene-recent pushing and subthrusting phase of the Microadria towards the Dinarides. The Sistiana and Kvarner Faults do not intersect the Dinarides, but only extend to the Istra-Friuli Thrust-Undrerthrust Zone. The Sistiana and Kvarner Flexural Zones have developed in their extensions in the Dinarides. The first is simpler and weaker, but can be followed on a digital relief model at least 50 km into the Dinarides. The second one is considerably stronger and forms an extensive flexural zone of sigmoidal shape, but its extent in the Dinarides is difficult to determine. According to a rough estimate, it extends at least 70 km to 80 km into the Dinarides. In its extension, the Idrija Fault is not bent in the same way as in the extension of the Sistiana Flexural Zone. Discussion of this issue is beyond the scope of this article; here it is sufficient to explain that the Idrija Fault is segmented in the area of the karst fields southeast of Mt. Hrušica and in this sense has not yet been investigated in detail, therefore its trace in Figures 1 and 22 is drawn dashed.

The course of the Sistiana Fault in the Gulf of Trieste is not clear. Carulli (2011, fig. 3) hypothetically stretched it from Sistiana Bay towards the southwest, based on the structural map of the contact between the carbonates and the flysch in the subsea of the Gulf of Trieste, which is based on the geophysical profiles. Carulli (2011) was guided by a saddle in the hinge of the Savudrija-Buzet Anticline extension drawn on the structural map. Determination of the Sistiana Flexural Zone in the External Dinarides to 60–56° (Placer et al., 2021b) offered a hypothetical possibility that the fault trace runs along the north-western edge of the extension of the Savudrija-Buzet Anticline, where Carulli (ib.) assumed the Aquilea Fault. According to this variant, there is a possibility that the Sistiana Fault runs from Sistiana Bay towards the west-southwest to the mentioned edge of the Savudrija-Buzet Anticline and continues along the south-western slope of the Friuli Mesozoic Carbonate Platform in the Lignano area. Such an interpretation could also mean that the previously uniform Mesozoic carbonate platform margin was cut along the Sistiana Fault, and its south-south-eastern part was moved together with the Istra block towards the Dinarides. In our opinion, the Aquileia Fault does not exist; the structural anomaly on the north-western margin of the Trieste-Komen Anticlinorium, to which Carulli linked the Aquileia Fault, is, according to our yet unpublished research, similar to the structural anomaly between

Dinamski model

Na sliki 22 je skicirana strukturna geometrija istrskega bloka in jugozahodni del istrskega potisnega območja. Že na prvi pogled je opaziti povezavo med avtohtonom (*sensu stricto* in *sensu lato*), torej Mikroadrijo in Dinaridi. Izvorni deformaciji avtohtona *sensu stricto* sta le Sesljanski in Kvarnerski prelom, oba ležita prečno na Dinaride, medtem ko je Bujski reverzni prelom, oziroma Bujska narivna luska, del dinarske narivne zgradbe, ki pa je v fazi neogensko-recentnega potiskanja in podrivanja Mikroadrije proti Dinaridom, postala del avtohtona (*sensu lato*). Sesljanski in Kvarnerski prelom ne sekata Dinaridov, temveč segata le do istrsko-furlanske narivno-podrivne cone, v Dinaridih sta se v njunih podaljških razvili sesljanska in kvarnerska upogibna cona. Prva je enostavnejša in šibkejša, vendar jo je mogoče na digitalnem modelu reliefa slediti vsaj 50 km v notranjost Dinaridov. Druga je bistveno močnejša in tvori obsežno upogibno cono sigmoidalne oblike, ki pa ji je težko določiti doseg v Dinaridih. Po grobi oceni sega vanje vsaj 70 km do 80 km. V njenem podaljšku Idrijski prelom ni upognjen tako kot v podaljšku sesljanske upogibne cone. Razprava o tem vprašanju presega okvir tega članka, tu zadostuje pojasnilo, da je Idrijski prelom na območju kraških polj jugovzhodno od Hrušice segmentiran in v tem smislu še ni detajlno raziskan, zato je njegova trasa na slikah 1 in 22 narisana črtkano.

Potek Sesljanskega preloma v Tržaškem zalivu ni jasen. Carulli (2011, sl. 3) ga je na podlagi strukturne karte stika med karbonati v podlagi in flišem v podmorju Tržaškega zaliva, ki je bila izdelana s pomočjo geofizikalnih profilov, hipotetično potegnil od Sesljanskega zaliva proti jugozahodu. Za vodilo mu je služilo sedlo v temenu podaljška Savudrijsko-Buzetske antiklinale, ki se je izrisala na strukturni karti. Potem, ko je bila določena smer sesljanske upogibne cone v Zunanjih Dinaridih, ki znaša okoli 60° do 65° (Placer et al., 2021b), se je ponudila hipotetična možnost, da poteka po severozahodnem robu podaljška Savudrijsko-Buzetske antiklinale, kjer je Carulli (ib.) domneval Oglejski prelom. Po tej varianti obstaja možnost, da poteka Sesljanski prelom od Sesljanskega zaliva proti zahodu-jugozahodu do omenjenega roba Savudrijsko-Buzetske antiklinale in se nadaljuje po jugozahodnem pobočju Furlanske mezozojske karbonatne platforme na območju Lignana (Lignano). Taka interpretacija pa bi lahko tudi pomenila, da je bil ob Sesljanskem prelomu prej enotni rob mezozojske karbonatne platforme

the Čičarija and Trieste-Komen Anticlinorium in the Val Glinščica/Rosandra area, only that the Trieste-Komen Anticlinorium meets a similar unit in the northwest, which is covered by fluvial deposits on the Friuli Plain. If the proposed interpretation of the Sistiana Fault trace turns out to be correct, it could represent the agreed boundary between the Adriatic and Friuli Mesozoic Carbonate Platforms. This assumption is supported by the consistency of the strike-slip direction along the Sistiana Flexural Zone and along the proposed route of the Sistiana Fault. The offset in both cases is left-lateral. The assumption that the Sistiana Fault has not been active recently (Placer et al., 2021b) speaks only in favour of the proposed hypothesis.

The location of the Kvarner Fault in the Adriatic Sea subsea was well determined by Špelić et al. (2021). At the same time, we must draw attention to the subsided block of the Microadria on the east-south-eastern side of the Kvarner Fault, with which the Kvarner islands, belonging to the External Dinaric Imbricated Belt, also subsided and which we have named the Kvarner block. It is the result of the Paleogene and Neogene-recent Microadria activities southeast of the Kvarner Fault, description of which exceeds the scope of this article. The formation of the East Istrian Anticline is also related to this same scheme (Korbar et al., 2020).

Formation of the Istra Pushed Area and the two flexural zones is therefore related to the movement of the Istra block towards the Dinarides. The difference in the size of the flexural zones and the submarine response of the Sistiana and Kvarner Faults shows that northwest of the Kvarner Fault the Istra block is only the most exposed object of this part of the Microadria, while the second in the series is the Friuli block. The Sistiana Fault is therefore less important than the Kvarner Fault. Based on this, we believe that the Kvarner Fault divides the Microadria into the Po and Adriatic segments. This assumption is also supported by the fact that southeast of the Kvarner Flexural Zone there is no structure that would surpass it in terms of size and importance, at least in the middle Adriatic area. The Istra block is therefore the most eastward-pushed part of the Po segment of the Microadria.

Three dynamic units lie opposite the Dinarides: the Trieste parallelepiped, the North Istra Extrusion Wedge, and the South Istra Pushed Wedge in the Istra Block. The formation of the Kraški rob - Mt. Hrušica Traverse can be explained by the blocking of the lateral extrusion of the North Istra Extrusion Wedge towards the Trieste parallelepiped. We assume that the Extrusion Wedge was therefore compressed and acted as a rigid

presekan, njegov jugo-jugovzhodni del pa premaknjen skupaj z istrskim blokom proti Dinaridom. Oglejski prelom po našem mnenju ne obstaja, strukturna anomalija na severozahodnem obrobju Tržaško-Komenskega antiklinorija, na katero je Carulli vezal Oglejski prelom, je po naših, vendar še neobjavljenih raziskavah, podobna strukturni anomaliji med Čičarijskim in Tržaško-Komenskim antiklinorijem na območju Glinščice, le da se tu stikata Tržaško-Komenski antiklinorij in podobna enota na severozahodu, ki pa je prekrita z naplavinami Furlanske nižine. Če se predlagana interpretacija poteka Sesljanskega preloma izkaže za pravilno, bi ta lahko predstavljal dogovorno mejo med Jadransko in Furlansko mezozojsko karbonatno platformo. V prid tej domnevi govori skladnost smeri zmika ob sesljanski upogibni coni in ob predlagani trasi Sesljanskega preloma. V obeh primerih je levi. Domneva, da Sesljanski prelom recentno ni aktiven (Placer et al., 2021b), govori le v prid predlagane hipoteze.

Lego Kvarnerskega preloma v podmorju Jadranskega morja so dobro določili Špelić et al. (2021). Ob tem moramo opozoriti na ugreznjeni blok Mikroadrije na vzhodno-jugovzhodni strani Kvarnerskega preloma s katerim so se ugreznili tudi Kvarnerski otoki, ki pripadajo Zunanjedinarskemu naluskanemu pasu. Poimenovali smo ga kvarnerski blok. Gre za posledico paleogenske in neogensko-recentne dejavnosti Mikroadrije jugovzhodno od Kvarnerskega preloma, katere opis presega okvir tega članka. S tem je povezan tudi nastanek Vzhodnoistrske antiklinale. O tej problematiki so pisali Korbar et al. (2020).

Nastanek istrskega potisnega območja in obeh upogibnih con je torej povezan s premikom istrskega bloka proti Dinaridom. Razlika v velikosti upogibnih con in podmorske odzivnosti Sesljanskega in Kvarnerskega preloma kaže, da je severozahodno od Kvarnerskega preloma istrski blok le najbolj izpostavljen objekt tega dela Mikroadrije, drugi v nizu je furlanski blok. Sesljanski prelom je torej manj pomemben od Kvarnerskega preloma. Glede na to menimo, da Kvarnerski prelom deli Mikroadrijo na padski in jadranski segment. Tej domnevi ustreza tudi podatek, da jugovzhodno od kvarnerske upogibne cone vsaj v območju srednjega Jadrana ni strukture, ki bi jo prekašala po velikosti in pomenu. Istrski blok je torej najbolj proti vzhodu potisnjeni del padskega segmenta Mikroadrije.

V istrskem bloku ležijo nasproti Dinaridom tri dinamske enote, tržaški paralelepiped, severnoistrski iztisni klin in južnoistrski potisni

insert between the active Microadria and the passive Dinarides, in which stress state trajectories grew thicker transversely to their direction. Specific deformations occurred in the area of thickening, presented on the correlation diagram in Figure 19. The lateral boundaries of the zones of these deformations are not sharp, but gradually die out more slowly toward the northwest and more quickly toward the southeast. The visible area of influence of the Kraški rob-Mt. Hrušica Traverse is 10 to 15 km wide and about 40 km long.

It is necessary to prove the assumption about the formation of the traverse experimentally, and to determine the mutual influence of three factors: the blocking of the North Istra Extrusion Wedge, the Črni Kal Anomaly, and the Senožeče Folds Splitting Zone.

The presented dynamic model should work from the beginning of the movement of the Microadria towards the Dinarides. More broadly, the process is related to the anticlockwise rotation of the Microadria (Weber et al., 2006), which is expressed in two components, in the hinterland of the Istra block, transpressive and shear (Placer et al., 2010). The question arises as to which status is recently active. Whether it is a transpressive or shear phase could only be determined from focal mechanisms and targeted surface surveys. However, it should be taken into account that one activity does not exclude the other, only that one is the prevailing one and the other is parallel, i.e., relieves the burden. It follows from the field data that the role of the Sistiana Fault in the recent dynamics is not important (Placer et al., 2021b), but the assumption needs to be proven. The presented dynamic model forms the basis for focused geodetic measurements.

The proposed dynamic model is supported by the following structural-geomorphological indicators: in the area of the Kraški rob-Mt. Hrušica Traverse, in addition to Mt. Selivec (619 m) and Mt. Vremščica (1027 m), are also the highest peaks of Mt. Nanos (Mt. Suhi vrh 1313 m), the north-western part of Brkini (Mt. Ajdovščina 804 m, Mt. St. Servul 817 m, above Artviže village) and the north-western part of Čičarija (Mt. Slavnik 1028 m). The existence of the South Istra Pushed Wedge is confirmed by the highest peaks of Mt. Učka (Mt. Vojak 1394 m), Čičarija (Mt. Veliki Planik 1272 m, Mt. Gomila 1241 m) and Snežnik hills (Mt. Veliki Snežnik 1796 m). In terms of geomorphology, the Čičarija Anticlinorium generally rises gradually from the northwest (Mt. Reva by Kozina 587 m) to the southeast (Mt. Veliki Planik). Mt. Slavnik, only some 7 km from Mt. Reva, would therefore be an anomaly if it did not lie in the area of the Kraški klin. Nastanek traverze Kraški rob - Hrušica je moč razložiti z blokado bočnega izrivanja severnoistrskega iztisnega klina proti tržaškemu paralelepipedu. Domnevamo, da se je iztisni klin zaradi tega komprimiral in deloval kot trd vložek med aktivno Mikroadrijo in pasivnimi Dinaridi, v katerih so se prečno na njihovo smer zgostile trajektorije napetostnega stanja. V območju zgostitve so nastale specifične deformacije, ki so predstavljene na korelacijskem diagramu na sliki 19. Bočne meje območij teh deformacij niso ostre, temveč postopoma zamirajo proti severozahodu počasneje in jugovzhodu hitreje. Vidno vplivno območje traverze Kraški rob - Hrušica je široko okoli 10 km do 15 km, v dolžino pa sega okoli 40 km.

Domnevo o nastanku traverze je potrebno eksperimentalno dokazati, pri tem pa določiti medsebojne vplive treh dejavnikov: blokade severnoistrskega iztisnega klina, črnokalske anomalije in senožeške cone cepljenja gub.

Predstavljeni dinamski model naj bi deloval vse od pričetka pomikanja Mikroadrije proti Dinaridom. Širše je proces povezan z rotacijo Mikroadrije v nasprotni smeri urinega kazalca (Weber et al., 2006), kar se v zaledju istrskega bloka, izraža v dveh komponentah, transpresivni in zmični (Placer et al., 2010). Postavlja se vprašanje, katero stanje je recentno dejavno. Ali gre za transpresivno ali zmično fazo bi se dalo ugotoviti le iz potresnih mehanizmov in z usmerjenimi površinskimi raziskavami. Treba pa je upoštevati, da ena aktivnost ne izključuje druge, le da je ena glavna, druga pa vzporedna, oziroma razbremenilna. Iz terenskih podatkov izhaja, da vloga Sesljanskega preloma v recentni dinamiki ni pomembna (Placer et al., 2021b), vendar je potrebno domnevo dokazati. Predstavljeni dinamski model je osnova za usmerjene geodetske meritve.

Predlagani dinamski model podpirajo naslednji strukturno-geomorfološki kazalci: v območju traverze Kraški rob - Hrušica ležijo poleg Selivca (619 m) in Vremščice (1027 m), tudi najvišji vrhovi Nanosa (Suhi vrh 1313 m), severozahodnega dela Brkinov (Ajdovščina 804 m, Sv. Servul v Artvižah 817 m) in severozahodnega dela Čičarije (Slavnik 1028 m). Obstoj južnoistrskega potisnega klina potrjujejo najvišji vrhovi Učke (Vojak 1394 m), Čičarije (Veliki Planik 1272 m, Gomila 1241 m) in Snežniškega hribovja (Veliki Snežnik 1796 m). Čičarijski antiklinorij se v geomorfološkem smislu na splošno polagoma dviguje od severozahoda (Reva pri Kozini 587 m) proti jugovzhodu (Veliki

rob – Mt. Hrušica Traverse. Mt. Veliki Snežnik lies in a structural block that has risen extremely high above the landscape. According to OGK, sheet Ilirska Bistrica, this process was helped along by the appropriate shape of the block, which probably narrows in depth in a wedge-shaped manner. In the intermediate space between the Snežnik hills and Čičarija lies the Brgudsko podolje (plane), a compressional trench. A complex view of the geomorphology of the Istra Pushed Area will be given in the following discussion.

The importance and existence of the Črni Kal Anomaly is also reflected in the geomorphology of the Istra Pushed Area, with important structural lines of this zone running parallel to the anomaly: the north-eastern boundary of the Istra-Friuli Thrust-Underthrust Zone, the north-western part of the Čičarija Anticlinorium axis, and the north-western part of the Brkini Synclinorium axis. Everything is nicely reflected in the course of the structural-geomorphological trajectories between the Sistiana and Kvarner Flexural Zones. In this scheme, the unresponsiveness of the Raša Fault stands out in the area of the Kraški rob - Hrušica Traverse, and there are two reasons for this: the Raša Fault was formed at a late stage in the development of the Istra Pushed Area (Placer et al., 2021b), and part of the lateral bending was compensated for by the formation of transpressive Vremščica Anticline.

The presented deformation model covers only Istra and its immediate hinterland, i.e. the Istra Block and the area of the External Dinaric Imbricated Belt between the Sistiana and Kvarner Flexural Zones. The area of the External Dinaric Thrust Belt is not covered in the discussion.

Conclusion

Istra is part of the Dinaric promontory (Microadria) on which the External Dinarides are thrusted. Thrusting of the Dinarides ended in the middle of Paleogene, and in the middle of Neogene, the movement of the Microadria towards the Dinarides began, which continues today. Istra lies in the Istra Block, which moved significantly towards the Dinarides between the left-lateral strike-slip Sistiana and right-lateral strike-slip Kvarner Faults. As it moved, it pushed the Dinarides in front of it, creating a large-scale arc-like structure called the Istra Pushed Area.

Part of the movement of the Microadria towards the Dinarides was also compensated by underthrusting, which took place and is still active along newly formed reverse faults. Along these, the hanging block was raised, and the Paleogene thrust planes within it were anticlinally folded. The Planik), Slavnik, le okoli 7 km od Reve, bi bil torej anomalija, če ne bi ležal v območju traverze Kraški rob - Hrušica. Veliki Snežnik leži v strukturnem bloku, ki se je ekstremno dvignil nad pokrajino. Po podatkih OGK, list Ilirska Bistrica, je k temu pripomogla ustrezna oblika bloka, ki se v globino verjetno klinasto zožuje. V vmesnem prostoru med Snežniškim hribovjem in Čičarijo leži Brgudsko podolje, ki je kompresijski jarek. Kompleksen pogled na geomorfologijo istrskega potisnega območja bo podan v naslednji razpravi.

Pomen in obstoj črnokalske anomalije se odraža tudi v geomorfologiji istrskega potisnega območja, vzporedno z anomalijo potekajo pomembne strukturne linije tega območja: severovzhodna meja istrsko-furlanske narivno-podrivne cone, severozahodni del osi Čičarijskega antiklinorija in severozahodni del osi Brkinskega sinklinorija. Vse se lepo odraža v poteku strukturno-geomorfoloških trajektorij med sesljansko in kvarnersko upogibno cono. V tej shemi izstopa neodzivnost Raškega preloma v območju traverze Kraški rob - Hrušica, vendar obstajata za to dva razloga, Raški prelom je nastal v poznem stadiju razvoja istrskega potisnega območja (Placer et al., 2021b), del bočnega upogiba se je kompenziral z nastankom Vremške transpresivne antiklinale.

Predstavljeni deformacijski model zajema le Istro in njeno neposredno zaledje, torej istrski blok in območje Zunanjedinarskega naluskanega pasu med sesljansko in kvarnersko upogibno cono. Območje Zunanjedinarskega narivnega pasu v razpravi ni zajeto.

Sklep

Istra je del dinarskega predgorja (Mikroadrija) na katerega so narinjeni Zunanji Dinaridi. Narivanje Dinaridov se je zaključilo sredi paleogena, sredi neogena pa se je pričelo premikanje Mikroadrije proti Dinaridom, ki traja še danes. Istra leži v istrskem bloku, ki se je med levozmičnim Sesljanskim in desnozmičnim Kvarnerskim prelomom, ekstremno premaknil proti Dinaridom. Med premikanjem je Dinaride potiskal pred seboj, da je nastala obsežna ločna struktura imenovana istrsko potisno območje.

Del premikanja Mikroadrije proti Dinaridom se je kompenziral tudi s podrivanjem, to se je dogajalo in se še vedno dogaja, ob novonastalih reverznih prelomih, ob katerih se je krovninsko krilo dvignilo, paleogenske narivne ploskve v njem pa so se antiklinalno usločile. Cona podrivanja se v Istri na površju prekriva z mejo

underthrusting zone in Istra on the surface overlaps with the Dinarides boundary, so it makes sense to speak of a thrust-underthrust zone (Istra-Friuli Thrust-Underthrust Zone). On the surface the Sistiana and Kvarner Faults only extend as far as the mentioned thrust-underthrust zone, and further to the northeast they continue under the units of the Dinaric thrust structure, so only the lateral and vertical response of the movements along both faults under the thrust units is visible on the surface. In the extension of the Sistiana Fault, a relatively simple Sistiana Flexural Zone was formed, while in the extension of the Kvarner Fault a complicated and far more extensive Kvarner Flexural Zone in the form of a large sigmoid was formed. This lends the Kvarner Fault exceptional importance in the breakdown of the Microadria block, which is why we think it divides it into its Po and Adriatic segments. The Istra block is the farthest eastward-pushed part of the Microadria Po segment.

The Istra block has a hybrid structure, consisting of the autochthonous *sensu stricto* and the aborted Buje Thrust Sheet, which was part of the Dinarides during the thrusting period and became a connected part of the Microadria (autochthonous *sensu lato*) during the underthrusting period. The Karški rob – Mt. Hrušica Traverse, which lies in the Istra Pushed Area transversely to the Dinarides, was created as a result of the hybrid structure of the Istra block. Its geomorphologically most prominent deformation is Mt. Vremščica.

Mt. Vremščica is a transpressive anticline that rose from the levelled karst surface. Its formation is a challenge for the study of the geomorphology of karst areas.

The direction of the Sistiana Flexural Zone indicates the course of the Sistiana Fault in the seabed of the Gulf of Trieste from Sistiana to the west-southwest. According to such course, it can be assumed that the external boundary of the Mesozoic carbonate platform in the area of Lignano is transversally shifted along the Sistiana Fault. If so, the Sistiana Fault could represent an agreed boundary between the Friuli and Adriatic Mesozoic Carbonate Platforms.

The hydrographic network of Istra is specific and entirely subordinated to the deformations of the South Istra Pushed and North Istra Extrusion Wedges. The Classical Karst (territory between the Gulf of Trieste and the Ljubljana Marshes) lies entirely in the Istra Pushed Area, where the development of the hydrographic network is mainly related to the deformations of shortening caused by the Neogene to recent movement of Istra towards the Dinarides.

Dinaridov, zato je smiselno govoriti o narivno-podrivni coni (istrsko-furlanska narivno-podrivna cona). Sesljanski in Kvarnerski prelom segata na površju le do omenjene narivno-podrivne cone, naprej proti severovzhodu pa se nadaljujeta pod enotami dinarske narivne zgradbe, zato je na površju viden le bočni in vertikalni odziv premikov ob obeh prelomih pod narivnimi enotami. V podaljšku Sesljanskega preloma je nastala razmeroma enostavna sesljanska upogibna cona, v podaljšku Kvarnerskega preloma pa komplicirana in po dimenzijah dosti obsežnejša kvarnerska upogibna cona v obliki velike sigmoide. Ta daje Kvarnerskemu prelomu v blokovni razčlenitvi Mikroadrije izjemen pomen, zato menimo, da jo deli na njen padski in jadranski segment. Istrski blok je najdlje proti vzhodu potisnjeni del padskega segmenta Mikroadrije

Istrski blok ima hibridno zgradbo, sestavljen je iz avtohtona *sensu stricto* in abortirane Bujske narivne luske, ki je bila v obdobju narivanja del Dinaridov, v obdobju podrivanja pa je postala priključeni del Mikroadrije (avtohton *sensu lato*). Traverza Kraški rob - Hrušica, ki leži v istrskem potisnem območju prečno na Dinaride, je nastala zaradi hibridne zgradbe istrskega bloka. Njena geomorfološko najbolj izstopajoča deformacija je Vremščica.

Vremščica je transpresivna antiklinala, ki se je dvignila iz uravnanega kraškega površja. Njen nastanek je izziv za študij geomorfologije kraških območij.

Smer sesljanske upogibne cone nakazuje potek Sesljanskega preloma v podmorju Tržaškega zaliva od Sesljana proti zahodu-jugozahodu. Na podlagi tega je moč domnevati, da je zunanja meja mezozojske karbonatne platforme na območju Legnana (Legnano) prečno premaknjena ob Sesljanskem prelomu. Če je tako, bi Sesljanski prelom lahko predstavljal dogovorno mejo med Furlansko in Jadransko mezozojsko karbonatno platformo.

Hidrografska mreža Istre je specifična in povsem podrejena deformacijam južnoistrskega potisnega in severnoistrskega iztisnega klina. Klasični kras (ozemlje med Tržaškim zalivom in Ljubljanskim barjem) leži v celoti v istrskem potisnem območju, kjer je razvoj hidrografske mreže pretežno povezan z deformacijami krčenja prostora, ki jih je izzvalo neogensko do recentno pomikanje Istre proti Dinaridom.

Acknowledgement

We would like to thank Petra Jamšek Rupnik (GeoZS) for kindly providing artwork which we modified in order to create Figure 1. This study benefited from funding provided by the Slovenian Research and Innovation Agency in the scope of project Z1-3195 and program group P1-0011.

Zahvala

Avtorji se prijazno zahvaljujemo Petri Jamšek Rupnik (GeoZS), ki je delila grafično osnovo za izdelavo Slike 1. Raziskava je bila deloma finančno podprta s strani ARIS v okviru projekta Z1-3195 in programske skupine P1-0011.

References / Literatura

Blašković, I. & Aljanović, B. 1981: Mikrotektonski elementi kao osnova za model tektonske građe šireg područja Kvarnera = Microtectonic elements as a basis for tectonic model of the broader Kvarner area. Simp. Kompleksna naftno-geološka problematika podmorja i priobalnih djelova Jadranskog mora, Split, Zbornik radova (Proceedings), 87–100, Zagreb.

Blašković, I. 1991: Raspored uzdužnih, reversnih i normalnih rasjeda i konstrukcija oblika i dubina ploha podvlačenja = Disposition of the longitudinal, reverse and normal faults and the construction of the forms and depths of the underthrusting surfaces. Geol. vjesnik, 44: 247–256.

Blašković, I. 1999: Tectonics of Part of the Vinodol Valley with in the Model of the Continental Crust Subduction. Geol. Croat., 52/2: 153–189. https://doi.org/10.4154/GC.1999.13

Brancolini, G., Civile, D., Donda, F., Tosi, L., Zecchin, M., Volpi, V., Rossi, G., Sandron, D., Ferrante, G. M. & Forlin, E. 2019: New insights on the Adria plate geodynamics from the northern Adriatic perspective. Marine and Petroleum Geology, 109: 687-697. https://doi.org/10.1016/j.marpetgeo.2019.06.049

Busetti, M., Volpi, V., Barison, E., Giustiniani, M., Marchi, M., Ramella, R., Wardell, N. & Zanolla, C. 2010a: Meso-Cenozoic seismic stratigraphy and the tectonic setting of the Gulf of Trieste (Northern Adriatic). GeoActa SP, 3: 1–14.

Busetti, M., Volpi, V., Nicolich, R., Barison, E., Romeo, R., Baradello, L., Brancatelli, G., Giustiniani, M., Marchi, M., Zanolla, C., Wardell, N., Nieto, D. & Ramella, R. 2010b: Dinaric tectonic features in the Gulf of Trieste (Northern Adriatic Sea). Bollettino di Geofisica Teorica ed Applicata, 51: 117–128.

Busetti, M., Zgur, F., Romeo, R., Sormani, L. & Pettenati, F. 2012: Caratteristiche geologico-strutturali del Golfo di Trieste. Meeting Marina ISPRA, Roma, 25-26 ottobre 2012. At: Roma, 6-8 novembre 2001. Volume: Atti Ondine.

Busetti, M., Zgur, F., Vrabec, M., Facchin, L., Pelos, C., Romeo, R., Sormani, L., Slavec, P., Tomini, I., Visnovich, G. & Žerjal, A. 2013: Neotectonic reactivation of Meso-Cenozoic structures in the Gulf of Trieste and its relationship with fluid seepings. Proceedings of the 32nd Gruppo Nazionale di Geofisica della Terra Solida (GNGTS) Congress, Trieste 19-21, November 2013, 29–34.

Carulli, G. B. 2006: Carta geologica del Friuli Venezia Giulia 1:150 000. Regione autonoma F.V.G., Direzione centrale ambiente e lavori publici, Servizio geologico. S.E.L.C.A. Firenze.

Carulli, G. B. 2011: Structural model of the Trieste Gulf: A proposal. Journal of Geodynamics, 51/2–3: 156–165. https://doi.org/10.1016/j.jog.2010.05.004

Diercks, M., Grützner, C., Vrabec, M. & Ustaszewski, K. 2021: A model for the formation of the Pradol (Pradolina) dry valley in W Slovenia and NE Italy. Geologija, 64/1: 21–33. https://doi.org/10.5474/geologija.2021.002

Fontana, A., Mozzi, P. & Bondesan, A. 2008: Alluvial megafans in the Venetian–Friulian Plain (north-eastern Italy): Evidence of sedimentary and erosive phases during Late Pleistocene and Holocene. Quaternary International, 189: 71–90. https://doi.org/10.1016/j.quaint.2007.08.044

Fontana, A., Mozzi, P. & Bondesan, A. 2010: Late pleistocene evolution of the Venetian–Friulian Plain. Rendiconti Lincei, 21: 181–196. https://doi.org/10.1007/s12210-010-0093-1

Fontana, A., Mozzi, P. & Marchetti, M., 2014. Alluvial fans and megafans along the southern side of the Alps. Sedimentary Geology, 301: 150–171. https://doi.org/10.1016/j.sedgeo.2013.09.003

Jurkovšek, B., Toman, M., Ogorelec, B., Šribar, Lu., Drobne, K., Poljak, M. & Šribar, Lj. 1996: Formacijska geološka karta južnega dela Tržaško-Komenske planote 1:50 000 = Geological Map of the Southern Part of the Trieste-Komen Plateau 1:50 000. Geološki zavod

Ljubljana = Geological Survey of Ljubljana, Ljubljana.

Jurkovšek, B. 2010: Geološka karta severnega dela Tržaško-komenske planote 1:25 000 = Geological Map of the Northern Part of the Trieste-Komen Plateau 1:25 000. Geološki zavod Slovenije = Geological Survey of Slovenia, Ljubljana.

Korbar, T., Markušić, S., Hasan, O., Fuček, L., Brunović, D., Belić, N., Palenik, D. & Kastelic, V. 2020: Active Tectonics in the Kvarner Region (External Dinarides, Croatia) – An Alternative Approach Based on Fokused Geological Mapping, 3D Seizmological, and Shallow Seismic Imaging Data. Front. Earth Sci., 25 November. https://doi.org/10.3389/feart.2020.582797

Merkù P. 2006: Krajevno imenoslovje na slovenskem zahodu. Založba ZRC - ZRC SAZU, Ljubljana: 215 p.

Mlakar, I. 1969: Krovna zgradba idrijsko žirovskega ozemlja = Nappe structure of the Idrija-Žiri region. Geologija, 12: 5–72.

Morelli, C. & Mosetti, F. 1968. Rilievo sismico continuo nel Golfo di Trieste Andamento della formazione arenacea (Flysch) sotto il fondo marino della zona tra Trieste, Monfalcone e Grado. Bolletino della Societa' Adriatica di Scienze, 1: 42–57.

Novak, A., Šmuc, A., Poglajen, S. & Vrabec, M. 2020. Linking the high-resolution acoustic and sedimentary facies of a transgressed Late Quaternary alluvial plain (Gulf of Trieste, northern Adriatic). Marine Geology, 419: 106061. https://doi.org/10.1016/j.margeo.2019.106061

OGK: Osnovna geološka karta Jugoslavije 1:100.000 = Basic geological map of Yugoslavia 1:100.000. Listi / Sheets: Tolmin in Videm, Kranj, Gorica, Postojna, Trst, Ilirska Bistrica, Rovinj, Labin, Pula, Cres. Savezni geološki zavod, Beograd.

Petrič, M., Ravbar, N., Gostinčar, P., Krsnik, P. & Gacin, M. 2020: Vzpostavitev prosto dostopne GIS zbirke rezultatov sledenj toka podzemne vode in možnosti njene uporabe = Establishment of a freely accessible GIS database containing the results of groundwater tracing and possibilities of its use. Geologija, 63/2: 203–220. https://doi.org/10.5474/geologija.2020.017

Placer, L. 1994: O zgradbi Soviča nad Postojno = On the structure of Sovič above Postojna. Geologija, 37/38 (1994/95): 551–560. https://doi.org/10.5474/geologija.1995.020

Placer, L. 1980: Tektonski razvoj idrijskega rudišča. Disertacija, Univerza v Ljubljani, Fakulteta za naravoslovje in tehnologijo, Montanistika, Odsek za geologijo, 172 p., tab. 33.

Placer, L. 2003: Strukturno-geološke značilnosti trase avtoceste Klanec-Srmin na odseku 11,500 – 19,500 m. Arhiv Geološkega zavoda Slovenije.

Placer, L. 2004: Strukturno-geološke značilnosti trase avtoceste Klanec-Srmin na odseku 19,500 – 26,400 m. Arhiv Geološkega zavoda Slovenije.

Placer, L., Košir, A., Popit, T., Šmuc, A. & Juvan, G. 2004: The Buzet Thrust Fault in Istria and overturned carbonate megabeds in the Eocene flysch of Dragonja Valley (Slovenia). Geologija, 47/2: 193–198. https://doi.org/10.5474/geologija.2004.015

Placer, L. 2005: Strukturne posebnosti severne Istre = Structural curiosity of the northern Istria. Geologija, 48/2: 245–251. https://doi.org/10.5474/geologija.2005.020

Placer, L. 2007: Kraški rob. Geološki prerez vzdolž AC Kozina – Koper = Kraški rob (landscape term). Geologic section along the motorway Kozina – Koper (Capodistria). Geologija, 50/1: 29–44. https://doi.org/10.5474/geologija.2007.003

Placer, L., Vrabec, M. & Celarc, B. 2010: The bases for undertanding of the NW Dinarides and Istria Peninsula tectonics. Geologija, 53/1: 55–86. https://doi.org/10.5474/geologija.2010.005

Placer, L. & Jamšek, P. 2011: Ilirskobistriški fosilni plaz – mesto na plazu = The Ilirska Bistrica fossil landslide – The town on the landslide. Geologija, 54/2: 223–228. https://doi.org/10.5474/geologija.2011.017

Placer, L. 2015: Simplified structural map of Kras. Kras (Slovene), Carso (Italian) = Geographical unit. Geologija, 58/1: 89–93. https://doi.org/10.5474/geologija.2015.008

Placer, L., Mihevc, A. & Rižnar, I. 2021a: Tectonics and gravitational phenomena (Nanos, Slovenia). Geologija, 64/1: 35–63. https://doi.org/10.5474/geologija.2021.003

Placer, L., Jamšek Rupnik, P. & Celarc, B. 2021b: Sistiana Fault and the Sistiana Bending Zone. Geologija, 64/2: 221–252. https://doi.org/10.5474/geologija.2021.013

Poljak, M. 2007: Strukturno-tektonska karta Slovenije 1:250 000 = Structural-Tectonic Map of Slovenia 1:250 000. Geološki zavod Slovenije = Geological Survey of Slovenia, Ljubljana.

Rižnar, I., Koler, B. & Bavec, M. 2007: Recentna aktivnost regionalnih geoloških struktur v zahodni Sloveniji = Recent activity of the

regional geologic structures in western Slovenia. Geologija, 50/1: 111-120. https://doi.org/10.5474/geologija.2007.009

Ronchi, L., Fontana, A., Novak, A., Correggiari, A. & Poglajen, S. 2023: Late-Quaternary Evolution of the Semi-Confined Alluvial Megafan of Isonzo River (Northern Adriatic): Where the Fluvial System of the Southern Alps Meets the Karst. Geosciences, 13/5: 135. https://doi.org/10.3390/geosciences13050135

Šebela, S. 2005: Tektonske zanimivasti Pivške kotline = Tectonic sights of the Pivka Basin. Acta carsologica, 34/3: 566-581.

Špelić, M., Del Ben, A. & Petrinjak, K. 2021: Structural setting and geodynamics of the Kvarner area (Northern Adriatic). Marine and Petroleum Geology 125C, 104857. Project: GEOSEK-VA - Geological and seismological aspects of geodynamics in Kvarner area - unveiling of the Kvarner fault. https://doi.org/10.1016/j.marpetgeo.2020.104857

Trobec, A., Šmuc, A., Poglajen, S. & Vrabec, M. 2017: Submarged and buried Pleistocene river channels in the Gulf of Trieste (Northern Adriatic Sea): Geomorphic, stratigraphic and tectonic interfaces. Geomorphology, 286: 110–120. https://doi.org/10.1016/j.geomorph.2017.03.012

Trobec, A., Busetti, M., Zgur, F., Baradello, L., Babich, A., Cova, A., Gordini, E., Romeo, R., Tomini, I., Poglajen, S., Diviacco, P. & Vrabec, M. 2018: Thickness of marine Holocene sediment in the Gulf of Trieste (northern Adriatic Sea). Earth System Science Data, 10: 1077–1092. https://doi.org/10.5194/essd-10-1077-2018

Vrabec, M., Pruner, P., Zupan Hajna, N., Mihevc, A. & Bosak, P. 2018: Unraveling neotectonic vertical-axis rotations in the AdriaEurasia collision zone: paleomagnetic data from Pliocene-Quaternary cave sediments (Slovenia). In: Ustaszewski, K., Grützner, Ch. & Navabpour, P. (eds.): TSK Jena 2018. 1st ed. Jena: Friedrich Schiller University Jena, Institute of Geological Sciences: 134 p.

Vrabec, M. & Rožič, B. 2014: Strukturne in sedimentološkr posebnosti obalnih klifov. In: Rožič, B., Verbovšek, T. & Vrabec, Mi. (eds.): Povzetki in ekskurzije = Abstracts and field trips, 84–91, 4. Slovenski geološki kongres, Ankaran, 2014.

Weber, J., Vrabec, M., Stopar, B. Pavlovčič Prešeren, P. & Dixon, T. H. 2006: The PIVO-2003 experiment: A GPS study of Istria peninsula and Adria microplate motion, and active tectonics in Slovenia. In: Pinter, N., Gyula, G., Weber, J., Stein, S. & Medak, D. (eds.): The Adria Microplate: GPS Geodesy, Tectonics and Hazards, 305-320. Nato Science Series IV, Earth and Environmental Sciences, 61. https://doi.org/10.1007/1-4020-4235-3_21

Weber, J., Vrabec, M., Pavlovčič Prešeren, P., Dixon, T., Jiang, Y. & Stopar, B. 2010: GPS-derived motion of the Adriatic microplate from Istria Peninsula and Po Plain sites, and geodynamic implications. Tectonophysics, 483/3–4: 214–222. https://doi.org/10.1016/j.tecto.2009.09.001

Žitko, S. (ur.) 1990: Kraški rob in Bržanija (zbornik). Pokrajinski muzej Koper, 152 p.

GEOLOGIJA 66/1, 73-85, Ljubljana 2023

https://doi.org/10.5474/geologija.2023.002

Geološka spremljava poskusnega odkopa uranove rude na Žirovskem vrhu

Geological control of trial excavation of Uranium ore in Žirovski vrh

Franci ČADEŽ

Gorje 7, SI-5282 Cerkno, e-mail: fcadez@gmail.com

Prejeto / Received 28. 12. 2022; Sprejeto / Accepted 20. 3. 2023; Objavljeno na spletu / Published online 4. 8. 2023

Ključne besede: uranova ruda, poskusno odkopavanje, grödenske klastične kamnine, Žirovski vrh
Key words: uranium ore, trial excavation, Val Gardena clastic rocks, Žirovski vrh

Izvleček

Leta 1981–1983 je bilo na Rudniku Žirovski vrh pred pričetkom redne proizvodnje izvedeno poskusno odkopavanje uranove rude za preverjanje metod geološke in radiometrične kontrole ter tehničnih metod pridobivanja. Poskusni odkop je bil v bloku 1, na skrajnem severozahodnem delu rudišča v zgornji gubi dvojne S strukture. V tem bloku se je orudenje nahajalo samo v horizontu sivega peščenjaka debeline 20–30 m. Z geološko spremljavo odkopavanja smo potrdili, da so bili peščenjaki odloženi v sekvencah debelih od par dm do več kot 2 m. Sekvenca je običajno pričenjala z debelozrnatim peščenjakom, večkrat so bili na bazi prisotni še klasti kremena in muljevca. Navzgor je debelozrnat peščenjak pogosto prehajal v srednjezrnatega, redkeje pa še v drobnozrnatega in meljevec. V peščenjakih je bila značilna prisotnost organskih drobcev, ki so v diagenezi ustvarjali redukcijsko okolje v katerem se je iz podtalnice izločal uran. Najpogosteje se je orudenje nahajalo v debelozrnatih peščenjakih, običajno v debelejših sekvencah. Orudenje se je zato pojavljalo v več nivojih debelih navadno pod 1m, kjer se je združevalo je skupna debelina presegla tudi 5 m. Dolžina sklenjenega orudenja v vzdolžni smeri je znašala do 150 m, širina od nekaj metrov do več kot 40 m. V vmesnih prekinitvah orudenja smo opazovali, da so peščenjaki iz temnosive in sive barve prehajali v svetlosive in zelenosive, ki so bili le siromašno orudeni ali jalovi. V vzdolžni smeri se je tak prehod zgodil med prerezi P-35 in P-35a, kjer se je tudi zaključilo odkopavanje. V jami sta bila raziskana še prereza P-36 in P-37, kjer pa se je pojavljal pretežno zelenosiv peščenjak z le redkimi lečami siromašnega orudenja. S površinskimi vrtinami sta bila dlje proti zahodu raziskana tudi še dva prereza oddaljena 1,3 in 2,8 km od jamske zgradbe. V teh vrtinah je bilo ugotovljeno nastopanje sivih in zelenosivih peščenjakov z zelo redkimi sledovi orudenja, ki so se menjavali z bolj drobnozrnatimi različki (muljevci), ostanki organske snovi pa so bili v njih zelo redki. Blok 1 je bil zato mejni blok na SZ strani rudišča, predviden za pridobivanje.

Abstract

In 1981-1983, before the start of full production, trial mining of uranium ore was carried out at the Žirovski vrh mine to test the methods of geological and radiometric control as well as the technical methods of extraction. The trial excavation was done in block 1, in the extreme NW part of the mine in the upper fold of the double S structure. In this block, the ore deposits bodies were found only in the horizon of grey sandstone about 20–30 m thick. Geological monitoring of the excavation confirmed that the sandstones were deposited in sequences from a few dm to more than 2 m thick. The sequence usually graded bed started with coarse-grained sandstone, with pebbles of quartz and mudstone occasionally present at the base. Upwards, coarse-grained sandstone often passed into medium-grained, and more rarely into fine-grained sandstone and siltstone. The sandstones were characterized by the presence of organic fragments, which created an anoxic environment during diagenesis and that in turn enabled uranium to precipitate from the groundwater and concentrate in the host rock. Most often, ore bodies were found in coarse-grained sandstones, usually in several sedimentary sequences. As such, ore bodies appear in several sequences, usually under 1 m thick. In some places ore bodies can join together, exceeding 5 m. The length of the uninterrupted ore body in the longitudinal direction was up to 150 m, the width ranges from a few meters to more than 40 m. In the intermediate areas where the ore body is interrupted, we observed that the sandstones changed from dark grey and grey to light grey and greenish grey. These sandstones were usually barren or contained only small concentrations of uranium. In the longitudinal direction, such a transition took place between cross-sections P-35 and P-35a, where excavation was completed. Cross-sections P-36 and P-37 were also investigated inside the mine, where predominantly greenish-grey sandstone with only rare lenses of poor uranium concentrations appeared. Further to the west, two cross-sections 1.3 and 2.8 km from the mine area were also explored with surface boreholes. Grey and greenish-grey sandstones with very rare remains of organic matter and very rare traces of mineralisation were found in these boreholes, alternating with siltstones. Block 1 is therefore considered the boundary block on the NW side of the mine, intended for extraction.

Uvod

Na severovzhodnih pobočjih Žirovskega vrha je bila leta 1960 odkrita uranska mineralizacija znotraj grödenskih klastičnih sedimentnih kamnin srednje permske starosti. Po skoraj dveh desetletjih raziskovanj je bil leta 1977 izdelan Investicijski program in naslednje leto sprejeta odločitev o izgradnji rudnika. Leta 1981 je bil izdelan Glavni rudarski projekt (Rudis Trbovlje) in v njegovem sklopu še Rudarski projekt poskusnega odkopavanja (Spasojević, 1981). Z izdelavo odkopnih priprav se je začelo še istega leta, se nadaljevalo s poskusnim odkopavanjem, ki se je zaključilo v letu 1983. S poskusnim odkopavanjem se je poleg rudarsko tehnoloških možnosti pridobivanja preverjalo tudi postopke načrtovane geološke in radiometrične spremljave. V tem članku podajamo ugotovljene značilnosti geološke sestave in z njo povezanega orudenja.

Kratek pregled predhodnih raziskav in poskusnih odkopavanj

Rudišče so po odkritju leta 1960 prvih 10 let raziskovali strokovnjaki Geoinstituta iz Beograda. Poleg površinskih radiometričnih raziskav so že v letu 1961 začeli z vrtanjem površinskih vrtin in izdelavo prvega podkopa. Naprej so raziskave potekale vzporedno. S površine so vrtali globoke strukturne vrtine s katerimi se je ugotavljalo prostorsko razprostiranje grödenskih plasti in prisotnost uranskega orudenja. Z detajlnimi raziskavami v jami so iz vzdolžne smerne proge izdelovali prečnike, iz njih pa izvajali strukturno in udarno vrtanje v mreži 50 × 50 m oziroma 50 × 5 m. S strukturnimi vrtinami so ugotavljali razvoj grödenskih plasti v prostoru in znotraj njih predvsem položaj orudenih plasti. Z udarnimi vrtinami pa so določali rudne intervale, ki so jih povezovali med seboj v rudna telesa pri čemer pa so bili velikokrat v dilemah, katere intervale povezovati med seboj. Rudne intervale se je določalo le z radiometričnimi meritvami, enako kot tudi v progah, kjer so ga našli. Menili so, da se rude na izgled ne da ločevati od jalovine. Sklenili so, da bodo do boljšega poznavanja in povezovanja orudenja v prostoru prišli le s poskusnim odkopavanjem.

Med leti 1964 in 1968 so izdelali dva poskusna odkopa na zgornjem obzorju 580, ki je bilo takrat edino razvito. Skupno so pridobili preko 10.600 t rude s povprečno vsebnostjo nekaj čez 1000 g U/t (0,1 %). Mejo ruda-jalovina so postavili pri 300 g U/t (0,03 %), kar je obveljalo za celotno obdobje delovanja rudnika. Njihova bistvena ugotovitev je bila, da orudenje načeloma sledi plastovitosti, njegova debelina pa da je zelo spremenljiva. Zaradi zapletenosti orudenja so menili, da ima oblika orudenja na prerezih vrtin le statistično vrednost (Omaljev, 1967a, 1969).

V letu 1970 je dotedanjo rudarsko in geološko ekipo Geoinstituta zamenjal Geološki zavod iz Ljubljane (GZL). Nadaljevali so s konceptom raziskav, ki so ga razvili Beograjčani. Ker pa se je ekipa zamenjala v celoti so poskusno odkopavanje v letih 1971–1975 izvedli tudi delavci in strokovnjaki GZL. S tem, ko so z odkopavanjem sledili orudenju, so pridobili praktična znanja o obliki in naravi orudenja, istočasno pa že tudi rudo za tehnološke teste njene predelave in preverjanje možnosti radiometričnega separiranja. Skupno je bilo v tej fazi na 5 različnih lokacijah na spodnjih dveh obzorjih 430 m in 480 m pridobljeno 5.900 t rude z vsebnostjo 1400 g U/t. Tudi tu so ugotavljali, da orudenje večinoma sledi plastovitosti vendar so navajali še primere prečnega poteka orudenja glede na plastovitost, kar pa je bila največkrat posledica dejstva, da v tem času še niso poznali strukture dvojne gube. V orudenih delih so prav tako opazili pomembno prisotnost organske snovi, hkrati pa so menili, da se ob orudenju poveča tudi delež karbonatov (Florjančič, A.P. et al., 1973).

Poskusno odkopavanje v letih 1981–1983

Z ustanovitvijo Rudnika urana Žirovski vrh v letu 1976 je ta postopoma prevzemal tudi izdelavo rudarskih in raziskovalnih del od Geološkega zavoda. V letu 1981 se je pričelo s poskusnim odkopavanjem v bloku 1, ki leži na skrajnem severozahodnem delu rudišča. Po njegovem zaključku leta 1983 se je nadaljevalo z rednim odkopavanjem, katerega obseg se je količinsko in prostorsko postopno povečeval tako, da je prav v letu njegovega prenehanja dosegel polno načrtovano proizvodnjo. V prvem polletju leta 1990 je bilo namreč odkopano 81.000 t uranove rude, kar je bilo polovica načrtovane letne proizvodnje 160.000 t. S poskusnim odkopavanjem v letih 1981–1983 se je pridobilo 36.542 t izkopane rude z vsebnostjo 827 g U_3O_8/t oziroma 30,218 t U_3O_8. Hkrati se je pridobilo še 10.427 t revne rude z vsebnostjo 220 g U_3O_8/t in 2,328 t U_3O_8. Ta izkopana ruda je bila pridobljena iz 24.202 t radiometrično izmerjene rude, ki je imela vsebnost 1280 g U_3O_8/t. Zaradi razredčenja radiometrično izmerjene rude z jalovino pri odkopavanju se je njena vsebnost v izkopani rudi znižala, količina pa povečala. S koncem sedemdesetih let se je s pričetkom izračunavanja zalog za potrebe Investicijskega programa, vsebnosti začelo prikazovati v g U_3O_8/t. Takrat se je tudi rez jalovina-ruda začel podajati v isti obliki, kar je predstavljalo delno znižanje vrednosti glede

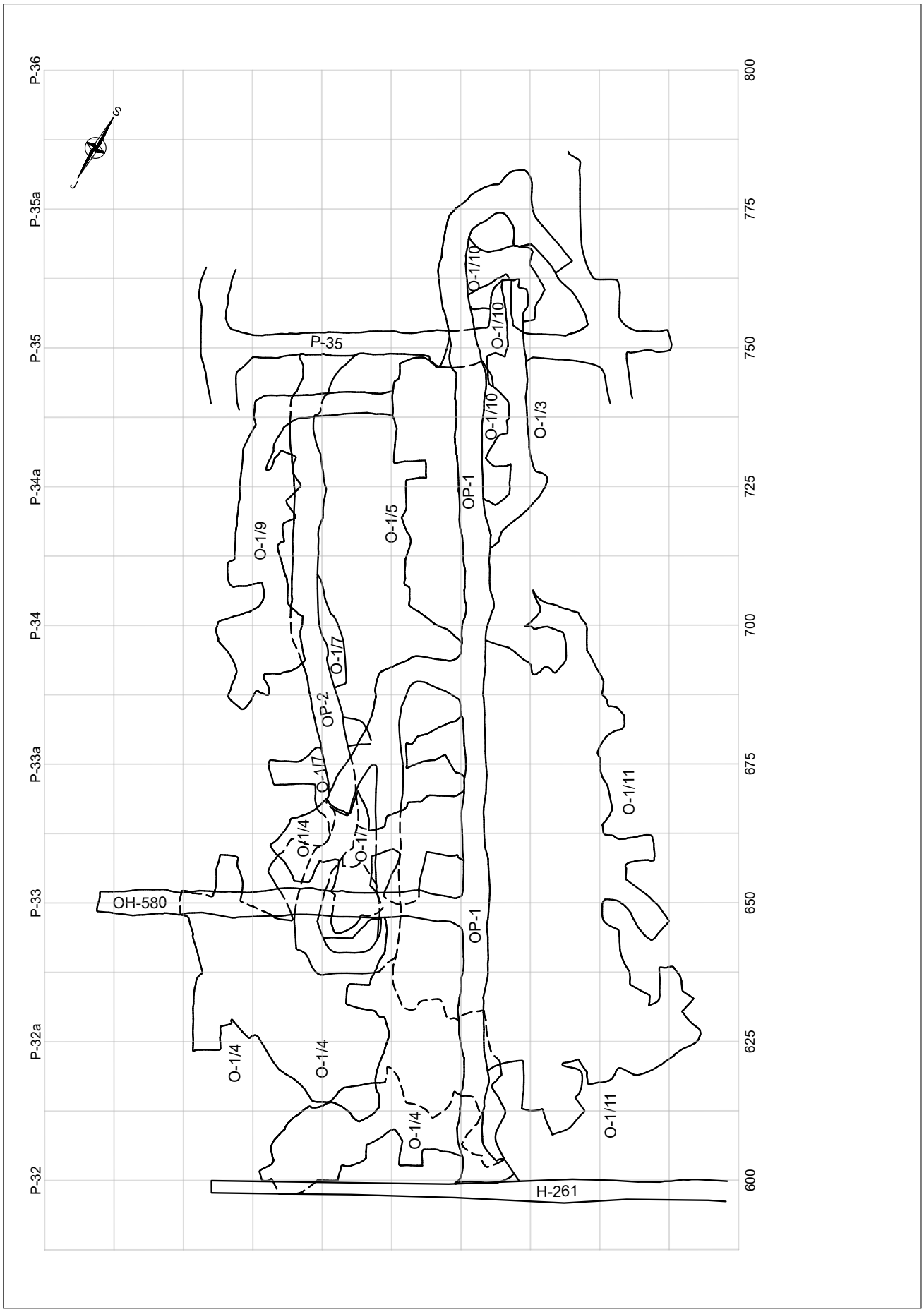

Sl. 1. Tlorisna karta odkopnih priprav in odkopov.
Fig. 1. Map-view of excavation areas.

na predhodno obliko podajanja koncentracij v g U/t (1 g U_3O_8 = 0,848 g U).

Po Rudarskem projektu (Spasojević, 1981) sta se najprej izdelali dve odkopni pripravi OP-1 in OP-2 ter zračilni prečnik OH-580. Te priprave so se navezovale na obstoječe jamske proge in z njimi se je rudonosno plast odprlo po dolžini, širini in višini (sl. 1). OP-1 se je pričela iz prečnika H-261 na obzorju 580 in prerezu P-32 ter se spuščala do višine 560 m v prerezu P-35a, kjer se je zaključila v prečniku P-35. Druga priprava je začenjala v tem istem prečniku le bolj jugozahodno in se dvigovala po orudeni plasti ter se med prerezoma P-33a in P-34 priključila na prvo. Odkopne priprave so bile locirane tako, da so v največji meri presekala predhodno raziskana orudenja. Iz teh odkopnih priprav so se potem izdelovali odkopi levo in desno do koder se je orudenje širilo (sl. 1).

Postopki geološke in radiometrične kontrole odkopavanja

Za orudenje z uranom je značilno, da ga s prostim očesom ne vidimo, ker je podobne sive barve kot prikamnina. Zato se njegovo prisotnost in količino ugotavlja z radiometričnimi meritvami. Tako pri izdelavi odkopnih priprav kot tudi pri poznejšem odkopavanju smo izvajali delovne operacije s katerimi smo ugotavljali obliko in kvaliteto orudenja na vsakokratnem čelu in pozneje v fazi miniranja, nakladanja in odvoza na deponijo (Lavrenčič et al., 1984). Ti postopki so vključevali:

- geološko kartiranje čela,
- radiometrično izmero čela,
- karotažo minskih vrtin,
- odločitev o obliki selektivnega odstrela,
- radiometrično izmero izkopnine.

Z geološkim kartiranjem smo ugotavljali barvo in zrnavost klastičnih kamnin, prisotnost organske snovi, sedimentne teksture in tektonske značilnosti. Radiometrična izmera se je izvajala z diferencialnimi merilniki gama sevanja, ki so pokazali na površinsko obliko orudenja na čelu. S tem se je lahko prilagajalo lego zalomnih vrtin in s tem obliko selektivnega odstrela. S karotažo minskih vrtin, kjer smo uporabljali merilnike z Geiger-Müllerjevo sondo, se je potem ugotavljalo obliko in kvaliteto orudenja po celotni globini odstrela (običajno 1,4 m). Podatki o vsebnosti urana iz minskih vrtin so služili za določanje vsebnosti radiometrično izmerjene rude in vsebnosti rudnega in jalovinskega odstrela ter določanje razredčenja in odkopnih izgub. Vsa izkopanina rudnega ali jalovinskega odstrela se je po izvozu iz jame na kamionih še enkrat radiometrično izmerila s pikanjem s T sondo in merjenjem v radiometričnih vratih, pozneje pa samo še v radiometričnih vratih, kjer se je vsak kamion še stehtal. S tem je bila vzpostavljena celovita evidenca odkopavanja od čela v jami do izkopanine na deponijah.

Geološke razmere pri odkopavanju

Blok 1, kjer se je izvajalo zadnje poskusno odkopavanje, leži na skrajnem severozahodnem delu rudišča. S predhodnimi raziskavami, od kartiranja raziskovalnih prog do raziskovalnih vrtin, je bilo ugotovljeno, da bo poskusno odkopavanje potekalo v zgornji gubi dvojne S strukture rudišča, ki sta jo dokazala Lukacs in Florjančič (1974). Orudenje je vezano le na najstarejši, sivi del grödenske formacije, kar so ugotavljali tako geologi Geoinstituta kot Geološkega zavoda. Budkovič (1980) jo je poimenoval siva formacija za razliko od višje ležečih pretežno rdeče obarvanih klastitov, ki jih je uvrstil v rdečo formacijo. Novejšo razčlenitev grödenskih klastitov je pozneje izdelal Mlakar, ki je celotno grödensko formacijo razdelil na 6 členov, od katerih je najstarejši Brebovniški člen, ki je ekvivalent Budkovičeve sive formacije (Mlakar & Placer, 2000). Najuporabnejšo nadaljnjo razčlenitev sive formacije oziroma Brebovniškega člena za potrebe rudarjenja je podal Budkovič (1980). Na osnovi različne zrnavosti in barve je sivi del grödenske formacije razdelil na 10 horizontov, orudenja z uranom pa nastopajo v 4., 5., 6. in 8. horizontu. Skupaj z vmesnim jalovim 7. horizontom tvorijo rudonosno cono (Budkovič, 1980). V bloku 1 se je orudenje nahajalo in odkopavalo le v 6. horizontu, v ostalih horizontih rudonosne cone orudenja tu ni bilo ali pa je bilo presiromašno za izkoriščanje. Iz raziskanih prečnih prerezov v bloku 1 izhaja, da je debelina 6. horizonta v bloku 1 znašala med 20 in 30 m (sl. 2 in sl. 3).

Pri izdelavi odkopnih priprav smo ugotovili, da so te skorajda v celoti potekale znotraj rudonosnega peščenjaka 6. horizonta, le OP-1 se je v spodnjem delu, kjer se je navezala na prečnik P-35 pričenjala še v talninskih rdečkastih in zelenkastih peščenjakih in konglomeratih, ki pripadajo 5. horizontu (sl. 2). Zračilni prečnik OH-580 je v začetnem delu, kjer se je pričenjal v OP-1, potekal v orudenem peščenjaku, v drugi polovici pa je nastopal najprej tanek horizont rdečkastih in zelenkastih peščenjakov in meljevcev (7. horizont), sledili so jim zelenosivi srednje in debelozrnati peščenjaki (8. horizont) in na koncu zopet zeleni in rdeči peščenjaki in meljevci, ki pa so bili že del 9. horizonta (sl. 3). Peščenjaki 8. horizonta v tem bloku niso vsebovali ekonomsko zanimivih vsebnosti urana.

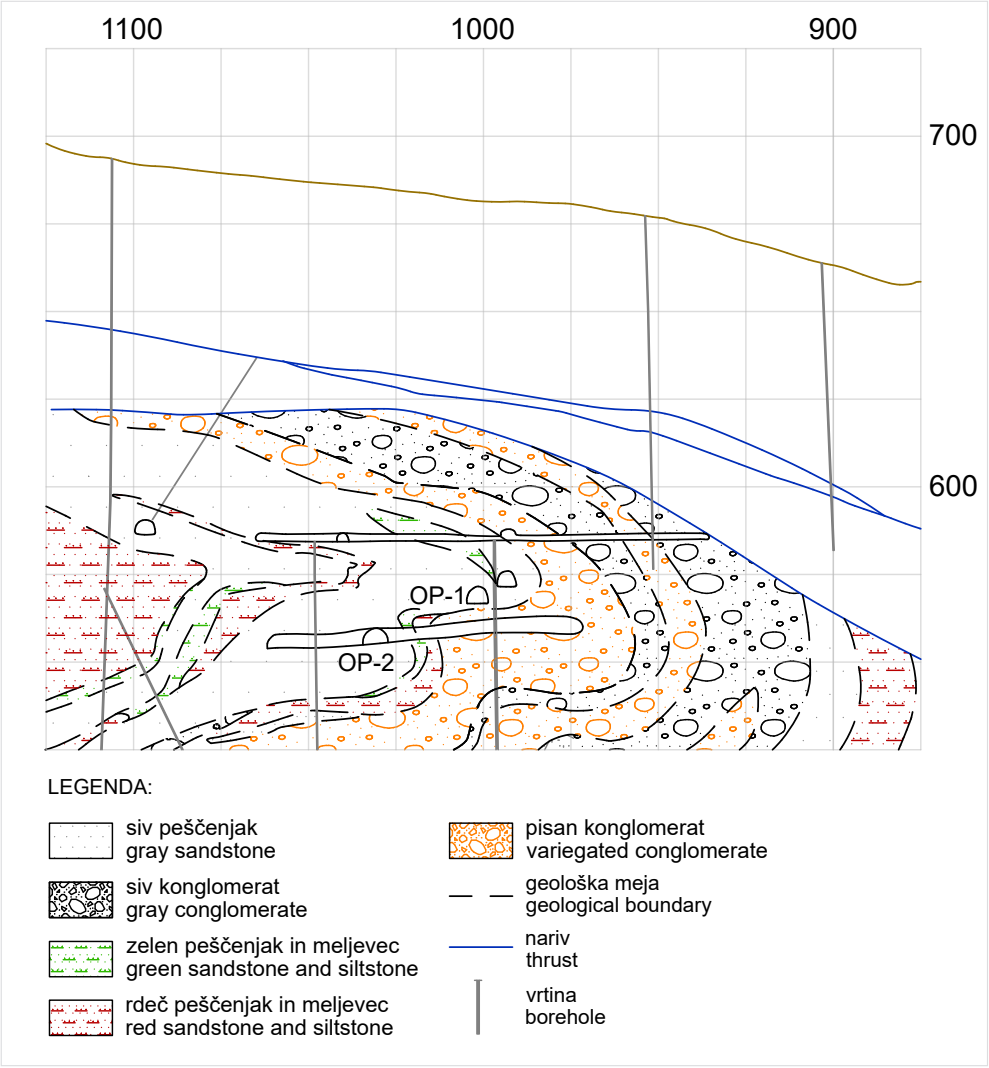

Sl. 2. Geološki prečni prerez P-35.

Fig. 2. Geological cross-section P-35.

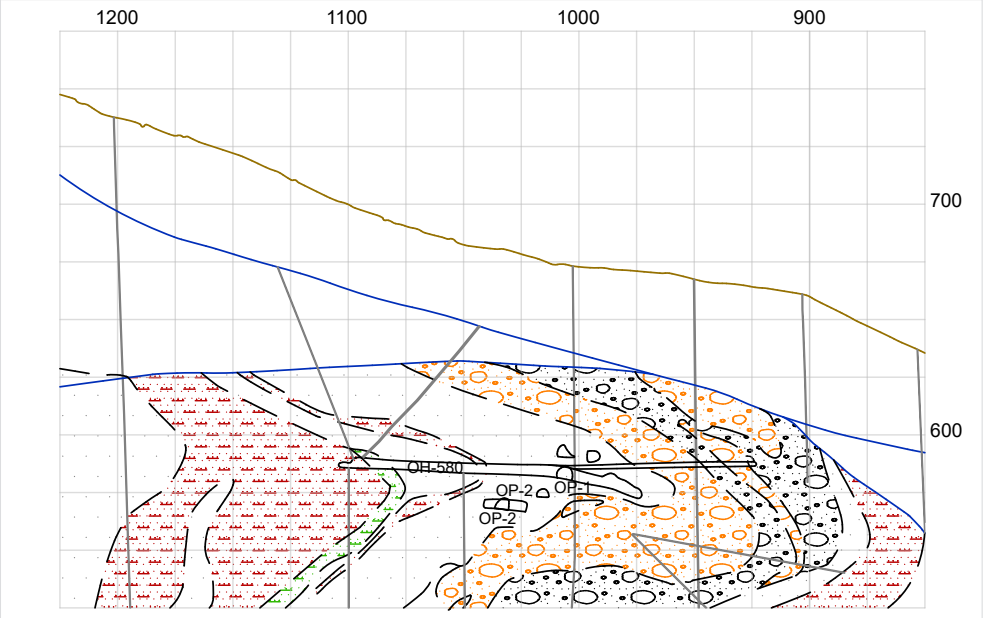

Legenda na sliki 2.

Legend on Figure 2.

Sl. 3. Geološki prečni prerez P-33.

Fig. 3. Geological cross-section P-33.

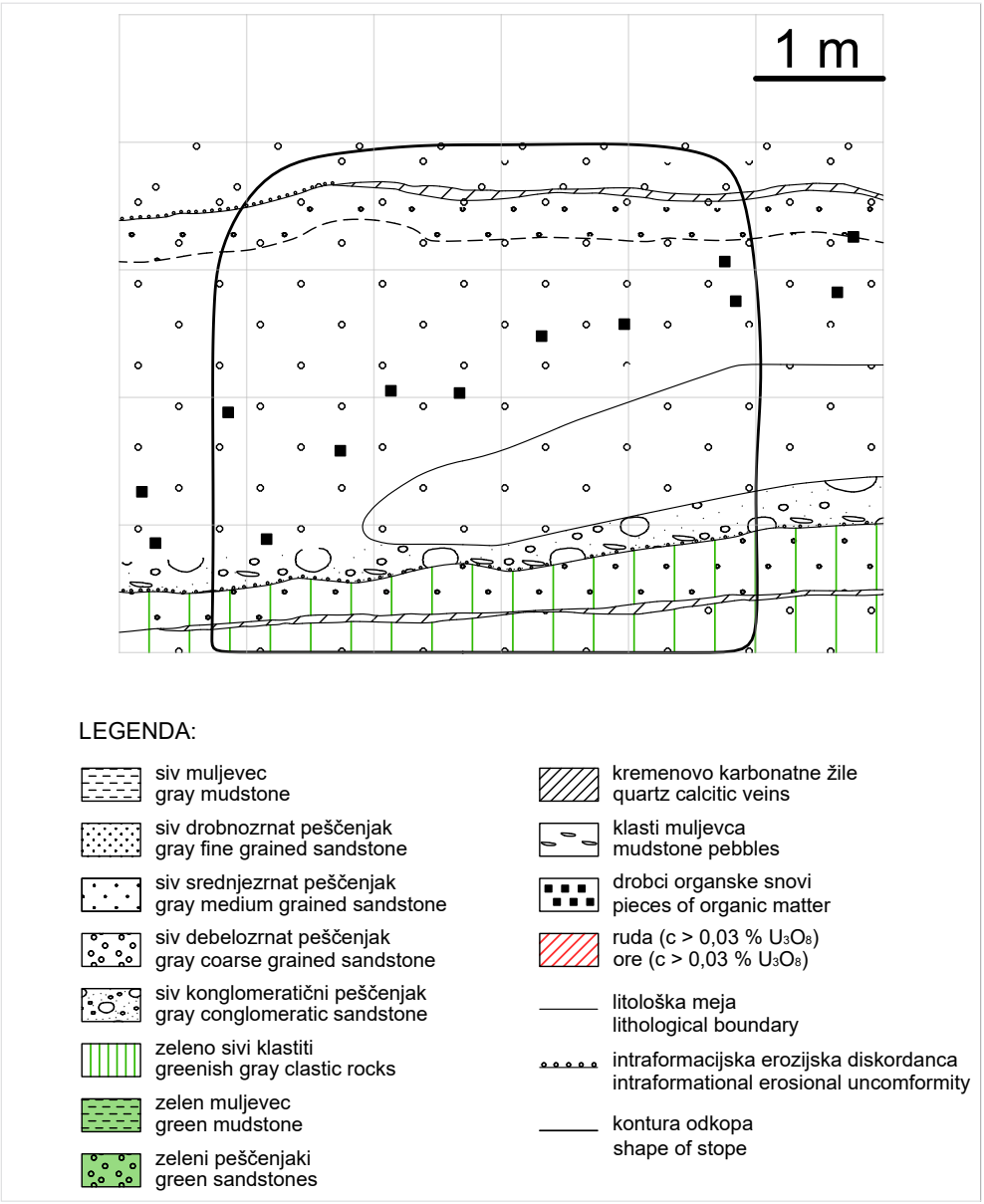

Sl. 4. Horizontalna tekstura v peščenih sekvencah (O-1/5-2, 14. odstrel).

Fig. 4. Horizontally bedding sequences (O-1/5-2, 14th blasting).

Pri kartiranju čel smo ugotavljali sedimentne teksture, ki so značilne za rečne sisteme prepletajoče reke (braided river) in jih je podrobno razčlenil Miall (1978, 2014), pozneje pa jih je v svoji disertaciji prav za klastite z Žirovskega vrha opisal in poimenoval Skaberne (1995). Pri kartiranju čel smo največkrat opazovali horizontalno teksturo (sl. 4), kjer so plasti v sekvencah oziroma same sekvence med seboj približno vzporedne. Večkrat je bila prisotna še masivna tekstura (sl. 5), kjer

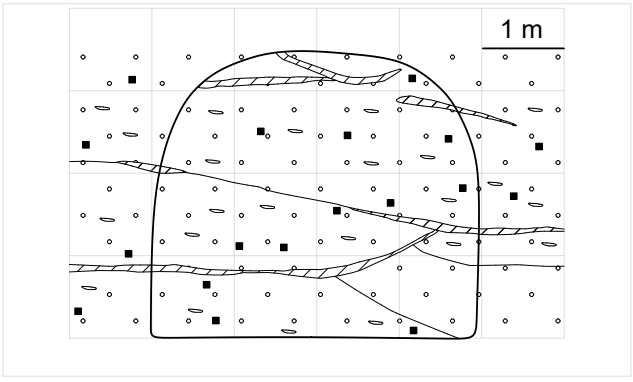

Sl. 5. Temnosiv oruden peščenjak z masivno teksturo (OP-1, 30. odstrel).

Fig. 5. Dark grey mineralised sandstone with massive structure (OP-1/ 30th blasting).

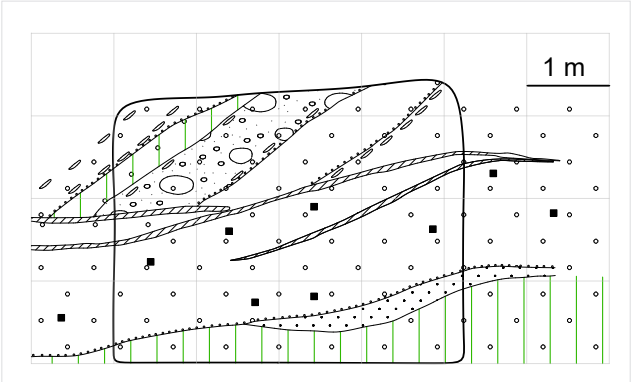

Sl. 6. Koritasta navzkrižna tekstura (O-1/11-2, 111. odstrel).

Fig. 6. Trough cross-bedding (O-1/11-2, 111st blasting).

plastovitost ni bila opazna in je nastopala le ena frakcija klastitov. Najredkeje smo srečali planarno in koritasto navzkrižno teksturo (sl. 6). Razne oblike laminacij, ki so značilne za bolj drobnozrnate sedimente (Skaberne, 1995), na odkopih nismo zasledili. Orudenje se je pojavljalo znotraj 6. horizonta, ki ga je v posameznem odkopnem čelu višine 3,5 do 4,5 m sestavljalo več sekvenc, največkrat 2–4 sekvence, kjer so te bile vidne. Debelina posameznih sekvenc je znašala od nekaj dm do več kot 2 m. Prevladujoči litološki različek v njih je bil sivi debelozrnati peščenjak. V njem so bili na začetku sekvence često prisotni klasti muljevca in karbonatnih konkrecij, redkeje drobni prodniki kremena tako, da je sekvenca lahko pričenjala z intraformacijskim konglomeratom oziroma konglomeratičnim peščenjakom. Na debelozrnatem peščenjaku je bil pogosto odložen še srednjezrnat, redkeje pa tudi drobnozrnat peščenjak in muljevec. Meje med temi litološkimi različki v isti sekvenci so bile postopne, med sekvencami pa navadno ostre, na njihovem stiku so bile pogosto razvite še medplastovne kremenovo karbonatne žile. Najlepše so bile te žile razvite v temenih gub, kjer so medplastovne spremljale še prečne karbonatno kremenove žile (sl. 7). Oba sistema žil sta nastala postdiagenetsko, v fazi gubanja in narivanja (Dolenec, 1983).

Na prehodu iz zelenega in rdečega konglomerata (5. horizont) se je 6. horizont pričenjal z zelenosivim debelozrnatim peščenjakom, ki pa je ponekod že takoj nad kontaktom postal temneje siv in oruden (sl. 8). Orudenje je bilo najpogosteje vezano na debelozrnate peščenjake, kjer se je pojavila organska snov ali povečal njen delež (sl. 9). Odkopna priprava OP-1 se je od prereza P-35a, kjer se je pojavil peščenjak z orudenjem proti prerezu P-32 dvigala in v splošnem sledila plastovitosti. Posamezne sekvence smo tako lahko sledili po dolžini na razdalji več 10 do preko 100 m, ko so se izklinjale ali zavile iz odkopnega profila. Predvsem v prevladujočem debelozrnatem peščenjaku je bilo pomembno pojavljanje organske snovi. Ta je nastopala v obliki drobnih delcev dimenzij do nekaj mm redkeje do več decimetrskih leč, ki so predstavljale ostanke drevesnih debel in ki so bili v diagenezi mineralizirani ali karbonizirani. Med mineraliziranimi različki so bili najbolj razširjeni okremeneli rastlinski ostanki, pojavljale pa so se tudi psevdomorfoze rudnih mineralov (Omaljev, 1967; Drovenik et al., 1980; Dolenec, 1983; Skaberne, 1995). Analiza organske snovi je pokazala, da je ta prisotna kot antracit in semiantracit s prehodom v grafit (Hadži-Popović, 1962). Povprečna vsebnost organske snovi v vzorcih iz sive grödenske formacije je znašala 0,14 %, v orudenih peščenjakih pa se je njena vsebnost povečevala (Drovenik et al., 1980). Omaljev je za vzorce, ki so jih odvzeli v prvem obdobju raziskav navajal povprečno vsebnost organske snovi 0,26 %, pri tem je še ločeval topno in netopno obliko. Orudenje z uranom je bilo bolj pogosto v peščenjakih s povečanim deležem organske snovi, še posebej tistih s topno obliko (Omaljev, 1982).

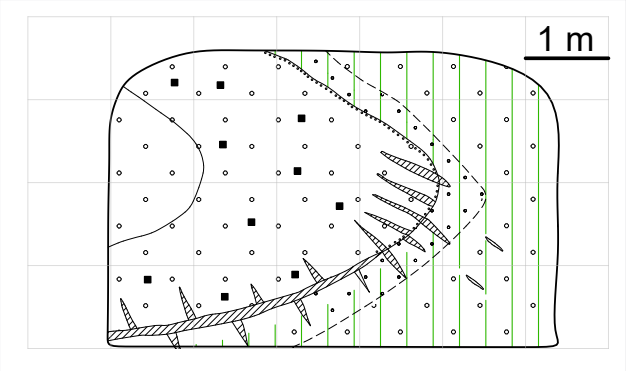

Sl. 7. Medplastovna in prečne kalcitno kremenove žile v peščenjaku (O-1/11-2).
Fig. 7. Interbedded and cross-bedded calcite-quartz veins in sandstone (O-1/11-2).

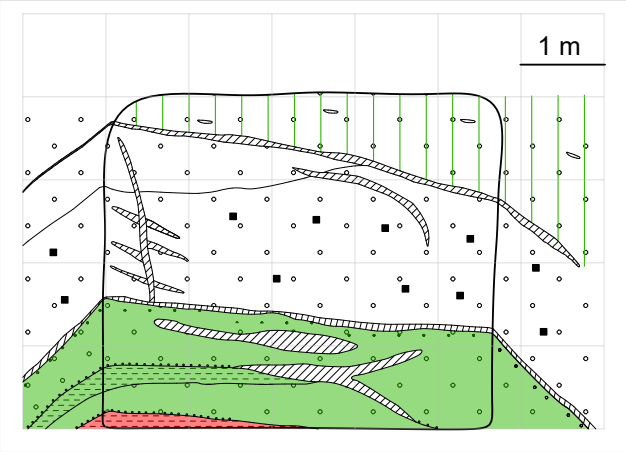

Sl. 8. Orudeni peščenjak nad pisanimi klastiti (O-1/10-1, 2. odstrel).
Fig. 8. Mineralised sandstone above variegated conglomerate (O-1/10-1, 2nd blasting).

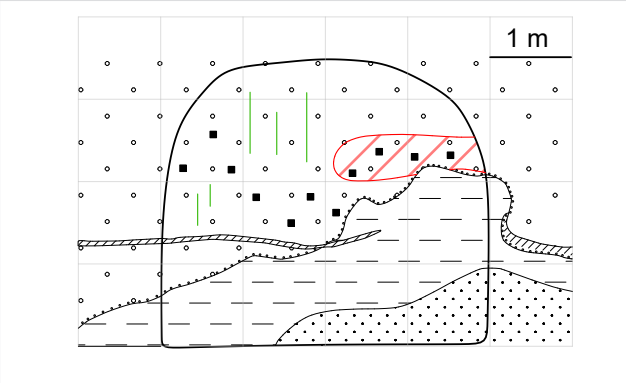

Sl. 9. Začetek orudenja ob povečani prisotnosti organske snovi (OP-1 zg., 18. odstrel).
Fig. 9. Beginning of higher ore concentrations coincides with higher content of organic matter (OP-1, 18th blasting).

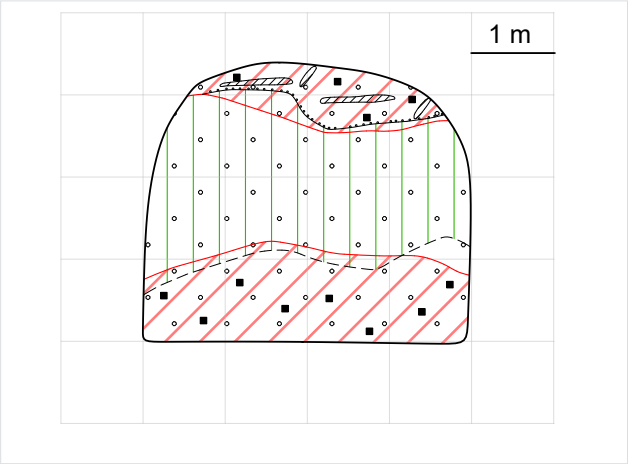

Sl. 10. Meja orudenja vezana točno na mejo temnosivega peščenjaka (OP-1 sp., 74. odstrel).
Fig. 10. Ore boundary corresponds to the boundary of dark grey sandstone (OP-1, 74th blasting).

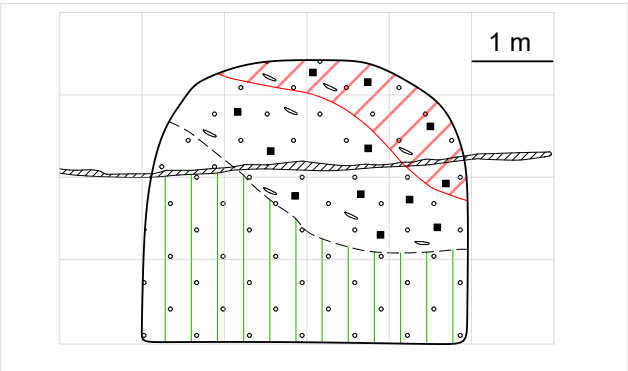

Sl. 11. Meja orudenja poteka znotraj sivega peščenjaka (OP-1 zg., 62. odstrel).
Fig. 11. Ore boundary runs within the grey sandstone (OP-1, 62nd blasting).

Pri spremljavi odkopavanja smo opazili, da je različen delež organske snovi pomembno vplival na barvni odtenek peščenjakov. Peščenjaki, ki so bili brez ali skoraj brez organske snovi so imeli zelenkast odtenek, kjer se je delež organske snovi povečeval pa se je barva spreminjala od svetlosive do sive in temnosive do skoraj že črne. Pri tem pa se je s temnejšo barvo povečevala tudi verjetnost bogatejšega orudenja. Meje orudenja so bile včasih vezane točno na meje temnosivega peščenjaka (sl. 10). Še večkrat pa se je orudenje končalo pred to mejo (sl. 11) ali pa se celo podaljšalo v svetleje sive ali zelenosive peščenjake. To si lahko razlagamo prav s pojavljanjem topne oblike organske snovi, ki se je premikala s podtalnico in ustvarjala geokemične pogoje za izločanje uranovih mineralov tudi izven območja pojavljanja vidne netopne organske snovi. V orudenih peščenjakih je bila pogosto prisotna tudi rjavkasta obarvanost (sl. 12), ki pa je predvsem posledica prisotnosti še drugih sulfidov (Fe) oziroma njihove oksidacije. Med organsko snovjo in uranskim orudenjem sicer ni bilo ugotovljene direktne korelacije (Omaljev, 1967; Dolenec,

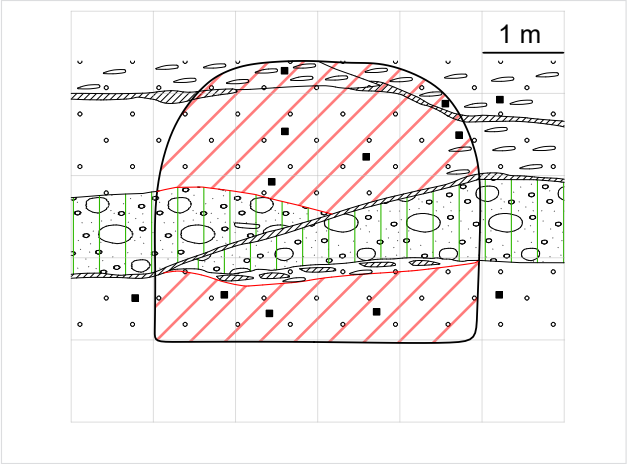

Sl. 12. Orudeni peščenjaki so večkrat nastopali v rjavkastih različkih (OP-1 sp., 67. odstrel).
Fig. 12. Brownish variations of sandstones are also usually mineralised (OP-1, 67th blasting).

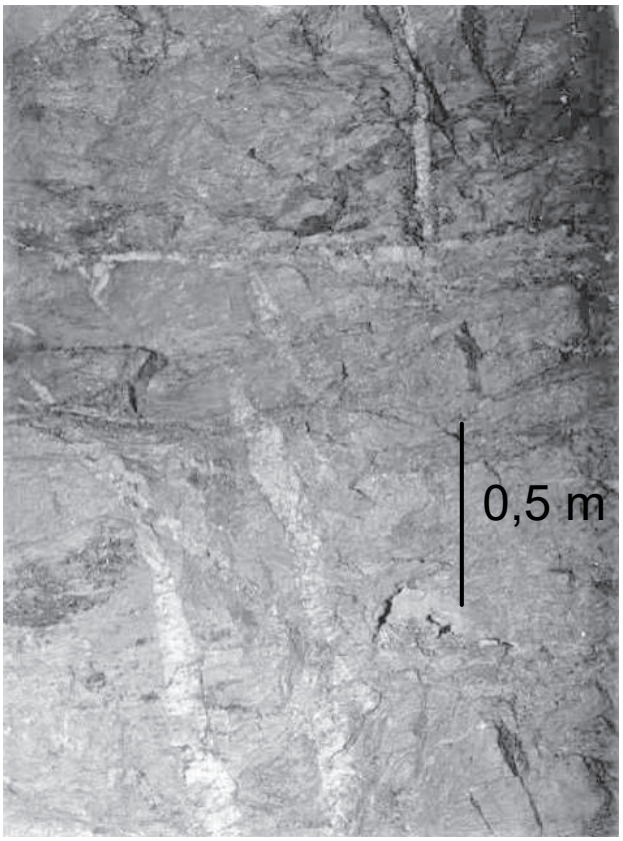

Sl. 13. Drobci organske snovi (črno) v orudenem peščenjaku (O-1/4-5, 33. odstrel).
Fig. 13. Organic detritus (black) in mineralised sandstone (O-1/4-5, 33rd blasting).

1983). Prisotnost organske snovi pa je bila predpogoj, da je v določenih delih sedimenta nastalo redukcijsko okolje, ki je povzročilo obarjanje uranilnih ionov iz podtalnice v medzrnske prostore.

Primerjava geološke sestave in pojavljanja orudenja je pokazala, da se je v bloku 1 pojavljala naslednja odvisnost:

barva/zrnavost	temnosiva	siva	svetlosiva	zelenosiva
konglomeratični peščenjak	ruda	mineralizacija	jalovina	jalovina
debelozrnati peščenjak	bogata ruda	ruda	mineralizacija	jalovina
srednjezrnati peščenjak	ruda	mineralizacija	jalovina	jalovina
drobnozr. pešč. in muljevec	mineralizacija	jalovina	jalovina	jalovina

Meje med posameznimi kategorijami orudenja so bile naslednje:

- jalovina: pod 100 g/t U_3O_8
- mineralizacija: 100–300 g/t U_3O_8
- ruda: 300–1000 g/t U_3O_8
- bogata ruda: nad 1000 g/t U_3O_8

Vzdolžni profil odkopne priprave OP-1 nam je pokazal skorajda sklenjen potek orudenja na celotni dolžini, ki se je pojavljalo na več mestih v dveh in celo treh nivojih oziroma v dveh oz. treh sekvencah, ki pa navadno niso bile orudene v celotni debelini. Le na enem odseku (P-32a+5 do P-32a+20) so bile sekvence orudene v celotni debelini in tu se je pojavljala največja debelina orudenja, ki je celo presegla 7 m (sl. 5 in sl. 14). Na tem delu se je pojavljal le debelozrnat peščenjak v katerem so bili pogostni drobci organske snovi. Verjetno je bilo tudi na teh mestih razvitih več sekvenc, ki pa jih zaradi zastopanosti le debelozrnatega peščenjaka ni bilo mogoče ločevati. Razvite medplastovno kremenovo kalcitne žile, ki smo jih kartirali in so zelo pogostne na stikih posameznih sekvenc, bi to lahko potrjevale. Omenili smo že, da je v tem delu prevladovala masivna tekstura. Na mestih s povečano debelino se je navadno pojavljala tudi bogatejša ruda. Bolj pogostni pa so bili primeri, da so bili orudeni le deli sekvenc, med njimi pa so se

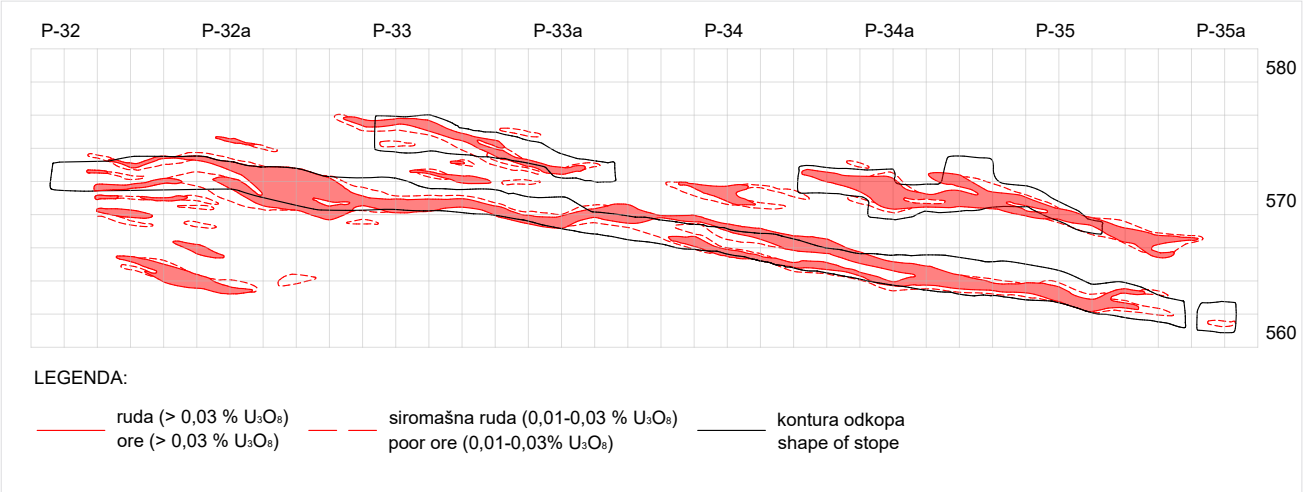

Sl. 14. Orudenje v vzdolžnem prerezu (OP-1).
Fig. 14. Ore bodies in longitudinal section (OP-1).

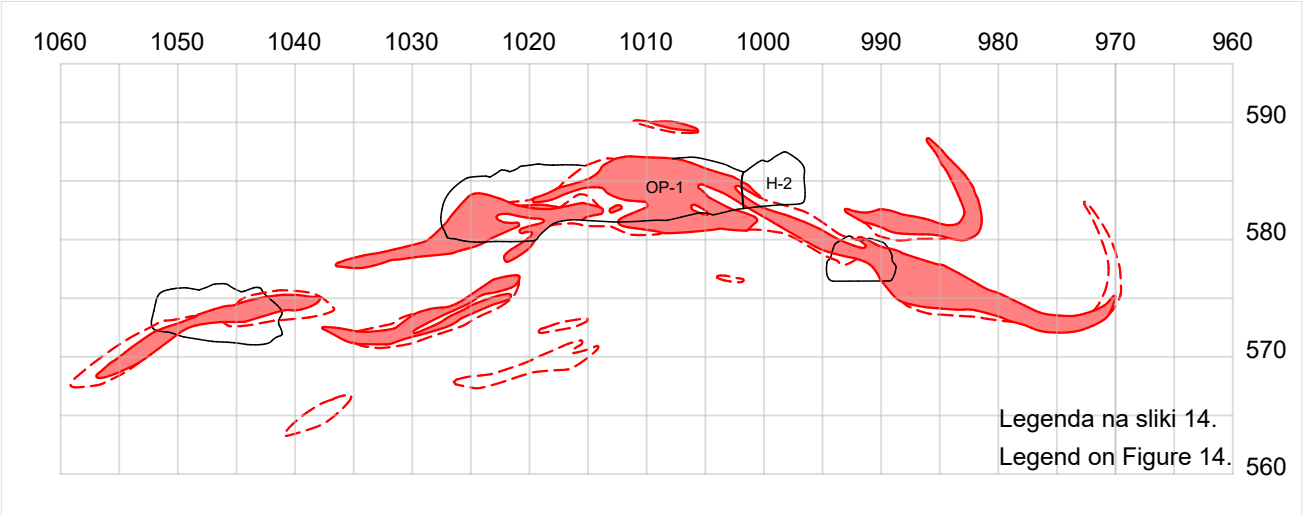

Sl. 15. Orudenje v prečnem prerezu P-32a+5.
Fig. 15. Ore bodies in cross section P-32a+5.

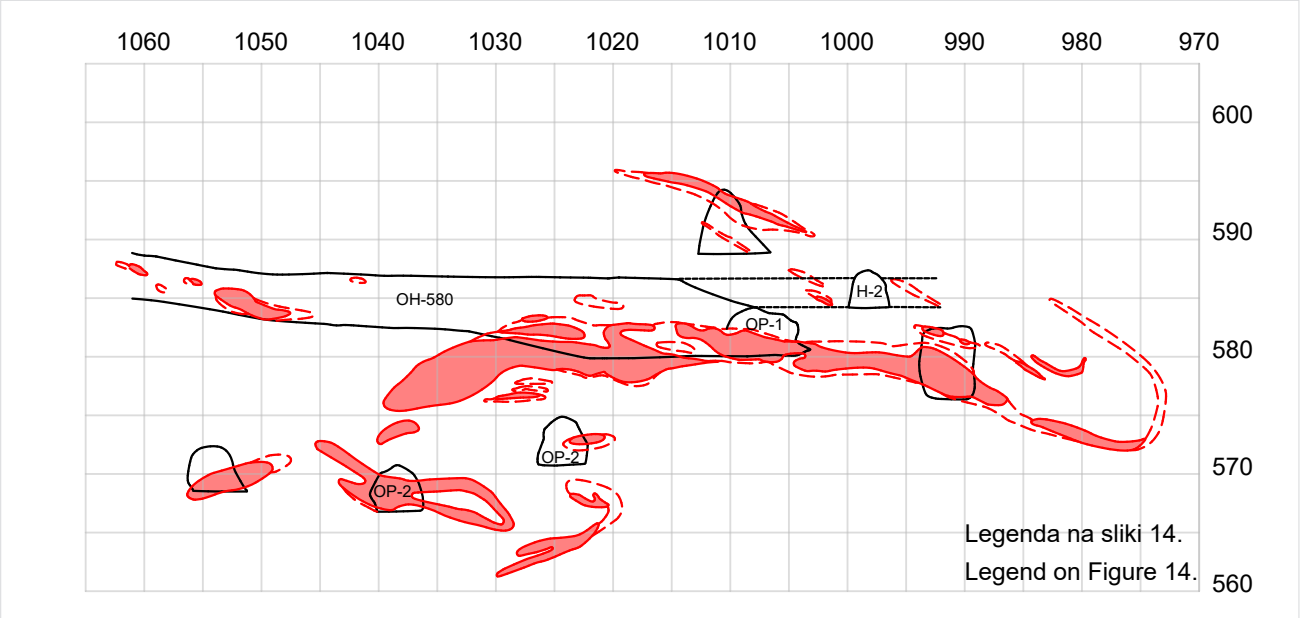

Sl. 16. Orudenje v prečnem prerezu P-33+5.
Fig. 16. Ore bodies in cross section P-33+5.

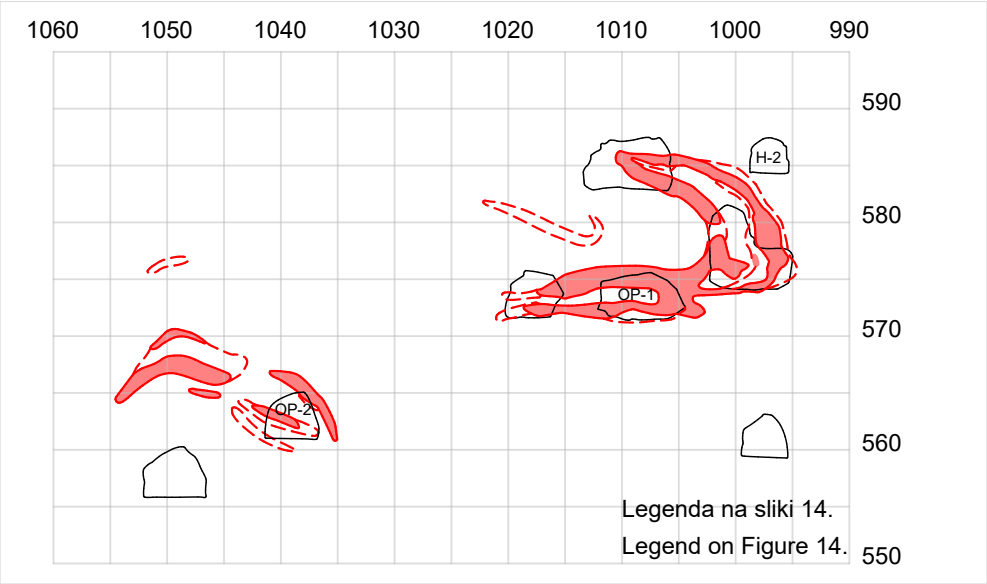

Sl. 17. Orudenje v prečnem prerezu P-34+15.
Fig. 17. Ore bodies in cross section P-34+15.

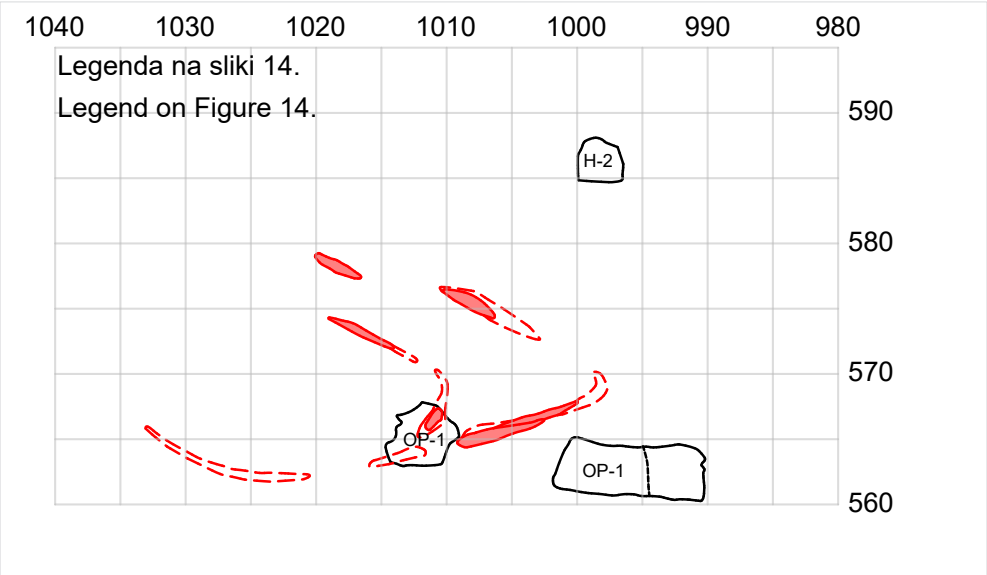

Sl. 18. Orudenje v prečnem prerezu P-35+20.
Fig. 18. Ore bodies in cross section P-35+20.

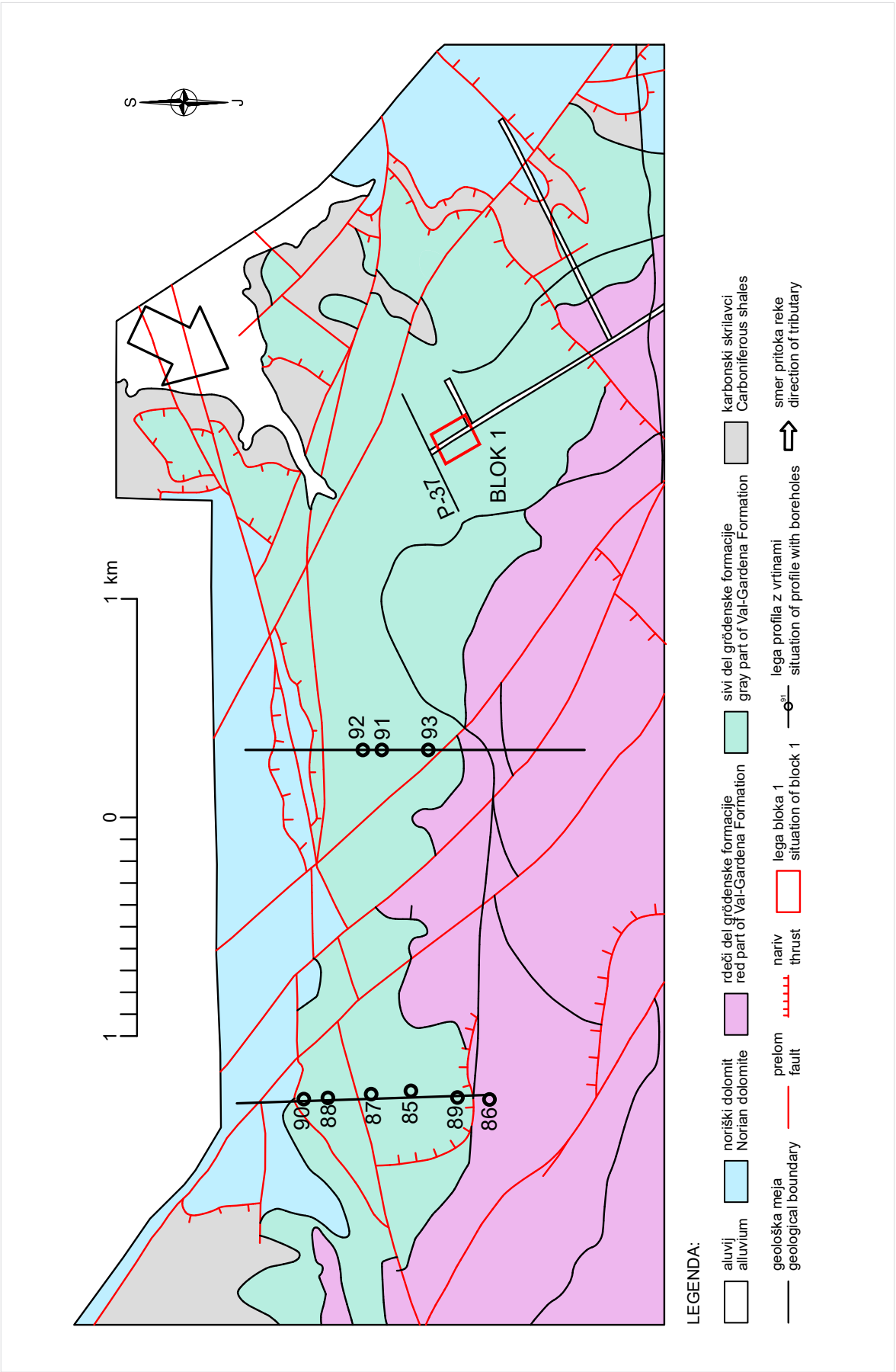

Sl. 19. Geološka karta severozahodnega podaljška (po I. Mlakarju).
Fig. 19. Geological map of the NW extension of the mine area (after I. Mlakar).

pojavljali jalovi deli ali je nastopala orudena le ena sekvenca. Sklenjena dolžina orudenja v bloku 1 je znašala največ 150 m merjeno vzdolž OP-1 (sl. 14). Med profiloma P-35 in P-35a se je orudenje pričelo postopno izklinjati in sicer se je zmanjševala njegova koncentracija kot tudi debelina. V zadnjem delu je orudenje postalo lečasto in tudi te leče so vsebovale vse manjše vsebnosti urana. Tudi na drugem koncu se je orudenje v smeri OP-1 izklinjalo (P-32+5) vendar pa se je v nekaterih odkopih (O-1/4-5) nadaljevalo vse do meje bloka (P-32) oziroma se je potem nadaljevalo neprekinjeno naprej v blok 2.

Širino rudnih teles smo opazovali v prečnih prerezih, kjer je ta znašala od nekaj metrov do preko 40 m. Med prerezi P-32a+5 (sl. 15) in P-33 se je pojavljal največji obseg orudenja tako po debelini kot tudi po padu. Za prerezom P-33 se orudenje stanjša in tudi dolžina orudenja v prečni smeri se začne skrajševati (sl. 16 in sl. 17). S približevanjem prerezu P-35a pa se orudenje še dodatno stanjša in zmanjšuje se tudi njegova koncentracija (sl. 18). Pri spremljavi odkopavanja smo opazili, da se je tam, kjer se je orudenje skrajševalo, prekinjalo ali izginjalo orudeni peščenjak postajal svetlejši in zelenosiv, v njem je bilo v splošnem vse manj organske snovi. Za prerezom P-35a se do prereza P-37, do kamor so se izvajala raziskovalna dela v jami, nikjer več ni pojavljalo orudenje v ekonomsko zanimivih količinah.

Severozahodni podaljšek rudišča

Peščenjaki, ki pripadajo 6. horizontu in so bili glavni nosilci orudenja v blokih, kjer se je odkopavalo uranovo rudo do leta 1990, se proti severozahodu še nadaljujejo, vendar so po barvi večinoma zelenosivi in le s sledovi orudenja. Prehod iz temnosivih in sivih peščenjakov z orudenjem v zelenosive smo opazovali v bloku 1 na njegovem SZ delu med prerezoma P-35 in P-36. Sprememba barve je bila povezana tudi z zmanjšanjem deleža organske snovi, ki je imela odločilno vlogo pri nastanku redukcijskega okolja in obarjanju urana. V jami je bil zadnji raziskan prerez P-37, kjer so bili torej peščenjaki 6. horizonta prevladujoče zelenosive barve. Pod njim pa so bili še prisotni pisani konglomerati, ki pa se navzdol (v prečni smeri) hitro izklinjajo in jih nadomeščajo sivi različki.

Severozahodno oziroma že zahodno od bloka 1 sta bila z vrtinami s površine raziskana še dva prereza oddaljena 1,3 in 2,8 km od zadnjega prereza v jami (sl. 19). Tudi tu so bile ugotovljene le redke in siromašne mineralizacije z uranom (Budkovič, 1986). Poleg tega se tu siva grödenska formacija močno stanjša saj se pričenja šele s 4. ali 5. horizontom, ki je zastopan le s sivim konglomeratom, pisanega konglomerata ni več. Peščenjaki 6. horizonta ostajajo prevladujoče zelenosive barve, vmes pa se pojavljajo tudi še sivi in celo temnosivi različki. Iz popisa vrtin izhaja, da se med temi debelozrnatimi peščenjaki pogosteje pojavljajo bolj drobnozrnati različki (drobnozrnati peščenjaki, meljevci, muljevci). Prisotnost organske snovi je bila zabeležena le redko. To bi kazalo na okolje prepletajoče reke z veliko poplavnih ravnic, kjer se je usedal drobnejši material.

Iz geološke karte I. Mlakarja (1981) je razvidno, da se na mestu, kjer se zaključuje jamska zgradba, smer grödenskih plasti obrača iz dinarske smeri v smer vzhod-zahod (sl. 19). O zavoju reke pri Gorenji vasi, ki je prinašala in odlagala peščeni material je pisal že Omaljev (1982). Sprememba v slemenitvi plasti in drugačen razvoj grödenskih plasti v smeri proti zahodu (Fužine) nam potrjuje predvidevanje Omaljeva, da je bil pri Gorenji vasi močan pritok v glavno reko. Ta pritok je moral prinašati material za pisane konglomerate, medtem ko je glavni tok reke iz zahoda prinašal material za sive konglomerate. V jamski zgradbi, ki se pričenja z blokom 1 in nadaljuje v dinarski smeri proti JJV je prav značilno, da se v 5. horizontu menjavata sivi in pisani konglomerat. Debelina in obseg slednjega se proti JV in JZ sicer manjšata, proti robovom bazena celo izklinjata. Raziskave prodniških združb so kazale na različno izvorno območje enega in drugega predvsem zaradi različne sestave prodnikov, njihove zaobljenosti in sortiranosti (Skaberne, 1995). Prodniki, ki gradijo pisane konglomerate so manj zaobljeni in slabše sortirani in jim je zato Skaberne (1995) pripisal aluvialno vršajno sedimentacijo s smerjo transporta od SV proti JZ glede na prevladujočo smer transporta SZ-JV. Glede na podoben potek teles pisanega konglomerata na obzornih kartah in vzdolžnih prerezih kot jih imajo ostali sedimenti, to je v smeri SZ-JV menimo, da je material zanj prinašal pritok reke iz smeri S do SV od Gorenje vasi in so se potem odlagali v prepletajočih koritih in ravnicah glavne reke, ki je tekla proti JV.

Zahvala

Za kritičen pregled vsebine in podane pripombe se najlepše zahvaljujem dr. Dragomirju Skabernetu. Grafične priloge mi je izdelala Nika Köveš, prevod povzetka in podnapisov k slikam pa Erazem Dolžan, za kar se jima prav tako lepo zahvaljujem.

Literatura

Budkovič, T. 1978: Litološka kontrola uranovega orudenja na obzorju 530 m v rudišču Žirovski vrh. Rudarsko-metalurški zbornik, 1: 25–34.

Budkovič, T. 1980: Sedimentološka kontrola uranove rude na Žirovskem vrhu. Geologija, 23/2: 221–226.

Budkovič, T. 1986: Raziskave severozahodnega podaljška rudišča Žirovski vrh med Karlovcem in Fužinami. Referati 2. jugoslovanskega posvetovanja o jedrskih surovinah, Škofja Loka.

Dolenec, T. 1983: Nastanek uranovega rudišča Žirovski vrh. Doktorska disertacija. Univerza v Ljubljani, Ljubljana: 2 zv. 287 str. + 48 tabel.

Drovenik, M., Pleničar, M. & Drovenik, F. 1980: Nastanek rudišč v SR Sloveniji. Geologija, 23/1: 1–159.

Florjančič, A.P. s sod. 1973: Poročilo o geološko-rudarskih raziskavah ležišča urana Žirovski vrh v letu 1972. Zgodovinski arhiv Ljubljana, enota v Škofji Loki.

Hadži-Popović, S. 1962: Organska materija v grodnu Žirovskega vrha. Tipkano poročilo, Zgodovinski arhiv Ljubljana, enota v Škofji Loki.

Lavrenčič, J., Florjančič, A.P., Čadež, F. & Šubelj, A. 1984: Uvajanje projektnih rešitev in poskusnega dela za najprimernejši sistem geološke kontrole pri poskusnem odkopavanju. Arhiv Ljubljana, enota v Škofji Loki.

Lukacs, E. & Florjančič, A.P. 1974: Uranium ore deposits in the Permian sediments of Northwest Yugoslavia. Formation of Uranium Ore Deposits, Proceedings of a Symposium, Athens, 6–10 May1974, IAEA, Wienna.

Miall, A.D. 1978: Lithofacies types and vertical profile models in braided river deposits: a summary. In: Miall, A. D. (ed.): Fluvial sedimentology. Can. Petrol. Geol. Mem., 5: 597–604.

Miall, A. D. 2014: Fluvial Depositional Systems. Springer Geology. https://doi.org/10.1007/978-3-319-00666-6

Mlakar, I. 1981: Geološki faktorji kontrole Hg, Cu in U mineralizacije (Žirovski vrh), IV. faza. Arhiv Geološki zavod Slovenije, Ljubljana: 82 str., 9 pril.

Mlakar, I. & Placer, L. 2000: Geološka zgradba Žirovskega vrha in okolice. In: Florjančič, A. P. (ed.): Rudnik urana Žirovski vrh, Didakta, Radovljica.

Omaljev, V. 1967a: Razvoj gredenskih slojeva i uranove mineralizacije u ležištu urana Žirovski vrh. Radovi IGRI 3, Beograd.

Omaljev, V. 1967b: Korelacija slojeva u ležištu Žirovski vrh. Radovi IGRI 3, Beograd.

Omaljev, V. 1969: Eksploatacijsko raziskovanje v uranovem rudišču Žirovski vrh. Geologija, 12: 107–152.

Omaljev, V. 1982: Metalogenetske karakteristike uranskog rudišta Žirovski vrh. Geoinstitut, Posebna izdanja, knjiga 7, Beograd.

Skaberne, D. 1995: Sedimentacijski in postsedimentacijski razvoj grödenske formacije med Cerknim in Žirovskim vrhom. Doktorska disertacija. Univerza v Ljubljani, Ljubljana: 1. del 500 str., 2. del 192 str. + 46 prilog.

Spasojević, L. 1981: Rudarski projekat za izvođenje radova pri probnom otkopavanju u Rudniku urana Žirovski vrh. Rudarski institut Beograd.

GEOLOGIJA 66/1, 87-105, Ljubljana 2023
https://doi.org/10.5474/geologija.2023.003

Taxonomic and stratigraphic remarks on *Placites urlichsi* Bizzarini, *Pompeckjites layeri* (Hauer), *Carnites floridus* (Wulfen) and *Sageceras haidingeri* (Hauer)

Taksonomija in stratigrafski razpon vrst *Placites urlichsi* Bizzarini, *Pompeckjites layeri* (Hauer), *Carnites floridus* (Wulfen) in *Sageceras haidingeri* (Hauer)

Andreas SPATZENEGGER[1] & Walter POLTNIG[2]

[1]A-5113 St. Georgen, Wetterkreuzstraße 16, Austria, e-mail: andreas.spatzenegger@outlook.com
[2]A- 8063 Eggersdorf, Feldweg 16, Austria, e-mail: walter.poltnig@gmx.at

Prejeto / Received 19. 8. 2022; Sprejeto / Accepted 12. 4. 2023; Objavljeno na spletu / Published online 4. 8. 2023

Key words: ammonoids, Triassic, Carnian, Wettersteinkalk, Bleiberger Sonderfazies, Upper San Cassian Formation
Ključne besede: amoniti, trias, karnij wettersteinski apnenec, pliberški facies, Zgornja San Cassianska formacija

Abstract

Investigations of an Lower Carnian Wettersteinkalk ammonoid fauna found in the Hochobir massif (Carinthia/Austria) gave rise to problems in the taxonomic relationship within the Triassic ammonoid Family Pinacoceratidae. The morphological parameters of the ammonoid genus *Pompeckjites* are rather unclear. Morphological variation of at least two ammonoid species as *Pompeckjites layeri* Hauer on one end, *Placites urlichsi* Bizzarini on the other end have to be take into account. Numerous field surveys, studies and excavations on upper Wettersteinkalk sites within the Karavank Mountains and Hallstatt-facies sites in the Northern Calcareous Alps were implemented and compared with the reference sites in the Dolomites. As a consequence of our investigations, the Hochobir Wettersteinkalk ammonite assemblage is thought to be equivalent in time to the ammonoid fauna of the Upper San Cassian Formation. The frequent occurrence of the Julian (Lower Carnian) ammonoid *Placites urlichsi* Bizzarini may be a powerful tool in field investigations for a refined correlation of the upper Wettersteinkalk reef limestone to the coeval basinal facies of the Upper San Cassian Formation (Lower Carnian/upper *Trachyceras aonoides* Zone). As a result of this study *Placites urlichsi* was included in the genus *Pompeckjites*. This paper could be an attempt to recognize the differences in juvenile forms of *Pompeckjites layeri* and *Placites urlichsi* and other similar disciform ammonoid genera like *Carnites floridus* and *Sageceras* sp. based on suture lines, polished transversal-sections and morphological features.

Izvleček

Rezultati raziskave amonitne favne v spodnjekarnijskem wettersteinskem apnencu, ki se pojavlja na Obirju, na avstrijskem Koroškem, odpirajo problem v taksonomskem razlikovanju triasnih amonitov družine Pinacoceratidae. Razlikovanje na podlagi morfoloških parametrov amonitov rodu *Pompeckjites* je precej nejasno, pri čemer je treba upoštevati morfološke variacije najmanj dveh vrst, in sicer *Pompeckjites layeri* Hauer na eni ter *Placites urlichsi* Bizzarini na drugi strani. Številni ogledi nahajališč v zgornjem wettersteinskem apnencu Karavank in hallstattskem faciesu Severno apneniških Alp, njihova izkopavanja ter raziskave, poleg tega pa tudi primerjava z referenčnimi najdišči v Dolomitih kažejo, da je zbrana amonitna združba wettersteinskega apnenca najverjetneje časovni ekvivalent amonitni favni zgornje San Cassian formacije. Pogosto pojavljanje julijskega (spodnji karnij) amonita *Placites urlichsi* Bizzarini je na terenu lahko močno orodje za oceno korelacije med grebenskim zgornjim wettersteiskim apnencem ter ekvivalentnim bazalnim faciesom zgornje San Cassian formacije (spodnji karnij/zgornji del *Trachyceras aonoides* cone). Kot rezultat te raziskave je bil *Placites urlichsi* vključen v rod *Pompeckjites*. Pričujoči članek na podlagi suturnih linij, poliranih rezov in morfoloških značilnosti, pomaga prepoznati razliko med juvenilnimi oblikami *Pompeckjites layeri in Placites urlichsi* ter drugimi amoniti diskoidne oblike kot sta *Carnites floridus* in *Sageceras* sp.

Introduction

The Julian (Lower Carnian) *Trachyceras aonoides* and *Austrotrachyceras austriacum* ammonoid zonation was originally established in the fossiliferous Hallstatt Limestones of the Northern Calcareous Alps (Mojsisovics 1892, 1893; Frech 1911a, 1912, subsequently better defined by Krystyn 1978 and verified by Hornung et al. 2007). Later on it was compared with the biostratigraphic framework of the San Cassian Formation of the Southern Calcareous Alps/Dolomites (see reference lists of Mietto et al. (2012) and Urlichs (2017). It was recognized that the San Cassian Formation spans more than the previously thought late Ladinian to earliest Carnian (*Trachyceras aon* Zone) age (Bizzarini 1987, 2000; Mastandrea 1995; Di Bari & Baracca 1998). Consequently, attempts were made to correlate both facies on the basis of occuring Trachyceratidae (Urlichs 1994, 2017). However, other co-occurring ammonoid genera (except *Lobites*, see Urlichs 2012) were never part of such studies. From the Julian part of the Wettersteinkalk (Bleiberger Sonderfazies of Holler 1960) such comparative ammonoid studies were not carried out until today. Current biostratigraphic studies in the UNESCO Geopark Karawanken/Karavanke (A/Slo) evidence a *T. aonoides* Zone age of these strata that is based on the occuring Trachyceratidae (Poltnig & Spatzenegger 2022). The co-occuring ammonoids of the Family Pinacoceratidae show striking similarities to the Pinacoceratidae of the Upper San Cassian Formation East of Cortina d' Ampezzo that were revised by Bizzarini (1987). A small disciform ammonoid fauna, found in the uppermost Wettersteinkalk (Bleiberger Sonderfazies, Holler 1960) caused severe taxonomic classification problems that hampered a clear Carnian/Julian ammonoid subzone (see Fig. 2, middle column) identification already in the field. Because of syndiagenetic dolomitization and recrystallization during lithogenesis, only very few ammonoids showed well preserved suture lines. This fact made it complicated to distinguish between the Julian contemporaneous ammonoid genera *Pompeckjites*, *Sageceras* and *Carnites*. To make matters worse, some juvenile growth stages of *Placites urlichsi* show strong homeomorphism to *Sageceras* sp. and *Pompeckjites layeri*.

To facilitate the classification on poorly preserved ammonoids of the genera above mentioned we provide our results based on polished hand specimens and morphological features.

Study areas

Fladung mining area on Obir massif/Austria

The abandoned Fladung lead-zinc mining area is located about 8 km west of Bad Eisenkappel on the southern slope of Hochobir (see Fig. 1, A). It is easily accessible via the toll road to the Eisenkappler Hütte. During several field excursions the majority of the ammonoids were sampled from the ravine directly east of the Fladung Berghaus (see Figs. 1, B and D with sites 1a, 1b, 1c). The western ravine wall (approximately 1200 m above sea level) crops out of a steeply dipping (55 degrees towards east-south-east) Wettersteinkalk succession that shows a slope angle parallel to the bedding. Therefore, all ammonoid locations (site 1 a-c) found in this wall originate from approximately the same stratigraphic layers. Location 2 is situated 500 m further eastwards of the Fladung Berghaus directly beside the toll road near a junction with a forest road (see Fig. 1, B). It is in tectonically stressed contact (not well visible in the field) with Cardita shale and Cardita limestone. Lipolt (1856:337f) mentions from the Fladung mining district light ore bearing "Hallstätter Kalk" (=Wettersteinkalk) and cited Carnian ammonoids from the locality ("*Ammonites Aon*, *Ammonites Joannis Austriae*, *Ammonites Jarbas* and *Ammonites Gaytani*"). The "Bleiberger Schichten des Ovir (=Obir)" with *Carnites floridus*, also mentioned in Lipolt (1856), correspond to the first Raibl shale horizon and should not be confused with today's Bleiberger Sonderfazies of Holler (1960). For further information we refer to Poltnig & Spatzenegger (2022).

Our newly discovered fossiliferous strata correspond to the Bleiberger Sonderfazies (Holler 1960) of the uppermost Wettersteinkalk and mark the area between the sediment hosted lead-zinc mineralization (Bechstaedt 1979; Mondillo et al. 2019) and the tectonically sheared off and subsequently eroded first Raibl shale horizon.

Unterpetzen mining area near Podpeca/Slovenia

The former mining district Unterpetzen/Podpeca is situated roughly 6.5 km southwest of the town Mežica/Slovenia. (see Fig. 1, A) on the south eastern slope of the Petzen massif. It should not be confused with the Helena mining district in the village Podpeca itself that is situated one kilometer eastwards. Two field campaigns were carried out in this area to verify our stratigraphic results from Hochobir. Main sampling was done alongside the forest road (sites Pod. 1-3, roughly E 46.476450, N 14.808636) to the abandoned Mariahilf mine

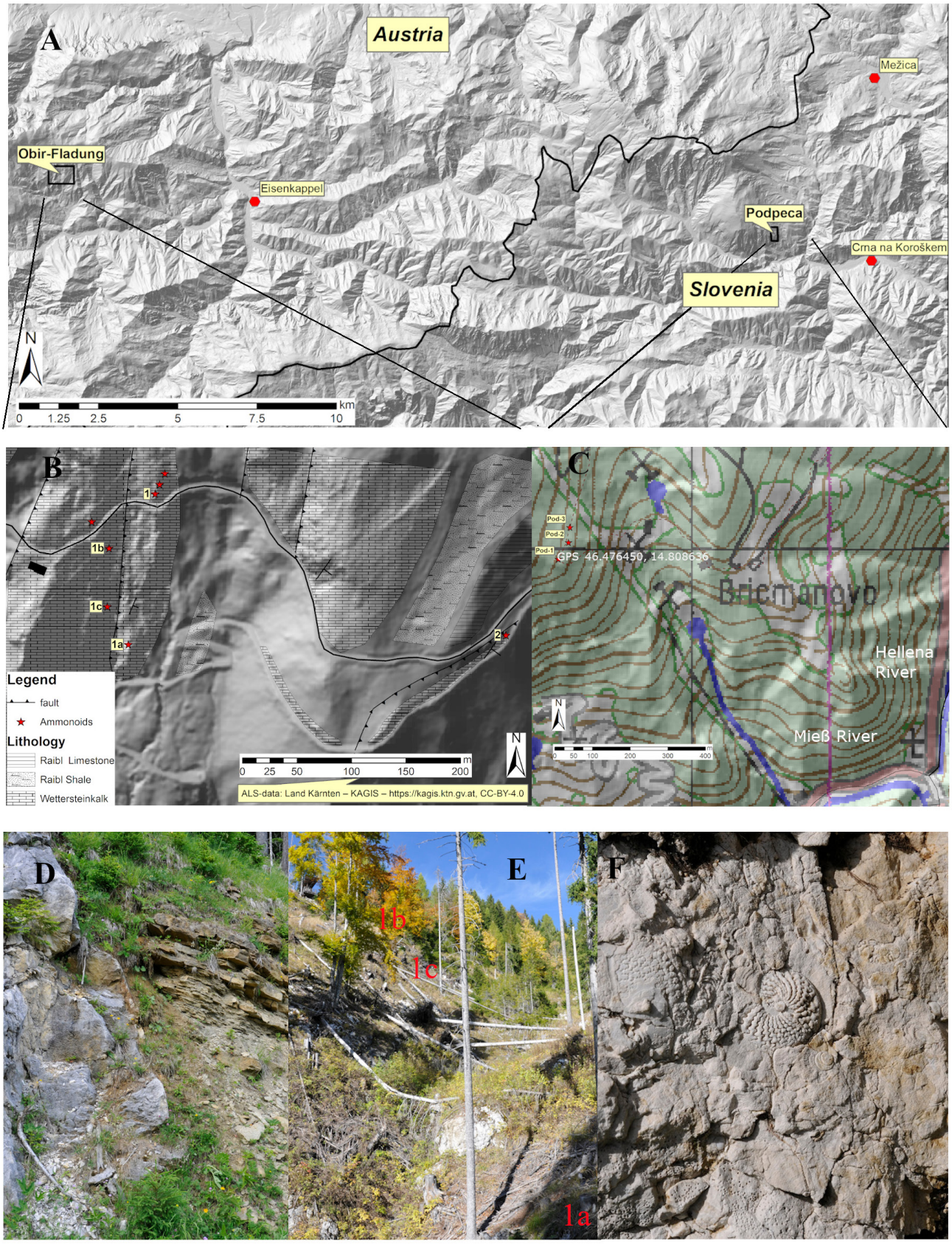

Fig. 1. Overview of the Studied Areas.

A, geographic situation of the Obir/Fladung area in Austria and of the Unterpetzen/Podpeca area in Slovenia. B, enlarged overview of the Fladung sites with mapped lithologic strata (debris and soil are not mapped). C, Unterpetzen/Podpeca mining area with sites Pod 1–3 alongside the forest road to the Mariahilf mine gallery. D, tectonically stressed contact of Wettersteinkalk (left) to Raibl shales (right) in the Fladung area. E, view from Fladung site 1a towards 1b and 1c. F, weathered in situ Wettersteinkalk ammonoid (*Joannites klipsteini*), Fladung, site 1c.

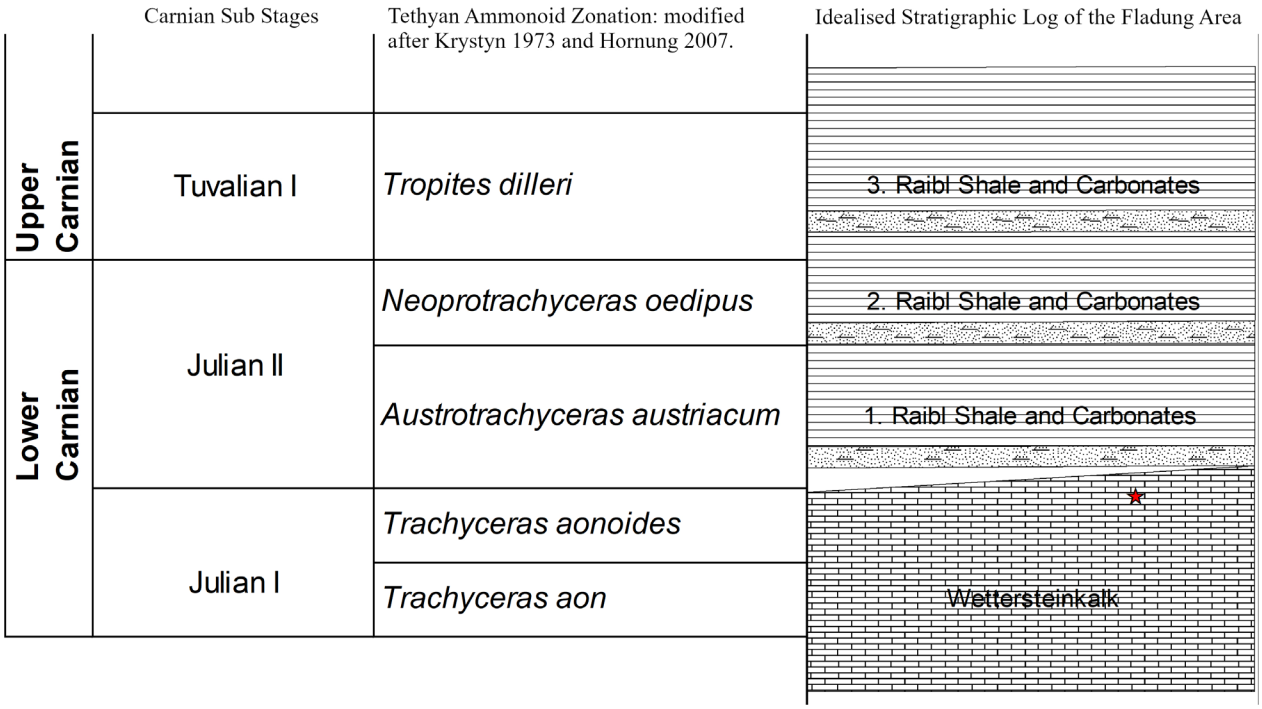

Fig. 2. Simplified stratigraphic log of the Fladung area.

The left column shows the Lower Carnian (Julian) sub-stages. The middle column shows the ammonoid zonation modified after Krystyn (1973) and Hornung et al. (2007). The right column shows an idealized lithologic log of the Fladung area and the stratigraphic position of the found ammonoid fauna (red star).

gallery (see Fig. 1, C). From Unterpetzen several ammonoid finds in Wettersteinkalk have been cited in Mojsisovics (1871, 1873, 1882, 1893, 1902).

Material and methods

All ammonoid concentrations found at both locations originate from the vicinity of algal laminites and do show a partial current sorting of the fossils. This suggests a deposition in the tidal to subtidal zone. Most ammonoids in this study were completely recrystallized and partially encrusted by a several millimeters thick dolomitic crust. Towards the surface and near mineralized layers better preservation was found. In some limestone parts the ammonoids showed calcitic shell replacement that was sometimes covered with a fine limonite crust between ammonoid shell and sediment. If this coating was missing, preparation was difficult and of poor result. Another common feature of ammonoids found near the surface was the dissolution of the ammonoid shell by humic acids. The result was an internal mold (steinkern) covered by a crumbled powder of the former ammonoid shell. The identification of ammonoids that showed steinkern preservation was also hindered by the lack of visible suture lines. Preparation was done by the authors exclusively. The best results were obtained by using coarse and fine pneumatic engravers. Limestone lacking preparable ammonoids was used for making polished transversal-sections (see Figs. 7, A, B, F and 9, C). Such sections gave good insights into the depositional conditions and were found to be very helpful in identification of some ammonoids.

All collected fossils originate from the Bleiberger Sonderfazies (Holler, 1960) of the mining district Fladung and are stored in the administration center of the UNESCO Geopark Karawanken/Karavanke in Tichoja and in the private collection of Andreas Spatzenegger (A-5113 St. Georgen). All fossils are accessible by prior appointment.

Systematics

More than 300 ammonoid specimens were collected during fieldwork. The general preservation of the ammonoid assemblages found was moderate to poor. Sample richness in ammonoid quantity was very high and similar to the ammonoid accumulations within the Hallstatt limestone. For the species mentioned in the systematic part, the most important synonyms provided in the literature and the original papers describing the holotypes were carefully reviewed. The systematic paleontology below is thus based upon a careful revisitation of previous Triassic ammonoid literature (Hauer 1846, 1847; Mojsisovics 1873, 1882; Hyatt 1884; Mojsisovics 1902; Gemmellaro 1904; Arthaber 1905; Hyatt & Smith 1905; Arthaber 1911; Frech 1911a; Welter 1914; Diener 1915a, 1915b, 1916; Smith 1927, 1932; Johnston 1941; Spath 1951; Tozer

1967; Silberling & Tozer 1968; Tozer 1971; Krystyn 1973, 1978, 1980; Tozer 1981; Krystyn 1982; Tozer 1984; Sestini 1992; Tozer 1994; Doguzhaeva et al. 2007; Balini 2008; Konstantinov 2008; Mietto et al. 2008; Balini et al. 2010, 2012; Hyatt & Smith 2012; Konstantinov 2012; Lukeneder & Lukeneder 2014; Ritterbush et al. 2014; Jenks et al. 2015) and our own investigations based on morphology and transversal sections. For each ammonoid species, remarks are provided with respect to the original identifications and descriptions provided in the literature. The main subject of the systematic part is the Lower Carnian/Julian genus *Pompeckjites* of the Family Pinacoceratidae Mojsisovics, 1879. The additionally described genus *Carnites* (Carnitidae Arthaber, 1911) is not a member of Pinacoceratidae but included with the latter in the Superfamily Pinacoceratoidea (Tozer, 1981). The genus *Sageceras* (Superfamily Sageceratoidea Hyatt, 1884) is shown here only for comparison purposes to highlight some morphological similarities with the above mentioned genera in transversal sections. For the higher taxonomic nomenclature of ammonoids the work of Hoffmann et al. (2022) was used. In regards to the taxonomy of ammonite families and subfamilies we used the classification of Tozer (1971, 1981) and Krystyn (1982). For the detailed descriptions of *Carnites floridus* and *Pompeckjites layeri,* we refer to the original descriptions (Hauer 1847; Mojsisovics 1873, 1902). The description of *Placites urlichsi* Bizzarini, 1987 is more detailed because of its importance for this work.

Superorder Ammonoida Haeckel 1866
Order Ceratitida Hyatt, 1884
Pinacoceratoidea Mojsisovics, 1879
Carnitidae Arthaber, 1911
Carnites Mojsisovics, 1879

Type species: *Carnites floridus* (Wulfen, 1793)

1793 *Nautilus bisulcatus* Wulfen, p. 103, fig. 10.

1793 *Nautilus floridus* Wulfen, p.113, fig. 16.

1793 *Nautilus nodulosus* Wulfen, p. 115, fig. 17.

1793 *Nautilus redivivus* Wulfen, p. 116, fig. 18.

1846 *Ammonites floridus* Hauer, p. 2, pl. 1, figs. 5-14.

1855 *Ammonites floridus* Hauer, p. 150.

1873 *Pinacoceras floridum* Mojsisovics, p.58, pl. 22, figs. 15, 16; pl. 25, figs. 1-6.

1882 *Carnites floridus*, Mojsisovics, p.228, pl. 50, figs. 5-8; pl. 51, figs. 1-8.

1911b *Carnites floridus*, Frech, p. 19, figs. 24 a, b, non c.

1911b *Carnites floridus*, Frech, p. 19, figs. 25 a, b, c.

non 1911b *"Carnites" falcifer*, Frech, p. 21, figs. 26, 27.

2007 *Carnites floridus*, Hornung et al., pl. 6, figs. b1-b4.

Description: For the detailed morphological description we refer to (Hauer, 1846) and (Mojsisovics, 1873, 1882).

Remarks: The juvenile development of *Carnites floridus* (Wulfen, 1793) was first described in detail in Hauer (1846) and is excellently pictured in his plate. Hauer recognized the different growth stages of *Carnites floridus* which were assigned by Wulfen (1793) to four different Nautilus species. Hauer (1846) established on contemporary nomenclature and the "ammonitic" suture line *Ammonites floridus*. Mojsisovics (1873) confirmed the growth development illustrated and described by Hauer (1846) and identified it as *Pinacoceras floridum*. Mojsisovics (1879a) first mentioned the genus name *Carnites* and formally established the genus *Carnites* in Mojsisovics (1879b) with *C. floridus* as its type species. The original type specimen of *C. floridus* was found in the first Cardita shale horizon of Bad Bleiberg. Its stratum typicum in the so called first Raibl shale horizon (= first Cardita shale horizon) was clearly named and described too.

The hitherto considered large stratigraphic range of *C. floridus* most probably has its origin in the descriptions of Hauer (1846) and Mojsisovics (1873) where both authors refer to a great morphologic variability in the mature growth stages of *C. floridus*. Alas, some subsequent authors (Leonardi & Polo, 1952) didn't focus on the juvenile development of *C. floridus* and mis-identified specimens showing divergent juvenile development and mature *Carnites* shape as *C. floridus*.

Carnites floridus (see Figs. 3, E-E2 and F-F1) found in the Hallstatt Limestone of the Rappoltstein hill (= historic „Mons Tuval", located in Bavaria) show the same development in juvenile

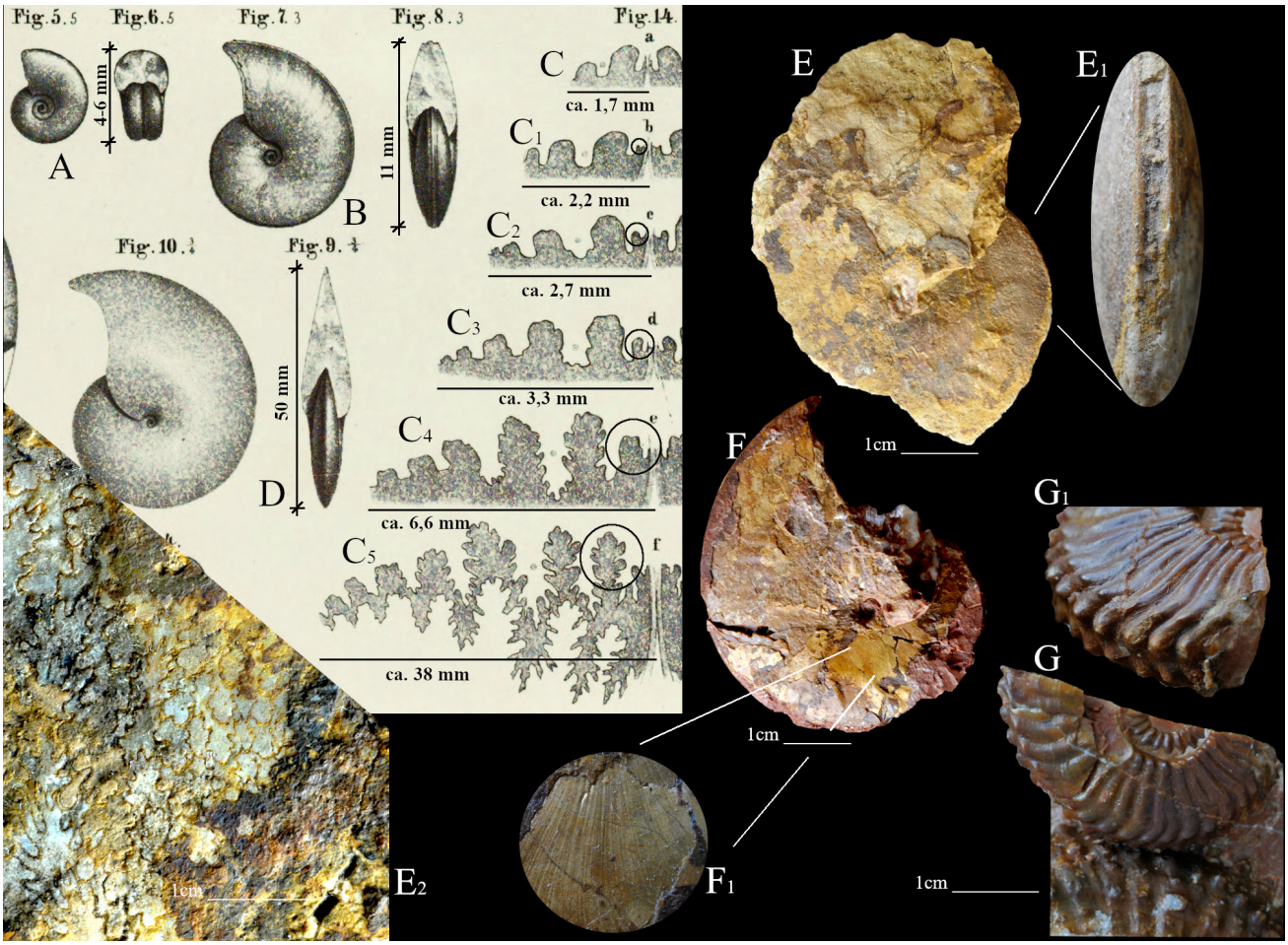

Fig. 3. *Carnites floridus*.

A, B, D, different growth stages of *C. floridus* with added metric measurements (modified after Hauer 1846: pl. 1, figs. 5-14). C–C5, original suture drawings in Hauer (1846). The development of an adventitious saddle is focused on the black circles. E–E1, side and venter view of *Carnites floridus* from Carnian Hallstatt Limestone of Rappoltstein. F, *C. floridus* from Rappoltstein in iridescent shell preservation. F1, enlargement of the faint growth lines on ammonoid F. G–G1, *Neoprotrachyceras thous*, found together with *Carnites floridus* on Rappoltstein. E2, sutureline of *C. floridus* from Rappoltstein.

stage as in *C. floridus* from the first shale horizon of Bad Bleiberg. At Rappoltstein *C. floridus* was found with *Austrotrachyceras* sp., and *Neoprotrachyceras thous* (see Figs. 3, G, G1) what allows a correlation with the beginning of the *A. austriacum* Zone (Hornung et al. 2007). This indicates that the first Raibl shale horizon can be correlated as well, which implies that the uppermost Wettersteinkalk (Bleiberger Sonderfazies) occurring below roughly corresponds to the upper *T. aonoides* Zone. Frech (1911b: 19ff) established *"Carnites" falcifer* as a new *Carnites* species from presumably Tuvalian (Upper Carnian) strata. Our own investigations on Rappoltstein revealed that *"C." falcifer* belongs to the genus *Parahauerites*. It is of early Tuvalian age and was found with *Pleurotropites* sp. and *Trachysagenites* sp. Therefore, we can exclude an occurrence of *Carnites* in lower Tuvalian (*Tropites dilleri* Zone) strata.

To illuminate the juvenile morphological development and the development of the suture line of *C. floridus* we have pictured the modified plate of Hauer (1846: pl. 1), (see Figs. 3, A-D) with additional metric measurements. The added black circles in the suture line drawings (see Figs. 3, C-C5) focus on the development of an adventitious lobe/saddle what is a diagnostic feature for *C. floridus*. Fully mature specimens of *C. floridus* show two adventitious elements that both emerged in the same way. In the largest suture (see Fig. 3, C5), the genesis of the second adventitious element is visible in the small adventitious bulgy saddle near the venter on the right side of the black circle. The juvenile specimen illustrated in Figure 3, A shows a ventral furrow with a faint keel in the middle (not visible in Hauers drawing). According to Hauer (1846) this is not the regular development. Most juvenile cores at this size show a normal rounded venter. The Figure 3, B in this text, shows the subsequent development of the tricarinate venter that is also an important morphological feature of *C. floridus* too (see Figs. 3, E1 and 9, A1).

Following this stage, the shape of *C. floridus* diverges considerably. There can occur equal sized

specimens with almost sharp (Fig. 3, D) or with rounded venter. Some specimens showed fold-like nodes at the mid flank, which were sometimes accompanied by nodes on the ventro-lateral margin. This is in contrast with other totally smooth specimens of the same size. Between these extremes, many variations exist. The suture line is identical in all of these variations. All these different forms are based on an identical juvenile stage showing similar measurements in ratio of diameter to thickness. This was not really taken into account in earlier classifications of similar ammonoids to *Carnites floridus*, which led to an enlarged stratigraphic range of true *C. floridus*.

The ammonoid fauna of the San Cassian Formation laid a base for an extended stratigraphic range of *C. floridus* as well. Early authors (Mojsisovics, 1869, 1882, Mojsisovics et al., 1895; Zittel, 1899) assigned the San Cassian layers as a whole into the former Cordevol (*T. aon* Zone). All ammonoid forms similar to *Carnites*, were assigned to *C. floridus*. This opinion prevailed until the 20th century and can be seen clearly in the identifications on the ammonoid plates in Leonardi and Polo (1952), where ammonoids from the upper San Cassian Formation East of Cortina d' Ampezzo (Boa Staolin, Boa Tamarin, Costalares) were compared and identified with upper Ladinian to lower Carnian ammonoid species of the classic San Cassian locations (Stuores Wiesen, Pralongia). For example, the genus *Sirenites* that begins in the upper *T. aonoides* Zone, was not recognized in Boa Staolin because it does not occur in San Cassian. It was identified as (*Pro)trachyceras ladinum* in Leonardi and Polo (1952: pl. 2, Figs. 32-35). Bizzarini (1987, 2000) took these differences into account and attempted to improve the identifications by establishing *Placites urlichsi* (for *C. floridus* in Leonardi and Polo 1952) and by enlarging the stratigraphic log of the upper San Cassian Formation to include the *T. aonoides* and *A. austriacum* ammonoid Zones. For further literature regarding to the San Cassian Formation, we refer to the reference lists of Mietto et al. (2012) and Urlichs (2017).

Occurrence: *Carnites floridus* occurs in Carnian Hallstatt Limestone of Feuerkogel/Austria and Rappoltstein/Germany, in the first Raibl shale in Austria and Germany (Bavaria), in the Reingraben shales in Austria (Frech 1911b; Lukeneder & Lukeneder, 2022). Hungary (Frech 1911b), Slovenia (Jurkovšek et al., 2002) and Italy.

Pinacoceratidae Mojsisovics, 1879

The Family Pinacoceratidae probably has its origin in the late Anisian to lower Ladinian age with *Praepinacoceras damesi* (Mojsisovics). In the subsequent Carnian stage the Family Pinacoceratidae is subdivided into several genera whose phylogenetic relationships to each other are not very clear. A close relationship exists among the genera *Pompeckjites* and *Eupinacoceras* in the development of the suture line and in some morphological parameters.

Genus *Pompeckjites* Mojsisovics, 1902

Type species: *Pompeckjites layeri*, (Hauer, 1847)

1847 *Ammonites layeri* Hauer, pl. 9, figs. 1-3.

1873 *Pinacoceras layeri*, Mojsisovics, pl. 23, figs. 1-6.
1902 *Pompeckjites layeri*, Mojsisovics, pl. 19, figs. 3-5; pl. 20, fig. 1.

Description: For detailed description see in (Hauer, 1847) and in (Mojsisovics, 1873, 1902)

Remarks: In the Hallstatt Limestone, *Pompeckjites layeri* (see Figs. 4, A-E) spans the entire Julian stage (*T. aon*, *T. aonoides* and *A. austriacum* ammonoid Zones). Our own measurements on *P. layeri* from the *T. aonoides* and *A. austriacum* Zones show slight differences in the development of the juvenile whorls. In the *A. austriacum* Zone the inner whorls are thicker and do show a somewhat persisting rounded venter stage (see white arrows in Fig. 7, C) than in the *T. aonoides* Zone where the early juvenile whorls are thinner and more fastigated (see Fig. 7, D) at equal size. According to Krystyn (1973: 125, see in faunal list of *T. aon* Zone) *P. philopater* is synonymous with *P. layeri*. In contrast to this opinion *Pinacoceras philopater* (Laube) was assigned to *Pompeckjites* by Bizzarini (1987).

Occurrence: According to Krystyn (1978), *P. layeri* occurs in the *T. aon*, *T. aonoides* and *A. austriacum* Zones of the Hallstatt Limestone. San Cassian Formation/Italy.

"Placites" urlichsi Bizzarini, 1987

Type species: *Placites urlichsi* Bizzarini, 1987, pl. 1 figs. 1, 2a,b, 3a,b, 6a,b, 7, 8. Holotype: pl. 1, fig. 1, from Boa Staolin. Paratypes: pl. 1, figs. 6-8, from Boa Staolin. Depository of types (see Bizzarini, 1987: 50).

1952 *Carnites floridus*, Leonardi & Polo, pl. 1 figs. 26, 44, 45, 47- 49, 55, 57; pl. 2, figs. 39, 40, 41, 42, 43.

2000 *Placites urlichsi* Bizzarini, pl. 3, figs. 3, 4.

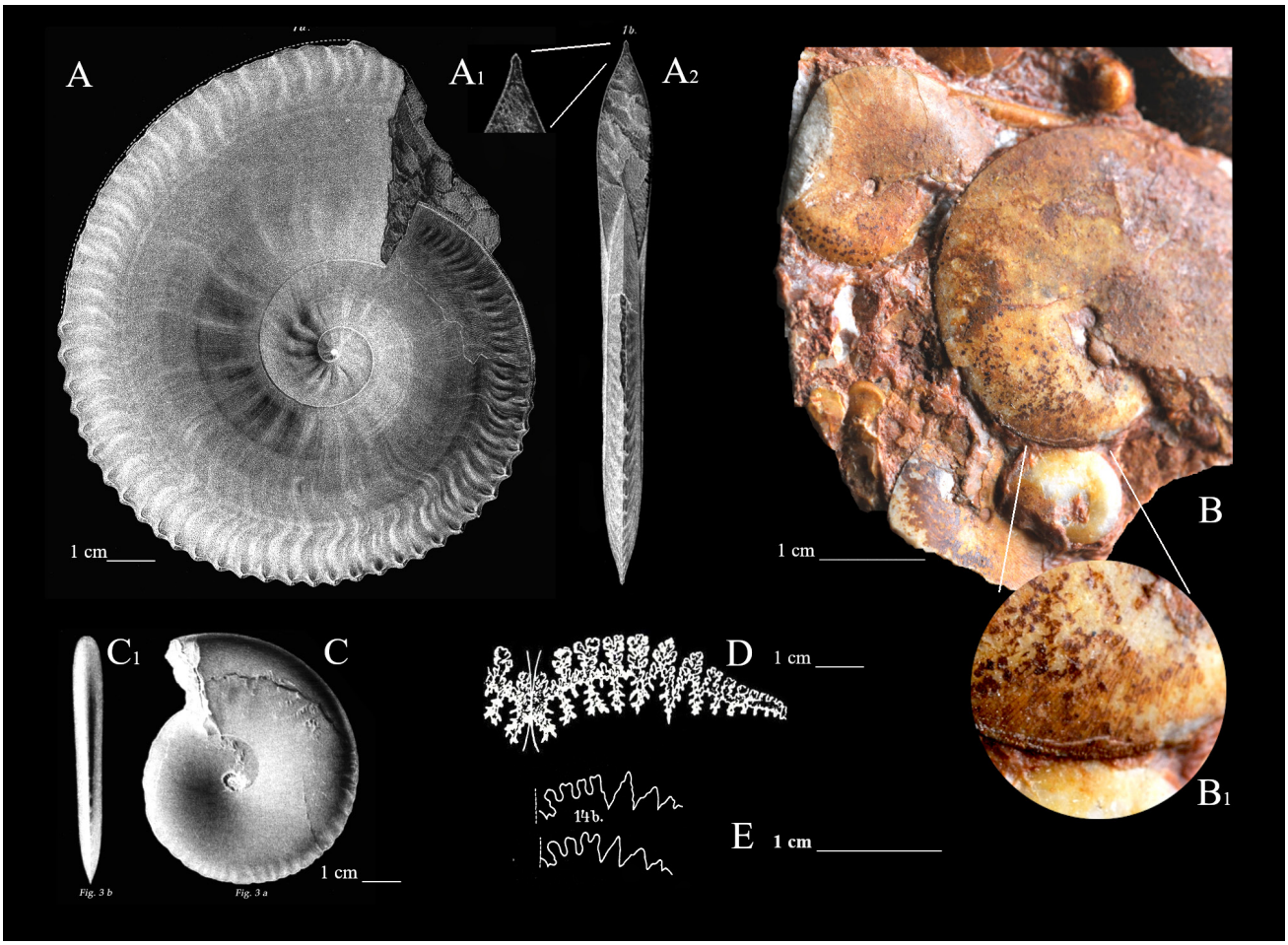

Fig. 4. *Pompeckjites layeri*.

A-A2, *Pompeckjites layeri* (Mojsisovics, 1902: pl. 20, fig. 1), side and venter view. B, *Pompeckjites layeri* from Hallstatt Limestone (*T. aonoides* Zone) of Rappoltstein. B1, enlarged detail of the preserved wrinkle layer. D, suture of *P. layeri* (Hauer, 1847: pl. 9, fig. 3). E, suture of *P. layeri* (Diener, 1915: pl. 2, figs. 14 a, b). C-C1, *P. layeri* (Mojsisovics, 1873: pl. 23, fig. 3) side and venter view.

Description: The early juvenile stage shows an open umbilicus and a rounded venter (Figs. 5, A1, B and C). Then the wide umbilicus narrows quickly, leaving a deep narrow navel. During further growth stages the venter is at first sub to high-trapezoidal rounded and finally develops a broad tabulate venter stage (see Figs. 7, A2, B1 and F1). At this growth stage *Placites urlichsi* resembles *Sageceras* sp. in form and cross-section (see Fig. 9, E1) but shows a totally different suture line. The suture line of *P. urlichsi* shown in Bizzarini, (1987: 51) is comparable with the suture lines of equal sized specimens from Fladung, site 2 in the Hochobir massif. Well preserved flanks of bigger specimens of *P. urlichsi* from the same site show faint growth lines with a distinct bend towards the aperture in the middle of the flank.

Remarks: Our specimens from Fladung, site 2 reach 25 mm in diameter (see Figs. 5, D and 6, D) and show a body chamber of about a half to three quarters of the coiling. Visible sutures were found on a few specimens only. In the Hochobir massif, two morphotypes of *Placites urlichsi* can be recognized. Both variants show the same tabulate venter in sub-mature growth stages. Morphotype 1 (see Figs. 5, A1, A2 and C) is somewhat thinner and shows a sharp high-trapezoidal venter development in juvenile stage at roughly 15 mm in diameter. At this stage, specimens of morphotype 1 (see Fig. 5, A2; Figs. 6, E and 7, E2) are difficult to distinguish with the naked eye from *Pompeckjites layeri* (see Fig. 6, A). In its juvenile stage morphotype 2 develops a thicker, more rounded sub-trapezoidal venter.

Placites urlichsi in Bizzarini (1987: figs. 3a, b) is identical to the same sized specimens of the morphotype 2 from Fladung, site 2. The Figures 2a, b in Bizzarini (1987) are identical to morphotype 1 from Fladung, site 1 a-c. The suture line is identical in both morphotypes. The steinkern of *Pompeckjites philopater* pictured in Bizzarini (2000: pl. 2, fig. 6) from Boa Tamarin is surmised to be a *Placites urlichsi* because on the steinkern the distinct ventro-lateral margins (compare to Fig. 5, A2) of *P. urlichsi* morphotype 1 are visible. From a stratigraphic point of view, the ammonoid fauna of

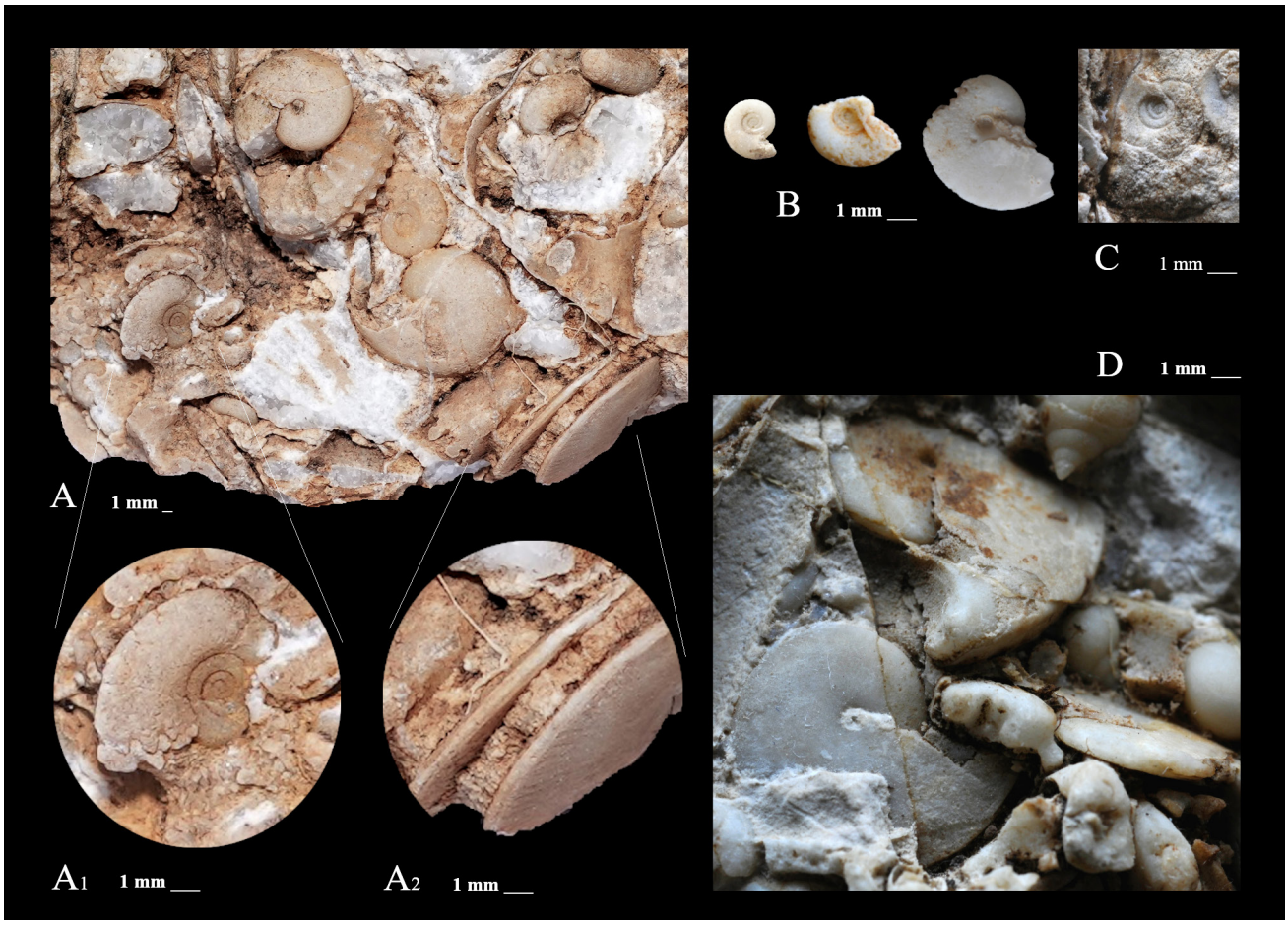

Fig. 5. *Placites urlichsi* from Obir.

A, ammonoid fauna from Fladung site 1c. A1, enlarged juvenile internal mold/steinkern of *P. urlichsi,* (morphotype 1). A2, enlarged venter (steinkern) of *P. urlichsi*, (morphotype 1). B, early juvenile growth stages of *Placites urlichsi* (morphotype 2). C, *Placites urlichsi* (morphotype 1) showing partial shell preservation. D, *Placites urlichsi* (morphotype 2) showing partial shell preservation.

Boa Tamarin in Bizzarini (2000: 22), is thought to be slightly older than the ammonoid fauna of Boa Staolin whence *Placites urlichsi* morphotype 2 occurs. Similar minor age and shape (from slender to thicker specimens) differences are also recognizable at the Hochobir sites. In *P. layeri* a similar development from slender to thicker specimens was observed from the *T. aonoides* Zone towards the *A. austriacum* Zone (see Figs. 7, C and D).

Occurrence: Morphotype 2 (see in Figs. 5, B and D) from Hochobir/Fladung exclusively at site 2 but is very common there. Morphotype 1 (see in Figs. 5, A1, A2 and C) occurs at Fladung, sites 1a, b and c. Unterpetzen/Podpeca and San Cassian Formation.

Arguments to replace *Placites urlichsi* Bizzarini to the genus *Pompeckjites*

The genus *Placites*, (Superfamily Pinacoceratoidea Mojsisovics, 1879, Family Gymnitidae Waagen, 1895) is characterized by its platycone cross-section and its rounded venter. According to (Mojsisovics, 1873) all species of *Placites* are distinguished mainly on their whorl sections and suture lines. Furthermore, all species descriptions of *Placites* in Mojsisovics (1873) were based on sub mature and mature stages of growth.

The type species *Placites platyphyllus* (Mojsisovics, 1873) as the closely related species *Placites polydactylus*, *P. oxyphyllus* and *P. myophorus* show all a closed umbilicus and an external saddle with one strong side branch on the ventral side. Their confirmed age is middle to late Norian. According to Diener (1915b) no real adventitious lobes/saddles occur. The same feature was noted by Spath (1951) who described in *Placites platyphyllus* a simple suture line as in *Gymnites* with an individualized outer branch of the external saddle. Subsequently this similarity to *Gymnites* led to a ranking of *Placites* within the Family Gymnitidae. *Paragymnites* (Hyatt, 1900), whose generic type is *Placites sakuntala* (Mojsisovics, 1896) was established for those species of *Placites* which do not show this strong side branch on the external saddle. *Placites placodes* and *Placites perauctus*, described in Mojsisovics (1873) are, according to

Krystyn and Siblik (1983), of late Carnian (Tuvalian 3) and early Norian (Lacian 1) age. They both differ from other *Placites* sp. and from *Paragymnites* sp. by a highly individualized external saddle and additionally in *P. placodes* by a small open umbilicus.

Based on the above mentioned differences, *Placites urlichsi* has to be compared to the type species *Placites platyphyllus* exclusively.

Already Bizzarini (1987: 45), mentioned the close relationship of his newly established species *Placites urlichsi* to the genus *Pompeckjites* and stated: "The two species described here present characteristics of the external saddle and the suspensory lobe that seem intermediate between the genera *Placites* and *Pompeckjites*". The above mentioned suture line characteristics were well recognized by Bizzarini (1987) in his own findings from the Upper San Cassian formation of Boa Staolin (horizon B, in Bizzarini, 1987) and in the pictured and classified specimens of "*Carnites floridus*" in Leonardi and Polo (1952). Unfortunately, Bizzarini (1987) recognized more analogies to the genus *Placites* than to *Pompeckjites*. The main reason for his supposed similarity to *Placites* was the use of exclusively juvenile specimens showing not fully developed suture lines.

As mentioned above, *Placites platyphyllus* is restricted to the upper Norian stage. This makes a comparison of juvenile suture lines of early Carnian *Placites urlichsi* with sub-mature suture lines of late Norian *Placites platyphyllus* not very realistic. *P. urlichsi* differs from *P. platyphyllus* in its strongly dissolved external saddle, its persistent open umbilicus and its sub-mature tabulate ventral stage.

Based on these differences *Placites urlichsi* is hereby transferred to the genus *Pompeckjites*.

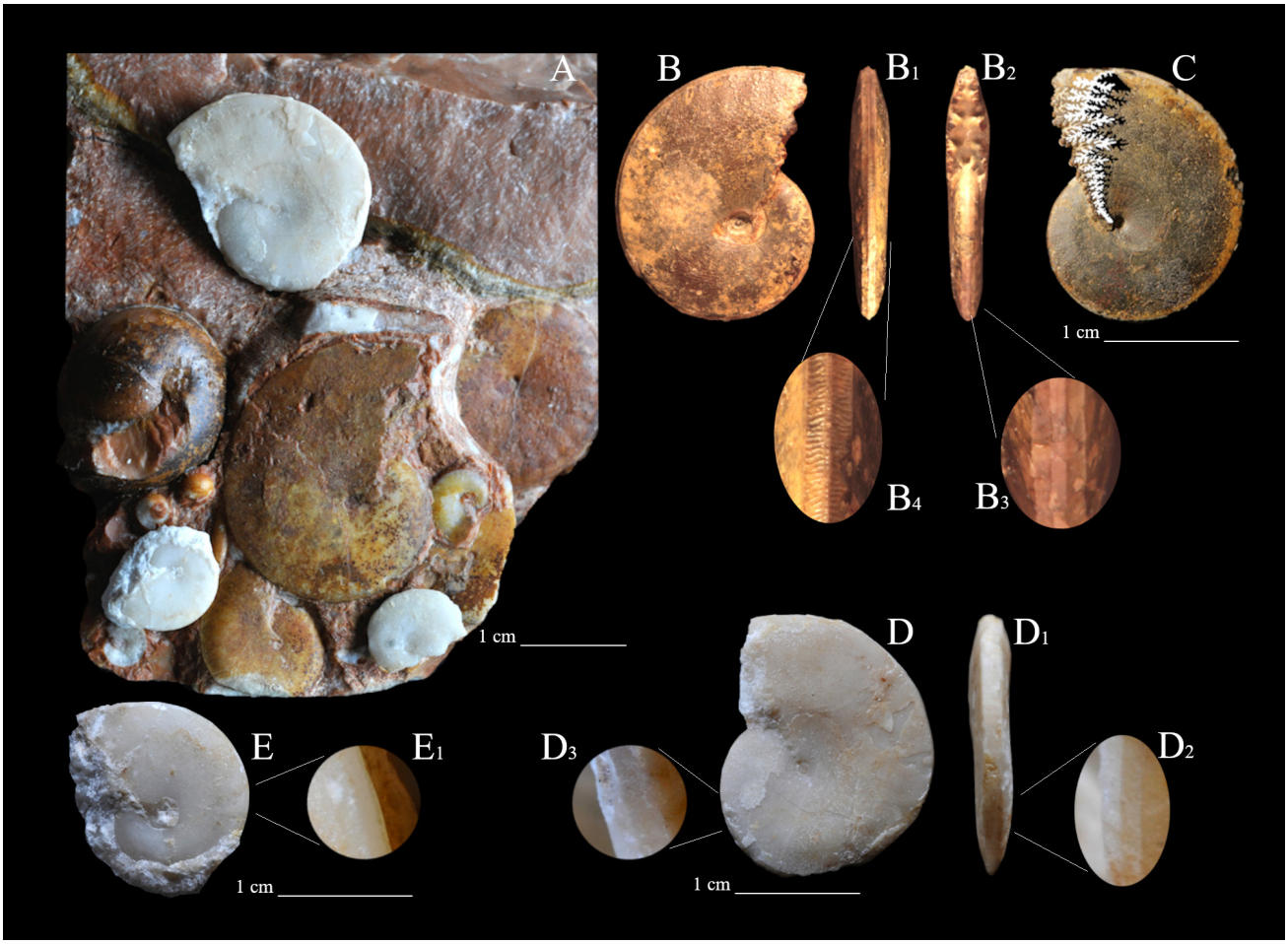

Fig 6. Comparison of *Pompeckjites urlichsi* from Wettersteinkalk to *P. urlichsi* from the upper San Cassian Formation.

A, direct comparison of *Pompeckjites layeri* in red Hallstatt Limestone from Rappoltstein to white specimens of *Pompeckjites urlichsi* (morphotype 1, from Fladung, site 1c). B, phragmocone (showing partial shell) of *Pompeckjites urlichsi* from the upper San Cassian Formation of Boa Staolin. B1 and B2, venter views of ammonoid B, B3 and B4, enlarged details of the trapezoidal venter development. C, backside of ammonoid B with marked suture lines. D, *Pompeckjites urlichsi* showing preserved shell on the body chamber and with parts of shell on the phragmocone. D1 - venter view of ammonoid D. D2 and D3, enlarged venter details (without shell) of ammonoid D. E - small specimen of *P. urlichsi* (morphotype 1, Fladung, site 1c) that is difficult to distinguish from same sized specimens of *P. layeri*. E1, enlarged trapezoidal venter detail of E.

Pompeckjites urlichsi (Bizzarini, 1987)

Type species: The designated holotype and the paratypes of *Placites urlichsi* in Bizzarini, 1987 are hereby accepted as holotype and as paratypes of *Pompeckjites urlichsi* (Bizzarini, 1987).

1987 *Placites urlichsi* Bizzarini, p. 50-52, pl. 1, figs. 1, 2a, b, 3a,b, 6a,b, 7, 8; text figs. 2b, 3; tab. p. 52.

1952 *Carnites floridus* (Wulfen), Leonardi & Polo, pl. 1 figs. 26, 44, 45, 47-49, 55, 57; pl. 2, figs. 39, 40, 41, 42, 43.

2000 *Placites urlichsi* Bizzarini, pl. 3, figs. 3, 4.

We propose the following characteristics to differentiate *Pompeckjites layeri* (Hauer) from *Pompeckjites urlichsi* (Bizzarini). Note that the early juvenile stage (up to 5 mm in diameter) in both species is identical in showing a round venter and an open umbilicus. In further growth both species show an eccentric umbilical ingression towards to a closed or nearly closed umbilicus. After the umbilicus is closed or nearly closed an eccentric umbilical egression evolves in both species.

***Pompeckjites layeri* (Hauer 1847):** Persisting sharp acute venter up to more than 30 mm diameter. Mature sculpture on body chamber is very variable but never showing a tabulate venter. The deeply incised external saddle shows four stems already in juvenile specimens. Large mature size up to 15 cm.

***Pompeckjites urlichsi* (Bizzarini 1987):** A rounded sub to high-trapezoidal ventral stage that persists to roughly 15 mm diameter. In morphotype 1 a distinct tabulate middle keel occurs at this size on steinkerns (Fig. 7, A1; Figs. 8, D, D2). Sometimes this tabulate part of the trapezoidal

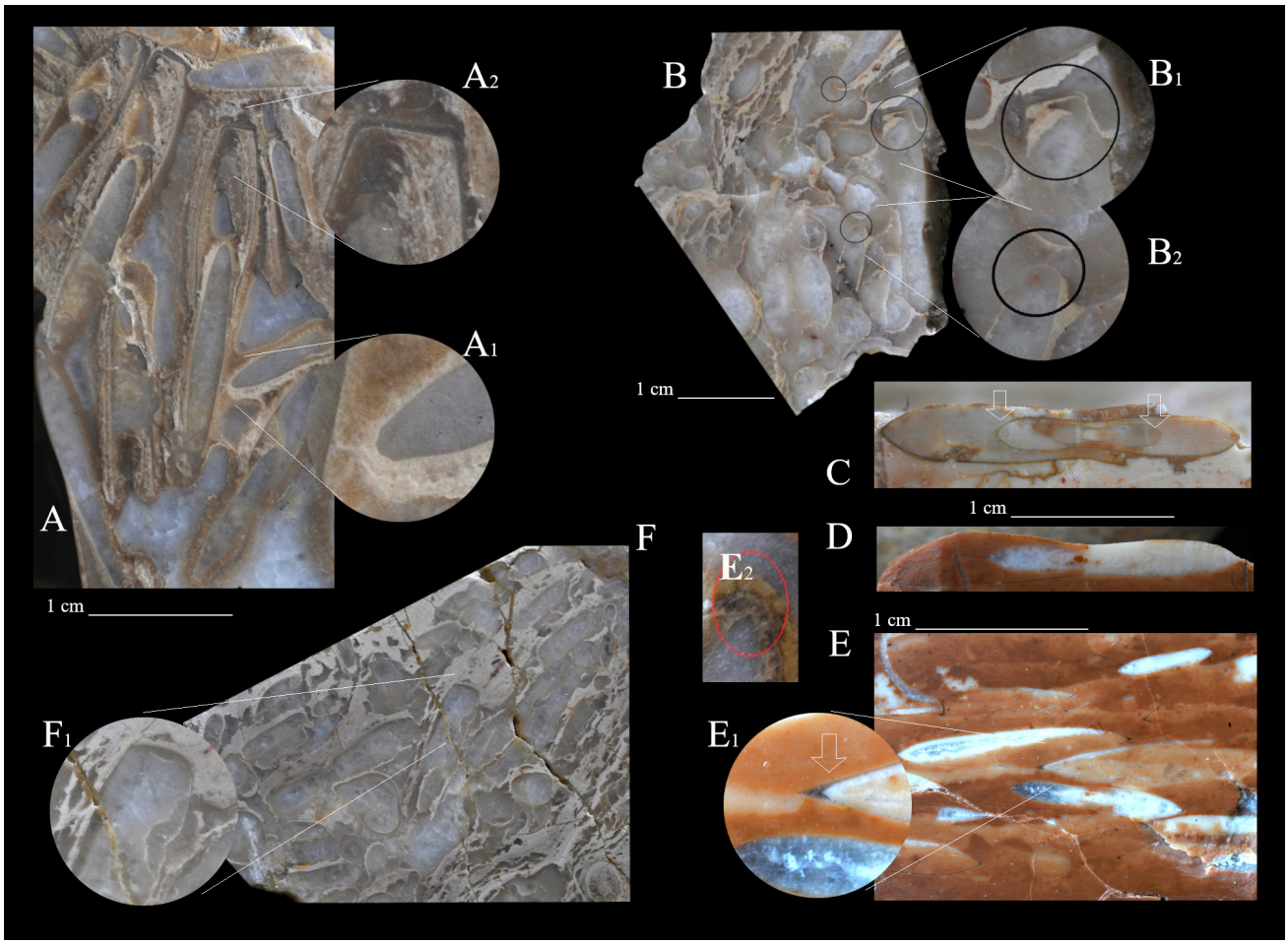

Fig. 7. Differences of *P. urlichsi* to *P. layeri* in transversal and cross-sections.

A, polished hand specimen showing frequent transversal-sections of *Pompeckjites urlichsi,* (morphotype 1, Fladung, site 1c). A1, enlarged trapezoidal venter detail of the internal mold/steinkern. A2, enlarged tabulate venter detail with preserved shell, B, transversal-sections of *P. urlichsi* (morphotype 2) from Fladung, site 2. B1 and B2, enlarged tabulate venter details. C, cross section of *Pompeckjites layeri* from the *A. austriacum* Zone (Hallstatt Limestone of Feuerkogel). D, cross section of *P. layeri* from the *T. aonoides* Zone of Rappoltstein. E, transversal-section with frequent juvenile specimens of *P. layeri* (*T. aonoides* Zone) of Rappoltstein. E1, the white arrow shows the two different venter preservation modes in *P. layeri*. Blunt triangular without shell (preserved in white calcite on the internal side) compared to the acute venter with shell (preserved in darker calcite). E2, shows a comparable venter development on a steinkern of *P. urlichsi* morphotype 1.

venter is very small (Fig. 7, E2). It is more rounded trapezoidal in morphotype 2 steinkerns (Fig. 7, B2) and in specimens of morphotype 1 preserved with shell. After that stage the sub-mature tabulate venter starts to evolve (Figs. 7, A2, B1). The incised external saddle shows three stems in juvenile morphs. The mature size of *P. urlichsi* remains unknown. Specimen found at Hochobir reached a size of 25-30 mm showing a body chamber length of roughly a half to three quarters of a whorl.

Species differentiation of *Pompeckjites urlichsi, Pompeckjites layeri, Sageceras haidingeri* and *Carnites floridus* based on morphology and polished transversal-sections

Morphological similarities between *Pompeckjites urlichsi* (Bizzarini, 1987), *Pinacoceras philopater* (Laube, 1869) and *Pompeckjites layeri* (Hauer, 1847)

The second species treated by Bizzarini (1987), was *Pinacoceras philopater* (Laube, 1869). Bizzarini (1987) tried to examine the type of *P. philopater* (Laube, 1869), together with Mojsisovics' (1882) samples, stored in the GBA (Geologische Bundesanstalt Austria). Unfortunately, the original specimens have not been found. Therefore, we compared our specimens of *P. urlichsi* morphotype 1 from Fladung/Obir exclusively with the specimens of *P. philopater* and *P. urlichsi* pictured in Bizzarini (1987: pl. 1) in regards to their form and suture line. Diener (1915b: 189) does not comment on *Pinacoceras philopater* as to whether it is synonymous to *Pompeckjites layeri*. He just stated that the small specimens are impossible to compare with other Pinacoceratidae at generic level. The same conclusion was reached by Mojsisovics (1882). According to Krystyn (1973: 125, see in faunal list of *T. aon* Zone) *Pinacoceras philopater* is synonymous with *Pompeckjites layeri*. Contrary to this opinion Bizzarini (1987) established *Pompeckjites philopater* as a separate species in *Pompeckjites*. Our own found specimens from Unterpetzen are well comparable to the specimens shown in Bizzarini (1987: pl. 1, figs. 4a, 4b, 5a, 5b). They mainly differ from *P. layeri* in less acute venter development.

Typical for both species are the similar adventitious saddle elements that according to Diener (1915b) evolved from a broadly developed external saddle. In further growth stages these adventitious saddle stems show a bifid ending in both species. The redrawn original suture line of *Pinacoceras philopater* (1869: pl. 41, fig. 10) pictured in Figure 8, C4, does not clearly show the position of the lateral saddle. It is not clear if there are three or four adventitious stems in the external saddle. The amount of suture line elements shown in Laube (1869) is similar to *Pompeckjites layeri*. In contrast the suture line of *Pinacoceras philopater* in Mojsisovics (1882: pl. 52, fig. 12a) show three stems (redrawn in Fig. 8, C2). The pictured suture line of *P. philopater* in Bizzarini (1987: p.49, Fig. 2, A) shows three stems in its external saddle also (redrawn in Fig. 8, C3).

In *Pompeckjites urlichsi* morphotype 1 from Fladung, site 1a-c, the suture line is nearly identical to the suture line of *P. philopater* in Bizzarini (1987: 49). Morphotype 1 of *P. urlichsi* shows a sub to high-trapezoidal juvenile venter and a tabulate sub-mature to mature ventral stage that isn't described in *P. philopater*. In fact, some juvenile specimens of *P. urlichsi* morphotype 1 (see figs. 6, E-E1) can show a very acute venter. Such specimens cannot be distinguished from *Pompeckjites layeri* or *Pinacoceras philopater* with the naked eye. This can mislead to a classification as *Pompeckjites layeri* when the tabulate venter is not evolved, broken off or not visible in the matrix. Under enlargement the venter on the steinkern of *Pompeckjites urlichsi* morphotype 1 is always trapezoidal, though the tabulate part of the trapezoidal venter is sometimes very small (see Fig. 5, A2; Figs. 6, B4, E, E1 and F 7 E2). In *Pompeckjites layeri* the venter is juvenile or sub-mature always acute. The most acute venter in *P. layeri* can be seen in specimens with well-preserved shell (see Fig. 7, E1).

The Figure 8, A shows a fully chambered steinkern of *P. urlichsi* from Boa Staolin, which was incorrectly classified as *Carnites floridus*. The clearly visible suture line is comparable to *P. urlichsi* morphotype 1 from Fladung/Obir. Figure 8, A1 show remains (white arrows) of an eccentric umbilicus in further growth like in *Pompeckjites layeri*. Here, *P. urlichsi* shows a body chamber length from a half to three quarters of a whorl which is similar to *P. layeri*. D and D1, (with small part of shell) in figure 8, show the ventral development in *Pompeckjites urlichsi*, morphotype 1 that differs clearly from *Pompeckjites layeri*. The wavy band (distinctly visible on the steinkern, less distinctly visible in shell preservation) on both sides of the venter show reminiscence to the sculpture of large mature specimens of *P. layeri* from the Hallstatt Limestone where a similar, broader wavy sculpture occurs on the ventral flanks (see Fig. 4, A). The enlarged cross-section of *P. layeri* in Fig. 7, E1 shows a blunt triangular internal venter development preserved in white calcite (see white arrow). This feature can create distinct ventro-lateral margins on steinkerns. Since similar ventro-lateral

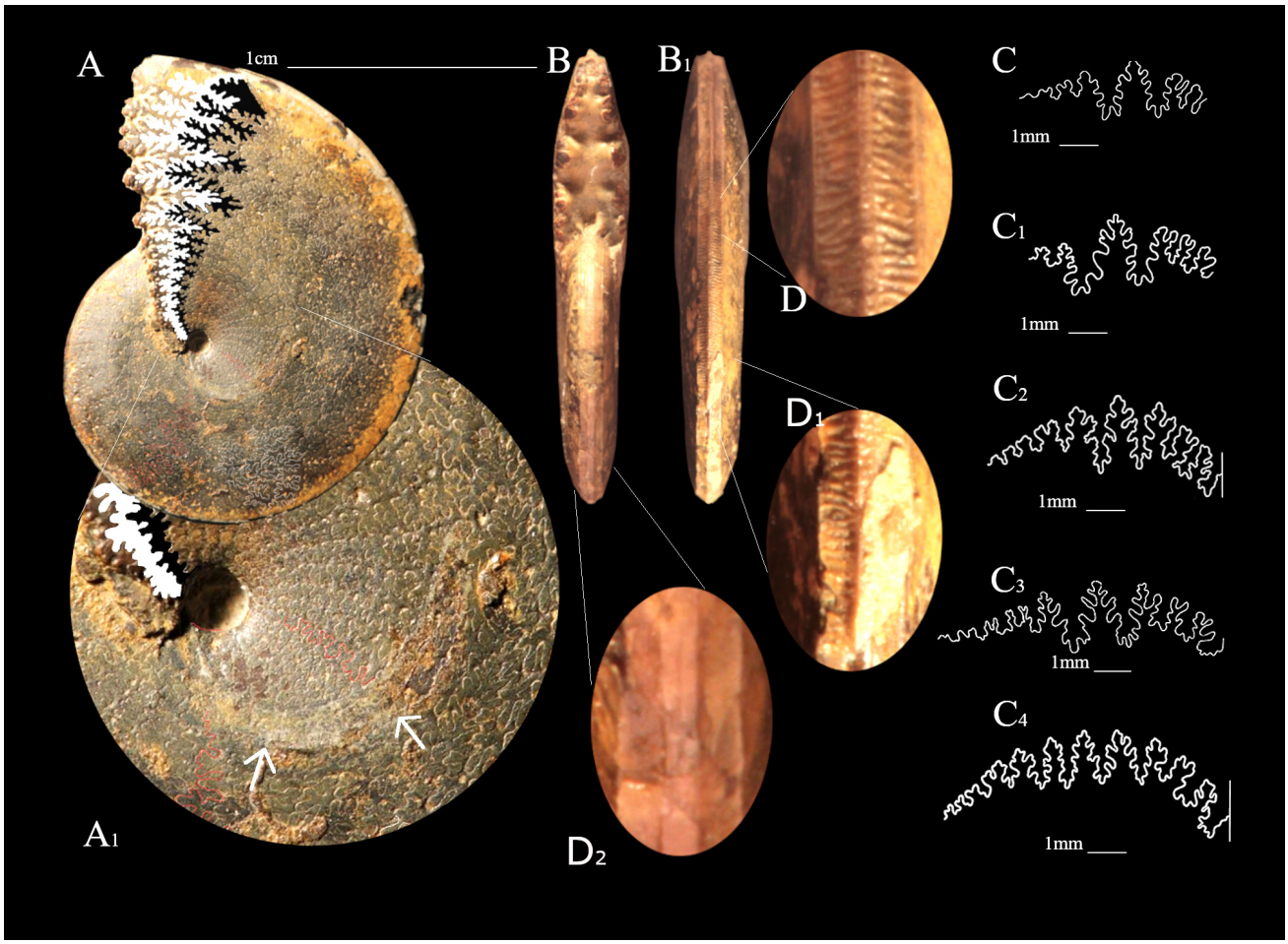

Fig. 8. *Pompeckjites urlichsi* from the San Cassian Formation.

A, interal mold/steinkern of *Pompeckjites urlichsi* from Boa Staolin (coll. Alberto Rubini). A1, reminiscence of an eccentric umbilicus (white arrows) in further growth of *P. urlichsi*. B-B1, venter views of ammonoid A. C-C1, suture of *"Placites" urlichsi* in Bizzarini (1987: p. 51, fig. 3, D and E). C2, redrawn suture of *"Pinacoceras" philopater* (Laube), in Mojsisovics (1882: pl. 52, fig. 12a). C3, suture of *Pompeckjites philopater* (Laube) in Bizzarini (1987: p. 49, fig. 2, A). C4, redrawn suture of *"Ammonites" philopater* Laube, 1869: pl. 41, fig. 10. D, enlarged detail of the wavy bands beside the small tabulate keel. D1, small part of shell that indicates a more rounded trapezoidal venter in specimens preserved with shell.

margins occur on steinkerns of *P. urlichsi* morphotype 1 too (see Figs. 5, A2 and 7, E2) this also may point at a common ancestor of *P. urlichsi* and *P. layeri*.

Morphological similarities between *Pompeckjites urlichsi* (Bizzarini, 1987), *Carnites floridus* (Wulfen, 1793) and *Sageceras* sp.

Diener (1915b) described in *Carnites floridus* a development of the adventitious elements from the external lobe, precisely from the ascending part of the external lobe to the median saddle (see black circles in Figs. 3, C-C5). *Pompeckjites* shows, according to Diener (1915b) no real adventitious elements. It shows a broadly created, deeply incised external saddle instead. The fundamental differences in *Carnites* and *Pompeckjites* are that the adventitious elements evolves in *Carnites* on the ventral side of the external lobus and in *Pompeckjites* on the ventral side of the external saddle.

Species differentiation of *P. urlichsi* from *C. floridus* and *Sageceras* sp.

The bifid stem endings in the adventitious external saddle elements of *Pompeckjites urlichsi* originate from a stronger growth of one side branch of former juvenile pyramidal stems. In *C. floridus* this bifid split of the saddle elements does not exist. In very small specimens of *P. urlichsi*, before this bifid growth feature takes place, the suture line of *P. urlichsi* is similar to the suture line of *Carnites floridus*. That may hint at a common ancestor of *Carnites* and *Pompeckjites*. The trapezoidal venter development in *P. urlichsi* may point in this direction too. But these similarities may be just homeomorphic features too. Therefore, it is not surprising that subsequent authors (Leonardi & Polo, 1952,) often assigned small specimens of *P. urlichsi* to *C. floridus*.

Both morphotypes of *Pompeckjites urlichsi* show in the sub-mature growth stage a tabulate venter which makes them look homeomorphic

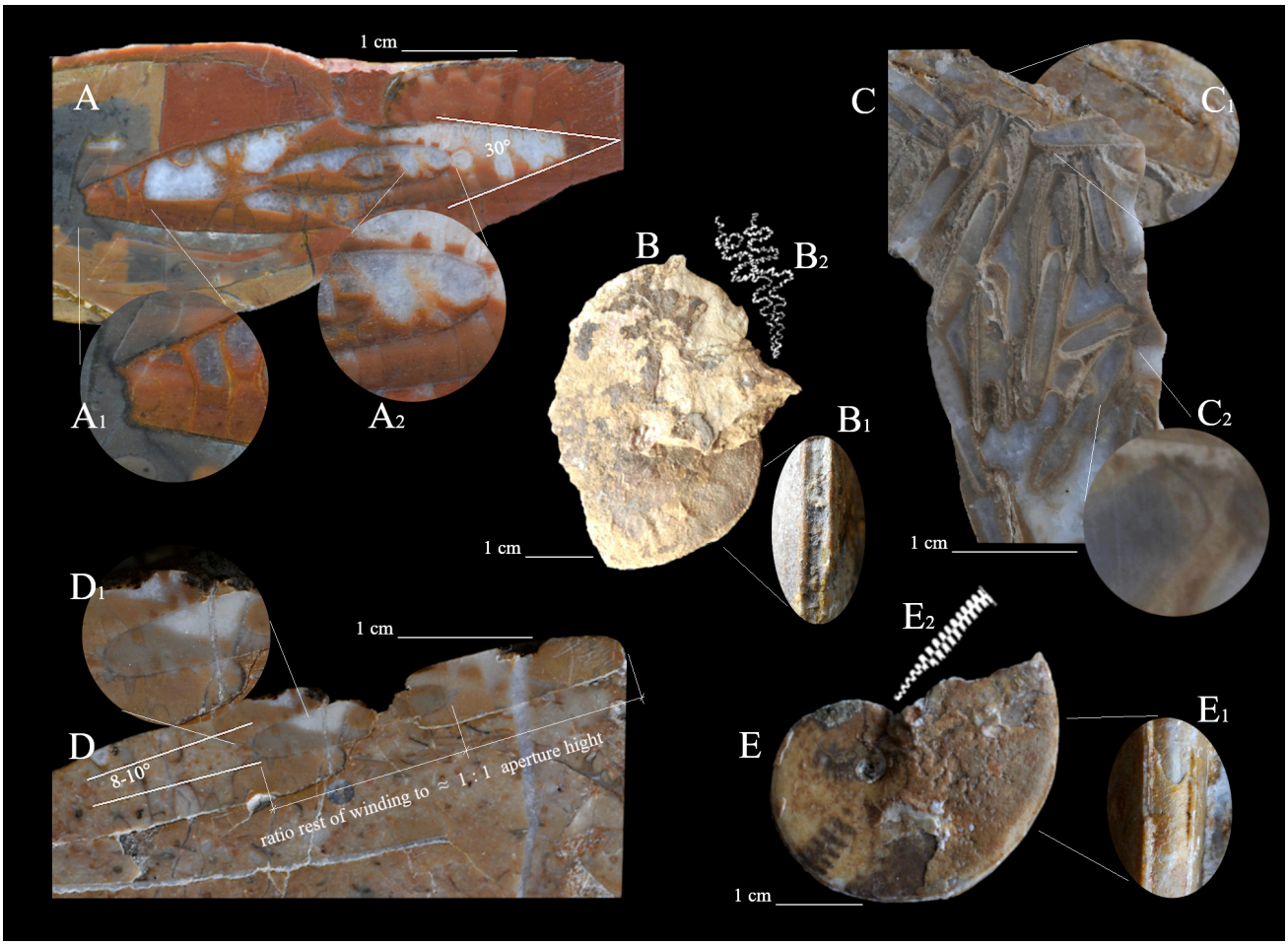

Fig. 9. Species differentiation of *P. urlichsi* from *C. floridus* and *Sageceras* sp.

A, polished cross-section of *Carnites floridus* from Hallstatt Limestone of Rappoltstein. A1 and A2, enlarged development of the tricarinate venter. B, *C. floridus* from Rappoltstein. B1, view of the tricarinate venter. B2, suture line of *C. floridus* in Mojsisovics (1873: pl. 25, fig. 4). C, transversal-sections of numerous *Pompeckjites urlichsi* (morphotype 1) from Fladung/Obir. C1 and C2, enlarged tabulate venter development of *P. urlichsi*. E, *Sageceras haidingeri* from the *T. aonoides* Zone of Rappoltstein. E1, venter of *Sageceras* sp., E2, suture line of *Sageceras*. D, cross-section of *Sageceras* sp. from Hallstatt Limestone of Rappoltstein with outlined flank angle and ratio of aperture height to the rest of the winding. D1, enlarged detail of the juvenile venter.

to *Sageceras* sp. (see Figs. 7, A2; 9 C1, E1). In cross-sections, *P. urlichsi* can be distinguished from *Sageceras* sp. by the different developments of the juvenile whorls (see Fig. 7, A1 compared to Fig. 9, D1). The height of the shell aperture is a helpful distinguishing feature in cross-sections too. *Sageceras* sp. shows roughly a proportion of 1:1 in the ratio of aperture height to the rest of the whorl (see Fig. 9 D). In *Carnites floridus* and *P. urlichsi* the ratio of aperture height to the rest of the whorl is closer to 1:2.

Juvenile whorls of *Sageceras* sp. and *Carnites floridus* are very similar in polished transversal-sections. The flatter angle of the flank is in *Sageceras* sp. (see in Fig. 9, D,) during growth relatively constant at 8-10°, whereas in *C. floridus* (see Fig. 9, A) the angle increases up to 30°. Both in figures. 9, A-A2 and B-B1, shown *C. floridus* originate from Hallstatt Limestone of Rappoltstein (Hornung et. al 2007) and were found together with a sparse *A. austriacum* Zone ammonoid fauna with *Neoprotrachyceras thous* and *Austrotrachyceras* sp.

If the suture lines can be checked, a confusion of *Sageceras* sp. with *Carnites floridus* or *Pompeckjites* sp. can be excluded.

Stratigraphic conclusions

Our data suggest that *Carnites floridus* Hauer is restricted to the first strong pulse of the CPE (Carnian Pluvial Episode) at the border *T. aonoides* Zone to *A. austriacum* Zone (for further literature regarding to the CPE we refer to the reference lists of Dal Corso et al. 2018; Hornung et al. 2007; Mueller et al. 2016 and Preto et al. 2019). An early Julian *T. aon* Zone age or an early Tuvalian *Tropites dilleri* Zone age of true *C. floridus* can be excluded. Based on true *Carnites floridus* the first Raibl shale horizon on Hochobir can be correlated with the beginning of the *A. austriacum* Zone. This is

evidenced in the Hallstatt Limestone of Rappoltstein where *Carnites floridus*, *Neoprotrachyceras thous* and *Austrotrachyceras* sp. were found (Hornung et al. 2007) and in the Reingraben shales of Austria where *Carnites floridus* was referred to the *A. austriacum* Zone in Lukeneder & Lukeneder (2022). Therefore, the underlying Bleiberger Sonderfazies (Holler 1960) with *Pompeckjites urlichsi* can indirectly be correlated with the upper *T. aonoides* Zone. A correct species recognition of *P. urlichsi*, allows a direct correlation of some parts/layers of the Upper San Cassian Formation with layers of the Bleiberger Sonderfazies (upper Wettersteinkalk). Minor morphologic differences in juvenile whorls of *P. urlichsi* further allow for a differentiation in a morphotype 1 and a slightly younger morphotype 2.

Furthermore, the onset of the *A. austriacum* Zone can be fixed with true *C. floridus* in strata where *Austrotrachyceras* sp., was not found. *Pompeckjites urlichsi* in contrast allows for a fixing of the upper *T. aonoides* Zone in strata where *Trachyceras* s. str. was not found or is missing.

Discussion

A transitional ammonoid fauna spanning the period from the *T. aonoides* to the *A. austriacum* ammonoid Zones is not adequately described at present. From an evolutionary view such a fauna should exist. *Pompeckjites urlichsi* (Bizzarini) seems to be an appropriate ammonoid species showing a close stratigraphic range that may fit as an index ammonoid to close this gap. It may be of future importance for a finer stratigraphic correlation between the basinal facies of the upper San Cassian Formation and the coeval algal rhytmites of the upper Wettersteinkalk. Within the condensed pelagic deposits of the Hallstatt Limestone *P. urlichsi* has not been found so far. This might have its origin in a collecting hiatus, in a confusion with small specimens of *Pompeckjites layeri* or *Carnites floridus* or in the possibility of a habitat restriction to the reef fronts and their directly adjacent basins. The above mentioned close morphologic similarity of *P. urlichsi* to small *Carnites floridus* raises some doubts on *Carnites floridus* classifications from the upper *T. aonoides* Zone of the Rio del Lago Formation (Preto et al. 2005). Such small *C. floridus* are surmised to be *Pompeckjites urlichsi* (Bizzarini) and thus may need further revision.

According to Krystyn (1978) *Pompeckjites layeri* spans the entire Julian stage and *Pinacoceras philopater* is thought to be synonymous (Krystyn 1973: 125, see in faunal list of *T. aon* Zone). Contrary to that opinion, Bizzarini (1987) established *Pompeckjites philopater* as a separate *Pompeckjites* species. Here we classify all *Pompeckjites* species that show a sub-mature tabulate venter as *Pompeckjites urlichsi*. The transfer from *Placites* to *Pompeckjites* in *P. urlichsi* is based on the similar sutureline, the similar juvenile venter development and the similar eccentric umbilical egression compared with *Pompeckjites layeri*. Especially juvenile specimens of *Pompeckjites urlichsi* morphotype 1 show a close similarity to *Pompeckjites layeri*. *Pompeckjites philopater* as pictured in Bizzarini (1987) is intermediate in shape between *P. layeri* and juvenile *P. urlichsi* morphotype 1 before evolving the tabulate venter. Juvenile specimens of *P. urlichsi* morphotype 2 do show some similarity in shape and suture line to *Pinacoplacites* Diener, 1916. A presumed evolutionary connection of Julian *Pompeckjites urlichsi* to upper Tuvalian *Pinacoplacites* sp. may exist via *"Placites" placodes* but it is not confirmed at present. Further research to this assumption was hindered by lacking data.

Acknowledgements

We sincerely thank the UNESCO Geopark Karawanken/Karavanke (A/Slo) for the permission to carry out fieldwork and research in its area, Matija Križnar (Slovenian Museum of Natural History, Ljubljana) and Ivan Ocepek (Mežica), for the possibility to visit the historical mining area Unterpetzen/Podpeca (Slovenia), Peter Englmaier, ECONSULT expert consultancy, Vienna and University of Vienna, for the help in the fieldwork, writing and literature search, Alberto Rubini (Italy) for the pictures of the ammonoid from Boa Staolin on Figures. 6 B-C, 8 A-D, Roger Furze (Germany), Heidi Henderson and Karen Lund (Vancouver/Canada) for their help to improve our English.

References

Arthaber, G. 1905: Die alpine Trias des Mediterran-Gebietes. In: Frech, F. (ed.): Lethaea geognostica, pt. II, Das Mesozoicum, Trias: 223–391, 417–472.

Arthaber, G. 1911: Die Trias von Albanien – Beiträge zur Paläontologie von Österreich. Mitteilungen des Geologischen und Paläontologischen Institutes der Universität Wien, 24: 169–277.

Balini, M. 2008: Discovery of upper Ladinian ammonoids at the type locality of the lower Carnian Desatoyense zone (South Canyon, New Pass range, Nevada). Journal of Paleontology, 82/1: 176–182. https://doi.org/10.1666/05-049.1

Balini, M., Lucas, S. G., Jenks, J. F. & Spielmann, J. A. 2010: Triassic ammonoid biostratigraphy: an overview. Geological Society, London, Special Publications: 334/1: 221–262. https://doi.org/10.1144/SP334.10

Balini, M., Jenks, J. & Martin, R. 2012: Taxonomy and stratigraphic significance of *Trachyceras silberlingi* n. sp., from the Lower Carnian of South Canyon (New Pass Range, central Nevada, USA. Bollettino della Società Paleontologica Italiana, 51/2: 127–136.

Bechstaedt, T. 1979: The lead-zinc deposit of Bleiberg-Kreuth (Carinthia, Austria): Palinspastic situation, paleogeography and ore mineralisation. Verh. Geol. B.-A., H. 3: 221–235.

Bizzarini, F. 1987: Revisione delle Pinacoceratidae (Cephalopoda, Ammonoidea) della Formazione di S. Cassiano (Traissico superiore). Boll. Mus. civ. St. nat. Venezia, 38: 43–54.

Bizzarini, F. 2000: Studio biostratigrafico delle tanatocenosi a cefalopodi della Formazione di S. Cassiano (Valle d'Ampezzo, Dolomiti orientali). Lavori della Società Veneziana di Scienze Naturali, 25: 15–28.

Dal Corso, J., Gianolla P., Rigo, M., Franceschi, M., Roghi, G., Mietto, P., Manfrin, S., Raucsik, B., Budai, T., Jenkyns, H.C., Reymond, C.E., Caggiati, M., Gattolin, G., Breda, A., Merico, A. & Preto, N. 2018: Multiple negative carbon-isotope excursions during the Carnian Pluvial Episode (Late Triassic). Earth-Science Reviews, 185: 732–750. https://doi.org/10.1016/j.earscirev.2018.07.004

Di Bari, D. & Baracca, A. 1998: Late Triassic (Carnian) Foraminifers of Northeastern Cortina d'Ampezzo (Tamarin, San Cassiano Fm., Dolomites, Italy). Ann. Mus. civ. Rovereto, Arch., St., Sc. nat., 12 (1996): 117–146.

Diener, C. 1915a: Fossilium Catalogus 1, Animalia, Pars 8, Cephalopoda Triadica, 369 p.

Diener, C. 1915b: Über Ammoniten mit Adventivloben. Denkschriften der Akademie der Wissenschaften. Math. Natw. Kl., 93: 139–199, incl. 2 Pls.

Diener, C. 1916: Einige Bemerkungen zur Nomenklatur der Triascephalopoden. Centralblatt für Mineralogie, Geologie und Paläontologie: 97–105.

Doguzhaeva, L.A., Mapes, R.H., Summesberger, H. & Mutvei, H. 2007: The preservation of body tissues, shell, and mandibles in the ceratitid ammonoid *Austrotrachyceras* (Late Triassic), Austria: 221–237.

Frech, F. 1911a: Neue Cephalopoden aus den Buchensteiner, Wengener und Raibler Schichten des südlichen Bakony mit Studien über die Wohnkammerlänge der Ammoniten und über die Lebensweise der Nautileen. Teil 4 in: Resultate der wissenschaftlichen Erforschung des Balatonsees. 1, 2. Anhang: Palaeontologie der Umgebung des Balatonsees, 3. Bd: 94 p., incl. 11 pls.

Frech, F. 1911b: Nachträge zu den Cephalopoden und Zweischalern der Bakonyer Trias (Werfener und Cassianer Estherienschichten. Teil 5 in: Resultate der wissenschaftlichen Erforschung des Balatonsees, 1, 2. Teil Anhang „Palaeontologie der Umgebung des Balatonsees" 3. Bd: 1–38, incl. 4 pls.

Frech, F. 1912: Die Leitfossilien der Werfener Schichten und Nachträge zur Fauna des Muschelkalkes der Cassianer und Raibler Schichten sowie des Rhät und des Dachsteindolomits (Hauptdolomit). - Res. d. wissenschaftlichen Erforsch. d. Balatonsees, 1, 1. Anhang, Paläontologie der Umgebung des Balatonsees, 2/6: 96 p., incl. 16 pls., Budapest.

Gemmellaro, G.G. 1904: I cefalopodi del Trias superior della regione occidentale della Sicilia. Giorn. Sc. Nat. Ec., 24: 1–319.

Haeckel, E. 1866: Allgemeine Entwicklungsgeschichte der Organismen. Berlin, Reimer.

Hauer, F. 1846: Über die Cephalopoden des Muschelmarmors von Bleiberg in Kärnten. Naturw. Abh. von W. Haidinger. 1: 10 p., incl. 1 pl.

Hauer, F. 1847: Neue Cephalopoden aus dem rothen Marmor von Aussee. Naturw. Abh. von W. Haidinger. 1: 24 p., incl. 3 pls.

Hauer, F. 1855: Beiträge zur Kenntnis der Cephalopoden-Fauna der Hallstätter Schichten. Denkschr. Akad. Wiss. Wien, 9/1: 141–166, incl. 5 pls.

Hoffmann, R., Howarth, M., Fuchs, D., Klug, C. & Korn D. 2022: The higher taxonomic nomenclature of Devonian to Cretaceous ammonoids and Jurassic to Cretaceous ammonites including their authorship and publication. N. Jb. Geol. Paläont. Abh. 305/2: 187–197. https://doi.org/10.1127/njgpa/2022/1085

Holler, H. 1960: Zur Stratigraphie des Ladin im östlichen Drauzug und in den Nordkarawanken. Carinthia II, 150/70: 63-75.

Hornung, T., Spatzenegger, A. & Joachimski, M. 2007: Multistratigraphy of condensed ammonoid beds of the Rappoltstein (Berchtesgaden, southern Germany): unravelling palaeoenvironmental conditions on 'Hallstatt deep swells' during the Reingraben Event (Late Lower Carnian). Facies, 53: 267–292. https://doi.org/10.1007/s10347-006-0101-1

Hyatt, A. 1884: The Evolution of the Cephalopoda. I. Science, 52: 122–127.

Hyatt, A. 1900: Cephalopoda in Zittel-Eastman, Textbook of Palaeontology, 502–604.

Hyatt, A. & Smith, J.P. 1905: The Triassic cephalopod genera of America. U.S Geological Survey, Professional paper No. 40: 394 p., incl. 85 pls.

Jenks, J.F., Monnet, C., Balini, M., Brayard, A. & Meier, M. 2015: Biostratigraphy of Triassic ammonoids. In Ammonoid Paleobiology: From macroevolution to paleogeography, 329–388.

Johnston, F.N. 1941: Trias at New Pass, Nevada (New Lower Karnic Ammonoids). Journal of Paleontology, 50: 447–491.

Jurkovšek, B., Kolar-Jurkovšek, T. & Jaecks, G.S. 2002: Macrofauna of the Carnian beds in the Mežica area. Geologija, 45/2: 413–418. https://doi.org/10.5474/geologija.2002.041

Konstantinov, A.G. 2008: Debatable questions of Boreal Triassic stratigraphy: boundary between middle and upper series. Russian Geology and Geophysics, 49/1: 64–71. https://doi.org/10.1016/j.rgg.2007.05.004

Konstantinov, A.G. 2012: A revision of the early Carnian Trachyceratidae (Ammonoidea) of northeastern Asia. Paleontological Journal, 46/5: 453–460. https://doi.org/10.1134/S0031030112050048

Krystyn, L. 1973: Zur Ammoniten- und Conodonten-Stratigraphie der Hallstätter Obertrias (Salzkammergut, Österreich). Verh. Geol. B.-A. Wien, 1973/1: 113–153.

Krystyn, L. 1978: Eine neue Zonengliederung im alpin-mediterranen Unterkarn. Schriftenreihe der Erdwissenschaftlichen Kommissionen. Österreichische Akademie der Wissenschaften, 4: 37–75, incl. 5 pls.

Krystyn, L. 1980: Stratigraphy of the Hallstatt region. Abh. Geol. B.-A. Wien, 35: 69–80.

Krystyn, L. 1982: Obertriassische Ammonoideen aus dem Zentralnepalesischen Himalaya. Abh. Geol. B.-A. Wien. 36: 63 p, incl. 18 pls.

Krystyn, L. & Siblik, M. 1983: *Austriellula robusta n. sp.* (Brachiopoda) from the Upper Carnian Hallstatt limestone of Timor (Indonesia). Schriftenreihe der Erdwissenschaftlichen Kommissionen. Österreichische Akademie der Wissenschaften, 5: 259–266.

Laube, G.C. 1869: Die Fauna der Schichten von St. Cassian. Ein Beitrag zur Paläontologie der Alpinen Trias. V. Abtheilung. Cephalopoden. Schlusswort. Denkschrift Math. Naturw. Kl. 30: 49–108, incl. 8 pls.

Lipold, M.V. 1856: Erläuterung geologischer Durchschnitte aus dem östlichen Kärnten. Jb. Geol. R.-A. 7: 332–345.

Leonardi, P. & Polo, C. 1952: La fauna Cassiana di Cortina d'Ampezzo. Parte II: Cefalopodi. Mem. Ist. Gel. min. Univ. Padova, 17: 1–28, incl. 5 pls.

Lukeneder, S. & Lukeneder, A. 2014: A new ammonoid fauna from the Carnian (Upper Triassic) Kasimlar Formation of the Taurus Mountains (Anatolia, Turkey). Palaeontology, 57/2: 357–396.

Lukeneder, A. & Lukeneder, P. 2022: Taphonomic history and trophic interactions of an ammonoid fauna from the Upper Triassic Polzberg palaeobiota. Scientific Reports, 12/1: 1–14. https://doi.org/10.1038/s41598-022-11496-y

Mastandrea, A. 1995: Carnian conodonts from upper Triassic strata of Tamarin section (San Cassiano Fm., Dolomites, Italy). Riv. It. Paleont. Strat. 100/4: 493–510, incl. 4 pls.

Mietto, P., Manfrin, S., Preto, N. & Gianolla, P: 2008: Selected ammonoid fauna from Prati di Stuores/Stuores Wiesen and related sections across the Ladinian-Carnian boundary (Southern Alps, Italy). Rivista Italiana di Palaeontologic e Stratigrafia, 114/3: 377–429, incl. 8 pls.

Mietto, P., Manfrin, S., Preto, N., Rigo, M., Roghi, G., Furin, S., Gianolla, P., Posenato, R., Muttoni, G. & Nicora, A. 2012: The Global boundary Stratotype Section and Point (GSSP) of the Carnian Stage (Late Triassic) at Prati di Stuores/Stuores Wiesen Section (Southern Alps, NE Italy). Episodes, 35/3: 414–430. https://doi.org/10.18814/epiiugs/2012/v35i3/003

Mojsisovics, E. 1869: Über die Gliederung der oberen Triasbildungen der östlichen Alpen. Jb. Geol. R.-A. 19: 91–150, incl. 4 pls.

Mojsisovics, E. 1871: Über das Belemnitiden-Geschlecht *Aulacoceras* Fr. v. Hauer. Abh. Geol. R.- A., 21: 41–57, incl. 4pls.

Mojsisovics, E. 1873: Die Mollusken Faunen der Zlambach und Hallstätter Schichten. Abh. Geol. R.-A., 6/1: 356 p, incl. 32 pls.

Mojsisovics, E. 1879a: Die Dolomit-Riffe von Südtirol und Venetien: Beiträge zur Bildungsgeschichte der Alpen. 551 p.

Mojsisovics, E. 1879b: Vorläufige kurze Uebersicht der Ammoniten-Gattungen der mediterranen und juvavischen Trias. Verh. k.u.k. Geol. R.-A., 7: 133–143.

Mojsisovics, E. 1882: Die Cephalopoden der mediterranen Triasprovinz. Abh. Geol. R.-A., 10, 322 p., incl. 94. pls.

Mojsisovics, E. 1892: Die Hallstätter Entwicklung der Trias. Sitzungsberichte der Akademie der Wissenschaften mathematisch-naturwissenschaftliche Klasse, 101: 769–780.

Mojsisovics, E. 1893: Die Cephalopoden der Hallstätter Kalke. Abh. Geol. R.- A. 6/2: 835 p, incl. 130 pls.

Mojsisovics, E. 1896: Beiträge zur Kenntniss der Obertriadischen Cephalopoden-Faunen des Himalaya. Denkschriften der Mathematisch-Naturwissenschaftlichen Klasse der Kaiserlichen Akademie der Wissenschaften, 63: 575–701, incl. 22 pls.

Mojsisovics, E. 1902: Die Cephalopoden der Hallstätter Kalke. Supplement Band. Abh. Geol. R.-A., 6/3: 177–356, incl. 23 pls.

Mojsisovics, E., Waagen, W. & Diener, C. 1895: Entwurf einer Gliederung der pelagischen Sediments des Trias-Systems. Sb. Akad. Wiss., math. naturw. Kl. 104: 1271–1302.

Mondillo, N., Lupone, F., Boni, M., Joachimski, M., Balassone, G., De Angelis, M., Zanin, S. & Granitzio, F. 2020: From Alpine-type sulfides to nonsulfides in the Gorno Zn project (Bergamo, Itay). Mineralium Deposita, 55/5: 953–970. https://doi.org/10.1007/s00126-019-00912-5

Mueller, S., Hounslow, M.W. & Kürschner, W.M. 2016: Integrated stratigraphy and palaeoclimate history of the Carnian Pluvial Event in the Boreal realm; new data from the Upper Triassic Kap Toscana Group in central Spitsbergen (Norway). Journal of the Geological Society, 173/1: 186–202.

Poltnig, W. & Spatzenegger, A. 2022: Carnian Ammonoids from the Wetterstein Limestone of Hochobir (North Karawanken, Carinthia). GEONAKU, 2: 41 p., incl. 6 pls.

Preto, N., Roghi, G. & Gianolla, P. 2005: Carnian stratigraphy of the Dogna area (Julian Alps, northern Italy): tessera of a complex palaeogeography. Bollettino della Società Geologica Italiana, 124/1: 269–279.

Preto, N., Bernardi, M., Dal Corso, J., Gianolla, P., Kustatscher, E., Roghi, G. & Rigo, M. 2019: The Carnian Pluvial Episode in Italy: history of the research and perspectives. Bollettino della Società Paleontologica Italiana, 58/1: 36.

Ritterbush, K.A., Hoffmann, R., Lukeneder, A. & De Baets, K. 2014: Pelagic palaeoecology: The importance of recent constraints on ammonoid palaeobiology and life history. J. Zool., 292: 229–241.

Sestini, N.F. 1992: The Middle Triassic new genus *Praepinacoceras* (Family Pinacoceratidae). Riv. It. Paleont. Strat., 97/3–4: 269–274.

Silberling, N.J. & Tozer, E.T. 1968: Biostratigraphic classification of the marine Triassic in North America. Geological Society of America Special Paper, 110: 1–63

Smith, J.P. 1927: Upper Triassic marine invertebrate faunas of North America. U.S Geological Survey, Professional Paper, 141: 262 p., incl. 121 pls.

Smith, J.P. 1932: Lower Triassic ammonoids of North America. U.S Geological Survey, Professional Paper, 167: 199 p., incl. 81 pls.

Spath, L.F. 1951: Catalogue of fossil Cephalopoda in the British Museum (Natural History), Part V: The Ammonoidea of the Trias II. 228 p.

Tozer, E.T. 1967: A standard for Triassic time. Geological Survey of Canada Bulletin, 156: 1–103.

Tozer, E.T. 1971: Triassic time and ammonoids: problems and proposals. Canadian Journal of Earth Sciences, 8: 989–1031. https://doi.org/10.1139/e71-088

Tozer, E.T. 1981: Triassic Ammonoidea: Geographic and stratigraphic distribution. Systematics Association Special Volume, 18: 397–431.

Tozer, E.T. 1984: The Trias and its ammonoids: the evolution of a time scale. Geological Survey of Canada Miscellaneous, Report, 35: 1–171. https://doi.org/10.4095/119548

Tozer, E.T. 1994: Canadian Triassic ammonoid faunas. Geological Survey of Canada, Bull. 467: 663 p, incl. 148 pls.

Urlichs, M. 1994: *Trachyceras* LAUBE 1869 (Ammonoidea) aus dem Unterkarn (Obertrias) der Dolomiten (Italien): Stuttgarter Beiträge zur Naturkunde: Reihe B (Geologie und Paläontologie), 217: 55 p incl. 4 pls.

Urlichs, M. 2012: Stunting in some invertebrates from the Cassian formation (Late Triassic, Carnian) of the Dolomites (Italy). Neues Jahrbuch für Geologie und Paläontologie-Abhandlungen, 265: 1–25. https://doi.org/10.1127/0077-7749/2012/0241

Urlichs, M. 2017: Revision of some stratigraphically relevant ammonoids from the Cassian Formation (latest Ladinian-early Carnian, Triassic) of St. Cassian (Dolomites, Italy). Neues Jahrbuch für Geologie und Paläontologie-Abhandlungen, 283: 173–204. https://doi.org/10.1127/njgpa/2017/0635

Waagen, W. 1895: Fossils from the Ceratite Formation. Memoirs Geological Survey of India, Palaeontologia Indica (ser. 13), Salt Range Fossils, 2: 1–323.

Welter, O.A. 1914: Die obertriadischen Ammoniten und Nautiliden von Timor. 258 p.

Wulfen, F.X. 1793: Abhandlung vom kärnthnernschen pfauenschweifigen Helmintholith oder dem sogenannten opalisierenden Muschelmarmor: 124 p., incl. 32 pls.

Zittel, C. 1899: Über die Entwickelung der Wengener, St. Cassianer und Raibler Schichten auf der Seiser Alp in Tirol. Z. dt. geol. Ges., Verh., 51: 102–114.

GEOLOGIJA 66/1, 107-124, Ljubljana 2023

https://doi.org/10.5474/geologija.2023.004

Microfossils from Middle Triassic beds near Mišji Dol, central Slovenia

Mikrofosili iz srednjetriasnih plasti pri Mišjem Dolu, osrednja Slovenija

Katja OSELJ[1,2], Tea KOLAR-JURKOVŠEK[3], Bogdan JURKOVŠEK[3,4] & Luka GALE[2,3]

[1]Trboje 104, 4000 Kranj, Slovenia; e-mail: katja.oselj@gmail.com;
[2]Department of Geology, Faculty of Natural Sciences and Engineering, University of Ljubljana, Aškerčeva cesta 12, 1000 Ljubljana, Slovenia; e-mail: luka.gale@ntf.uni-lj.si
[3]Geological Survey of Slovenia, Dimičeva ulica 14, SI-1000 Ljubljana, Slovenia; e-mail: tea.kolar-jurkovsek@geo-zs.si; luka.gale@geo-zs.si;
[4]Kamnica 27, 1262 Dol pri Ljubljani, Slovenia; e-mail: geolog.bj@gmail.com

Prejeto / Received 13. 3. 2023; Sprejeto / Accepted 29. 5. 2023; Objavljeno na spletu / Published online 4. 8. 2023

Key words: Dinarides, Sava Folds, Middle Triassic, upper Anisian, lower Ladinian, basin, volcaniclastics, conodonts, foraminifera
Ključne besede: Dinaridi, Posavske gube, srednji trias, zgornji anizij, spodnji ladinij, bazen, vulkanoklastiti, konodonti, foraminifere

Abstract

Middle Triassic beds exposed along the road between Mišji Dol and Poljane pri Primskovem (Posavje Hills) comprise marlstone, tuff, volcaniclastic sandstone, and thin- to medium-bedded limestone and dolostone. The succession was logged and sampled for conodonts. A relatively rich conodont assemblage was determined, consisting of *Budurovignathus gabrielae* Kozur, *Budurovignathus* sp., *Cratognathodus kochi* (Huckriede), *Gladigondolella malayensis* Nogami, *Gladigondolella tethydis* Huckriede, *Gladigondolella* sp., *Neogondolella balkanica* Budurov & Stefanov, *Neogondolella* cf. *excentrica* Budurov & Stefanov, *Neogondolella constricta* (Mosher & Clark), *Neogondolella cornuta* Budurov & Stefanov, *Neogondolella* sp., *Paragondolella excelsa* Mosher, *Paragondolella liebermani* (Kovacs & Kozur), *Paragondolella trammeri* (Kozur), *Paragondolella* cf. *alpina* (Kozur & Mostler), and *Paragondolella* sp. The assemblage correlates with the upper Anisian and lowermost Ladinian assemblages from the Global Boundary Stratotype Section and Point (GSSP) of the Ladinian at Bagolino in the Southern Alps in northern Italy. Along with conodonts, numerous specimens of benthic foraminifera *Nodobacularia*? *vujisici* Urošević & Gaździcki were recovered from the lowermost part of the succession. Previous research on this taxon is critically evaluated.

Izvleček

Zaporedje srednjetriasnih plasti, ki so razgaljene ob cestnem useku med Mišjim Dolom in Primskovim (Posavsko hribovje), sestavljajo laporovec, tuf, vulkanoklastični peščenjak in tanko do srednje plastnat apnenec in dolomit. Zaporedje je bilo popisano in vzorčeno za konodontne analize. Določena je bila relativno bogata združba, ki sestoji iz vrst *Budurovignathus gabrielae* Kozur, *Budurovignathus* sp., *Cratognathodus kochi* (Huckriede), *Gladigondolella malayensis* Nogami, *Gladigondolella tethydis* Huckriede, *Gladigondolella* sp., *Neogondolella balkanica* Budurov & Stefanov, *Neogondolella* cf. *excentrica* Budurov & Stefanov, *Neogondolella constricta* (Mosher & Clark), *Neogondolella cornuta* Budurov & Stefanov, *Neogondolella* sp., *Paragondolella excelsa* Mosher, *Paragondolella liebermani* (Kovacs & Kozur), *Paragondolella trammeri* (Kozur), *Paragondolella* cf. *alpina* (Kozur & Mostler) in *Paragondolella* sp. Združbo lahko koreliramo z zgornjeanizijsko do spodnjeladinijsko združbo iz globalnega mejnega stratotipskega profila in točke (GSSP) za ladinij v Bagolinu v Južnih Alpah, severna Italija. Poleg konodontov so bili v spodnjem delu zaporedja najdeni številni primerki bentoških foraminifer *Nodobacularia*? *vujisici* Urošević & Gaździcki. Podajamo kritični pregled dosedanjih raziskav tega taksona.

Introduction

The Middle Triassic tectonic and paleogeographic evolution of the present-day Southern Alps, Dinarides, Northern Calcareous Alps, and Transdanubian Range was strongly affected by crustal extension that accompanied the opening and spreading of the western Neotethys (Meliata-Maliac) Ocean (Schmid et al., 2008; Kovács et al., 2011). As a result, several smaller basins were created, mainly between late Anisian and early Ladinian (Buser, 1989; Haas & Budai, 1999; Budai & Vörös, 2006; Berra & Carminati, 2010; Stefani et al., 2010; Velledits et al., 2011; Gawlick et al., 2012; Celarc et al., 2013; Smirčić et al., 2020).

Tectonic activity was accompanied by volcanism, which is reflected in the local deposition of volcaniclastic and/or volcanic rocks, mostly within the basinal areas (Buser, 1989; Gianolla et al., 2019). Upper Anisian to Ladinian basinal successions are relatively widespread in the territory of Slovenia (see Dozet & Buser, 2009 and Kolar-Jurkovšek & Jurkovšek, 2019 for summary). Local differences among the successions evidence the existence of several basins of different depths and characters, ranging from open marine environments (Rakovec, 1950; Buser, 1986; Skaberne et al., 2003; Rožič et al., 2021), to ephemeral marshes, river systems, freshwater lakes, and shallow restricted lagoons (Čar, 2013). The ruggedness of the relief is well exemplified in the Idrija area, where at least three Ladinian sedimentary basins separated by topographic ridges were recognised (Čar, 2013). Determination of age is crucial for exact stratigraphic position and correlation of this plethora of different depositional environments. Limestones from open marine and well-aerated basins often contain conodonts (Celarc et al., 2013; Kolar-Jurkovšek & Jurkovšek, 2019), radiolarians (Goričan & Buser, 1990; Ramovš & Goričan, 1995; Skaberne et al., 2003; Celarc et al., 2013), and bivalves (Jurkovšek, 1984), while ammonoids are rarely found (Čar, 2010). Foraminifera are also present, but they are usually not abundant (Jurkovšek, 1984). Numerous Middle Triassic deposits, however, remain poorly dated (e.g., the shale- and sandstone-dominated Pseudozilian beds in the central and western Slovenia; Rakovec, 1950; Buser, 1986; Čar et al., 2021).

A Middle Triassic volcanoclastic unit between Mišji Dol and Poljane pri Primskovem in the central Posavje Hills was previously mentioned by Lipold (1858), Germovšek (1955), and Buser (1974). Some ammonoid and bivalve taxa were determined (Lipold, 1858; Germovšek, 1955; Buser, 1974; also Jurkovšek, 1984 for localities in vicinity). A detailed description of a volcano-sedimentary succession from Obla Gorica in the vicinity was given by Dozet (2006), who divided the succession into (from bottom/older to top/younger): bedded tuff with interbeds of limestone (1), lower platy dolostone with chert and tuff interbeds (2), light grey bedded dolostone with tuff interbeds (3), upper platy dolostone with cherts and tuff interbeds (4), dark marly limestone and marlstone (5); tuff with interbeds of volcaniclastic sandstone (6), and bedded and platy grained limestone (7). A renewed sampling of Middle Triassic beds between Mišji Dol and Poljane pri Primskovem yielded a relatively rich and well-preserved conodont and foraminiferal fauna. The aim of this paper is to present the recovered conodont and foraminiferal assemblages for a better stratigraphic assignment of the Upper Anisian to Ladinian beds in the researched area. The conodont assemblage is compared to other assemblages from the region.

Geological setting

According to Placer (1998a, 2008), the studied area structurally belongs to the External Dinarides and the Sava Folds (Placer, 1998b). The studied succession is a part of the Litija Anticline (Placer, 1998b), created by post-Miocene compression (Placer, 1998b; Tomljenović & Csontos, 2001). The pre-folding structure of the External Dinarides was largely governed by Oligocene–early Miocene thrusting in the NE-SW direction

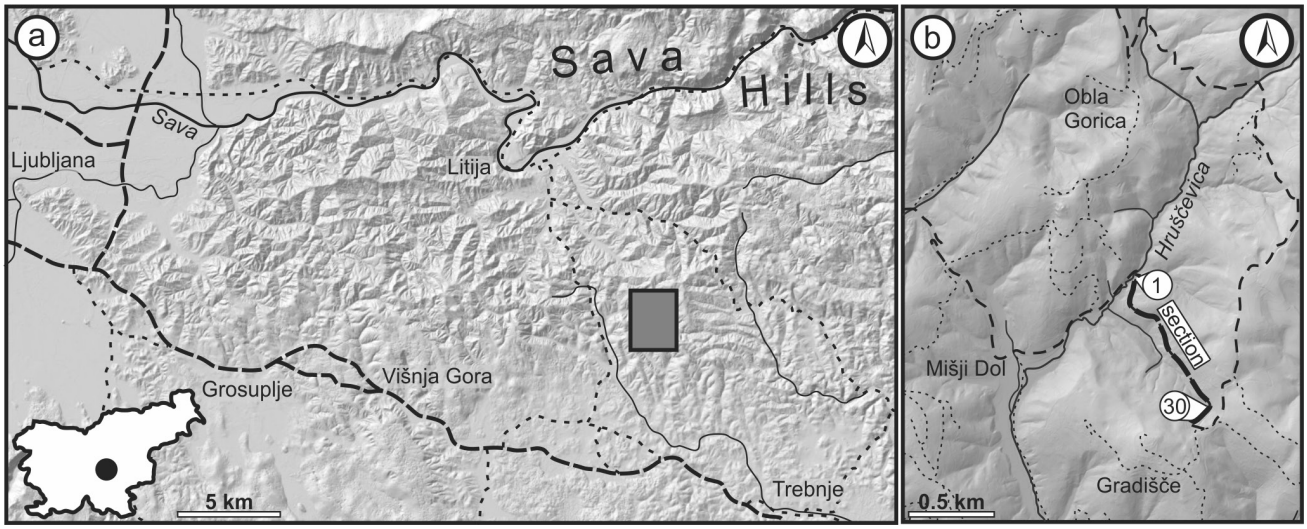

Fig. 1. Geographic position of the studied section. a: Position of area depicted in Fig. 1b. b: Position of the section along the road from Mišji Dol to Poljane pri Primskovem. LIDAR digital model of the relief, 2015. Data source: Slovenian Environment Agency. Accessed via Geopedia portal (Sinergise d.o.o.) in November 2022.

(Placer, 1998a, 1998b; Vrabec & Fodor, 2006). The logged succession of Middle Triassic beds lies along the road between Mišji Dol and Poljane pri Primskovem (Fig. 1), starting at 45°59′28.43′′N, 14°54′37.56′′E and ending at 45°59′0.71′′N, 14°54′54.15′′E. The succession is folded, dissected by numerous minor faults, and partly covered. According to Buser (1968) and Dozet (2006), the investigated succession unconformably overlies massive Anisian dolostone and is succeeded upwards by the massive Ladinian dolostone.

Material and methods

Due to the partial coverage of the succession, we were only able to reconstruct the succession by combining the outcropping segments. Thirty-one conodont samples were collected along the succession, weighting between 1.5 and 2.5 kg. The rock was dissolved in 10–15 % acetic acid and the residue was separated into light and heavy fractions with the use of bromoform. Conodonts from the heavy fraction and foraminifera from the light fraction were hand-picked under a binocular microscope. In some instances, the interior of foraminifera could be viewed by immersing them in glyceryl. We also prepared some oriented thin sections of foraminifera. Selected specimens of conodonts and foraminifera were photographed with a scanning electron microscope (SEM) JEOL JSM 6490LV. The macroscopic lithological description was supplemented by micropetrographic analysis of 49 thin sections using a polarizing optical microscope. Carbonate rocks were classified according to Dunham (1962), Embry and Klovan (1972), and Wright (1992). The terminology of volcaniclastics follows Di Capua et al. (2022). Similarities with other conodont assemblages from the same time interval were evaluated using the Dice similarity index using PAST v. 2.17c statistics software (Hammer et al., 2001). Preparatory work and SEM microscopy were performed at the Geological Survey of Slovenia. The conodont samples are stored at the Geological Survey of Slovenia under repository numbers 6247–6264. The thin sections are stored in repository of the co-author L.G. at the Department of Geology, Faculty of Natural Sciences and Engineering in Ljubljana.

Results

Description of section

The succession was investigated along 1100 m long road section. The contact with the massive Anisian dolostone is not exposed. The general orientation of bedding changes from 235/42 in the lower part of the succession, to 190/40 halfway along the roadcut, and to 200/50 near the top. Despite this relative consistency in the general orientation of the bedding, small-scale folds and faults are present, which makes the estimate of the thickness of individual sub-sections very difficult. We estimate that the entire succession is between 100 and 200 m thick. Figure 2 shows some better exposed parts of the succession, and Figure 3 the reconstructed generalized succession and position of conodont samples within it. The general succession starts with a variegated succession of marlstone, tuff, and thin-bedded limestone. Higher up in the succession thin- to medium-bedded limestone and dolostone predominate, commonly interchanging with volcaniclastic sandstone. The top of the roadcut is again dominated by poorly exposed variegated succession of tuff, volcaniclastic sandstone, marlstone, and limestone. The lithological composition of each sector along the road and the actual thickness of each part of the succession is presented in Table 1.

Fig. 2. Middle Triassic beds between Mišji Dol and Poljane pri Primskovem. a: Dolomitized cherty limestone with thin interbeds of volcaniclastic sandstone; sector 13. b: Thin bedded limestone (radiolarian-filament wackestone/packstone); sector 21.

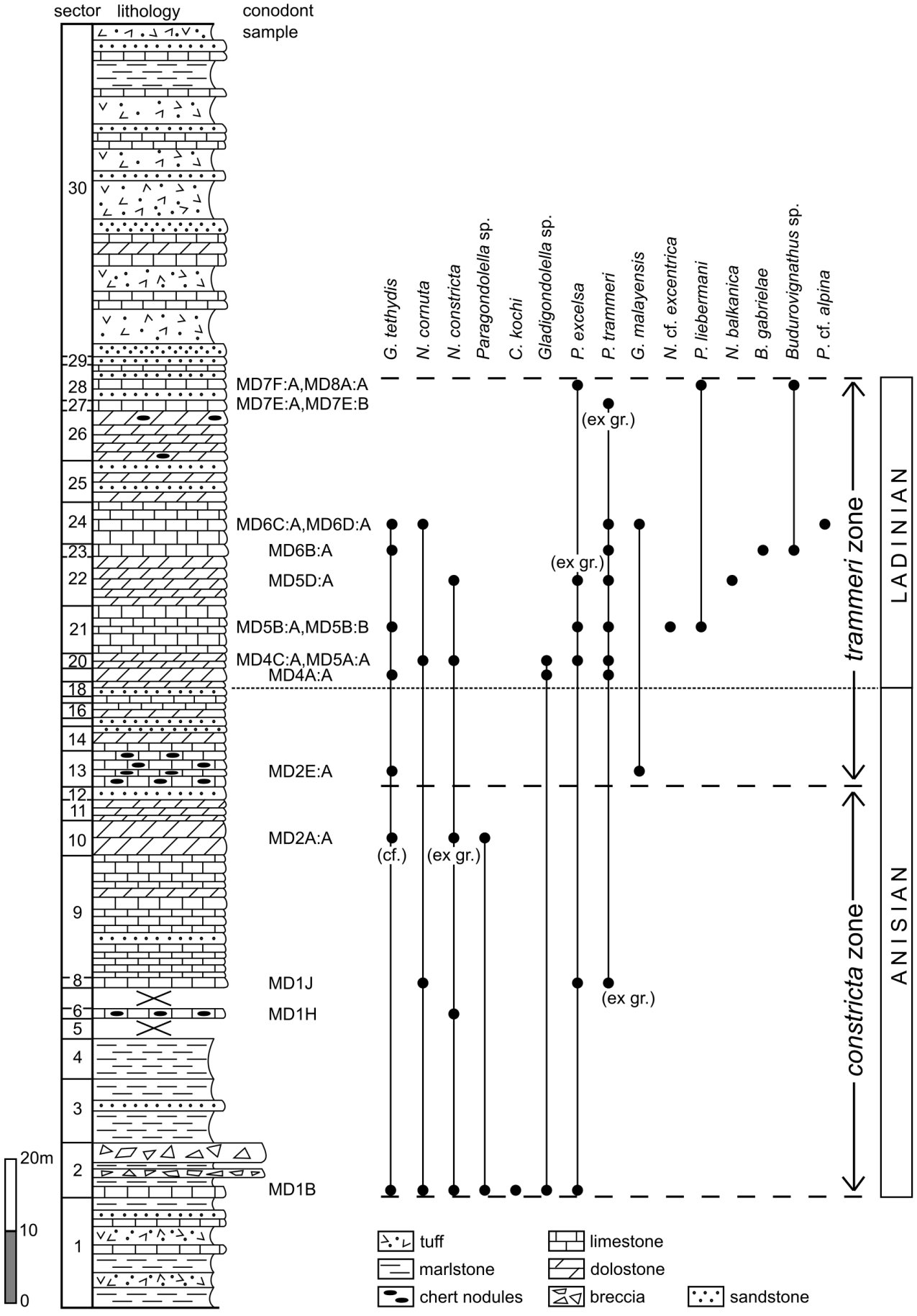

Fig. 3. Reconstruction of the Middle Triassic succession along the road between Mišji Dol and Poljane pri Primskovem. The true stratigraphic thickness of each sector is shown (see thicknesses in Table 1). The right-hand side presents the position of the conodont samples and the stratigraphic distribution of the conodont species. The Anisian/Ladinian boundary is within the *trammeri* zone.

Table 1. Lithological composition of Middle Triassic beds between Mišji Dol and Poljane pri Primskovem.

Sector	Lithology	Total thickness	Microfacies
1	Covered by soil. Marlstone and pelitic tuff (80 %) in 1–5 cm thick beds, locally with chert and thin-shelled bivalves, concordant to bedding. -Dark limestone in up to 7 cm thick beds (18 %); locally with bands with thin-shelled bivalves, concordant to bedding. Locally silicified. -Volcaniclastic sandstone (2 %) forms up to 3.5 cm thick beds. Weathered pieces are light yellow in colour.	16 m (estimated)	Limestone: -radiolarian-filament-peloid packstone; -bioclastic-intraclastic grainstone; -peloid-bioclastic packstone/grainstone
2	The lower part (1.2 m) is dominated by limestone, the next 4.2 m by tuff and volcaniclastic sandstone. Micritic limestone and breccia (45 cm thick) follow, then a 1.5 m thick bed of marlstone, and two more beds (20 cm and 25 cm thick) of breccia. -Limestone is dark grey to black, locally selectively silicified. Bed thickness is from 1 cm to 15 cm. Bivalve shells and radiolarians were recognised with a hand-lens. -Tuff and volcaniclastic sandstone is present in 1–15 cm thick beds. The colour is yellow, green, brownish green or greenish grey. -Marlstone is dark brown in colour and laminated. -Breccia is poorly sorted; the largest clasts from the top of the bed are 4 cm across.	8.2 m (logged in detail)	Limestone: -calcimudstone; -radiolarian-filament wackestone/packstone; -bioclastic-intraclastic rudstone Clastics: -calcareous mudstone; -volcaniclastic sandstone; -mud-supported sandy breccia
3	Mostly covered. Marlstone dominates (90 %) over a few beds of volcaniclastic sandstone and black pelitic tuff.	9 m (estimated)	Clastics: -calcareous mudstone; -volcaniclastic sandstone
4	Mostly covered. Marlstone.	6 m (2 m exposed, the rest estimated)	/
5	Covered.	? (estimated 3 m)	/
6	Black marly limestone, locally with chert.	1 m	/
7	Covered.	? (estimated 3 m)	/
8	Three beds of black micritic limestone.	1.5 m	/
9	Mostly covered. Fragments of black micritic limestone are found over 75 % of this interval; the rest is probably grey dolostone and volcaniclastic sandstone.	18 m (estimated)	/
10	Light grey dolostone, fractured and folded. Bedding is not clear.	? (estimated 5 m at most)	Dolostone: -dolomitized intraclastic grainstone/rudstone?; subhedral
11	Grey dolostone in 1.5–8 cm thick beds.	? (estimated 3 m)	Dolostone: -dolomitized intraclastic grainstone/rudstone?; subhedral
12	Covered. Fragments of volcaniclastic sandstone and dolostone.	? (estimated 2 m)	/
13	Bedded dolomitized cherty limestone with cleavage. Beds are 0.5–34.5 cm thick. They interchange with beds of volcaniclastic sandstone.	6 m	Dolostone: -subhedral; locally with chert
14	Covered. Fragments of dolostone and volcaniclastic sandstone.	? (estimated 3 m)	Clastics: -volcaniclastic sandstone; grains of volcanics, quartz, feldspar, microsparitic lithoclasts
15	Volcaniclastic sandstone.	? (estimated 1 m)	Clastics: -sandstone with grains of poli- and monocrystal quartz, chloritized volcanics, feldspar; sericitic matrix and dolomitic cement
16	Covered. Fragments of dolostone and limestone.	? (estimated 2 m)	Dolostone: - subhedral; 10% of terrigenous quartz, rare echinoderms are preserved
17	Dolomitized limestone in app. 5 cm thick beds.	1 m	/
18	Covered. Fragments of dolostone and volcaniclastic sandstone.	? (estimated 1–3 m)	/
19	Dolostone in 2–34 cm thick beds. Laterally pinching out and lateral amalgamation of beds suggest slumping.	2 m	Dolostone: - subhedral; dolomitized grainstone or rudstone (remains of echinoderms and intraclasts) and packstone with filaments
20	Folded thin-bedded (0.5–2 cm) dolostone, subordinately limestone.	2 m	Dolostone: -subhedral; chert nodules Limestone: -radiolarian-filament wackestone/packstone
21	Dark grey to black limestone in 3.5–12 cm thick beds. Parallel lamination and silicification are locally present. Subordinate are thin marlstone interlayers.	7 m	Limestone: -radiolarian-filament wackestone/packstone

Sector	Lithology	Total thickness	Microfacies
22	Dolostone in 5.5–19 cm thick beds. One bed shows cross-lamination. Subordinate are thin marly interlayers. Cleavage is present.	7 m	Dolostone: -dolomitized filament packstone/grainstone and intraclastic rudstone; subhedral
23	Covered. Fragments of limestone and volcaniclastic sandstone.	? (estimated 1.5 m)	Limestone: -peloid-bioclastic packstone/grainstone
24	Partly covered. Dolomitized limestone in 2–7.5 cm thick, folded beds. Large part of the succession covered by a concrete wall.	3 m + unknown + 3 m	Dolostone: -subhedral; remains of brachiopods/bivalves and echinoderms; selective silicification
25	Thin beds of dolostone (1.5–13 cm), interchanging with volcaniclastic sandstone.	6 m	Dolostone: -subhedral; remains of echinoderms, filaments; 5 % of terrigenous quartz
26	Dolostone in 4–22 cm thick beds. Nodules of chert and laminae are locally present.	7 m	Dolostone: -subhedral; selective silicification
27	Dark grey to black limestone in 4–20 cm thick beds. Cross-lamination is locally present.	1.5 m (estimated)	Limestone: -peloid-bioclastic packstone/grainstone
28	Mostly covered. Fragments of volcaniclastic sandstone and limestone. Exposed beds of limestone are 2–29 cm thick. Parallel lamination is locally visible.	? (estimated 5 m)	Limestone: -peloid-bioclastic packstone/grainstone; -bioclastic-intraclastic-peloid grainstone with terrigenous admixture
29	Volcaniclastic sandstone in 0.5–10 cm thick beds.	1 m	Clastics: -volcaniclastic sandstone
30	Covered. Variegated succession of tuff, volcaniclastic sandstone, limestone, dolostone.	? (estimated 50 m)	Clastics: -volcaniclastic sandstone

Table 2. Limestone microfacies types from Middle Triassic beds between Mišji Dol and Poljane pri Primskovem.

Microfacies	Description
Calcimudstone	Texture is homogenous. Micritic matrix strongly predominates. Only 5 % of the area is occupied by grains (radiolarians).
Radiolarian-filament wackestone/packstone	Texture is heterogenous, locally bioturbated. Matrix represents 50–70 % of the area, grains 30–50 %. Grains are well sorted, supported by matrix or in point contacts. The average grain size is 0.4 mm. Among grains, bioclasts predominate (90 % of grains). These are mostly filaments and radiolarians, while ostracods and benthic foraminifera (*Frondicularia woodwardia* Howchin, Lagenida) are rare.
Peloid-filament-radiolarian packstone	This microfacies interchanges with bioclastic-intraclastic grainstone in wide laminae. Texture is homogenous. Grains represent 85 % of the area, whereas matrix and spar represent 15 % of the area of thin section. Sorting is moderate. Grains are in point and long contacts, and they measure 0.03–1 mm in size. Spherical forms are the most common. Peloids and pellets represent 80 % of grains. Filaments (10 %) and radiolarians (7 %) are subordinate. Less abundant are echinoderms and foraminifera (*Krikoumbilica* sp.). Echinoderm plates are overgrown by syntaxial calcite cement. The calcite cement in intergranular space is fine-grained, locally drusy mosaic.
Bioclastic-peloid packstone/grainstone	Texture is homogenous. Grains form 80 % of the area, matrix and cement 20 %. Sorting is moderate. Grains are 0.11–4.9 mm large. They are in point and long contacts. Geopetal structures are present within gastropod shells. Biogenic grains represent 40–50 % of the grains. Peloids (35–40 %), aggregate grains (5–10 %), and intraclasts (5–15 %) are also commonly present. Less abundant are bivalves, echinoderms, foraminifera (sessile agglutinated foraminifera, *Glomospirella* sp., *Palaeolituonella meridionalis* (Luperto), *Endoteba* sp., *Endotriadella* sp., *Variostoma* sp., Duostominidae), microproblematica (*Plexoramea cerebriformis* Mello, *Tubiphytes obscurus* Maslov), gastropods (locally more common), brachiopods, *Terebella* tubes, and dasycladacean algae. Radiolarians are present where the micritic matrix is present. Terrigenous component is subordinate to allochems. Monocrystal quartz with uniform extinction is present in angular grains measuring 0.5–0.6 mm in size. Lithic grains of chert are locally also present. The cement is fine-grained and drusy mosaic calcite. Echinoderms are overgrown by syntaxial calcite.
Bioclastic-intraclastic grainstone	This microfacies interchanges with peloid-filament-radiolarian packstone in wide laminae. Texture is homogenous. Grains represent 80 % of the area; intergranular space is filled by fine-grained, locally drusy mosaic calcite cement. Sorting is poor. Grains are mostly in point or long contacts. Grains range from 0.06 to 1.55 mm in size. Filaments and radiolarians strongly predominate (80 % of grains). Intraclasts, peloids and pellets are subordinate (10 % and 8 %, respectively). Very rare are ostracods and problematic algae.
Peloid-intraclastic-bioclastic grainstone with terrigenous admixture	Texture is homogenous. Grains form 50 % of the area. Of these, terrigenous grains represent 20 % and allochems 30 %. Grains range 0.15–1 mm in size. They are moderately sorted. Small intraclasts and peloids are the most abundant among allochems. Approximately 5 % of the allochems are small bioclasts, which are partly or completely micritized. Benthic foraminifera (*Palaeolituonella meridionalis* (Luperto)) and echinoderms are recognisable. Terrigenous grains comprise chert, rhyolite-like volcanics, monocrystal quartz and plagioclase, and carbonate lithoclasts. Terrigenous grains are angular to very angular, between 0.15 mm and 0.55 mm in size. Plagioclase grains are partly sericitizied. Echinoderm plates are overgrown by syntaxial calcite cement.
Bioclastic-intraclastic rudstone	Texture is homogenous. Grains form 80 % of the area. They are very poorly sorted and measure 1 mm to 18.5 mm in size [within the thin section; several cm large clasts were observed in the field]. Subrounded clasts dominate. Grains are in stylolitic contacts. Allochems are dominated by intraclasts (oolithic packstone, wackestone with radiolarians and filaments, peloidal-bioclastic packstone, mudstone). Subordinate are echinoderm plates, ooids, peloids, benthic foraminifera and bivalve shells. Lithic grains are represented by recrystallised limestone. Other terrigenous grains are monocrystal quartz, plagioclase, and chert. These grains are angular to subangular, up to 5 mm large. The intergranular space is filled with spar. Silicification is locally present.

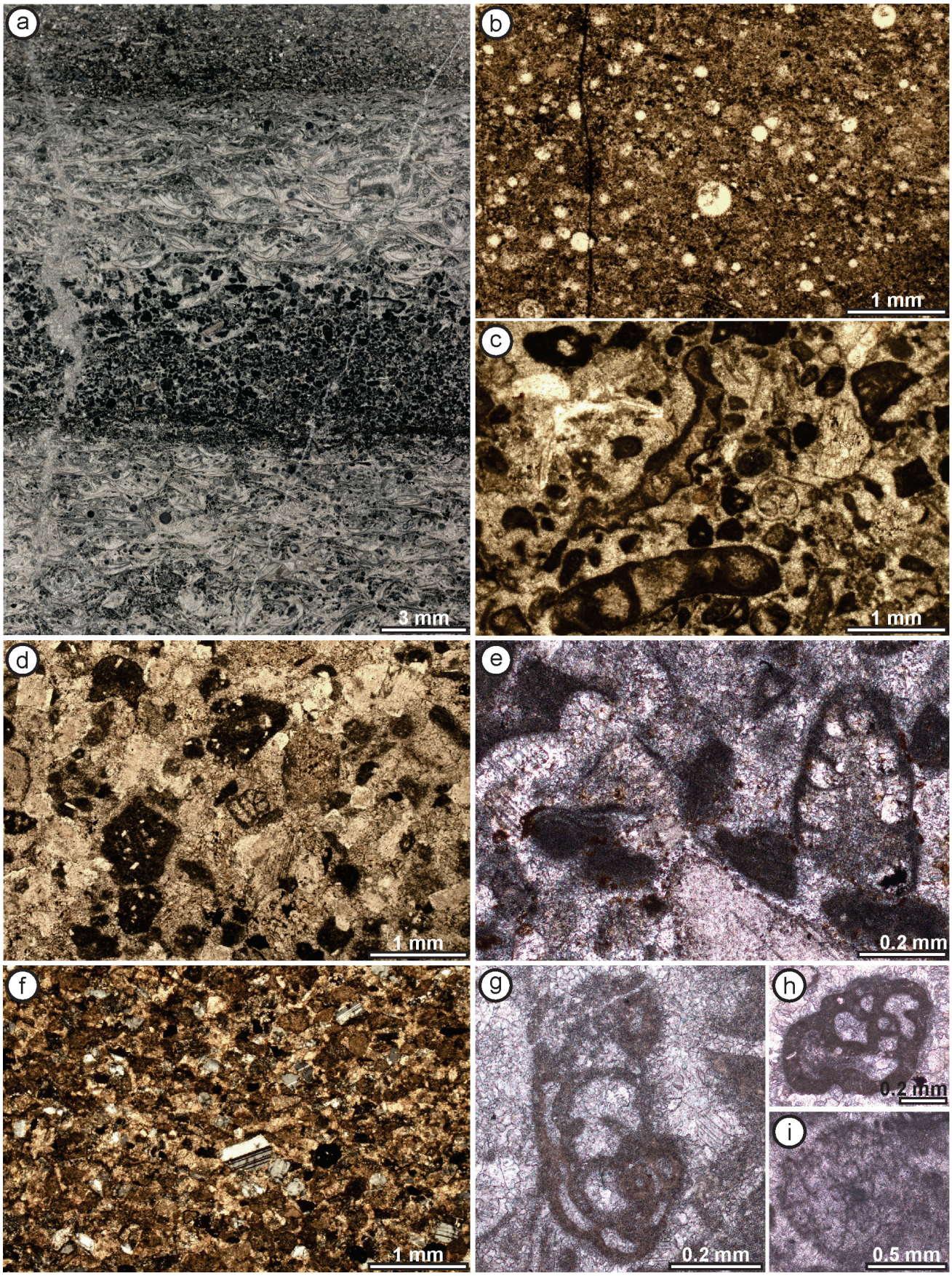

Fig. 4. Selected microfacies types and microfossils from Middle Triassic beds between Mišji Dol and Poljane pri Primskovem. a: Interchanging laminae of radiolarian-filament wackestone/packstone and peloid-filament-radiolarian packstone. Thin section 1758 (sample MD1A:B). b: Radiolarian-filament wackestone-packstone. Thin section 1790 (sample MD5A:A). c: Bioclastic-peloid grainstone. Thin section 1763 (sample MD1A:C). d: Peloid-intraclastic-bioclastic grainstone with terrigenous admixture. Note foraminifer *Palaeolituonella meridionalis* (Luperto) in the centre. Thin section 1796 (sample MD7F:B). e: *Variostoma* sp. (right) and *Ophthalmidium* sp. (left) in bioclastic-peloid grainstone. Thin section 1763 (sample MD1A:C). f: Volcaniclastic sandstone. Thin section 1766 (sample MD1C:B). g: *Endotriadella* sp. in bioclastic-peloid grainstone. Thin section 1763 (sample MD1A:C). h: *Endoteba* sp. in bioclastic-peloid grainstone. Thin section 1763 (sample MD1A:C). i: *Plexoramea cerebriformis* Mello in bioclastic-peloid grainstone. Thin section 1786 (sample MD8A:A).

Carbonate microfacies

The textures and composition of the limestone samples are described in more detail in Table 2. Selected microfacies types and microfossils from thin sections are shown in Figure 4.

Microfossil assemblage

The microfossil assemblage from the residue consists of conodonts, benthic foraminifera, gastropods, echinoderms, brachiopods, green algae, radiolarians, microproblematica, and ostracods. A total of 16 conodont taxa were determined (Fig. 5):

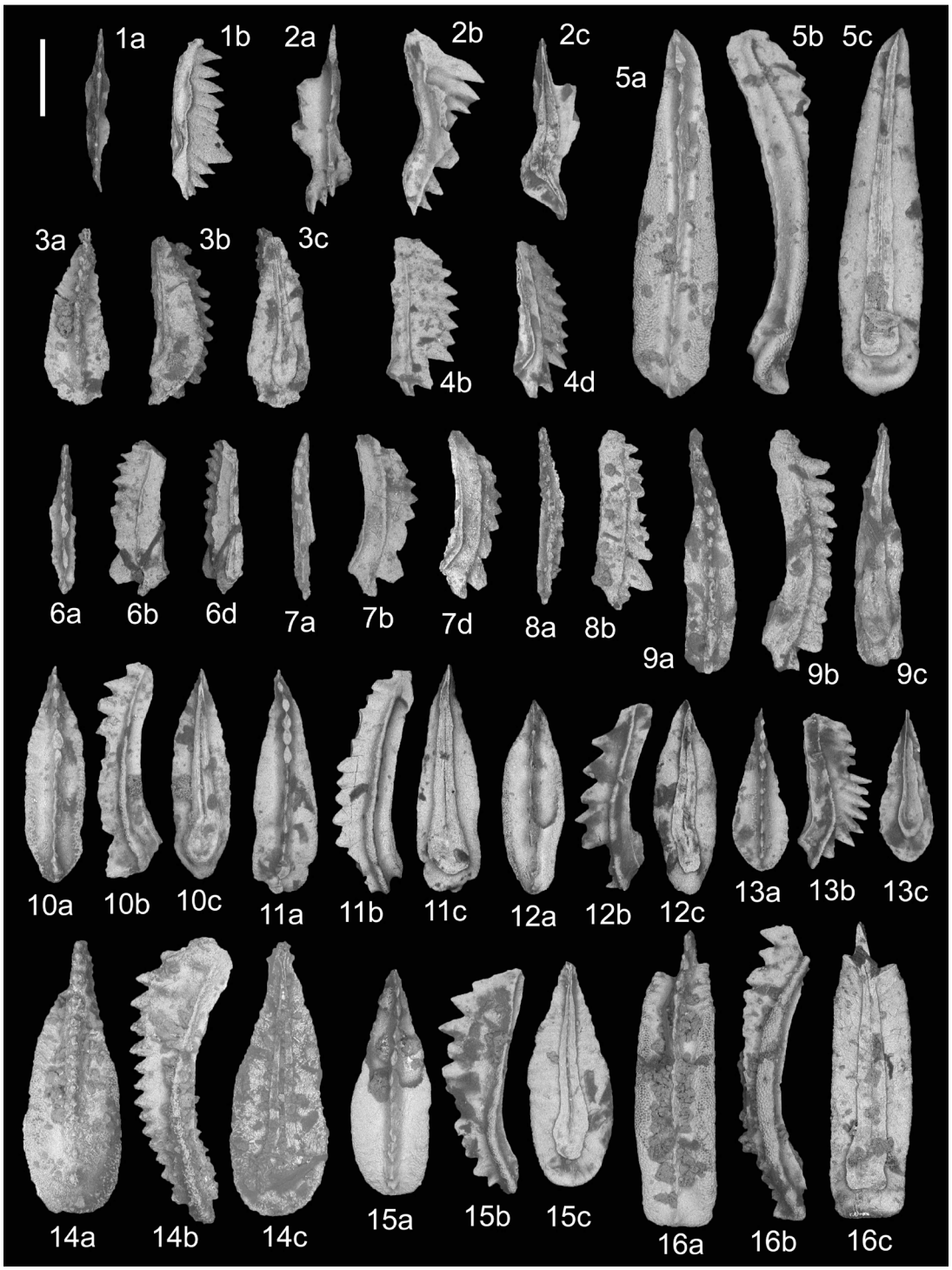

Fig. 5. Conodont taxa from Middle Triassic beds between Mišji Dol and Poljane pri Primskovem. SEM images. 1 – *Budurovignathus* sp., juvenile specimen, sample MD 6B:A (GeoZS 6260). 2 – *Budurovignathus* sp., sample MD 7F:A (GeoZS 6263). 3 – *Paragondolella excelsa* Mosher, sample MD 1J (GeoZS 6251). 4 – *Paragondolella* sp., juvenile specimen, sample MD 1B komp 0–0.25 (GeoZS 6247). 5 – *Neogondolella cornuta* Budurov & Stefanov, sample MD 1B komp 0–0.25 (GeoZS 6247). 6 – *Paragondolella* ex gr. *trammeri* (Kozur), sample MD 1J (GeoZS 6251). 7–9 – *Paragondolella trammeri* (Kozur), sample MD 5B:B (GeoZS 6258). 10 – *Paragondolella trammeri* (Kozur), samples MD 6C:A and MD 6D:A (GeoZS 6261). 11 – *Paragondolella* ex gr. *trammeri* (Kozur), samples MD 7E:A and MD 7E:B (GeoZS 6262). 12 – *Budurovignathus gabrielae* Kozur, sample MD 6B:A (GeoZS 6260). 13, 15 – *Paragondolella* ex gr. *excelsa* Mosher, sample MD 5D:A (GeoZS 6259). 14 – *Paragondolella liebermani* (Kovacs & Kozur), sample MD 5B:B (GeoZS 6258). 16 – *Neogondolella balkanica* Budurov & Stefanov, sample MD 5D:A (GeoZS 6259). Scale bar: 200 μm; a – upper, b – lateral, c – lower, d – oblique lower views.

Budurovignathus gabrielae Kozur (Fig. 5.12), *Budurovignathus* sp. (Fig. 5.1–5.2), *Cratognathodus kochi* (Huckriede), *Gladigondolella malayensis* Nogami, *G. tethydis* Huckriede, *Gladigondolella* sp., *Neogondolella balkanica* Budurov & Stefanov (Fig. 5.16), *N.* cf. *excentrica* Budurov & Stefanov, *N. constricta* (Mosher & Clark), *N. cornuta* Budurov & Stefanov (Fig. 5.5), *Neogondolella* sp., *Paragondolella excelsa* Mosher and *P.* ex gr. *excelsa* (Fig. 5.3, 5.13, 5.15), *P. liebermani* (Kovacs & Kozur) (Fig. 5.14), *P. trammeri* (Kozur) and *P.* ex gr. *trammeri* (Fig. 5.6–5.11), *P.* cf. *alpina* (Kozur & Mostler), and *Paragondolella* sp. (Fig. 5.4). Juveniles dominate, while adult specimens are mostly fragmented. Conodont elements are black and have a Colour Alteration Index (CAI) of 5.5 (Epstein et al., 1977).

The foraminiferal assemblage is relatively sparse, except for a high number of *Nodobacularia? vujisici* Urošević & Gaździcki recovered from the residue of dissolved limestone from the lower part of the succession (sector 2; see Table 1). *Ophthalmidium exiguum* Koehn-Zaninetti and very rare *Pseudonodosaria* sp. were present in the same sample. Along with the mentioned species, foraminifera include sessile agglutinated foraminifera, *Palaeolituonella meridionalis* (Luperto), *Glomospirella* sp., *Endoteba* sp., *Endotriadella* sp., *Krikoumbilica* sp., *Variostoma* sp., Duostominidae, and small Lagenida. All were determined from thin sections. A taxonomic description of *Nodobacularia? vujisici* Urošević & Gaździcki, which is a rarely noted species, is given below.

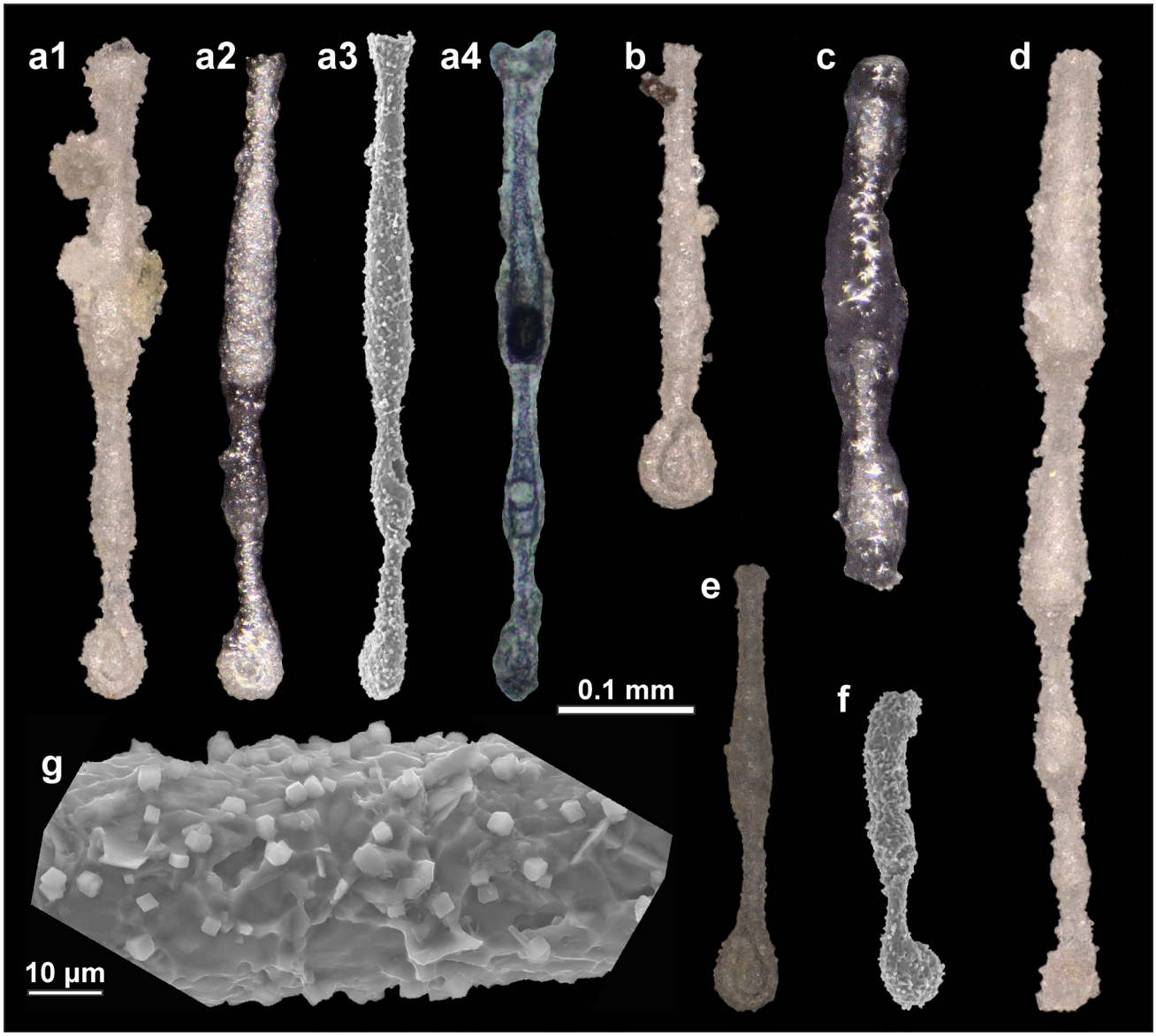

Fig. 6. *Nodobacularia? vujisici* Urošević & Gaździcki from Middle Triassic beds between Mišji Dol and Poljane pri Primskovem. a: The same specimen viewed in reflected light (a1), immersed in glyceryl (a2), under SEM (a3), and in thin section (a4). b–f: Different specimens showing variability in size and length of the chambers. g: Detail of the wall seen under SEM. All specimens are from sample MD1B (GeoZS 4268).

Subphylum Foraminifera d'Orbigny, 1826
Class Tubothalamea Pawlowski et al., 2013
Order Miliolida (Delage & Hérouard, 1896), emend Pawlowski et al., 2013
Superfamily Cornuspiroidea Schultze, 1854
Family Nubeculariidae Jones in Griffith and Henfrey, 1875
Subfamily Nodobacullariinae Cushman, 1927
Genus ?*Nodobacularia* Rhumbler, 1895
Nodobacularia? vujisici Urošević & Gaździcki, 1977
Fig. 6a–g

1977 *Nodobacularia vujisići* nov. sp., Urošević & Gaździcki, p. 97, pl. 1, fig. 1–6.
1980 *Nodophthalmidium elenae* n.sp., Gheorghian, p. 38, pl. 1, fig. 1–11; pl. 2, fig. 1–6; pl. 3, fig. 1–2.
1983 *Nodobacularia vujisići* Urošević et Gaździcki, 1977 – Salaj et al., p. 113, pl. 141, fig.1–2.
1984 *Nodophthalmidium vujisici* (Urošević & Gazdzicki, 1977) – Kristan-Tollmann, p. 285, fig. 8.1–8.7; pl. 11, fig. 1–29; pl. 8, fig. 9.
1987 *Nodobacularia vujisici* Urošević et Gaźd. – Oravecz-Scheffer, pl. 31, fig. 4.
1988 *Nodophthalmidium vujisici* Urošević et Gaździcki – Salaj et al., pl. 3, fig. 25, 26, 34.
1991 *Nodobacularia vujisici* Urošević et Gaździcki – Kolar-Jurkovšek, pl. 2, fig. 3–4.
1993 *Gheorghianina vujisici* (Urošević & Gaździcki, 1977) – Trifonova, p. 50, pl. 8, fig. 1–2.
1996 *Gheorghianina vujisici* (Urosevic et Gazdzicki, 1977) – Bérczi-Makk, p. 435, pl. 1, fig. 6–7.

Material: Approximately 500 isolated specimens from the residue of radiolarian-filament wackestone/packstone from the bottom of sector 2 (Sample MD1B; GeoZS 4268; see Table 1).

Description: The foraminiferal test is free, unattached, and very elongated. Ovoid proloculus (diameter 0.018 mm, length 0.032 mm) is followed by two (?) elongated tubular chambers. The first of these is one-half of the whorls long, and shaped like in *Ophthalmidium*. The second chamber leads to a rectilinear or curvilinear part of the test, which consists of up to four elongated chambers. These are pyriform or flask-like in shape, but with the largest constriction two-thirds of the way up the chamber, so that the chamber again gains in width towards the simple circular aperture. The third chamber in the uniserial part measures approximately 0.041–0.054 mm in width and 0.135–0.230 mm in length. Although both, the length and width of the chambers increase continuously, they do so at different and inconstant rates. However, since the chambers are always much longer than they are wide, the test is always very elongated and narrow. Specimens with three chambers in the linear part are between 0.39 and 0.63 mm long, whereas the specimens with four chambers in the linear part measure 0.40 to 0.695 mm in length. The largest length of the chamber is 0.31 mm. The widest (usually third or fourth) chamber in the linear part is usually equal in width to the planispiral part. However, deviations are possible in both directions. The wall is silicified.

Remarks: The first description of *N. vujisici* was based on specimens in the thin sections, and was originally thought to have lived fixed to a substrate. It was also interpreted that the planispiral part, which follows the proloculus, consists of a single tubular chamber, which later straightens up to form the initial part of the linear series of chambers (Urošević & Gaździcki, 1977). The new species was placed in the genus *Nodobacularia*, which, however, is characterised by two chambers in the planispiral part, and has some agglutinated particles within its wall (Loeblich & Tappan, 1988). Gheorghian (1980) later introduced two new species from the Middle and Upper Triassic of Romania, with both attributed to the genus *Nodophthalmidium* Macfayden, 1939; of these species, *Nodophthalmidium elenae* Gheorghian represents a junior synonym of *N. vujisici*, but *Nodophthalmidium anae* Gheorghian represents a distinct species characterised by longitudinal costae. Gheorghian (1980, pl. 2) provided hand-drawings of the specimens, showing a tubular second chamber, that completely envelops the proloculus and continues to the linear part of the test. These illustrations led Loeblich and Tappan (1986) to establish a new genus, *Gheorghianina*, that differs from *Nodobacularia* in the mentioned feature, and from *Nodophthalmidium* in having more elongated chambers and a simple circular aperture. Both valid species, *Nodobacularia vujisici*, and *Nodophthalmidium anae* were attributed to this genus. However, we believe that the microphotograph in Gheorghian's (1980) plate 3 shows two chambers in the planispiral part, and that the second chamber is only one-half of a whorl long. Trifonova (1993) also noted that there are two chambers in the planispiral part of *Nodobacularia vujisici* and *Nodophthalmidium anae*. Moreover, this observation can be confirmed in the specimens from Mišji Dol. Bérczi-Makk (1996) stated that *Gheorghianina* possesses a long, tapered neck, which is absent in both *Nodobacularia* and

Nodophthalmidium. Bérczi-Makk (1996) still considered *Gheorghianina* to have a planispiral part one-chamber long, and also stated that the planispiral part is much smaller in *Gheorghianina* than in the other two genera.

Whatever the generic assignment, *Gheorghianina* has been reported from the literature quite rarely. This could also be due to its small size and the brittle nature of its test. Imperfect sections could lead to confusion with *Earlandia amplimuralis* (Pantić). Salaj et al. (1983) described another species, *Nodobacularia cylindriformis* Salaj, Borza & Samuel, from Anisian beds, which lacks costae but is otherwise similar to *N. anae*. On the same plate, they figured also *Nodophthalmidium cylindriformis* n. sp. (perhaps a misnomer for *Nodobacularia cylindriformis*), creating some confusion, as no description is given under this name. *Nodobacularia? vujisici* is often found in facies with daonellids or some undetermined thin-shelled bivalves (Urošević & Gaździcki, 1977; Gheorghian, 1980; Kristan-Tollmann, 1984; Kolar-Jurkovšek, 1991).

Stratigraphic range: Illyrian to upper Carnian of Carpathians; Ladinian of Himalayas; Ladinian of Transdanubian Range and the Alsó Hill in Hungary; lower Ladinian to Carnian of Balkan Mountains and Dobrogea; and upper Anisian and Ladinian of Slovenia.

Discussion

Biostratigraphy and comparison with other conodont assemblages

All of the studied conodont samples are marked by *P. excelsa* that is present throughout the sampled succession. This species is accompanied by *G. tethydis*, *N. cornuta* and *N. constricta* that occur in most samples, except in the three samples from the uppermost part of the succession. *Paragondolella excelsa* ranges from the Illyrian to the Fassanian (Chen et al., 2015). The species *N. constricta* (sensu Kozur), ranges in the Illyrian, and possibly even in the Pelsonian; *N. cornuta*, with a distinct cusp fused with the posterior platform end, is also common in the Illyrian faunas (Kozur et al., 1994).

The upper part of the section is marked by the first occurrence of *G. malayensis*. Moreover, a successive appearance of *N.* cf. *excentrica*, *P. liebermani*, *N. balkanica* and *P.* cf. *alpina* is noted in this zone; all of these species range in the Illyrian and the Fassanian (Chen et al., 2015). Moreover, an introduction of budurovignathids is noteworthy. They first appear in the sample MD6B:A, from which a single specimen of *B. gabrielae* is determined. It reveals a slightly sigmoidal platform, bent, and a forward shifted basal cavity. This species was first described from the upper Fassanian of Karavanke, Southern Alps, and was interpreted to be the oldest *Budurovignathus* representative as it retained some features of *Neogondolella*, i.e., broadly rounded platform end and relatively separated carina denticles (Kozur et al., 1994). The *Budurovignathus* specimens from the uppermost part of the section are more advanced, having typical high carina with fused denticles, as well as significant sigmoidal bending and thus a forward-shifted basal cavity.

The specimens of *P. trammeri* predominate in the faunas of the upper part of the section. Juvenile and intermediate forms prevail over adults. It should be noted here that some other taxa (*P. eotrammeri* Krystyn, *P. preaetrammeri* (Kozur)) were described from the *P. trammeri* group, where only adult specimens can be distinguished among each other. For a long time, *P. trammeri* was one of the most important Ladinian markers found in open pelagic and more restricted settings of the Tethys.

Based on the composition of the faunas, two conodont zones can be distinguished. The older is the *constricta* Zone that encompasses the interval from the sample MD1B to the sample MD2A:A. The zonal marker *N. constricta* is accompanied by *C. kochi*, *G. tethydis*, *N. cornuta*, *P. excelsa*, *P.* ex gr. *trammeri* (juvenile), and *Paragondolella* sp. The range of this zone in Slovenia is lower Illyrian (Kolar-Jurkovšek & Jurkovšek, 2019).

Upward follows the *trammeri* Zone. It is characterized by the index species in association with some holdover species from the previous zone, which are *G. tethydis*, *N. cornuta*, *N. constricta*, and *P. excelsa*. The lower boundary of this zone is identified by the first appearance of *G. malayensis* in the sample MD2E:A. Other species that are introduced in this zone are: *B. gabrielae*, *N. balkanica*, *N.* cf. *excentrica*, *P. liebermani*, *P.* cf. *alpina*. The *trammeri* zone in Slovenia ranges from the upper Illyrian to the lower Fassanian (Kolar-Jurkovšek & Jurkovšek, 2019). The colour of the conodont elements suggests that the rocks were subjected to temperatures between 300 °C and 550 °C (Epstein et al., 1977).

The conodont assemblage from the Mišji Dol section is similar to the assemblage recorded from Bagolino in the Southern Alps of the northern Italy, the GSSP for the Ladinian (Brack & Nicora, 1998; Brack et al., 2005). The similarity is especially

Table 3. Illyrian – Fassanian conodont assemblages from Slovenia (based on Kolar-Jurkovšek & Jurkovšek, 2019). Localities Slugovo and Rižnikar feature slightly younger, late Fassanian, and Fassanian – Longobardian assemblages, respectively.

	Mišji Dol	Topla	Prisojnik	Kamna Gorica	Idrijske Krnice	Šentjošt	Hrastenice	Šmarna gora	Jagršče	Rižnikar	Rob & Ortnek	Bučka	Sremič	Loke	No.
Budurovignathus sp.	•										•		•		3
Budurovignathus gabrielae Kozur	•														1
B. hungaricus Kozur										•	•				2
B. mirautae (Kovacs)										•					1
B. mungoensis (Diebel)										•					1
Cratognathodus kochi (Huckriede)	•												•		2
Gladigondolella malayensis Nogami	•		•												2
G. tethydis Nogami	•				•				•	•		•			5
Gondolella hanbulogi (Sudar & Budurov)					•										1
Neogondolella balkanica Budurov & Stefanov	•		•												2
N. bifurcata (Budurov & Stefanov)					•										1
N. bulgarica (Budurov & Stefanov)					•				•						2
N. constricta (Mosher & Clark)	•						•	•				•		•	5
N. cornuta Budurov & Stefanov	•	•					•	•					•		5
N. excelsa (Mosher)					•							•		•	3
N. excentrica Budurov & Stefanov	•	•			•										3
N. mombergensis (Tatge)		•												•	2
N. transita (Kozur & Mostler)							•						•		2
Paragondolella alpina (Kozur & Mostler)	•										•		•		3
P. excelsa Mosher	•					•	•	•		•					5
P. liebermani (Kovacs & Kozur)	•														1
P. navicula (Huckriede)		•												•	2
P. prealpina Ramovš & Goričan							•	•							2
P.? pridaensis posteroacuta Kozur, Krainer & Mostler			•					•							2
P. trammeri (Kozur)	•		•	•				•		•	•				6
P. praeszaboi bystricky Kovács et al.										•					1
Total no. species at locality:	13	4	4	1	6	1	5	6	2	7	4	3	5	4	

evident for the elements belonging to the latest Anisian *constricta* zone, and in the presence of budurovignathids in the Ladinian part. Eight taxa are common to both sections: *N. balkanica, N. constricta, N. cornuta, P. excelsa, P. liebermani, P. trammeri, P.* ex gr. *alpina*, and *G. malayensis*. Their occurrence is similar in both sections. It should be noted here that different taxonomies have been used for the determination of some neogondolellids, and in Bagolino some of them were determined at subspecies level: *N. constricta cornuta* Budurov & Stefanov, *N. constricta postcornuta* (Kovacs), *N. constricta balkanica* Budurov & Stefanov (Brack & Nicora, 1998). The lower part of the *reitzi* Zone in the Bagolino section yields *N. constricta, N. cornuta* and *P. excelsa* that can be compared to the lower part of the Mišji Dol section belonging to the *constricta* Zone. The upper part of the *reitzi* Zone and the *secedensis* Zone of the Bagolino section is marked by the appearance of *G. malayensis* and *P. trammeri*; this part is also characterized by the occurrence of the precursor of *B. gabrielae*, determined as *N.* sp. A, whereas early budurovignathids are represented by three taxa in the Ladinian part of the section. The difference between the composition of the faunas in the two sections is the earlier appearance of *P. liebermani* in the Bagolino section, where *P.* ex gr. *alpina* is present in most of the Anisian part of the section and continues also in the *curionii* Zone; in the Mišji Dol section, *P.* ex gr. *alpina* is very rare and has been encountered only in the *trammeri* Zone.

Based on the conodont faunas the age of the studied section thus is Illyrian-Fassanian. Exact position of the base of the *trammeri* zone cannot be determined based on the recovered material, but it is tentatively marked by the first occurrence of *G. malayensis*. The Anisian-Ladinian boundary could be therefore placed between samples MD2E:A and MD4A:A, most probably after the facies change within the sector 18 (Fig. 3). The fauna of the upper part of the *trammeri* zone reveals Ladinian character due to the presence of budurovignathids. In the studied Mišji Dol section they are first encountered approximately 20 m above the occurrence of *G. malayensis*, whereas in the Bagolino section budurovignathids (*B. truempyi, B. hungaricus*) occur in the layers corresponding the Ladinian level (Brack et al., 2005).

Table 3 lists other localities from Slovenia with common conodont species from the Illyrian – Fassanian interval (see Kolar-Jurkovšek and Jurkovšek, 2019 for an overview of the localities and existing references). These successions were deposited in different palaeogeographic situations

Table 4. The Dice similarity index for different localities with latest Anisian – earliest Ladinian conodont assemblages in Slovenia (based on Kolar-Jurkovšek & Jurkovšek, 2019).

	Mišji Dol	Topla	Prisojnik	Kamna Gorica	Šentjošt	Hrastenice	Šmarna gora	Jagršče	Rižnikar	Rob & Ortnek	Bučka	Sremič	Loke	Idrijske Krnice
Mišji Dol	1	0.24	0.35	0.14	0	0.33	0.42	0.13	0.3	0.35	0.25	0.44	0.11	0.21
Topla	0.24	1	0	0	0	0.22	0.2	0	0	0	0	0.22	0.4	0.2
Prisojnik	0.35	0	1	0.4	0	0	0.4	0	0.18	0.25	0	0	0	0
Kamna Gorica	0.14	0	0.4	1	0	0	0.29	0	0.25	0.4	0	0	0	0
Šentjošt	0	0	0	0	1	0	0	0	0	0	0.5	0	0.29	0.29
Hrastenice	0.33	0.22	0	0	0	1	**0.73**	0	0.17	0	0.25	0.4	0.18	0
Šmarna gora	0.42	0.2	0.4	0.29	0	0.73	1	0	0.31	0.2	0.22	0.18	0.17	0
Jagršče	0.13	0	0	0	0	0	0	1	0.22	0	0.4	0	0	0.5
Rižnikar	0.3	0.18	0.25	0.4	0	0.17	0.31	0.22	1	0.36	0.2	0	0	0.15
Rob & Ortnek	0.35	0	0.25	0.4	0	0	0.2	0	0.36	1	0	0.44	0	0
Bučka	0.25	0	0	0	0.5	0.25	0.22	0.4	0.2	0	1	0	0.44	0.44
Sremič	0.44	0.22	0	0	0	0.4	0.18	0	0	0.44	0	1	0	0
Loke	0.11	0.4	0	0	0.29	0.18	0.17	0	0	0	0.44	0	1	0.17
Idrijske Krnice	0.21	0.2	0	0	0.29	0	0	0.5	0.15	0	0.44	0	0.17	1

Table 5. The Dice similarity index for the correlation among the determined conodont taxa.

	Budurovignathus sp.	*B.mirautae*	*B.gabrielae*	*B.hungaricus*	*B.mungoensis*	*C.kochi*	*G.malayensis*	*Go.hanbulogi*	*G.tethydis*	*N.balkanica*	*N.bifurcata*	*N.bulgarica*	*N.constricta*	*N.cornuta*	*N.excelsa*	*N.excentrica*	*N.mombergensis*	*N.transita*	*P.alpina*	*P.excelsa*	*P.liebermani*	*P.navicula*	*P.prealpina*	*P.pridaensis*	*P.trammeri*	*P.praeszaboi*
Budurovignathus sp.	1	0	0.5	0.4	0	0.8	0.4	0	0.25	0.4	0	0	0.25	0.5	0	0.33	0	0.4	1	0.3	0.5	0	0	0	0.44	0
B.mirautae	0	1	0	0.67	1	0	0	0	0.33	0	0	0	0	0	0	0	0	0	0	0.4	0	0	0	0	0.29	1
B.gabrielae	0.5	0	1	0	0	.67	0.67	0	0.33	0.67	0	0	0.33	0.33	0	0.5	0	0	0.5	0.4	1	0	0	0	0.29	0
B.hungaricus	0.4	0.67	0	1	0.67	0	0	0	0.29	0	0	0	0	0	0	0	0	0	0.4	0.33	0	0	0	0	0.5	0.67
B.mungoensis	0	1	0	0.67	1	0	0	0	0.33	0	0	0	0	0	0	0	0	0	0	0.4	0	0	0	0	0.29	1
C.kochi	0.8	0	0.67	0	0	1	0.5	0	0.29	0.5	0	0	0.29	0.57	0	0.4	0	0.5	0.8	0.33	0.67	0	0	0	0.25	0
G.malayensis	0.4	0	0.67	0	0	0.5	1	0	0.29	1	0	0	0.29	0.29	0	0.4	0	0	0.4	0.33	0.67	0	0	0.5	0.5	0
Go.hanbulogi	0	0	0	0	0	0	0	1	0.33	0	1	0.67	0	0	0.4	0.5	0	0	0	0	0	0	0	0	0	0
G.tethydis	0.25	0.33	0.33	0.29	0.33	0.29	0.29	0.33	1	0.29	0.33	0.57	0.4	0.2	0.44	0.5	0	0	0.25	0.44	0.33	0	0	0	0.36	0.33
N.balkanica	0.4	0	0.67	0	0	0.5	1	0	0.29	1	0	0	0.29	0.29	0	0.4	0	0	0.4	0.33	0.67	0	0	0.5	0.5	0
N.bifurcata	0	0	0	0	0	0	0	1	0.33	0	1	0.67	0	0	0.4	0.5	0	0	0	0	0	0	0	0	0	0
N.bulgarica	0	0	0	0	0	0	0	0.67	0.57	0	0.67	1	0	0	0.33	0.4	0	0	0	0	0	0	0	0	0	0
N.constricta	0.25	0	0.33	0	0	0.29	0.29	0	0.4	0.29	0	0	1	0.6	0.44	0.25	0.29	0.29	0.25	0.67	0.33	0.29	0.57	0.29	0.36	0
N.cornuta	0.5	0	0.33	0	0	0.57	0.29	0	0.2	0.29	0	0	0.6	1	0	0.5	0.29	0.57	0.5	0.67	0.33	0.29	0.57	0.29	0.36	0
N.excelsa	0	0	0	0	0	0	0	0.4	0.44	0	0.4	0.33	0.44	0	1	0.29	0.33	0	0	0	0	0.33	0	0	0	0
N.excentrica	0.33	0	0.5	0	0	0.4	0.4	0.5	0.5	0.4	0.5	0.4	0.25	0.5	0.29	1	0.4	0	0.33	0.29	0.5	0.4	0	0	0.22	0
N.mombergensis	0	0	0	0	0	0	0	0	0	0	0	0	0.29	0.29	0.33	0.4	1	0	0	0	0	1	0	0	0	0
N.transita	0.4	0	0	0	0	0.5	0	0	0	0	0	0	0.29	0.57	0	0	0	1	0.4	0.33	0	0	0.5	0	0	0
P.alpina	1	0	0.5	0.4	0	0.8	0.4	0	0.25	0.4	0	0	0.25	0.5	0	0.33	0	0.4	1	0.29	0.5	0	0	0	0.44	0
P.excelsa	0.29	0.4	0.4	0.33	0.4	0.33	0.33	0	0.44	0.33	0	0	0.67	0.67	0	0.29	0	0.33	0.29	1	0.4	0	0.67	0.33	0.6	0.4
P.liebermani	0.5	0	1	0	0	0.67	0.67	0	0.33	0.67	0	0	0.33	0.33	0	0.5	0	0	0.5	0.4	1	0	0	0	0.29	0
P.navicula	0	0	0	0	0	0	0	0	0	0	0	0	0.29	0.29	0.33	0.4	1	0	0	0	0	1	0	0	0	0
P.prealpina	0	0	0	0	0	0	0	0	0	0	0	0	0.57	0.57	0	0	0	0.5	0	0.67	0	0	1	0.5	0.25	0
P.pridaensis	0	0	0	0	0	0	0.5	0	0	0.5	0	0	0.29	0.29	0	0	0	0	0	0.33	0	0	0.5	1	0.5	0
P.trammeri	0.44	0.29	0.29	0.5	0.29	0.25	0.5	0	0.36	0.5	0	0	0.36	0.36	0	0.22	0	0	0.44	0.6	0.29	0	0.25	0.5	1	0.29
P.praeszaboi	0	1	0	0.67	1	0	0	0	0.33	0	0	0	0	0	0	0	0	0	0	0.4	0	0	0	0	0.29	1

and presently belong to different structural units. The conodont assemblage from Prisojnik, Šentjošt, Hrastenice, Šmarna gora, Sremič, Idrijske Krnice, and Bučka derive from red nodular limestone deposited within smaller grabens on top of a drowned upper Anisian carbonate platform. Successions from Kamna Gorica, Jagršče, Rižnikar, Rob and Ortnek, and Loke are lithologically more similar to the succession at Mišji Dol, namely featuring grey hemipelagic limestone in association with volcaniclastics and marlstone. The succession from Topla comprises bedded limestone with chert. It must be reminded that samples were (at least partly) collected by different authors, at different times, and that the size of the exposures and the number of collected samples vary as well. In addition, assemblages from Hrastenice, Loke and Idrijske Krnice represent only one conodont zone (*constricta*), section at Kamna Gorica only spans Fassanian, whereas sections at Rižnikar, Rob and Ortnek contain elements from the *trammeri*, as well as the succeeding *hungaricus* zones. The diversity of the conodont assemblages from these localities is generally low to moderate (Kolar-Jurkovšek & Jurkovšek, 2019). The diversity and composition of the conodont assemblages seems unrelated to the lithological composition of the sampled sites. Based on the current data and without regard for the issues mentioned above, the assemblage from Mišji Dol has a notably more diverse range of conodonts (13 species) than other sampled assemblages. The beta diversity of the conodont assemblages seems rather large, since only five species are present in a significant number of sampling sites: out of 14, *Paragondolella trammeri* has been found at 6 localities, and *Gladigondolella tethydis*, *Neogondolella constricta*, *N. cornuta* and *Paragondolella excelsa* at 5 localities. Consequently, the similarity between localities is relatively low (Table 4). The largest similarity can be found between the localities of Šmarna gora and Hrastenice (Dice index 0.73), the first being late Anisian – early Ladinian in age, the latter late Anisian. The assemblage from Mišji Dol is most similar to the assemblages from Sremič and Šmarna gora (Dice indices 0.44 and 0.42, respectively), both spanning the same, late Anisian – early Ladinian time interval.

Table 5 shows correlation among species. Some of the species seem to associate (e.g., *Paragondolella alpina* and *Budurovignathus* sp., *Paragondolella liebermani* and *Budurovignathus gabrielae*, *Neogondolella mombergensis* and *Paragondolella navicula*; Table 5), which indicates that they had similar ecological preferences. However, said correlation would be more reliable if it were based on data obtained from samples of the same weight and collected in a similar density. The correlation also cannot be confirmed for the pairs of species that are listed in the Table 5 only once, for example *Budurovignathus mungoensis*, *Budurovignathus mirautae* and *Paragondolella praeszaboi, Neogondolella balkanica* and *Neogondolella bifurcata*.

Depositional environment

The investigated succession roughly consists of segments, in which there is a variable mixture of lithologies, namely the thin-bedded limestone, marlstone, tuff and volcaniclastic sandstone, and segments that are dominated by thin- to medium-thick beds of carbonates (limestone and/or dolostone). The first are attributed to times of more intense volcanic activity and/or deposition in a more distal part of the basin, while the latter indicate periods of substantial platform production and export of the material down-slope to the more proximal parts of the basin, and/or periods of the quiescence of volcanic activity. The mudstone and radiolarian-filament wackestone-packstone present background hemipelagic/pelagic sedimentation. Other microfacies types are interpreted as sediments of distal (in the case of rudstone also more proximal) turbidity currents, which brought some platform-derived material (biogenic grains with micritised margins, green algae) into the basin and mixed it with components characteristic for open-marine waters (e.g., radiolarians, thin-shelled bivalves). The volcaniclastic sandstone also results from mass flow deposition, but the source of the material was volcanic rocks or tuff layers. The paleogeographic extent of the basin cannot be determined, but numerous smaller basins with a similar type of sedimentation can be envisioned for the late Anisian – early Ladinian for the External Dinarides (e.g., Kolar-Jurkovšek, 1983; Jurkovšek, 1983; Kolar-Jurkovšek, 1991; Demšar & Dozet, 2003; Čar, 2010; Kocjančič et al., 2022).

Conclusions

A succession of marlstone, tuff, volcaniclastic sandstone, and thin- to medium-bedded limestone and dolostone between Mišji Dol and Poljane pri Primskovem contains a relatively rich assemblage of conodonts of the lower Illyrian *constricta* Zone and the upper Illyrian to lower Fassanian *trammeri* Zone. The associated foraminifera include numerous representatives of the species *Nodobaculariа*? *vujisici* Urošević & Gaździcki. The conodont assemblage is similar to the assemblage recorded from Bagolino in northern Italy. On the other hand, assemblages from other localities in

Slovenia have few taxa in common, which is in accordance with the presence of numerous smaller basins characterised by different conditions and communities.

Acknowledgements

The presented paper is the result of the master thesis written by the first author (K. Oselj). The thesis was defended at the Department of Geology, Faculty of Natural Sciences and Engineering. Preparation of the material and the field work was financed by the Slovenian Research Agency (research core funding No. P1-0011; authors T. Kolar-Jurkovšek, B. Jurkovšek and L. Gale). Thin sections were prepared and the microfossils were photographed at the Geological Survey of Slovenia. We thank the reviewers for the thorough reading of the manuscript and constructive remarks.

References

Bérczi-Makk, A. 1996c: Foraminifera of the Triassic formations of Alsó Hill (Northern Hungary). Part 3: Foraminifer assemblage of the basinal facies. Acta Geol. Hungarica, 39/4: 413–459.

Berra, F. & Carminati, E. 2010: Subsidence history from a backstripping analysis of the Permo-Mesozoic succession of the Central Suthern Alps (northern Italy). Basin Res., 22/6: 952–975. https://doi.org/10.1111/j.1365-2117.2009.00453.x

Brack, P. & Nicora, A. 1998: Conodonts from the Anisian-Ladinian succession of Bagolino, Brescian Prealps (Brescia, Lombardy, Northern Italy). Giornale Geol., 60/3: 314–325.

Brack, P., Rieber, H., Nicora, A. & Mundil, R. 2005: The Global boundary Stratotype Section and Point (GSSP) of the Ladinian Stage (Middle Triassic) at Bagolino (Southern Alps, Northern Italy) and its implications for the Triassic time scale. Episodes, 28/4: 233–244. https://doi.org/10.18814/epiiugs/2005/v28i4/001

Budai, T. & Vörös, A. 2006: Middle triassic platform and basin evolution of the Southern Bakony mountains (Transdanubian Range, Hungary). Riv. Ital. Paleontol. Strat., 112/3: 359–371. https://doi.org/10.13130/2039-4942/6346

Buser, S. 1969: Osnovna geološka karta SFRJ 1: 100 000. List Ribnica. Zvezni geološki zavod, Beograd.

Buser, S. 1974: Osnovna geološka karta SFRJ 1: 100 000. Tolmač lista Ribnica. Zvezni geološki zavod, Beograd: 60 p.

Buser, 1986: Osnovna geološka karta SFRJ 1: 100 000. Tolmač za lista Tolmin in Videm (Udine). Zvezni geološki zavod, Beograd: 103 p.

Buser, S. 1989: Development of the Dinaric and the Julian carbonate platforms and of the intermediate Slovenian Basin (NW Yugoslavia). Boll. Soc. Geol. Ital., 40: 313–320.

Celarc, B., Goričan, Š. & Kolar-Jurkovšek, T. 2013: Middle Triassic carbonate-platform breakup and formation of small-scale half-grabens (Julian and Kamnik-Savinja Alps, Slovenia). Facies, 59: 583–610. https://doi.org/10.1007/s10347-012-0326-0

Chen, Y.L., Krystyn, L., Orchard, M.J., Ali, X.L. & Richoz, S. 2015: A review of the evolution, biostratigraphy, provincialism and diversity of Middle and early Late Triassic conodonts. Pap. Palaeontol., 2/2: 235–263. https://doi.org/10.1002/spp2.1038

Cushman, J.A. 1927: An outline of a re-classification of the foraminifera. Contributions from the Cushman Laboratory for Foram. Res., 3: 1–105. https://doi.org/10.1126/science.65.1689.473.b

Čar, J. 2010: Geological structure of the Idrija – Cerkno hills: Explanatory book to the Geological map of the Idrija – Cerkljansko hills between Stopnik and Rovte 1: 25 000. Geological Survey of Slovenia, Ljubljana: 127 p.

Čar, J. 2013: Ladinian skonca beds of the Idrija Ore Deposit (W Slovenia). Geologija, 56/2: 151–174. https://doi.org/10.5474/geologija.2013.010

Čar, J., Jež, J. & Milanič, B. 2021: Structural setting at the contact of the Southern Alps and Dinarides in western Cerkljansko region (western Slovenia). Geologija, 64/2: 189–203. https://doi.org/10.5474/geologija.2021.011

Delage, Y. & Hérouard, E. 1896: Traité de Zoologie Concrète, Volume 1, La Cellule et les Protozoaires. Schleicher Frères, Paris: 584 p. https://doi.org/10.5962/bhl.title.11672

Demšar, M. & Dozet, S. 2003: Anisian and Ladinian beds in the cross-section above Srednik Valley at Križna Gora, central Slovenia. Geologija, 46/1: 41–48. https://doi.org/10.5474/geologija.2003.002

Di Capua, A., De Rosa, R., Kereszturi, G., Le Pera, E., Rosi, M. & Watt, S.F.L. 2022: Volcanically-derived deposits and sequences: a unified terminological scheme for application in modern and ancient environments. Geol. Soc. London, Spec. Publ., 520: 11–27. https://doi.org/10.1144/SP520-2021-201

Dozet, S. 2006: Ladinian beds in the Obla Gorica area, central Slovenia. RMZ – Mater. Geoenviron., 53/3: 367–383.

Dozet, S. & Buser, S. 2009: Triassic. In: Pleničar, M., Ogorelec, B. & Novak, M. (eds.): Geology of Slovenia. Geological Survey of Slovenia, Ljubljana: 161–214.

Dunham, R.J. 1962: Classification of carbonate rocks according to depositional texture. In: Han, W.E. (ed.): Classification of carbonate rocks, A symposium. American Ass. Petrol. Geol. Mem., Tulsa: 108–121.

Embry, A.F. & Klovan, J.E. 1972: Absolute water depth limits of late Devonian paleoecological zones. Geol. Rundschau, 61: 672–686. https://doi.org/10.1007/BF01896340

Epstein, A.G., Epstein, J.B. & Harris, L.D. 1977: Conodont colour alteration – an index to organic metamorphism. Geol. Survey Am. Prof. Paper, 995: 1–27.

Gawlick, H.-J., Goričan, Š., Missoni, S. & Lein, R. 2012: Late Anisian platform drowning and radiolarite deposition as a consequence of the opening of the Neotethys ocean (High Karst nappe, Montenegro). Bull. Soc. géol. France, 183: 349–358. https://doi.org/10.2113/gssgfbull.183.4.349

Germovšek, C. 1955: O geoloških razmerah na prehodu Posavskih gub v Dolenjski kras med Stično in Šentrupertom. Geologija, 3: 116–135.

Gheorghian, D. 1980: Note concernant quelques espèces de *Nodophthalmidium* dans le Trias Moyen-Supérieur de Roumanie. Dări de Seamă ale Şedinţelor, Institutul de Geologie si Geofizica, Paleontologie, 65/3: 37–41.

Gianolla, P., Caggiati, M. & Pecorari, M. 2019: Looking at the timing of Triassic magmatism in the Southern Alps. Geo.Alp, 16: 65–68.

Goričan, Š. & Buser, S. 1990: Middle Triassic radiolarians from Slovenia (Yugoslavia). Geologija, 31–32 (1988/1989): 133–197.

Griffith, J.W. & Henfrey, A. 1875: The micrographic dictionary: a guide to the examination and investigation of the structure and nature of microscopic objects. Van Voorst, London.

Haas, J. & Budai, T. 1999: Triassic sequence stratigraphy of the Transdanubian Range (Hungary). Geol. Carpathica, 50/6: 459–475.

Hammer, Ø., Harper, D.A.T. & Ryan, P.D. 2001: PAST: Paleontological statistics software package for education and data analysis. Palaeontol. electronica, 4/1: 1–9.

Jurkovšek, B. 1983: Fassanian beds with daonellas in Slovenia. Geologija, 26/1: 29–70.

Jurkovšek, B. 1984: Langobardian beds with daonellas and posidonias in Slovenia. Geologija, 27/1: 41–95.

Kocjančič, A., Rožič, B., Gale, L., Vodnik, P., Kolar-Jurkovšek, T. & Celarc, B. 2022: Facies analysis of Ladinian and Carnian beds in the area of Rute Plateau (External Dinarides, central Slovenia). In: Rožič, B. & Žvab Rožič, P. (eds): 15th Emile Argand Conference on Alpine Geological Studies: 12–14 September 2022, Ljubljana, Slovenia: abstract book & fieldtrip guide. Faculty of Natural Sciences and Engineering, Department of Geology, Ljubljana: 37. https://doi.org/10.5194/egusphere-alpshop2022-37

Kolar-Jurkovšek, T. 1983: Middle Triassic conodonts from Slovenia. Rudarsko-metalurški zbornik, 30/4: 323–364.

Kolar-Jurkovšek, T. 1991: Microfauna of Middle and Upper Triassic in Slovenia and its biostratigraphic significance. Geologija, 33/1: 21–170. https://doi.org/10.5474/geologija.1990.001

Kolar-Jurkovšek, T. & Jurkovšek, B. 2019: Conodonts of Slovenia. Geological Survey of Slovenia, Ljubljana: 259 p.

Kovács, S., Sudar, M., Grădinaru, E., Gawlick, H.-J., Karamata, S., Haas, J., Péro, C., Gaetani, M., Mello, J., Polák, J., Aljinović, D., Ogorelec, B., Kolar-Jurkovšek, T., Jurkovšek, B. & Buser, S. 2011: Triassic evolution of the tectonostratigraphic units of the Circum-Pannonian Region. Jb. Geol. B.-A., 151: 199–280.

Kozur, H., Krainer, K. & Mostler, H. 1994: Middle Triassic Conodonts from the Southern Karawanken Mountains (Southern Alps) and Their Stratigraphic Importance. Geol.-Paläontol. Mitt. Innsbruck, 19: 165–200.

Kristan-Tollmann, E. 1984: Trias-Foraminiferen von Kumaun im Himalaya. Mitt. Österr. Geol. Ges., 77: 263–329.

Lipold, M. 1858: Bericht über die geologische Aufnahmen in Unter-Krain im Jahnre 1857. Jb. Geol. Reichsanst., 9/2: 257–276.

Loeblich, A.R.Jr. & Tappan, H. 1986: Some new and redefined genera and families of Textulariina, Fusulinina, Involutinina, and Miliolina (Foraminiferida). J. Foram. Res., 16/4: 334–346. https://doi.org/10.2113/gsjfr.16.4.334

Macfayden, W.A. 1939: On *Ophthalmidium*, and two new names for Recent foraminifera of the family Ophthalmidiidae. J. Royal Microscop. Soc., 59: 162–169.

Oravecz-Scheffer, A. 1987: Triassic foraminifers of the Transdanubian Central Range. Geol. Hungarica, 50: 3–134.

Orbigny, A. d' 1826: Tableau méthodique de la classe des Céphalopodes. Ann. Sci. Natur., 7: 245–314.

Pawlowski, J., Holzmann, M. & Tyszka, J. 2013: New supraordinal classification of Foraminifera: Molecules meet morphology. Marine Micropal., 100: 1–10. https://doi.org/10.1016/j.marmicro.2013.04.002

Placer, L. 1998a: Structural meaning of Sava Folds. Geologija, 41/1: 191–221. https://doi.org/10.5474/geologija.1998.012

Placer, L. 1998b: Contribution to the macrotectonic subdivision of the border region between Southern Alps and External Dinarides. Geologija, 41/1: 223–255. https://doi.org/10.5474/geologija.1998.013

Placer, L. 2008: Principles of the tectonic subdivision of Slovenia. Geologija, 51/2: 205–217. https://doi.org/10.5474/geologija.2008.021

Rakovec, I. 1950: Pseudozilian strata in Slovenia (NW Yugoslavia). Geogr. Vestnik, 22: 1–24.

Ramovš, A. & Goričan, Š. 1995: Late Anisian – Early Ladinian radiolarians and conodonts from Šmarna gora near Ljubljana, Slovenia. Razprave IV. razreda SAZU, 36/9: 179–221.

Rhumbler, L. 1895: Entwurf eines naturlichen Systems des Thalamophoren. Nachrichten Gesell. Wiss. Göttingen, Math.-Physik, 1: 51–98.

Rožič, B., Kocjančič, A., Gale, L., Popit, T., Žvab Rožič, P., Vodnik, P., Zupančič, N., Kolar-Jurkovšek, T. & Celarc, B. 2021: Arhitektura in sedimentarni razvoj ladinijskega bazena na območju Rutarske planote. Geol. zbornik, 26: 111–116.

Salaj, J., Borza, K. & Samuel, O. 1983: Triassic foraminifers of the West Carpathians. Geol. ústav Dionýsa Štúra: 213 p.

Salaj, J., Trifonova, E., Gheorghian, D. & Coroneou, V. 1988: The Triassic foraminifera microbiostratigraphy of the Carpathian – Balkan and Hellenic realm. Mineralia slov., 20/5: 387–415.

Schmid, S. M., Bernoulli, D., Fügenschuh, B., Matenco, L., Schefer, S., Schuster, R., Tischler, M. & Ustaszewski, K. 2008: The Alpine-Carpathian-Dinaridic orogenic system: correlation and evolution of tectonic units. Swiss J. Geosci. (Geol. Rundsch.), 101/1: 139–183. https://doi.org/10.1007/s00015-008-1247-3

Schultze, M.S. 1854: Über den Organismus der Polythalamien (Foraminiferen), nebst Bermerkungen über die Rhizopoden im Allgemeinen. Wilhelm Engelmann, Leipzig: 68 p.

Skaberne, D., Goričan, Š. & Čar, J. 2003: Kamnine in fosili (radiolariji) iz kamnoloma Kamna Gorica. Vigenjc, glasilo Kovaškega muzeja v Kropi, 3: 85–96.

Smirčić, D., Aljinović, D., Barudžija, U. & Kolar-Jurkovšek, T. 2020: Middle Triassic syntectonic sedimentation and volcanic influence in the central part of the External Dinarides, Croatia (Velebit Mts.). Geol. Quarterly, 64/1: 220–239. https://doi.org/10.7306/gq.1528

Stefani, M., Furin, S. & Gianolla, P. 2010: The changing climate framework and depositional dynamics of Triassic carbonate platforms from the Dolomites. Palaeogeogr., Palaeoclimatol., Palaeoecol., 290: 43–57. https://doi.org/10.1016/j.palaeo.2010.02.018

Tomljenović, B. & Csontos, L. 2001: Neogene–Quaternary structures in the border zone between Alps, Dinarides and Pannonian Basin (Hrvatsko zagorje and Karlovac Basins, Croatia). Int. J. Earth Sciences (Geol. Rundsch.), 90: 560–578. https://doi.org/10.1007/s005310000176

Trifonova, E. 1993: Taxonomy of Bulgarian Triassic foraminifera. II. Families Endothyriidae to Ophthalmidiidae. Geol. Balcanica, 23/2: 19–66.

Urošević, D. & Gaździcki, A. 1977: *Nodobacularia vujisici* nov. sp. ladinskog kata unutrašnjeg-karpatskog pojasa (istočna Srbija). Bull. Mus. Hist. Natur., Ser. A, 32: 97–101.

Velledits, F., Péró, C., Blau, J., Senowbari-Daryan, B., Kovács, S., Piros, O., Pocsai, T., Szügyi-Simon, H., Dumitrică, P. & Pálfy, J. 2011: The oldest Triassic platform margin reef from the Alpine-Carpathian region (Aggtelek, NE Hungary): platform evolution, reefal biota and biostratigraphic framework. Riv. Ital. Paleontol. Stratigr., 117/2: 221–268. https://doi.org/10.13130/2039-4942/5973

Vrabec, M. & Fodor, L. 2006: Late Cenozoic tectonics of Slovenia: Structural styles at the northeastern corner of the Adriatic microplate. In: Pinter, N., Grenerczy, G., Weber, J., Stein, S. & Medek, D. (eds.): The Adria microplate: GPS geodesy, tectonics and hazards. NATO Sci. Ser., IV, Earth Environ. Sci., 61: 151–168.

Medak, D. & Stein, S. (eds.): The Adria Microplate: GPS geodesy, tectonics and hazards. Kluwer Academic Publ.: 151–168.

Wright, V.P. 1992: A revised classification of limestones. Sed. Geology, 76: 177–185. https://doi.org/10.1016/0037-0738(92)90082-3

GEOLOGIJA 66/1, 125-150, Ljubljana 2023

https://doi.org/10.5474/geologija.2023.005

Overview of the thermal properties of rocks and sediments in Slovenia

Pregled toplotnih lastnosti kamnin in sedimentov v Sloveniji

Dušan RAJVER & Simona ADRINEK

Geological Survey of Slovenia, Dimičeva ul. 14, SI-1000 Ljubljana, Slovenia; e-mail: dusan.rajver@geo-zs.si

Prejeto / Received 30. 3. 2023; Sprejeto / Accepted 10. 7. 2023; Objavljeno na spletu / Published online 4. 8. 2023

Key words: thermal conductivity, thermal diffusivity, borehole, tunnel, surface, rock, sediment, radioactive heat generation, Slovenia

Ključne besede: toplotna prevodnost, toplotna difuzivnost, vrtina, predor, površje, kamnina, sediment, radiogena tvorba toplote, Slovenija

Abstract

The use of geothermal energy, which comes from both deep geothermal systems and the shallow underground, has been developing rapidly in the last few decades. The purpose of the paper is to present the results of measurements of the thermal properties of all rock samples and sediments that were available from boreholes, two tunnels and numerous surface locations in Slovenia in the period from 1982 to the end of 2022. In relation to the shallow geothermal potential, a special effort is needed to characterize the thermal properties of the rocks and sediments and to implement thermal energy transfer technology. In this sense, knowledge of the thermal conductivity of rocks and sediments is required to assess the possibility of low-enthalpy heat exchange in a given local area. The largest number of measurements was taken to determine thermal conductivity. Determinations of thermal diffusivity were carried out on a much smaller number of rock and sediment samples, as well as determinations of radiogenic heat production in rocks. The results of thermal conductivity measurements on 430 samples from 119 wells, 20 samples from two tunnels and 156 samples from surface locations are shown. The highest thermal conductivities are shown by samples of dolomite, quartz conglomerate and conglomerate, phyllonite, quartz phyllite and gneiss, while the lowest are measured in sediments such as clay, lignite with clay, peat and dry sand. The determined radioactive heat generation is the lowest for milonitized dolomite and highest for dark grey sandstone with shale clasts. Our results are comparable to those already published worldwide, and they could be the basis for the possible future Slovenian standard for the thermal properties of measured rocks and sediments.

Izvleček

Raba geotermalne energije, ki izhaja iz globokih geotermalnih sistemov kot tudi iz plitvega podzemlja, se v zadnjih nekaj desetletjih hitro razvija. Namen prispevka je prikazati rezultate meritev toplotnih lastnosti vseh vzorcev kamnin in sedimentov, ki so bili na voljo iz vrtin, dveh predorov in številnih površinskih lokacij v Sloveniji v obdobju od 1982 do konca 2022. V zvezi s plitvim geotermalnim potencialom je potrebno posebno prizadevanje za karakterizacijo toplotnih lastnosti tal in plitvega podtalja ter za izvedbo tehnologije prenosa toplotne energije. V tem smislu je potrebno poznavanje toplotne prevodnosti kamnin in tal za oceno možnosti izmenjave toplote z nizko entalpijo na določenem lokalnem območju. Številčno največ meritev je bilo za določitev toplotne prevodnosti. Določitve toplotne difuzivnosti so bile izvedene na precej manjšem številu vzorcev kamnin in sedimentov, prav tako določitve produkcije radiogene toplote v kamninah. Prikazani so rezultati meritev toplotne prevodnosti na 430 vzorcih iz 119 vrtin, na 20 vzorcih iz predorov in na 156 vzorcih iz površinskih lokacij. Najvišje toplotne prevodnosti kažejo vzorci dolomita, kremenovega konglomerata in konglomerata, filonita, kremenovega filita in gnajsa, najniže pa so izmerjene v sedimentih, kot so glina, lignit z glino, šota in suh pesek. Ugotovljena radiogena tvorba toplote je najmanjša pri milonitiziranem dolomitu in največja pri temno sivem peščenjaku s klasti skrilavega glinavca. Naši rezultati so primerljivi z že objavljenimi v svetu in lahko predstavljajo osnovo za morebitni bodoči slovenski standard toplotnih lastnosti merjenih kamnin in sedimentov.

Introduction

The energy potential that exists due to the large temperature difference between the inner parts of our planet and its surface, in theory, far exceeds all existing conventional sources (Ravnik, 1991). The total thermal energy in the Earth, calculated above the default average surface temperature of 15 °C, is of the order of $12.6 \cdot 10^{12}$ EJ, and only that thermal energy in the Earth's crust up to a depth of 50 km amounts to $5.4 \cdot 10^{9}$ EJ (Dickson & Fanelli, 2004; Clauser, 2006; Rajver et al., 2012). The exploitation of geothermal energy, in addition to some technical problems, has certainly natural limitations due to the low thermal conductivity and diffusivity of rocks, but the available energy is still huge.

The depths that are of importance for geothermal energy utilization today are a maximum of 10 km, while geodynamics and theoretical geothermics investigate thermal conditions up to a few thousand kilometers depth (Ravnik & Uran, 1984; Uyeda, 1988; Pollack & Sass, 1988). The accumulation of heat, which is today or will be technologically and economically usable in the near future, is located only at depths of less than 10 km, and in most cases less than 4 km. The exploitation of heat and geothermal fluid in low (<90 °C)-, medium (90-150 °C)- and high (>150 °C)- temperature fields (e.g. after Muffler & Cataldi, 1978) for district heating, thermal tourism, greenhouse heating, electricity and thermal energy production requires the knowledge of geological, hydrogeological and thermal characteristics of the area (Di Sipio et al., 2014). In such a context, low enthalpy geothermal energy with its ubiquitous potential is one of the most useful renewable energy sources for heating and cooling of buildings. The successful implementation of low enthalpy geothermal systems, such as ground source heat pump (GSHP) systems (open or groundwater HP and closed-loop or ground-coupled HP systems), operating in the heating-cooling mode entails a better characterization of the thermal and petrophysical properties of subsoil (Di Sipio et al., 2014). Since all this research refers to different depths, we must also know these properties at different temperatures and pressures.

This paper deals predominantly with the results of measurements of thermal conductivity on rocks and loose sediments from numerous boreholes, two tunnels and numerous surface locations in Slovenia, all performed at the Geological Survey of Slovenia (GeoZS) since 1982. The results of thermal diffusivity measurements carried out on rock samples from eight Slovenian boreholes and many surface locations since 2017 are also mentioned. In addition, the results of radiogenic heat production determination in the sampled rocks are presented. It does not go into the study of thermal properties at extremely high pressure and temperature (pT) conditions. The purpose of the paper is to show the values of the thermal conductivity of the sampled rocks in Slovenia, which should be used on a regional scale to provide the necessary information for the dimensioning of closed-loop systems with heat pumps (BHEs, pipes, horizontal collectors), and to better predict the geothermal conditions for the planning of deep boreholes. Our purpose was also to test how well the thermal conductivities measured on rocks from Slovenia match the ranges of values measured on rocks from the other parts of the world, which are mentioned in standards and literature.

Three aspects are required to be taken into consideration when a new closed-loop GSHP system is designed (Dalla Santa et al., 2020): (1) climate and location of the building, (2) building characteristics, such as its use, size and insulation level, and (3) ground (subsoil) conditions. The first two aspects determine the heating and cooling demand of the building while the thermal exchange potential depends on the geological and hydrogeological conditions (Sarbu & Sebarchievici, 2014). Therefore, the determination of ground thermal parameters is crucial in designing the total borehole length to be installed, the borehole heat exchangers (BHEs) spacing and layout, the number of BHEs and mutual position, all of which affect the short-term installation costs and the long-term maintenance of adequate energy efficiency of the GSHP system (Di Sipio et al., 2014; Dalla Santa et al., 2020). The most essential thermal properties of the local underground to be considered when designing a new closed-loop geothermal system are (Dalla Santa et al., 2020):

1. *thermal conductivity* (λ), defined as the ability to transfer heat, usually expressed in W/(m·K). In addition to the temperature gradient, thermal conductivity is the most important parameter in calculating the regional heat-flow density (the basic parameter for evaluating the geothermal potential of a territory), the heat transfer between underground and engineering solutions and the potential of geothermal reservoirs. Thermal conductivity is usually used for geothermal modelling and for validating data obtained by indirect control methods (geoelectrical sounding, magnetotelluric methods, etc.) applied in situ (Banks, 2008; Galson et al., 1987; Di Sipio et al., 2014).

2. *heat capacity* (C), defined as the ability to store heat. It is the ratio between the amount of heat to be transferred to a certain mass or volume to achieve 1 K change in temperature, thus it is expressed in J/K. It depends on the material but also on the mass/volume and, hence, the "specific" heat capacity (c) is usually used, in J/(kg·K) or J/(m^3·K).

3. *thermal diffusivity* (a), that is the ratio of the thermal conductivity and specific heat capacity, defined as the physical property governing the heat diffusion in transient conditions measuring the penetration of temperature changes into a material.

4. *undisturbed ground temperature profile*, which varies in the shallower layers due to annual variation of the ground surface temperature, while from about 10 m, is stable throughout the year and increases with depth based on the local geothermal

heat flux. Regarding determination of the annual mean ground temperature, if this cannot be measured it can be assessed using an alternative approach presented by Rajver et al. (2019) in four ways according to the available data at a given location.

Additionally, the local groundwater flow in the aquifers can significantly affect the heat exchange capability by adding a significant contribution of heat transported by convection, which is not accounted for in the thermal conductivity value, measured in the laboratory (Clauser & Huenges, 1995; Banks, 2008; Dalla Santa et al., 2020).

Knowledge of the thermal properties of rocks and sediments is also increasingly important in various human activities, such as in mining, geotechnical, civil and underground engineering. According to Popov et al. (2016), this knowledge has a crucial role in environmentally sensitive projects such as the disposal of high-level radioactive waste in deep underground sites and repositories, or various engineering projects such as the design of buried high-voltage power cables, oil and gas pipelines and ground modification techniques employing heating and freezing. Much attention in the past years was dedicated to the studies of thermal properties of geologic materials due to growing interest in underground storage. Heat transfer is namely an important consideration when building underground structures (tunnels, subway stations), for underground storage of natural gas and energy and in mining engineering (problem of ventilation for deep mine operation). Detailed data on the thermal conductivity and volumetric heat capacity for relevant geologic formations are needed for thermo-hydrodynamic models to evaluate oil recovery from heavy oil reservoirs and for thermo-hydrodynamic modelling including basin and petroleum systems (Popov et al., 2016).

Thermal conductivity of rocks and sediments – worldwide compilations

For the large number of different rocks thermal conductivity data are available and classified according to rock name and origin in several extensive compilations (Birch, 1942; Clark Jr., 1966; Desai et al., 1974; Kappelmeyer & Haenel, 1974; Roy et al., 1981; Čermák & Rybach, 1982; Robertson, 1988; Sundberg, 1988; Schön, 1996, 2011). It is important to realize that these compilations comprise rocks which are heterogenous in many aspects, such as mineral composition, porosity, water saturation and experimental conditions (Clauser, 2006). Consequently, the great variability of thermal conductivity exists within most rock types. Indeed, rock type as such is a rather poor descriptor for thermal and most other physical rock properties. This limits the usefulness of such tabulations, except for the rare instance when they comprise data for the exact location of particular interest. In all other cases, predictions based only on data collated according to general rock type may be in error. For all practical applications, it is therefore strongly recommended to obtain genuine, representative data of thermal conductivity, either by direct measurement or by inference from geophysical logs. When no measured data are available or no direct measurements can be performed, thermal conductivity can be inferred indirectly, either from data on mineralogical composition together with data on saturating fluids (e.g. Beck, 1988; Horai, 1991; Somerton, 1992; Schön, 1996), or from correlations with other physical properties, in particular those measured in well-logs (e.g. Vacquier et al., 1988; Blackwell & Steele, 1989; Brigaud et al., 1990; Hartmann et al., 2005; Goutorbe et al., 2006). While some of these methods are based on well-defined physical models, others are purely empirical (Clauser, 2006).

Clauser & Huenges (1995) extended their complementary approach of thermal conductivity data compilation with new data. In his attempt to adequately collect and arrange data of the measured thermal conductivity of rocks, Clauser (2006) supplemented data from earlier compilations (Birch & Clark, 1940; Clark Jr., 1966; Touloukian et al., 1970; Desai et al., 1974; Kappelmeyer & Haenel, 1974; Roy et al., 1981; Čermák & Rybach, 1982; Buntebarth, 1984; Robertson, 1988) by a large amount of new data. The data have become available (e.g. Kobolev et al., 1990; Popov et al., 2002, 2003; Mottaghy et al., 2005), and arranged as in the article by Clauser & Huenges (1995) according to four basic rock types: sedimentary, volcanic, plutonic and metamorphic. It is worth noting that older and more recent databases exist on the measured thermal conductivities in several countries or regions, for instance, by Lyubimova & Popova (1967), Lyubimova (1968), Majorowicz & Jessop (1981), Reiter & Tovar (1982), Gable (1986), Robertson (1988), Dövényi & Horváth (1988), Kobolev et al. (1990), Pandey (1991), Fuchs & Förster (2010), Pasquale et al. (2011), Di Sipio et al. (2014), Hamza et al. (2020), Gomes et al. (2021) and others. The thermal conductivity of minerals is much better constrained than that of rocks, due to the well-defined crystal structure and chemical formula for each mineral (Clauser, 2011). Substantial collections of mineral thermal conductivities were

compiled, for instance, by Birch (1942), Clark Jr. (1966), Horai & Simmons (1969), Touloukian et al. (1970), Horai (1971), Roy et al. (1981), Čermák & Rybach (1982), Carmichael (1984), Popov et al. (1987), Diment & Pratt (1988), Somerton (1992), Clauser & Huenges (1995), Romushkevich & Popov (1998) and Clauser (2006). Thermal conductivity measurements were also carried out on rock and sediment samples from lakes and seabeds, and also as *in situ* sea-floor and lake-floor measurements around the world (e.g. Haenel, 1979; Fujisawa et al., 1985; Davis, 1988; Dorofeeva & Duchkov, 1995; Dorofeeva, 1998). Thermal conductivities of common rocks measured at room temperature are given also in suitable graphs and tables, for instance, by Kappelmeyer (1979), Zoth & Haenel (1988), Kappelmeyer & Haenel, (1974), Jessop (1990) and a comparison of published compilations of thermal conductivities by Beardsmore and Cull (2001). Recently, Dalla Santa et al. (2020) developed the thermal properties database by integrating and comparing data (a) provided by the most important international guidelines, (b) acquired from an extensive literature review and (c) obtained from more than 400 direct measurements, mainly of thermal conductivity of rocks and sediments. On the other hand, for closed-loop system designers, the most common thermal conductivity values are available from standard tables, such as the German standard VDI 4640 (VDI, 2001). However, they do not list values for all known types of rocks.

Overview of thermal conductivity measurement methods

Thermal conductivity can be measured in the laboratory on rock (cores or cuttings) and sediment samples. It can also be measured *in situ* either in boreholes or with shallow penetration needle probes (e.g. marine heat flow probes 3 to 20 m long). The available and commercial methods for measuring thermal conductivity can be classified into *steady-state* methods (guarded hot plate, heat-flow meter, divided-bar) and *transient* methods (plane source, hot wire, needle probe, laser flash, optical scanning, modulated DSC, thermocouple method, 3ω method – the last three are important for thermal energy storage materials), presented in Figure 1. All of them are also suitable to determine the anisotropy of thermal conductivity of rocks (Clauser, 2006, 2011). These methods are discussed and described in detail in numerous textbooks and review articles, e.g. by Parker et al. (1961), Beck (1965, 1988), Lyubimova (1968), Kappelmeyer & Haenel (1974), Roy et al. (1981), Davis (1988), Kobolev et al. (1990), Somerton (1992), Popov et al. (1999, 2012), Beardsmore & Cull (2001), Blumm & Lemarchand (2002) and Palacios et al. (2019). Among these techniques, the transient ones are also suitable for determining thermal diffusivity (Drury et al., 1984; Clauser, 2011). The laser flash method can be used for very low (down to -150 °C) and very high (above 500 °C) operating temperatures.

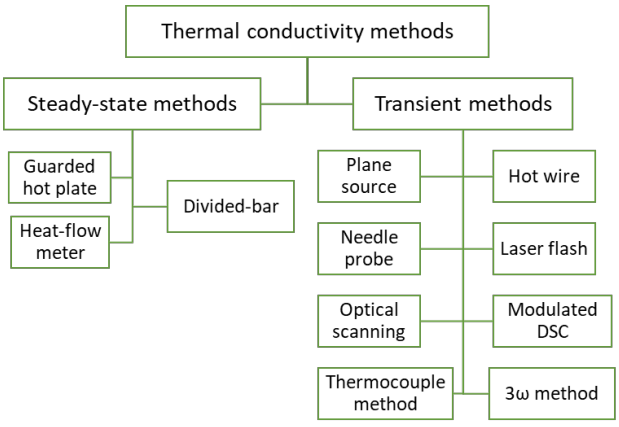

Fig. 1. Thermal conductivity measurement methods classification (modified after Palacios et al., 2019).

Steady-state thermal conductivity measurements are usually made using a divided-bar apparatus – a device designed to measure the thermal conductivity of discs or cylindrical plugs of material (Beardsmore & Cull, 2001). The device, first described by Benfield (1939), is easy to construct and operate, and results are usually accurate to within 5 % (Beck, 1957; Beck, 1988; Beardsmore & Cull, 2001). A similar device, used by scientists, notably from the former Soviet Union, especially in Siberia, is called a thermal (conductivity) comparator (Kalinin, 1981). The thermal conductivity λ is defined as (Carslaw & Jaeger, 1959; Kappelmeyer & Haenel, 1974; Haenel et al., 1988):

$$q = -\lambda \cdot grad\, T = -\lambda \cdot \frac{\partial T}{\partial z} \quad (1)$$

where q is heat-flow density, and T is the local temperature in the sample. With the known geometry of the sample, which is usually plane-parallel, and the known constant power of the heater, the thermal conductivity λ is determined from the measured temperature differences (Prelovšek et al., 1982). Steady-state methods have few disadvantages, consequently, faster transient methods flourished in the 1970s (Prelovšek et al., 1982). Besides, steady-state techniques are unsuitable for loose sediments or *in situ* measurements. Yet in many cases, especially sea-floor measurements, such situations are encountered where a thermal conductivity estimate is required to convert temperature data into a heat flow measurement. For

these cases, a technique for *transient* measurement has evolved (Beardsmore & Cull, 2001). Initially, the transient hot wire method with radial heat flow was developed. The beginnings of this absolute method date back to 1949, when it was used to measure the thermal conductivity of liquids (Van der Held, 1949). Later, the use was extended to solids as well (Ravnik & Uran, 1984). The most commonly used transient device is the *line-source needle probe*, first described by DeVries & Peck (1958), and then by Von Herzen & Maxwell (1959). Among transient methods, the *line-source hot wire* method has become established because it determines the thermal conductivity directly (Carslaw & Jaeger, 1959; Cull, 1974). This method is also the basis of an *improved hot wire* method developed by experts from the Japanese company Showa Denko K.K. (Sumikawa & Arakawa, 1976). Among the transient linear heat flow techniques also few other methods have been developed, such as the method with an *instantaneous source* (Hanley et al., 1978), the "Mongelli" method with a *constant plane heat source* (Mongelli, 1968) and the Ångstrom method using a *periodic heating technique* (Drury et al., 1984). Among the techniques using radial (2-dimensional) heat flow the one with an *instantaneous line-source* was used especially by Lyubimova et al. (1961), while the method with *constant linear or cylindrical heat sources* is the one with typical *needle* probe arrangement (Beck, 1988). One of the more recent methods is the *optical scanning* technology developed by prof. Yuri Popov in the 1980s (Popov, 1983; Popov et al. 1983, 2012, 2017).

The studies comparing the results between the steady-state and transient line-source method of thermal conductivity measurements showed a very good agreement (Čermák et al., 1984; Sass et al., 1984; Galson et al., 1987; Popov et al., 1999). The advantages and disadvantages of both groups of methods are listed in Table 1. Popov et al. (1999) also compared the results between the transient line-source method and the optical scanning method, which showed good agreement. Many studies on the thermal properties of rocks and sediments have taken place with the main goal to increase the number of heat-flow density determinations worldwide (e.g. Roy et al., 1981; Clauser & Huenges, 1995).

However, several difficulties exist when measuring the thermal conductivity of rocks and sediments, since the values are extremely dependent on mineralogical composition, porosity, density, water content (degree of saturation), anisotropy of the material under investigation and pressure and temperature of the surrounding environment. Recent studies have also confirmed the strong influence of solar radiation, soil texture and soil moisture on the soil (or sediment) thermal conductivity down to a depth of 3 m (Dédeček et al., 2012; Di Sipio et al., 2014; Čermák et al., 2016). At a laboratory scale, thermal conductivity measurements are usually performed on samples belonging to rock cores or surface outcrops. Each specimen is non-homogeneous and anisotropic on a scale of a few centimeters, according to its orientation, due to changes in the mineralogical composition, porosity, foliation, bedding, filling of discontinuities and weathering. A difference in thermal conductivity is registered if data are collected between directions parallel (λ_{par}) and perpendicular (λ_{perp}) to the layering, where the former is usually greater than the latter (Davis et al., 2007; Clauser, 2011; Di Sipio et al., 2014).

Upscaling the laboratory data from mesoscale to macroscale entails considering the various lithologies that make up the stratigraphic formations represented on a geological map along with their variability with depth. A geological model must be created where the thermophysical properties of the main lithologies are defined on the basis of real data, obtained from laboratory measurements and supplemented by literature and well-log data (Di Sipio et al., 2014).

Short history of measurements of thermal properties and on geothermal maps in Slovenia

Geothermal research in Slovenia began in the 1950s with hydrogeological studies focusing on hot springs mainly for balneological needs, and to

Table 1. Advantages (A) and disadvantages (D) of thermal conductivity/thermal diffusivity measurement methods (after Palacios et al., 2019).

Steady-state methods		**Transient methods**	
Complex sample preparation	D	Simple sample preparation	**A**
Long measuring time	D	Short measuring time	**A**
Complex realization, thermal constant resistance	D	Small samples	**A**
Clear mean value & simple evaluation of thermal conductivity (simple theory)	**A**	Complex evaluation, solution of heat equations	D
Low cost	**A**	High cost	D

a lesser extent for recreation. They were carried out by the Geological Survey of Ljubljana - GZL (predecessor of today's GeoZS). During their research on hot springs, hydrogeologists obtained a lot of data on water temperature (usually at the source or the wellhead), water yield, chemistry and pressure. However, the results of the temperature measurements were only described descriptively. Geophysical methods, especially geoelectrical soundings and well loggings, soon began to be used in research (Ravnik, 1991). The first systematic geothermal measurements were initiated in Slovenia in 1982–1984 with the manufacture of electric thermometers and equipment for measuring the thermal conductivity of rocks. One of the first results of thermal conductivity measurements on rock samples from a geothermal borehole in Slovenia, using the MTP-1 meter, were presented by Ravnik et al. (1982). Later the results of thermal conductivity measurements on rock samples from the boreholes at four Slovenian geothermal locations, using both line-source meters, were presented by Rajver (1986). These geothermal measurements were supplemented by analyses of the concentration of radiogenic isotopes of elements U, Th and K^{40} at the Jožef Stefan Institute in Ljubljana on prepared (properly ground) rock samples (Ravnik, 1991). In research already done by Ravnik et al. (1995), no clear relationship was found between near-surface heat-flow density and radiogenic heat generation, which was probably due to the predominantly Cenozoic age of the samples, and the irregular vertical distribution of heat producing elements in the near-surface layers.

In 1985, the GZL took over the editing of the preparation of geothermal maps of the former Yugoslavia for the new Geothermal Atlas of Europe. These maps were completed in the first phase in 1987 (Ravnik et al., 1987) and finally in 1989-1990 (Ravnik et al., 1992) and present the results of all previous research, supplemented by new data. The Atlas was published in 1992 under the auspices of the International Association for Seismology and Physics of the Earth's Interior (IASPEI) (Hurtig et al., 1992).

The report by Ravnik & Rajver (1990) was the first transparent result of geothermal research in Slovenia up to that time. The basic research methodology was established and the first two basic maps were produced: 1) a map of formation temperatures at a depth of 1000 m and 2) a map of surface heat-flow density (HFD). Even then, it was planned to create several similar geothermal maps, containing data up to a depth of 5000 m. The aim of the research was to enable the assessment of the geothermal potential of the entire Slovenia as soon as possible, which also required appropriate hydrogeological data. Both aforementioned maps were updated and presented by Ravnik et al. (1995). Every few years, the maps were updated and corrected according to new data (Ravnik, 1991; Rajver, 2018).

Methods

Thermal conductivity measurement methods at GeoZS

The thermal conductivity of rocks has been measured at GeoZS since 1982, when we acquired the first measuring device, based on the transient hot wire method. Considering the basic idea of the Japanese Sumikawa and Arakawa (1976), this method was used also in Slovenia based on the initiative of the Department of Geophysics at GZL (Uran, 1982; Prelovšek & Uran, 1984). At the same time, in cooperation with geophysicists from GZL, the first thermal conductivity meter MTP-1 was produced for GZL at the Department of Physics (Faculty of Natural Sciences at University of Ljubljana) (Prelovšek et al., 1982). It was the first meter of its kind produced in former Yugoslavia (Fig. 2). The results of thermal conductivity obtained with our MTP-1 meter were compared by prof. Prelovšek on the same samples measured with a similar meter at the Department of Geophysics of the Eötvös Loránd University in Budapest (dr. Horváth), then with a similar Japanese QTM (Quick Thermal conductivity Meter) device in the geothermal laboratory of prof. Rybach at ETH in Zurich, and with especially detailed measurements by the standard divided-bar (DB) method (Kappelmeyer & Haenel, 1974; Haenel et al., 1988) at the Geophysical Institute of the Czechoslovak

Fig. 2. Thermal conductivity meter MTP-1 (photo taken in 2022 during measurement on silicified brick).

Academy of Sciences in Prague (dr. Čermák), described by Ravnik & Uran (1984) and Ravnik (1988). Later, controls were also made at the International Institute for Geothermal Research in Pisa (Rajver, 1990) on samples from two deep Slovenian boreholes and during the 4th International Heat Flow meeting in Czechia in 1996, where experts from the State Geological Research Academy in Moscow checked our measurement results with their optical scanning IR device (prof. Popov).

According to these control measurements and according to the literature (Čermák et al., 1984; Sass et al., 1984; Galson et al., 1987), generally insignificant differences were indicated, as the difference between QTM and DB measurements does not exceed ±10 %. Two years later, in 1984 the GZL bought from the same faculty another meter MTP-4 of the same hot wire method, which was slightly improved with more time and power selection options (Fig. 3). At least ten such meters were produced by the mentioned faculty and sold all over former Yugoslavia.

Fig. 3. Thermal conductivity meter MTP-4 (photo taken in 2022 during measurement on lacquered marble).

The proper functioning of both line-source devices was constantly monitored by standard calibration material, like fused quartz and some appropriately prepared rocks, such as marble pieces, limestone and quartz diorite (tonalite). The imprecision of the conductivity data was about 3 %, whereas inaccuracy is estimated to be not more than 10 % (Ravnik et al., 1995). Measurements were performed at normal pressure and room temperature and, if possible, on intact rock samples, using both line-source meters in the period 1982 to 2006. Typically, 10 to 15 individual measurements were performed with the MTP-1 and MTP-4 devices on each rock sample, placing the measuring probes at different positions on the sample.

Since January 2007, we use a TCS device (Fig. 4), which works with the optical scanning method. The *optical scanning* technology is available in the commercial device named "Thermal Conductivity Scanner" (TCS), produced by TCS - Lippmann and Rauen GbR, Germany (Popov et al., 2016, 2017, 1999). The optical scanning technology is based on scanning using a focused, mobile and continuously operated near-point-like heat source in combination with infrared temperature sensors. Infrared sensors measure the temperature before and after focused heating. Determination of thermal properties is based on the comparison of temperature differences measured on *standard samples* (reference samples) with temperature differences measured on one or more *unknown samples*:

$$\lambda = \lambda_R \left(\frac{\Theta_R}{\Theta}\right) \quad (2)$$

where:
λ = thermal conductivity (TC) of sample
λ_R = TC of standard
Θ_R = temperature rise in the standard
Θ = temperature rise in the sample

Fig. 4. The TCS device in a TC+TD mode with a set of rock samples along the scanning line (photo taken in 2022).

The TCS meter also displays the following two values after each TC measurement: G factor (G = standard deviation / mean TC) and Inhomogeneity factor = (max TC – min TC) / mean TC. When the TCS meter is set in the TC+TD mode then also thermal diffusivity (TD) is measured (e.g. Marx, 2014; Haenel et al., 1988):

$$\alpha = \frac{\lambda}{\rho \cdot c} \quad (3)$$

where:
α = TD of sample
λ = TC of sample
ρ = sample density
c = specific heat capacity

The density of rocks were determined by the geomechanics laboratory at GZL by determining the volumetric weight using the mercury method, where the weight of the sample W (in pounds, p) and the weight of displaced mercury W_{Hg} (p) were first measured. Knowing the specific weight of mercury γS_{Hg} (13.546 p/cm^3), the sample volume $V = W_{Hg} / \gamma S_{Hg}$ (cm^3) is calculated, and from this the volumetric weight of the rock sample $\gamma S = W / V$ (p/cm^3). Three such consecutive analyses have been always performed on each sample. The average of the three analyses (p/cm^3) is taken into account, which is multiplied by 10 to get the average in kN/m^3. If this is divided by 9.81 we get the density (g/cm^3). A map of the volumetric (specific) heat capacity (MJ/m^{3}K) of rocks and sediments in Slovenia has also been prepared (Prestor et al., 2018), for which the input data are the basic geological map of Slovenia on a scale of 1:100,000 and average measured values of the volumetric heat capacity of rocks and sediments, which are taken from two standards (SIA and VDI).

Fig. 5. The longer TR-1 single-needle probe and the shorter SH-1 dual-needle probe of the KD2 Pro Thermal Properties Analyzer.

For the TC measurements of the loose sediments, we have been using the KD2 Pro portable device (Decagon Devices, 2016) (Fig. 5) since spring 2017. Depending on the physical properties of the tested sediment samples, two needle probes are used (TR-1 and SH-1).

Comparison of thermal conductivity values by line-source and optical scanning methods on reference standards at GeoZS laboratory

Control measurements of thermal conductivity (TC) were performed with both methods (line-source and optical scanning) on reference standards in the GeoZS geothermal laboratory. The

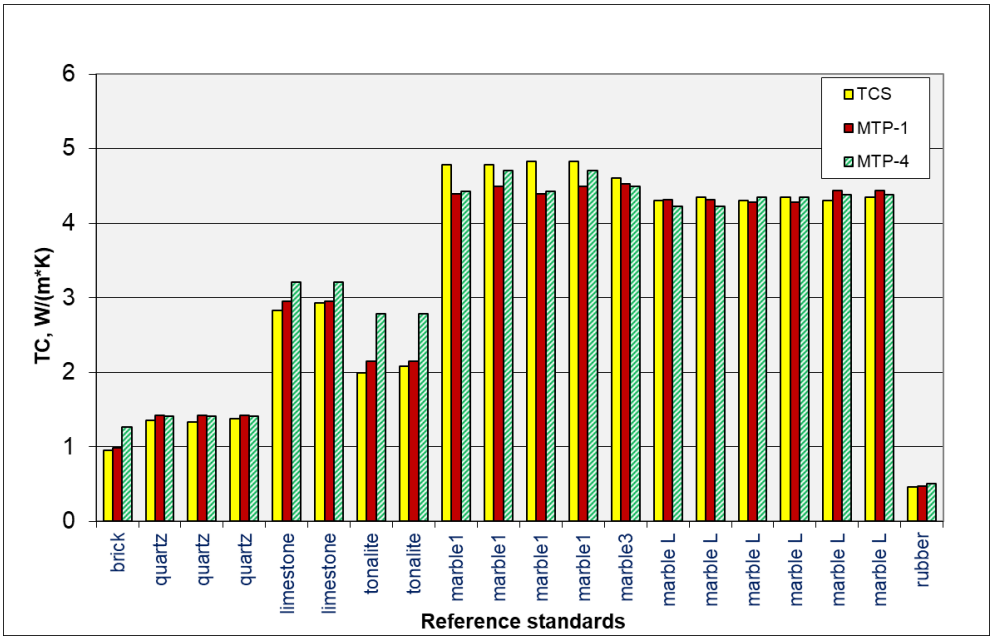

Fig. 6. Comparison of measured TC on reference standards at the GeoZS by the optical scanning (TCS meter) and line-source (MTP-1 and MTP-4 meters) methods.

results showed comparable values of thermal conductivity (Figs. 6 and 7). The measurements on reference standards with the MTP-1 and MTP-4 meters were occasionally carried out over a longer time period (from 1984 to 2007). The used reference standards were (in order from highest to lowest thermal conductivity): polished marble (3 samples), polished lacquered marble (marble L), limestone, tonalite, fused quartz, silicified brick and rubber. Figure 6 shows a comparison between the measured thermal conductivities with the TCS meter (either individual measurements or the averages of 2 to 5 individual measurements, which are different for each standard sample) and the measured TCs with the MTP-1 and MTP-4 meters (averages of a higher number of individual measurements, minimum 4 and maximum 234 measurements on each standard sample), which were performed in different time periods.

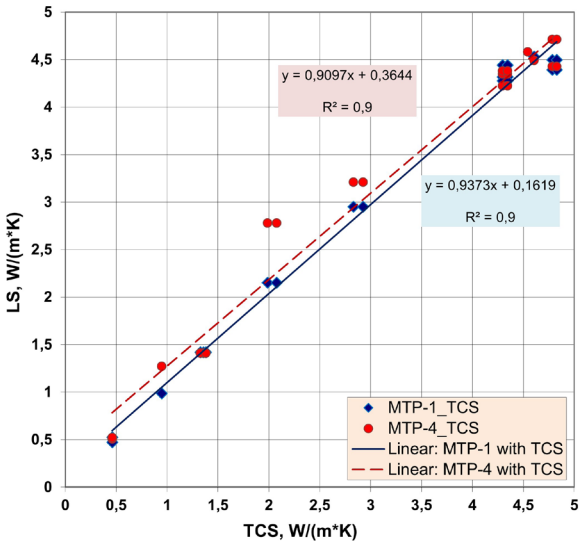

Fig. 7. Correlation between measured TC values (from Fig. 6) on reference standards with the TCS device and the line-source (LS) method (MTP-1 and MTP-4 meters), with trend lines shown.

One may notice a deviation in Figures 6 and 7, showing that higher TC values were obtained by the MTP-4 meter on tonalite, a little higher also on limestone and brick. Perhaps not completely suitable settings of this meter were selected for these particular measurements, or there was some other unexplained reason. Since the TC originally determined by the manufacturer on tonalite was 2.29 and on limestone 2.94 W/(m·K), probably measured with the MTP-1 meter, which were assumed to have declared values, the measurements with the MTP-4 were excluded in further correlation analysis. It turned out that the TCS measured lower TC values on the low conductivity standard (fused quartz) than the two line-source meters (Fig. 8). On the other hand, the TCS measured higher values mainly on the marble 1 standard, especially compared to the results with the older meter MTP-1 (Fig. 7). Of course, more comparative measurements should be made for more appropriate conclusions but both line-source devices don't operate properly anymore or they do only occasionally. Yet, according to Figures 6–8, the agreement of the measured values by both methods is quite satisfactory.

Calculation of radiogenic heat generation

An important source of the Earth's heat is the decay of radioactive isotopes. All natural radioactive isotopes generate heat to a certain extent but only the contributions of the decay series of uranium ^{235}U and ^{238}U, thorium ^{232}Th and of the isotope potassium ^{40}K are geologically significant. In this process, the kinetic energy of the alpha and beta particles and the gamma photons almost entirely convert into heat (Ravnik, 1991). Radioactive heat production H is calculated according to the equation (Rybach, 1988):

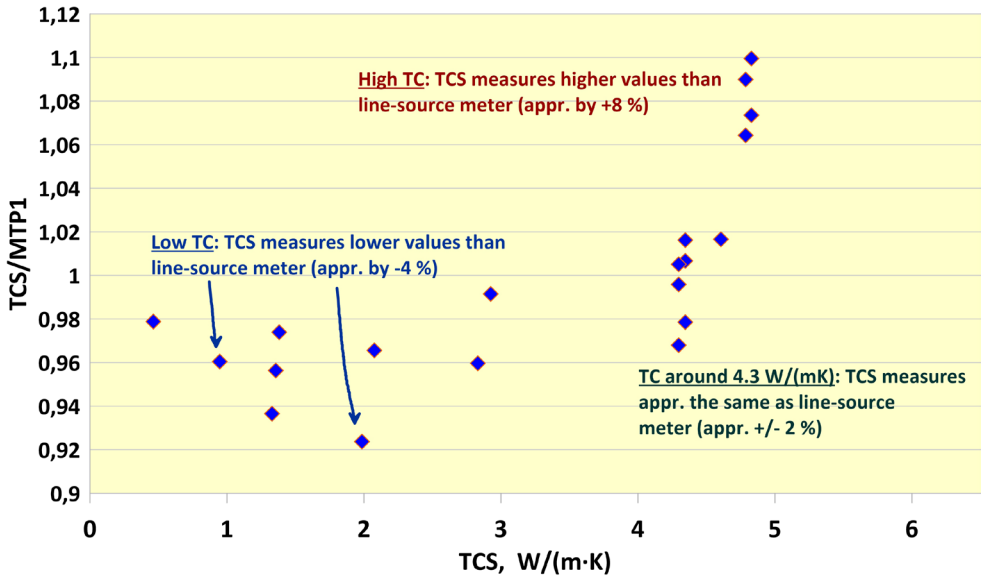

Fig. 8. Correlation between measured TC values (from Fig. 6) with the TCS device and the ratio of values measured with the TCS and MTP-1 meters.

$$H = \rho\,(9.52\,c_U + 2.56\,c_{Th} + 3.48\,c_K)\,10^{-5}\ (\mu W/m^3) \quad (4)$$

where:

c = concentration in ppm for U and Th and in % for K,

ρ = density of the rock (kg/m^3)

μ = micro (10^{-6})

Most samples were analysed at the Institute Jožef Stefan in Ljubljana where the concentration of radioactive isotopes in Slovene rock samples has been determined with a gamma-ray spectrometer equipped with a Ge/Li detector (Ravnik et al., 1995). The remaining 11 samples were analysed at the Geophysical Institute in Bucharest with a gamma spectrometer equipped with a NaI (Ti) detector. All mentioned analyses have been done over the period 1982 to 1995. Knowledge of heat generation is necessary to understand the relationship between geological conditions and the thermal field in the crust.

Results of measurements of thermal properties of rocks and sediments from Slovenia

Thermal conductivity and thermal diffusivity of rocks and sediments

The present paper discusses the results on a total of 606 rock and sediment samples that have been measured since 1982. Of these, 430 were cored rock samples from 119 boreholes, 20 rock samples from two tunnels (17 from the Karavanke highway tunnel and 3 from the Malence highway tunnel SE of Ljubljana) and 156 rock and sediment samples from surface locations (among the latter also four samples from a depth of 1 m in very shallow holes). The rock samples were of different sizes, mostly with a minimum length of 12 or 14 cm (a strict condition for both line-source devices) and minimum thickness of 2 cm, but in most cases, the samples, especially cored samples, were longer (up to 60 cm) and thicker.

The first 35 surface samples and 4 samples from very shallow holes were measured by the line-source method (Appendix A), while the remaining 103 surface samples were measured by the optical scanning method (TCS meter) and 14 sediment samples by the needle probe method (KD2 Pro). Out of 450 samples from the boreholes and two tunnels, 61 samples (13.6 %) were measured by the optical method (TCS meter), 388 samples (86.2 %) were measured by the line-source method, using both meters (MTP-1, MTP-4), and one sample (0.2 %) by the needle probe method (KD2 Pro). The vast majority, 549 measured samples (90.6 %) were sedimentary rocks and sediments, while 23 samples were metamorphic rocks (3.8 %) and 34 samples were igneous rocks (5.6 %) (Fig. 9 and Table 2).

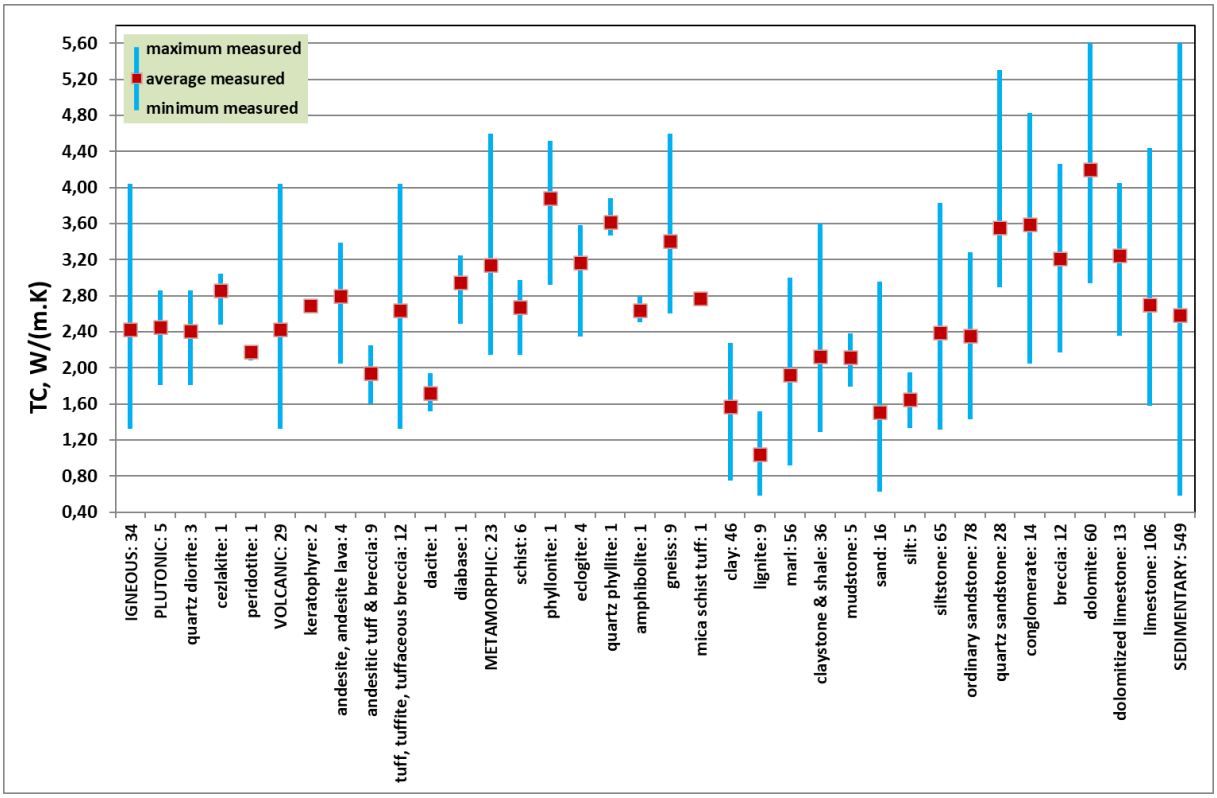

Fig. 9. Thermal conductivity (TC) of total 606 rock and sediment samples from the boreholes, two tunnels and numerous surface locations in Slovenia, with the number of samples by lithology and a total number of samples by main groups of rocks (status: March 2023); red points: mean values; the vertical lines show the range of measured TC values.

Table 2. Values of arithmetic mean TC with standard deviation and median TC of total 606 rock and sediment samples from Slovenia, grouped by lithology and main groups of rocks.

Lithology	No. of samples	Mean TC, W/(m·K)	s.d. TC, W/(m·K)	Me TC, W/(m·K)
Igneous rocks	**34**	**2.43**	**0.66**	**2.27**
Plutonic rocks	**5**	**2.45**	**0.46**	**2.56**
Quartz diorite (tonalite)	3	2.41	0.54	2.56
Cezlakite	1	2.86	/	2.86
Peridotite	1	2.18	/	2.18
Volcanic rocks	**29**	**2.43**	**0.69**	**2.25**
Keratophyre	2	2.69	0.04	2.69
Andesite, andesite lava	4	2.80	0.62	2.87
Andesitic tuff, andesitic breccia	9	1.94	0.22	1.89
Tuff, tuffite, tuffaceous breccia	12	2.64	0.83	2.52
Dacite	1	1.72	/	1.72
Diabase	1	2.95	/	2.95
Metamorphic rocks	**23**	**3.14**	**0.58**	**3.05**
Schist (green, amphibolitic, chloritic, etc.)	6	2.67	0.30	2.74
Phyllonite	1	3.88	/	3.88
Eclogite	4	3.17	0.56	3.36
Quartz phyllite	1	3.62	/	3.62
Amphibolite	1	2.64	/	2.64
Gneiss	9	3.41	0.59	3.31
Mica schist tuff	1	2.77	/	2.77
Sedimentary rocks	**549**	**2.57**	**0.49**	**2.53**
Clay, clay with impurities	46	1.57	0.38	1.57
Lignite, lignite with clay	9	1.04	0.37	0.97
Marl, marlstone with impurities	56	1.92	0.43	1.90
Claystone & shale, with impurities	36	2.13	0.74	1.89
Mudstone	5	2.12	0.26	2.15
Sand, sand with impurities	16	1.51	0.48	1.39
Silt, silt with impurities	5	1.65	0.48	1.68
Siltstone, siltstone with impurities	65	2.39	0.50	2.27
Sandstone (calcareous, marly, silty,...)	78	2.36	0.45	2.38
Quartz sandstone	28	3.56	0.56	3.46
Conglomerate (dolomitic, quartz)	14	3.59	0.88	3.59
Breccia (dolomitic, limestone)	12	3.21	0.70	3.21
Dolomite	60	4.20	0.60	4.11
Dolomitized limestone, limestone grading into dolomite	13	3.25	0.54	3.21
Limestone	106	2.70	0.39	2.68

Localities of the boreholes, two road tunnels and numerous points on the surface where the rock samples have been taken for the thermal conductivity measurements are shown in Figure 10. The boreholes are distributed according to the maximum depth in which the rock sample has been cored. In the GRETA project the rocks were sampled in the Municipality of Cerkno (Casasso et al., 2017, 2018) and in the GeoPLASMA-CE project in the Municipality of Ljubljana - MOL (Janža et al., 2017). Another project focused on geothermal potential assessment in the Municipality of Velenje (Janža et al., 2022). Other groups of rocks were sampled in two distinctive areas for the RockSense project (Jemec Auflič & Šegina, 2022; Rajver, 2022; Research project ARRS PROJEKT

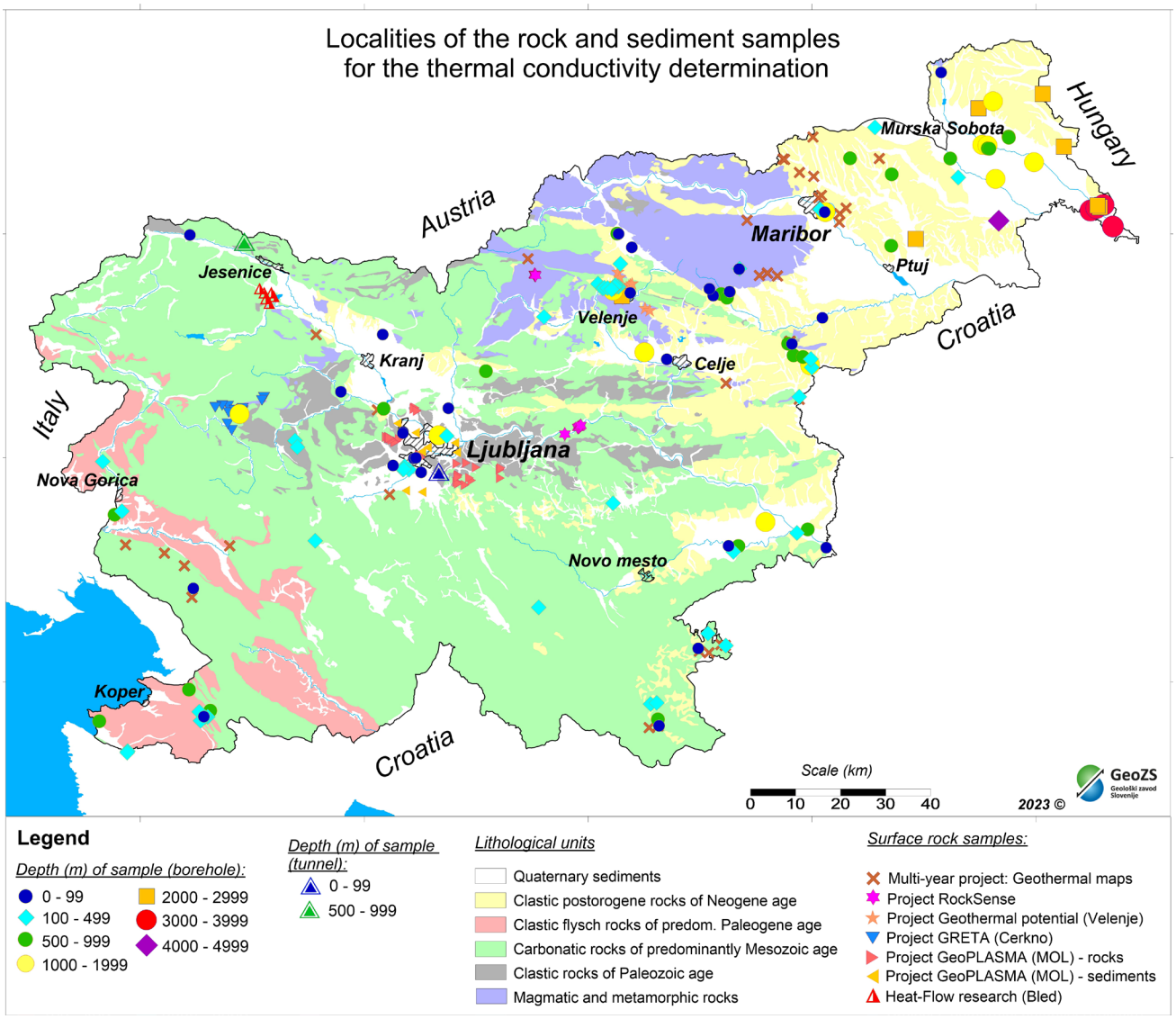

Fig. 10. Localities of the 119 boreholes, two road tunnels and numerous points on the surface where the rock samples have been taken for TC measurements. The boreholes are distributed according to maximum depth of the cored rock samples. The map of lithologic units is simplified after Bavec et al. (2013).

J1-3024) and for the heat flow research (Adrinek et al., 2019; Serianz, 2022). Many surface rocks were already sampled since 1983 for the multi-year project "Geothermal maps of Slovenia" (Ravnik & Rajver, 1990; Ravnik, 1988, 1991; Ravnik et al., 1995).

It should be emphasized that many rock samples and especially sediments, which were cored in boreholes, were brought to the laboratory with mostly preserved pore water content. They were properly wrapped, often even protected with paraffin. So, we took the measurements as soon as we unwrapped them from the protection. For these critical samples, especially samples of sand, sand with impurities, silt and also some sandstones, we characterized the condition of the sediment (and rock) as saturated, semi-dry or dry (Appendix A). It is worth noting that the mean TC values in Table 2 do not show all the diversity of sediments and rocks, for this it is recommended that the user looks at Appendix A and the corresponding graphs for individual rock and sediment types to get a sense that many things affected the larger range of measured TC values, for example, the state of the samples itself (saturated, semi-dry, dry) or whether they were crumbled, fissured and similar.

In the following graphs (Figs. 11–19), the values of measured TC on rock samples, including sediments (such as sand and clay), are shown against the depths of the coring of rocks from the boreholes and depths of sampling below the surface in two tunnels. Samples from numerous surface locations are included (drawn at a depth level of 0 m). In each graph, the arithmetic mean and median of all values together with a range of measured values is presented (Fig. 9, Table 2).

Details of the state of the rock samples and sediments during measurements are shown in Appendix A. It is important to emphasize that thermal diffusivity has only been measured since 2017, when the TCS meter was upgraded. Thermal diffusivity (TD) was measured on a total of 27 rock samples from eight boreholes and on 104 samples from surface locations (Appendix A).

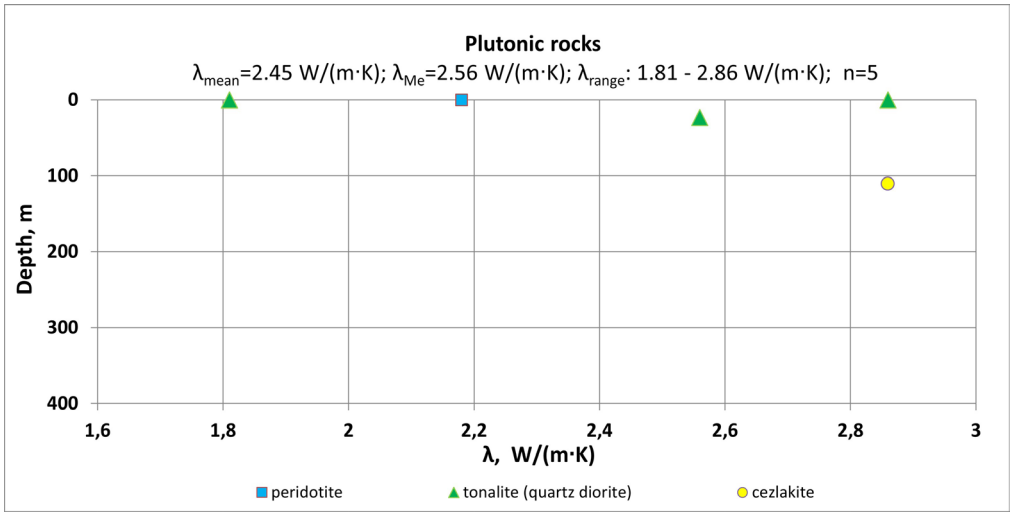

Fig. 11. Thermal conductivity of five samples of plutonic rocks.

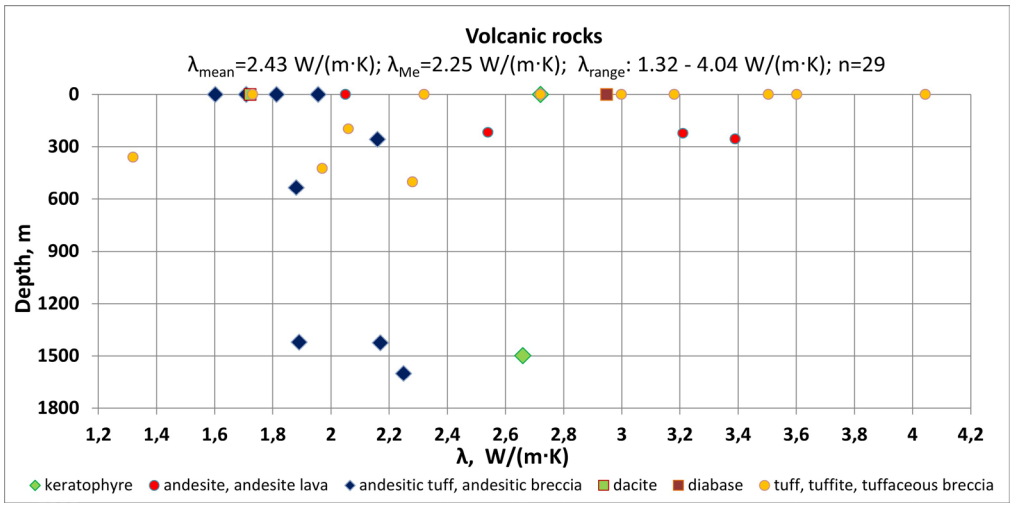

Fig. 12. Thermal conductivity of 29 samples of volcanic rocks.

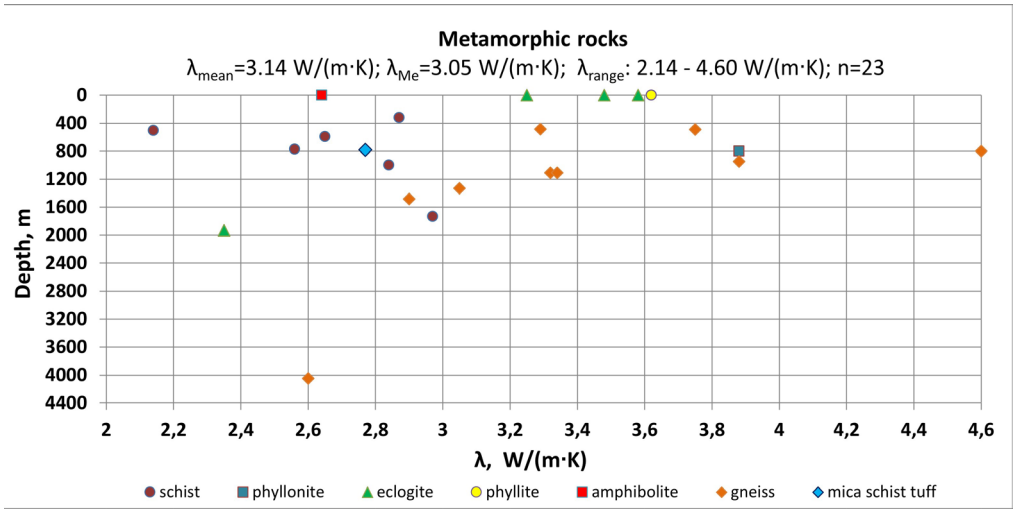

Fig. 13. Thermal conductivity of 23 samples of metamorphic rocks.

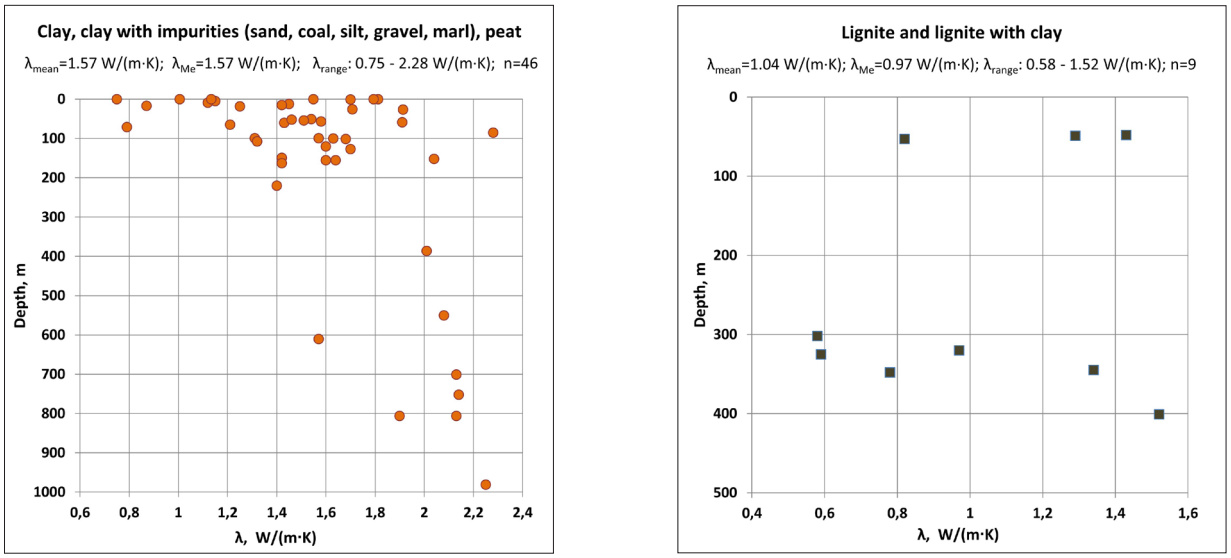

Fig. 14. TC of 46 samples of clay, clay with impurities and peat on the left and on the right TC of nine samples of lignite and lignite with clay.

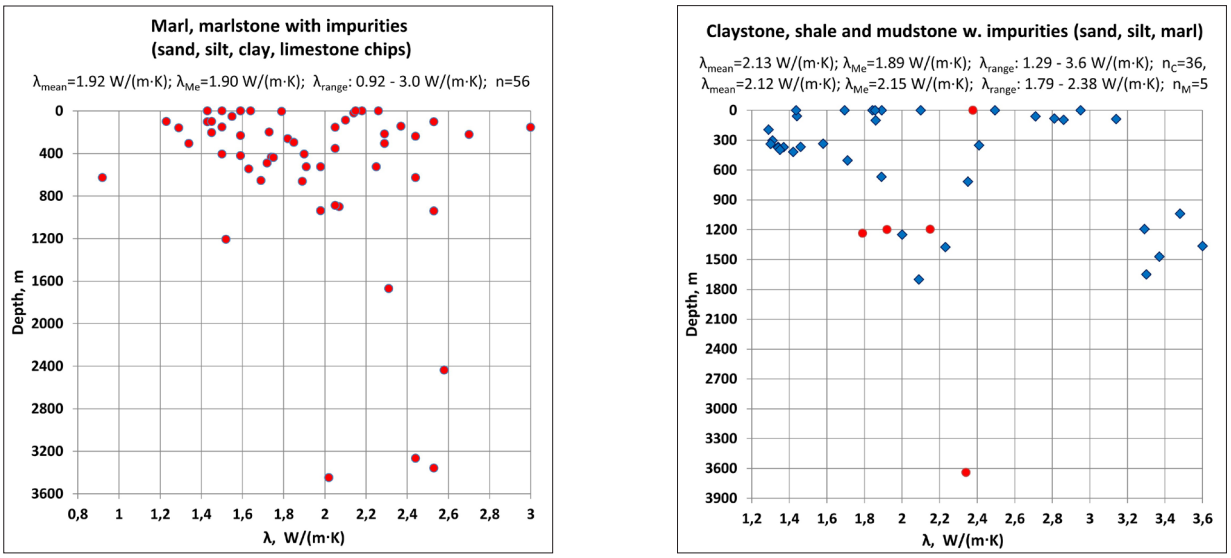

Fig. 15. TC of 56 samples of marl and marl with impurities on the left and on the right TC of 36 samples of claystone and shale (rombs) and five samples of mudstone (circles); some samples also include impurities.

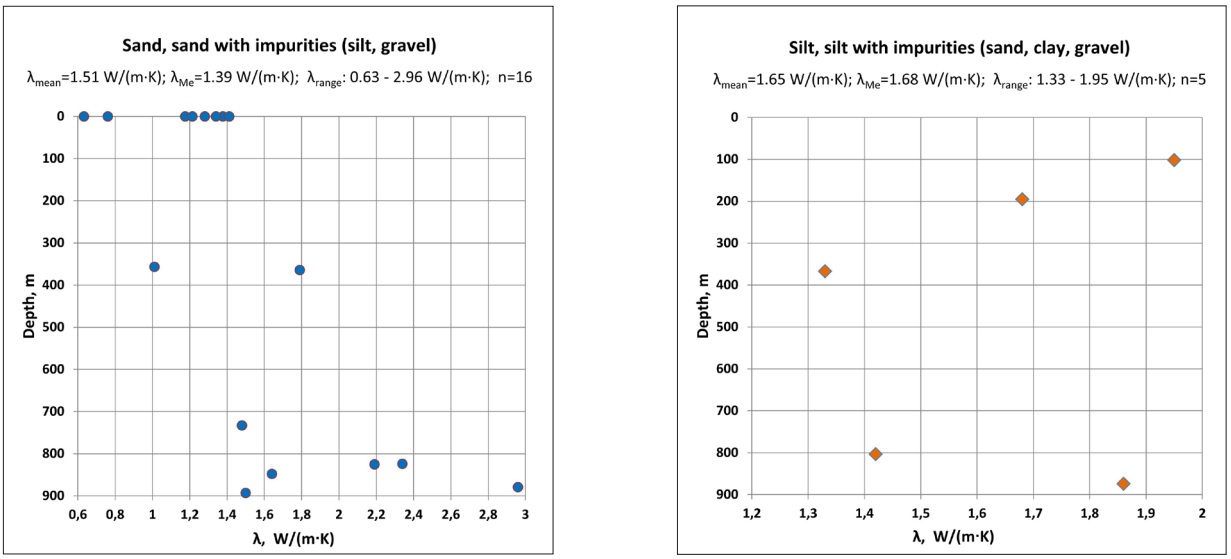

Fig. 16. TC of 16 samples of sand and sand with impurities on the left and on the right TC of five samples of silt and silt with impurities.

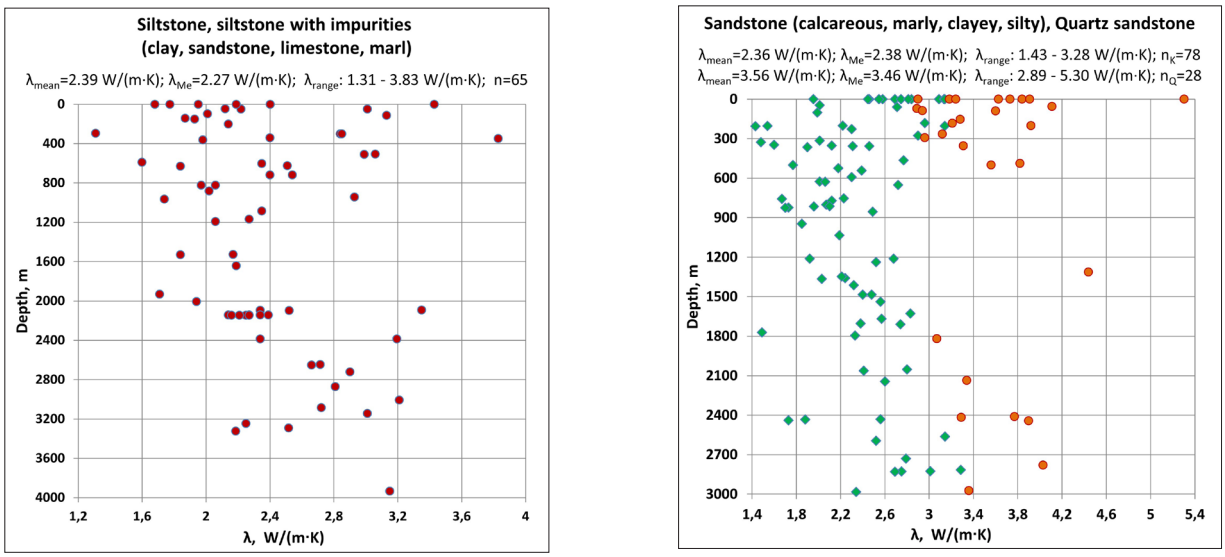

Fig. 17. TC of 65 samples of siltstone and siltstone with impurities on the left and on the right TC of 106 samples of sandstone; of them 78 samples are calcareous or marly, clay, silty sandstones (rombs), some of them with impurities, and 28 are quartz sandstones (circles).

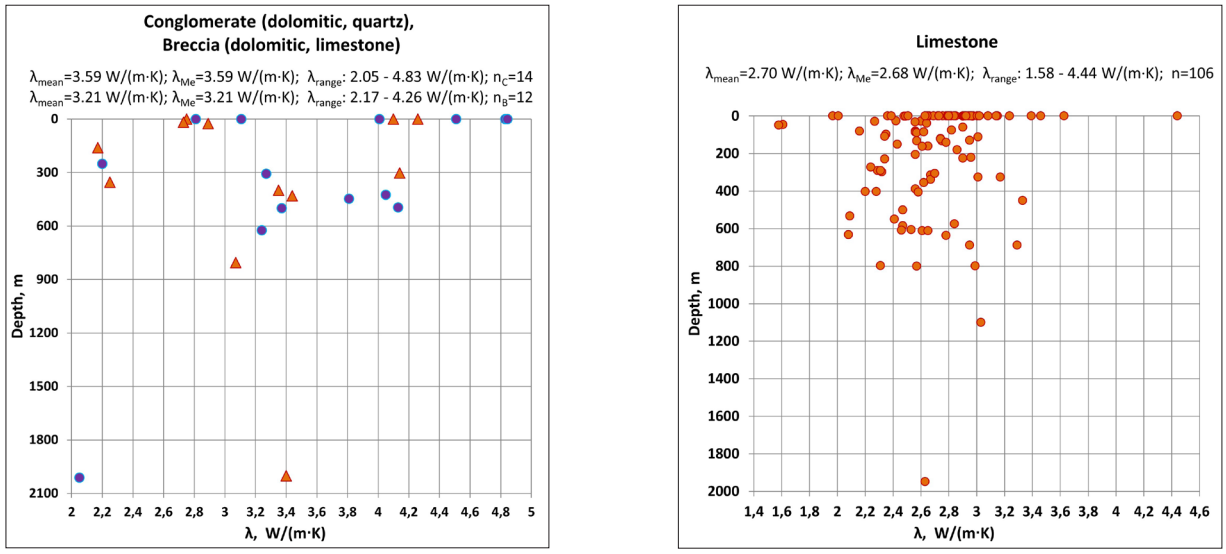

Fig. 18. TC of 14 samples of conglomerate (circles) and 12 samples of breccia (triangles), both of different compositions, on the left and on the right TC of 106 samples of limestone.

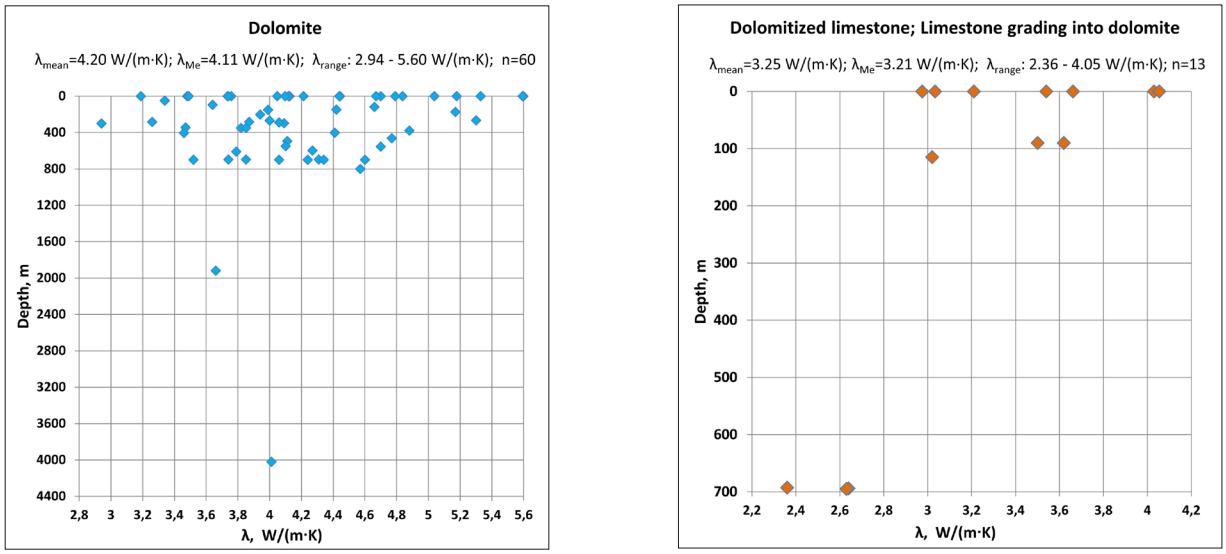

Fig. 19. TC of 60 samples of dolomite on the left and on the right TC of 13 samples of dolomitized limestone and limestone grading into dolomite.

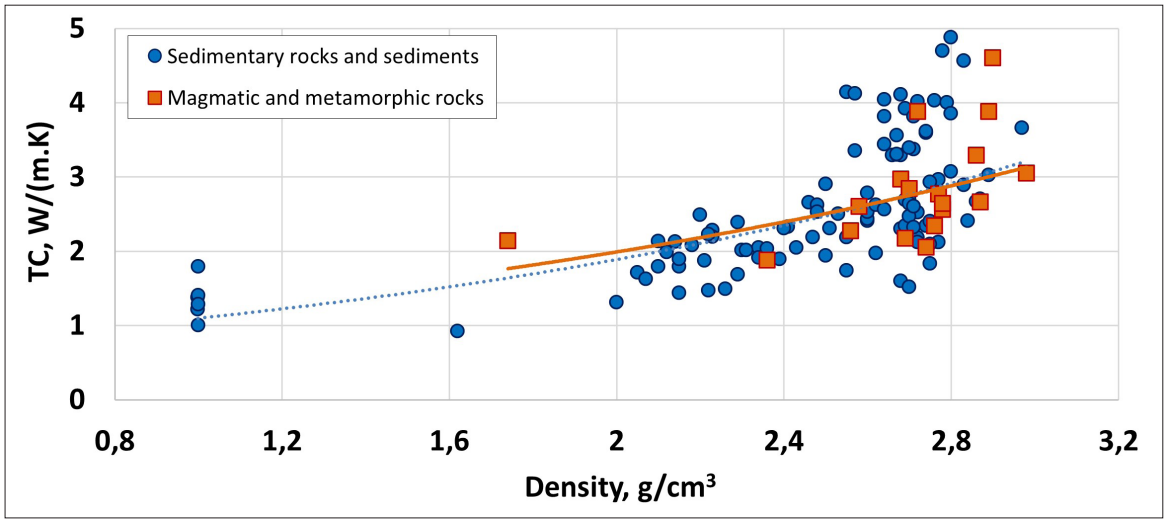

Fig. 20. Relation between TC and density for sedimentary rocks and sediments (blue) and for magmatic and metamorphic rocks (orange).

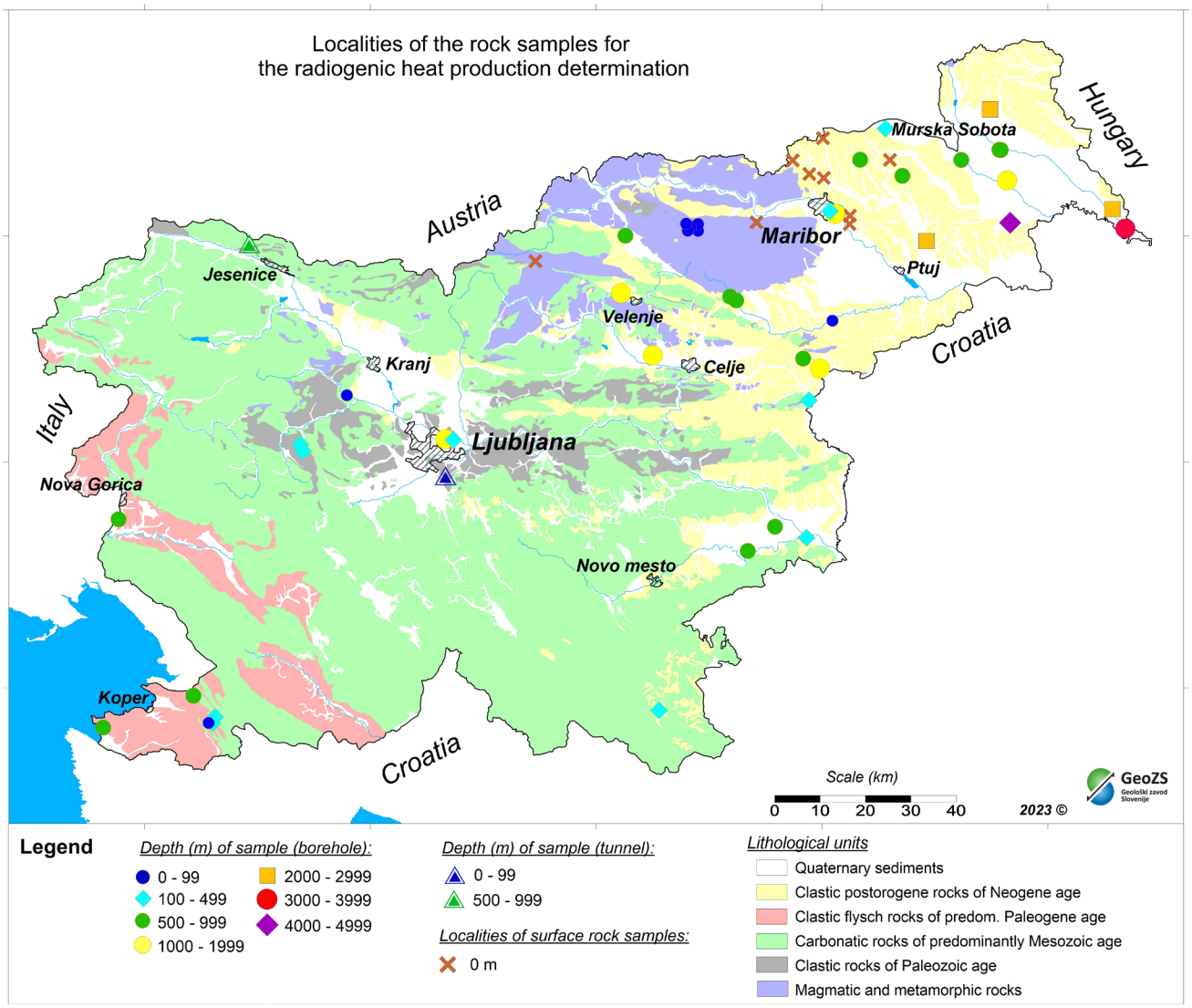

Fig. 21. Localities of the 39 boreholes, two road tunnels, 9 surface localities and 9 very shallow boreholes where the rock samples have been taken for radioactive heat production determination. Boreholes are distributed according to maximum depth of the cored rock samples, and both tunnels are distributed according to maximum depth of extracted rock below the surface (above the tunnel). From very shallow boreholes the samples were taken at a depth of 1 m, and only in one borehole from a depth of 5 m. The map of lithologic units is simplified after Bavec et al. (2013).

A relationship between measured density and TC is shown for 126 rock and sediment samples. Of these, 18 samples are igneous and metamorphic rocks, the rest are sedimentary rocks and sediments (Fig. 20). We found a good relationship between TC and density, with TC increasing with density. Both quartz and olivine play an important role in the relationship between TC and density. In the first case, TC usually decreases with density, and in the second case, TC increases, as already discussed by Pasquale et al. (2015). Also, there is a noticeable scatter in our results. The fact is that not all the samples (in Fig. 20) contain quartz, but only some igneous and metamorphic rocks as well as sandstones and conglomerates. Therefore, TC is not observed to decrease with density in the case of quartz-bearing rocks. At most, we observe that the trend is neutral if we exclude the chlorite carbonaceous schist (phyllite) sample with the lowest density (1.74) and quite low TC (2.14). We can only assume that the relationship is influenced by rock compaction, which is related to mineral composition, as many samples were taken from shallower or greater depths.

Radiogenic heat production of rocks in Slovenia

Localities of the boreholes, two road tunnels and points on the surface from where the rock samples have been taken for the radioactive heat production determinations are shown in Fig. 21. Altogether 144 rock samples were analysed for the concentrations of the mentioned radioisotopes, of them 112 samples from the 39 boreholes, 14 samples from both tunnels (13 from the Karavanke tunnel and 1 from the Malence tunnel SE of Ljubljana) and 18 samples from surface locations, nine of them from depths of 1 m in very shallow boreholes. Their density was first measured and then properly ground into small particles (appr. as small as silt).

In Appendix B, we also show the results of TC measurements of some rock samples (already listed in Appendix A under the same database numbers), which showed distinct layering (sandstone, siltstone, marl) and foliation (gneiss). With this, the effect of anisotropy in heat conduction was verified and, using the same equations as Jorand et al. (2013) have done for TC measured perpendicular and parallel to bedding or foliation, the anisotropy values for certain rock types were found roughly similar to those presented by Kappelmeyer & Haenel (1974) and Di Sipio et al. (2014).

Discussion

It is known that the physical properties of the rocks, such as porosity (e.g. water content), texture and homogeneity of the material, can be significantly modified by tectonic events acting on the territory together with the climate and environmental conditions, for example igneous rocks may be affected by different weathering conditions. All these facts can lead to more or less different TC values from those mentioned in the literature (Di Sipio et al., 2014). Therefore, we strive to create geological and geothermal models, in which the thermo-physical properties of the main lithologies are defined based on real data obtained through laboratory or in-situ measurements and, when necessary, supplemented with data from the literature and well-logging data (Norden et al., 2012). Most of the measured TC values are also accompanied by the standard deviation data, which is a good indicator of the quality of the measurement and how heterogeneous and/or tectonically broken the rock is.

Heat exchanger designers and planners in Slovenia most often use TC values from standard tables in the following standards (Prestor et al., 2020): the German standard VDI 4640 (VDI, 2001), the Swiss standard SIA (Eugster et al., 2010), the British standard MIS 3005 and the American ASHRAE standard. It is assumed that the latter two are less used in Slovenia. The comparison of the results of our measurements on rocks within the projects GRETA and GeoPLASMA with the TC values in four standards (UNI standard 2012 according to VDI 2001, SIA 384/6, MIS 3005 and ASHRAE) is given in the link (page 152 in Prestor et al., 2020). The range of measured TC values complies with those in the cited standards and also with results published in other literature (e.g. Kappelmeyer & Haenel, 1974; Zoth & Haenel, 1988; Beardsmore & Cull, 2001). Possible minor deviations between our results and other foreign values of TC are caused due to differences in mineral composition within the samples of the individual lithological types.

We believe that our results could form the basis for a possible future Slovenian standard for thermal properties of measured rocks and sediments, as they also cover some lithological types that are not presented in the existing foreign standards, but appear on the Slovenian territory, like dolomitized limestone, dacite, phyllonite and lignite. For several rock types our results are more constrained than the values in the mentioned standards, as they fall within a narrower range of TC values than reported in other sources.

The results of TC and TD measurements on 32 rock samples from the municipality of Cerkno (project GRETA) have already been presented by Casasso et al. (2017) with maps of shallow geothermal potential intended for the design of closed-loop HP systems with the BHEs. The rock types sampled were claystone and shale, siltstone, sandstone, quartz sandstone, quartz conglomerate, dolomite, dolomitized limestone, limestone, marl and marly limestone, tuff and diabase, all with an age from Carboniferous to Upper Triassic.

In the MOL area, rocks were sampled mainly in the western and eastern parts and on the Ljubljana castle hill (project GeoPLASMA). The rock types of a total of 47 representative measured samples were claystone and shale, siltstone, mudstone, sandstone, sandstone with siltstone and claystone, quartz sandstone, conglomerate, quartz conglomerate, limestone, Dachstein limestone (with grading into dolomite), marl (marly dolomite) and tuff, with ages ranging from Upper Carboniferous to Upper Cretaceous. In addition, in central and southern parts of the MOL, also *in situ* measurements were done using the needle probe method. The measured sediments of Quaternary age were clay with sand and silt, sand with gravel, gravel with sand, river sand, gravel with sand and silt, clay with silt, and peat. The results of all measurements on rocks and sediments from the MOL area have already been presented by Janža et al. (2017).

As part of geothermal heat flow research, six rock samples were measured from the Lake Bled area (Adrinek et al., 2019; Serianz, 2022), comprising the following rock types from Upper Permian to Ladinian age: limestone, massive dolomite, organogenic limestone, massive dolomite with oncoids and stromatolites, dolomite breccia, micritic limestone and marly limestone with mica. The collected outcrop samples were dried in an oven for 24h on 60°C before measuring. Later, the dried samples were saturated by submerging them in distilled water inside a sealed vacuum exsiccator. The values for thermal conductivity and diffusivity fall within the expected values for these rock types.

For the LIFE ClimatePath2050 project, an analysis of the potential of shallow geothermal energy in Slovenia until 2050 was performed. The final report (Prestor et al., 2018) shows two maps – the thermal conductivity and volumetric heat capacity of rocks and sediments on the surface of Slovenia. For the first map, however, it was necessary to upgrade data from laboratory results to lithological units. The TC values of rocks and sediments on the TC map were attributed on the basis of mean TC values obtained from measurements on many different rocks and sediments, mainly from boreholes (435 samples from 118 boreholes and 2 tunnels) and less from surface locations (35 samples). Thus, the mean TC values were used to create the TC map of Slovenia. For Quaternary, Neogene, and Paleogene sediments, different mean values for several different types of sediments were used, from Lower Paleocene to Quaternary in age. They were assigned from different surface locations and boreholes with a proper care as regard to the lithological formations. Therefore, the assigned TC values are not a mixture of different types of sediments. The TC values were assigned to the lithological units of the basic geological map of Slovenia at a scale of 1:100,000. The same basic geological map served as the basis for the second map, where the average values of the volumetric heat capacity of rocks and sediments were taken from two standards, SIA (Eugster et al., 2010) and VDI (2001).

The largest number of measured samples for TC is that of sedimentary rocks and sediments, followed by volcanic rocks, metamorphic and plutonic rocks (Fig. 9). The range of measured TC values for plutonic rocks (Fig. 11) is between 1.81 and 3.04, with a TC mean of 2.45 W/(m·K). Higher TC value is shown by plutonic rock of gabbro group (cezlakite). The range of measured TC values for volcanic rocks (Fig. 12) is between 1.32 and 4.04, with a TC mean of 2.43 W/(m·K). Some rock types show quite high range of values, with the highest TC values measured on andesite, tuff and tuffaceous breccia and diabase. The range of measured TC values for all metamorphic rocks (Fig. 13) is between 2.14 and 4.60, with a TC mean of 3.14 W/(m·K). The highest TC values are shown by phyllonite, some gneisses and phyllite. Among the gneiss samples is also one sampled until now in a deepest (4048 m) borehole LJUT-1/88 at its base.

As expected, the highest range of measured TC values is represented by sedimentary rocks and sediments, being between 0.58 and 5.60, with a TC mean of 2.58 W/(m·K). In the lower part of this range, there are sediments, such as clay and clay with impurities (Fig. 14), with a range of 0.75 to 2.28 and a mean TC of 1.57 W/(m·K), and lignite (Fig. 14) with a range of 0.58 to 1.52 and a TC mean of 1.04 W/(m·K). The samples of sand, when dry, also show low TC values, and in total the range of TC values for all sand samples, also sand with impurities (Fig. 16) is between 0.63 and 2.96, with a mean TC of 1.51 W/(m·K). The samples of marl and marlstone (Fig. 15) were quite numerous (56 in number), showing the range of values

between 0.92 and 3.00, with a TC mean of 1.92 W/(m·K). The samples of claystone and shale (Fig. 15) present higher range of TC values, 1.29 to 3.6 W/(m·K), with a mean TC of 2.13 W/(m·K), while the mudstone samples (Fig. 15) show the range between 1.79 and 2.38, with almost the same mean TC of 2.12 W/(m·K). Only five samples of silt (Fig. 16) were measured, showing the range of 1.33 to 1.95, with a mean TC of 1.65 W/(m·K). The samples of siltstone and siltstone with impurities (Fig. 17) were also numerous (65 in number), their TC range is between 1.31 and 3.83, with a mean TC of 2.39 W/(m·K). The range of measured TC values on numerous sandstone samples (Fig. 17) is visibly different for calcareous, marly, clayey and silty sandstones (78 in number) on one side and for quartz sandstones (28 in number) on the other side. For the first ones it is between 1.43 and 3.28 W/(m·K), with a mean TC of 2.36 W/(m·K), while for the quartz sandstone it is between 2.89 and 5.30, with a mean TC of 3.56 W/(m·K). The range of measured TC values for the samples of conglomerate and breccia (Fig. 18) is not so much different. For the conglomerate samples (14 in number) it is between 2.05 and 4.83, with a mean TC of 3.59 W/(m·K), and for the breccia samples (12 in number) it is between 2.17 and 4.26, with a mean TC of 3.21 W/(m·K). The range of measured TC values for the numerous samples of limestone (106 in number, Fig. 18) is between 1.58 and 4.44, with a mean TC value of 2.70 W/(m·K). Samples of dolomite (Fig. 19) were also numerous (60 in number) with a sample from the second greatest depth (4020 m) in the country. Their range of TC values is between 2.94 and 5.60, with a mean TC of 4.20 W/(m·K). Lastly, the range of measured TC values for the samples of dolomitized dolomite and limestone grading into dolomite (Fig. 19) is from 2.36 to 4.05, with a mean TC of 3.25 W/(m·K).

The range for measured thermal diffusivity of rocks and sediments varies between 0.22 mm^2/s for peat with organic clay and 0.42 mm^2/s for clayey sediment of Quaternary (Holocene) age on low side and 2.31 mm^2/s and 3.62 mm^2/s for quartz sandstone of Ladinian and Upper Carboniferous age, respectively, on high side.

The range for determined radiogenic heat generation in the rocks varies between 0.26 $\mu W/m^3$ for milonitized dolomite of Triassic age to 7.09 $\mu W/m^3$ for dark grey sandstone with black shale clasts of Middle Permian age. The latter rock sample was cored in the borehole V-931/88 in the Uranium mine Žirovski vrh (database number 37 in Appendix A), where the production of uranium ore was closed in 1992. The density of the rock was also measured for all those rock samples on which radiogenic heat generation was determined (Ravnik et al., 1995). For one group of surface rock samples with determined radiogenic heat, their density was not measured but only assumed. The measured rock densities vary from as low as 1.651 g/cm^3 for silty marl of Lower Badenian or Karpathian age to 3.042 g/cm^3 for granat-muscovite-biotite gneiss of Precambrian age.

Conclusions

With the presented measurement results on rock and sediment samples from Slovenia, we have presumably covered more than 90 % of all lithological types that occur on the surface of the country. The question is, what other lithological types would be encountered at depths of up to 4 or 5 km, if such boreholes were made in certain areas of Slovenia, especially in areas with metamorphic and igneous rocks, not only as surface rocks but also in the subsurface. For example, thermal conductivity has not yet been measured on any of the following interesting rock types, most of which occur very locally on the surface in Slovenia: poorly metamorphosed slate, quartzite, calc-phyllite, calc-schist, granite gneiss, serpentinite, granite, rhyolite, rhyodacite, syenite and granodiorite.

Nowadays, various users of data on the thermal parameters of rocks and sediments rely on data from the literature. However, direct measurement of thermal parameters on representative samples for a certain territory is necessary to provide real data to energy and infrastructure planners, public authorities and operators involved in the exploitation of geothermal energy resources in low, medium and high enthalpies (Di Sipio et al., 2014). Although it is known that the thermal response test (TRT) is the most reliable method for determining in-situ thermal properties in the shallow underground, as it also includes local hydrogeological conditions and physical parameters of the specific lithological units, it is expensive and time-consuming. Therefore, it is advisable to perform it in cases where large scale closed-loop systems are planned (e.g. more than 10 BHEs), and the use of literature data is sufficient when small scale closed-loop system are planned (individual houses). A good alternative to the field method are precise laboratory measurements, which could be used on a regional scale to provide necessary information for the dimensioning of closed-loop systems with the heat pumps and to better predict the geothermal conditions for the planning of deep boreholes.

We are confident that the thermal property results of Slovenian rocks and sediments are within the expected range for each lithological type, which is confirmed by literature data, thus highlighting the quality of our methodology and measurements. We believe that by presenting the results of TC and TD measurements in a manner as they are in Appendix A, the requirements of the IHFC Global Heat Flow Database Renovation Group (Fuchs et al., 2021) are satisfied also for the compilation and collection of metadata. Our results could be the basis for the possible future Slovenian standard of thermal properties of measured rocks and sediments.

Acknowledgements

The authors are grateful to dr. L. Z. Lenkey and dr. N. Rman for their very appropriate and constructive suggestions, and for improvements in text clarity. This research was partly funded by the Slovenian Research Agency through programme groups "Regional geology P1-0011" and "Groundwater and geochemistry P1-0020". The authors are also grateful for discussions with several scientists at the Geological Survey of Slovenia (Kristina Ivančič, Mateja Jemec Auflič, Jernej Jež, Polona Kralj, Matevž Novak) as well as for their participation in the surface rock sampling.

Appendix A and B: Supplementary data associated with this article can be found in the online version at https://doi.org/10.5474/geologija.2023.005

References

Adrinek, S., Janža, M., Rajver, D. & Brenčič, M. 2019: Thermal conductivity and diffusivity of geological units around Lake Bled, NW Slovenia. In: 10th European Geothermal PhD Day, 25–27 Feb. 2019, Potsdam: poster.

Banks, D. 2008: An introduction to thermogeology. Ground source heating and cooling. 1st ed. Blackwell Publ. Ltd, Oxford: 339 p.

Bavec, M., Novak, M. & Poljak, M. 2013: Geological Map of Slovenia 1:1 million. GeoZS, Ljubljana.

Beardsmore, G.R. & Cull, J.P. 2001: Crustal heat flow: A guide to measurement and modelling. Cambridge University Press, Cambridge: 324 p.

Beck, A.E. 1957: A steady state method for the rapid measurement of the thermal conductivity of rocks. J. Sci. Instr., 34: 185–189.

Beck, A.E. 1965: Techniques of measuring heat flow on land. In: Lee, W.H.K. (ed.): Terrestrial heat flow. Monograph No. 8, Am. Geophys. Union, Washington D.C.: 24–57.

Beck, A.E. 1988: Thermal properties. Methods for determining thermal conductivity and thermal diffusivity. In: Haenel, R., Rybach, L. & Stegena, L. (eds.): Handbook of terrestrial heat-flow density determination. Kluwer Academic Publishers: Dordrecht: 87-124.

Benfield, A.E. 1939: Terrestrial heat flow in Great Britain. Proc. Roy. Soc., A 173: 428–450. https://doi.org/10.1098/rspa.1939.0157

Birch, F. 1942: Thermal conductivity and diffusivity. In: Birch, F., Schairer, J.F. & Spicer, G.C. (eds.): Handbook of physical constants. Special paper 36, Geol. Soc. of America, Baltimore: 243–266.

Birch, F. & Clark, H. 1940: The thermal conductivity of rocks and its dependence upon temperature and composition. Am. J. Sci., 238/8: 529–558. https://doi.org/10.2475/ajs.238.8.529

Blackwell, D.D. & Steele, J.L. 1989: Thermal conductivity of sedimentary rocks: Measurement and significance. In: Naeser, N.D. & McCulloh, T.H. (eds.): Thermal history of sedimentary basins. Methods and case histories. Springer-Verlag, Berlin: 13–36.

Blumm, J. & Lemarchand, S. 2002: Influence of test conditions on the accuracy of laser flash measurements. High Temp.-High Pres., 34/5: 523–528. https://doi.org/10.1068/htjr062

Brigaud, F., Chapman, D.S. & Le Douran, S. 1990: Estimating thermal conductivity in sedimentary basins using lithologic data and geophysical well logs. AAPG Bulletin, 74/9: 1459–1477.

Buntebarth, G. 1984: Geothermics. An Introduction. Springer-Verlag, Berlin: 144 p.

Carmichael, R.S. (ed.) 1984: CRC Handbook of physical properties of rocks III, CRC Press, Boca Raton, FL: 354 p.

Carslaw, H.S. & Jaeger, J.C. 1959: Conduction of heat in solids. Clarendon Press, Oxford: 517 p.

Casasso, A., Prestor, J., Zosseder, K., Capodaglio, P., Bottig, M., Maragna, C., Zambelli, P., Huggenberger, P. et al. 2018. Local-scale maps of the NSGE potential in the case study areas. GRETA project Deliverable D4.2.1., Interreg Alpine Space: 137 p.

Casasso, A., Pestotnik, S., Rajver, D., Jež, J., Prestor, J. & Sethi, R. 2017: Assessment and mapping of the closed-loop shallow geothermal potential in Cerkno (Slovenia). Energy Procedia, 125: 335–344. https://doi.org/10.1016/j.egypro.2017.08.210

Čermák, V. & Rybach, L. 1982: Thermal conductivity and specific heat of minerals and rocks.

In: Angenheister, G. (ed.): Landolt-Börnstein: Numerical data and functional relationships in science and technology. New series, V(1a), Springer, Berlin: 305–343.

Čermák, V., Krešl, M., Šafanda, J., Nápoles-Pruna, M., Tenreyro-Perez, R., Torres-Paz, L.M. & Valdés, J.J. 1984: First heat flow density assessments in Cuba. Tectonophysics, 103: 283–296, https://doi.org/10.1016/0040-1951(84)90090-8

Čermák, V., Bodri, L., Krešl, M., Dédeček, P. & Šafanda, J. 2016: Eleven years of ground–air temperature tracking over different land cover types. Int. J. Climatology, 37/2: 1084–1099. https://doi.org/10.1002/joc.4764

Clark Jr., S.P. 1966: Thermal conductivity. In: Clark Jr., S.P. (ed.): Handbook of physical constants. Memoir 97, Geol. Soc. of America, New York: 459–482.

Clauser, C. & Huenges, E. 1995: Thermal conductivity of rocks and minerals. In: Ahrens, T.J. (ed.): Rock physics and phase relations - A handbook of physical constants. AGU reference shelf 3, Amer. Geophys. Union, Washington D.C.: 105–126.

Clauser, C. 2006: Geothermal energy. In: Heinloth, K. (ed.): Landolt-Börnstein, Group VIII: Advanced Materials and Technology, 3: Energy Technologies, subvol. C Renewable Energies, Springer Verlag, Heidelberg-Berlin: 493–604.

Clauser, C. 2011: Thermal storage and transport properties of rocks, II: Thermal conductivity and diffusivity. In: Gupta, H. (ed.): Encyclopedia of Solid Earth Geophysics, 2nd ed., Springer, Dordrecht, preprint: 31 p. https://doi.org/10.1007/978-90-481-8702-7_67

Cull, J.P. 1974: Thermal conductivity probes for rapid measurements in rock. J. Phys. E.: Sci. Instrum., 7: 771. https://doi.org/10.1088/0022-3735/7/9/026

Dalla Santa, G., Galgaro, A., Sassi, R., Cultrera, M., Scotton, P., Mueller, J., Bertermann, D., Mendrinos, D., Pasquali, R., Perego, R., Pera, S., Di Sipio, E., Cassiani, G., De Carli, M. & Bernardi, A. 2020: An updated ground thermal properties database for GSHP applications. Geothermics, 85: 1–13, https://doi.org/10.1016/j.geothermics.2019.101758

Davis, E.E. 1988: Oceanic heat-flow density. In: Haenel, R., Rybach, L. & Stegena, L. (eds.): Handbook of terrestrial heat-flow density determination. Kluwer Academic Publishers, Dordrecht, Boston, London: 223–260.

Davis, M.G., Chapman, D.S., Van Wagoner, T.M. & Armstrong, P.A. 2007: Thermal conductivity anisotropy of metasedimentary and igneous rocks. J. Geophys. Res.: Solid Earth, 112 (B05216): 1–7. https://doi.org/10.1029/2006JB004755

Decagon Devices, Inc. 2016: KD2 Pro Thermal Properties Analyzer. Operator's Manual. Decagon Devices, Inc., Pullman WA99163: 67 p.

Dédeček, P., Šafanda, J. & Rajver, D. 2012: Detection and quantification of local anthropogenic and regional climatic transient signals in temperature logs from Czechia and Slovenia. Climatic Change, 113: 787–801. https://doi.org/10.1007/s10584-011-0373-5

Desai, P.D., Navarro, D.A., Hasan, S.E., Ho, C.Y., DeWitt, D.P. & West, T.R. 1974: Thermophysical properties of selected rocks. CINDAS report 23, Center for Information and Numerical Data Analysis and Synthesis (CINDAS), Purdue Univ., West Lafayette, IN.

DeVries, D.A. & Peck, A.J. 1958: On the cylindrical probe method of measuring thermal conductivity with special reference to soils. 1. Extension of theory and discussion of probe characteristics. Australian Journal of Physics, 11: 255–271. http://hdl.handle.net/102.100.100/334002?index=1

Dickson, M.H. & Fanelli, M. 2004: What is geothermal energy? International Geothermal Association, Bochum: 47 p. http://iga.igg.cnr.it/geo/geoenergy.php

Diment, W.H. & Pratt, H.R. 1988: Thermal conductivity of some rocks-forming minerals: A tabulation. Open file report 88–690, U.S. Geol. Survey, Denver, CO.

Di Sipio, E., Galgaro, A., Destro, E., Teza, G., Chiesa, S., Giaretta, A. & Manzella, A. 2014: Subsurface thermal conductivity assessment in Calabria (southern Italy): a regional case study. Environ. Earth Sci., 72: 1383-1401. https://doi.org/10.1007/s12665-014-3277-7

Dorofeeva, R.P. 1998: Thermal conductivity of bottom sediments measured in deep water boreholes in Lake Baikal. In: Popov, Y.A. & Pimenov, V. (eds.): Proc. Intl. Conference "The Earth's thermal field and related research methods", May 19-21, 1998, Moscow, Russia.

Dorofeeva, R.P. & Duchkov, A.D. 1995: A new geothermal study in underwater boreholes on Lake Baikal (Continental Rift Zone). In: Barbier, E., Frye, G., Iglesias, E. & Palmason, G. (eds.): Proc. World Geothermal Congress 1995, Florence, Italy.

Dövényi, P. & Horváth, F. 1988: A review of temperature, thermal conductivity and heat flow data for the Pannonian basin. In: Royden, L.H.

& Horváth, F.: The Pannonian basin. AAPG Memoir 45, 195–210, Tulsa.

Drury, M.J., Allen, V.S. & Jessop, A.M. 1984: The measurement of thermal diffusivity of rock cores. Tectonophysics, 103: 321–333. https://doi.org/10.1016/0040-1951(84)90094-5

Eugster, W., Pahud, D., Rohner, E. & Signorelli, S. 2010: Sondes géothermiques. SIA 384/6:2010 Bâtiment, génie civil. Norme suisse SN 546 384/6. Valable dès 2010-01-01. Société suisse des ingénieurs et des architectes, CH-8027 Zurich: 76 p.

Fuchs, S. & Förster, A. 2010: Rock thermal conductivity of Mesozoic geothermal aquifers in the Northeast German Basin. Chem. Erde Geochem., 70: 13–22, https://doi.org/10.1016/j.chemer.2010.05.010

Fuchs, S., Beardsmore, G., Chiozzi, P., Espinoza-Ojeda, O.M., Gola, G., Gosnold, W., Harris, R., Jennings, S., Liu, S., Negrete-Aranda, R., Neumann, F., Norden, B., Poort, J., Rajver, D., Ray, L., Richards, M., Smith, J., Tanaka, A. & Verdoya, M. 2021: A new database structure for the IHFC Global Heat Flow Database. Int. J. Terr. Heat Flow Appl. Geotherm. (IJTHFA), 4/1: 1–14. https://doi.org/10.31214/ijthfa.v4i1.62

Fujisawa, H., Nagao, T., Uyeda, S., Honda, S. & Tsunoda, T. 1985: Heat flow measurements in Lake Biwa, Central Japan. A preliminary study. Proc. Japan Academy, V.61, Ser.B, N 4, 145-148.

Gable, R. 1986: Température, gradient et flux de chaleur terrestre. Mesures. Interprétation. Thèse présentée à l'Université Pierre et Marie Curie. Documents du B.R.G.M. No. 104: 187 p.

Galson, D.A., Wilson, N.P., Schaerli, U. & Rybach, L. 1987: A comparison of the divided-bar and QTM methods of measuring thermal conductivity. Geothermics, 16/3: 215–226. https://doi.org/10.1016/0375-6505(87)90001-0

Gomes, J.L.S., Vieira, F.P. & Hamza, V.M. 2021: Reappraisal of heat flow variations in mainland Africa. Int. J. Terr. Heat Flow Appl. Geotherm. (IJTHFA), 4/1: 26-78. https://doi.org/10.31214/ijthfa.v4i1.64

Goutorbe, B., Lucazeau, F. & Bonneville, A. 2006. Using neural networks to predict thermal conductivity from geophysical well logs. Geophys. J. Int., 166(1): 115–125. https://doi.org/10.1111/j.1365-246X.2006.02924.x

Haenel, R. 1979: A critical review of heat flow measurements in sea and lake bottom sediments. In: Čermák, V. & Rybach, L. (eds.): Terrestrial heat flow in Europe, Berlin: 49–73.

Haenel, R., Rybach, L. & Stegena, L. 1988: Fundamentals of geothermics. In: Haenel, R., Rybach, L. & Stegena, L. (eds.): Handbook of terrestrial heat-flow density determination. Kluwer Academic Publishers, Dordrecht: 9–57.

Hamza, V., Vieira, F., Gomes, J., Guimaraes, S., Alexandrino, C. & Gomes, A. 2020: Update of Brazilian heat flow data, within the framework of a multiprong referencing system. Int. J. Terr. Heat Flow Appl. Geotherm. (IJTHFA), 3/1: 45–72. https://doi.org/10.31214/ijthfa.v3i1.42

Hanley, E.J., DeWitt, D.P. & Roy, R.F. 1978: The thermal diffusivity of eight well-characterized rocks for the temperature range 300–1000 K. Engineering Geol., 12: 31–47. https://doi.org/10.1016/0013-7952(78)90003-0

Hartmann, A., Rath, V. & Clauser, C. 2005: Thermal conductivity from core and well log data. Int. J. Rock Mech. Min. Sci., 42: 1042–1055. https://doi.org/10.1016/j.ijrmms.2005.05.015

Horai, K. 1971: Thermal conductivity of rock-forming minerals. J. Geophys. Res., 76/5: 1278–1308. https://doi.org/10.1029/JB076i005p01278

Horai, K. 1991: Thermal conductivity of Hawaiian basalt: A new interpretation of Robertson and Peck's data. J. Geophys. Res.: Solid Earth, 96 (B3): 4125–4132. https://doi.org/10.1029/90JB02452

Horai, K. & Simmons, G. 1969. Thermal conductivity of rock-forming minerals, Earth Planet. Sci. Lett., 6/5: 359–368. https://doi.org/10.1016/0012-821X(69)90186-1

Hurtig, E., Čermák, V., Haenel, R. & Zui, V. (eds.) 1992: Geothermal Atlas of Europe. GeoForschungsZentrum Potsdam, Publ. No 1: 156 p., 25 maps.

Janža, M., Lapanje, A., Šram, D., Rajver, D. & Novak, M. 2017: Research of the geological and geothermal conditions for the assessment of the shallow geothermal potential in the area of Ljubljana, Slovenia. Geologija, 60/2: 309–327. https://doi.org/10.5474/geologija.2017.022

Janža, M., Jež, J., Rajver, D., Milanič, B., Markič, M., Atanackov, J., Mencin Gale, E., Ivančič, K., Uršič Arko, A., Lapanje, A., Adrinek, S. & Peternel Rikanovič, R. 2022: Ocena geotermalnega potenciala na območju Mestne občine Velenje = Assessment of the geothermal potential in the area of the Municipality of Velenje. Final report for the Municipality of Velenje. Geological Survey of Slovenia, Ljubljana: 28 p. (in Slovene).

Jemec Auflič, M. & Šegina, E. 2022: Study of rockfall activity in the Alpine and Pre-Alpine environment outside permafrost areas. In: MGM

22 & AK Permafrost 22, Nov. 24.-27. 2022, Kaprun, Austria. Kaprun: [Org. Comm.], 51–52.

Jessop, A.M. 1990: Thermal geophysics. Developments in Solid Earth Geophysics 17, Elsevier, Amsterdam: 306 p.

Jorand, R., Vogt, C., Marquart, G. & Clauser, C. 2013: Effective thermal conductivity of heterogeneous rocks from laboratory experiments and numerical modelling. J. Geophys. Res.: Solid Earth, 118/10: 5225–5235. https://doi.org/10.1002/jgrb.50373

Kalinin, A.N. 1981: An instrument for direct measurements of thermal conductivity on solid samples of arbitrary shape. Promyshlennaya Teplotekhnika, 3/1: 48–53 (in Russian).

Kappelmeyer, O. 1979: Implications of heat flow studies for geothermal energy prospects. In: Čermák, V. & Rybach, L. (eds.): Terrestrial heat flow in Europe. Springer-Verlag, Berlin etc.: 126–135. https://doi.org/10.1007/978-3-642-95357-6_11

Kappelmeyer, O. & Haenel, R. 1974: Geothermics with special reference to application. Gebrüder Borntraeger, Berlin, Stuttgart: 238 p.

Kobolev, V.P., Kutas, R.I. & Popov, Y.A. 1990: Method and results of research of thermal properties of Ural region rocks with laser scanning. Geophysical J., 12/4: 29–37 (in Ukrainian).

Lyubimova, E.A. 1968: Termika Zemli i Luny (Thermal conditions of the Earth and Moon). Nauka Press, Moscow: 278 p. https://doi.org/10.1594/pangaea.809800

Lyubimova, E.A. & Popova, A.K. 1967: Measurement of thermal conductivity of Lake Baikal sediments by a ball probe method. Izv. Earth Sci., 5: 71–74; English transl., Am. Geophys. Union 5: 309–311.

Lyubimova, E.A., Lusova, L.M., Firsov, F.V., Starikova, G.N. & Shushpanov, A.P. 1961: Determination of surface heat flow in Mazesta (USSR), Ann. Geophys., 14: 157–167.

Majorowicz, J.A. & Jessop, A.M. 1981: Regional heat flow patterns in the Western Canadian sedimentary basin. Tectonophysics, 74: 109–238. https://doi.org/10.1016/0040-1951(81)90191-8

Marx, H.-W., 2014: Thermal diffusivity and conductivity – an introduction to theory and practice. Thermal Analysis & Thermophysical Properties. Linseis Messgeräte GmbH WoTS_2-10-2014. Utrecht: 29 p.

Mongelli, F. 1968: Un metodo per la determinazione in laboratorio della conducibilità termica delle rocce. Boll. Geof. Teor. Appl. X: 51–58.

Mottaghy, D.C., Schellschmidt, R., Popov, Y.A., Clauser, C., Kukkonen, I.T., Nover, G., Milanovsky, S. & Romushkevich, R.A. 2005: New heat flow data from the immediate vicinity of the Kola superdeep borehole: vertical variation in heat flow density confirmed and attributed to advection. Tectonophysics, 401/1–2: 112–142. https://doi.org/10.1016/j.tecto.2005.03.005

Muffler, L.J.P. & Cataldi, R. 1978: Methods for regional assessment of geothermal resources. Geothermics, 7/2–4: 53–89. https://doi.org/10.1016/0375-6505(78)90002-0

Norden, B., Förster, A., Behrends, K., Krause, K., Stecken, L., Meyer, R. 2012: Geological 3-D model of the larger Altensalzwedel area, Germany, for temperature prognosis and reservoir simulation. Environ. Earth Sci., 67/2: 511–526. https://doi.org/10.1007/s12665-012-1709-9

Palacios, A., Cong, L., Navarro, M.E., Ding, Y. & Barreneche, C. 2019: Thermal conductivity measurement techniques for characterizing thermal energy storage materials – A review. Renewable Sustainable Energy Reviews, 108: 32–52. https://doi.org/10.1016/j.rser.2019.03.020

Pandey, O.P. 1991: Terrestrial heat flow and lithospheric geothermal structure in New Zealand. In: Čermák, V. & Rybach, L. (eds.): Terrestrial heat flow and the lithosphere structure. Springer-Verlag, Berlin etc.: 338–380.

Parker, W.J., Jenkins, R.J., Butler, C.P. & Abbott, G.I. 1961: Flash method of determining thermal diffusivity, heat capacity, and thermal conductivity. J. Appl. Phys., 32/9: 1679–1684. https://doi.org/10.1063/1.1728417

Pasquale, V., Gola, G., Chiozzi, P. & Verdoya, M. 2011: Thermophysical properties of the Po Basin rocks. Geophys. J. Int., 186/1: 69–8. https://doi.org/10.1111/j.1365-246X.2011.05040.x

Pasquale, V., Verdoya, M. & Chiozzi, P. 2015: Measurements of rock thermal conductivity with a Transient Divided Bar. Geothermics, 53: 183–189. https://doi.org/10.1016/j.geothermics.2014.05.008

Pollack, H.N. & Sass, J.H. 1988: 8. Crust and mantle geothermics 8.1. Thermal regime of the lithosphere. In: Haenel, R., Rybach, L. & Stegena, L. (eds.): Handbook of terrestrial heat-flow density determination. Kluwer Academic Publishers, Dordrecht: 301–308.

Popov, Y. 1983: Theoretical models of the method of determination of the thermal properties of rocks on the basis of moveable sources. Geologiya i Razvedka (Geology and Prospecting), p(I): 97-103.

Popov, Y. A., Semionov, V. G., Korosteliov, V.M. & Berezin, V. V. 1983: Non-contact evaluation of thermal conductivity of rocks with the aid of a mobile heat source. Izvestiya, Physics of the Solid Earth, 19: 563–567.

Popov Y.A., Berezin, V.V., Soloviov, G.A., Romushkevich, R.A., Korosteliov, V.M., Kostiurin, A.A. & Kulikov, A.V. 1987: Thermal conductivity of minerals, Izvestiya, Physics of the Solid Earth, 3: 83–92.

Popov, Y.A., Pribnow D.F.C., Sass, J.H., Williams, C.F. & Burkhardt, H. 1999: Characterization of rock thermal conductivity by high-resolution optical scanning. Geothermics, 28/2: 253–276. https://doi.org/10.1016/S0375-6505(99)00007-3

Popov, Y.A. & Romushkevich, R.A. 2002: The Earth's thermal field and related research methods. In: Popov, Y.A., Khutorskoy, M. & Korobkov, D.: Proc. Intl. Conference, June 13-17.

Popov, Y.A., Tertychnyi, V., Romushkevich, R.A., Korobkov, D. & Pohl, J. 2003: Interrelations between thermal conductivity and other physical properties of rocks: Experimental data. Pure Appl. Geophys., 160: 1137–1161. https://doi.org/10.1007/PL00012565

Popov, Y.A., Bayuk, I., Parshin, A., Miklashevskiy, D., Novikov, S. & Chekhonin, E. 2012: New methods and instruments for determination of reservoir thermal properties. Proc., 37th workshop on Geothermal Reservoir Engineering, Stanford Univ., Stanford, CA, SGP-TR-194.

Popov, Y., Beardsmore, G., Clauser & C., Roy, S. 2016: ISRM Suggested methods for determining thermal properties of rocks from laboratory tests at atmospheric pressure. Rock. Mech. Rock. Eng., 49/10: 4179-4207. https://doi.org/10.1007/s00603-016-1070-5

Popov, Y.A., Lippmann, E. & Rauen, A. 2017: TCS – Manual. Thermal conductivity (TC) and thermal diffusivity (TD) scanner, ver. 31.01.2017. TCS Lippmann and Rauen GbR, Schaufling: 53 p.

Prelovšek, P., Babič, M. & Uran, B. 1982: Meritve toplotne prevodnosti kamenin z izboljšano metodo grelne žice = Thermal conductivity measurements on rocks by improved hot wire method. Geologija, 25/2: 335–339 (in Slovene).

Prelovšek, P. & Uran, B. 1984: Generalised hot wire method for thermal conductivity measurements. J. Phys. E.: Sci. Instrum., G. Britain 17: 674–677. https://doi.org/10.1088/0022-3735/17/8/012

Prestor, J., Pestotnik, S., Rajver, D., Jež, J., Gerčar, D., Klančič, K. & Svetina, J. 2018: Analize potenciala plitve geotermalne energije v Sloveniji do leta 2050, za projekt LIFE ClimatePath2050 (Analyzes of the potential of shallow geothermal energy in Slovenia until 2050, for the LIFE ClimatePath2050 project) (LIFE 16 GIC/SI/000043), GeoZS, Ljubljana: 59 p. (in Slovene).

Prestor, J., Rajver, D., Svetina, J., Janža, M., Šram, D., Rman, N. & Lapanje, A. 2020: Raba geotermalne energije v Sloveniji (Geothermal energy use in Slovenia). In: A. Senegačnik (ed.), Mineralne surovine v letu 2019, Bulletin, GeoZS, Ljubljana: 141–157 (in Slovene). https://www.geo-zs.si/PDF/PeriodicnePublikacije/Bilten_2019.pdf.

Rajver, D. 1986: Merjenje toplotne prevodnosti kamnin iz nekaterih slovenskih geotermalnih nahajališč = Measurement of thermal conductivity of rocks from some Slovenian geothermal locations. Diploma work. FNT, University of Ljubljana, Ljubljana: 73 p. (in Slovene).

Rajver, D. 1990: New heat flow data in Slovenia, Yugoslavia. Final report of the 20th International Course in Geothermics, International school of geothermics, NRC IIRG, Pisa: 73 p.

Rajver, D. 2018: Geothermal maps. Surface heat-flow density. In: Novak, M. & Rman, N. (eds.): Geological Atlas of Slovenia. Second, revised and supplemented edition, GeoZS, Ljubljana.

Rajver, D., 2022: Poročilo o meritvah toplotne prevodnosti in toplotne difuzivnosti na 10 vzorcih kamnin iz lokacij Smrekovec, Renke in Pasjek, Slovenija = Report on thermal conductivity and thermal diffusivity measurements on 10 rock samples from Smrekovec, Renke and Pasjek locations, Slovenia. Geological Survey of Slovenia, Ljubljana: 23 p. (in Slovene).

Rajver, D., Lapanje, A. & Rman, N. 2012: Možnosti proizvodnje elektrike iz geotermalne energije v Sloveniji v naslednjem desetletju = Possibilities for electricity production from geothermal energy in Slovenia in the next decade. Geologija, 55/1: 117–140. https://doi.org/10.5474/geologija.2012.009

Rajver, D., Pestotnik, S. & Prestor, J. 2019: Primeri ocene temperature na površini trdnih tal pri projektiranju zajetij plitve geotermalne energije = Examples of the assessment of temperatures on the surface of solid ground in the design of the shallow geothermal energy extractions. Geologija, 62/1: 101–120. https://doi.org/10.5474/geologija.2019.005

Ravnik, D. 1988: Osnovne količine toplotnega toka v geotermiji = Basic parameters of heat flow in geothermics. Doctoral thesis. FNT, University of Ljubljana, Ljubljana: 253 p. (in Slovene, with English summary).

Ravnik, D., Verbovšek, R. & Premru, U. 1982: Gostota Zemljinega toplotnega toka v konjiški udorini = Heat flow density in the fault basin of Slovenske Konjice. Geologija, 25/2: 327–334 (in Slovene, with English abstract).

Ravnik, D. & Uran, B. 1984: Geotermične meritve II. Metodologija in interpretacija meritev toplotne prevodnosti in gostote Zemljinega toplotnega toka (Raziskovalna naloga za l. 1983) = Geothermal measurements II. Methodology and interpretation of measurements of thermal conductivity and Earth's heat-flow density (Research paper for y. 1983). Geološki zavod Ljubljana TOZD-I. Archive of Geological Survey of Slovenia: 119 p. (in Slovene).

Ravnik, D., Kolbah, S., Jelić, K., Milivojević, M., Miošić, N., Tonić, S. & Rajver, D. 1987: Geotermalne karte Jugoslavije. In: Ravnik, D. (ed.): Geothermal Atlas of Europe. Yugoslavia. Geothermal regime in Yugoslavia. Geološki zavod Ljubljana, TOZD GGG, Archive of Geological Survey of Slovenia: 17 p. and 7 maps.

Ravnik, D. & Rajver, D. 1990: Geotermalne karte Slovenije. 1. Baza podatkov geotermičnih količin, 2. Geotermalne karte = Geothermal maps of Slovenia. 1. Database of geothermal quantities, 2. Geothermal maps. Unpubl. Report of GZL: 70 p. and 77 fig. (in Slovene).

Ravnik, D. 1991: Geotermične raziskave v Sloveniji = Geothermal investigations in Slovenia. Geologija, 34/1: 265–303 (in Slovene, with English summary). https://doi.org/10.5474/geologija.1991.006

Ravnik, D. (National Editor), Kolbah, S., Jelić, K., Milivojević, M., Miošić, N., Tonić, S. & Rajver, D. 1992: Yugoslavia. In: Hurtig, E., Čermak, V., Haenel, R. & Zui, V. (eds.): Geothermal Atlas of Europe. Geoforschungszentrum Potsdam Publ.,1: 102–104: 152–153.

Ravnik, D., Rajver, D., Poljak, M. & Živčić, M. 1995: Overview of the geothermal field between the Alps, the Dinarides and the Pannonian basin. Tectonophysics, 250/1–3: 135–149. https://doi.org/10.1016/0040-1951(95)00031-X

Reiter, M.A. & Tovar, R.J.C. 1982: Estimates of terrestrial heat flow in Northern Chihuahua, Mexico. Canadian Journal of Earth Sciences, 22: 1503-1517.

Research project ARRS PROJECT J1-3024: Deciphering the sensitivity of rock walls to climate change and freeze-thaw cycles in non-permafrost areas = Raziskovalni projekt ARRS PROJEKT J1-3024: Dešifriranje občutljivosti skalnih sten na podnebne spremembe in cikle zmrzovanja in odtaljevanja na območjih brez permafrosta.

Robertson, E.C. 1988: Thermal properties of rocks. U.S.G.S. Open-file report 88-441, U.S. Geol. Survey, Reston, VA.: 106 p.

Romushkevich, R.A. & Popov, Y.A. 1998: Study of thermal conductivity of ore samples. In: Popov, Y.A. & Pimenov, V. (eds.): Proc. Intl. Conference "The Earth's thermal field and related research methods", May 19–21, Moscow, Russia.

Roy, R.F., Beck, A.E. & Touloukian, Y.S. 1981: Thermophysical properties of rocks. In: Touloukian, Y.S., Judd, W.R. & Roy, R.F. (eds.): Physical properties of rocks and minerals. McGraw-Hill, New York: 409–502.

Rybach, L. 1988: Determination of heat production rate. In: Haenel, R., Rybach, L. & Stegena, L. (eds.): Handbook of terrestrial heat-flow density determination. Kluwer Academic Publishers: Dordrecht, Boston, London: 125–142.

Sarbu, I. & Sebarchievici, C. 2014: General review of ground-source heat pump systems for heating and cooling of buildings. Energy and Buildings, 70: 441–454. https://doi.org/10.1016/j.enbuild.2013.11.068

Sass, J.H., Lachenbruch, A.H. & Munroe, R.J. 1971: Thermal conductivities of rocks from measurements on fragments and its application to heat flow determinations. J. Geophys. Res., 76: 3391–3401. https://doi.org/10.1029/JB076i014p03391

Sass, J.H., Stone, C. & Munroe, R.J. 1984: Thermal conductivity determinations on solid rock – A comparison between a steady-state divide-bar apparatus and a commercial transient line-source device. J. Volcan. Geotherm. Res., 20: 145–153.

Schön, J.H. 1996: Physical properties of rocks. Fundamentals and principles of petrophysics. Pergamon, Oxford: 583 p.

Schön, J.H. 2011: Physical properties of rocks: a workbook. Handbook of petroleum exploration and production. Volume 8, 1st edition, Elsevier, Amsterdam, Boston: 494 p.

Serianz, L. 2022: Hidrogeološka analiza iztoka termalne vode iz karbonatnega vodonosnika vzhodnega dela Julijskih Alp = Hydrogeological analysis of thermal water outflow from a carbonate aquifer in the eastern part of the Julian Alps. Doctoral dissertation.

University of Ljubljana. Ljubljana: 138 p. https://repozitorij.uni-lj.si/IzpisGradiva.php?lang=slv&id=137195

Somerton, W.H. 1992: Thermal properties and temperature-related behavior of rock/fluid systems. Developments in Petroleum Science 37, Elsevier, Amsterdam etc.: 257 p.

Sumikawa, S. & Arakawa, Y. 1976: Quick thermal conductivity meter. Instr. Autom. 4/4: 60–66.

Sundberg, J. 1988: Thermal properties of soils and rocks. SGI report 35, Swedish geotechnical institute (SGI), Linköping: 47 p.

Touloukian, Y.S., Powell, R.W., Ho, C.Y. & Klemens, P.G. 1970: Thermal properties of matter, vol. 2, Thermal conductivity, Non-Metallic Solids. New York and Washington: IFI/Plenum.

Uran, B. 1982: Merilnik toplotne prevodnosti na grelno žico = Thermal conductivity meter on the heating wire. Dipl. Thesis. VTO Fizika, University of Ljubljana: 72 p. (in Slovene).

Uyeda, S. 1988: 9. Implications 9.1. Geodynamics. In: Haenel, R., Rybach, L. & Stegena, L. (eds.): Handbook of terrestrial heat-flow density determination. Kluwer Academic Publishers, Dordrecht: 317–351.

Vacquier, V., Mathieu, Y., Legendre, E. & Blondin, E. 1988: Experiments on estimating thermal conductivity of sedimentary rocks from oil well logging. Am. Ass. Petrol. Geol. Bull., 72/6: 758–764.

Van der Held, E.F.M., Herdebol, J. & Kalshoven, J. 1949: On the measurement of the thermal conductivity of liquids by a non-stationary method. Physica, 208–216.

VDI 2001: VDI 4640, Part 1 – Thermal use of the underground. Fundamentals, approvals, environmental aspects. Düsseldorf: 32 p.

Von Herzen, R. & Maxwell, A. 1959: The measurement of thermal conductivity of deep-sea sediments by a needle-probe method. J. Geophys. Res., 64/10: 1557–1563. https://doi.org/10.1029/JZ064I010P01557

Zoth, G. & Haenel, R. 1988: Appendix. 10.1. Thermal conductivity. In: Haenel, R., Rybach, L. & Stegena, L. (eds.): Handbook of terrestrial heat-flow density determination. Kluwer Academic Publishers: Dordrecht, Boston, London: 449–466.

GEOLOGIJA 66/1, 151-166, Ljubljana 2023

https://doi.org/10.5474/geologija.2023.006

Hydrogeological characterization of karst springs of the white (*Proteus anguinus anguinus*) and black olm (*Proteus anguinus parkelj*) habitat in Bela krajina (SE Slovenia)

Hidrogeološka karakterizacija kraških izvirov na območju habitata belega (*Proteus anguinus anguinus*) in črnega močerila (*Proteus anguinus parkelj*) v Beli krajini (JV Slovenija)

Katja KOREN[1] & Rok BRAJKOVIČ[1]
Manca BAJUK[2], Špela VRANIČAR[2] & Vesna FABJAN[2]

[1]Geological Survey of Slovenia, Dimičeva ulica 14, SI-1000, Ljubljana, Slovenia;
e-mail: katja.koren@geo-zs.si, rok.brajkovic@geo-zs.si
[2]High school Črnomelj, Gimnazija Črnomelj, Kidričeva ulica 18a, SI-8340, Črnomelj, Slovenia

Prejeto / Received 19. 5. 2022; Sprejeto / Accepted 10. 7. 2023; Objavljeno na spletu / Published online 4. 8. 2023

Key words: hydrogeology, olm, ecology, nitrate, monitoring
Ključne besede: hidrogeologija, močeril, ekologija, nitrat, monitoring

Abstract

The springs west of Črnomelj, in SE Slovenia, are the habitat of the black (*Proteus anguinus parkelj*) and the white olm (*Proteus anguinus anguinus)*. Some of these springs are also the only known habitat in the world of endemic species of black olm. A steady decline in olm populations has been observed in this area over the past decades. Owing to the rapid runoff and groundwater flow high-resolution monitoring is essential in providing better insight into the hydrogeological characterization of the catchment area of springs. Specific factors and critical parameters of water behind said olm degradation have not yet been defined. Because the olm's environment is largely aquatic, one potential critical parameter could be the higher water temperatures (>12 °C) or higher nitrate concentration (>9.2 mg/l). The six-month observation of the springs (July – December 2021) point to water temperature as a potential critical parameter since the water temperature of the springs exceeded 12 °C in months July and August. Nitrate concentrations could also be a second critical parameter in the degradation of the olm's habitat. Maximum nitrate concentrations above 9.2 mg/l throughout much of the observation period (except for Dobličica spring). Due to less agricultural activity in December in the spring catchment area and a higher dilution rate due to reduced evapotranspiration and increased effective precipitation during this time of the year, the nitrate concentrations are decreased. The results of the measured parameters of groundwater could show the hydrogeological connection between the Otovski and Pački breg springs and between Šotor, Jamnice and Dobličica. The Obršec spring has an independent catchment area. A detailed estimation of the springs catchment area is possible due to a detailed geologic map. It is necessary to determine the origin of the nitrate (nitrate isotope analysis), to quantify the threshold values of the critical parameters, to define precisely all the causes of the olm deterioration, and to make proposals for appropriate measures to limit or even stop the decline of the olm population.

Izvleček

Izviri zahodno od Črnomlja, v JV Sloveniji so habitat črnega (*Proteus anguinus parkelj*) in belega močerila (*Proteus anguinus anguinus)*. Nekateri od teh izvirov so tudi edini znan habitat te endemične vrste črnega močerila. V zadnjih desetletjih je opazen upad populacije močerilov. Za boljši vpogled in ocenitev hidrogeoloških značilnosti prispevnega območja izvirov, je zaradi hitrega odtoka in toka podzemne vode pomembno pogosto spremljanje stanja. Potencialni vplivni dejavniki in parametri podzemne vode, ki bi lahko vplivali na slabšanje stanja ohranjenosti močerila še niso opredeljeni. Ker močeril večino časa živi v vodi, bi lahko potencialni kritični dejavnik bila višja temperatura vode (>12 °C) ali višja vsebnost nitrata v vodi (>9.2 mg/l). Izsledki šestmesečnega spremljanja kažejo, da bi potencialni kritični parameter za slabšanje stanja ohranjenosti močerila bila temperature vode nad 12 °C v mesecih julij in avgust v opazovanem obdobju. Vsebnost nitrata bi prav tako lahko bil kritični parameter oz. razlog za upad števila močerilov in slabšanje stanja tega habitata. Najvišje vsebnosti nitrata so mejno vrednost za močerila presegale skoraj čez celotno opazovalno obdobje (z izjemo izvira Dobličice), razen v mesecu decembru. Vzrok za to je zelo verjetno zmanjšana kmetijska dejavnost oz. višja stopnja razredčenja v tem delu leta zaradi zmanjšane evapotranspiracije in višjih količin efektivnih padavin. Rezultati izmerjenih parametrov podzemne vode kažejo, na verjetno hidrogeološko povezavo med izviri Otovski in Pački breg ter med izviri Šotor, Jamnice in Dobličica. Izvir Obršec ima samostojno prispevno območje. V prihodnje bo podrobnejša opredelitev prispevnega območja izvirov mogoča z detajlnim geološkim kartiranjem. Potrebno je ugotoviti izvor nitrata (izotopske analize nitrata), kvantificirati mejne vrednosti kritičnih parametrov, določiti vse možne vzroke za slabšanje stanja ohranjenosti populacije močerila in opredeliti predloge ukrepov za preprečevanje oz. ustavitev upada populacije močerilov.

Introduction

Some springs and caves in the Bela krajina region (SE Slovenia), in the area west of Črnomelj, are especially important and should be kept in good hydrogeological and geochemical condition (or work towards improvement), since they are the habitat of the black (*Proteus anguinus parkelj*) and white olm (*Proteus anguinus anguinus*). The black olm is an endangered endemic subspecies known only from a few springs over less than 3 km^2 in the W part of Bela krajina. Based on Annex 6 (Red List of Amphibians) of the Habitats Directive (Council Directive 92/43/EEC), the white and black olm are classified as rare and vulnerable species. The classification of the white and black olm as rare and vulnerable species was made based on a long-term scientific research of the distribution and decline in the olm population in the Bela krajina area. The problem of deterioration of the olm's habitat has also been noted by locals, among them the students of the Črnomelj secondary school, who work to raise awareness among the wider local community and draw attention to the problem. Cave pollution and the consequent polluted groundwater affects these groundwater-dependant ecosystems (Mezga et al., 2016). In the long term, this could cause the decline of one of the most important symbols of subterranean biodiversity, the white olm, as well as the black olm in Bela krajina (Sket, 1997; Aljančič et al., 2014; Ribeiro & Tičar, 2017).

Olm lives in aquatic environments, in still and oxygen-rich waters with stable temperatures of 8 to 11 °C. Occasionally, enters the phreatic and epiphreatic zones at high water levels (Aljančič et al., 2014; Mezga et al., 2015). Based on the conditions under which olm lives, water temperature above 12 °C could also be a potentially critical parameter for its degradation.

Potential factors and related critical parameters affecting the preservation status of the olm's habitat have not yet been properly defined. Past research (NLZOH, 2017) has determined the nitrate threshold value for olms, which consists of the predicted no-effect concentration (PNEC), the natural background concentration, and the expected variation of the natural background concentration. The main toxic effect of nitrate on aquatic animals appears to be the conversion of oxygen-carrying pigments (hemoglobin, hemocyanin) into forms incapable of transporting oxygen (methemoglobin, methemocyanin) (Jensen, 1996; Scott & Crunkilton, 2000).

If the assessed critical parameters are found to have a significant influence, the next step is to find the causes behind certain excessive critical parameter in groundwater and to limit or lower them using appropriate measures.

The aims of this study are (I) to assess the basic hydrogeological characteristics (water level, water temperature and electrical conductivity) of the observed springs as a response to water levels and water temperatures to precipitation (II) to determine whether water temperatures and nitrate concentrations are in a range suitable for the olm, (III) to determine whether long-term national monitoring would provide a realistic assessment of the quality of spring water, and (IV) to determine whether there is a possible geological or hydrogeological connection between the studied springs.

The study area

Geographical settings

The study area lies in SE Slovenia, in Bela krajina, west of the town of Črnomelj (Fig. 1), with a focus on six springs that are the habitat of white and black olm. The black olms were detected in the springs of Obršec, Šotor, Jamnice (also known as Jelševnik spring) and Dobličica, while only the white olm is known from Otovski breg and Pački breg springs (Gorički, 2017). In the catchment area of these six springs are village settlements, which have regulated water supplies but no sewage system. On the slopes west of the springs (Doblička gora, Stražni vrh, Rodine) there are homes with vineyards and permanently inhabited houses spread over a wider area of the catchment area of the studied springs. The potential sources of anthropogenic impacts in this part of the karst area mainly consist of illegal landfills, the use of septic tanks in households, and the use of manure. Furthermore, in the immediate vicinity of the Obršec spring an illegal settlement with uncontrolled sewage disposal.

Geological settings

Bela krajina can be geotectonically divided into its NE part, which belongs to the transition area between the Internal and External Dinarides, and the remaining part, which belongs to the External Dinarides (Placer, 2008), where our study area is located. The lithostratigraphic succession of the study area is largely characterized by shallow marine limestones and dolomites of Jurassic and Cretaceous age (Fig. 2) (Bukovac et al., 1984a, 1984b; Vlahović et al., 2005). The studied area is characterised by outcrops of Jurassic and Cretaceous carbonates. The Upper Jurassic bedded limestones and bedded to massive dolomites are tectonically fractured and exhibit strong secondary porosity.

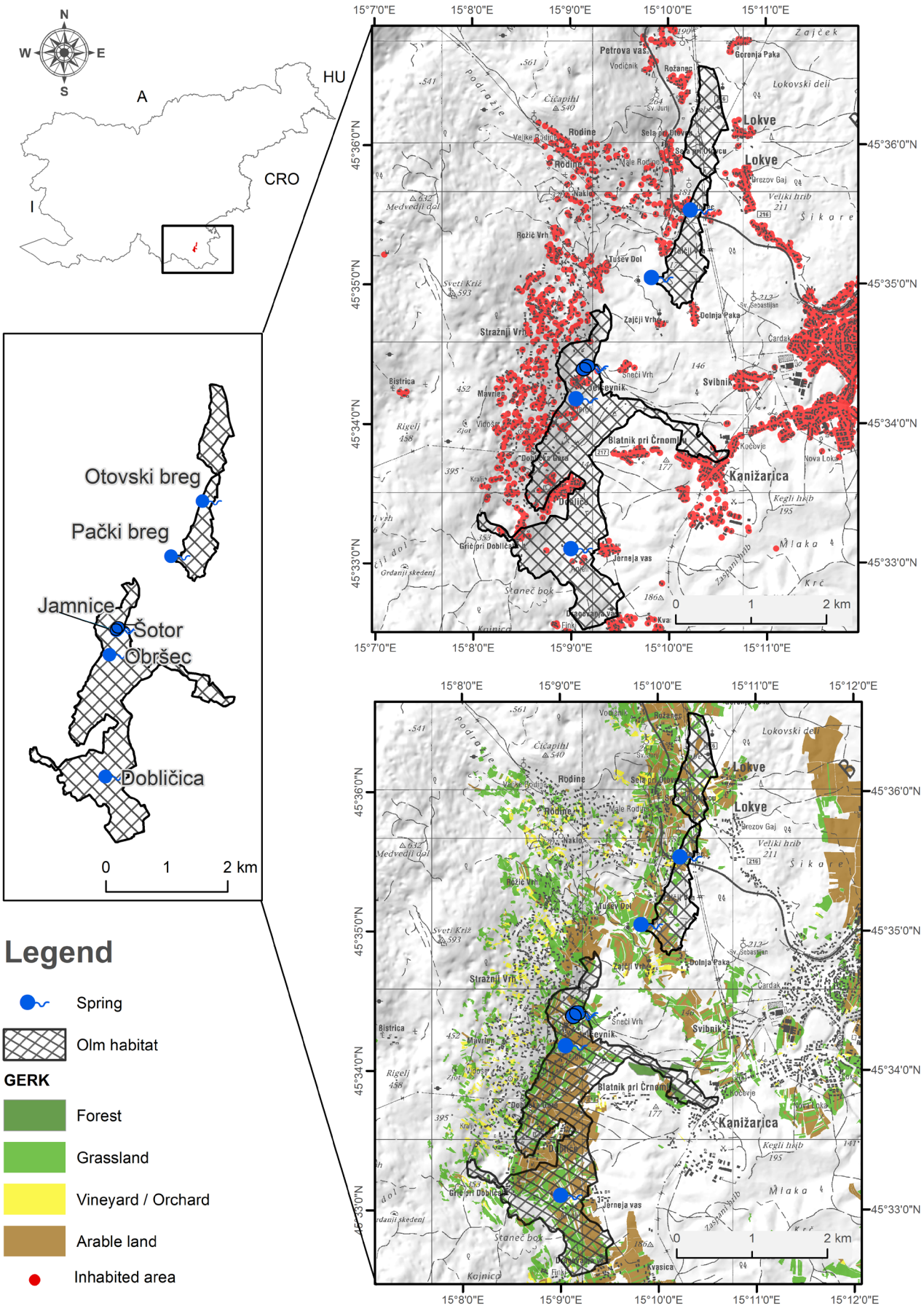

Fig. 1. Geographical location with observation springs, inhabited area (GURS, 2016) and land use (GERK, 2023) in the study area.

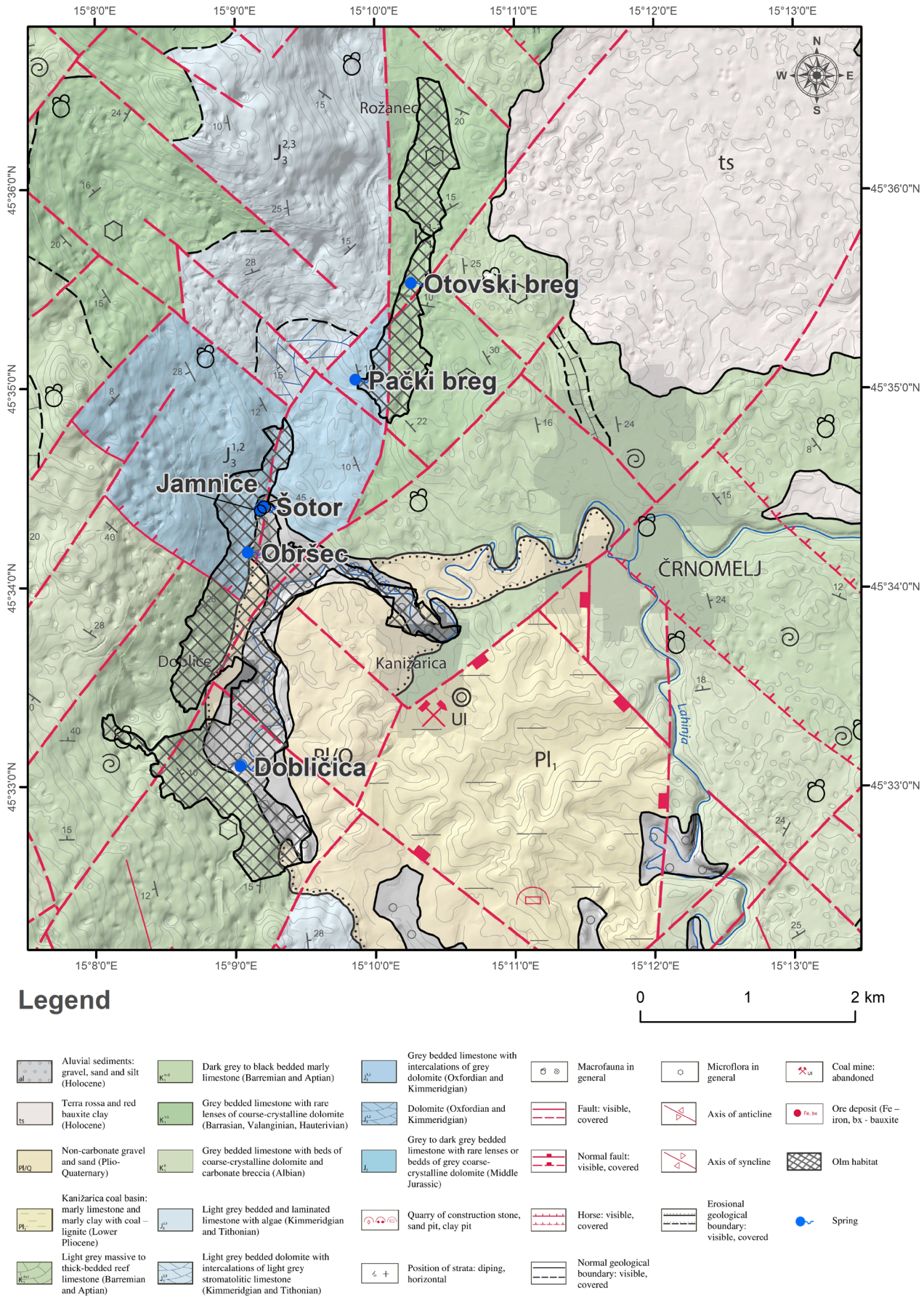

Fig. 2. The geological settings of the study area (modified after Bukovac et al., 1984a, 1984b).

Lower Cretaceous limestones (Bukovac et al., 1984a, 1984b) in some parts also contain lenses of dolomite and a breccia horizon. The entire Cretaceous succession exhibits strong and deep karstification, which is reflected in a large number of karst dolines, vertical shafts, and caves. To the east, the study area is bounded by the tectonic contact with the Kanižarica coal basement, which formed in the Pliocene and was filled with fine-grained lake sediments and organic matter (coal) (Šinigoj et al., 2012). The Jurassic, Cretaceous and Neogene rocks and their contacts in the lower parts of the shallow karst are covered by clays of the Plio-Quaternary age, a thick (2–6 m) cover of residual and resedimented terra rossa and Quaternary sediments of the Dobličica and Jelševniščica floodplains. Structurally, the wider area of Bela krajina is characterized by NW–SE trending Dinaric longitudinal structures (folds and faults). The fault planes are mostly characterized as reverse faults with their dip towards the SW (Bukovac et al., 1984a, 1984b). The springs of the study area lie on the potential continuation of the reverse fault, defined on the basic geological map as the "Bosiljevo-Črnomelj" thrust (Bukovac et al., 1984a, 1984b; Habič et al., 1991b; Novak, 1996; Šinigoj et al., 2012). From the Dobličica spring towards the Šotor, Obršec, and Jamnice springs, this zone is covered by the Quaternary flood plain of the Dobličica River. N–S orientated fault zone outcrops only in some locations E of the village of Dobliče and W of village Otovec. Different structural trends can be observed NW of the village Dobliče (Šinigoj et al., 2012). There the fault system shows NW–SE orientation. The structural relations between these two fault systems are not clear, as the possible fault intersection is covered by Quaternary sediments. These fault zones could be an important factor for groundwater conduction (Čar, 2018). The springs studied are classified as karst springs. Dobličica and Otovski breg flow from Lower Cretaceous limestone and could not be directly connected to any of the known fault systems, while Obršec, Šotor, Jamnice and Pački breg springs flow from the Upper Jurassic limestone and dolomite and are probably located in a tectonic zone running in the NNE–SSW direction (Bukovac et al., 1984b; Habič et al., 1991b; Šinigoj et al., 2012).

Observation springs

Otovski breg is a spring in an unroofed cave from which the water flows to the surface through two syphons. Close by, another monitored spring is located (approximately 1 km SW from Otovski breg) called Pački breg. The white olm is present in these two (Pački breg & Otovski breg) observed springs. Both springs are located in the northern part of the studied area near the villages of Otovec and Tušev dol (Fig. 1). In Pački breg there are three smaller springs that are a mere one meter apart and never run dry. The water flows to the surface in two horizontal syphon springs. In the third, the water springs vertically, which is obvious when observed at high water level.

The habitat of the black olm consists in the four observed springs located in the southern part of the studied area (Fig. 1) near the villages of Jelševnik and Dobliče. Šotor is a spring located on the Zupančič farm in Jelševnik, only 50 m away from the Jamnice spring. It is about 4.5 m wide, and the water comes to the surface in several syphons. The Šotor spring is covered with a tent to simulate a dark environment and a camera is installed to observe the olms. The Jamnice spring is a funnel-shaped spring some about 2 m wide from where water outflows to the lake at the Zupančič farm. The Obršec spring is located 500 m south of the village of Jelševnik with two larger syphons 5 m apart. The southernmost and observably largest is the Dobličica spring. The spring Dobličica is located 2.4 km SE from the village Jelševnik (springs Šotor and Jamnice) and is a spring with a depth of more than 100 m (Novak, 1996). The spring is protected by a groundwater protection zone and is part of the public drinking water supply system.

Material and Methods

Effective precipitation (P_{ef}), evapotranspiration (ETR)

Data on hourly measurements of precipitation and daily potential evapotranspiration were obtained from the meteorological station Črnomelj-Dobliče (SEA 2022a, 2022b). The effective precipitation (P_{ef}) is the amount of total precipitation without runoff and evapotranspiration. Based on hourly measurements of precipitation and daily evapotranspiration we calculated the highest amount of precipitation (P_{tot}) in one day, in a one-hour event, and the monthly volume. We also calculated the daily evapotranspiration (ETR) and effective precipitation. Based on the daily total precipitation (P_{tot}) and the daily potential evapotranspiration (ETR) in the meteorological station Črnomelj – Dobliče, we simplified and assessed the amount of daily effective precipitation (Eq. 1).

$$P_{ef} = P_{tot} - ETR\ [mm] \qquad \text{[Eq. 1]}$$

Table 1. Characteristics of sensors for water level, temperature and electrical conductivity measurements (Eltratec GSR 130NTG).

Observation point	Monitoring period	Interval	Water level	Temperature	Electrical conductivity
Obršec	July – December 2021	1 h	0 – 9.99 m	0 – 50 °C ± 0.3 °C	10 – 2000 µS/cm ±50 µS/cm (< 2 %)
Šotor	July – December 2021	1 h	0 – 9.99 m	0 – 50 °C ± 0.3 °C	10 – 2000 µS/cm ±50 µS/cm (< 2 %)
Pački breg	August – December 2021	1 h	0 – 99.99 m	0 – 50 °C ± 0.4 °C	0.1 – 10 mS/cm ± 400 µS/cm

Field measurements

Field measurements of water levels, temperature, and electrical conductivity were carried out using the water level measurement logger Eltratec GSR 130NTG with sensors for water level, temperature, and electrical conductivity (Table 1). The loggers were installed at the Obršec and Šotor springs from July to December 2021 and at the Pački breg spring from August to December 2021. The loggers recorded measurements at one-hour intervals. The water level, electrical conductivity and water temperature in Jamnice and Otovski breg were not monitored, we only measured nitrate content.

Data on water levels and temperature is recorded every five minutes at the Dobličica spring and was provided by Komunala Črnomelj, a public utility company. Due to the wide measurement range and high measurement uncertainty of the electrical conductivity probe installed at Pački breg (± 400 µS/cm), the data obtained during the study for this spring was omitted. In this case, we monitored only the relative fluctuations in electrical conductivity.

Response of water level (WLR) on rainfall event

We defined the rain event as a maximum daily amount of precipitation (P_{tot}) of more than 25 mm. This rainfall amount (25 mm/day) was determined based on a significant simultaneous rise in water level in the observed springs, which occurred as a peak just a few hours after the rain event began. All rain events began with a rainfall rate greater than 0.2 mm/hour. The time of the beginning of the rainfall event (t_{start}) is the so-called beginning of the rainfall event. During this time, the water level does not change (WL_{start}). After some time during the rain event (t_{max}), the peak or maximum spring water level (WL_{max}) is measured. Based on the rainfall events and the water level rise in response to the rainfall event, we calculated the response rates or water level rise rate (WLR), which is a very simplified tool to roughly evaluate the response of the karst spring to rainfall events (Eq. 2).

$$WLR = \frac{WL_{max} - WL_{start}}{t_{max} - t_{start}} \ [m/h] \qquad \text{[Eq. 2]}$$

Water sampling

Sampling for nitrate concentrations was carried out at weekly intervals between July and December 2021 at the Obršec, Šotor, Jamnice, Otovski breg, Pački breg and Dobličica springs (Fig. 1). Sampling was performed in collaboration with students from Črnomelj High school (Gymnasium Črnomelj), that were included into research as citizen science members. For sampling, we used 100 ml plastic bottles or two 50 ml plastic tubes for each sampling location and stored at 2–5 °C. Before collecting the water samples, the bottles were washed with water from the individual spring. Then the samples were taken to the Geological Survey of Slovenia laboratory to a dark and cool place.

Nitrate measurements

Measurements of nitrate concentrations in water were carried out in the hydrogeological laboratory of the Geological Survey of Slovenia using a UV-VIS Spectro:IyserTM spectrometer. Based on the reflection of laser beams, the spectrum and nitrogen content of nitrate (NO_3-N) are determined. Measurements were performed no later than 72 hours after sampling. The spectrometer is calibrated to the primary standards using known values. For a quality control check prior to sample measurement, the in-house standard (ultrapure water) was measured first, and the second in-house standard (tap water) was measured at the end of the measurement process. The same sample from one bottle was measured three times. All measured values are corrected with the correction equation obtained using primary standards with known values and checked with in-house standards.

Results

Effective precipitation (P_{ef}) and evapotranspiration (ETR) and rain events

In the observation period July – December 2021, the highest monthly amount of precipitation (P_{tot}) came in July (141.99 mm) and the lowest in September (79.17 mm). The highest evapotranspiration (ETR) coincided with higher air

Table 2. Precipitation, evapotranspiration and effective precipitation in Črnomelj – Dobliče meteorological station (July – December 2021) (SEA 2022a, 2022b).

	Precipitation (P_{tot}) N=9169			**Evapotranspiration) (ETR) N=185**	**Effective precipitation ($P_{ef} = P_{sum}$-ETR_{sum})**
Month/Year	Max [mm/h]	Sum [mm/month]	Max [mm/day]	Sum [mm/month]	Sum [mm/month]
7/21	50.9	141.99	6.8	137.2	4.79
8/21	23.5	108.25	5.3	106.0	2.25
9/21	34.4	79.17	3.5	73.7	5.47
10/21	27.0	105.83	2.6	31.2	74.63
11/21	23.6	131.77	1.4	14.4	117.37
12/21	33.9	97.57	1.2	9.4	88.17

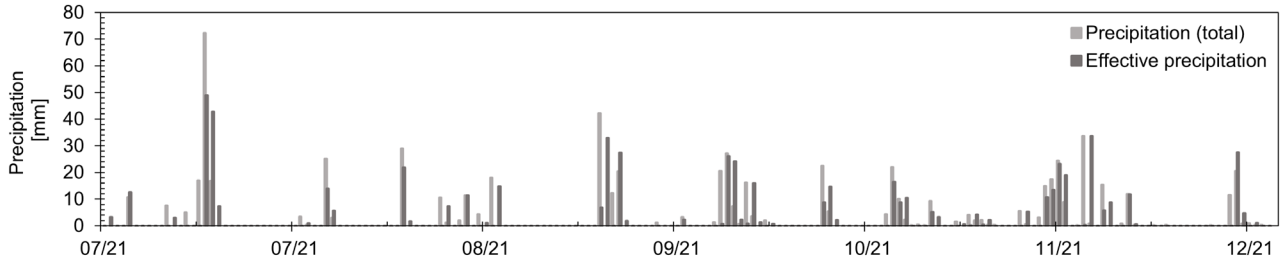

Fig. 3. Total daily precipitation and effective precipitation in Črnomelj-Dobliče meteorological station (July – December 2021) (SEA 2022a, 2022b).

temperatures and higher plant transpiration, in July (137.2 mm), with the lowest volumes in December (9.4 mm). The lowest monthly amount of effective precipitation (P_{ef}) was in August (2.25 mm), and the highest in November (117.37 mm) (Table 2).

In the period July – December 2021 we defined five rain events: at July 16 (72.3 mm/day), August 17 (29 mm/day), September 17 (42.1 mm/day), October 6 (27.1 mm/day) and December 2 (33.6 mm/day).

Water level, temperature, and electrical conductivity in the observed springs

In the period July – December 2021 we observed the hourly change in water level (WL), temperature (T), and electrical conductivity (EC) in three springs – Pački breg, Obršec, and Šotor. The measured values are presented in Figure 4, 5, 6, and 7. The highest and lowest water level values, temperatures, and electrical conductivity of these four springs are presented in Table 3.

Table 3. Highest and lowest water level, electrical conductivity water temperature in observed springs (July – December 2021).

	Pački breg						**Obršec**						**Šotor**						**Dobličica**			
	WL [m]		EC [µS/cm]		T [°C]		WL [m]		EC [µS/cm]		T [°C]		WL [m]		EC [µS/cm]		T [°C]		WL [m]		T [°C]	
	N=3430		N=3430		N=3409		N=3930		N=3709		N=3958		N=3926		N=3954		N=3954		N=41318		N=51780	
Month/ Year	Max	Min	Max	Min	Max	Min	Max	Min	Max	Min	Max	Min	Max	Min	Max	Min	Max	Min	Max	Min	Max	Min
07/21	/	/	/	/	/	/	1.91	0.76	452	424	13.9	11.5	1.47	0.48	535	357	17.3	10.5	1.43	0.37	25.6	10.7
08/21	0.53	0.33	930*	620*	11.8	11.5	1.44	0.56	451	420	14.7	11.5	0.71	0.40	442	403	11.3	10.5	0.42	0.37	14.1	11
09/21	0.59	0.25	970*	920*	12.0	11.7	1.63	0.29	474	431	14.1	11.4	1.03	0.41	435	418	10.7	10.5	0.83	0.43	13	10.9
10/21	0.76	0.27	990*	890*	11.9	11.4	1.63	0.3	507	430	12.8	11.2	1.9	0.54	549	418	11	10.4	1.82	0.39	12.4	9.7
11/21	0.85	0.41	970*	900*	11.7	10.9	1.82	1.19	489	452	11.6	11.3	2.09	0.81	625	435	11.8	10.2	1.96	0.49	10.7	9.0
12/21	0.86	0.42	960*	900*	11.5	10.9	1.8	1.36	461	450	11.5	11.4	2.08	0.91	695	442	11.9	10.1	1.91	0.49	10.7	8.3

*wide measuring range – deviations of ± 400 µS/cm

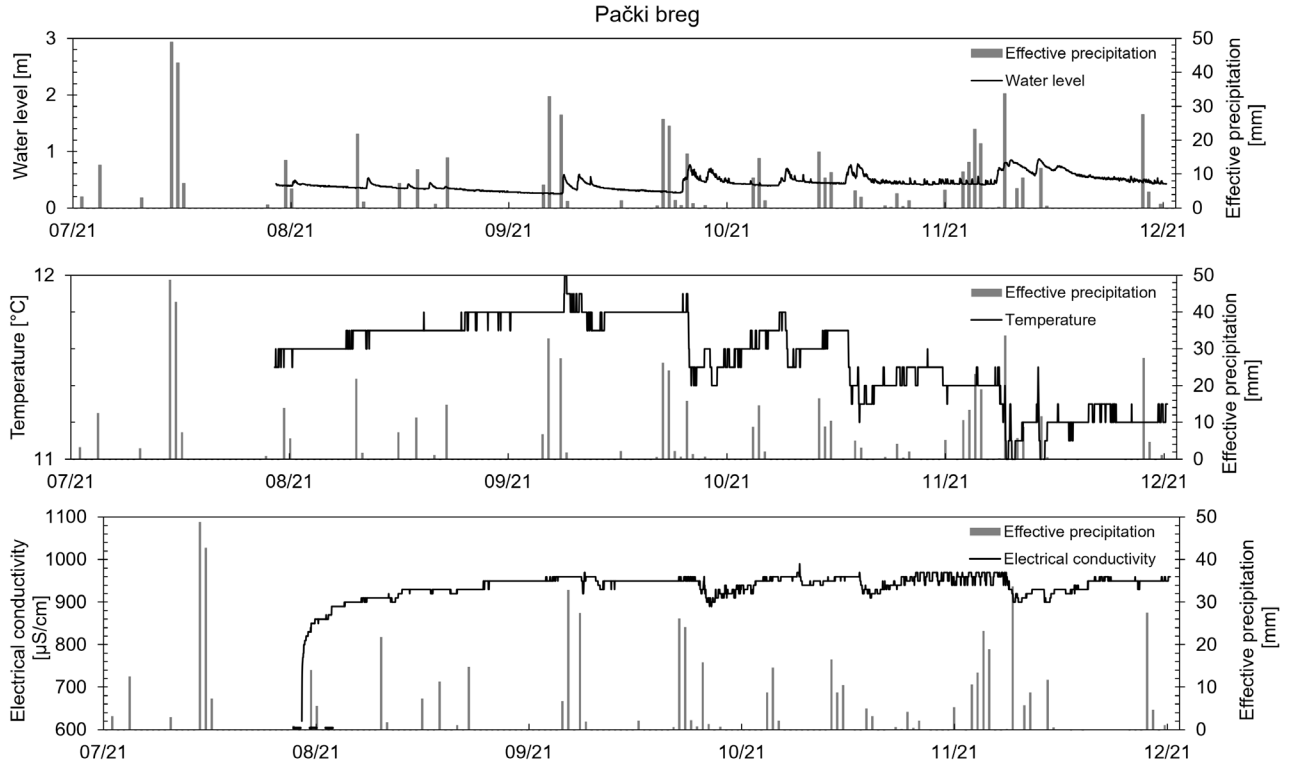

Fig. 4. Water level, temperature and electrical conductivity in Pački breg in comparison with effective precipitation.

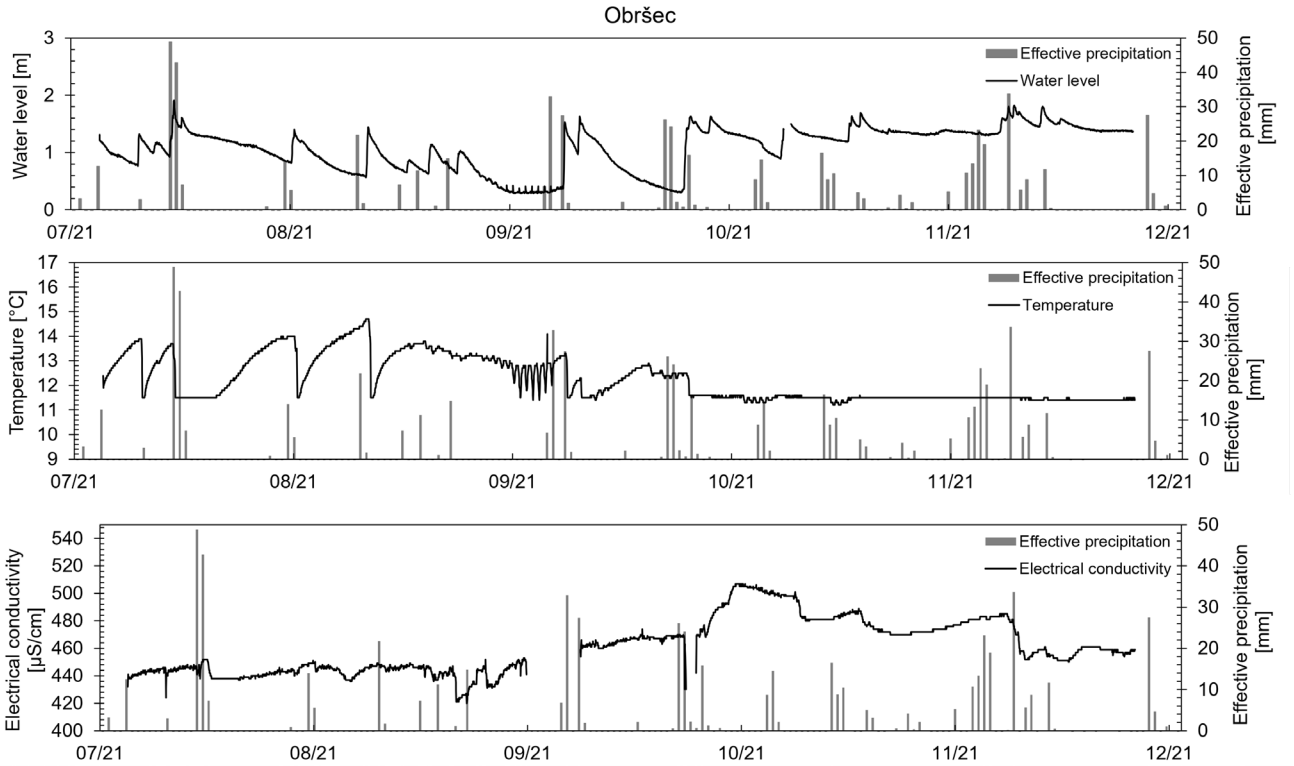

Fig. 5. Water level, temperature and electrical conductivity in Obršec in comparison with effective precipitation.

The highest water level in Pački breg spring (Fig. 4) was recorded in December (0.86 m) with the minimum evapotranspiration, and the lowest water level (0.25 m) in September, when the lowest total precipitation and highest water temperature were recorded. The highest water level in Obršec (1.91 m) (Fig. 5) was measured in July, when evapotranspiration and effective precipitation also reached their maximum. The lowest water level in Obršec (0.29 m) was recorded in September,

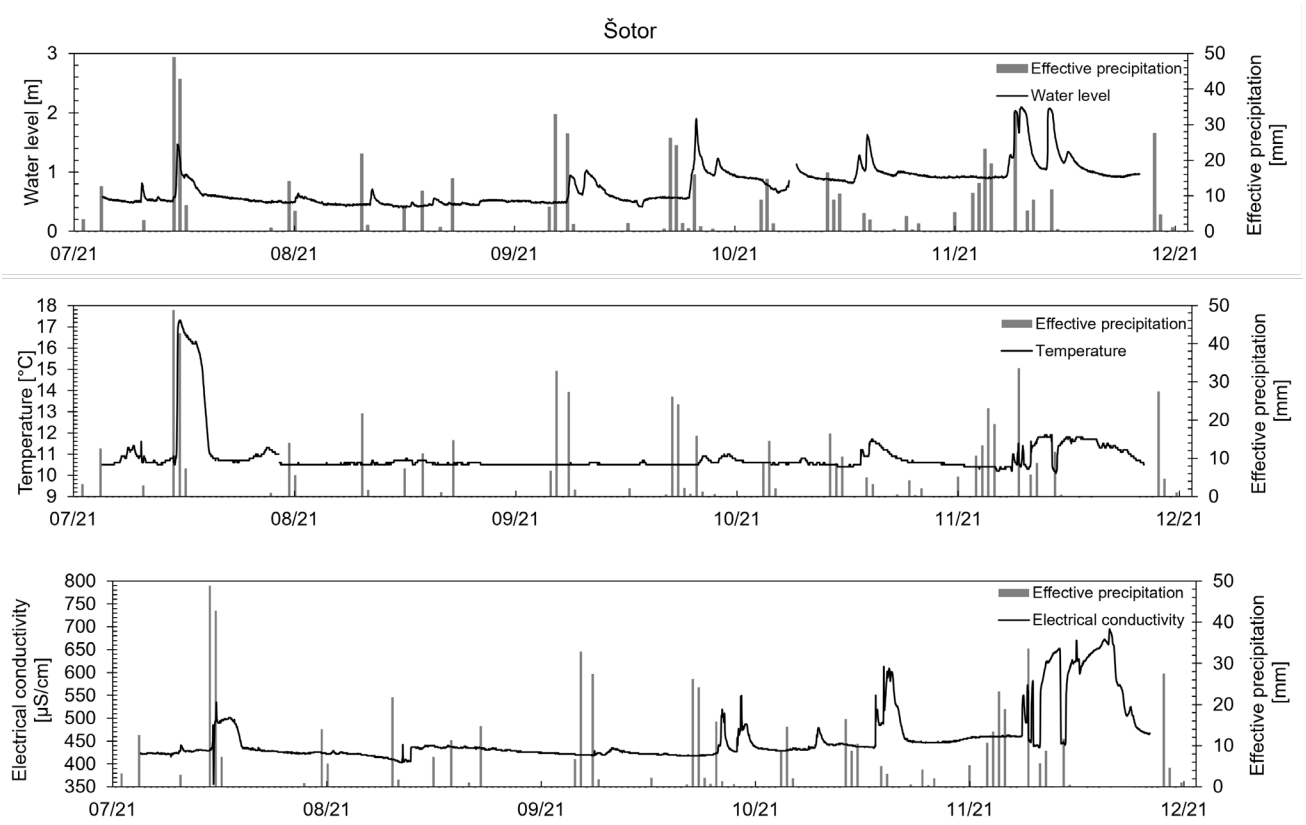

Fig. 6. Water level, temperature and electrical conductivity in Šotor in comparison with effective precipitation.

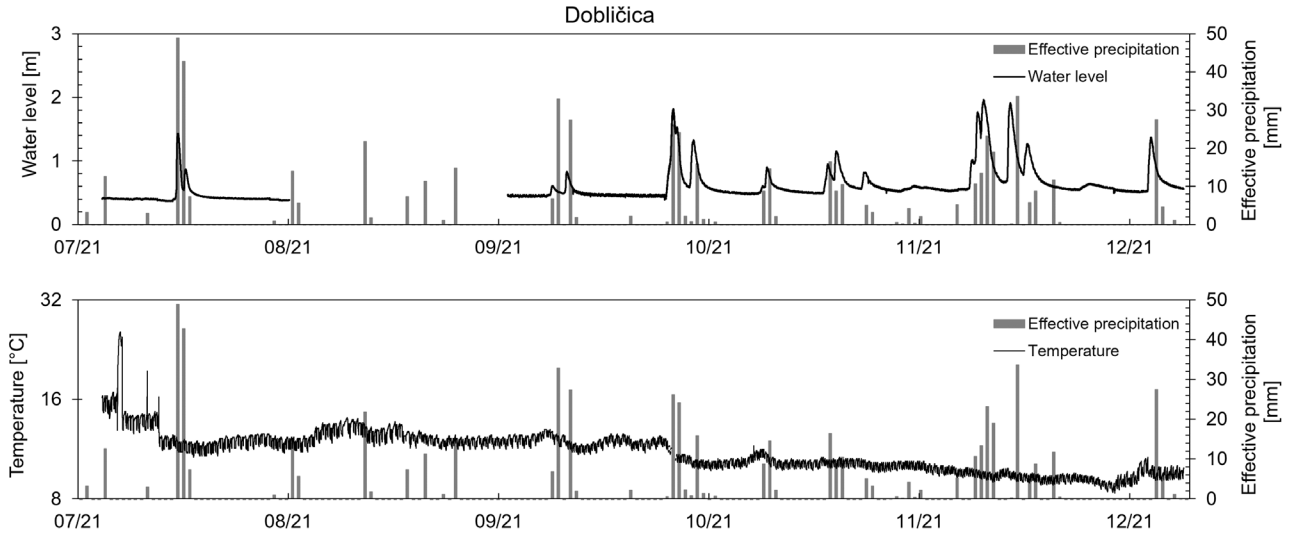

Fig. 7. Water level and temperature in Dobličica in comparison with effective precipitation.

like in Pački breg, when the lowest total precipitation was measured. The highest water level in Šotor (Fig. 6) was recorded in November (2.09 m) as well as in Dobličica spring (1.96 m) (Fig. 7), when maximum effective precipitation was also recorded. The lowest water level in Šotor (0.4 m) and Dobličica (0.37 m) was observed in August, coinciding with the lowest effective precipitation.

The maximum water temperature of the Šotor (Fig. 6) and Dobličica springs (Fig. 7) was recorded in July, and the minimum in December, along with the highest and lowest evapotranspiration rates. The highest water temperature in Pački breg (Fig. 4) was recorded in September (12.0 °C) in Šotor (Fig. 6) (17.3 °C) and Dobličica (Fig. 7) (25.6 °C - logger likely dry; other

maximum 12.4 °C) in July, and in Obršec in August (14.7 °C). The maximum water temperature exceeded the limit of 12 °C in Šotor spring in July (17.3 °C), several times in Obršec between July and October (14.7–12.8 °C) and in Dobličica also between July and October. Highest water temperatures were measured simultaneously with the highest evapotranspiration (Table 3).

The highest electrical conductivity in Pački breg was recorded in October (990 µS/cm). The lowest electrical conductivity in Pački breg (620 µS/cm) was in July, during the period of highest evapotranspiration. The highest electrical conductivity in Obršec (507 µS/cm) was, as in Pački breg, also recorded in October. In this spring the lowest electrical conductivity was detected in August (420 µS/cm), during the period of lowest effective precipitation. The highest electrical conductivity in Šotor was recorded in December (695 µS/cm), when minimum water temperatures and evapotranspiration were recorded. The lowest electrical conductivity in Šotor (357 µS/cm) was recorded in July, during the period of maximum evapotranspiration.

Response of water level to rainfall events

Based on the rainfall events determined in the period July – December 2021 and water level rise in a spring after a short time at the beginning of the rain event we calculated the water level rise rate (WLR) (Table 4). In average, among other springs in Obršec water level rise is the fastest (0.1 m/h) and in Pački breg the slowest (0.04).

Concentration of nitrates in springs

Nitrate concentrations measured weekly in collected water samples from the six monitored springs over a six-month period (July-December 2021) are shown in Figure 8. The basic statistical analysis and the highest and lowest maximum concentrations in the springs are shown in Table 5.

The highest concentration of nitrates in Pački breg (25.3 mg/l) and Otovski breg (29.2 mg/l) was recorded in September, when the lowest amount of total precipitation was recorded. The highest nitrate concentration in Pački breg (20.8 mg/l) was in October. In Šotor the highest concentration of nitrates was recorded in July (15.1 mg/l), as in Jamnice (29.2 mg/l), during the period of maximum evapotranspiration.

Since spring 2010, Jamnice (also named Jelševnik), Otovski breg, Pački breg, and Dobličica are included in the national monitoring of the qualitative status of groundwater. At the beginning, the national monitoring included sampling twice

Table 4. Water level rise rate (WLR) in Pački breg, Obršec, Šotor and Dobličica spring (July – December 2021) as a response to a rainfall event.

	Pački breg					**Obršec**					**Šotor**					**Dobličica**				
Month/ Year	WL_{start}	WL_{max}	Δt [h]	ΔWL [m]	**WLR [m/h]**	WL_{start}	WL_{max}	Δt [h]	ΔWL [m]	**WLR [m/h]**	WL_{start}	WL_{max}	Δt [h]	ΔWL [m]	**WLR [m/h]**	WL_{start}	WL_{max}	Δt [h]	ΔWL [m]	**WLR [m/h]**
07/21	/	/	/	/	/	16/7, 18:00	17/7, 11:00	17	0.99	**0.06**	16/7, 17:00	17/7, 10:00	17	0.96	**0.06**	16/7, 18:15	17/7, 14:15	23	1.04	**0.05**
08/21	17/8, 04:00	17/8, 10:00	6	0.16	**0.03**	17/8, 02:00	17/8, 10:00	8	0.88	**0.11**	17/8, 00:00	17/8, 08:00	8	0.26	**0.03**	/		/	/	/
09/21	17/9, 15:00	17/9, 18:00	3	0.29	**0.10**	17/9, 14:00	17/9, 19:00	5	1.12	**0.22**	17/9, 07:00	17/9, 20:00	13	0.45	**0.03**	17/9, 15:00	17/9, 21:00	6	0.12	**0.02**
10/21	6/10, 20:00	8/10, 00:00	28	0.47	**0.02**	6/10, 19:00	7/10, 17:00	22	1.24	**0.06**	6/10, 18:00	7/10, 21:00	27	1.31	**0.05**	6/10, 21:00	8/10, 01:00	29	1.33	**0.05**
12/21	2/12, 14:00	3/12, 00:00	10	0.26	**0.03**	2/12, 12:00	2/122, 23:00	11	0.35	**0.03**	2/12, 14:00	2/12, 20:00	6	0.99	**0.17**	2/12, 14:00	3/12, 02:00	12	1.22	**0.10**
Average WLR				0.04				0.1					0.07					0.05		

$\Delta t = t_{max} - t_{start}$ [h]

$\Delta WL = WL_{max} - WL_{start}$ [m]

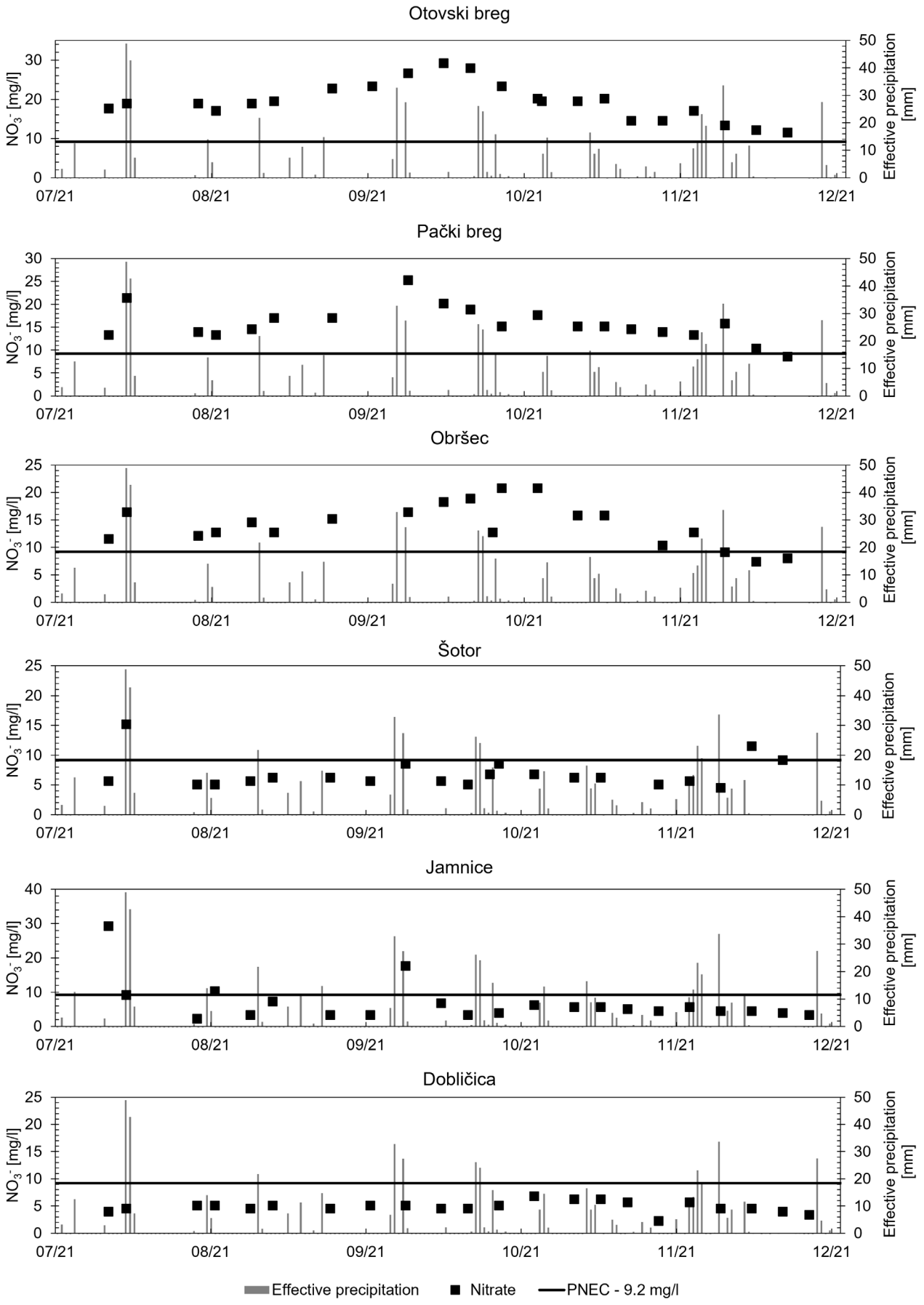

Fig. 8. Nitrate concentration in all observed springs with PNEC for olm.

Table 5. Highest and lowest monthly nitrate concentration in Pački breg, Otovški breg, Obršec, Šotor, Jamnice and Dobličica in the period of July – December 2021.

	Pački breg		Otovški breg		Obršec		Šotor		Jamnice		Dobličica	
	N=21		N=22		N=22		N=21		N=22		N=22	
Month/Year	Max	Min	Max	Min	Max	Min	Max	Min	Max	Min	Max	Min
07/21	21.4	13.3	18.9	17.6	16.4	11.5	15.1	5.6	29.2	9.1	4.5	3.9
08/21	17	14.5	19.5	18.9	14.5	12.1	6.2	5.6	7.3	3.3	5.1	4.5
09/21	25.3	17	29.2	22.7	18.2	15.1	8.5	5.6	17.6	3.3	5.1	4.5
10/21	18.9	15.1	27.9	19.5	20.8	15.8	8.5	5.1	6.2	3.3	6.8	4.5
11/21	15.8	13.3	27.9	13.3	15.8	9.1	6.8	4.5	5.6	4.5	6.2	2.2
12/21	10.3	8.5	12.1	11.5	9.1	7.4	11.5	9.1	4.5	3.3	4.5	3.3

Table 6. Basic statistical analysis and comparison of nitrate concentration of short-term observations (July – December 2021) and nitrate concentrations of national monitoring (2010–2018). Higher nitrate concentrations are marked in bold).

	median		mean		max	
NO_3^- (mg/l)	Jul–Dec 2021	(SEA 2022c) (2010–2018)	Jul–Dec 2021	(SEA 2022c) (2010–2018)	Jul–Dec 2021	(SEA 2022c) (2010–2018)
Jamnice	**4.76**	3.20 (Jelševnik)	**6.76**	3.27 (Jelševnik)	**29.22**	4.25 (Jelševnik)
Otovški breg	**19.18**	16.50	**19.36**	16.55	**29.22**	19.90
Pački breg	15.14	**15.20**	**15.71**	14.75	**25.27**	17.70
Dobličica	**4.76**	3.19	**4.79**	3.31	**6.78**	5.55

in a year. In the last few years sampling was performed just one time in a year. We compared, where possible, long-term national monitoring nitrate concentrations (2010–2018) in these springs, with the results of our weekly observations and performed a basic statistical analysis of the data (Table 6). We calculated the median, mean, and maximum value of nitrate concentrations for all data obtained for the long-term (2010–2018) and the short-term (July – December 2021). The higher values of nitrate concentration are represented in bold.

Discussion

Evapotranspiration, the sum of bare soil evaporation, plant transpiration, and evaporation from precipitation intercepted by the canopy (Pollard & Thompson, 1995) and rainfall determine the spatial and temporal distribution of groundwater recharge (Jukić & Jukić, 2015). Land cover, like vegetation, changes the evapotranspiration and consequently has an influence on groundwater recharge (Kovačič et al., 2020). Due to vegetation cover, evapotranspiration in that area has a higher impact on groundwater recharge.

Anthropogenic impact in this part of the karst area consists of some illegal landfill, the use of septic tanks in households and pouring manure on agricultural land. Decomposition under anaerobic conditions produces leachate saturated with organic matter, which is characterized by a relatively high temperature, different from the temperature of the surrounding surface (Breg Valjavec & Zega, 2017). Additionally, in complex karst aquifers, significant temperature changes under a variety of hydrological conditions are a consequence of the inflow of water from different parts of the recharge area (Petrič & Kogovšek, 2010). So water temperature can be considered as a natural tracer of groundwater flow (Saar, 2010).

The electrical conductivity of water could also be used as a groundwater tracing tool. Electrical conductivity is determined by the dilution by precipitation during rain events and can also be reflected in higher concentrations of pollutants. The peaks in the electrical conductivity of monitored springs are likely controlled by the washing of pollutants from unsaturated zone during rain event (Kogovšek, 2011; Chang et al., 2021). Intensive transfer of contaminants occurred when the more permeable fissures were flushed out, while some of the pollutants were retained in the less permeable part of the thick vadose zone (Kogovšek, 2011).

The rough estimation of water level response (WLR) in Šotor and Dobličica springs shows us the fast response in water level rise during a rain event in December, when the minimum evapotranspiration was recorded, which was considered as an indicator of the high impact of evapotranspiration on the Šotor and Dobličica spring recharge

dynamics. The highest (November) and lowest (July) effective monthly precipitation and water levels in Šotor and Dobličica spring were recorded in the same month. This basic assessment again demonstrates the important role of land cover in the Šotor and Dobličica recharge area. The highest (July) and lowest (September) amounts of total precipitation and the highest and lowest water levels in the Obršec spring further indicate less impact from evapotranspiration and more direct infiltration, as well as the existence of a small independent catchment area of the Obršec spring, as previously proposed by Habič (1991a) and Novak (1996).

The nitrate ion (NO_3^-), and consequently, nitrate toxicity for aquatic animals, is due to nitrate ions (Camargo & Alonso, 2006). Based on these facts nitrate could be one of the potential critical parameters affecting the proposed threshold concentration (PNEC), estimated at 9.2 mg/l NO_3^- (NLZOH, 2017). The nitrate ion occurs naturally in the nitrogen cycle and during nitrification but is also present in fertilizers in various forms. The most common anthropogenic sources of nitrate in groundwater are livestock and other agricultural production, wastewater, old landfills and illegal dumps, and fertilization with artificial fertilizers or digestate (NLZOH, 2017). The nitrate concentration above PNEC could be a major problem in Otovski breg, Pački breg, and Obršec, as concentrations throughout most of the entire monitoring period (July – November) was exceeded, and occasionally also in Šotor and Jamnice (July 2021). There are no problems with high nitrate concentrations in Dobličica, as its catchment area is protected by the decree on water protection, wherein certain environmental interventions are not allowed (e.g. agriculture). The highest concentration of nitrates was recorded in October in Dobličica, which did not exceed a concentration level of 7 mg/l (6.8 mg/l). Based on the geological and hydrogeological characteristics of Dobličica, low nitrate concentrations could be the result of the higher dilution rate seeing as it has the largest catchment area of all studied springs (Habič et al., 1991; Šinigoj et al., 2012). The main factor behind the high nitrate concentrations in the July – November period in Otovski breg and Pački breg could be agriculture, as in the case of Obršec, which includes an unregulated communal system (Habič et al., 1991a) in the catchment area. In most of the springs, the lowest maximum nitrate concentrations were recorded in December, which could be the result of little or no agricultural activity at that time of the year. A potential measure that could serve to ease nitrate concentrations would be to protect the springs with a decree limiting activities that contribute to high nitrate concentrations in the catchment area of such springs. One of the proposed measures should be the regulation of wastewater drainage or the arrangement of a public sewage system. Also working with farmers on developing new fertilization techniques could contribute to a solution.

We also compared the median, mean, and maximum nitrate concentrations of long-term national monitoring of the qualitative status of groundwater with low frequency of water sampling and short-term high-resolution sampling and measurements of nitrate concentrations. The comparison shows higher nitrate concentrations in the case of high-resolution sampling. In three of the compared springs – Jelševnik, Obršec and Otovski breg – nitrate concentrations are higher in the case of high-resolution sampling, whereas the median nitrate concentration in Pački breg is the exception. Owing to their high solubility and mobility, nitrates respond far more quickly and strongly to changes in hydrologic conditions and land use (Hem, 19985). So, in karst aquifers, low-resolution monitoring of nitrates is unlikely to adequately characterize the system, especially during rainfall events (Pu et al., 2011).

To assess the possible hydrogeological connection between the studied springs, preliminary results of detailed geological mapping at a scale of 1:5000 were used (Mušič et al., 2023). These data show some inconsistencies with previous geological maps of the area (Bukovac et al., 1984a, 1984b; Šinigoj et al., 2012) in terms of stratigraphy and structural relationships between fault zones. Therefore, only field verified (Mušič et al., 2023) fault zones were included in our interpretation. Thus, the majority of the connections currently evaluated are based primarily on the hydrogeologic data collected. The basic hydrogeological characteristics of the Otovski breg are similar with that of Pački breg, as variations in nitrate concentrations in these two springs are similar over the entire observation period. The connection between Otovski breg and Pački breg has already been confirmed by previous tracer tests (Habič, 1991b). Although in Otovski breg and Jamnice only nitrate concentrations were monitored, a hydrogeological connection is also likely between the springs of Jamnice and Šotor. Nitrate concentrations fluctuate similarly in both springs and are low compared to the rest of the monitored springs. Comparisons of water levels, WLR, as well as nitrate concentrations in Šotor and Dobličica springs also show

similar spring dynamics. The Obršec spring has its own smaller catchment area and reacts quickly to precipitation, which drains in the NNE–SSW oriented fault zone (Bukovac et al., 1984a, 1984b; Šinigoj et al., 2012; Mušič et al., 2023).

Conclusion

The results of this study support the established knowledge of the dynamics that characterize the karst springs in Bela Krajina, habitat of the black and white olm, and help to reveal the main problems that affect its conservation status. In order to try and solve the problem of the decline of the olm, it was first necessary to assess the basic hydrogeological characteristics of the six observed springs west of Črnomelj in Bela krajina – the habitat of the black and white olm – and to determine whether there were any possible geological or hydrogeological connections between the observed springs.

Due to their different hydrogeological characteristics, the springs react to weather phenomena differently, but some, like Pački and Otovski breg, have very similar dynamics, as do the Šotor and Dobličica springs. In the next step we evaluated the potential critical factors and water-related parameters (nitrate concentration and temperature). The next step would require finding and specifically defining the causes or critical water parameters using quantified threshold values and to take appropriate measures to slow or even halt entirely the decline of the olm. Nitrate concentrations throughout most of the entire monitoring period exceed the maximum threshold in Otovski breg, Pački breg and Obršec, and occasionally also in Šotor and Jamnice. During July – August (2021), the water temperature of the springs exceeded 12 °C in all four of the monitored springs.

The comparison of high and low-resolution sampling indicates the importance of the high-resolution monitoring in karst areas, where the runoff and groundwater flow are much faster compared to the flow in the intergranular aquifer.

Further research is needed to constrain the hydrogeological parameters over longer periods and to supplement our data using additional springs in the area. Said detailed hydrogeological data should also be further supplemented with a new detailed geological map of the area. It is necessary to define the origin of nitrate (nitrate isotope analysis), quantify threshold values of the critical parameters, specifically define all the causes of olm deterioration, and make proposals for the appropriate measures to limit or even stop the olm population decrease.

Authors contributions

The authors' contribution is as follows: Katja Koren and Rok Brajkovič contributed to the conceptualization, analysis of data, writing, and review of the article. Authors Manca Bajuk, Špela Vraničar, and Vesna Fabjan, who participated in the present research as a Citizen Science Team, contributed through field observations, measurements, sampling, and participated in the discussion of the measurements. All authors read and agreed to the published version of the manuscript.

Acknowledgments

This study was financially supported by the Slovenian Research Agency (research core funding Groundwaters and Geochemistry (P1-0020), Mineral Resources (P1-0025) and by the Slovenian Water Agency with the project Development of a support system for decision-making on the use of groundwater (2555-20-470115) regarding groundwater-dependent ecosystems, including olms. For access to the sampling sites, we extend special thanks to the Zupančič farm and tourism Jelševnik and Komunala Črnomelj (Public Utility Company). Additionally, we would like to thank the Reviewers for their valuable comments, which significantly contributed towards the improvement of the manuscript.

References

Aljančič, G., Gorički, Š., Năpăruş, M., Jeffery, W., R., Kuntner, M. & Lokovšek, T. 2014: A survey of distribution of Proteus Anguinus by environmental DNA sampling. Društvo za jamsko biologijo/ Society for Cave Biology. 10 p. Internet: https://www.cepf.net/sites/default/files/edna_prezentacijacitluk.pdf (1. 2. 2022).

Breg Valjavec, M. & Zega, M. 2017: Zasute vrtače – Potencialna nevarnost za vodne vire. In: Globevnik, L. & Širca, A. (eds.): Voda povezuje, Drugi slovenski kongres o vodah, Podčetrek 19.–20. 4. 2017.

Bukovac, J., Poljak, M., Šušnjar, M. & Čakalo, M. 1984a: Osnovna geološka karta SFRJ 1:100 000. Tolmač lista Črnomelj. Zvezni geološki zavod, Beograd: 63 p.

Bukovac, J., Poljak, M., Šušnjar, M. & Čakalo, M. 1984b: Osnovna geološka karta SFRJ 1:100.000. List Črnomelj. Zvezni geološki zavod, Beograd.

Camargo, J.A. & Alonso, A. 2006: Ecological and toxicological effects of inorganic nitrogen pollution in aquatic ecosystems: A global assessment. Environment International,

32: 831–849. https://doi.org/10.1016/j.envint.2006.05.002

Chang, Y., Hartmann, A., Liu, L., Jiang, G. H. & Wu, J. C. 2021: Identifying More Realistic Model Structures by Electrical Conductivity Observations of the Karst Spring. Water Resources Research, 57. https://doi.org/10.31219/osf.io/gw876

Council Directive 92/43/EEC of 21 May 1992 on the conservation of natural habitats and of wild fauna and flora (Habitats directive).

Čar, J. 2018: Geostructural mapping of karstified limestones. Geologija, 61/2: 133–162. https://doi.org/10.5474/geologija.2018.010

Gorički, Š., Stanković, D., Snoj, A., Kuntner, M., Jeffery, W.R., Trontelj, P., Pavićević, M., Grizelj, Z., Năpăruş-Aljančič, M. & Aljančič, G. 2017: Environmental DNA in subterranean biology: range extension and taxonomic implications for Proteus. Sci. Rep. 7, 4505. https://doi.org/10.1038/srep45054

GERK 2023: Javni pregledovalnik grafičnih podatkov MKGP. https://rkg.gov.si/GERK/WebViewer/ (February 2023).

GURS 2016: Inhabited area. Kataster stavb. https://eprostor.gov.si/imps/srv/slv/catalog.search#/metadata/5aa2b97b-2ea3-427f-a9fb-d7827c61c115 (February 2023).

Habič, P., Kogovšek, J., Bricelj, M. & Zupan, M. 1991a: Izviri Dobličice in njihovo širše kraško zaledje. Acta carsologica, 17/19: 5–100.

Habič, P., Kranjc, A., Kogovšek, J., Bricelj, M., Zupan, N., Drole, F., Drame, L. & Zadel, M. 1991b: Raziskovanje Dobličice in Krupe, 5. del, poročilo za leto 1990. Znanstvenoraziskovalni center SAZU, Postojna: 82 p.

Hem, J.D. 1985: Study and interpretation of the chemical characteristics of natural water. US Geological Survey, Water Supply Paper, 2254: 1–263.

Jensen, F.B. 1996: Uptake, elimination and effects of nitrite and nitrate in freshwater crayfish (Astacus astacus). Aquatic Toxicology, 34, 95–104.

Juberthie, C., Durand, J. & Dupuy, M. 1996: Reproduction of Proteus anguinus: results of 35 years of rearing in laboratory-caves of Moulis and aulignac (France). Mémoires de biospéologie, 23: 53–56.

Jukić, D. & Denić-Jukić, V. 2015: Investigating relationships between rainfall and karst-spring discharge by higher-order partial correlation functions. Journal of Hydrology, 530: 24–36. https://doi.org/10.1016/j.jhydrol.2015.09.045

Kogovšek, J. 2000: Ugotavljanje načina pretakanja in prenosa snovi s sledilnim poskusom v naravnih razmerah. Annales, 10/19: 133–142.

Kogovšek, J. 2011: The role of the vadose zone in the transfer of pollution through karst aquifers to karst springs. In: Gabrovšek, F. (eds.): Karstology and development challenges on karst - Water, Karst Research Institute ZRC SAZU, Postojna: 21–37.

Kovačič, G., Petrič, M. & Ravbar, N. 2020: Evaluation and Quantification of the Effects of Climate and Vegetation Cover Change on Karst Water Sources: Case Studies of Two Springs in South-Western Slovenia. Water, 12/11: 3087. https://doi.org/10.3390/w12113087

Mezga, K., Janža, M., Prestor, J., Koren, K. & Šram, D. 2016: Groundwater dependent ecosystems – groundwater status indicators. Natura Sloveniae, 18: 35–42.

Mezga, K., Janža, M., Šram, D. & Koren, K. 2015: Pregled ekosistemov odvisnih od stanja podzemnih vod. Priprava strokovnih podlag in strokovna podpora pri izvajanju vodne direktive za področje podzemnih voda (Direktiva 2000/60/EC); 2. UKREP DDU26: Analiza razpoložljivih zalog podzemne vode in površinske vode ter obstoječe in predvidene rabe vode za obdobje do 2021. Ljubljana: Geološki zavod Slovenije.

Mušič, M., Dvorščak, L., Fariselli, S., Rome, T., Štern, M., Grum Verdinek, L., Brajkovič, R., Rožič, B. & Žvab Rožič, P. 2023: Student geological mapping of the Black olm habitat and its catchment area in Bela krajina. In: Švara, A., Zupan Hajna, N. & Gabrovšek, F. (eds.): 30th International Karstological School "Classical Karst", ZRC SAZU: 135-136.

NLZOH, 2017: Ocena tveganja, ki ga predstavlja nitrat za ekosisteme podzemne vode in za človeško ribico na projektnem območju LIFE Kočevsko. 25. Nacionalni laboratorij za zdravje, okolje in hrano, Center za okolje in zdravje Maribor: 20 p.

Novak, D. 1996: Padavinsko zaledje izvira Jelševniščice. Naše jame, 38: 105–110.

Petrič, M. & Kogovšek, T. 2010: Water temperature as a natural tracer – a case study of the Malenščica karst spring (SW Slovenia). Geologia Croatica, 63/2: 171–177. https://doi.org/10.4154/gc.2010.14

Petrič, M., Ravbar, N. & Kogovšek, T. 2011: Characteristics of karst aquifers, their vulnerability and endangerment. In: Gabrovšek, F. (eds.): Karstology and development challenges on

karst - Water, Karst Research Institute ZRC SAZU, Postojna. 8–19.

Placer, L. 2008: Principles of the tectonic subdivision of Slovenia. Geologija, 51/2: 205–217. https://doi.org/10.5474/geologija.2008.021

Pollard, D. & Thompson, S.L. 1995: Use of a land-surface-transfer scheme (LSX) in a global climate model: the response to doubling stomatal resistance. Global and Planetary Change, 10:129–161. https://doi.org/10.1016/0921-8181(94)00023-7

Pu, J., Yuan, D., He, Q., Wang, Z., Hu, Z. & Gou, P. 2011: Highresolution monitoring of nitrate variations in a typical subterranean karst stream, Chongqing, China. Environtal Earth Science, 64: 1985–1993. https://doi.org/doi:10.1007/s12665-011-1019-7

Ribeiro, D. & Tičar, J. 2017: The problematics of cave pollution in Bela krajina / »SOS Proteus« – Field Note. Natura Sloveniae, 19/1: 43–45.

Saar, M.O. 2010: Review: Geothermal heat as a tracer of large-scale groundwater flow and as a means to determine permeability fields. Hydrogeology Journal, 19: 31–52. https://doi.org/10.1007/s10040-010-0657-2

Scott, G. & Crunkilton, R.L. 2000: Acute and chronic toxicity of nitrate to fathead minnows (Pimephales promelas), ceriodaphnia dubia, and Daphnia magna. Environmental Toxicology and Chemistry, 19: 2918–2922. https://doi.org/10.1002/etc.5620191211

SEA 2022a: Črnomelj – Dobliče. Referenčna evapotranspiracija in padavine samodejnih postaj (dnevni podatki od leta 2017). Internet: https://meteo.arso.gov.si/met/sl/agromet/data/arhiv_etp/ (10. 2. 2022).

SEA 2022b: Meteorološki parametri Črnomelj – Dobliče. ARHIV – opazovani in merjeni meteorološki podatki po Sloveniji. Internet: https://meteo.arso.gov.si/met/sl/archive/ (10. 2. 2022).

SEA 2022c: Kakovost podzemnih voda. Internet: https://gis.arso.gov.si/portal/apps/webappviewer/index.html?id=a16308bd37344559b1c5d5e515468f49 (10. 2. 2022).

Sket, B. 1997: Distribution of *Proteus* (Amphibia: Urodela: Proteidae) and its possible explanation. Journal of Biogeography, 24/3: 263–280. https://doi.org/10.1046/j.1365-2699.1997.00103.x

Šinigoj, J., Lapanje, A. & Poljak, M. 2012: Geologija območja zaledja Dobličice. Dolenjski kras, 6: 46–52.

Vlahović, I., Tišljar, J., Velić, I. & Matičec, D. 2005: Evolution of the Adriatic Carbonate Platform: Palaeogeography, main events and depositional dynamics. Palaeogeography, Palaeoclimatology, Palaeoecology, 220/3–4: 333–360. https://doi.org/10.1016/j.palaeo.2005.01.011

Voituron, Y., de Fraipont, M., Issartel, J., Guillaume, O. & Clobert, J. 2011: Extreme lifespan of the human fish (Proteus anguinus): a challenge for ageing mechanisms. Biology letters, 7/1: 105-107. https://doi.org/10.1098/rsbl.2010.0539

GEOLOGIJA 66/1, 167-183, Ljubljana 2023
https://doi.org/10.5474/geologija.2023.007

Geological-genetic structure of Irpin city, the role of lithological factors during engineering-geological zoning and construction assessment

Geološko-genetska zgradba mesta Irpin, vloga litoloških dejavnikov pri inženirsko-geološkem določanju con in oceni gradnje

Pavlo ZHYRNOV[1] & Iryna SOLOMAKHA[2]

[1]Design Institute of Security Service of Ukraine, str. Zolotovorytska, 5, 01030 Kyiv, Ukraine;
e-mail: sbu-misto@ukr.net
[2]Ukrainian State Scientific Research Institute of Cities' Design "DIPROMISTO" named after Y.M. Bilokonya,
blvd.LesiUkrainky, 26, 01133 Kyiv, Ukraine;
e-mail: gis@dipromisto.gov.ua

Prejeto / Received 21. 9. 2022; Sprejeto / Accepted 4. 4. 2023; Objavljeno na spletu / Published online 4. 8. 2023

Key words: engineering-geological zoning, engineering-geological units, geological-genetic structure, engineering-geological map, construction assessment
Ključne besede: inženirsko-geološka rajonizacija, inženirsko-geološke enote, geološko-genetska zgradba, inženirsko-litološka karta, gradbena ocena

Abstract

The scheme of engineering-construction assessment created based on engineering-geological zoning of the city's territory is desirable among additional graphic materials in the design of master plans projects as determined by building regulations. Engineering-geological zoning provides for different ranks' selection of engineering-geological units (EG units), which have a particular range of common engineering-geological conditions that ultimately determine the construction sites' affiliation to a specific suitability category. Geological-genetic structure of Irpin city of Kyiv region (Ukraine) is explored in this article. A variant of the creation of a large-scale engineering-geological map and corresponding geological-lithological sections by supporting boreholes in the borders of the city based on the engineering-geological survey conducted is presented. The obtained result allowed the selection of engineering geological zoning units – engineering geological districts by general conditions of geological development and subdistricts by engineering-geological complexes of Quaternary rocks' thickness. The analysis of soils' geomechanical properties (engineering-geological elements) lays the foundations for the selection of engineering-geological sites based on the comparison of this information with geomorphological, hydrogeological and geodynamic data. Accounting of geological-lithological factors in the preparation of the construction assessment scheme in the project of Irpin city's master plan has become the ultimate result.

Izvleček

Shema inženirsko-gradbene presoje, ki je ustvarjena na podlagi inženirsko-geološkega razvrščanja mestnega ozemlja, je zaželena informacija, ki bi bila na voljo projektantom pri izdelavi gradbenega projekta. Inženirsko geološko razvrščanje predvideva različno rangiranje inženirsko geoloških enot (EGE), ki imajo skupne nekatere osnovne inženirsko-geološke lastnosti, ki vplivajo na gradnjo objektov. V tem članku je raziskana inženirsko-geološka sestava tal mesta Irpin v Kijevski regiji (Ukrajina). Predstavljena je varianta izdelave obsežne geološko-litološke karte in ustreznih geoloških litoloških prerezov z vključenimi podatki iz raziskovalnih vrtin, izvedenimi za inženirsko-geološke raziskave različnih predelov mesta. Dobljeni rezultat je omogočil rangiranje tal glede na inženirsko-geološke zahteve glede temeljenja objektov. V naslednjem koraku se tla rangirajo še na debelino kvartarnih plasti. Analiza geotehničnih lastnosti zemljin (inženirsko-geoloških elementov) postavlja osnovo za izbiro primernih lokacij za gradnjo na osnovi inženirsko-geoloških podatkov pridobljenih z geomorfološkimi, hidrogeološkimi in geosezmičnimi podatki. Končni rezultat raziskave je ocena tal glede na primernost gradnje v mestu Irpin.

Introduction

In the design of projects' master plans building regulations determine that among some additional town-planning documentation the engineering construction assessment scheme is desirable and that scheme takes into account natural and anthropogenic factors that define construction sites' suitability for urban development (Building regulations B.1.1-15:2012, 2012). Estimated natural and technogenic factors (geological processes triggered by civil engineering activity that harm building structures: technogenic waterlogging, eutrophication, technogenic landslides, water erosion, ground subsidence, etc. (Shnyukov et al., 1993) of engineering-construction assessment should include geomorphological characteristics, geologic-lithological structure, geomechanical properties of rocks, hydrogeological circumstances, microseismic circumstances, etc. (Zhyrnov et al., 2019).

Engineering-geological maps are a generalized image on a topographic base of a complex of geological parameters, the interaction of which determines the engineering-geological conditions, the specifics of surveys, construction and operation of engineering structures. The most important of engineering-geological conditions in the maps are the basis for the engineering construction scheme's elaboration, namely the geological structure of the territory, lithological composition, hydrogeological conditions and current natural and technogenic geological processes. Engineering-geological zoning maps have particular importance among engineering-geological maps for engineering construction assessment. They are drawn up as a result of identification in the space based on theoretical positions' combination and methodological procedures of objectively existing territorial elements that have common engineering-geological features of their delineation from territories that haven't such features, their mapping and description. Different-order engineering-geological units are allocated during the regional type of engineering-geological zoning and each next unit is allocated from the previous (larger) by dividing it into separate parts based on specific classification features (Trofimov & Krasilova, 2008).

A significant role belongs to EG units that are allocated by geological-genetic and lithological features during engineering-geological zoning. Geological-genetic and lithological structure of the territory plays the main and crucial role in the engineering-geological substantiation of construction projects, determination of the type of buildings' foundations, planning the features of building operation and their reverse impact on the ecological state of the geological environment (Bell, 2007). Therefore, there is an urgent need to characterize the geological-genetic and lithological structure of the deposits used for construction.

Identification of engineering-geological districts and subdistricts, as well as preconditions for the selection of engineering-geological sites based on detailed geomorphological, geological-genetic and lithological characteristics using the example of Irpin city, Kyiv region (Ukraine) is the purpose of this article. Determination of the place of lithological factors in the structure of engineering-geological zoning and complexity categories of geologic-lithological conditions for construction assessment are also the objectives of this article.

Attempts of engineering-geological zoning detailing with geologic-lithological features' accounting have been implemented in Tunis city, (El May et al., 2010) Split city (Šestanović et al., 2012) Moscow city, (Osipov et al., 2012) Velopolja region, (Muceku, 2010) Fortaleza region, (Zuquette et al., 2004). We took into account the scientific experience of the predecessors and offer our opinion on the consideration of geologic-lithological factors in the engineering-geological zoning for urban planning.

One of the previous articles (Zhyrnov & Solomakha, 2022) provides an example of a completed engineering-geological zoning of the Irpin city. However, in this study, there is not enough information about the geomechanical properties of engineering-geological elements, there are no recommendations for choosing the types of foundations for buildings and structures, and protective measures for buildings located in areas with a high level of groundwater are not introduced. In previous work is no accounting for the category of complexity of geological-lithological conditions for engineering-construction assessment. In addition, here we will dwell in more detail on the principles for selection such important engineering-geological units as districts and subdistricts. The current article aims to fill these important gaps.

Study area

Irpin city administratively is situated in the central part of the Kyiv region at a distance of 7 km northwest of Kyiv, which is Ukraine's capital (Fig. 1).

Irpin city is situated in the southwest part of the East European Plain in the limits of Kyiv Polesia as a part of the Polesian Lowland. According

Fig. 1. Irpin city in the central part of Kyiv region, Ukraine.
Sl. 1. Mesto Irpin v osrednjem delu Kijevske regije, Ukrajina.

to the geomorphological map (scale 1: 55 000) of Ukraine, the investigated territory corresponds to Makariv moraine fluvioglacial wavy slightly dissected plain between Irpin's, Buchanka's, Teteriv's and Zdvyzh's River valleys. Knowing the physical-geographical and administrative location of the city, it is easy to identify that according to principles of engineering and geological classification, Irpin is situated in the limits of East-European Craton, the north-east slope of Ukrainian Shield province, Kyiv Polesia subprovince, engineering geological region of Makariv moraine fluvioglacial wavy slightly dissected plain (Paton et al., 2007). There are such engineering geological districts in the limits of Irpin according to engineering geomorphological zoning of Kyiv city district's map: erodible and depositional alluvial plain and denudation-depositional watershed moraine and fluvioglacial plain (Barshchevsky et al., 1989).

Upper- and Holocene Quaternary Q_{III}-Q_{IV} erodible and depositional alluvial plain with absolute altitudes of 107–118 m. Middle Quaternary Q_{II} denudation-depositional watershed moraine fluvioglacial plain with absolute altitudes of 120–160 m. In the borders of the erodible and depositional alluvial plain are allocated: 1) Alluvial floodplain flat inundated terrace of Buchanka and Irpin Rivers of Holocene age with swamped areas and peat depressions of Holocene age; 2) Alluvial upper Holocene, slightly dissected first above-flood terrace of Buchanka and Irpin Rivers. In the borders of the denudation-depositional watershed moraine, fluvioglacial plain is allocated: 1) Plateau and highland of moraine fluvioglacial wavy and slightly dissected plain of Dnipro age with corresponding absolute altitudes of 135–160 m; 2) Lowland part of moraine fluvioglacial wavy and slightly dissected plain of Dnipro age with absolute altitudes of 120–135 m; 3) Arroyos' bottoms and detrital cones of Holocene age; 4) Sites with artificially modified relief (Tsybko, 2020).

Flooding in the Buchanka and Irpin Rivers' floodplains, waterlogging in the borders of the floodplain and the first terrace of the Buchanka and Irpin Rivers are part of the dangerous hazards in the Irpin. Waterlogging is connected with a naturally high level of groundwater, floodplain flooding during spring and also the unloading of aquifers in permanent and temporary watercourses. Eutrophication occurs in the Buchanka and Irpin Rivers' floodplain and is connected with spring floods and unloading of aquifer related to Middle-Quaternary fluvioglacial deposits of dividing range. River erosion is generally weak along the Irpin and Buchanka Rivers and occurs at local sites during spring. Eolian sand deflation is observed on some sites of the floodplain and first terraces of the Irpin and Buchanka Rivers (northeast and northwest city outskirts) (Tsybko, 2020).

Significant hydration of Quaternary deposits and high groundwater level, which provokes flooding, waterlogging and eutrophication are the main obstacles to urban development (Rudenko et al., 1971).

Comparison of data on the territory's morphogenetic structure and areas of development of natural hazards made it possible to build a geomorphological map of Irpin city (Zhyrnov & Solomakha, 2022) (Fig. 2).

The morphogenetic and morphological structure of the relief lays the foundations for the selection of engineering-geological districts and subdistricts, but it is necessary to distinguish corresponding geological-genetic complexes of Quaternary sediments within the erosion-accumulative alluvial plain and the denudation-accumulative watershed moraine water-glacial plain and determine the lithological composition of the mentioned Quaternary deposits for the relief's morphological elements.

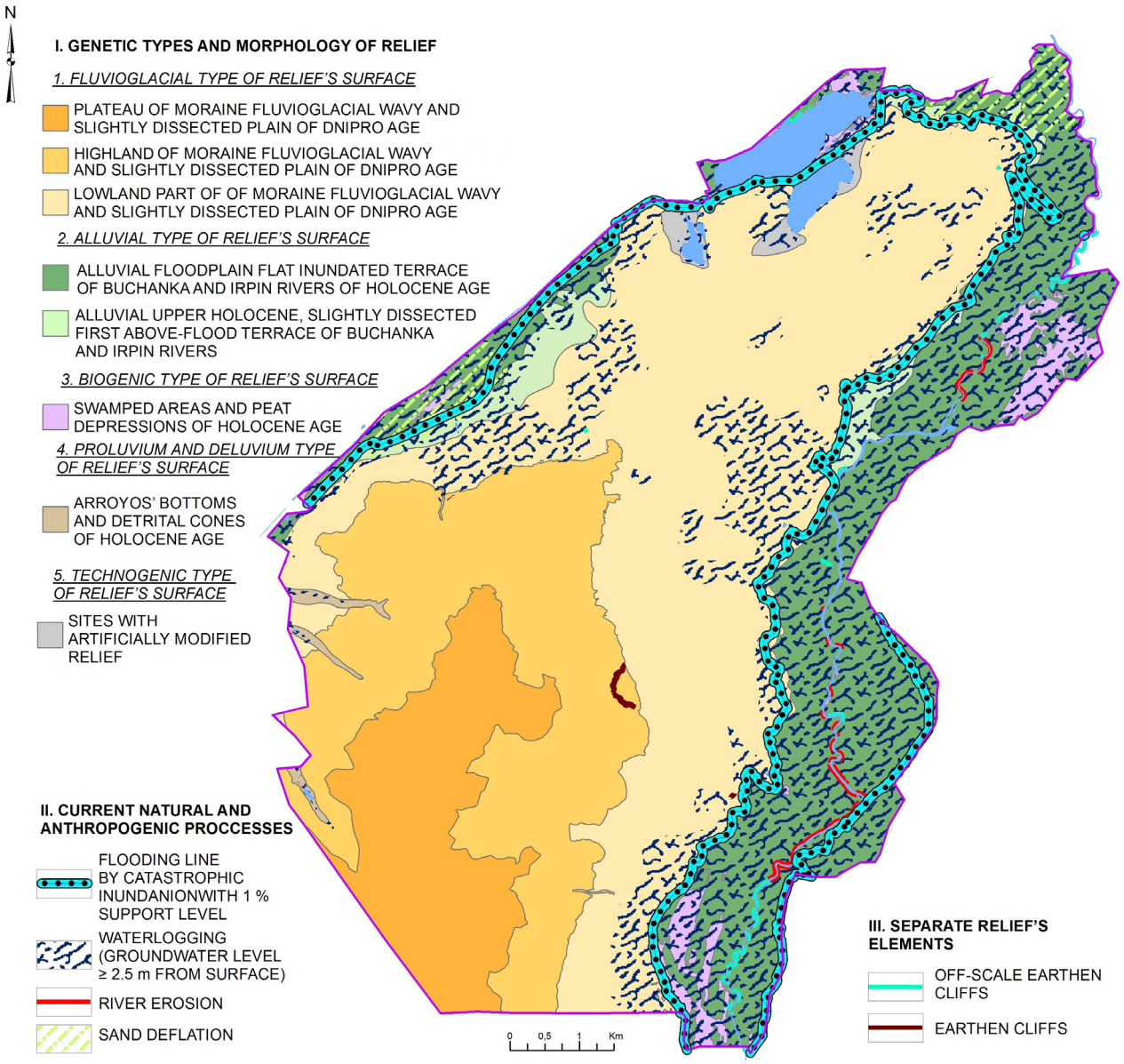

Fig. 2. Geomorphological map of Irpin city (Zhyrnov & Solomakha, 2022).
Sl. 2. Geomorfološka karta mesta Irpin (Zhyrnov & Solomakha, 2022).

Materials and methods

There are such initial data for engineering-geological mapping: a topographic survey of Irpin city on a scale of 1: 5000, a geological map on a scale of 1: 50 000 on sheets of Kyiv region, (Solovytsky & Vozgryn, 1990) project of the master plan of Irpin city (Gubenko et al., 2017), state geological map of Ukraine – 200 (Ivanenko, 2020), a geological map of Ukraine (Panchenko, 2019), materials of engineering-geological investigations between 1990 and 2020 years under construction for residential and public buildings that have been made by different design organization and companies. 154 geotechnical reports were analyzed, and those materials were collected and systematized at SE "Ukrainian Institute of Engineering Technical Exploration for Construction" (UKRIINTR) (Tsybko, 2020).

The principles of engineering-geological zoning were most fully developed by Ivan Popov, who proposed to distinguish engineering-geological regions, oblasts, districts and subdistricts of various orders as independent taxonomic units.

Engineering-geological regions are distinguished by structural-tectonic features. The engineering-geological region of the first order is the largest taxonomic unit. The second-order region, namely the engineering-geological province, is distinguished by its morphostructure and hydrogeological structure. The region of the third order (subprovince) is distinguished based on the morphogenetic type of the territory of the first order (Popov, 1951).

Popov proposed to distinguish engineering-geological areas within one region based on geomorphological features. With this approach, the geomorphological features of the territory are a consequence of the history of its geological development, mainly in recent times. We can say that engineering-geological regions are territories that are distinguished by geostructural features as a result of the analysis of the history of the geological development of this territory for the entire time available to us, and engineering-geological oblasts are parts of regions that have had different development in recent times, which was reflected in their geomorphological features (Popov, 1951). So, engineering-geological oblasts are distinguished based on the IInd order morphogenetic type.

Engineering-geological districts in the engineering-geological oblasts are distinguished on the territory of which the uniformity of the geological structure is noted, which is expressed in the same sequence of rocks' occurrence, their thickness and petrographic composition. Such relatively small territories can be formed under the conditions that they experienced tectonic movements of the same sign and intensity over their entire area and were in the same paleoclimatic conditions throughout their development history, which goes beyond the latest stage of the Earth's geological development (Popov, 1951). Therefore, engineering-geological districts are distinguished based on the common conditions of geological development.

Engineering-geological subdistricts can be allocated within one engineering-geological district according to a different state of rocks, and the manifestation of modern and ancient geological processes, if necessary (Popov, 1951). For example, within one engineering-geological area, there may be different strata of rocks located in a stratigraphic sequence and characterized by similarity or natural variability of engineering-geological characteristics. So, engineering-geological subdistricts are distinguished based on engineering-geological complexes of rocks of a certain age geological layer.

Engineering-geological sites are allocated within subdistricts during a large-scale engineering-geological study of the territory, within which engineering-geological subsites can be allocated as well. As a rule, engineering-geological sites are distinguished according to the conditions of construction, that is, according to the assessment of a complex of natural and technogenic factors (Popov, 1951) (Fig. 3).

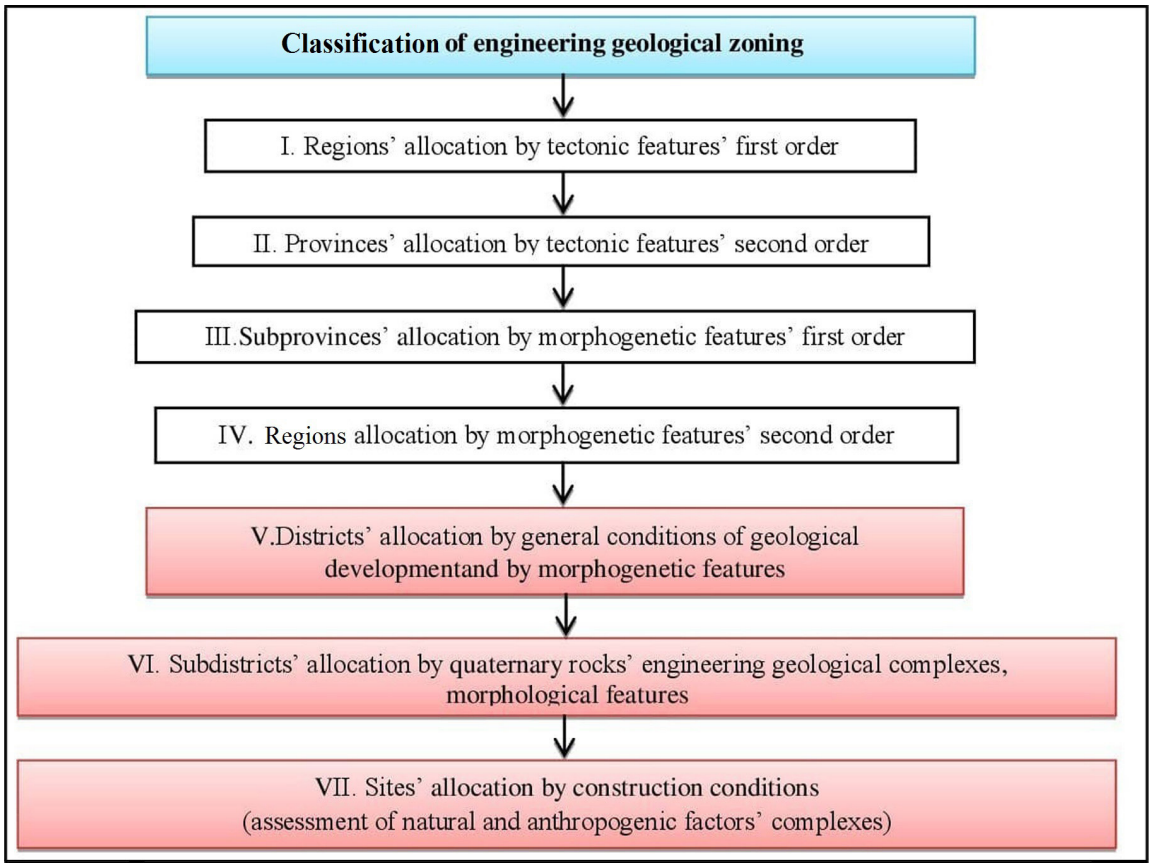

Fig. 3. Procedure of engineering-geological zoning (adapted after Zhyrnov & Solomakha, 2022).
Sl. 3. Postopek inženirsko-geološkega razvrščanja (prirejeno po Zhyrnov & Solomakha, 2022).

The following methods were used in the current research: field engineering-geological researches (geomorphological, geological and hydrogeological survey, identification of natural hazards) methods of interpretation of remote sensing data (analysis of satellite images Sentinel-2 (scale 1: 40 000, period - 2017–2020 years) of the study area in order to fix natural hazards) methods of mining and drilling operations: 72 wells were drilled by percussion-rope method with a depth of 1.6 to 94 m, 9 points of cone penetration test were made (studying the geological structure, indication of tectonic processes and rock fracturing, conducting field experimental work, sampling rocks with an undisturbed structure and water samples, organization of observations of the regime of groundwater and exogenous geological processes) hydrogeological research (research of state of rocks, depth of groundwater level and the level of soils' permeability) methods of engineering-geomorphological (engineering-geomorphological maps are narrow-purpose maps that serve engineering purposes in construction, reflect the structural and geomorphological characteristics, dynamics and stability of the relief, its qualitative and quantitative features and development forecast elements (Palienko, 1978) and engineering-geological mapping (creation of engineering-geomorphological (scale 1: 55 000) and engineering-geological maps (scale 1: 55 000) for the purposes of urban planning) laboratory methods for obtaining data on the geomechanical properties of soils (selection of engineering-geological elements, research of granulometric composition, description of strength, deformation properties, compressibility indicators, etc.) as well as the method of conjugated cartographic analysis (complex comparison of cartographic data into a single multicomponent synthetic map) (Fig. 4).

Results

As noted earlier borders of genetic types and relief morphology were delineated during the engineering-geological survey using GPS equipment, made relief's morphologic description, research of natural hazards and made a detailed description

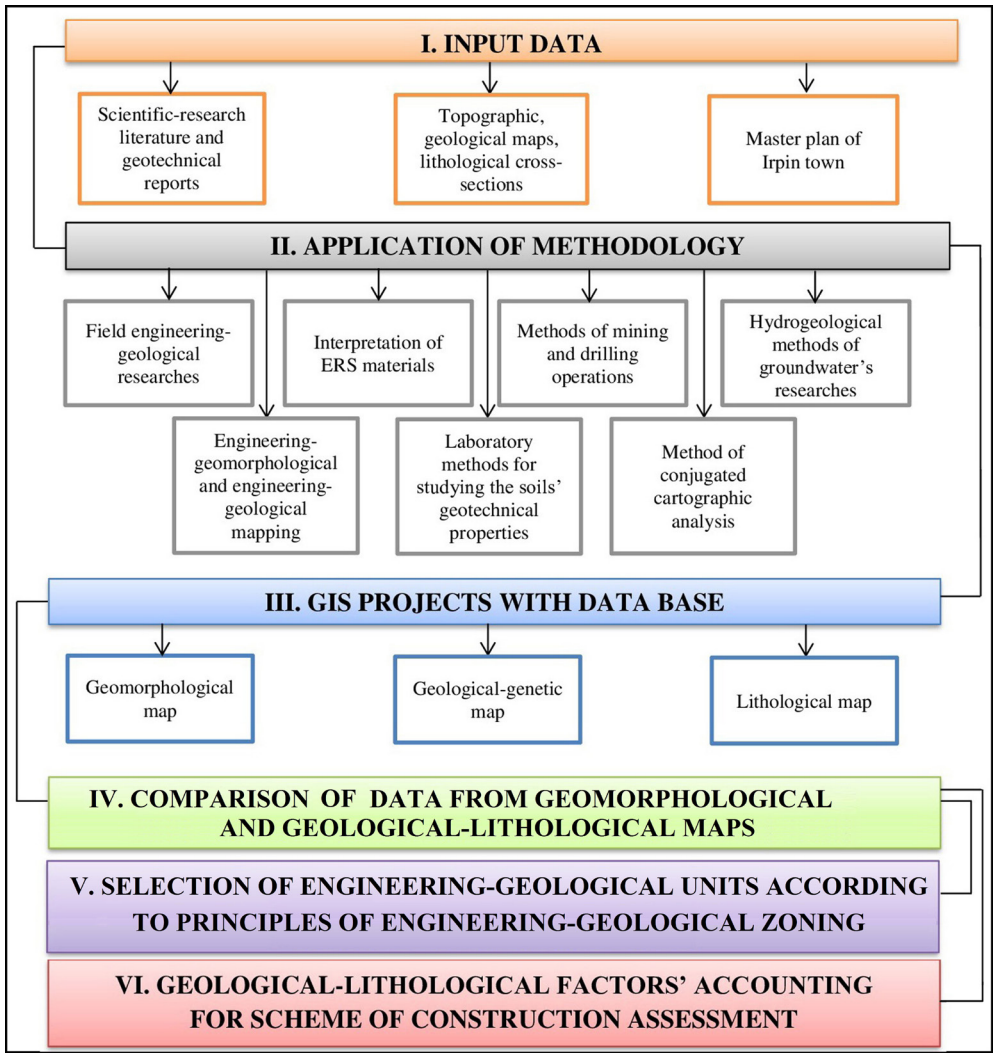

Fig. 4. Data and methodology of current research (adapted after Zhyrnov & Solomakha, 2022).

Sl. 4. Podatki in metodologija trenutne raziskave (prirejeno po Zhyrnov & Solomakha, 2022).

of sediments, that are involved in construction, selected soil samples for determination of their geomechanical properties in the geotechnical laboratory. All this information was exported from GPS equipment and referenced to the existing topographic survey. Geotechnical reports' analysis allowed to specify Quaternary deposits' lithological composition and correct the areas of hydrological and hydrogeological hazards' manifestation in particular flooding, waterlogging and eutrophication (Tsybko, 2020).

Irpin is situated on the borders of the Ukrainian Shield's northern-east slope in geostructural terms, which gradually dips in a north-easterly direction to the side of the Dnieper-Donets Rift. The sediments of the Cretaceous, Paleogene and Quaternary systems lie on the eroded surface of the Precambrian basement. Deposits of the Cenomanian layer, represented by sands and sandstones on siliceous cement are the oldest sedimentary formations exposed in the territory of Irpin. The sand is greenish-gray, fine- and medium-grained, quartz-glauconite. Deposits of the Upper Cretaceous are on the rocks of the Cenomanian layer represented by white, light gray chalk with an average thickness of 9.0 m. The Kaniv, Bucha, Kyiv and Kharkiv suites are established as part of the Paleogene sediments. Rocks of the Kaniv Formation (P_2kn) lie on chalk rocks and are represented by shallow marine formations: dark gray fine- and fine-grained glauconite-quartz, micaceous sand with underlying layers of aleurites and clays, and sometimes sandstones. The thickness of the Kaniv suite varies from 20.4 to 30.5 m with an average thickness of 25 m.

The sediments of the Bucha suite (P_2bc) lie on the Kaniv sediments and are overlain by clays and marls of the Kyiv suite, they are represented by shallow marine formations: greenish-gray, fine- and fine-grained sands of quartz-glauconite composition and dark green and greenish-gray clays with thickness from 8.0 to 20.0 m.

Deposits of the Kyiv suite (P_2kv) are represented by a layer of greenish-gray clayey marls, which pass into marly clays with a thickness of 4.0-30.0 m. A significant change in the capacities of the Kyiv suite is due to its erosion in the Irpin and Buchanka Rivers' riverine zones for which the Kyiv suite's deposits are a water-resistant layer. Deposits of the Kharkiv suites (P_3ch) are limitedly distributed on the territory of the city's south-western part, where they are confined to the most mountainous part of the watershed between the Irpin and Buchanka Rivers, they are blurred in the rest of the area in Quaternary time. The sediments of the Kharkiv suite are gray, greenish-gray, shallow- and fine-grained sands of quartz-glauconite composition with a thickness of 4.5-5.0 m.

Quaternary sediments completely cover pre-Quaternary formations. They are represented by the following genetic types: water-glacial, glacial, alluvial, marsh and technogenic. Quaternary deposits in terms of age are represented by Middle Quaternary, Upper Quaternary and modern sediments.

Mid-Quaternary water-glacial submarine sediments ($f_{II}dn_1$) lie on formations of the Kharkiv and Kyiv suites. They are widely distributed on the city's territory and consist of the highlands between the Irpin and Buchanka Rivers. They are represented by yellow-gray, gray, ochreous, fine- and medium-grained, quartz sands with admixtures of feldspars with layers and lenses of clays. They overlap with moraine and water-glacial moraine sands with a capacity of 12 m.

Mid-Quaternary glacial (moraine) deposits ($g_{II}dn_2$) are represented by glacial deposits with red-brown loams and clays, sometimes greenish-gray with ochre spots of ferrugination with inclusions of gravel and pebbles of crystalline rocks. Coarse-grained material is represented by granites, gneisses, limestones and sandstones. Moraine sediments were not widely distributed, they were preserved only in upland watershed areas and remnant mounds. The moraine deposits are covered everywhere by fluvioglacial deposits, their thickness ranges from 3.0 to 11.5 m.

Mid-Quaternary water-glacial over-moraine deposits ($f_{II}dn_3$) are the most widely distributed on the city's territory, they are the basis for the foundations of most buildings and structures. They are represented by light-gray, brown-yellow and yellow-gray quartz sands. Sands are multi-grained, medium-grained prevail. Sandstone layers and lenses are often found in gravel-pebble material with a thickness of 0.2–2.7 m, including boulders of crystalline rocks. The total thickness of fluvioglacial deposits varies from 5 to 20 m with an average thickness of 10 m.

Alluvial Upper Quaternary a_{III} deposits are represented by alluvial formations of the Irpin and Buchanka Rivers' floodplain terraces – quartz, fine-grained, light-gray and yellow-gray sands with a thickness of 8–12 m with interlayers and lenses of sands with a thickness of 0.2–0.5 m. Alluvial deposits lie on the washed-out surface of Kyiv suite's marls.

Modern Quaternary alluvial a_{IV} and biogenic deposits b_{IV} consist of the floodplain of the Irpin and Buchanka Rivers. They are represented by

fine-grained light-yellow and gray-yellow quartz sands with a thickness of 10–16 m with lenses and interlayers of sandy loams and silts with a thickness of 0.13–0.9 m. Biogenic deposits are represented by peat with a thickness of 0.3-5.0 m, which covers alluvial deposits in most of the flood-

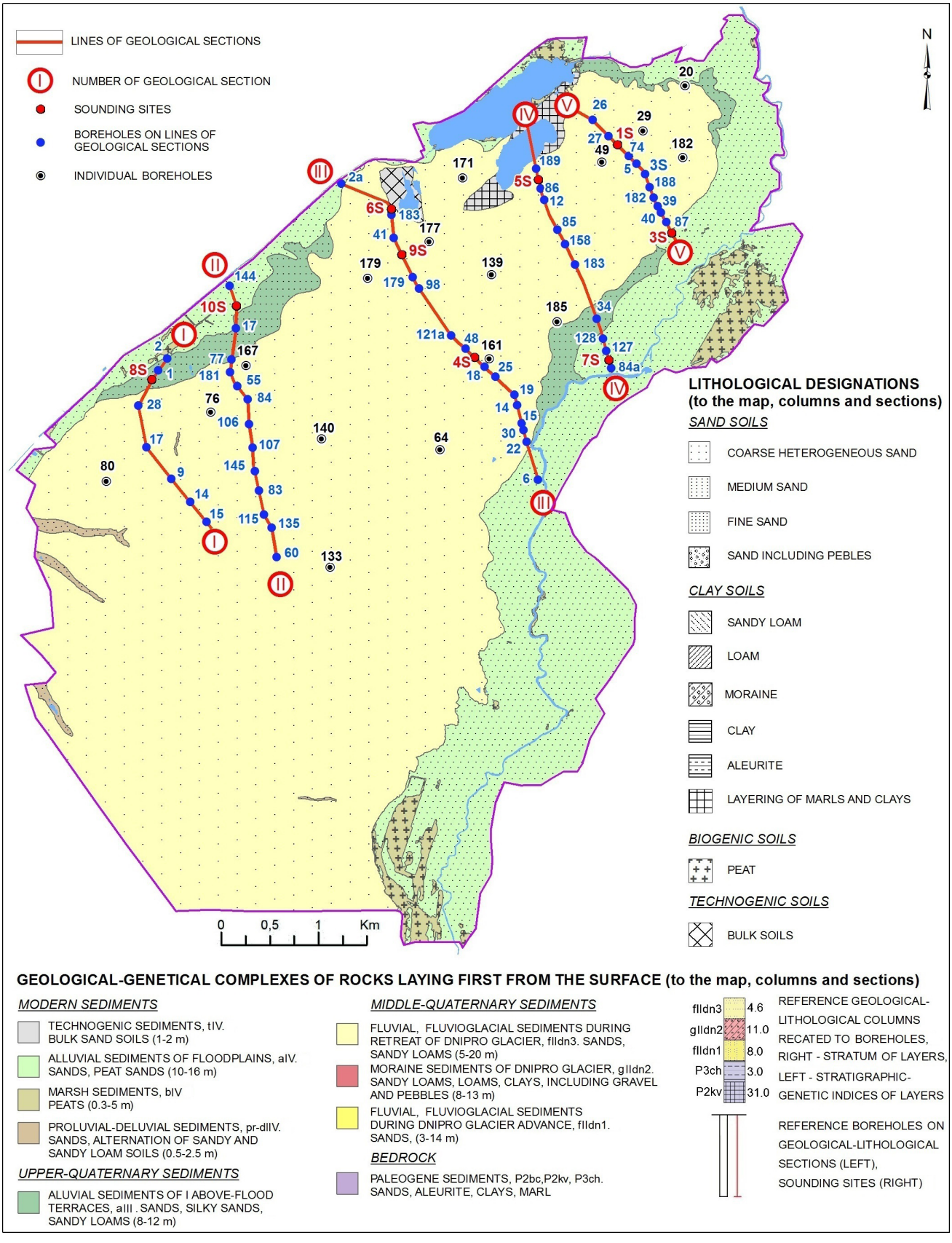

Fig. 5. Geological-lithological map of Irpin city (Zhyrnov & Solomakha, 2022).
Sl. 5. Geološko-litološka karta mesta Irpin (Zhyrnov & Solomakha, 2022).

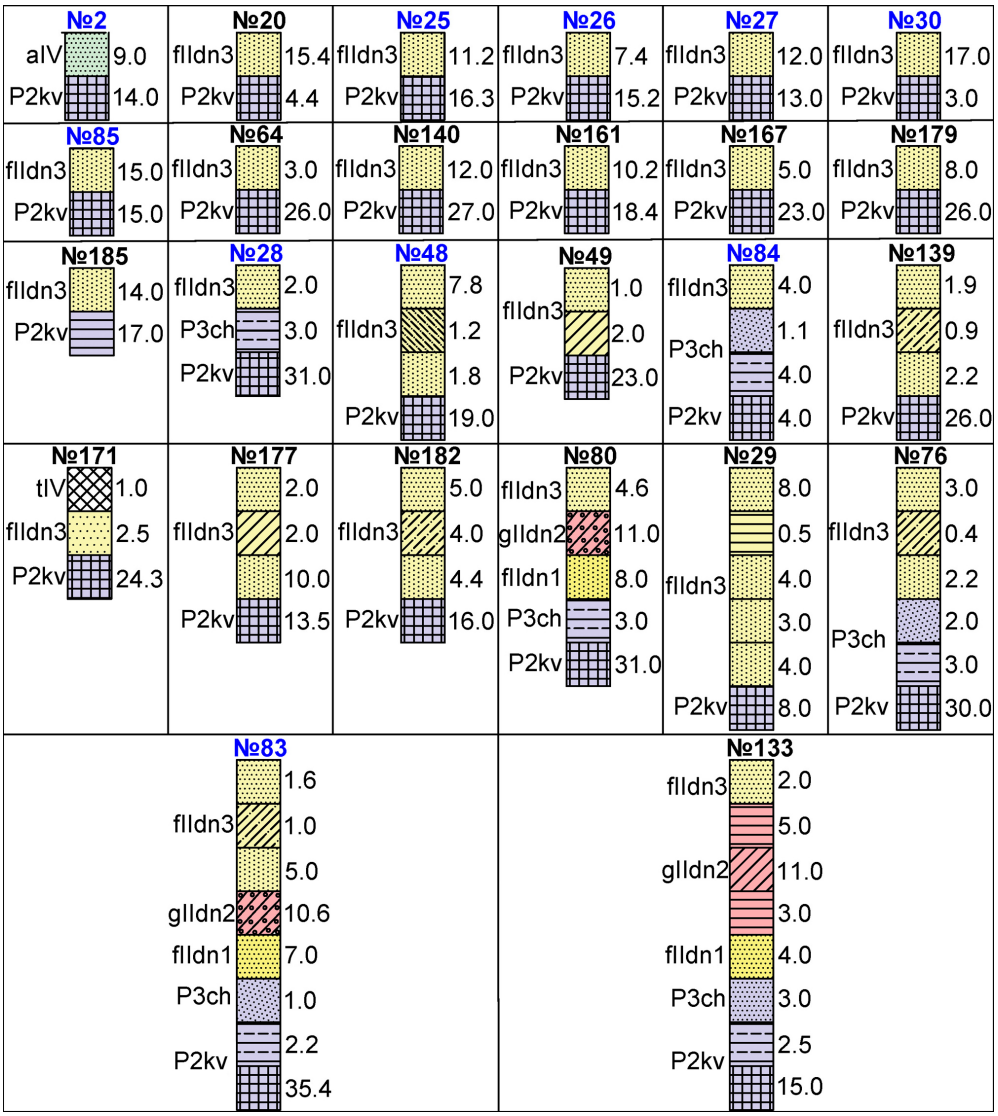

Fig. 6. Geological-lithological columns by boreholes on lines of geological sections and by individual boreholes (Zhyrnov & Solomakha, 2022).

Sl. 6. Geološko-litološki popisi vrtin na linijah geoloških prerezov in po posameznih vrtinah (Zhyrnov & Solomakha, 2022).

plain. Peat is mainly poorly decomposed, brown and brownish-brown in colour. The composition of peat is dominated by reed material. Peat is often sandy, which is the result of washing out the organic component from its mass (Tsybko, 2020; Veklych, 1958; Zhyrnov & Solomakha, 2022).

Therefore, the analysis of the territory's geomorphological features and geological structure made it possible to distinguish four geological-geneti crock complexes on the territories of Irpin's city.

1. A complex of modern alluvial sandy-clay deposits (a_{IV}) with a thickness of 10–16 m represented by fine-grained quartz sands of light yellow and gray-yellow colour with lenses and interlayers of sandy loams and loams with a thickness of 0.3–0.9 m;
2. A complex of Upper Quaternary alluvial sandy-clay deposits (a_{III}) with a thickness of 8–12 m, represented by quartz medium-grained sands of light gray and yellow-gray colour with lenses and layers of sand with a thickness of 0.2–0.5 m;
3. A complex of Upper Quaternary water-glacial sand-clay deposits ($f_{II}dn$) with a thickness of 5–20 m represented by granular quartz sands of a light gray colour with lenses and interlayers of sands, loams and clays with a thickness of 0.2–2.7 m with the inclusion of gravel and weakly rolled pebbles of crystalline rocks;
4. A complex of Upper Quaternary moraine deposits ($g_{II}dn$) with a thickness of 8–13 m, represented by boulder loams and clays, in places with layers of sand (Figs. 5, 6).

The analysis of the geomechanical properties of the soils according to SSU B V.2.1-2-96 made it possible to divide the selected complexes into 12 engineering-geological elements (EGE) which are presented in the geological-lithological sections (Fig. 7).

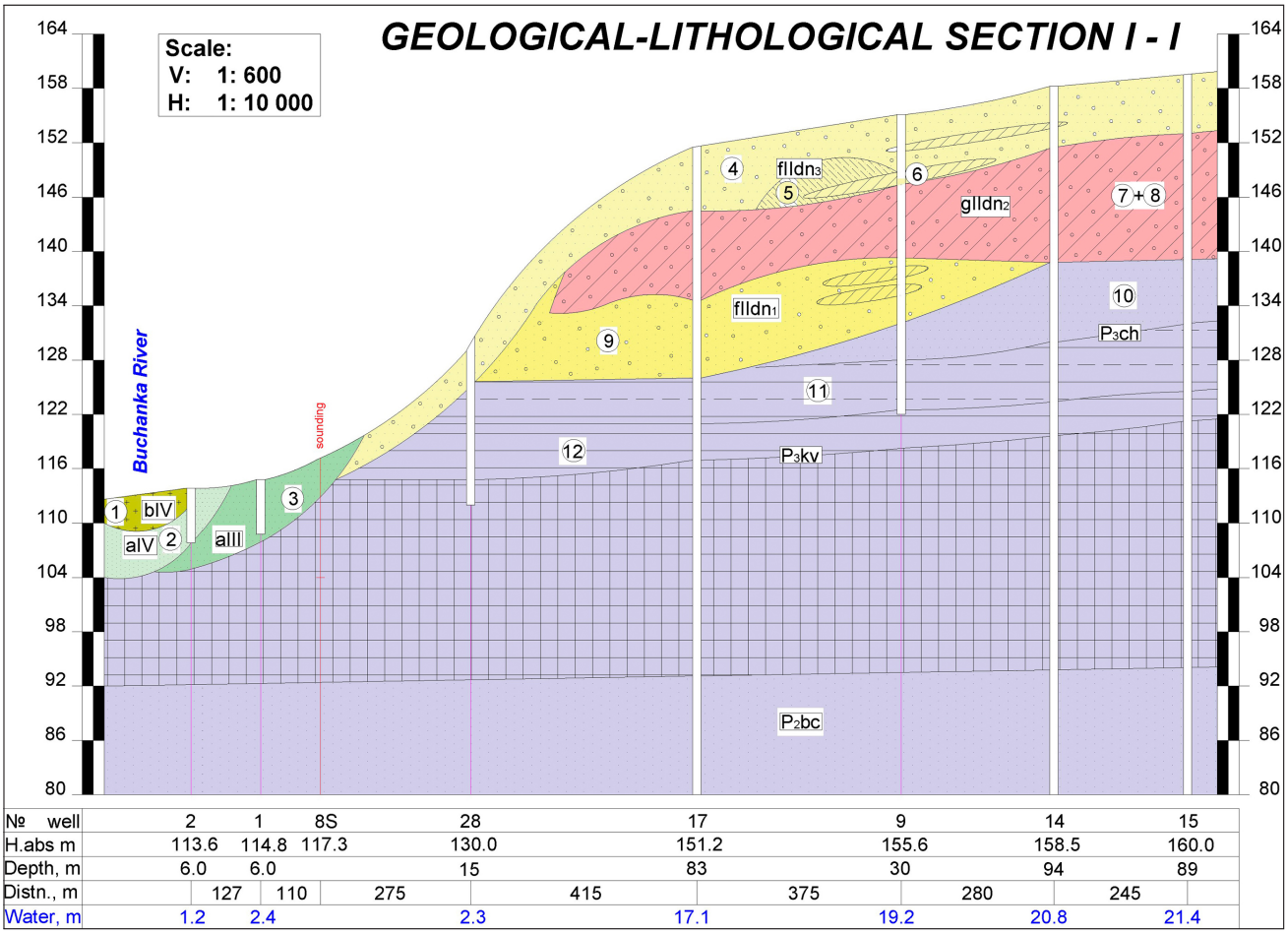

№ well	2	1	8S	28	17	9	14	15
H.abs m	113.6	114.8	117.3	130.0	151.2	155.6	158.5	160.0
Depth, m	6.0	6.0		15	83	30	94	89
Distn., m	127	110	275	415	375	280	245	
Water, m	1.2	2.4		2.3	17.1	19.2	20.8	21.4

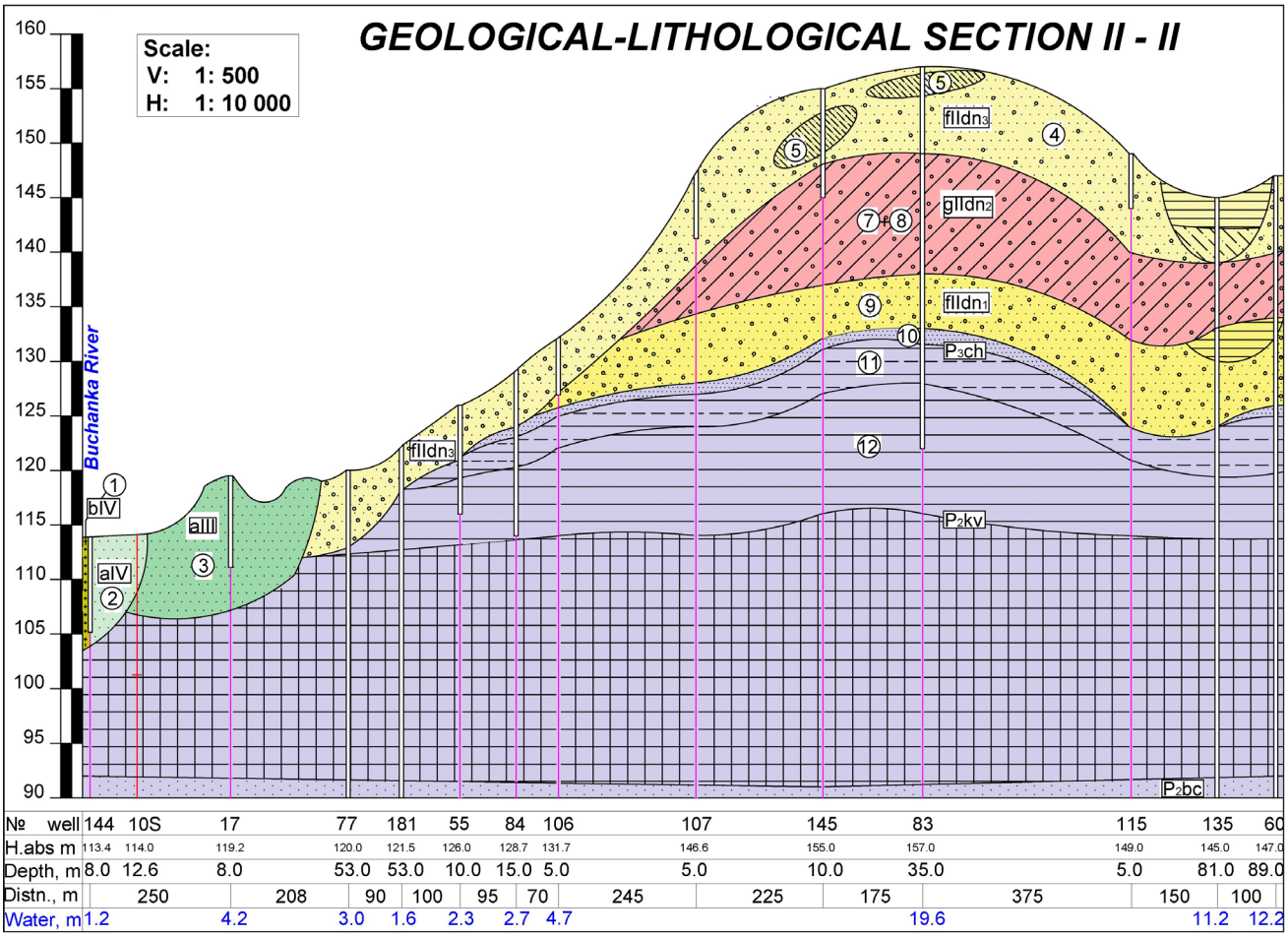

№ well	144	10S	17	77	181	55	84	106	107	145	83	115	135	60
H.abs m	113.4	114.0	119.2	120.0	121.5	126.0	128.7	131.7	146.6	155.0	157.0	149.0	145.0	147.0
Depth, m	8.0	12.6	8.0	53.0	53.0	10.0	15.0	5.0	5.0	10.0	35.0	5.0	81.0	89.0
Distn., m	250		208	90	100	95	70	245	225	175	375	150	100	
Water, m	1.2		4.2	3.0	1.6	2.3	2.7	4.7			19.6		11.2	12.2

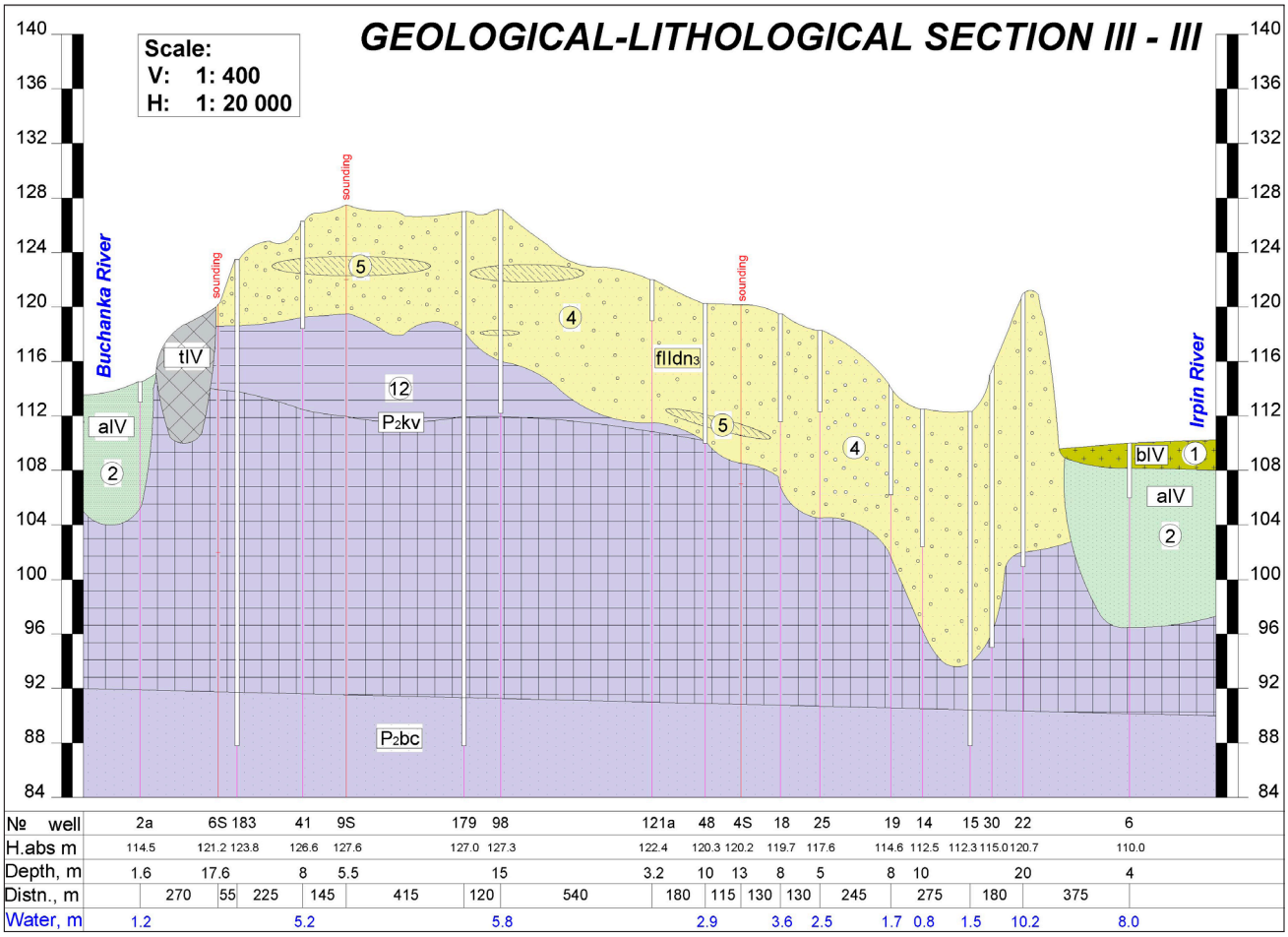
GEOLOGICAL-LITHOLOGICAL SECTION III - III
Scale:
V: 1: 400
H: 1: 20 000
Buchanka River
Irpin River
tlV
alV
bIV
fIldn3
P2kv
P2bc
sounding
№ well 2a 6S 183 41 9S 179 98 121a 48 4S 18 25 19 14 15 30 22 6
H.abs m 114.5 121.2 123.8 126.6 127.6 127.0 127.3 122.4 120.3 120.2 119.7 117.6 114.6 112.5 112.3 115.0 120.7 110.0
Depth, m 1.6 17.6 8 5.5 15 3.2 10 13 8 5 8 10 20 4
Distn., m 270 55 225 145 415 120 540 180 115 130 130 245 275 180 375
Water, m 1.2 5.2 5.8 2.9 3.6 2.5 1.7 0.8 1.5 10.2 8.0

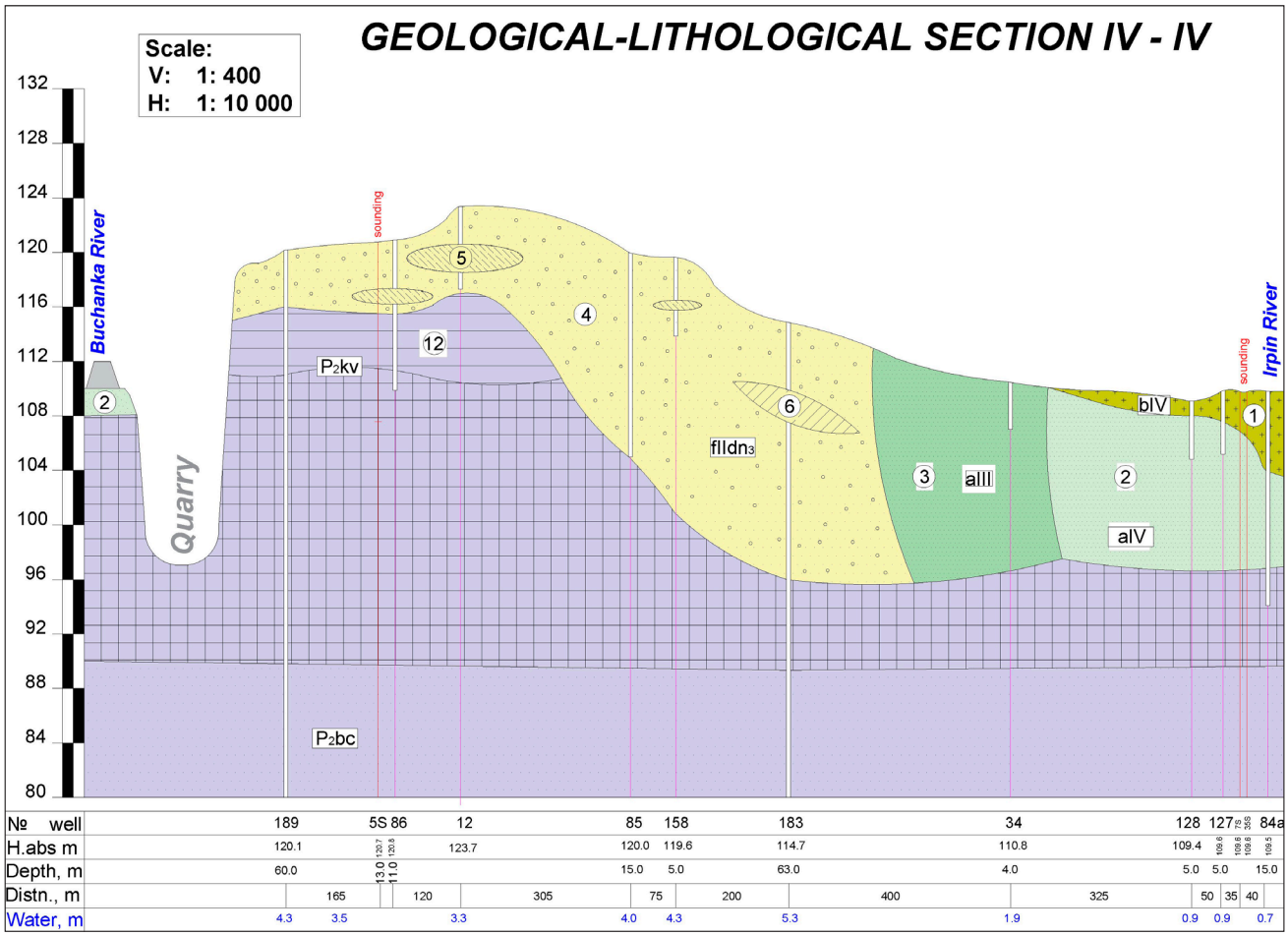
GEOLOGICAL-LITHOLOGICAL SECTION IV - IV
Scale:
V: 1: 400
H: 1: 10 000
Buchanka River
Irpin River
Quarry
P2kv
P2bc
fIldn3
alII
alV
bIV
sounding
№ well 189 5S 86 12 85 158 183 34 128 127 84a
H.abs m 120.1 123.7 120.0 119.6 114.7 110.8 109.4
Depth, m 60.0 13.0 11.0 15.0 5.0 63.0 4.0 5.0 5.0 15.0
Distn., m 165 120 305 75 200 400 325 50 35 40
Water, m 4.3 3.5 3.3 4.0 4.3 5.3 1.9 0.9 0.9 0.7

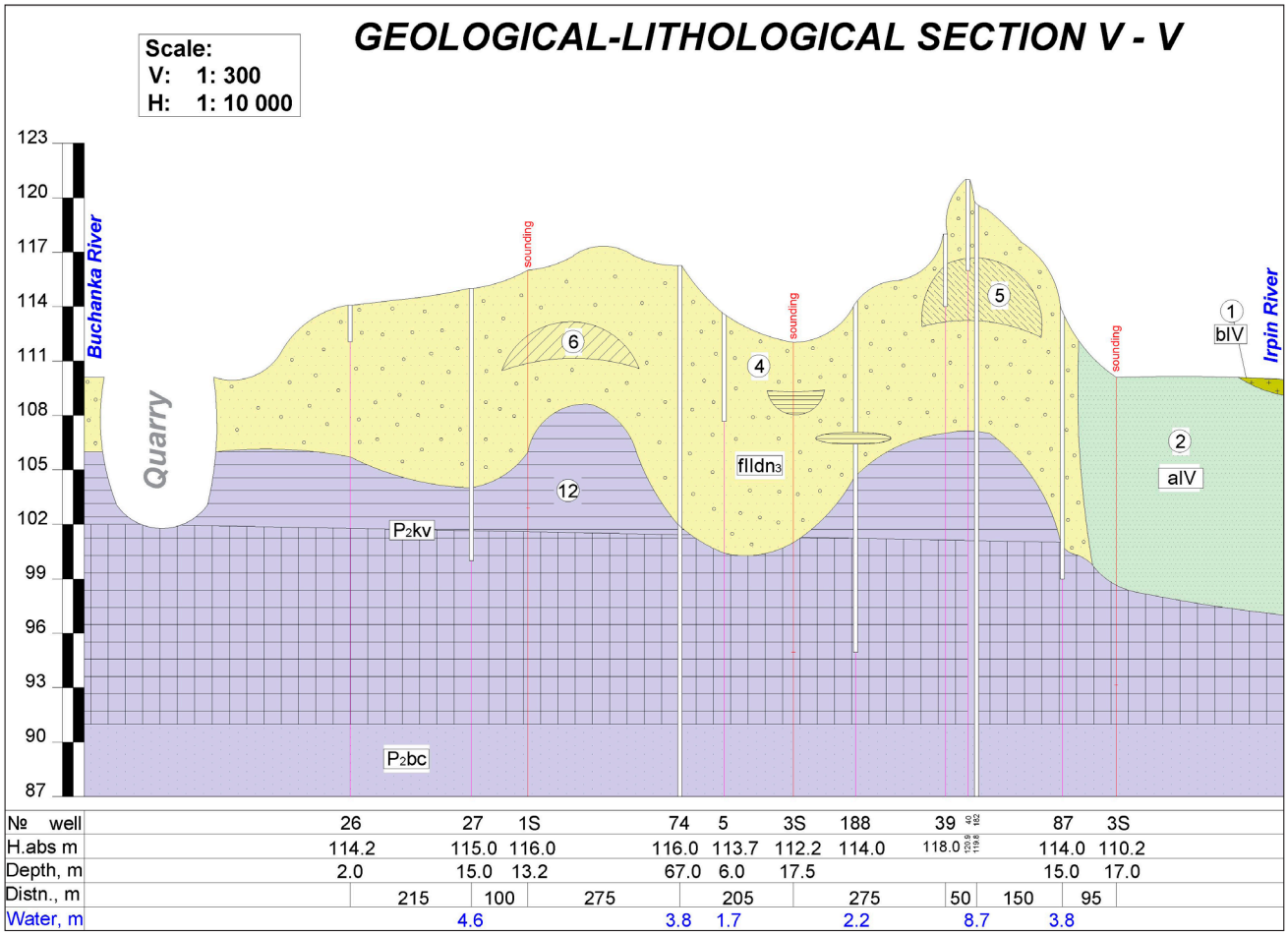

Fig. 7. Geological-lithological sections I-V on Irpin city's territory along conditional lines (Zhyrnov & Solomakha, 2022).
Sl. 7. Geološko-litološki profili I-V na območju mesta Irpin (Zhyrnov & Solomakha, 2022).

Table 1. Engineering-geological elements (EGE) are presented in the geological-lithological sections.
Tabela 1. Inženirsko-geološki elementi (IGE), ki so predstavljeni na geološko-litoloških profilih.

№ EGE	Description
1	Peat, mainly finely decomposed, brown and brownish-brown in colour. Reed material is present in the composition of peat, and sedge material plays a secondary role. Peat is often sandy, which is the result of the washing-out of organic components from its mass. The peat is medium ashy, strongly moist, plasticity and very compressible. Peat is characterised by poor geomechanical properties and cannot be the basis for buildings and structures.
2	Quartz sand with the inclusion of weakly rounded quartz grains. Lenses and layers of sandy loam, loam and silt are found at various depths. The sand is heterogeneous, of poor density, fine and fine-grained, horizontally layered, low water permeability, medium deformability, compressibility and strength.
3	Medium-grained quartz sand of light gray and yellow-gray colour, with lenses and layers of sand 0.2–0.5 m thick. Sand is heterogeneous, poorly compacted, medium permeable, medium deformability, compressibility and strength.
4	Light-gray multi-grained quartz sands with brown and red-brown layers and spots of ferruginization. The sand is layered with the inclusion of weakly rounded quartz grains with separate inclusions of gravel and pebbles, as well as with layers of gravel-pebble material with a thickness of 5 to 25 cm. The sand is homogeneous, with a low degree of compactibility, high permeable, medium deformability, compressibility and strength.
5	Light-yellow and brown-yellow sandy loam. The soil is thin-layered, sometimes with layers of sand, loam and clay. Statistical processing of the granulometric composition gave the following content of fractions: sand – 64 %, dust – 28 %, clay – 8 %. Sandy loam is solid, dense, weakly compressible and medium deformability.
6	Moraine loam of light composition. Loam is dense, stiff, low water permeability, weakly compressible and medium deformability.
7	Moraine clay of dark brown colour with inclusions of pebbles and boulders. Clay is dense, stiff, impermeable, weakly compressible and medium deformability.
8	Moraine loam. Loam is dense, stiff, low water permeability, weakly compressible and slightly deformable.
9	Quartz sand. The sand is homogeneous, with a high permeable, medium deformability, compressibility and strength.
10	Quartz sand. Sand is heterogeneous, poorly compacted, medium permeable, medium deformability, compressibility and strength.
11	Sandy aleurite, thinly laminated, of low strength, medium-deformable.
12	Marl.

Table 2. Geomechanical properties of biogenic soils.
Tabela 2. Geomechanske lastnosti biogenih tal.

№	Indicators of geomechanical properties	EGE-1
1	Degree of soil decomposition, R (%)	> 20
2	Soil ash content, %	24
3	Weighted soil moisture, w (%)	390
4	Plasticity index	143
5	Density of wet peat γ_o (g/cm^3)	1.01
6	Density of dry peat, γ_d (g/cm^3)	0.22
7	Solid particles density, γ_s (g/cm^3)	1.57
8	Porosity, e	19
9	Volume shrinkage, ε_{shV}	34
10	Specific adhesion, C (KPa)	0.33
11	Modulus of deformation, E_o (MPa)	2.6

Table. 3. Geomechanical properties of sandy soils.
Tabela. 3. Geomechanske lastnosti peščenih tal.

№	Indicators of geomechanical properties	EGE-2	EGE-3	EGE-4	EGE-9	EGE-10
1	Coefficient of non-uniformity, Cu	1.7	2.1	3.4	4.0	1.9
2	Compaction coefficient, Cc (%)	7–15	8–12	8–12	-	7–10
3	Density, γ_o (g/cm^3)	2.02	2.00	2.00	1.99	1.97
4	Bulk density, γ_c (g/cm³)	1.70	1.70	1.72	1.66	1.68
5	Natural slope's angle dry (°)	33	32	33	-	29
6	Natural slope's angle underwater (°)	25	25	29	-	23
7	Internal friction's angle, φ (°)	34	37	27	33	33
8	Specific adhesion, C (KPa)	2.94	0.98	1.96	2.94	0.98
9	Modulus of deformation, E_o (MPa)	23.5	27.5	31.4	22.6	23.5

Table. 4. Geomechanical properties of clayey soils.
Tabela. 4. Geomehanske lastnosti glinenih tal.

№	Indicators of geomechanical properties	EGE-5	EGE-6	EGE-7	EGE-8	EGE-11	EGE-12
1	Moisture content, w (%)	16	13	22	14	29	31
2	The upper limit of plasticity, w_l (%)	22	26	44	35	50	34
3	Plasticity index, P_l	4	10	22	14	18	25
4	Density, γ_o (g/cm³)	1.92	2.14	1.99	2.08	1.91	1.89
5	Bulk density, γ_c (g/cm³)	1.69	1.89	1.63	1.80	1.48	1.44
6	Porosity, e	0.58	0.43	0.67	0.51	0.84	0.90
7	Internal friction's angle, φ (°)	27	23	18	22	20	18
8	Specific adhesion, C (KPa)	15.7	25.9	49.0	32.4	42.2	72.6
9	Modulus of deformation, E_o (MPa)	29.4	45.1	34.3	53.9	23.5	25.5

Engineering-geological districts and subdistricts can be distinguished based on the geomorphological and engineering-geological maps' comparison (Figs. 2, 5) by the procedure of engineering-geological zoning. Geomechanical properties of engineering-geological elements are the basis for the selection of engineering-geological sites, however, hydrogeological data are needed for this, so the selection of engineering-geological sites is not possible yet. However, the soils' geomechanical characteristics determine the lithological component of Irpin city's construction assessment, which will be discussed later.

So, the I district is represented by Upper- and Holocene Quaternary Q_{III}-Q_{IV} erodible and depositional alluvial plain with absolute altitudes of 107–118 m. Alluvial deposits with a thickness of 8–16 m lie on the Kyiv suite's marls, which are a water-resistant layer for this area. Two engineering-geological subdistricts are allocated in the first district: 1) Alluvial floodplain inundated flat terrace with swamped areas and peaty

depressions of Holocene age that composed modern alluvial deposits a_{IV} with a capacity of 10–16 m, that covered by modern organogenic formations (silt, peat) b_{IV} with a capacity of 0.3–5.0 m. Alluvial deposits are represented by quarts of fine-grained sands of light yellow and grey-yellow colours with a layer of sandy loams and loam with a capacity of 0.3–0.9 m. The alluvial complex lies on the washed-out surface of the Kyiv suite's marls P_2kv; 2) Alluvial Upper Holocene slightly dissected first above-flood terrace that composed by alluvial sandy and clayey deposits a_{III} with a capacity of 8–12 m, that represented by alluvial quarts fine-grained sands of light grey and yellow-grey colours with lens and layers of sandy loams with a capacity of 0.2–0.5 m. The alluvial complex lies on the washed-out surface of the Kyiv suite's marls P_2kv.

The II district is represented by the Middle Quaternary Q_{II} denudation-depositional watershed moraine fluvioglacial plain with absolute altitudes of 120–160 m. Fluvioglacial and glacial deposits with a thickness of 5 to 23 m lie on the marls of the Kyiv suite, which is a regional water-resistance layer for this area. Two engineering-geological subdistricts are allocated in the II district: 1) Lowland part of moraine fluvioglacial wavy and slightly dissected plain of Dnipro age with absolute altitudes of 120–135 m. Subdistrict composed of complex of Middle Quaternary fluvioglacial sandy-clayey deposits ($f_{II}dn_3$) with a capacity of 5–20 m at 10 m medium capacity. The complex is represented by middle-grained quarts of sands of light grey colour with lens and layers of sandy loams, loams and clays with a capacity of 0.5–2.7 m with the inclusion of crystal rocks' gravel

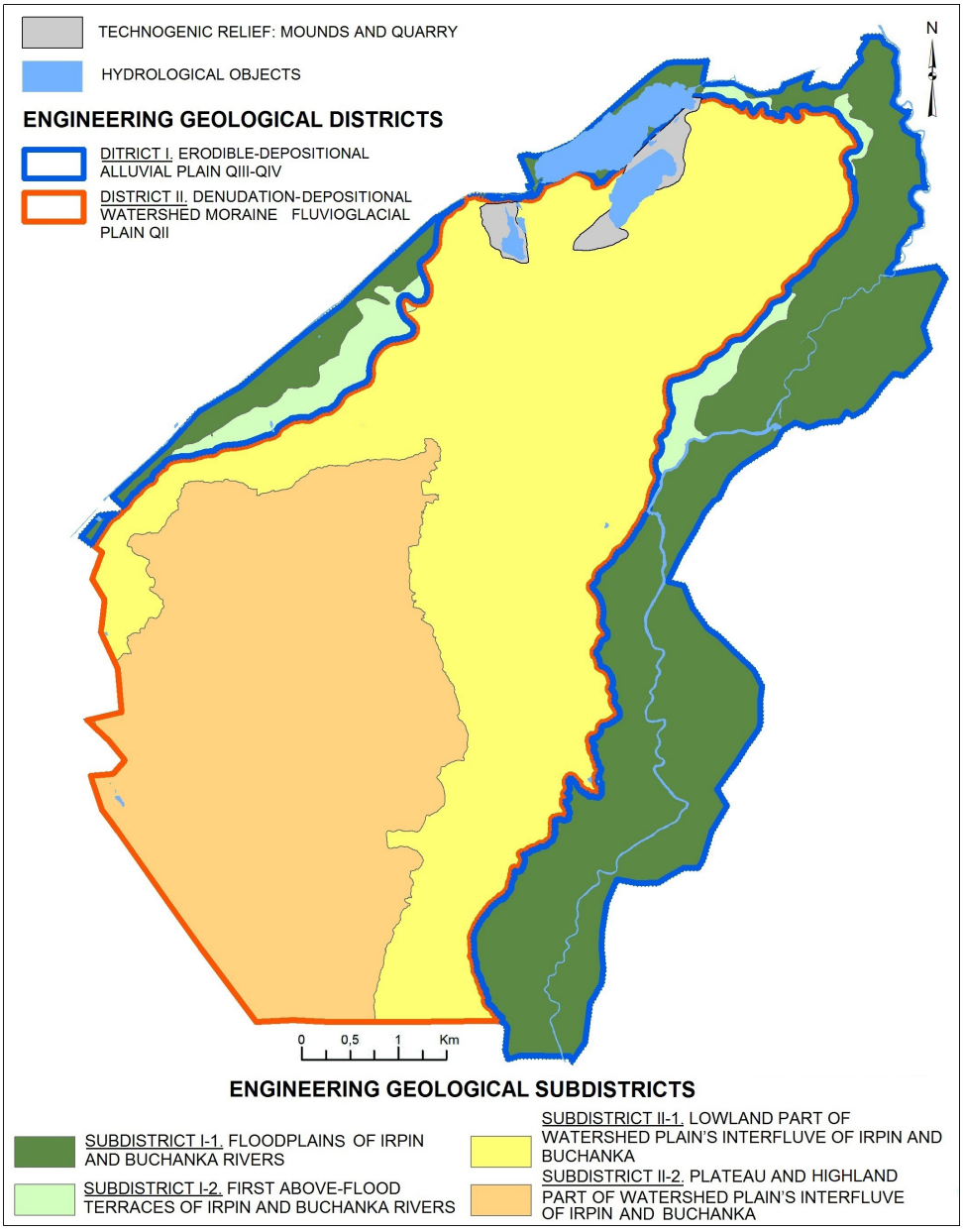

Fig. 8. Engineering-geological districts and subdistricts of Irpin city.

Sl. 8. Inženirsko-geološka okrožja in podokrožja mesta Irpin.

and pebble. Sometimes the gravel-pebble material is collected in the form of lenses and layers; 2) Plateau and elevated portion of moraine fluvioglacial wavy and slightly dissected plain of Dnipro age with absolute altitudes of 135–160 m. Subdistrict consists of moraine complexes ($g_{II}dn_2$) with a capacity of 8–13 m, which cover and underlie with fluvioglacial sandy-clayey deposits of advance and retreat of Dnipro glacier ($f_{II}dn_1$ and $f_{II}dn_3$). Moraine deposits are represented by loams and clays with the inclusion of pebbles and boulders, fluvioglacial deposits are represented by average-grained quarts sands with layers of sandy loams and loams including gravel and pebbles. (Fig. 8) (Tsybko, 2020; Zhyrnov & Solomakha, 2022).

Sites with artificially modified relief and arroyo's bottoms and detrital cones of the Holocene age will relate to engineering-geological sites due to the small size and local spread.

Discussion

The conducted research on the geological-genetic structure map of Irpin city allows us to determine two topics for discussion:

- Disadvantages of studying soil properties (engineering-geological elements) within Irpin city;
- Geological-lithological factors' accounting for drawing up schemes of construction assessment in the project of the master plan of Irpin city.

1. Disadvantages of studying soil properties (engineering-geological elements) within Irpin city;

The main disadvantages in the determination of soils' geomechanical properties (engineering-geological elements) within Irpin city are the absence of the following studies: a) determination of chemical soils' properties, in particular, missing data on solubility, acid-base properties and soils' chemical aggressiveness; b) determination of soils' physical properties, in particular, missing information on thermophysical (thermal capacity, soils' frost resistance) and electrical properties (electrical conductivity, soils' corrosive activity); c) determination of soils' biotic properties (biological activity, bioaggressiveness and biocorrosion in soils);d) determination of certain geomechanical properties of soils (rheological properties: creep, relaxation of stresses in soils, soils' long-term strength; dynamic properties: soils' behavior under vibration and impulsive effects, soils' liquefaction)(Trofimov et al., 2005). The categories of soils according to seismic properties according to the construction sites' normative seismicity are not defined (Building regulations B.1.1-12:2014, 2014). It is worth noting that the construction of geological-lithological sections and the determination of soils' geomechanical properties took place only in the high-density area and most developed northern, north-eastern and north-western city's parts, while the rest of Irpin's territory has not been explored, which is a significant disadvantage for the urban development in the distant future.

2. Geological-lithological factors' accounting for drawing up schemes of construction assessment in the project of the master plan of Irpin city. The compiled geological-lithological map and sections can be used to determine the territory with different degrees of geological conditions' complexity for the city's construction assessment at this stage. (tab. 5; Building regulations A.2.1-1-2008, 2008).

The study of the geological-lithological structure of Irpin city allows us to conclude that the engineering-geological conditions for the development of the city's territory are simple and the soils that consist of the Quaternary and Paleogene rock strata suitable for their use by their geomechanical properties as a natural base for laying foundations, except the peat layer, which must be removed or which must be excluded during construction development (Amaryan, 1990).

Table 5. Category of geological-lithological conditions' complexity for construction assessment.
Tabela 5. Kategorija zahtevnosti inženirsko-litoloških razmer za oceno gradnje.

Factors	I (easy)	II (average)	III (difficult)
Geological-lithological	No more than four different geological-lithologicalunitsof rocks with horizontal laying lithological layers. Soil characteristics by plan or by depth with natural changes. Absence of soils with poor geomechanical properties.	No more than six different geological-lithological units of rocks with sloping laying lithological layers. Soil characteristics as per plan or according to depth with natural changes. Absence of soils with poor geomechanical properties.	More than six different geological-lithological units of rocks. Capacity suddenly changed, lens' soil laying. There are a high diversity index's soil characteristic, which vary with out-of-specification changes. Presence of soils with poor geomechanical properties (peak, silt).

Conclusion

1. Qualitative engineering-construction assessment as part of the project of the urban master plan should be based on the engineering-geological zoning of the territory with the determination of engineering-geological units. Consideration of geological-lithological estimated factors in engineering construction assessment is the basis for the selection of engineering-geological units (districts and subdistricts) and also sets the preconditions for the selection of engineering-geological sites based on the geomechanical properties of engineering-geological elements (EGE).
2. The morphogenetic and morphological structure of the relief forms a basis for engineering-geological districts and subdistricts selection. It is necessary to distinguish the geological-genetic complexes of Quaternary deposits, that constitute them, while relief's morphological elements determine the lithological composition of the mentioned Quaternary deposits.
3. The analysis of the territory's geomorphological features and their geological structure made it possible to distinguish four geological-genetic rocks' complexes on the territories of Irpin's city: 1) complex of modern alluvial sandy-clayey deposits (a_{IV}) with a thickness of 10–16 m (sands with lenses and layers of sandy loams, loams); 2) complex of Upper Quaternary alluvial sandy-clay deposits (a_{III}) with a thickness of 8–12 m (sands with lenses and layers of sandy loams); 3) complex of Upper Quaternary water-glacial sand-clay deposits ($f_{II}dn_1$) with a thickness of 5–20 m (sands with lenses and layers of sandy loams, loams and clays with inclusion of gravel, boulders, pebbles); 4) complex of Upper Quaternary moraine deposits ($g_{II}dn_2$) with a thickness of 8–13 m (boulder loams, clays and clays with layers of sand).
4. The analysis of the soils' geomechanical properties made it possible to divide the selected complexes into 12 engineering-geological elements (EGE) with appropriate geomechanical properties, of which only EGE-1 (peat) is unsatisfactory as a natural basis for laying foundations. The peat layer must be removed during construction.
5. There are engineering-geological districts according to morphogenetic features and common conditions of geological development and engineering-geological subdistricts according to morphological features and engineering-geological complexes of Quaternary rocks based on the conjugate cartographic analysis' method of geomorphological and engineering-geological maps. So, the first district is represented by an erodible-depositional alluvial plain with two engineering-geological subdistricts: floodplain terraces of the Irpin and Buchanka rivers with swamped areas and peat depressions with alluvial (sands, sandy loams, loam) and biogenic (peat) deposits and first above-flood terraces of mentioned rivers with alluvial deposits (sands, sandy loam. The second district is represented by a denudation-depositional watershed moraine water-glacial plain with two engineering-geological subdistricts: lowland part, highland part and plateau of moraine fluvioglacial plain with fluvioglacial and glacial deposits, (sands, sandy loams, loam with inclusion of gravel, pebbles and boulders).
6. Geological-lithological estimated factors of Irpin city are simple in complexity and soils, in general, are suitable for use as a natural basis for laying foundations. Engineering-geological elements (EGE) 3, 4, 7, 8, 9, 11, 12 can serve as a natural basis for laying foundations. The development of the floodplains of the Buchanka and Irpin Rivers is not recommended for environmental reasons, therefore EGE-2 is excluded from use. A deep strip foundation is recommended for low-rise buildings, taking into account the geomechanical properties of soils. The best type of foundation is the pile type for multi-storey buildings. It is necessary to use waterproofing materials, when arranging foundations. It is necessary to equip horizontal drainage and rainwater drainage for areas with a high level of groundwater, for aggressive waters appropriate grades of concrete and anti-corrosion protection for underground metal reinforcement should be used. (Building regulations B.2.1-10:2018, 2018).

Acknowledgments

The authors express their gratitude to the leadership of the Ukrainian Institute of Engineering Scientific and Technical Exploration (UKRIINTR) and Ukrainian State Scientific Research Institute of Cities' Design "DIPROMISTO for the provided geotechnical reports, a master plan of Irpin city and corresponding graphic materials.

References

Amaryan, L.S. 1990: Poor soils' properties and methods for their studying. Moscow, Nedra: 220 p.

Barshchevsky, M.E., Kuprash, R.P. & Shvidky, Y.M. 1989: Geomorphology and relief-forming deposits of Kyiv's district. Kyiv, Naukova dumka: 196 p.

Bell, F.G. 2007: Engineering Geology, Second Edition. Oxford, Elsevier: 593 p.

Building regulations A.2.1-1-2008, 2008: Engineering exploration for construction. Kyiv, Minregion: 72 p.

Building regulations B.1.1-12:2014, 2014: Construction in the seismic regions of Ukraine. Kyiv, Minregion: 110 p.

Building regulations B.1.1-15:2012, 2012: Structure and contents of master plan's settlement. Kyiv, Minregion: 33 p.

Building regulations B.2.1-10:2018, 2018: Bases and foundations of buildings and structures. Kyiv, Minregion: 36 p.

El May M., Diala M. & Chenini I. 2010: Urban geological mapping: geotechnical data analysis for rational development planning. Engineering Geology, 116/1-2: 129–138. https://doi.org/10.1016/j.enggeo.2010.08.002

Šestanović, S., Toševski, A., Mihalić, S., Dečman, A. & Ferić, P. 2012: Preliminary data for the development of the engineering geological map of the city of Split (Croatia). Environmental Earth Sciences, 66: 1547–1556. https://doi.org/10.1007/s12665-011-1394-0

Gubenko, T.V., Mukha, V.G. & Kozyna N.P. 2017: Master plan of Irpin city. Kyiv, DIPROMISTO: 180 p.

Ivanenko, P.I. 2020: State geological map of Ukraine– 200. Kyiv, Ukrgeoinform: 67 p.

Muceku, Y. 2010: Land evaluation and site assessment-engineering geological mapping for Regional planning and urban development in Velipoja area. Journal of Albanian Sciences Academy, 27, 1: 101–114.

Osipov, V. I., Burova, V.N., Zaikanov, V.G., Molodykh, I.I., Pyrchenko, V.A. & Savisko I.S. 2012: A map of large-scale (detail) engineering geological zoning of Moscow territory. Water Resources, 39: 737–746. https://doi.org/10.1134/S0097807812070093

Palienko, E.T. 1978: Exploration and engineering geomorphology. Kyiv, Vyshcha shkola: 200 p.

Panchenko, T.S. 2019: Geological map of Ukraine. Kyiv, Ukrgeoinform: 75 p.

Paton, B.E., Shpak, A.P., Rudenko, L.G. & Bochkovska, A.I. 2007: National atlas of Ukraine. Kyiv, Kartografiya: 440 p.

Popov, I.V. 1951: Engineering geology. Moscow, State Publishing House of Geological Literature: 444 p.

Rudenko, F.A., Solyakov, I.P. & Mesyats I.A. 1971: Hydrogeology of USSR. Moscow, Nedra: 614 p.

Shnyukov, E.F., Shestopalov, V.M. & Yakovlev, E.A. 1993: Ecological geology of Ukraine. Kyiv, Naukova dumka:407 p.

Solovytsky, V.N. & Vozgryn, B.D. 1990: Geological map on the scale 1:50 000 by sheets of Kyiv region. Kyiv, Ukrgeolstrom: 10 p.

State standard of Ukraine B V.2.1-2-96, 1997: Soils. Classification. Kyiv, State Committee of Ukraine for urban planning and architecture: 47 p.

Trofimov, V.T., Korolev, V.A., Voznesensky, E.A., Golodkovskaya, G.A., Vasylchuk, Y.K. & Ziangirov R.S. 2005: Soil science. Moscow, Moscow State University: 1024 p.

Trofimov, V.T. & Krasilova, N.S. 2008: Engineering geological maps. Moscow State University, Moscow: 383 p.

Tsybko, V.A. 2020: Engineering-geological atlas of Irpin city on the scale 1:5000. Kyiv, UKRIINTR: 97 p.

Veklych, M.F. 1958: Quaternary deposits of the right bank of the Middle Dnieper. Kyiv, Academy of Science of USSR: 200 p.

Zhyrnov, P.V., Sadoviy, Y.V. & Tomchenko, O.V. 2019: Methodology for the territories' engineering construction assessment with difficult geological conditions. Proceedings of 10th International Academic Conference "Geodesy, Architecture & Construction": 71–77. https://doi.org/10.23939/lea

Zhyrnov, P. & Solomakha, I. 2022: Engineering-geological zoning as a scientific-methodical basis for scheme's development of engineering-construction assessment (on the example of Irpin town Kyiv region). Geodynamics, 2/33: 115–132. https://doi.org/10.23939/jgd2022.02.115

Zuquette, L.V., Osni Pejon, O.J. & Santos Collares, J.Q. 2004: Engineering geological mapping developed in the Fortaleza Metropolitan Region, State of Ceara, Brazil. Engineering Geology, 71/3–4: 227–253. https://doi.org/10.1016/S0013-7952(03)00136-4

GEOLOGIJA 66/1, 185-198, Ljubljana 2023
https://doi.org/10.5474/geologija.2023.008

Borers and epizoans on oyster shells from the upper Tortonian, Lower Chelif Basin, NW Algeria

Vrtalci in epizoji na zgornjetortonijskih ostreidnih lupinah iz Spodnjega Chelif bazena, SZ Alžirija

Rachid KHALILI, Linda SATOUR & Saci MENNAD

University of Oran 2 - Mohamed Ben Ahmed, Algeria, Laboratory of Palaeontology, Stratigraphy and Palaeoenvironments, El M'Naouer, BP 1015, ex IAP, Es Senia 31000 Oran, Algeria;
e-mail: rachido1990@gmail.com, satourlind@gmail.com, sassiy2@gmail.com

Prejeto / Received 18. 4. 2022; Sprejeto / Accepted 27. 3. 2023; Objavljeno na spletu / Published online 4. 8. 2023

Key words: Miocene, borings, encrustation, *Entobia*, *Gastrochaenolites*, *Caulostrepsis*, *Trypanites*, *Maeandropolydora*, foreshore, shoreface

Ključne besede: miocen, vrtanje, inkrustacija pas bibavice, *Entobia, Gastrochaenolites, Caulostrepsis, Trypanites, Maeandropolydora*, plitvi podplimski pas

Abstract

The three oyster lenses of the upper Tortonian of Djebel Touaka site which are described herein contain three species, *Crassostrea gryphoides* (Schlotheim), *Ostrea lamellosa* (Brocchi) and *Hyotissa squarrosa* (De Serre). The density of shell packing between the lenses is dissimilar. Most of the specimens are disarticulated and poorly fragmented; they exhibit a random distribution and orientation, without any distinct sorting. Bioerosion and encrustation are featured on both surfaces of left and right valves.

The identified ichnogenera are *Entobia* (Bronn), *Gastrochaenolites* (Leymarie, 1842), *Caulostrepsis* (Clarke, 1908), *Trypanites* (Mägdefrau, 1932) and *Maeandropolydora* (Voigt, 1965). Encrusters are scared, represented by juvenile oysters/other bivalves, bryozoans and barnacles. The coexistence of borings on both sides of valves means that they probably occur not only while alive, but they keep happening after death. The oyster beds were deposited in a foreshore to shoreface environment, from the combined action of wave currents and sedimentation rate.

Izvleček

Opisane so tri ostreidne akumulacije iz zgornjega tortonija Djebel Touka v Alžiriji. Ostreidne plasti vsebujejo vrste *Crassostrea gryphoides* (Schlotheim), *Ostrea lamellosa* (Brocchi) in *Hyotissa squarrosa* (De Serre). Gostota ostreidnih lupin variira. Večina primerkov je disartikuliranih in nekoliko fragmentiranih. Razporejeni so naključno in brez preferenčne orientacije. Prav tako niso sortirane. Sledovi bioerozije in preraščanja so prisotni na obeh straneh levih in desnih loput. Prepoznani so bili *Entobia* (Bronn), *Gastrochaenolites* (Leymarie), *Caulostrepsis* (Clarke), *Trypanites* (Mägdefrau) in *Maeandropolydora* (Voigt). Preraščanja se stojijo iz juvenilnih primerkov ostrig in drugih školjk, mahovnjakov in ciripednih rakov. Hkratna prisotnost izvrtin na obeh straneh lupin pomeni, da je do preraščanj prišlo tudi po smrti ostreidnih školjk. Ostreidne akumulacije so nastale v širšem območju plimovanja in v plitvem podplimskem pasu pod skupnim vplivom valovanja in hitrostjo odlaganja sedimenta.

Introduction

Many papers have debated the fossil oyster's paleoecological and biostratinomic properties (e.g., El-Hedeny, 2005, 2007; El-Sabbagh, 2008; Lopes, 2011; Domènech et al., 2014; El-Sabbagh et al., 2015; El-Sabbagh & El-Hedeny, 2016; Breton et al., 2017). The stratigraphic studies of Miocene deposits of the Lower Chelif Basin had been the purpose of several anterior authors (Mansour, B, 2004; Belekebir et al., 2008; Belhadji et al., 2008; Atif et al., 2008; Saint-Martin, 2008; Satour et al., 2011, 2013, 2020). According to Neurdin-Trescartes, (1995), the paleogeography of Lower Chelif Basin during the Miocene changed through the

time and the space, dependant on different supplies of sediment, coming into the basin either from the north (uplifted coastal block) from the east (shore currents bringing detrital materials from the Krouminie), and from the south from the area of Medea and Bou Hanifa.

The upper Tortonian outcrop of Sig Valley reveals three main oyster lenses with different repartition and orientation. The oyster shells are among the most favourable substrates for attachment and settlement of organisms. The effect of this latter may be simulated as encrustation or boring traces, which are very common in all the geological time epochs, and they are considered as the result of trace makers behavior, engraved on organic or rocky substrates (Gibert et al., 2004).

The purpose of this paper is to bring out and record the main traces produced by endoskeletozoa and episkeletozoa, in hopes of better understanding the environmental conditions during life and after death of oysters.

Geographic and geologic context

The stratigraphic studies of Miocene deposits of the Lower Chelif Basin had been the purpose of several earlier authors (Neurdin-Trescarte, 1992; Mansour, 2004; Belekebir et al.,2008; Belhadji et al., 2008; Atif et al., 2008; Saint-Martin, 2008; Satour et al., 2011, 2013, 2020; Satour,2021). The upper Miocene deposits are more distinguished in the center of the basin and contain many discontinuities, allowing a large variety of facies (Perrodon, 1957).

The studied outcrop belongs to the anticline of Djebel Touaka. It is located at approximately 1.5 km, south of the Sig City (Fig. 1). It is exposed

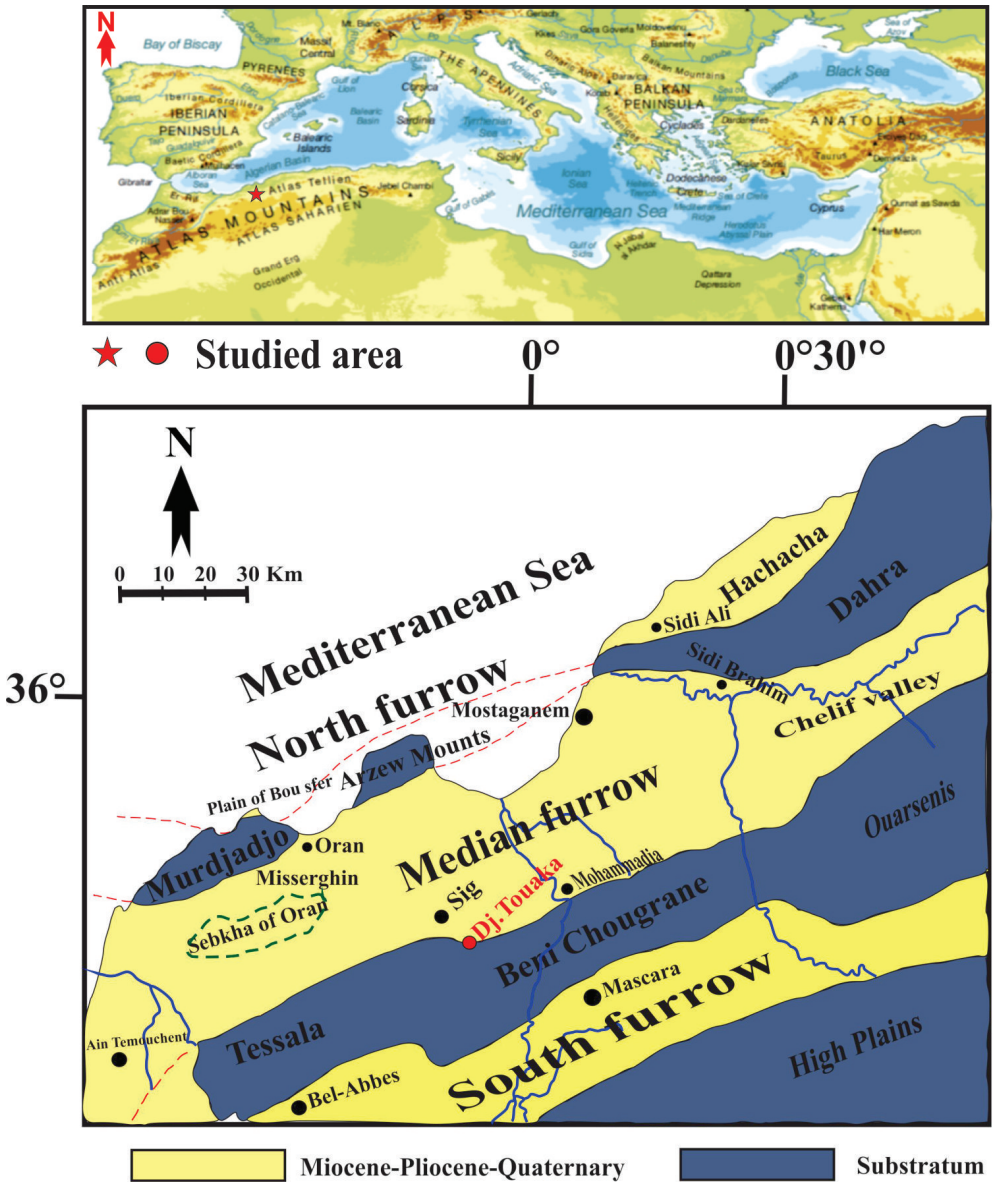

Fig. 1. Geographic and geologic localization of the studied area.

on the eastern side of the Sig Valley and belongs to the Beni Chougrane mounts. The upper Tortonian section is unconformly overlies the red sandstones of the second post-nappe cycle (Saint Martin, 1990). From bottom to top, it comprises numerous sandstones layers at the base showing horizontal, oblique and cross bedding, sandy yellowish marls contain three larger oyster's beds, blue marl, and alternation of fossiliferous limestone and marls, followed by the Messinian diatomites and El Bordj sands (Bessedik et al., 1997; Mansour, 2004) (Fig. 2).

Methodology

After washing and cleaning, 186 specimens were identified and analysed from the three oyster beds: 30 specimens were recovered from the first bed, 127 from the second bed, and 29 specimens from the third bed. The oyster shell beds were collected directly from the surface or by digging about 30 cm in sediments. The shells have different sizes (less than 70 mm for small shells and more than 70 mm for medium and large shells). They were described in the field by measuring the lateral extension, thickness; packing density and

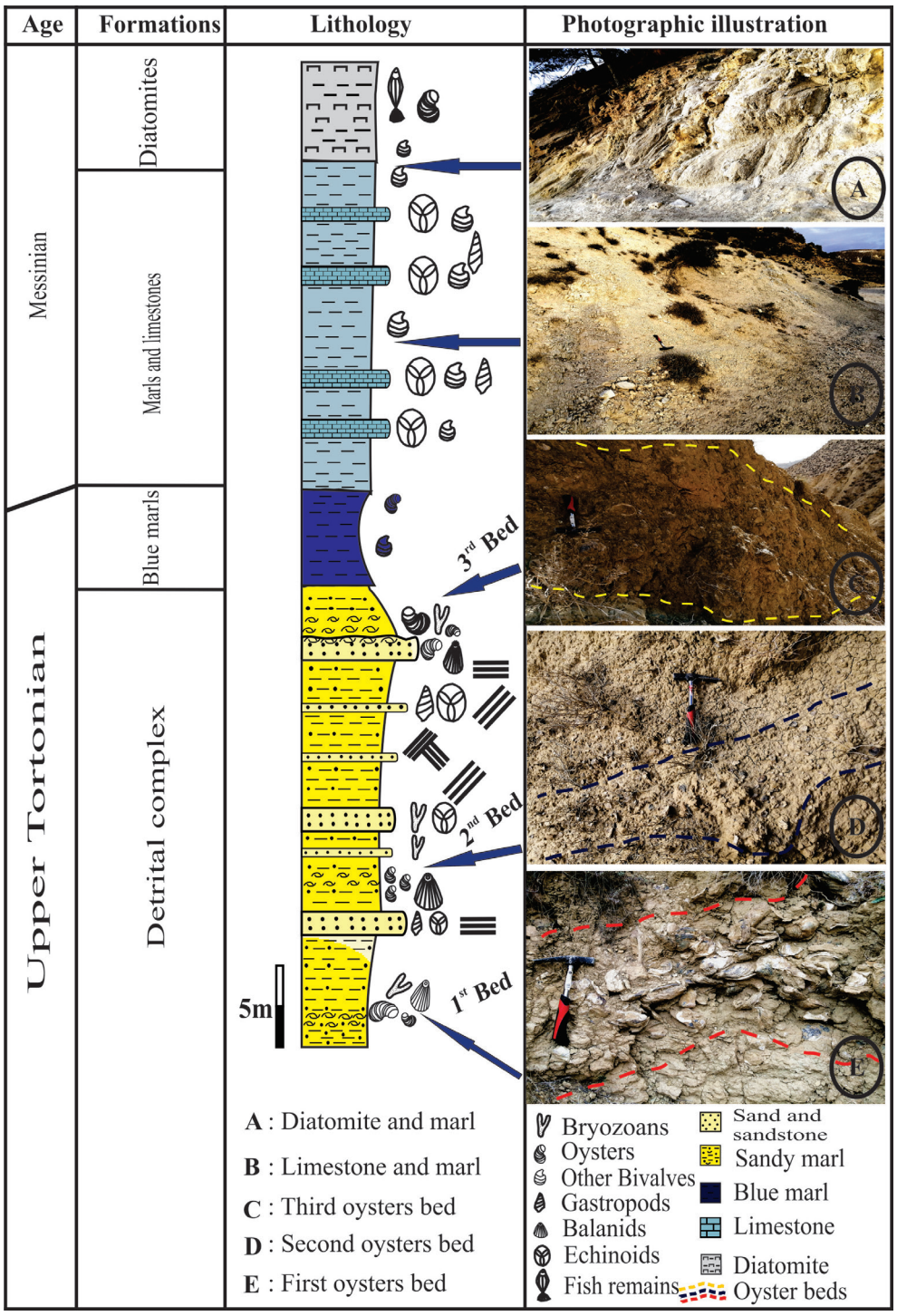

Fig. 2. Lithostratigraphic section of the upper Tortonian beds of Djebel Touaka (Sig).

shell orientation, taphonomic properties (disarticulation, borings and encrustation) were analysed in the laboratory.

The oyster specimens are stored at the Laboratory of paleontology, stratigraphy and paleoenvironments of the University of Oran 2.

Results

Description of oyster's beds

The collected oysters are almost disarticulated. However, two specimens from the third lens are preserved with valves still connected and showing vertical aggregates in the first and second beds (in french: Crassat d'huitres). They are adult forms, belonging to two families, Ostreidae and Gryphaeidae (Fig. 3).

The first lens takes place at the base of the marls, sometimes yellowish and sandy, with a lateral extension of about 40 m and variable thickness (30 to 70 cm), represented essentially by *Ostrea lamellosa* (16 left valves; LV), *C. gryphoides* (6 left valves, 3 right valves; RV) and *H. squarrosa* (5 LV). The distribution of the specimens shows a strong concentration in the center (more than 60 percent) and becomes less dense (rarely seen) when we move toward the northeast and the southwest directions (less than 15 percent). They have a random distribution and slightly slanted with a predominance of concave-down valves compared to convex-up ones.

The second lens appears toward the middle of the detrital complex, in the yellowish sandy marls with a metric extension (about 70 m). The assemblage of oysters belongs to *O. lamellosa* (112 LV) and *H. squarrosa* (15 LV), characterized by small size and homogenous repartition (without any defined orientation of shells).

The third lens sets down at the surface of the last indurated sandstones bar (hard ground), appears like a tabular bed, with a lateral extension of 30 m. The collected shells were assigned to *O. lamellose* (24 LV, 3 RV), *H. squarrosa* (2 articulated shells) and *Spondylus crassicosta* (one articulated shell). The specimens distributed at the surface of the sandstone bar (the last sandstone layer), show significant dominance of convex-up valves and without any observed direction.

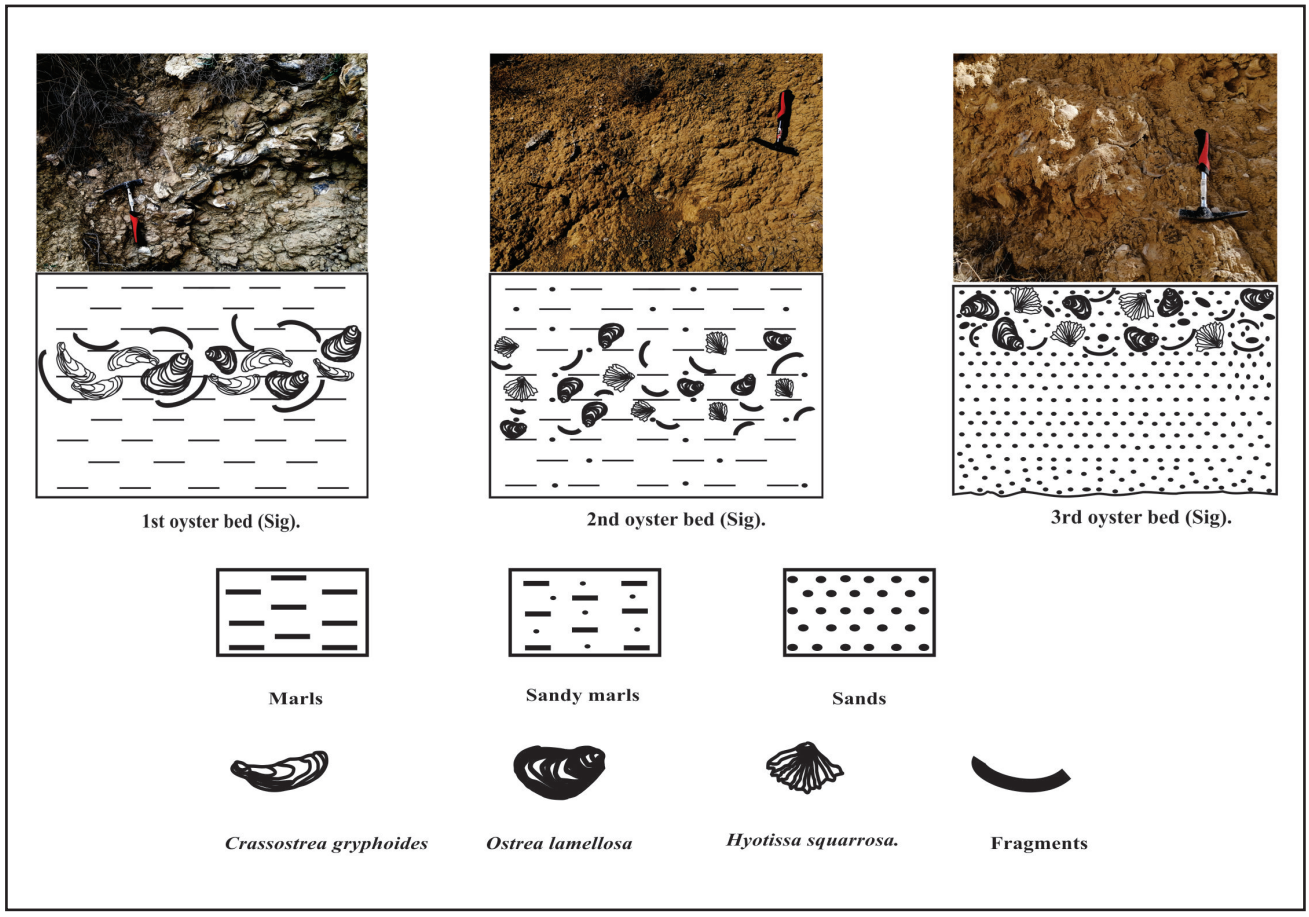

Fig. 3. The three beds identified from the upper Tortonian of Djebel Touaka (Sig).

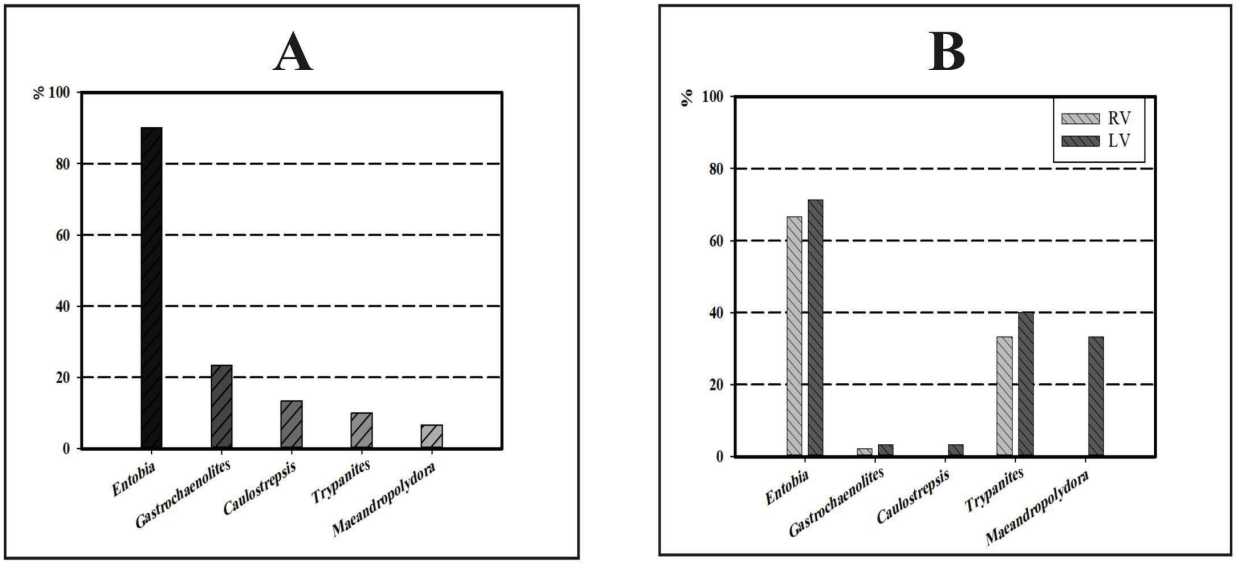

Fig. 4. Relative proportion of determined ichnogenus. **A**: All ichnogenera present in the three beds. **B**: All ichnogenera present in the three beds depending on valves (RV: right valves, LV: left valves).

Bioerosion

Both, the left and right valves are generally bioeroded (Fig. 4). Most of the bioerosion occurs on the external side, with fewer occurrences on the interior of the shells. The traces produced by endoskeletozoans are present on 60 % of the analyzed valves, recorded often on *C. gryphoides* and *O. lamellosa*; this may be due to the limited occurrence of *H. squarrosa*.

The most prominent trace marks produced by predators in the different valves from the three lenses are *Entobia* (90 %), *Gastrochaenolites* (23.33 %), *Caulostrepsis* (13.33 %), *Trypanites* (10 %) and *Maeandropolydora* (6.66 %).

Systematic ichnology

Ichnogenus *Entobia* (Bronn, 1837-38)
Ichnospecies type: *Entobia retiformis* (Stephenson, 1952)
Entobia cretacea (Portlock, 1843)

Material: Left and right valves of *C. gryphoides, O. lamellosa* and *H. squarrosa*.

Localities: Djebel Touaka at Sig, on the South-West border of the Lower Chelif Basin (Mascara province, North-West Algeria).

Description: According to Bromley and D'Alessandro (1984), these traces correspond to round apertures connected between each other with cylindrical galleries on subsurface drilled by the siliceous sponges (oftenly *Cliona*). The diameter of these apertures measures between 0.1 and 1.5 mm, and sometimes with different diameters on the same shell (Lopes, 2011).

Two ichnospecies had been identified.

Entobia retiformis (Stephenson, 1952): This ichnospecies corresponds to perforations with millimetric diameter, organized following a right, oblique or sinuous lines (Fig. 5d).

Entobia cf. *cretacea* (Portlock, 1843): It differs from the precedent by apertures and chambers less wide and extension without wall, also by one canal interconnecting the chambers. This ichnospecies forms a network of long and right tunnels, connected with the surface by several aligned apertures (Figs. 6g, 6i).

Remarks: The ichnogenus *Entobia* is the most frequent in the recorded material. The opening chambers are distributed over both the right and the left valves of *C. gryphoides, O. lamellosa* and *H. squarrosa*, in about 90 % of specimens from the three beds, but are significantly more distinct at the external surface of the left valves (71.43 %) of all the determined species compared with the right valves (66.66 %). The intense exposure to *Entobia* contributes to the destruction of most of the right valves, due to their smaller thickness.

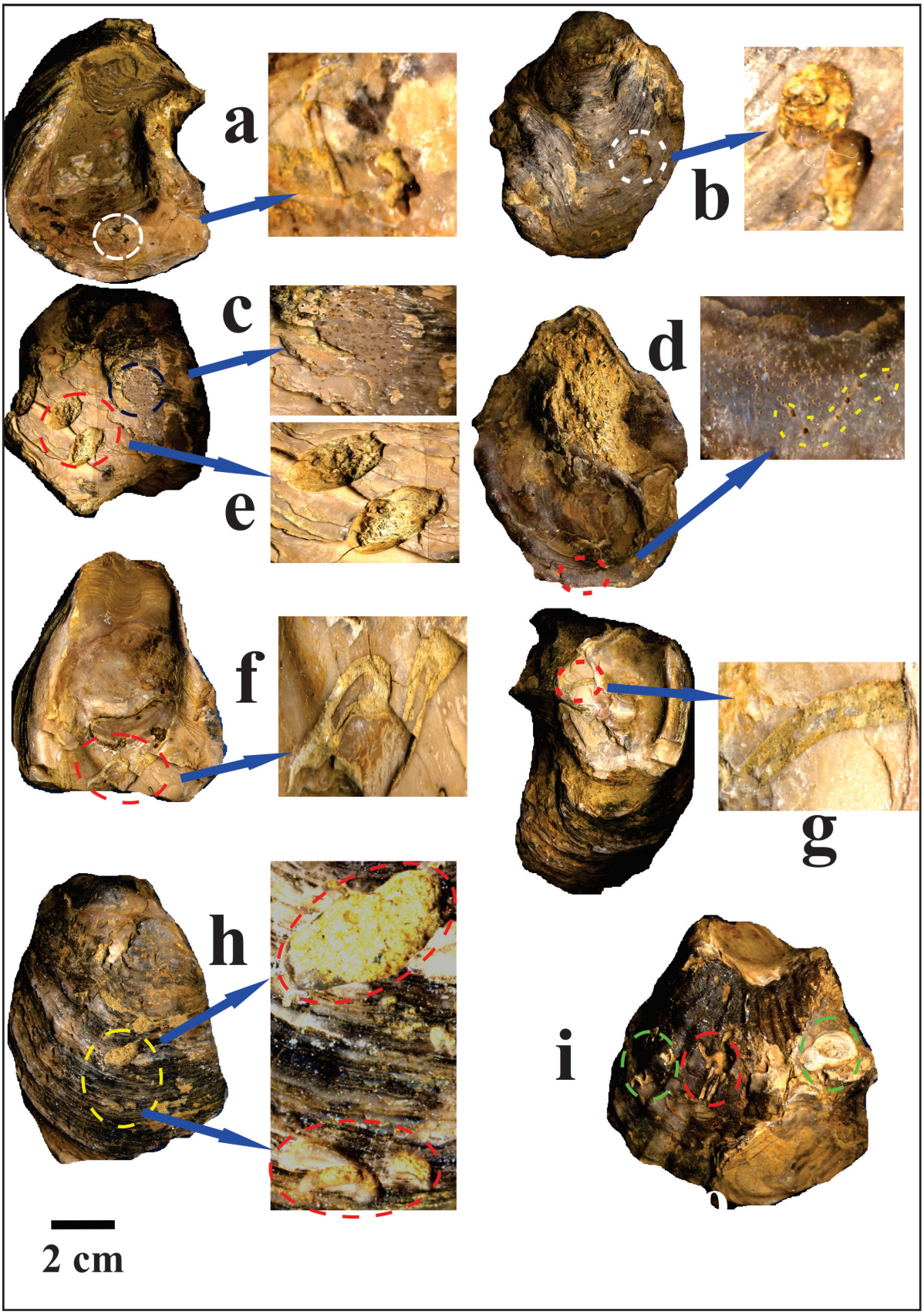

Fig. 5. **Ichnofossils: a** - *C. taeniola* on the internal surface of left valve of *C. gryphoides*; **b**, **d** - *Gastrochaenolithes* cf. *dijugus* on the external side and *E. retiformis* on the internal side of right valve of *C. gryphoides*; **c**, **e** – *Entobia ichnosp.* and *Gastrochaenolithes* cf. *dijugus* on the external face of left valve of *C. gryphoides*; **f** - *M. sulcans* on the inner side of left valve of *C. gryphoides:* **g** - *Gastrochaenolithes* cf. *dijugus* and cluster of *G. torpedo* on the outer side of *C. gryphoides;* **h** - *C. taeniola* over encrusted bivalve on the of left valve of *C. gryphoides*; **i** – *Caulostrepsis* ichnosp. on the outer surface of left valve of *H. squarrosa*, and encrustation by juvenile / adult oysters and balanids (eroded).

Ichnogenus *Gastrochaenolites* (Leymerie, 1842)
Ichnospecie type: *Gastrochaenolites torpedo* (Kelly & Bromley, 1984)
Gastrochaenolites cf. *dijigus* (Kelly & Bromley, 1984)

Material: Left and right valves of *C. gryphoides, O. lamellosa* and *H. squarrosa*.

Localities: Djebel Touaka at Sig, on the South-West border of the Lower Chelif basin (Mascara province, North-West Algeria).

Description: This ichnogenus is typically produced by bivalves and attributed to multiple taxons, *Lithophaga* (Rios, 1994; Mauna et al., 2005), *Hiatella* and mytilids (Kelly & Bromley,1984), also suspensivorous gastrochenids and pholadids (Tapanila & Hutchings, 2012). The openings are large and elongated, tilted toward the host substrate. They are simple and not aligned, solitary or in cluster, rarely with a striped parabolic base. The diameter is between 7 and 43 mm with 19 mm in average (Santos et al., 2011). In the case where these apertures are round and the neck unobservable, these characters are typical for the species.

Remarks: This ichnogenus was found frequently on the outer side of the left valves, except for some specimens of *C. gryphoides,* where it was produced on the right valves (Fig. 5.b). It is present on 23.33 % of the specimens, with 2.12 % on the right valves and 3.25 % on the left valves. The ichnospecies that were determined are: *Gastrochaenolites* cf. *dijugus* (Figs. 5b, 5e, 5h, 6.f) and *G. torpedo* (Figs. 5h, 6c, 6h).

Ichnogenus *Caulostrepsis* (Clarke, 1908).
Ichnospecies type: *Caulostrepsis taeniola* (Clarke, 1908).
Caulostrepsis taeniola (Clarke, 1908)
(Figs. 5a, 5g, 6f)

Material: Left and right valves of *C. gryphoides, O. lamellosa* and *H. squarrosa*.

Localities: Djebel Touaka at Sig, on the South-West border of the Lower Chelif basin (Mascara province, North-West Algeria).

Description: *Caulostrepsis* is the product of different families of marine polychaets (Bromley, 1978, 1994) or spionids (Barrier & D'Alessandro, 1985). It can be elongated, U-shaped, sinuous or straight. Occasionally, it appears in a figure 8-form.

Remarks: This ichnogenus appears only in the inner face of thicker left valves, in 13.33 % of the specimens, frequently parallel to the growth lamellae of oyster valves. It is represented here by one species: *C. taeniola* (Clarke, 1908). It is absent from the second bed.

Ichnogenus *Trypanites* (Mägdefrau, 1932)

Material: Left and right valves of *C. gryphoides, O. lamellosa* and *H. squarrosa*.

Localities: Djebel Touaka at Sig, on the South-West border of the Lower Chelif basin (Mascara province, North-West Algeria).

Description: Generated by polychaetes and sipunculids (Bromley, 1994; Wilson, 2007). It has a shape of a complicated network of thin shallow tubes with a cylindrical to sub-cylindrical form, straight or sinuous, characterized by a single entry.

Remarks: The ichnogenus featured here occurs on the outer side of left valve of 10 % of the specimens from the first and the second bed (Fig. 6d).

Ichnogenus *Maeandropolydora* (Voigt, 1965)
Ichnospecies type: *Maeandropolydora sulcans* (Voigt, 1965)
Maeandropolydora sulcans (Voigt, 1965)

Material: Left and right valves of *C. gryphoides, O. lamellosa* and *H. squarrosa*.

Localities: Djebel Touaka at Sig, on the South-West border of the Lower Chelif basin (Mascara province, North-West Algeria).

Description: Generally long and meandering tubes excavated by several forms of polychaetes, mostly Spionidae (Bromley & D'Allessandro,1983). It was also interpreted as traces of suspensivorous annelids from different families (Bromley, 1994). These tubes have a diameter between 0.5 and 3 mm. They are frequently found parallel to the structure of growth layers of oyster valves.

Remarks: It is the less prominent ichnogenus, occurring on the inner face of left valve from the first and the second bed, present in 6.66 % of the specimens. One ichnospecies has been named and has the morphology of *M. sulcans* (Voigt, 1965) (Figs. 5f, 6b, 6d).

Encrustation

The total of encrusters in the three beds is very scarce: 5.95 % by barnacles, 6.48 % by bryozoans and 21.62 % by juvenile oysters and other bivalves (Fig. 7). Most of the analyzed specimens were found encrusted on the outer side of the left valves, and few of them exhibit encrusters on the inner side.

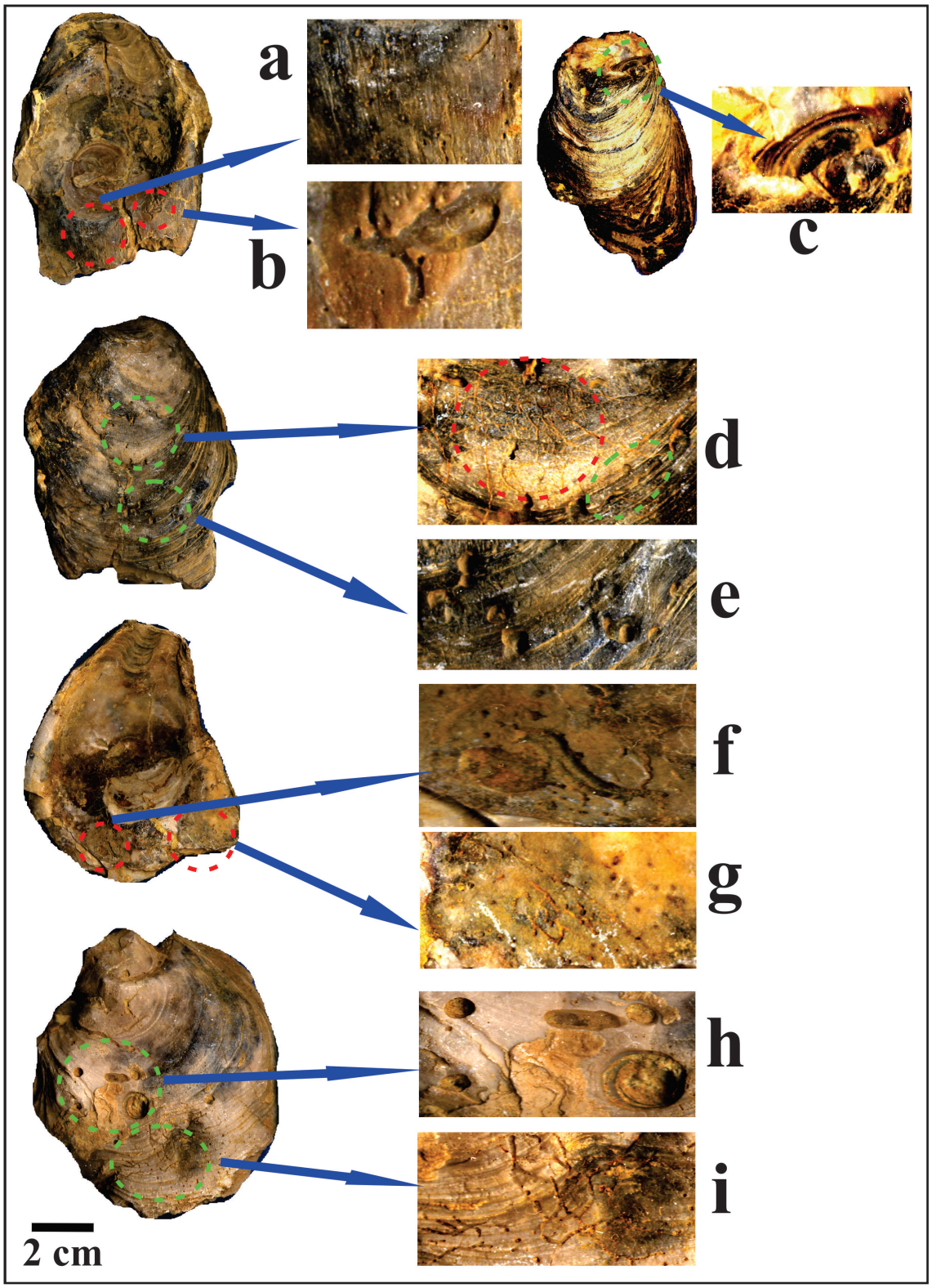

Fig. 6. **Ichnofossils:** *O. lamellosa*: **a** - *Entobia ichnosp., Caulostrepsis ichnosp.;* **b** - *M. sulcans*, on the internal surface of left valve; **c** - *G. torpedo* on the external side of *O. lamllosa* left valve, *O. lamellose*; **d** – *Trypanites ichnosp*., *M. sulcans*; **e** - *Gastrochaenolithes ichnosp*., on the external face of left valve; *O. lamellosa*: **f** - *C. taeniola*, *Gastrochaenolithes*. cf. *dijugus* and *Entobia ichnosp.;* **g** - *Entobia cretacea*, on the inner side of left valve of *O. lamellosa*; *O. lamellosa*: **h** - Cluster of different sizes of *G. torpedo*, *Entobia ichnosp.;* **i** - *E. cretacea* on the outer face of right valve.

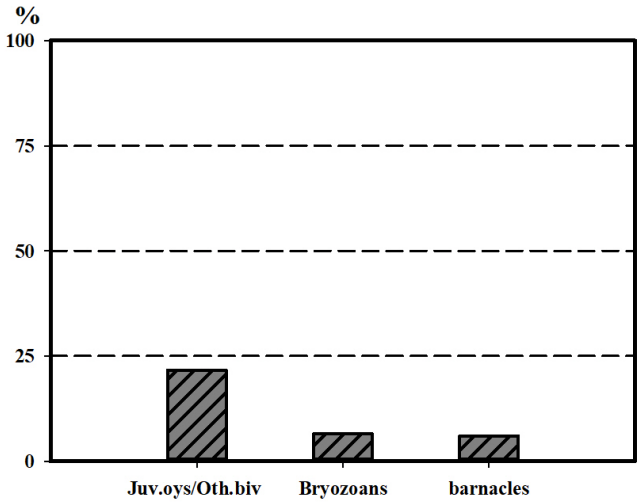

Fig. 7. Relative proportion of identified encrusters in the three beds.

The packed and dense bryozoans colonizing the internal surface of left valve; belong to the cheilostoma type (Figs. 8d–h). These thin carbonate network colonies were found only on oysters from the first and the third bed. Barnacles are recorded in several individuals of *O. lamellosa* from the second bed and one specimen of *C. gryphoides* from the first bed (Fig. 8e). They grow on the outer face of left valves, frequently forming clusters with few solitary specimens. Encrustation by juvenile oysters and other bivalves was observed from the first bed and more clearly from the second bed (Fig. 5i).

Discussion

The immense quantity of marls series interrupted by sands is the result of the upper Tortonian transgression (Belhadji et al., 2008). The intense ratio of disarticulation on oyster shells, combined with moderate fragmentation, signifies an extended time-averaging during deposit (Kidwell & Bosence, 1991; Brett & Baird, 1993). However, in the opinion of Allen (1992), disarticulated valves may serve as a sign of rapid burial episodes. These conditions may indicate that oyster shells were remobilized at a limited distance.

The scarcity of right valves suggests that they suffered from multiple sorting and reworking, because of their thinner nature, small size and low resistance to fragmentation (Lescinsky et al., 2002; El-Sabbagh et al., 2015) which led to easy decomposition after death. However, the abundance of left valves reflects the mode of life among oysters, by attaching themselves to hard substrate by means of left valves (Stenzel, 1971), which renders their remobilizing by wave currents more difficult.

The second bed is distinguished by oysters having smaller size and thinner left valves, in comparison with the two other beds. The specimen's assemblage shows a mixture of adult and younger individuals, with predominance of adults. This might indicate that they deposited during a period of deepening in a lower energy environment, affecting the shell growth.

In this area, borings were generated by predators such as sponges, polychaetes, bivalves and gastropods, they are assigned to Domichnia and Fodinichnia ethological groups, while that encrustation belongs to juvenile oysters (and other bivalves), bryozoans and balanids (cirripedes).

The abundant occurrence of *Entobia* in oyster shells from the different beds, especially on the second bed, could indicate lower energy conditions within the subtidal environment, such as low sedimentation rate and limited duration exposure on the seafloor; preferred by clinoid sponges, producer of this ichnogenus (Calcinai et al., 2005). Alternatively, it could be due to the relative absence of other organisms remains or to the occurrence of large submarine assemblage of shells (Lopes, 2011); which represent the favorable substrate available for settlement.

The rare occurrence of *Gastrochaenolites* may be due to the fact that mytilids and lithophages, which are responsible for this kind of boring, prefer to colonize lithified, hard rocky structure and large size shells (Lopes, 2011). Their record is more observable on the outer surface of left and right valves compared to the inner surface, signifying that they were produced probably during the lifetime and after the death of oysters.

On the other hand, the ichnogenera *Caulostrepsis*, *Trypanites*, and *Maeandropolydora* are found on the left valves from the first and the third beds, both on external and internal sides of large size shells. This may indicate that the larger size polychaetes created these borings and they favor large oyster shells for their settlement. As stated by Lopes and Buchmann (2008), the ichnogenus *Caulostrepsis* is infrequent amid small size bivalves.

The activity of encrusters was generally rare. Bryozoans were found only in the first bed, but barnacles are present in all beds mostly. This is probably due to the unstable environmental conditions causing sea level variations, which ranged from high to low wave currents. Oyster shells buildings forming vertical aggregates (in French, "Crassat d'huîtres") are numerous, especially on *C. gryphoides*, of the first bed, which was reported

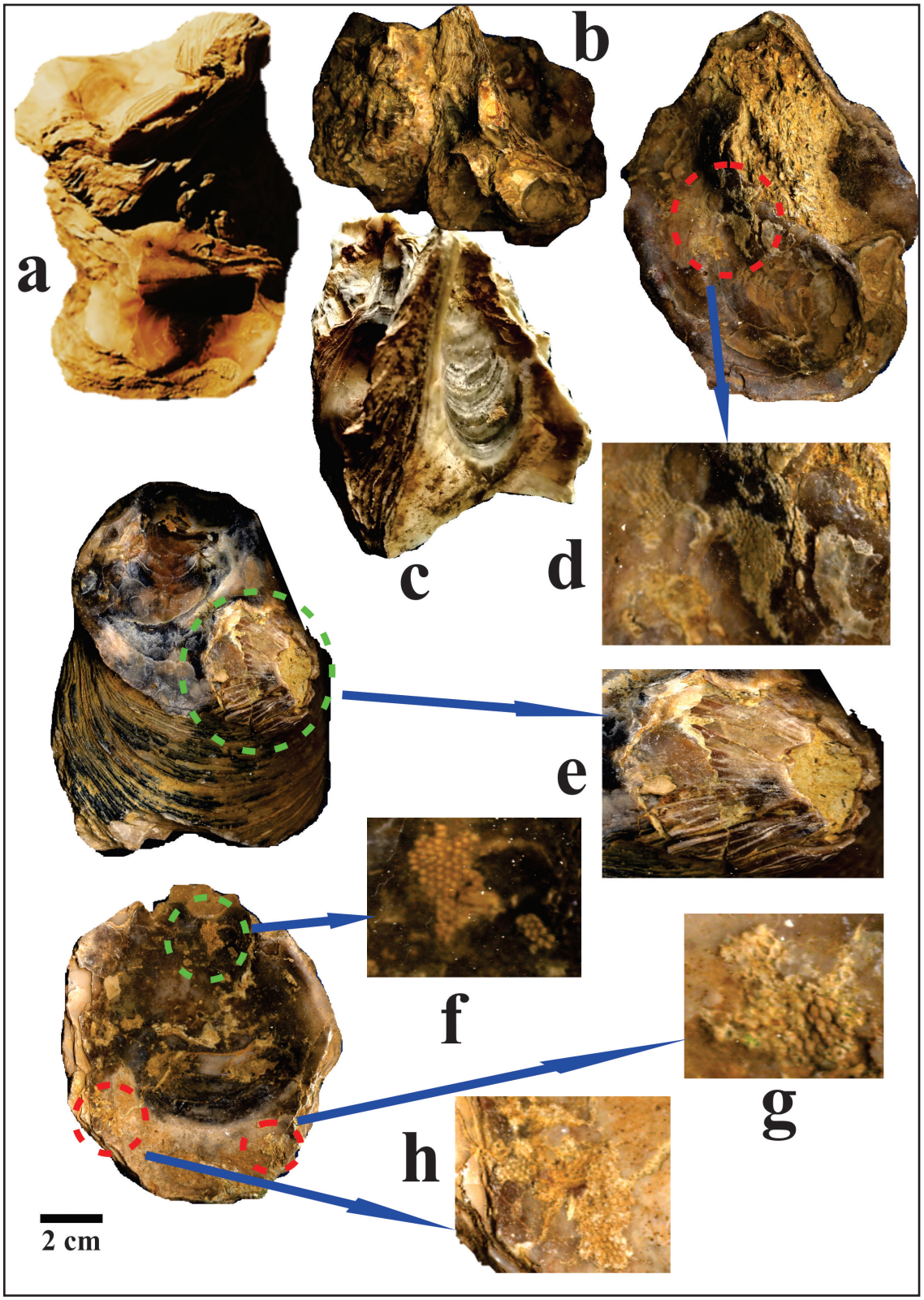

Fig. 8. **Encrustation:** Oysters aggregate: **a** - *C. gryphoides*, **b**, **c** - *H. squarrosa*; **d** - Bryozoans colonies on the internal side of right valve of *C. gryphoides*; **e** -the external surface of left valve of *O. lamellosa*, encrusted by solitary barnacle and other oyster bivalve; **f**, **g**, **h** - Bryozoans colonies distributed over the inner face of right valve of *O. lamellosa*.

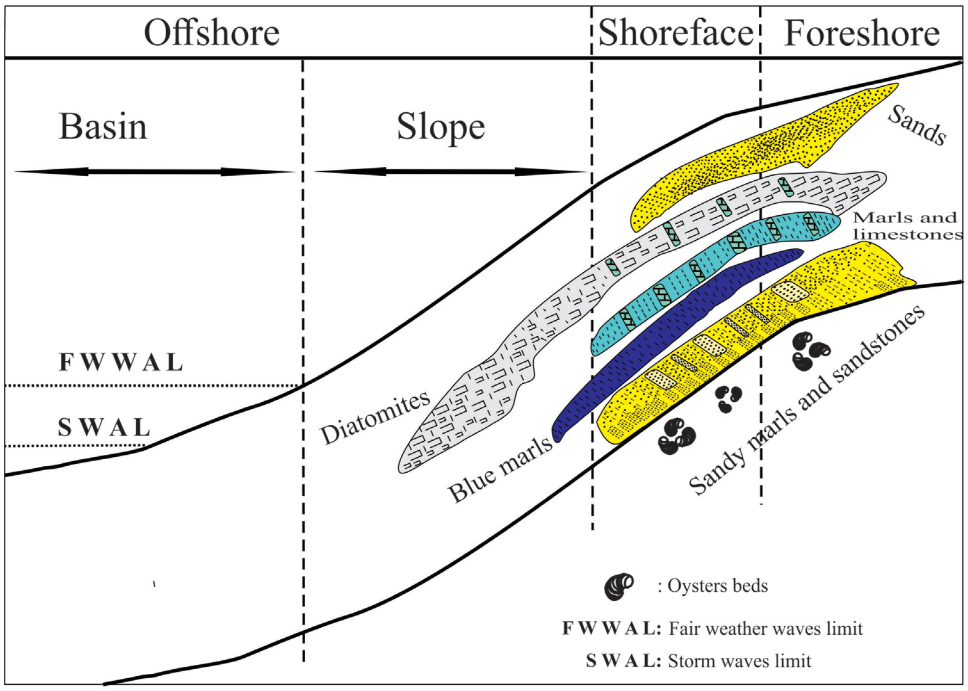

Fig. 9. Bathymetric and spatial distribution of the upper Tortonian of Djebel Touaka (Sig), marine deposits environments.

previously on oyster shells by Hocquet (1995 in Videt, 2004), El-Hedeny, 2005) and El-Sabbagh & El-Hedeny (2016). They are also observed on the species *O. lamellosa*, *H. squarrosa* of the second bed. Their occurrence is limited to the first bed, probably due to sediment input that obstructs their forming. However, they are quite recurring on the second bed, possibly in reference to the lightweight and the small size of oyster's species, which may prevent their shells from sinking rapidly after death into the substrate. These buildings are absent on the third bed. According to Hocquet (1995) the size and surface occupied by this construction are controlled by three main factors: environment hydrodynamics (must be calm and low energy), sea level (low marine level periods) and sedimentation supply (low sedimentation rate).

The features of the upper Tortonian deposits reflect paleoecological conditions coincides an environment which range from foreshore to shoreface, emphasized by turbulent, high energy and quiet periods (Fig. 9).

Conclusion

Three species of oysters were determined in the studied area, distributed over three beds, *Ostrea lamellosa*, *Hyotissa squarrosa*, and *Crassostrea gryphoides*. The first two are present in all beds, whereas the last species is limited to the lowest one. Shells show varied orientations and distribution in the space. The shells are mostly disarticulated and affected by moderate fragmentation and abrasion.

The epizoans activities are numerous, but their frequency ranges from weak to moderate. The most dominant activity is bioerosion traces, reflecting multiple shapes, round, sub-round elongated and meandering. Five ichnogenera were defined: *Entobia*, *Gastrochaenolites*, *Caulostrepsis*, *Trypanites* and *Maeandropolydora*. These boring processes are registered commonly on the external side of valves, with fewer occurrences on the internal side. This later may confirm that they are produced while oysters were alive and after death and disarticulation.

The higher percentage of *Entobia* among identified ichnogenera is perhaps due to the abundance of oyster specimens, which represent the available favored substrate for installation.

The existence and the diversity of encrusters are proportionally limited; they include juvenile oysters/other bivalves, bryozoans and barnacles, recorded on both outer and inner surfaces of left and right valves.

The complicated modality of borings and bioincrusations indicate that oysters underwent many phases of burial and uncovering resulted from the fluctuation of sea level, causing probably shells displacement at a short distance. From a paleoecological point of view, a foreshore to a shoreface environment reigned during the upper Tortonian of Djebel Touaka at Sig and it was characterized by low energy currents, interrupted by agitated and high energy intervals. This latter maybe confirmed by the recurring installments of sands layers showing sedimentary structures and the presence of the species *Spondylus crassicosta*, which indicates a nearest reef activity.

Acknowledgment

This work is done under the framework of the doctoral training of 3rd cycle, entitled: Geology of Marine and Continental Environments, Integrated Stratigraphy, Chronology and Dynamics of Paleoenvironments. This study is carried out with the support of the DGRS-DT (Ministry of Higher Education and Scientific Research). We also thank the observers for their constructive criticism.

References

Allen, J.R.I. 1992: Transport hydrodynamics. In: Briggs, D.E.G. & P.R. Crowther (eds.): Palaeobiology: A synthesis. Backwell Scientific Publications, 237–230.

Atif, K., Bessedik, M., Belkebir, L. & Mansour, B. 2008: Le passage Mio-Pliocène dans le bassin du bas Chélif (Algérie). Biostratigraphie et Paléoenvironnement. Geodiversitas, 30/1: 97–116.

Belkebir, L., Labdi, A., Bessedik, M., Mansour, B. & Saint Martin, J.P. 2008: Biostratigraphie et lithologie des séries serravallo-tortoniennes du massif du Dahra et du bassin du Chélif (Algérie). Implication sur la position de la limite serravallo-tortonienne. Geodiversitas, 30/1: 9–19.

Belhadji, A., Belkebir, L., Saint Martin, J.P., Mansour, B., Bessedik, M. & Conesa, G. 2008: Apports des foraminifères planctoniques à la biostratigraphie du Miocène supérieur et du Pliocène de Djebel Diss (bassin du Chélif, Algérie). Geodiversitas, 30/1: 79–96.

Bessedik, M., Benammi, M., Jaeger, J.J., Ameur-Chehbeur, R., Belkebir, L. & Mansour, B. 1997: Gisement à rongeurs d'âge tortonien dans des dépôts lagunaires etmarins de transition en oranie: corrélation marin continental. Actes du congrès BiochroM'97, Aguilar J P, Legendre S, Michaux J (eds.): Mém Trav E P H E, Inst. Montpellier, 21: 293–300.

Breton, G., Wisshak, M., Néraudeau, D. & Morel, N. 2017: Parasitic gastropod bioerosion trace fossil on Cenomanian oysters from Le Mans, France and its ichnologic and taphonomic context. Acta Palaeontologica Polonica, 62/1: 45–57. https://doi.org/10.4202/app.00304.2016

Brett, C.E. & Baird, G.C. 1993: Taphonomic approaches to temporal resolution in stratigraphy. In: Kidwell, S.M. & Behrensmeyer, A.K. (eds.): Taphonomic approaches to time resolution in fossil assemblages. Paleontological Society, Short Course, 6: 250–274.

Brocchi, G. 1814: Conchiologia fossili subapennina con osservazioni geologiche sugli Apennini e sul adiacente. Stamp. Reale, Milano, 1–2: 712 p.

Bromley, R.G. & D'Alessandro, A. 1983: Bioerosion in the Pleistocene of southern Italy: ichnogenera *Caulostrepsis* and *Maeandropolydora*. Rivista Italiana di Paleontologia e Stratigrafia, 89: 283–309.

Bromley, R.G. & D'Alessandro, A. 1984: The ichnogenus *Entobia* from the Miocene, Pliocene and Pleistocene of southern Italy. Rivista Italiana di Paleontologia e Stratigrafia, 90/2: 227–296.

Bromley, R.G. 1994: The palaeoecology of bioerosion. In: Donovan, S.K. (ed.): The Palaeobiology of trace fossils. John Wiley and Sons, Chichester: 134–154.

Bronn, H. G. 1837–1838: Lethaia Geognosticaoder Abbildungenund Beschreibungen der für die Gebirgs-Formationen bezeichnendsten-Versteinerungen. Schweizerbart, Stuttgart: 1350 p.

Calcinai, B., Bavestrello, G. & Cerrano, C. 2005: Excavating sponge species from the Indo-Pacific Ocean. Zool. Stud., 44/1: 5–18.

Clarke, J.M. 1908: The beginnings of dependent life. New York State Museum, Bulletin, 121: 146–196.

De Serres M. 1843: Observations sur les grandes huîtres fossiles des terrains tertiaires des bords de la Méditerranée. Annls Sci. Nat. Zool., 2e sér., 19: 143–168, pl. 2–3.

Domènech, R., Farinati, E.A. & Martinell, J. 2014: Crassostrea patagonica (d'Orbigny, 1842) shell concentrations from the late Miocene of Río Negro province, NE Patagonia, Argentina. Span. J. Palaeontol., 29/2: 165–182.

El-Hedeny, M. 2005: Taphonomy and paleoecology of the Middle Miocene oysters from Wadi Sudr, Gulf of Suez, Egypt. Revue de Paléobiologie, 24: 719–733.

El-Hedeny, M. 2007: Encrustation and bioerosion on Middle Miocene bivalve shells and echinoid skeletons: Paleoenvironmental implications.

El-Hedeny, M. & El-Sabbagh, A.M. 2007: Macro-borings on late Cretaceous oysters of Egypt. N. Jb. Geol. Paleontol. Abh., 244/3: 273–286.

El-Sabbagh, A.M., Mansour, H. & El-Hedeny, M. 2015: Taphonomy and paleoecology of Cenomanian oysters from the Musabaa Salama area, southwestern Sinai, Egypt. Geosciences Journal, 19/4: 655–679. https://doi.org/10.1007/s12303-015-0014-5

El-Sabbagh, A.M. & El-Hedeny, M. 2016: A shell concentration of the Middle Miocene Crassos-

trea gryphoides (Schlotheim, 1813) from Siwa Oasis, Western Desert, Egypt. Journal of African Earth Sciences, 120: 1–11. https://doi.org/10.1016/j.jafrearsci.2016.04.007

El-Sabbagh, A.M., El Hedeny, M., Rashwan, M.A. & Aal, A. 2016: The bivalve Placuna (Indoplacuna) miocenica from the Middle Mioceneof Siwa Oasis, Western Desert of Egypt: Systematic paleontology, paleoecology, and taphonomic implications. Journal of African Earth Sciences, 116: 68–80. https://doi.org/10.1016/j.jafrearsci.2015.12.022

Gibert, J.M., Domènech, R. & Martinell, J. 2004: An ethological framework for animal bioerosion trace fossils upon mineral substrates with proposal of a new class, Fixichnia. Lethaia, 37: 429–437. http://dx.doi.org/10.1080/00241160410002144

Hocquet, S. 1995: Enregistrement morphologique et chimique des paramètres du milieu dans la coquille de *Crassostrea gigas* Thunberg. Modèle actuel en milieu naturel et expérimental. DEA «Paleontologie, Dynamique Sédimentaire et Chronologie», Université de Dijon. 50 p. (inédit).

Kelly, S.R.A. & Bromley, R.G. 1984: Ichnological nomenclature of clavate borings. Palaeontology, 27/4: 793–807.

Kidwell, S.M. 1986: Models for fossil concentrations: paleobiologic implications. Paleobiology, 12/1: 6–24.

Kidwell, S. M. & Bosence, D.W.J. 1991: Taphonomy and time-averaging of marine shelly faunas. In: Allison, P.A. & Briggs, D.E.G. (eds.): Taphonomy: releasing the data locked in the fossil record. Topics in Geobiology, 9: 115-209.

Lescinsky, H.L., Ledesma-Vazquez, J. & Johnson, M.E. 1991: Dynamics of Late Cretaceous Rocky Shores (Rosario Formation) from Baja California, Mexico. Palaios, 6: 126–41. https://doi.org/10.2307/3514878

Lescinsky, H.L., Edinger, E. & Risk, M.J. 2002: Mollusc shell encrustation and bioerosion rates in a modern peiric sea: taphonomy experiments in the Java Sea, Indonesia. Palaios, 17/2: 171–191. https://doi.org/10.1669/0883-1351%282002%29017%3C0171%3AMSEABR%3E2.0.CO%3B2

Leymarie, A. 1842: Suite du mémoire sur le terrain Crétacé du Département de l'Aube. Mémoires de la Société Géologique de France, 5: 1–34.

Lopes, R.P. 2011: Ichnology of fossil oysters (Bivalvia, Ostreidae) from the southern Brazilian coast. Gaea, 7/2: 94–103. https://doi.org/10.4013/gaea.2011.72.02

Lopes, R.P. & Buchmann, F.S.C. 2008: Comparação tafonômica entre duas concentrações fossilíferas (shell beds) da Planície Costeira do Rio Grande do Sul, Brasil. Gaea, 4/2: 65–77. https://doi.org/10.4013/gaea.20082.03

Mansour, B. 2004: Les diatomées messiniennes du bassin du Bas Chélif (Algérie nord occidentale). Thèse de doctorat d'Etat. Université d'Oran., 286 p. 106 fig., 2 tabl., pl. IX.

Neurdin-Trescartes, J. 1995: Paléogéographie du Bassin du Chélif (Algérie) au Miocène. Causes et conséquences. Géologie Méditerranéenne, 22/2: 61–71. https://doi.org/10.3406/geolm.1995.1569

Portlock, J.E. 1843: Report on the geology of the county of Londonderry and of parts of Tyrone and Fermanagh. Dublin & London (Milliken): 784 p.

Saint Martin, J.P. 1990: Les formations récifales coralliennes du Miocène supérieur d'Algérie et du Maroc. Mémoires du Muséum National d'Histoire Naturelle, Sér. C, Sciences de la Terre, 56: 351 p.

Saint Martin, J.-P. 2008: Biodiversité dans les calcaires micritiques blancs des plates-formes messiniennes d'Algérie. Geodiversitas, 30/1: 165–179.

Satour, L., Lauriat Rage, A., Belkebir, L., Mansour, B., Saint Martin, JP. & Bessedik, M. 2011: Les bivalves ptériomorphes du Tortoniensupérieur du Dahra: systématique et paléoécologie. Bulletin duservice géologique national, Algérie, 22: 119–139.

Satour, L., Lauriat-Rage, A., Belkebir, L. & Bessedik, M. 2013: Biodiversity and taphonomy of bivalves assemblages ofthe Pliocene of Algeria (Bas Chelif basin). Arabian journal of Geosciences, 7: 5295–5308. https://doi.org/10.1007/s12517-013-1154-4

Satour, L., Saint Martin, J.P., Belkebir, L. & Bessedik, M. 2020: Evolution de la diversité des bivalves messiniens de la bordure méridionale du bassin du Bas Chélif (Algérie nord occidentale).

Schlotheim, E.F. 1813: Beitrage zur Naturgeschichte der Versteinerungen in geognostischer Hinsicht. Leonhard's Jahrbuch für Mineralogie, t. 7.

Stenzel, H.B. 1971: Oysters. In: Moore R.C. (ed.): Treatise on Invertebrate Paleontology. Part N., Mollusca 6, Bivalvia. Geological Society of America & University of Kansas Press, 3: i-iv, N953-N1224.

Stephenson, L.W. 1952: Larger invertebrate fossils of the Woodbine Formation (Cenomanian) of

Texas. United States Geological Survey, Professional Papers, 242: iv + 226 pp.

Videt, B. 2004: Dynamique des paléoenvironnements à huîtres du Crétacé Supérieur nord aquitain (SO France) et du Mio-Pliocène andalou (SE Espagne): biodiversité, analyse séquentielle, biogéochimie. Mémoire Géosciences, Rennes, 108: 1–261

Voigt, E. 1965: Über parasitische Polychaeten in Kreide-Austern sowie einige andere in Muschelschalen bohrende Würmer. Paläontologische Zeitschrift, 39: 193–211.

Appendix A. The mean TC and TD values of the rock and sediment samples from the boreholes, two tunnels and many surface locations, together with determined heat generation on several samples.

TC: Thermal conductivity, λ; TD: Thermal diffusivity, a; Heat generation (heat production rate), H; s.d.: standard deviation

TVD: true vertical depth of the cored rock samples from the boreholes: measured from the surface. - In the boreholes inside the mines: TVD from the surface above the mine. - In the tunnels: TVD from the surface above the tunnel. - *Karavanke highway tunnel: 1143 m is the altitude of the surface above the middle point of the Slovenian section of the tunnel; the underlined numbers indicate distance from the south entrance to the west tube of this tunnel.

- TVD: 0 m: surface sample.

- Rock state:

Saturated: as recovered, with natural humidity kept inside the rock (such rocks have been preserved and measured in close to their natural saturation state). – Semi-dry (partly wet): some wetness on the surface of the sample and a little bit moist inside the sample. – Dry: mostly naturally dry. – Sat-t: technically almost completely water saturated before the measurement.

Data Base No.	Borehole name	Locality	Lat. WGS84	Lon. WGS84	Altit. z	TVD	Rock or sediment type	Chrono-stratigraphy	TC λ	TC s.d.	Rock state	TC year of meas.	TC meas. device	TD a	Rock density ρ	Radiog Heat Prod. H	H year of det.
					m	m			W/(m·K)	W/m·K				mm^2/s	g/cm^3	$\mu W/m^3$	
1	SG-1/54	Hrastje Mota	46,6021	16,0735	212	120	marly clay & sand	Upper Pontian	1,60	0,09	Semi-dry	1984	MTP-1				
						220	clay & sand		1,40	0,07	Semi-dry						
4	BS-2/76	Benedikt	46,6101	15,8801	243	155	marlstone	Sarmatian	3,00	0,25	Dry	1983	MTP-1				
						230	sandy, silty marl	Badenian	1,59	0,1	Dry						
						405	sandy, silty marl	Lower Badenian	1,90	0,39	Dry	1985	MTP-4				
						420	sandy marl		1,59	0,10	Dry						
						465	sandstone		2,77	0,15	Dry						
						772	amphibolitic green schist	Ordovician-Silurian	2,56	0,11	Semi-dry	1986	MTP-1, MTP-4		2,834	0,75	1985
						781	mica schist tuff		2,77	0,03	Semi-dry				2,824	0,91	
5	Pg-6/81	Petišovci	46,5316	16,4572	159	2983	sandstone	Badenian	2,34	0,51	Dry	1987	MTP-4				
						3144	siltstone-sandstone with mica	Lower Badenian	3,01	0,17	Dry	2020	TCS	1,16			
6	B-1/81	Zreče	46,3726	15,3813	387	45	silty sandstone	Miocene	2,01	0,17	Saturated	1982	MTP-1				
						112	siltstone		3,13	0,07	Saturated						
						151	clayey siltstone		1,93	0,14	Saturated						
						202	calcitic, clayey siltstone		2,14	0,17	Saturated						
						239	calcitic marl	Upper Cretaceous	2,44	0,02	Saturated						
						299	dolomite	Middle Triassic	4,09	0,59	Saturated						
						344	dolomite		3,47	0,21	Saturated						
						401	dolomite		4,41	0,54	Saturated						
						502	phyllite-chloritic schist	Silurian-Devonian	2,14	0,16	Semi-dry				1,74	0,28	1982
7	R-1/82	Motel Rižana	45,5286	13,8840	69	87	marl	Middle Eocene	2,10	0,18	Sat./fissur.	1986	MTP-1, MTP-4				
						205	limestone	Paleocene	2,56	0,08	Saturated						
8	Mt-6/83	Moravske Toplice	46,6828	16,2221	187	806	clay	Pontian	1,90	0,09	Semi-dry	1983	MTP-1				
						848	sand, sandy marl	Pontian	1,64	0,38	Saturated						
						874	clayey silt		1,86	0,27	Semi-dry						
						879	sand		2,96	0,15	Saturated						
						893	sand		1,5	0,06	Semi-dry						
						900	sandy marl, marly clay		2,07	0,21	Saturated						
						981	sandy clay		2,25	0,21	Saturated						

10	V-38/84	Kanižarica	45,5495	15,1739	172	111	marl	Pliocene							2,15	0,56	1987
						124	marl								2,15	0,44	
						149	clay, carbonate particles		1,42	0,08	Saturated	1986	MTP-4, MTP-1				
						152	silty marl		1,50	0,04	Saturated						
						155	clay & some coal		1,64	0,04	Saturated						
						160	silty marl		1,29	0,09	Saturated						
						325	limestone	Lower Cretaceous	3,01	0,08	Semi-dry						
						325	limestone		3,17	0,08	Semi-dry						
12	B-2/85	Zreče	46,3650	15,3983	374	101	sandstone	Miocene	1,99	0,25	Semi-dry	1985	MTP-1		2,161	0,80	1985
						201	sandstone with conglomerate		2,22	0,26	Dry				2,752	1,50	
						302	dolomitic breccia		4,14	0,17	Dry				2,599	0,95	
						400	dolomitic breccia with claystone		3,35	0,28	Dry				2,620	0,99	
						500	polimicritic conglomerate		3,37	0,29	Dry				2,762	0,72	
						500	sandstone with breccia		3,56	0,37	Dry				2,721	1,74	
						556	dolomite, milonitized	Triassic	4,70	0,06	Dry				2,833	0,26	
						800	dolomite, milonitized		4,57	0,03	Dry				2,885	0,73	
13	ŠT-1/85	Štatenberg	46,3232	15,6746	250	5	marl	Upper Miocene	1,79	0,04	Semi-dry	1985-1986	MTP-1, MTP-4		2,10	1,53	1985
						98	siltstone (aleurolite)	Middle Miocene	2,01	0,08	Semi-dry				2,30	1,72	
14	V-7/85	Topličnik near Kostanjevica	45,8549	15,4130	152	52	marl or clayey marl	Upper Miocene	1,55	0,13	Semi-dry	1985-1986	MTP-4, MTP-1				
						100	marl or clayey marl		1,23	0,05	Semi-dry						
15	L-1/86	Mostec near Čatež	45,8990	15,6268	143	102	marl or clayey marl	Upper Miocene	1,43	0,29	Saturated	1986	MTP-4				
						200	marl		1,73	0,30	Saturated						
						262	sandy marl		1,82	0,34	Semi-dry						
						462	dolomite	Upper Triassic	4,77	0,93	Semi-dry						
						599	dolomite		4,27	1,34	Semi-dry						
						700	dolomite		4,24	0,90	Semi-dry						
16	SI-1/86	Sajevce near Kostanjevica	45,8660	15,4277	153	101	marly clay (soft)	Miocene	1,68	0,13	Saturated	1986	MTP-1, MTP-4				
						205	clayey marl (soft)		1,45	0,10	Saturated						
						305	clayey marl		1,34	0,05	Semi-dry						
						406	marl (clayey?)		1,50	0,08	Semi-dry						
						501	carbonatic sandstone		1,77	0,14	Semi-dry						
						592	carbonatic sandstone		2,30	0,09	Semi-dry				2,732	0,82	1987
						636	limestone	Jurassic	2,78	0,07	Dry						
						688	limestone		2,95	0,12	Semi-dry						
						799	limestone	Jurassic or Triassic?	2,99	0,18	Semi-dry						

17	CE-1/86	Levec near Celje	46,2417	15,2231	243	99	clay, some sand & pebbles	Oligocene	1,31	0,07	Saturated	1986	MTP-1, MTP-4				
18	V-8/86	Malence near Kostanjevica	45,8667	15,3992	152	1	clay with some sand	Quaternary	1,70	0,10	Saturated	2003	TCS				
						99	clayey marl	Miocene	1,50	0,04	Semi-dry	1986	MTP-4				
19	BR-1/86	Brdo near Kranj	46,2902	14,4003	464	60	clay	Oligocene	1,43	0,16	Saturated	1986	MTP-4				
20	K-2A/86	Spodnja Kostrivnica	46,2482	15,5898	247	502	tuff with sandy marl	Oligocene	2,28	0,10	Semi-dry	1987	MTP-4, MTP-1		2,610	n.d.	
						534	andesitic tuff		1,88	0,22	Semi-dry				2,406	0,90	1987
24	BZ-2/87	Brezovica	46,0276	14,4322	308	0	quartz sandstone	Permo-Carboniferous	3,84	0,25	Dry	1987	MTP-1, MTP-4				
26	PR-2/87	Prelesje near Soča river	46,0279	13,5956	79	133	limestone	Upper Cretaceous	2,75	0,32	Dry/ fissured	1987	MTP-4				
32	GT-1/88	Šentjakob near Ljubljana	46,0874	14,5869	275	56	quartz sandstone	Upper Carboniferous	4,11	0,15	Semi-dry	1988	MTP-1, MTP-4		2,732	1,47	1988
						127	sandstone, marly or carbonatic?	Middle-Upper Carboniferous							2,742	1,64	
						201	quartz sandstone		3,92	0,10	Semi-dry				2,742	1,46	
						267	sandstone	Middle Carboniferous							2,793	1,89	
						488	quartz mica sandstone		3,82	0,23	Semi-dry				2,762	1,7	
33	SOB-1/87	Murska Sobota	46,6597	16,1612	190	550	marly clay	Upper Pontian	2,08	0,04	Saturated	1987	MTP-1, MTP-4		2,181	1,65	1988
						701	sandy clay		2,13	0,04	Saturated				2,141	1,37	
						752	sandy clay	Pannonian-Pontian	2,14	0,22	Saturated				2,100	1,41	
34	GB-1/87	Gabrnik	46,4798	15,9476	220	888	sandy marl	Lower Pannonian	2,05	0,10	Semi-dry	1988	MTP-1, MTP-4		2,385	1,62	1988
						1796	sandstone	Middle Badenian	2,33	0,03	Semi-dry				2,458	1,03	
						2006	clayey siltstone	Badenian	1,94	0,04	Semi-dry				2,548	1,75	
						2011	dolomitic conglomerate		2,05	0,49	Semi-dry / fissured						
35	ŠL-1/88	Škofja Loka	46,1745	14,2803	370	0	dolomitic limestone	Upper Triassic	4,03	0,33	Semi-dry	1988	MTP-1, MTP-4		2,813	1,62	1990
37	V-931/88	Žirovski vrh Uranium mine	46,0755	14,1486	706	266	red quartz sandstone	Middle Permian	3,12	0,25	Dry	1988	MTP-4				
						292	red quartz sandstone & siltstone		2,96	0,22	Dry				2,824	2,96	1990
						352	dark grey sandstone with black shale clasts		2,12	0,16	Dry				2,824	7,09	
38	V-934/88	Žirovski vrh Uranium mine	46,0758	14,1493	700	306	colorful conglomera-te w. black siltstone	Middle Permian	3,27	0,38	Dry	1988	MTP-4				
						425	quartz conglomerate		4,05	0,12	Dry				2,691	1,97	1988
						447	grey-green conglomerate		3,81	0,21	Dry				2,691	1,00	
39	T-4/87	Radenci	46,6406	16,0509	198	542	sandstone with mica	Badenian-Sarmatian	2,39	0,23	Semi-dry	1988	MTP-1, MTP-4		2,334	0,97	1988
						624	conglomerate	Middle Badenian	3,24	0,49	Semi-dry						
						668	sandy claystone	Lower Badenian	1,89	0,04	Semi-dry				2,436	1,57	
						797	phyllonite	Paleozoic	3,88	0,48	Dry				2,773	1,57	

40	PDG-1/87	Podgorje near Cmurek	46,7049	15,8330	228	57	sandy claystone	Sarmatian	1,44	0,33	Semi-dry	1988	MTP-1, MTP-4		2,192	1,51	1988
						142	sandy siltstone	Upper Badenian	1,87	0,07	Semi-dry				2,253	1,13	
						217	sandy marl or claystone	Badenian	2,29	0,15	Semi-dry				2,273	1,5	
						250	conglomerate		2,20	0,04	Semi-dry				2,355	1,02	
						276	sandstone, siltstone, some marl		2,90	0,18	Semi-dry				2,548	0,64	
						296	siltstone or laminated sandstone		1,31	0,21	Dry				2,039	1,15	
						315	sandstone & pebbles or conglomerate		2,01	0,02	Dry				2,355	1,37	
						327	sandstone with marl		1,48	0,10	Dry				2,263	1,32	
41	LJUT-1/88	Ljutomer	46,5142	16,1897	250	1235	carbonaceous mudstone	Upper Pontian	1,79	0,08	Semi-dry	1988	MTP-1, MTP-4		2,192	1,01	1988
						1772	sandstone, fine-grained	Upper Pannonian-Lower Pontian	1,49	0,04	Semi-dry				2,304	1,46	
						2386	calcareous siltstone with sandstone	Upper Pannonian	2,66	0,10	Dry				2,508	1,91	
						2386	calcareous siltstone with sandstone		3,73	0,19	Saturated						
						2386	siltstone & sandstone		2,34	0,10	Semi-dry						
						2647	calcareous siltstone, sandstone		2,72	0,13	Semi-dry				2,752	1,91	
						2651	calcareous siltstone with sandstone		2,66	0,09	Semi-dry						
						2825	sandstone, fine-grained	Lower Pannonian	2,62	0,08	Dry				2,528	1,16	
						2825	sandstone, fine-grained		3,39	0,17	Saturated						
						2827	sandstone		2,75	0,13	Semi-dry						
						2830	sandstone, siltstone		2,69	0,07	Semi-dry				2,742	2,17	
						3087	siltstone, sandstone	Sarmatian?	2,72	0,24	Semi-dry						
						3293	calcareous siltstone		2,52	0,10	Semi-dry				2,773	1,82	
						3639	calcareous mudstone	Lower Badenian	2,34	0,22	Semi-dry				2,742	1,68	
						3935	calcareous siltstone	Karpatian? or Lower Badenian	3,15	0,25	Semi-dry						
						4020	silicified brecciated dolomite, dolosparite	Upper Triassic	4,01	0,47	Dry				2,773	0,66	
						4048	gneiss (biotite-sillimanite)	PreOrdovician	2,60	0,41	Dry				2,630	1,92	
42	SOB-2/88	Murska Sobota	46,6591	16,1654	190	733	sand	Pontian	1,48	0,07	Saturated	1988	MTP-1, MTP-4				
						802	marly sandstone		2,07	0,03	Semi-dry						
						854	sandstone		2,49	0,04	Semi-dry				2,243	2,07	1990
43	P-29/88	Praproče	45,5315	13,9153	422	297	limestone	Middle Eocene	2,32	0,15	Dry	1988	MTP-1, MTP-4				
						315	limestone		2,67	0,11	Dry				2,936	3,33	1990
						338	limestone	Lower Eocene	2,67	0,10	Dry						
						388	limestone		2,56	0,14	Dry						
						500	limestone		2,47	0,10	Dry						

45	ŠD-2/88	Špitalska Draga near Metlika	45,6611	15,3108	183	60	limestone	Upper Jurassic	2,9	0,17	Dry	2003	MTP-1				
						85	limestone	Lower Jurassic	2,62	0,04	Dry						
						90	dolomitic limestone, limestone, breccia		3,5	0,18	Dry						
46	V-14/83	Vaseno	46,2180	14,6996	437	202	dolomite	Middle Triassic	3,94	0,15	Dry	1983	MTP-1				
						300	dolomite		2,94	0,08	Dry/ fissured						
						349	dolomite		3,82	0,31	Dry/ fissured						
						496	dolomite		4,11	0,20	Dry/slightly fissured						
						550	dolomite		4,10	0,25	Dry/ fissured						
						610	dolomite		3,79	0,73	Dry						
47	V-2/79	Avber near Sežana	45,7764	13,8616	232	0	limestone	Upper Cretaceous	2,85	0,12	Dry	1986	MTP-1, MTP-4				
48	ČV-1/86	Črna vas near Ljubljana	46,0142	14,5136	288	5	clay	Quaternary	1,15	0,16	Saturated	1986	MTP-1, MTP-4				
						9	clay		1,12	0,45	Saturated						
						12	clay		1,45	0,55	Saturated						
51	Pg-7/88	Petišovci	46,5375	16,4849	158	1360	sandstone (laminated)	Lower Pontian	2,24	0,17	Dry	1988-1989	MTP-1, MTP-4				
						1365	sandstone	Upper Pannonian or Lower Pontian	2,03	0,10	Dry				2,406	1,99	1990
						1628	sandstone & siltstone	Upper or Lower Pannonian	2,61	0,15	Dry						
						1628	sandstone & siltstone		3,05	0,04	Saturated						
						1642	marly siltstone		2,19	0,28	Dry				2,610	1,63	
						1704	sandstone & siltstone		2,01	0,10	Dry						
						1704	sandstone & siltstone		2,74	0,08	Saturated						
						1710	sandstone		2,21	0,13	Dry						
						1710	sandstone		3,27	0,20	Saturated						
						2136	sandstone & siltstone	Sarmatian	2,97	0,20	Dry						
						2136	sandstone & siltstone		3,7	0,16	Saturated						
						2144	sandstone, marl and siltstone	Sarmatian or Badenian	2,6	0,18	Semi-dry				2,762	4,06	
						2412	sandstone with mica	Badenian	3,77	0,50	Semi-dry						
						2418	siltstone & sandstone		3,29	0,38	Semi-dry						
						2779	sandstone & siltstone	Lower Badenian	4,03	0,43	Semi-dry						
						2973	sandstone & siltstone	Badenian or Karpatian	3,36	0,19	Semi-dry						

52	DOK-1/88	Dokležovje	46,5984	16,1826	182	1348	sandstone with marl	Middle Badenian	2,21	0,04	Dry	1988	MTP-1, MTP-4				
						1539	sandstone		2,56	0,14	Semi-dry						
						1667	sandstone		2,57	0,24	Semi-dry						
						1670	silty marl with sandstone		2,31	0,19	Dry				2,559	1,38	1988
						1731	greenschist (sericite-chlorite)	Paleozoic	2,97	0,21	Dry				2,732	2,95	
						1933	eclogite		2,35	0,11	Dry				2,814	0,75	
53	Mg-6/85	Murski gozd	46,4985	16,5216	155	2063	sandstone	Badenian	2,41	0,05	Semi-dry	1985-1986	MTP-4, MTP-1		2,600	1,15	1985
						2595	silty marl & sandstone		2,52	0,10	Semi-dry				2,600	2,11	
						2730	sandstone & siltstone	Lower Badenian	2,79	0,14	Semi-dry				2,600	2,14	
						3266	silty marl		2,44	0,07	Semi-dry				2,600	1,29	
						3358	silty marl	Karpatian or Lower Badenian	2,53	0,07	Semi-dry				2,600	1,48	
						3448	calcitic silty marl		2,02	0,23	Semi-dry						
54	LK-1/89	Nadgorica near Ljubljana	46,0889	14,5630	279	203	sandstone, fine grained	Carboniferous	3,14	0,28	Dry	1989	MTP-4, MTP-1				
						351	silty shale with quartz		2,41	0,27	Dry				2,841	2,41	1990
						651	sandstone, fine-grained		2,72	0,35	Dry						
						717	shale with quartz veins		2,35	0,31	Dry				2,793	1,82	
						943	siltstone or sandstone, quartz veins		2,93	0,10	Dry				2,803	2,39	
						1038	silty claystone		3,48	0,24	Dry						
						1194	silty claystone or siltstone		3,29	0,65	Dry				2,707	2,29	
						1363	silty claystone or siltstone		3,60	0,26	Dry				2,789	2,41	
						1471	silty claystone or clayey siltstone		3,37	0,22	Dry						
						1649	silty claystone		3,30	0,28	Dry	2007	TCS		2,724	1,47	
55	SGT-1/90	Šmartno near Slovenj Gradec	46,4945	15,0794	445	319	graphitic schist	Paleozoic	2,87	0,08	Dry	1990	MTP-1, MTP-4				
						320	graphitic schist								2,559	1,57	1990
						591	amphibolitic schist with marble		2,65	0,36	Dry				2,836	1,33	
						998	chloritic biotite schist (diopside)		2,84	0,54	Dry				2,756	2,12	
56	P-27/87	Podpeč near Rižana	45,5189	13,9084	305	306	limestone	Paleocene	2,70	0,18	Dry	1987	MTP-1, MTP-4				
						355	limestone		2,62	0,08	Dry				2,671	0,78	1988
						450	limestone		3,33	0,40	Dry						

58	V-4/84	Podčetrtek	46,1652	15,6054	196	101	marl	Oligocene	2,53	0,04	Saturated/ fissured	1984	MTP-1		2,480	2,18	1984
						198	spilitic diabase tuff (metamorphosed porphyr. breccia)	Middle Triassic	2,06	0,08	Dry/ fissured				2,740	0,58	
61	Holes in the western tunnel tube wall	Karavanke Highway Tunnel	46,4678	13,9967	1143* 390	90	dolomitic limestone	Lower Triassic	3,62	0,48	Semi-dry	1987-1988	MTP-1, MTP-4		2,793	0,66	1988-1990
					426	115	limestone & dolomite		3,02	0,11	Dry/ fissured						
					508	160	limestone		2,65	0,19	Semi-dry				2,742	0,68	
					660	270	dolomite	Anisian	4,00	0,17	Semi-dry				2,844	0,62	
					700	285	red silty dolomite	Lower Triassic	3,87	0,21	Semi-dry						
					700	285	grey dolomite		3,26	0,19	Semi-dry						
					869	340	dolomite and siltsto-ne with gypsum		2,40	0,08	Semi-dry				2,814	1,85	
					911	350	black dolomite	Upper Permian?	3,85	0,36	Semi-dry				2,854	1,47	
					952	354	calcitic breccia	Middle Permian?	2,25	0,50	Semi-dry						
					1043	378	dolomite with calcite	Middle Permian-Triassic	4,88	0,48	Semi-dry				2,854	0,69	
					1210	430	dolomitic breccia & conglomerate	Middle Permian	3,44	0,54	Semi-dry				2,691	0,72	
					1690	496	dolomitic conglome-rate with sandstone	Upper Carboniferous -Lower Permian	4,13	0,60	Dry/partly crumbled				2,620	0,42	
					1755	502	black claystone with calcite	Carboniferous – Permian	1,71	0,10	Dry/partly crumbled				2,09	1,75	
					1855	525	sandstone, siltstone	Upper Carbon. -Lower Permian	2,18	0,11	Semi-dry				2,773	2,27	
					1970	544	siltstone, sandstone, limestone	Upper Carboniferous							2,691	2,22	
					2100	575	calcarenite		2,84	0,16	Semi-dry						
					2145	590	siltstone, claystone, clay		1,60	0,24	Semi-dry				2,732	2,53	
					2261	688	silty (?) limestone		3,29	0,19	Semi-dry				2,732	2,11	
63	P-8r/86	Družmirje near Velenje	46,3846	15,0697	380	356	carbonate pebble sandstone	Pliocene	2,46	0,94	Saturated	1986	MTP-4				
						357	gravel silty sand		1,01	0,06	Sat./partly crumbled						
						366	claystone with sand & pebbles		1,46	0,36	Saturated						
						367	silt with sand, clay & pebbles		1,33	0,37	Saturated						
						368	claystone		1,34	0,27	Saturated						
						369	silty and siderite claystone		1,37	0,31	Saturated						
						375	silty claystone		1,34	0,42	Saturated						

64	B-105/89	Uranium mine Žirovski vrh	46,0627	14,1563	703	72	pinky red sandstone or siltstone	Middle Permian	2,89	0,24	Semi-dry	1989	MTP-4, MTP-1		2,882	2,57	1990
						153	grey sandstone		3,28	0,22	Semi-dry						
						355	grey sandstone		3,31	0,92	Semi-dry				2,726	3,60	
66	ŠOM-1/88	Šomat near Plodršnica	46,6431	15,7589	270	357	marly sandstone	Lower Badenian	2,31	0,17	Saturated	1988	MTP-1, MTP-4		2,447	1,89	1990
						627	silty marl or marly siltstone	Lower Badenian or Karpatian	0,92	0,13	Dry				1,651	0,37	
						628	silty marl		2,44	0,19	Semi-dry						
						805	tectonic breccia of sandstone silt matrix	Karpatian	3,07	0,26	Semi-dry				2,854	2,55	
67	TB-1/89	Ljubljana, Regional waste center	46,0192	14,4789	288	152	dolomite	Triassic	3,99	0,49	Semi-dry	1989	MTP-4				
68	TB-2/89	Ljubljana, Spodnji Log	46,0258	14,4664	293	100	dolomite with lot of clay, tectonic. fissured	Upper Triassic	1,63	0,25	Semi-dry / fissured	1989	MTP-4				
70	MT-1/89	Mokrice	45,8619	15,6801	152	96	dolomite	Triassic	3,64	0,95	Dry/partly crumbled	1989	MTP-1, MTP-4				
72	TB-3/89	Ljubljana marsh, Curnovec creek	46,0196	14,4612	293	51	clay with sand & pebbles	Pleistocene	1,54	0,04	Saturated	1989	MTP-1, MTP-4				
						102	silt with sandy clay		1,95	0,09	Saturated						
						152	silty clay		2,04	0,28	Semi-dry						
						175	dolomite	Upper Triassic	5,17	0,52	Semi-dry						
						267	dolomite		5,30	0,27	Semi-dry						
						346	clayey sandstone with pebbles	Middle Triassic or Carnian?	1,60	0,11	Saturated						
77	SG-1/89	Slovenj Gradec	46,4942	15,0836	436	85	clay & sand	Pliocene	2,28	0,10	Saturated	1989	MTP-1, MTP-4				
78	DRN-1/89	Drnovo	45,9139	15,5056	150	195	carbonaceous silt & grey-brown clay	Lower Pliocene	1,68	0,45	Saturated	1989-1990	MTP-1, MTP-4				
						297	silty marl with mica		1,85	0,14	Semi-dry						
						435	silty marl	Pannonian	1,74	0,09	Semi-dry						
						437	clayey marl		1,75	0,31	Dry						
						490	silty (clayey) marl		1,72	0,03	Semi-dry						
						544	silty marl		1,63	0,07	Semi-dry				2,110	1,08	1990
						661	marly limestone	Badenian	1,89	0,06	Semi-dry				2,189	1,04	
						754	sandstone, silty clay with sand & pebbles (5%)	Ottnangian	2,23	0,07	Saturated				2,262	1,27	
						806	silty clay, silt	Ottnangian	2,13	0,07	Saturated						
						1250	silty claystone (80%), limestone & chert (20%)	Upper Cretaceous	2,00	0,22	Saturated						

79	O-1/91	Osp	45,5730	13,8533	27	306	marl	Middle Eocene	2,29	0,15	Semi-dry	1990-1991	MTP-1, MTP-4				
						405	marly limestone		2,58	0,47	Semi-dry						
						533	marly limestone		2,09	0,13	Semi-dry						
						549	marly limestone		2,41	0,22	Semi-dry						
						583	limestone	Paleocene							2,699	0,58	1995
						584	limestone		2,47	0,03	Semi-dry						
						606	limestone		2,53	0,18	Semi-dry						
						632	limestone, marly limestone		2,08	0,18	Semi-dry						
80	S-1/89	Polom near Kočevje	45,7437	14,8537	373	180	limestone	Lower Cretaceous	2,86	0,14	Semi-dry	1990	MTP-1, MTP-4				
						220	limestone		2,96	0,15	Semi-dry				2,723	n.d.	
82	MB-1/90	Maribor	46,5357	15,6836	256	19	sandy marl	Miocene	2,14	0,44	Saturated	1990	MTP-4		2,280	n.d.	
86	Holes in the tunnel tube wall	Debeli hrib Tunnel, Ljubljana	46,0091	14,5659	337* 170	47	siltstone with sandstone	Permo-Carboniferous	2,12	0,17	Semi-dry	1990	MTP-1, MTP-4		2,776	2,76	1990
					180	49	siltstone with sandstone		2,22	0,26	Sat. / perp. to bedding						
					181	49,3	siltstone with sandstone		3,01	0,16	Sat. / paral. to bedding						
87	MB-1/91	Maribor	46,5356	15,6855	256	154	sandy marl	Badenian	2,05	0,12	Saturated	1990-1991	MTP-1, MTP-4				
						353	marl	Badenian or Karpatian	2,05	0,20	Semi-dry				2,475	1,05	1992
						624	siltstone with sandstone	Karpatian?	2,51	0,31	Semi-dry				2,578	0,82	
						801	granat-muscovite gneiss, tectonized	PreCambrian	4,60	0,52	Dry				2,951	2,17	
						945	muscovite gneiss with granats		3,88	0,34	Dry				2,950	2,29	
						1331	granat-muscovite-biotite gneiss		3,05	0,31	Dry				3,042	2,37	
88	PB-5/90	Ljubljana marsh, Curnovec creek	46,0201	14,4633	292	65	clay (light brown)	Pleistocene	1,21	0,30	Saturated	1990	MTP-1, MTP-4				
						71	peat (black organic clay)		0,79	0,03	Saturated						
						127	silty sandy clay		1,70	0,28	Saturated						
						155	clay (dark grey)		1,60	0,06	Saturated						
						163	clay (red)		1,42	0,03	Saturated						
90	ŽT-1/91	Žalec	46,2561	15,1584	259	361	tuffaceous breccia and sandstone	Oligocene	1,32	0,16	Semi-dry	1990-1991	MTP-1, MTP-4		1,800	n.d.	1992
						654	silty marl (or sandstone)		1,69	0,26	Semi-dry				2,332	1,24	
						1100	calcarenite=limy tuffac. sandstone	Middle Triassic: Ladinian	3,03	0,22	Semi-dry				2,943	0,47	
						1499	keratophyre (alkali--albit trachyte)	Middle Triassic: Anisian	2,66	0,21	Semi-dry				2,922	2,97	

91	Tr-3/90	Rogaška Slatina	46,2235	15,6429	216	0	sandstone	Ottnangian-Karpatian	2,46	0,60	Dry	1990	MTP-1, MTP-4				
						228	sandstone with tuff		2,3	0,85	Dry						
92	PB-4/89	Ljubljana, Kolezija	46,0421	14,4926	292	88	quartz sandstone	Permo-Carboniferous	2,94	0,52	Semi-dry	1991	MTP-4, MTP-1				
98	PEČ-1/91	Pečarovci	46,7402	16,1361	234	1086	marly siltstone	Sarmatian	2,35	0,19	Semi-dry						
						1193	marly siltstone	Sarmatian or Badenian	2,06	0,17	Saturated						
						1211	sandstone with siltstone	Badenian	2,68	0,35	Sat./paral. to bedding						
						1212	sandstone, slightly marly		1,92	0,17	Dry				2,380	1,81	1992
						1920	dolomite	Mesozoic	3,66	0,13	Dry				3,028	1,00	
						2001	dolomite breccia with pyrites		3,40	0,51	Dry				2,752	2,27	
99	VG-1/90	Grčarevec	45,8749	14,2105	490	120	dolomite with calcite veins	Lower Jurassic	4,66	0,54	Dry	1991	MTP-4, MTP-1				
102	D-2/90	Dragonja	45,4474	13,6812	24	81	limestone	Eocene	2,16	0,12	Semi-dry	1991	MTP-4, MTP-1				
						150	marly limestone	Paleocene	2,43	0,24	Semi-dry						
106	MB-2/91	Maribor	46,5411	15,6703	256	486	gneiss	PreCambrian	3,29	0,36	Dry	1992	MTP-1, MTP-4		2,910	1,50	1992
						487	gneiss		3,75	0,64	Dry						
113	DAN-3/90	Dankovci - Moščanci	46,7543	16,1782	308	946	clayey-marly sandstone	Lower Pontian or Upper Pannonian	1,85	0,06	Saturated	1991	MTP-4, MTP-1				
						1237	sandstone	Sarmatian	2,52	0,40	Saturated						
						1314	sandstone		4,44	0,23	Saturated						
114	SGT-2/92	Mislinjska Dobrava	46,4668	15,1221	505	99	clay with quartz pebbles	Pliocene	1,57	0,16	Saturated	1992	MTP-1, MTP-4				
121	GM-1/93	Gozd Martuljek	46,4858	13,8373	742	0	quartz shale sandstone	Upper Carboniferous	2,90	0,07	Dry	1995	MTP-1				
122	RT-1/92	Rogaška Slatina	46,2286	15,6372	221	610	marly clay	Oligocene – Upper Egerian	1,57	0,08	Saturated	1992-1993	MTP-4, MTP-1		2,452	n.d.	1995
						1035	arkose sandstone	Oligocene – Lower Egerian	2,19	0,23	Semi-dry				2,470	1,28	
						1206	marl		1,52	0,06	Sat./fissur.				2,696	1,28	
						1412	tecton. sandstone, black mudstone	Middle Triassic	2,32	0,56	Semi-dry				2,713	1,72	
						1700	shale with quartz pebbles, pyrites	Permo-Carboniferous	2,09	0,25	Dry/partly crumbled				2,750	1,98	

123	KA-1/92	Dragonja	45,4445	13,6796	25	80	limestone	Paleocene-Eocene	2,56	0,10	Dry	1993	MTP-4				
						86	limestone	Paleocene	2,56	0,07	Dry						
						89	limestone		2,57	0,10	Dry						
						97	limestone with claystone		2,35	0,14	Dry						
						100	claystone with limestone pebbles		1,86	0,22	Dry						
						109	limestone with claystone		2,34	0,47	Dry						
						111	limestone, karstified		3,01	0,07	Dry						
						120	limestone		2,74	0,21	Dry						
						123	limestone		2,74	0,07	Dry						
						129	limestone		2,95	0,17	Dry						
						133	limestone	Upper Cretaceous	2,57	0,24	Dry						
						141	limestone		2,78	0,31	Dry						
						402	limestone (Hyppurites)		2,28	0,11	Dry						
						403	limestone		2,20	0,38	Dry						
124	P-12o/92	Družmirje near Velenje	46,3800	15,0672	373	758	mica sandstone and siltstone	Eggenburgian	1,67	0,25	Semi-dry	1992-1993	MTP-1, MTP-4				
						772	silty sandstone		2,12	0,22	Saturated						
						881	mica siltstone, sandstone		2,02	0,22	Saturated						
						966	sandy siltstone	Eggenburgian?	1,74	0,15	Semi-dry				2,552	1,10	1995
						1168	marly siltstone	Oligocene-Miocene: Egerian	2,27	0,32	Semi-dry						
						1375	mica siltstone, silty marlstone	Egerian	2,23	0,19	Saturated						
						1422	andesitic tuffaceous breccia		1,89	0,13	Dry						
						1425	andesitic tuffaceous breccia								2,693	0,77	
						1426	andesitic tuffaceous breccia		2,17	0,06	Dry						
						1528	black siltstone		2,17	0,10	Dry						
						1529	siltstone		1,84	0,06	Dry				2,749	1,57	
						1600	andesitic tuff (breccia)								2,656	1,17	
						1602	andesitic tuff (breccia)		2,25	0,18	Dry						
125	ČV-1/91	Čatež at Brežice	45,8916	15,5958	193	221	limy marlstone and claystone	Upper Cretaceous	2,70	0,14	Semi-dry	1992	MTP-4, MTP-1		2,931	1,50	1992
128	Mt-7/93	Moravske Toplice	46,6804	16,2229	186	824	sand	Pontian	2,34	0,21	Saturated	1993	MTP-4				
						825	sand		2,19	0,14	Saturated						

141	MK-1/93	Mark above Šempeter near Gorica	45,9287	13,6535	226	181	sandstone	Lower Eocene	2,96	0,37	Semi-dry	1993	MTP-4, MTP-1				
						183	sandstone with silty marl		3,21	0,19	Semi-dry						
148	Mrt-1/93	Sveti Martin, Kobilje breg	46,6606	16,3834	173	1931	marly siltstone	Lower Pontian?	1,71	0,14	Semi-dry / par. to bedding	1993	MTP-4				
						2092	marly siltstone, mica sandstone		3,35	0,49	Semi-dry						
						2096	marly siltstone		2,34	0,25	Semi-dry / perp. to bedding						
						2098	marly siltstone		2,52	0,14	Semi-dry						
155	Sre-1/91	Središče	46,7674	16,3240	229	2431	sandstone w. mica	Badenian	2,56	0,50	Semi-dry	1993	MTP-1, MTP-4				
						2434	sandstone w. mica		1,88	0,67	Semi-dry						
						2438	silty marlstone, mudstone?		2,58	0,10	Semi-dry						
						2439	sandstone w. mica		1,73	0,32	Semi-dry						
162	R-14/93	Področje near Hrastovlje	45,5183	13,9005	115	290	limestone	Paleocene-Eocene	2,29	0,21	Dry	1994	MTP-4				
						291	limestone		2,31	0,23	Dry						
163	LU-1/94	Lucija	45,5065	13,5988	2	204	silty carbonate sandstone	Middle Eocene	1,54	0,13	Dry/ fissured	1994	MTP-4				
						205	silty carbonate sandstone		1,43	0,07	Dry/ fissured						
						609	limestone	Upper Cretaceous	2,46	0,23	Semi-dry						
						611	limestone (fluidal sedimentation)		2,61	0,18	Semi-dry						
						611	limestone (shell)		2,65	0,19	Semi-dry						
						798	limestone (shell)		2,31	0,10	Semi-dry						
						800	limestone (bituminosed?)		2,57	0,14	Semi-dry			2,642	0,48	1995	
169	ŠE-1/94	Šempeter near Gorica	45,9216	13,6326	68	524	marl, calcareous marl (claystone?)	Middle Eocene	1,98	0,28	Dry/ fissured	1995	MTP-1				
						525	silty (calcareous) marl or shale		2,26	0,21	Dry/ fissured						
						526	marl (marly shale)		1,91	0,19	Dry/fissur.						
						938	silty (calcareous) marl		1,98	0,14	Dry/ fissured			2,622	0,51	1995	
						940	silty (calcareous) marl		2,53	0,07	Dry/paral. to bedding						
179	To-1/94	Okonina	46,3270	14,8669	393	160	breccia (dolo-limestone, marly)	Upper Oligocene: Chattian	2,17	0,14	Dry	1994	MTP-4				
189	Ce-2/95	Cerkno	46,1277	13,9881	318	693	dolomitized limestone	Upper Triassic: Norian & Rhaetian	2,36	0,20	Dry/ fissured	1995	MTP-1				
						694	dolom. limestone		2,64	0,24	Dry/fissur.						
						695	dolom. limestone		2,63	0,11	Dry/fissur.						
						1948	limestone	Upper Jurassic	2,63	0,06	Dry						

209	G-10/95	Zgornji Gabrnik	46,2718	15,5744	290	425	dolomitized tuff	Oligocene	1,97	0,06	Dry/fissur.	1996	MTP-1				
						602	calcareous siltstone		2,35	0,07	Dry						
233	PC-3/84	Topolšica	46,3939	15,0240	378	195	claystone	Pliocene	1,29	0,45	Saturated	1986	MTP-4				
247	PI-3/84	Šoštanj-Metleče	46,3847	15,0378	359	303	claystone	Pliocene	1,31	0,17	Saturated	1986	MTP-4				
252	Ng-1/18	Spodnje Negonje	46,2450	15,6172	268	300	mica siltstone and sandstone	Lower Oligocene	2,84	0,06	Semi-dry	2019	TCS	0,94			
						301	mica siltstone and sandstone		2,85	0,15	Semi-dry			0,60			
						508	siltstone with andesitic tuff		3,06	0,09	Semi-dry			0,94			
						509	siltstone with andesitic tuff		2,99	0,09	Semi-dry			1,11			
275	S-1j/83	Leženj	46,3880	15,0838	460	386	sandy clay	Pliocene	2,01	0,25	Saturated	1986	MTP-4				
276	P-2n/86	Gaberke	46,3883	15,0791	404	302	lignite	Pliocene	0,58	0,15	Semi-dry	1986	MTP-1, MTP-4				
						320	lignite		0,97	0,60	Semi-dry						
						325	lignite		0,59	0,16	Semi-dry						
						345	lignite		1,34	0,22	Semi-dry						
						348	lignite		0,78	0,20	Semi-dry						
277	P-2ut/87	Gaberke	46,3909	15,0743	377	290	dolomite	Middle Triassic	4,06	0,42	Dry	1987	MTP-1, MTP-4				
278	S-6s/83	Gaberke	46,3864	15,0717	382	337	claystone	Pliocene	1,30	0,37	Saturated	1986	MTP-1, MTP-4				
279	P-6t/84	Gaberke	46,3868	15,0709	384	401	lignite with clay	Pliocene	1,52	0,27	Saturated	1986	MTP-4, MTP-1				
280	P-5t/84	Gaberke	46,3877	15,0719	384	404	hydrothermally metam. dolomite (millonite)	Middle Triassic	3,46	0,24	Saturated/ fissured	1986	MTP-4				
281	S-60/86	Deberca near Velenje	46,3752	15,1172	406	48	lignite with clay	Pliocene	1,43	0,19	Saturated	1987	MTP-1, MTP-4				
						49	lignite with clay		1,29	0,20	Saturated						
						52	clay		1,46	0,17	Saturated						
						53	lignite, lignite with clay		0,82	0,14	Saturated						
						54	clay, lignite with clay		1,51	0,13	Saturated						
						57	clay		1,58	0,14	Saturated						
						59	clay with sand		1,91	0,19	Saturated						
282	J-1g/05	Velenje lake, Restaurant Jezero	46,3689	15,0929	370	2142	siltstone or mudstone	Lower Oligocene	2,34	0,18	Dry	2007	TCS				
						2143	siltst. or mudstone		2,39	0,15	Dry						
						2144	siltst. or mudstone		2,14	0,20	Dry						
						2144	siltst. or mudstone		2,27	0,06	Dry						
						2145	siltst. or mudstone		2,16	0,07	Dry						
						2145	siltst. or mudstone		2,25	0,05	Dry						
						2145	siltst. or mudstone		2,27	0,12	Dry						
						2146	siltst. or mudstone		2,21	0,11	Dry						
283	PJ-4/83	Šoštanj - Metleče	46,3855	15,0422	375	335	claystone	Pliocene	1,58	0,21	Saturated	1986	MTP-1, MTP-4				

284	PL-6/84	Šoštanj	46,3852	15,0514	360	397	claystone	Pliocene	1,35	0,24	Saturated	1986	MTP-4				
285	P-12u/85	Šoštanj - Družmirje	46,3824	15,0633	373	418	claystone, sandy siltstone	Pliocene	1,42	0,20	Saturated	1986	MTP-4, MTP-1				
407	BKV-1/98	Krmačina near Draši̇či	45,6664	15,3897	180	145	flysch marlstone	Upper Cretaceous	2,37	0,16	Dry	2003	MTP-1				
408	Rd-1/93	Radovica	45,6908	15,3387	330	225	limestone	Upper Jurassic	2,9	0,04	Dry	2003	MTP-1				
430	Jan-1/04	Janežovci	46,4666	15,8761	244	363	marly siltstone with bioturbations	Pontian	1,98	0,26	Semi-dry	2004	MTP-1, MTP-4				
						364	sand or very loosely sandstone		1,79	0,14	Saturated						
						365	sandstone, fine-grained		1,90	0,10	Semi-dry						
						626	sandstone, fine-grained (bioturb.)		2,01	0,15	Semi-dry						
						628	sandstone, fine-grained		2,06	0,18	Saturated						
						629	marly siltstone		1,84	0,15	Semi-dry						
						822	marly siltstone		2,06	0,13	Semi-dry						
						823	sandstone, fine-grained		1,73	0,14	Saturated						
						823	clayey siltstone w. calcite clasts		1,97	0,10	Semi-dry						
						824	sandstone, calcitic marly clasts		1,70	0,14	Saturated						
432	To-2/04	Mala Lahinja near Nerajec	45,5061	15,1982	155	50	dolomite, tectonic. crumbled	Upper Jurassic	3,34	0,19	Dry	2004	MTP-1				
442	Pg-8/89	Petišovci	46,5415	16,4782	159	2816	sandstone, with mica	Lower Badenian	3,10 3,47	0,11 0,19	Dry Saturated	2020	TCS	1,39			
443	Pg-5/87	Petišovci	46,5365	16,4746	158	2563	sandstone, with mica	Middle Badenian	3,00 3,29	0,11 0,13	Dry Saturated	2020	TCS	1,34			
						2722	siltstone or sandstone, mica	Lower Badenian	2,90	0,26	Dry			1,30			
						2871	siltstone or sandstone, mica		2,81	0,18	Dry			1,38			
						3247	siltstone with mica	Karpathian	2,25	0,15	Dry			1,15			
						3323	siltstone or sandstone, mica		2,19	0,30	Dry			1,09			
444	Pg-9/89	Petišovci	46,5422	16,4955	160	1819	sandstone	Sarmatian	3,07	0,32	Semi-dry	1991	MTP-4, MTP-1				
						2053	sandstone and siltstone	Sarmatian	2,81	0,31	Saturated						
						2443	sandstone	Badenian	3,9	0,47	Semi-dry						
						3008	marly siltstone	Badenian or Karpathian	3,21	0,33	Saturated						

482	TVPG-1/07	Pusti Gradec	45,5187	15,1944	152	75	limestone	Lower Cretaceous	2,82	0,10	Dry	2019	TCS	1,02			
						697	dolomitic breccia	Upper Jurassic	3,74	0,37	Semi-dry	2007	TCS				
						698	dolomitic breccia		3,85	0,23	Semi-dry						
						698	dolomitic breccia		4,31	0,18	Semi-dry						
						699	dolomitic breccia		4,34	0,22	Semi-dry						
						699	dolomitic breccia		4,60	0,20	Semi-dry						
						699	dolomitic breccia		3,52	0,42	Semi-dry						
						700	dolomitic breccia		4,24	0,42	Semi-dry						
						700	dolomitic breccia		4,06	0,33	Semi-dry						
486	TVM-2/08	Medvode	46,1415	14,4045	316	350	silt (siltstone)	Oligocene	3,83	0,14	Saturated	2009	TCS				
						803	silt		1,42	0,10	Dry/ crumbled						
515	Re-1g/11	Renkovci	46,6308	16,2952	174	1484	poorly quartz sandstone	Pontian	2,40	0,11	Saturated	2012	TCS				
						1485	poorly quartz sandstone		2,48	0,12	Saturated						
516	SOB-3g/12	Murska Sobota	46,6669	16,1454	191	718	calcareous clayey siltstone	Pontian	2,4	0,10	Saturated	2012	TCS				
						719	calcareous clayey siltstone		2,54	0,17	Saturated						
						1108	gneiss, w. quartz - calcite veins	Paleozoic	3,32	0,70	Dry						
						1109	gneiss, w. quartz - calcite veins		3,34	0,29	Dry						
						1484	gneiss, with quartz	Paleozoic or PreCambrian	2,90	0,32	Dry						
517	SOB-4g/13	Murska Sobota	46,6657	16,1604	191	814	poorly quartz sandstone w. mica	Pontian	2,1	0,08	Semi-dry	2014	TCS				
						815	poorly quartz sandstone w. mica		1,96	0,11	Semi-dry						
						1197	mudstone (sandy siltstone)	Lower Pannonian	2,15	0,09	Semi-dry						
						1198	mudstone (sandy siltstone)		1,92	0,13	Semi-dry						
530	Niko-1/08	Nuskova	46,8133	16,0276	237	45	lithotamnian limestone	Badenian or Sarmatian	1,61	0,07	Saturated	2008	TCS				
						48	lithotamnian limestone	Badenian or Sarmatian	1,58	0,06	Saturated						
535	D-1/71	Drevenik	46,2714	15,5855	415	17,5	breccia limestone	Permian	2,73	0,08	Dry	2008	TCS				
						24,8	breccia limestone		2,89	0,08	Dry		MTP-4				
544	D-2/05	Mirna na Dolenjskem	45,9527	15,0673	245	148	dolomite	Middle Triassic: Ladinian	4,42	0,62	Semi-dry	2005	MTP-4, MTP-1				
550	CZ-5/20	Ljubljana, Trnovo	46,0429	14,4985	292	15	clay	Quaternary	1,42	0,10	Saturated	2020	TCS	0,45			
						17	peat with clay		0,87	0,08	Semi-dry			0,22			
						18	peat with clay		1,25	0,09	Saturated			0,33			

551	VSG-803-V3p	Podgorje near Slovenj Gradec	46,4336	15,0888	689	16	conglomerate	Badenian	3,70	0,45	Dry	2020	TCS	1,65			
						17	conglomerate		3,77	0,32	Dry			1,67			
						41	claystone		2,21	0,10	Dry			1,03			
						87	sandstone		2,56	0,23	Dry			1,03			
						116	siltstone w. pyrite		2,34	0,14	Dry			0,99			
						129	siltstone		2,20	0,18	Dry			0,78			
						139	sandstone		2,25	0,13	Dry			1,07			
						145	siltstone		2,11	0,11	Dry			0,80			
556	ZDD-RV-3/21	Domžale	46,1431	14,5911	299	26	clay with gravel	Q: Pleistocene	1,71	0,00	Semi-dry	2021	KD2Pro				
						27	clay with gravel		1,91	0,12	Semi-dry		TCS	0,48			
						29	black micritic limestone, black claystone	Upper Triassic	2,27	0,18	Semi-dry			0,68			
						32	black micritic limestone		2,56	0,26	Dry			0,97			
						39	dark grey limestone with black claystone		2,64	0,12	Semi-dry			1,05			
557	PŠ-3/91	Ljubljana, Šentvid-Pržan	46,0946	14,4611	401	81	silty shale with quartz	Permo-Carboniferous	2,81	0,21	Dry	1991	MTP-1, MTP-4				
						88	silty shale and sandstone		3,14	0,36	Dry						
						90	quartz silty sandstone		3,60	0,29	Dry				2,834	n.d.	
						95	silty shale, black		2,86	0,19	Dry						
558	PŠ-4/91	Ljubljana, Šentvid-Pržan	46,0924	14,4601	387	60	silty shale	Permo-Carboniferous	2,71	0,30	Dry	1991	MTP-4		2,758	n.d.	
559	V-46/87	Kanižarica, Eastern coal-mine field	45,5517	15,1913	178	108	sandy clay with some pebbles	Pliocene	1,32	0,09	Saturated	1987	MTP-4, MTP-1				
						163	limestone	Lower Cretaceous	2,61	0,14	Semi-dry		MTP-4				
560	C-2/82	Cezlak, Pohorje	46,4231	15,4350	649	111	cizlakite (intrusive of gabbro group)	Miocene or Oligocene	2,86	0,16	Dry	1990	MTP-4, MTP-1				
561	C-8/83	Cezlak, Pohorje	46,4226	15,4337	634	23,4	tonalite	Oligocene	2,56	0,12	Dry	1990	MTP-4		2,701	n.d.	
562	V-6/67	Rogaška Slatina	46,2405	15,6399	231	217	andesite	Oligocene?	2,54	0,16	Dry	1990	MTP-4				
563	RGS-2/90	Rogaška Slatina	46,2406	15,6399	231	223	andesite with pyrite & tuff	Upper Oligocene	3,21	0,28	Dry	1990-1991	MTP-1, MTP-4				
						256	andesite with pyrite		3,39	0,55	Dry						
						258	andesitic tuff		2,16	0,30	Dry						
564	R-10/86	Rižana-Podračje	45,5193	13,8972	98	26	limestone, marly	Paleocene-Eocene	2,42	0,12	Dry	1987	MTP-4				
						27	limestone, marly		2,60	0,08	Dry				2,711	0,55	1987
565	P-41/90	Valley between Kubed and Hrastovlje	45,5107	13,8880	165	229	limestone	Upper Cretaceous or Eocene?	2,34	0,46	Dry/ crumbled	1990	MTP-1, MTP-4				
						273	limestone		2,24	0,40	Dry						

Surf. No.	Sample label	Surface rock samples – Multi-year project: Geothermal maps of Slovenia															
1		Turiška vas, NW of Slov. Bistrica	46,4140	15,5159	636	0	eclogite, second. metamorphosed	PreCambrian or Cambrian	3,25		Dry	1983	MTP-1				
2		Turiška vas, NW of Slov. Bistrica	46,4142	15,5158	632	0	eclogite, second. metamorphosed		3,58		Dry						
3		Nova Gora, N of Slov. Bistrica	46,4082	15,5451	413	0	eclogite		3,48		Dry						
4		Fošt, NW of Slov. Bistrica	46,4093	15,4927	599	0	harzburgite, serpentinized		2,18		Dry						
5		Tomaj	45,7582	13,8583	346	0	limestone	Upper Cretaceous	2,66		Dry	1986	MTP-4, MTP-1				
6		Podpeč near Ljubljana	45,9688	14,4229	473	0	limestone	Lower, Middle Jurassic	2,78		Dry						
7		Šentilj	46,6864	15,6516	308	0	marl	Badenian	1,59		Dry	1986	MTP-1, MTP-4		2,400	1,22	1987
8		Maribor, Meljski hrib	46,5151	15,7263	280	0	sandy marl	Badenian - Sarmatian	1,43		Dry				2,400	0,57	
9			46,5324	15,7278	306	0	sandy marl		2,18		Dry				2,400	1,15	
10			46,5429	15,7462	398	0	sandy marl	Ottnangian - Karpathian	2,26		Dry						
11			46,5641	15,6669	300	0	sandy marl & claystone		1,50		Dry						
12			46,5694	15,6748	349	0	sandy marl & claystone		2,15		Dry						
13		Zgor. Kungota, Sveti Jurij	46,6428	15,5638	303	0	sandstone		2,84		Dry				2,600	0,49	
14		Morski jarek, Rošpoh creek	46,6157	15,6116	336	0	quartz phyllite	Lower Paleozoic: Ordovician-Silurian	3,62		Dry				2,700	0,46	
15		Sveta Ana, Krivi Vrh	46,6421	15,8445	347	0	sandstone	Sarmatian	3,09		Dry				2,600	0,53	
16		Spod. Kungota	46,6077	15,6526	306	0	silty sandy marl	Ottnangian - Karpathian	1,59		Dry				2,400	1,15	
17		Zgor. Kungota, Sveti Jurij	46,6421	15,5681	358	0	sandstone		2,69		Dry						
18		Šumik on Pohorje Mt.	46,5203	15,4580	470	0	amphibolite	Ordovician-Silurian?	2,64		Dry				2,700	0,15	
19		NP Bistra near Črna/ Koroškem	46,4439	14,8205	842	0	tonalite (diorite)	Paleogene	2,86		Dry				2,630	1,12	

20		Harina Zlaka near Podčetrtek	46,1599	15,6054	203	0	limy dolomite	Middle Triassic: Ladinian	3,21		Dry	1991	MTP-1, MTP-4				
21		Gabrnik below Boč, quarry	46,2756	15,5784	389	0	dolomitic breccia	Upper Triassic: Carnian	4,10	1,04	Dry						
22		Gabrnik below Boč, quarry	46,2771	15,5807	493	0	dolomite		4,70	0,43	Dry						
23		Quarry, S of Šentjur at Celje	46,1931	15,3940	291	0	keratophyre	Middle Triassic: Ladinian?	2,72		Dry		MTP-4				
24		along the road Drašiči-Krmačina	45,6688	15,3759	181	0	carbonate sandstone, calcarenite, calclutite	Upper Cretaceous	2,58		Dry	2003	MTP-1				
25		Krmačina, near borehole	45,6667	15,3883	197	0	breccia, of limestone with calcarenite		2,75	0,04	Dry / partly crumbled						
26		Metlika center, school parking	45,6556	15,3136	180	0	dolomite	Upper Triassic	4,67		Dry						
27		Radoviči at Kolpa, near Rosalnice	45,6520	15,3410	156	0	shell limestone	Upper Jurassic	2,90	0,05	Dry						
28		Vipava valley	45,8629	13,9647	158	0	micrite limestone	Upper Cretaceous	2,72		Dry	1987	MTP-1, MTP-4				
29			45,8216	13,8354	309	0	micrite limestone, with rare rudists		2,92		Dry						
30			45,8461	13,7773	349	0	sparite limestone		3,15		Dry						
31			45,8616	13,6652	412	0	micrite limestone		2,94		Dry						
32		Mala Lahinja	45,5054	15,1953	164	0	(bio)sparitic limestone	Lower Cretaceous	2,69		Dry	1987	MTP-1				
33		Zapudje, near Dragatuš	45,5021	15,1698	234	0	micritic limestone		2,81		Dry						
34		Goričane-Sora, near Medvode	46,1389	14,3866	381	0	dolomitic conglomerate	Middle Oligocene	2,81		Dry	2005	MTP-4				
35		Kropa, along the road to Češnjica	46,2888	14,2073	638	0	claystone	Lower Cretaceous	2,95	0,12	Dry	1986	MTP-4, MTP-1				

Surf. No.	Sample label	Surface rock samples - The "GRETA project" - INTERREG Alpine Space Programme															
		The town of Cerkno and the surrounding area															
36	Ko-1_ab	Košec homestead	46,1292	13,9810	374	0	dolomite	Lower Triassic	3,76	0,19	Dry	2016-2017	TCS	1,36			
37	Lab-2	Magajna farm	46,1341	13,9958	420	0	dolomite		5,60	0,20	Dry			1,34			
38	Hom-1	W of the Homec hill	46,1375	13,9947	573	0	dolomite	Middle Triassic: Anisian	5,33	0,08	Dry			-			
39	Hot-1_ab	Hotel Cerkno	46,1277	13,9885	317	0	limestone, slightly dolomitized	Lower Triassic	3,03	0,10	Dry			1,02			
40	Ra-1	Rače, along the creek	46,1284	13,9784	353	0	limestone		2,65	0,10	Dry			1,18			
41	Ra-2_a		46,1274	13,9800	334	0	limestone		2,63	0,22	Dry			1,15			
42	Ra-2_b		46,1274	13,9800	334	0	marlstone to limestone, tecton.		1,97	0,30	Dry			1,00			
43	SvJ-1_a	Sv. Jernej, Pot v Čelo	46,1266	13,9811	325	0	limestone	Upper Permian	2,36	0,25	Dry			0,97			
44	SvJ-1_b		46,1266	13,9811	325	0	black marly limestone, almost passing into coal		2,01	0,22	Dry			0,85			
45	Lab-1	along the road to Labinje	46,1321	13,9946	364	0	limestone, tectonized	Lower Triassic	2,51	0,11	Dry			0,96			
46	Lab-3	to the Mill, Labinje	46,1366	13,9939	531	0	marly limestone		2,82	0,12	Dry			0,90			
47	Hom-2	Homec hill	46,1391	13,9970	637	0	black limestone	Middle Triassic: Ladinian	2,96	0,07	Dry			-			
48	Mak-1	Maketon homestead	46,1416	13,9776	437	0	sericitized lithocrystalline tuff		3,18	0,19	Dry			1,36			
49	Mak-2_ab	Maketon homestead	46,1332	13,9780	464	0	hydrothermally altered keratophyric and porphyritic tuff		4,04	0,13	Dry			1,60			
50	St-1_ab	Strana	46,1252	13,9913	343	0	sandstone (Val Gardena) and fine-grained siltstone	Middle Permian	1,95	0,11	Semi-dry			1,56			
51	B-1_bc	Brdca, at NOB monument	46,1302	13,9891	344	0	siltstone to mudstone	Upper Triassic: Carnian (Amphicl.)	1,95	0,15	Semi-dry			1,23			
52	B-1_a		46,1302	13,9891	344	0	sandstone		2,75	0,24	Semi-dry			1,09			
53	Kc-1_def	Kacan homestead	46,1278	13,9845	349	0	clay shale (muddy shale)	Carboniferous	1,84	0,10	Semi-dry			1,59			
54	Mlin-2_abcde	Mlin, Pot pod Bregom	46,1255	13,9846	326	0	quartz conglomerate		4,83	0,25	Semi-dry			1,87			
55	Mlin-1_abcd		46,1253	13,9839	316	0	quartz sandstone w. conglomerate		3,91	0,14	Semi-dry			1,88			

Surf. No.	**Sample label**	**The wider area of the municipality of Cerkno**														
56	Je-1_ab	Jesenica, Zakriž	46,1438	13,9538	688	0	clay shale	Upper Triassic: Carnian (Amphicl.)	1,89	0,18	Dry			-		
57	Je-2		46,1435	13,9547	693	0	limestone		2,76	0,10	Dry			-		
58	ČV-1_a	Črni Vrh	46,1620	14,0582	1262	0	siltstone and clay shale (Pseudozil.)	Middle Triassic: Ladinian	1,78	0,20	Semi-dry			0,99		
59	Ot_ab	Otaležˇ	46,0947	13,9660	307	0	siltstone, light brown	Lower Triassic	3,43	0,17	Semi-dry			-		
60	ČV-1_bc	Črni Vrh	46,1618	14,0579	1254	0	tuffaceous sandstone (Pseudozilian)	Middle Triassic: Ladinian	2,45	0,13	Dry			1,35		
61	ČV-2_ab	Črni Vrh	46,1620	14,0582	1263	0	quartz sandstone (Pseudozilian)		5,30	0,19	Dry			2,31		
62	Nov_ab	Gorenji Novaki	46,1554	14,0522	951	0	tuff (Pseudozilian)		3,00	0,13	Semi-dry			-		
63	Rav	Ravne, Zakriž	46,1305	13,9571	712	0	tuff		2,32	0,10	Dry			-		
64	Zk_ab	Zakriž	46,1356	13,9741	579	0	diabase		2,95	0,14	Semi-dry			-		
65	Koj_ab	Kojca	46,1445	13,9375	639	0	dolomite (Bača), thin-bedded	Upper Triassic: Norian & Rhaetian	4,12	0,29	Dry			1,20		
66	Ža	Žabče	46,1404	13,9178	535	0	massive crystalline dolomite	Upper Triassic: Carnian (Cordevol)	5,59	0,12	Dry			1,52		
67	Žel	Želin	46,1075	13,9541	263	0	layered dolomite	Middle Triassic: Anisian	4,84	0,07	Dry			1,44		
Surf. No.	**Sample label**	**Surface rock samples - The "GeoPLASMA-CE project" – INTERREG Central Europe programme**														
68	25a	Rašica hill, NW slope	46,1434	14,4931	495	0	red calcareous sandstone grading into siltstone	Lower and Upper Cretaceous	3,13	0,06	Semi-dry	2017	TCS	1,25		
69	25bc		46,1434	14,4931	495	0	red to pink limestone		3,24	0,07	Semi-dry			1,26		
70	24abcd		46,1436	14,4961	507	0	conglomerate		3,11	0,09	Semi-dry			1,24		
71	18ab	Podutik, quarry Podutik	46,0761	14,4432	345	0	limestone & limestone breccia	Lower Jurassic (Lias)	2,79	0,09	Semi-dry			1,23		
72	26ab	Rašica hill, NW slope	46,1413	14,4913	476	0	Dachstein limestone (thick-bedded) grading into dolomite	Upper Triassic: Norian & Rhaetian	2,98	0,07	Semi-dry			1,21		
73	14ab	Podutik, Dolnice, along the road to Kamna Gorica	46,0804	14,4500	326	0			3,66	0,12	Semi-dry			1,40		
74	13abc	Podutik, Bike park	46,0758	14,4366	349	0	Main dolomite (thick-bedded)		5,18	0,13	Semi-dry			2,10		
75	29ab	N of Repče, near quarry along the road	45,9931	14,6233	408	0			4,21	0,11	Dry			1,43		

76	35ab	ESE of Mali Vrh at Prežganje, S of Veliko Trebeljevo	46,0032	14,7423	631	0	limestone & marly limestone	Upper Triassic: Carnian	2,84	0,10	Semi-dry			1,17			
77	40a	S of Mali Lipoglav, between Mali Lipoglav and Zgornja Slivnica	45,9893	14,6403	484	0	limestone (a bit tuffaceous)		2,73	0,05	Semi-dry			0,98			
78	40bc		45,9893	14,6403	484	0	tuffite		1,73	0,07	Semi-dry			0,56			
79	40d		45,9893	14,6403	484	0	limestone (tuffaceous?)		2,92	0,10	Semi-dry			1,05			
80	5a	Podutik, Toško Čelo, E of Požgane doline	46,0850	14,4128	542	0	non bedded limestone	Middle & Upper Triassic: Ladinian-Carnian	3,01	0,10	Semi-dry			1,49			
81	10a	Podutik, Prevalnik, Toško Čelo	46,0825	14,4240	503	0	marly limestone with chert	Upper Triassic: Carnian	3,46	0,15	Semi-dry			1,53			
82	34ab	between Selo near Pance and Pance	45,9986	14,6599	400	0	Schlern dolomite	Middle & Upper Triassic: Ladinian-Carnian	4,79	0,16	Semi-dry			1,74			
83	7abc	Podutik, S of Bike park	46,0751	14,4374	348	0	tuff (pieces & we-athered matrix)	Middle Triassic: Ladinian	2,72	0,16	Semi-dry			1,21			
84	8b		46,0743	14,4371	390	0	tuff		3,50	0,15	Semi-dry			1,45			
85	11ab	Toško čelo	46,0791	14,4288	366	0	limestone with cherts & marly limestone		3,14	0,13	Semi-dry			1,37			
86	31abc	Malo Trebeljevo, on open meadow	46,0208	14,7410	569	0	dolomitic marlstone & marly dolomite		3,19	0,13	Semi-dry			1,42			
87	36a	Malo Trebeljevo (N part)	46,0201	14,7410	569	0	dolomite		4,44	0,13	Semi-dry			1,25			
88	12a	W of Podutik, SE of Toško Čelo	46,0815	14,4245	485	0	dolomite	Middle Triassic: Anisian	4,44	0,15	Semi-dry			1,83			
89	6a	Toško Čelo, S of restaurant "Pri Bitencu"	46,0819	14,4183	544	0	oolite limestone (marlstone?)	Lower Triassic (Werfen fm)	2,39	0,13	Semi-dry			0,82			
90	15abc	road to Toško Čelo	46,0839	14,4215	540	0	dolomite		3,74	0,15	Semi-dry			1,83			
91	16a	road to top of the hill on Toško Čelo	46,0823	14,4182	551	0	oolite limestone		2,92	0,05	Dry			1,03			
92	17abc		46,0846	14,4194	576	0	sandstone & siltstone		2,81	0,18	Semi-dry			1,02			
93	19abcd		46,0831	14,4227	525	0	dolomitic marlstone & marly dolomite		3,48	0,14	Semi-dry			1,37			
94	32ab	along the road Repče - Pleše	45,9953	14,6167	472	0	marlstone, marly limestone	Lower Triassic	1,64	0,08	Semi-dry			1,02			
95	32c		45,9953	14,6167	472	0	limestone		2,80	0,05	Semi-dry			1,01			
96	32d		45,9953	14,6167	472	0	dolomite		4,05	0,11	Semi-dry			1,50			

97	21a	Rašica hill, SW slope to Srednje Gameljne	46,1377	14,5014	420	0	red sandstone & shale	Middle Permian (Val Gardena fm)	3,14	0,20	Semi-dry			1,76			
98	22a	W of Repče, along the road Repče - Pleše	45,9921	14,6210	467	0	siltstone (aleurolith)		2,19	0,17	Semi-dry			0,80			
99	22b		45,9921	14,6210	467	0	tuffite, light brown	Middle Triassic	3,60	0,15	Semi-dry			1,88			
100	23ab	Rašica hill, SW slope to Srednje Gameljne	46,1377	14,5014	420	0	quartz sandstone	Middle Permian (Val Gardena fm)	3,18	0,14	Semi-dry			1,44			
101	33ab	SE of Šentpavel	46,0091	14,6207	315	0	quartz-dolomitic sandstone	Middle Permian	3,24	0,12	Semi-dry			1,38			
102	33c		46,0091	14,6207	315	0	mudstone	Middle Permian	2,38	0,09	Semi-dry			0,90			
103	30b	SE of Šentpavel, along the road to the South	46,0081	14,6197	320	0	red siltstone	Middle Permian	2,40	0,11	Semi-dry			0,72			
104	30cd		46,0081	14,6197	320	0	red quartz sandstone	Middle Permian	3,63	0,36	Semi-dry			0,96			
105	27abd	Brezje near Podlipoglav	46,0049	14,6196	322	0	shale	Middle Permian	1,86	0,22	Semi-dry			0,84			
106	28ab	NW of Češnjica, SE of Sostro	46,0317	14,6165	375	0	shale	Upper Carboniferous	1,44	0,10	Semi-dry			1,09			
107	41ab	Javor above Besnica, NW of Javor	46,0247	14,6718	584	0	sandstone		2,55	0,10	Semi-dry			0,99			
108	37ab	NE of Malo Trebeljevo	46,0233	14,7437	542	0	quartz conglomerate		4,84	0,68	Semi-dry			3,62			
109	38ab	NE of Veliki Lipoglav, W of Selo near Pance	46,0037	14,6532	370	0	quartz conglomerate		4,51	0,22	Semi-dry			2,32			
110	39ab	WNW of the Radio-amateurs' Mt. hut	46,0334	14,6442	535	0	quartz conglomerate		4,01	0,11	Semi-dry			2,19			
111	1a	Ljubljana Castle, W part of the circular route	46,0488	14,5077	363	0	shale, partly siltstone (aleurolith)		2,49	0,14	Semi-dry			0,93			
112	2ab	Ljubljana Castle, SE part of the circular route at the bridge	46,0483	14,5089	368	0	shale		2,10	0,05	Semi-dry			0,76			
113	3ab		46,0483	14,5089	368	0	shale		1,70	0,05	Semi-dry			0,61			
114	4ab	Ljubljana Castle, NE corner of the castle vineyard	46,0440	14,5143	327	0	siltstone (claystone?)		1,68	0,06	Semi-dry			0,80			

Surf. No.	Sample label	Surface soil samples – The "GeoPLASMA-CE project" – INTERREG Central Europe programme														
115	4	Ljubljana, Zalog, at the GLS building	46,0739	14,6109	283	0	clay, sand & silt	Holocene	1,81		Semi-dry	2017	KD2Pro				
116	5	Ljubljana, Spodnji Kašelj, S of Sv. Andrej church	46,0542	14,6167	269	0	gravel & sand (younger backfillings)	Holocene & Pleistocene	0,76		Semi-dry						
117	6	Ljubljana, Tabor, S of the Health Center	46,0559	14,5156	296	0	gravel, sand, silt & soil	Holocene	1,38		Saturated			0,46	0,999		
118	7a	Ljubljana, Jarški prod, S of Črnuče industr. zone	46,0840	14,5447	278	0	sand & plant residues		1,18		Semi-dry			0,53			
119	7b		46,0840	14,5447	277	0	river sand		1,41		Saturated			0,42	1,001		
120	8	Ljubljana, Šmartno, 300 m E of the football field	46,0812	14,5619	278	0	gravel, sand & silt		1,21		Semi-dry			0,38	0,999		
121	16	Ljubljana Moor, Iška Loka, Ložca creek	45,9745	14,5165	290	0	peat		1,01		Saturated			0,26	1,000		
122	17	Ljubljana Moor, Podkraj - Strahomer	45,9768	14,4700	289	0	peat		0,75		Semi-dry						
123	29	Šentvid, Dvor-Stanežiče sand pit & separation	46,1121	14,4441	311	0	gravel & sand (younger backfillings)	Pleistocene	1,34		Semi-dry						
124	30	Ljubljana, Kleče, Urške Zatlerjeve street	46,0935	14,4969	307	0	Silty clay (younger gravel backfillings)	Pleistocene	1,79		Semi-dry			0,60	1,000		
125	32	Ljubljana, Torkarjeva street	46,0642	14,5318	296	0	gravel & sand (younger gravel backfillings)	Pleistocene	0,63		Dry						
126	33	Ljubljana, Jarše, Orehov Gaj	46,0802	14,5497	283	0	gravel & sand (younger backfillings)	Holocene & Pleistocene	1,28		Semi-dry			0,46	1,000		

Surf. No.	Sample label	Surface rock samples – The project "ROCKSENSE"															
127	S1	between Mts of Bezovec and Komen (Smrekovec locality)	46,4116	14,8398	1314	0	andesitic hyaloclastic breccia	Middle-Upper Oligocene: Chattian	1,60	0,06	Dry	2022	TCS	0,63			
128	S2		46,4107	14,8411	1324	0	pyroclastic fine-grained andesitic tuff		1,81	0,19	Dry			0,77			
129	S3		46,4124	14,8398	1354	0	autobrecciated andesitic lava		2,05	0,24	Dry			0,83			
130	S4		46,4123	14,8412	1415	0	andesitic hyaloclastic breccia		1,96	0,12	Dry			0,78			
131	S5		46,4106	14,8423	1371	0	andesite tuff with fine lapilli		1,71	0,04	Dry			0,68			
132	R1	NE from Renke, E of the main road	46,1052	14,9658	304	0	limestone	Triassic-Jurassic	2,91	0,24	Dry			1,08			
133	R2		46,1058	14,9682	324	0	limestone, dolom. limestone?		3,08	0,07	Dry			1,16			
134	R3		46,1076	14,9705	285	0	limestone		2,98	0,09	Dry			1,16			
135	R4		46,1092	14,9739	314	0	limestone		2,95	0,11	Dry			1,17			
136	P5	Pasjek, ESE from Spodnji Log - Tepe crossroad	46,0917	14,9276	288	0	dolomite	Middle Triassic: Ladinian	5,04	0,18	Dry			1,92			
Surf. No.	Sample label	Surface rock samples – The project "Geothermal potential of the Municipality of Velenje"															
137	T1	Pirešica 18d near Velenje	46,3434	15,1603	395	0	quartz sandstone, fine-grained	Oligocene	3,73	0,26	Dry	2022	TCS	1,26			
138	T2	Ravne 123 near Velenje	46,4164	15,0813	579	0	tonalite	Paleogene	1,81	0,26	Dry			0,50			
139	T3	Gaberke 244 near Velenje	46,4058	15,0868	429	0	dolomite, (fine) grained	Lower Triassic	3,74	0,15	Dry			1,25			
140	T4	Hrastovec 51 near Velenje	46,3888	15,1131	456	0	limestone, partly brecciated, dolomitized, tectonized		3,54	0,32	Dry			1,12			
141	T5	Hrastovec 43 near Velenje	46,3905	15,1177	502	0	chert	Middle Triassic: Anisian	4,44	0,25	Dry			1,65			
142	T5		46,3905	15,1177	502	0	massive (plate?) dolomite		4,13	0,16	Dry			1,35			
143	T6	Škalske Cirkovce near Velenje	46,3933	15,1228	656	0	crystalline limestone, dolomitized	Middle Triassic: Ladinian	4,05	0,26	Dry			1,25			
144	T7	Cemetery Podkraj near Velenje	46,3620	15,0848	386	0	dacite	Oligocene	1,72	0,11	Dry			0,69			
145	T8	Vinska Gora 20 east of Velenje	46,3395	15,1739	344	0	clayey soil	Alluvium	1,13		Saturated	2022	KD2Pro	0,42			
146	T9	N of Škale Lake near Velenje	46,3775	15,1067	392	0,4	clay	Plio-Quaternary	1,55		Saturated			0,53			

Surf. No.	Shallow hole name	Rock samples from very shallow boreholes – Multi-year project: Geothermal maps of Slovenia															
147	PG1	Josipdol on Pohorje Mt.	46,5177	15,2892	771	5	tonalite	Paleogene							2,930	3,2	1982
148	K-1	Stranice, Quarry, Slov. Konjice	46,3696	15,3582	638	1	limestone	Upper Cretaceous	2,97		Dry	1987	MTP-1, MTP-4				
149	K-2	Pečevje, Štrkla creek, Slov. Konjice	46,3834	15,3468	522	1	limestone	Cretaceous	2,90		Dry						
150	K-3	Brinjeva Gora, Slovenske Konjice	46,3767	15,4065	621	1	limestone, hydrometamorph.		2,48		Dry/ fissured						
151	K-4		46,3769	15,4058	620	1	limestone		2,49		Dry						
152	J-1	Petelinovka, Ribnica on Pohorje Mt.	46,5133	15,2782	958	1	tonalite	Paleogene							2,697	2,74	1982?
153	J-2		46,5132	15,2797	948	1	tonalite								2,677	2,13	
154	T-1	Javorič	46,5038	15,2897	1140	1	tonalite								2,697	2,29	
155	T-2	Globaški graben	46,5171	15,2898	795	1	tonalite								2,700	3,26	
156	K-41/1	Lepšnik	46,5042	15,2597	1218	1	tonalite								2,674	2,94	
157	K-41/2		46,5114	15,2676	1145	1	tonalite								2,673	2,46	
158	K-41/3		46,5044	15,2597	1211	1	tonalite								2,668	2,14	
159	K-42/2	Pesnik	46,5182	15,2551	964	1	tonalite								2,621	2,39	
Surf. No.	surface rock samples - Research for Heat-Flow modelling of the Lake Bled area																
160		Bled, W of the Lake Bled	46,3650	14,0830	547	0	massive dolomite, with oncoids & stromatolites	Middle Triassic: Anisian	3,27	0,13	Dry	2019	TCS	1,38			
									3,71	0,10	Sat-t			1,38			
161		Bohinjska Bela, 100 m N of the Church	46,3508	14,0700	476	0	organogenic limestone	Upper Permian	2,92	0,14	Dry			1,16			
									3,12	0,07	Sat-t			1,26			
162		Krnica, between Radovna Valley and Pokljuka gorge	46,3800	14,0420	686	0	limestone, micritic	Triassic	3,44	0,16	Dry			1,29			
									3,81	0,10	Sat-t			1,23			
163		Poljšica pri Gorjah, W of Apartm. Franc	46,3720	14,0760	610	0	massive dolomite	Triassic	3,71	0,23	Dry			1,40			
									4,48	0,19	Sat-t			1,50			
164		Krnica 63, SW of Apartment Natur	46,3720	14,0550	676	0	dolomitic breccia	Middle Triassic: Ladinian	3,97	0,21	Dry			1,65			
									4,55	0,16	Sat-t			1,48			
165		Poljšica pri Gorjah, 1.7 km W of Velika Zaka	46,3600	14,0600	730	0	marly limestone, with mica and peloidic limestone	Lower Triassic	3,18	0,15	Dry			1,29			
									3,60	0,12	Sat-t			1,27			

Appendix B. The mean TC values of some rock samples from Appendix A (from the boreholes and one tunnel) with determined anisotropy of TC.

DataBase No.	Borehole name	Locality	Lat. WGS84	Lon. WGS84	Altit. m	TVD m	Rock or sediment type	Chrono-stratigraphy	Rock state	TC measured	TC mean W/m·K	ANISOTROPY: TCpar/TCperp
54	LK-1/89	Nadgorica near Ljubljana	46,0889	14,5630	279	651	sandstone, fine grained	Carboniferous	Dry	parallel to bedding	3,05	1,28
						651			Dry	perp. to bedding	2,39	
86	Holes in the tunnel tube wall	Debeli hrib Tunnel, Ljubljana	46,0091	14,5659	337	49,3	siltstone with sandstone	Permo-Carboniferous	Semi-dry	parallel to bedding	3,01	1,36
						49			Semi-dry	perp. to bedding	2,22	
87	MB-1/91	Maribor	46,5356	15,6855	256	1331	granat-muscovite--biotite gneiss	PreCambrian	Dry	parallel to foliation	3,48	1,33
						1331			Dry	perp. to foliation	2,62	
124	P-12o/92	Družmirje near Velenje	46,3800	15,0672	373	758	mica sandstone and siltstone	Eggenburgian	Saturated	parallel to bedding	2,11	1,72
						758			Dry	perp. to bedding	1,23	
						772	silty sandstone	Eggenburgian	Saturated	parallel to bedding	2,17	1,05
						772			Saturated	perp. to bedding	2,07	
						881	mica siltstone, sandstone	Eggenburgian	Saturated	parallel to bedding	1,99	0,97
						881			Saturated	perp. to bedding	2,05	
						966	sandy siltstone	Eggenburgian?	Saturated	parallel to bedding	2,15	1,62
						966			Dry	perp. to bedding	1,33	
148	Mrt-1/93	Sveti Martin, Kobilje breg	46,6606	16,3834	173	1931	marly siltstone	Lower Pontian?	Semi-dry	parallel to bedding	1,71	2,14
						1931			Semi-dry	perp. to bedding	0,80	
						2096	marly siltstone	Lower Pontian?	Semi-dry	parallel to bedding	2,42	1,03
						2096			Semi-dry	perp. to bedding	2,34	
169	ŠE-1/94	Šempeter near Gorica	45,9216	13,6326	68	524	marl, calcareous marl (claystone?)	Middle Eocene	Dry / fissured	parallel to bedding	2,31	1,41
						524			Dry / fissured	perp. to bedding	1,64	
						525	silty (calcareous) marl or shale	Middle Eocene	Dry / fissured	parallel to bedding	2,39	1,13
						525			Dry / fissured	perp. to bedding	2,12	
444	Pg-9/89	Petišovci	46,5422	16,4955	160	2053	sandstone and siltstone	Sarmatian	Saturated	parallel to bedding	3,05	1,19
						2053			Saturated	perp. to bedding	2,56	

GEOLOGIJA

št.: 66/1, 2023

www.geologija-revija.si

5 Gosar, M.
Uvodnik - 70 let revije Geologija

9 Placer, L., Rižnar, I. & Novak, A.
Transverse Dinaric zone of increased compression between the Kraški rob and Hrušica Regions, NE Microadria

73 Čadež, F.
Geološka spremljava poskusnega odkopa uranove rude na Žirovskem vrhu

87 Spatzenegger, A. & Poltnig, W.
Taxonomic and stratigraphic remarks on *Placites urlichsi* Bizzarini, *Pompeckjites layeri* (Hauer), *Carnites floridus* (Wulfen) and *Sageceras haidingeri* (Hauer)

107 Oselj, K., Kolar-Jurkovšek, T., Jurkovšek, B. & Gale, L.
Microfossils from Middle Triassic beds near Mišji Dol, central Slovenia

125 Rajver, D. & Adrinek, S.
Overview of the thermal properties of rocks and sediments in Slovenia

151 Koren, K., Brajkovič, R., Bajuk, M., Vraničar, Š. & Fabjan, V.
Hydrogeological characterization of karst springs of the white (*Proteus anguinus anguinus*) and black olm (*Proteus anguinus parkelj*) habitat in Bela krajina (SE Slovenia)

167 Zhyrnov, P. & Solomakha, I.
Geological-genetic structure of Irpin city, the role of lithological factors during engineering-geological zoning and construction assessmenta

185 Khalili, R., Satour, L. & Mennad, S.
Borers and epizoans on oyster shells from the upper Tortonian, Lower Chelif Basin, NW Algeria

70 LET

ISSN 0016-7789

GeoZS
Geološki zavod Slovenije